Heterogeneity in melanoma and the microenvironment

Cerys Sian Manning

University College London

and

Cancer Research UK London Research Institute

PhD Supervisor: Dr Erik Sahai

A thesis submitted for the degree of

Doctor of Philosophy

University College London

January 2013

Declaration

I Cerys Manning confirm that the work presented in this thesis is my own. Where information has been derived from other sources, I confirm that this has been indicated in the thesis.

Abstract

This thesis addresses the signalling pathways and gene networks associated with melanoma cell motility in vivo and heterogeneity in tumour-associated vasculature. Melanoma metastasis begins with the acquisition of motility in the primary tumour, however, there is little characterisation of signalling pathways or microenvironments associated with melanoma motility in vivo. Intra-vital imaging of clonal signalling reporter cell-lines showed heterogeneous cell behaviour in vivo and increased Notch, TGF-β and SRF dependent transcription in motile cells. Further investigations into Notch signalling in melanoma metastasis showed that Notch promotes metastasis through cell-autonomous and non-cell autonomous mechanisms. The reporter cell-lines were used to enrich for the motile melanoma cell population and genes up-regulated in this population were identified. Many cell-cycle regulators, including regulators of cytokinesis, were up-regulated in the B16 F2 melanoma population enriched for motile cells. Bioinformatic analysis indicated that EZH2, a histone methyltransferase in the Polycomb repressor 2 complex, can regulate the genes associated with motile cells and EZH2 depletion decreased melanoma cell motility in vitro and metastasis in vivo. EZH2 was also shown to regulate cell morphology and the actin cytoskeleton through regulating activation of a subset of ERM proteins. Due to association between melanoma metastasis and differentiation, the role of EZH2 in melanoma differentiation state was investigated. EZH2 depletion did not significantly affect expression of melanoma differentiation markers but increased *Oca2* mRNA expression leading to increased pigment.

This thesis also investigates heterogeneity in the tumour microenvironment. Morphologically and dynamically distinct regions of the tumour vasculature were identified by intra-vital imaging and quantitative image analysis, and these regions could be followed over time using imaging windows. The tumour vasculature showed a heterogeneous response to the anti-angiogenic drug, Sunitinib, possibly due to microenvironmental factors. Aspects of vascular morphology and dynamics correlated with melanoma motility and may be used to describe microenvironments favourable for motility.

Acknowledgement

I would like to thank the many people who have helped me during my PhD. Foremost, I would like to sincerely thank Erik for the continuous support, patience, and motivation. His immense knowledge, guidance and teaching have helped me throughout the whole PhD. Secondly, thanks go to Steve who has answered every question I could throw at him, with a friendly face and without complaint. Thanks also to Rob for helping with data analysis in the angiogenesis project. The Tumour Cell Biology Lab has been a great place to work and that is down to the people in it, past and present. Thank you for being fun and friendly but also great role models and teaching me a lot (not just about science!). The work has been greatly aided by members of the Biological Resources Unit, Experimental Histopathology Lab, FACS Lab and Bioinformatics department, so thank you to everyone who has helped. Finally I would like to thank Fay, my long-suffering partner (now wife) and my family for the encouragement and distraction at times when it all seemed too much.

Table of Contents

Abbreviations

α-MSH	α-Melanocyte stimulating hormone
ANOVA	Analysis of variance
CBFRE	C-promoter binding factor responsive element
EMT	Epithelial to mesenchymal transition
ERM	Ezrin/Radixin/Moesin family
FACS	Fluorescence activated cell sorting
F-actin	Filamentous actin
FDR	False discovery rate
FITC	Fluorescein isothiocyanate
G-actin	Monomeric globular actin
GFP	Green fluorescent protein
MC1R	melanocortin-1 receptor
MITF	microphthalmia-associated transcription factor
MLC	myosin light chain
MMP	Matrix metalloprotease
mRFP	monomeric red fluorescent protein
MYLK	myosin light chain kinase
NICD	Notch intracellular domain
PBS	Phosphate buffered saline
PKA	cAMP-dependent kinase
PRC2	Polycomb repressor complex 2
Q RT-PCR	Quantitative real-time polymerase chain reaction
Rho	Ras-homologue family
ROCK	Rho- kinase
SMAD	Small mothers against decapentaplegic
SRF	Serum response factor
TGF-β	Transforming growth factor-beta
TRITC	Tetramethylrhodamine isothiocyanate
VEGF-A	Vascular endothelial growth factor A

Table of figures

List of tables

Supplementary movies and files

Supplementary movie 1 B16 F2 melanoma single cell motility in vivo.
Intra-vital movie of B16 F2 melanoma with cell membrane labelling shown in white. Images taken over a 51 minute time period. Note singly motile cells in the middle and top right corner.

Supplementary movie 2 B16 F2 melanoma streaming and collective cell motility in vivo
Intra-vital movie of B16 F2 melanoma with cell membrane labelling shown in white. Images taken over a 19 minute time period. Movie has been subject to smoothing with a Gaussian filter. Note streaming cells and a group of cells moving collectively in centre.

Supplementary movie 3 B16 F2 melanoma streaming motility in vivo
Intra-vital movie of B16 F2 melanoma with cell membrane labelling shown in white. Images taken over a 22 minute time period. Movie has been subject to smoothing with a Gaussian filter. Note 2-3 streaming cells in the left centre.

Supplementary movie 4 B16 F2 clonal Notch reporter in vivo
Intra-vital movie of clonal B16 F2 Notch reporter cell-line. Cell membranes shown in red and Notch reporter activity shown in green. Autofluorescence also visible in green channel. Images taken over a 19 minute time period. Movie has been subject to smoothing with a Gaussian filter. Note a GFP positive cell moving singly in top left and 3 GFP positive cells moving in the bottom left.

Supplementary movie 5 B16 F2 clonal TGF-β reporter in vivo
Intra-vital movie of clonal B16 F2 TGF-β reporter cell-line (with linker). Cell membranes shown in red and TGF-β reporter activity shown in cyan. Images taken over a 19 minute time period. Movie has been subject to smoothing with a Gaussian filter.

Supplementary movie 6 B16 F2 clonal SRF reporter in vivo

Intra-vital movie of clonal B16 F2 SRF reporter cell-line. Cell membranes shown in red and SRF reporter activity shown in green. Autofluorescence also visible in green channel. Images taken over a 13 minute time period.

Supplementary movie 7 B16 F10 motility in vitro

B16 F10 cells were treated with control or EZH2 targeted siRNA, plated on Fibronectin coated glass bottomed cell cultre plates and stimulated with 5 ng/ml HGF. Lowlight images were taken every 10 minutes. Note tail retraction problems on EZH2 siRNA treatment.

Supplementary movie 8 Normal vessels

Movie of a 3D-reconstruction of a normal vessel. Endothelial cell membranes shown in green and Collagen fibres shown in blue.

Supplementary movie 9 Tumour vessels showing sprouting ends

Movie of a 3D-reconstruction of tumour-associated sprouting vessels. Endothelial cell membranes shown in green, Collagen fibres shown in blue and B16 F2 melanoma cells shown in red. Autofluorescent cells also visible in red channel.

Supplementary movie 10 Tumour and associated vessels overview

Movie of a 3D-reconstruction of a B16 F2 melanoma and associated vessels. Endothelial cell membranes shown in green and B16 F2 melanoma cells shown in red. Autofluorescent cells also visible in red channel. Angiosense, shown in purple, indicates the extent of blood flow.

Supplementary movie 11 Endothelial cells with filopodia protrusions

Intra-vital movie of tumour-associated vessels in a VE-Cadherin:GFPCAAX transgenic mouse. Endothelial cell membranes labelled in green. Images taken over a 51 minute time period. Movie is a maximum intensity projection of 6 z-stacks covering 24 µm. Note filopodial protrusions.

Supplementary movie 12 Endothelial cells with bleb-like protrusions

Intra-vital movie of tumour-associated vessels in a VE-Cadherin:GFPCAAX transgenic mouse. Endothelial cell membranes labelled in green. Images taken

over a 40 minute time period. Note blebbing behaviour of endothelial cells and bleb-like protrusions.

Supplementary movie 13 Endothelial cells undergoing intra-vessel wall motility

Intra-vital movie of tumour-associated vessels in a VE-Cadherin:GFPCAAX transgenic mouse. Endothelial cell membranes labelled in green. Images taken over a 38 minute time period. Note group of endothelial vessels moving within the vessel wall. Movie has been subject to smoothing with a Gaussian filter.

Supplementary movie 14 Endothelial cells undergoing amoeboid-like motility distant to vessels

Intra-vital movie of tumour-associated vessels in a VE-Cadherin:GFPCAAX transgenic mouse. Endothelial cell membranes labelled in green. Images taken over a 28 minute time period. Note endothelial cells undergoing rounded amoeboid-like motility distant to vessels.

Supplementary file 1

List of genes used in overlap analysis of PRC2 regulated genes and the genes up-regulated in the B16 population enriched in motile cells.

Chapter 1. Introduction

1.1 Chapter overview

This thesis describes investigations into heterogeneity in melanoma cell motility in vivo and examination of the signalling pathways that correlate with, and may act to control, melanoma motility and metastasis. It also reports on analysis of the tumour vasculature in the melanoma microenvironment and response to anti-angiogenic therapy. The work uses melanoma cells, so this introduction will have a focus on melanoma and normal melanocyte biology. It will also cover cell motility and metastasis in vivo and control of gene expression via the Notch, SRF and TGF-β pathways, together with chromatin mediated control of gene transcription. In addition, the tumour microenvironment will be discussed, including the tumour vasculature and the effects of the microenvironment on motility and invasion.

1.2 Melanocyte and melanoma biology

Melanoma is a skin cancer arising from the uncontrolled proliferation and invasion of melanocytes. Melanoma is an aggressive disease, but if metastasis is limited to local invasion of the skin, surgical resection is adequate. However, if distant metastasis has occurred, prognosis is poor and only 5 -22 % of patients survive beyond 5 years (http://info.cancerresearchuk.org/cancerstats/). Therefore the study of melanoma metastasis is important to try to further understand the pathways involved and find novel treatments.

1.2.1 Melanocytes

Melanocytes are the pigment producing cells in the skin and exist in the lower levels of the epidermis at regular intervals. They send out long dendritic processes into the epidermis which enable the transport and transfer of melanin to keratinocytes (Figure 1.2). The extent of melanin production and transport determines skin colour. Melanin is synthesised in a melanocyte specific organelle called the melanosome where tyrosine is processed into melanin in a number of

steps that require the enzymes Tyrosinase (TYR), DOPAchrome tautomerase (DCT) and 5,6-dihydroxyindole-2-carboxylic acid oxidase (TYRP1) (Kondo and Hearing, 2011). The P-protein, encoded by *Oca2*, is localised to melanosomes, and although its specific role is currently unknown, it is thought to stimulate pigment production by regulation of melanosomal pH (Sitaram et al., 2009). Melanosomes are transported to the cell periphery by kinesin motor proteins on the microtubule network. Melanosomes are subsequently transferred to the actin network at the distal region of the dendrite by a complex containing Rab-27A and Myosin-Va (Hara et al., 2000) (Strom et al., 2002). An interaction between Rab-27A, SLP2A and phosphatidylserine enables docking of melanosomes at the plasma membrane before melanin release and distribution through the epidermis (Kuroda and Fukuda, 2004).

1.2.2 Melanin production

Melanin production is mainly stimulated by UV-induced secretion of α-Melanocyte Stimulating Hormone (α-MSH) by keratinocytes. This activates Melanocortin receptor 1 (MC1R), a G-protein coupled receptor on melanocytes, which leads to an increase in melanocyte cAMP (Figure 1.1). cAMP activates PKA, which in turn phosphorylates and activates cAMP response element-binding transcription factor (CREB) (Kondo and Hearing, 2011). CREB activation results in increased transcription of Microphthalmia-associated Transcription Factor (MITF) which subsequently induces transcription of target genes such as TYR, DCT and TYRP1 (Bentley et al., 1994) (Bertolotto et al., 1998) (Yasumoto et al., 1997). Rab-27A expression is also increased by cAMP, which leads to an increase in the rate of melanosome transport and melanin export (Chiaverini et al., 2008). cAMP can also affect the dendritic morphology of melanocytes by stimulating Rac and inhibiting RhoA activity (Scott and Leopardi, 2003). Furthermore, the inhibition of RhoA is thought to be required for melanogenesis (Busca et al., 1998). In this way, UV radiation acts to increase melanin in the skin and protect cells from further UV-induced free-radicals and DNA damage.

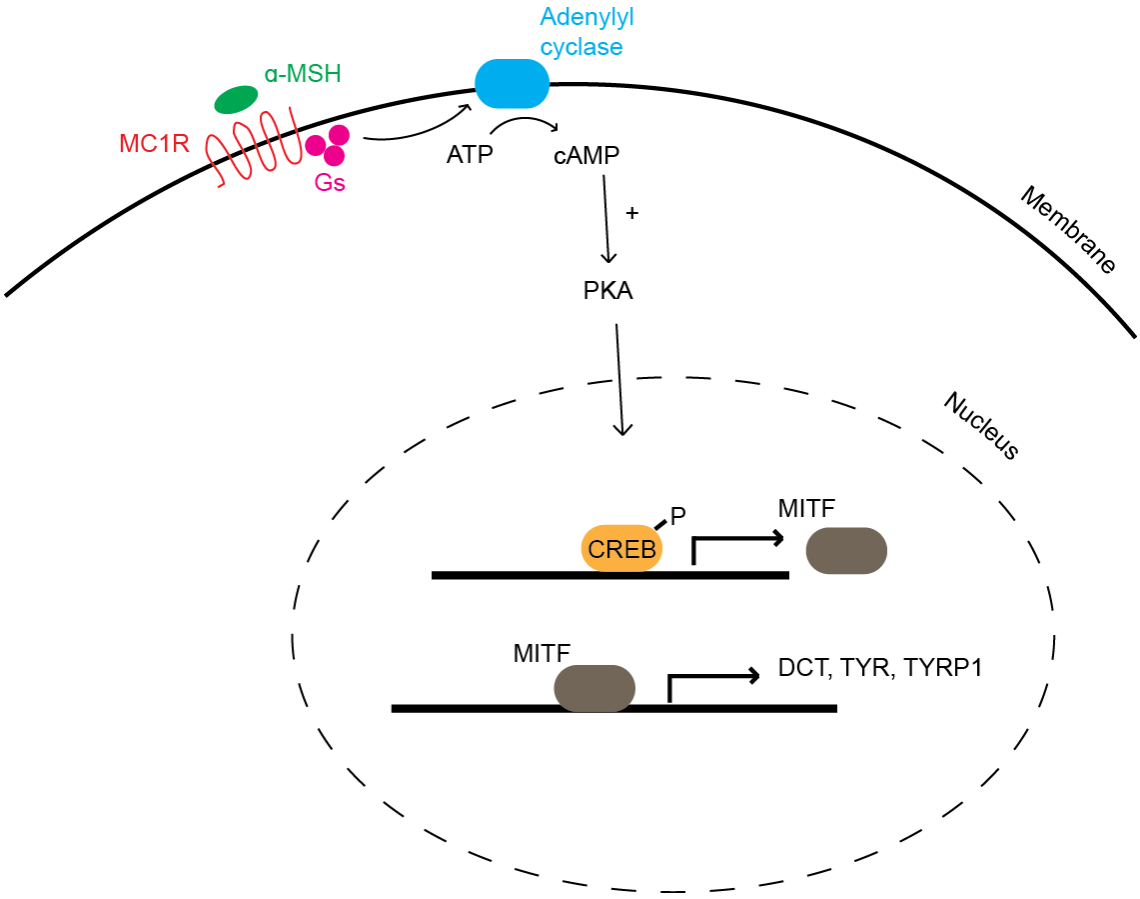

Figure 1.1 Signalling downstream of α-MSH.

α-MSH binds to and activates the G protein-coupled MC1R. The G_s family of G proteins subsequently transmits the signal to Adenylyl cyclase, which catalyzes the conversion of ATP to cAMP. Increased levels of cAMP activate PKA, which in turn, translocates to the nucleus and phosphorylates CREB. Phosphorylated CREB then induces transcription of genes including MITF. MITF can subsequently activate transcription of DCT, TYR and TYRP1.

1.2.3 Melanocyte natural history and differentiation

Melanocytes are derived from the neural crest, a highly motile population of cells that arise from the neural tube in development. Neural crest cells migrate extensively throughout the embryo to form neurons, glia, melanocytes, smooth muscle cells and cells of the craniofacial connective tissue (Sauka-Spengler and Bronner-Fraser, 2008). Melanocytes are thought to arise from the migration of melanoblasts to the skin, however, recent work suggests that a significant proportion also originate from neural crest derived nerves in the skin (Adameyko et al., 2009). The differentiation of neural crest cells into melanoblasts and subsequently melanocytes is dependent on the interactions between MITF, SOX-10, Wnt signalling and Pax-3. *Mitf* expression is specific to melanocyte lineages and is thought to promote melanocyte differentiation. Mutation of *Mitf* results in a decrease in melanoblasts early in development and ectopic expression of *Mitf* promotes a pigment cell phenotype (Hornyak et al., 2001) (Tachibana et al., 1996). SOX-10, Pax-3 and β-catenin all activate *Mitf* expression and mutations in these genes leads to pigment defects and disease (Cooper and Raible, 2009). The current model for melanocyte differentiation during development involves Pax-3 as both an activator of *Mitf* expression but also a competitor for MITF binding on the *Dct* promoter, such that it promotes MITF expression but prevents MITF dependent transcription of *Dct*. On activation of Wnt signalling, Pax-3 is displaced from the *Dct* promoter and MITF drives *Dct* transcription and hence pigment production (Lang et al., 2005). In this model Pax-3 acts to both determine cell fate and to maintain cells in a less differentiated state.

1.2.4 Melanoma and metastasis

Melanoma is largely attributable to somatic mutations caused by ultraviolet (UV) radiation exposure. More than 80 % of melanomas arising in the skin have activating mutations in either *Braf* or *Nras*, highlighting the importance of MAPK pathway in melanoma (Curtin et al., 2005). However, these mutations rarely occur together (Gray-Schopfer et al., 2005). *Braf* mutations are also found in benign melanocytic nevi (Pollock et al., 2003), but most nevi have undergone oncogene-induced senescence (Michaloglou et al., 2005), suggesting that further mutations

are required to initiate melanoma. Despite this, BRAF is a major regulator of oncogenic behaviour in melanoma including regulation of cell survival and invasion (Cartlidge et al., 2008) (Arozarena et al., 2011). In addition, genetic polymorphisms in the *Cdkn2a* (Hussussian et al., 1994), *Mc1r* (Beaumont et al., 2005) and *Mitf* (Yokoyama et al., 2011) genes can result in a predisposition to the disease

Melanoma progression and invasion is characterised by pathologists into a number of stages (Figure 1.2) (Miller and Mihm, 2006). Initially dysplastic nevi are formed, the nevi proliferates within the epidermis and advances to a radial growth phase. Then the lesion switches to a vertical growth phase and invades into the lower epidermis, dermis and underlying basement membrane. As the disease progresses, angiogenesis increases vascular density and promotes spread to distant organs, resulting in metastatic melanoma. Invasion in the vertical growth phase represents acquisition of a metastatic phenotype as the melanoma cells move and invade their surroundings (Miller and Mihm, 2006). Distant metastases are subsequently initiated through the motility and invasion of melanoma cells into lymphatic or blood vessels, transit in the vessels and successful growth at secondary organs. Melanomas are not only comprised of melanoma cells but also stromal cells such as cancer-associated fibroblasts (CAFs), macrophages, T cells, adipocytes, blood and lymphatic endothelial cells and pericytes, which all form the melanoma microenvironment.

Until the last five years, treatment for melanoma had not changed for decades, but the identification of mutant BRAF as a driver of melanoma provided a molecular target to inhibit melanoma growth (Davies et al., 2002). Vemurafenib, a BRAF kinase inhibitor with specificity for mutant BRAF was approved in the US in late 2011 after a phase III trial had to be stopped early when the overall survival benefit for vemurafenib became apparent (Chapman et al., 2011). Despite the positive response almost all patients showed resistance with subsequent disease progression (Chapman et al., 2011) (Fedorenko et al., 2011). Multiple mechanisms of resistance have been proposed, including increased receptor tyrosine kinase expression, *Nras* and *Map2k1* mutations and a RAF kinase switch (Nazarian et al., 2010) (Greger et al., 2012) (Villanueva et al., 2010).

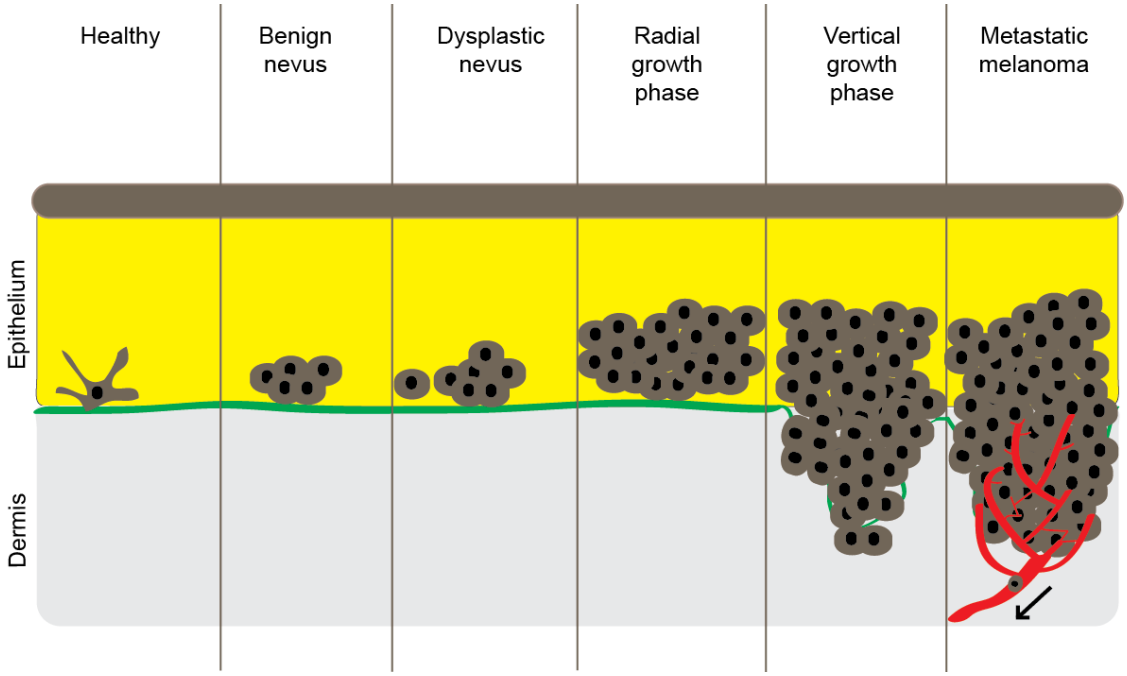

Figure 1.2 Melanoma progression.

Healthy melanocytes reside in the lower levels of the epidermis and extend dendritic protrusions to distribute melanin to keratinocytes. Melanoma progresses through a series of steps starting with a nevus displaying uncontrolled growth. The nevus initially grows radially but then switches to a vertical growth phase invading into the underlying dermis. The last stage, metastatic melanoma, has increased vascular density and melanoma cells have colonised distant sites.

1.2.5 Melanoma differentiation and metastasis

Melanoma is a particularly aggressive disease and once it has become metastatic it is difficult to treat. A potential explanation for the aggressive nature of melanoma is melanocyte natural history. Although melanocytes are stationary, they derive from highly motile neural crest cells and melanoma cells may revert to a neural crest-like state that promotes motility and metastasis. When a panel of cell-lines from different origins were transformed with the same oncogenes, only the transformed melanocytes were metastatic (Gupta et al., 2005). This correlated with slug expression, a transcription factor that drives neural crest motility, and slug was found to co-operate with oncogenic transformation to drive metastasis. Nevi were also found to express a number of neural crest related motility factors suggesting that melanoma may retain characteristics of the less differentiated neural crest cells (Gupta et al., 2005).

Reversion to a neural-crest-like state suggests changes in differentiation and there is a long standing interest in the relationship between differentiation and melanoma invasion and metastasis. Work in the B16 murine melanoma model together with other models has argued that differentiation is associated with both increased and decreased metastasis (Bennett et al., 1994) (Kameyama et al., 1990). The confusion may arise from the classification of differentiation. Most studies used increased pigment as a read-out for increased differentiation as differentiated cells of the melanocyte lineage produce pigment. However, as discussed in later chapters the two do not always correlate. More recent work using intra-vital imaging of the B16 model has shown that the motile cells in the primary tumour are less pigmented and have increased Brn2 promoter activity, a transcription factor expressed in melanoblasts (Pinner et al., 2009). This is suggestive of the motile cell population being less differentiated.

MITF, an important transcription factor for melanocyte differentiation has also been associated with motile behaviour (Carreira et al., 2006). Cells with low levels of MITF, suggestive of less differentiated melanoma cells, are more invasive and this is thought to be due to a decrease in the MITF target DIA1, and a subsequent increase in ROCK mediated contractility (Carreira et al., 2006). In addition, hypoxia

results in a down-regulation of MITF and a subsequent increase in the metastatic potential of melanoma cells (Cheli et al., 2012). Interestingly, Brn2 has been shown to repress MITF expression and analysis of human tumours showed distinct MITF+/Brn2- and MITF-/Brn2+ sub-populations (Goodall et al., 2008). This has lead to the hypothesis that cells may switch between these different states, potentially as a result of extracellular signals, leading to changes in motility (Hoek and Goding, 2010). Genome-wide analysis of melanoma cell-lines supports this model and proposes that melanoma cells can exist in two states, proliferative or invasive, and that a "phenotype switch" between the two may drive invasion and metastasis (Hoek et al., 2006) (Hoek et al., 2008). The differentiation markers TYR, TYRP1 and DCT are up-regulated in the proliferative phenotype, indicative of high MITF (Widmer et al., 2012). This implies that the invasive phenotype has low expression of differentiation associated genes and potentially represents a less differentiated state.

Less differentiated cells in melanoma may arise from loss of the differentiation program (de-differentiation), possibly mediated by cell-autonomous factors or factors from the microenvironment. Alternatively, less differentiated cells may represent the cancer stem cell population in melanoma. The field of melanoma stem cells is complex due to a variety of reports describing different markers and using mice of various immune competencies to demonstrate melanoma stem-like cells (Fukunaga-Kalabis et al., 2011). The proposed frequency of melanoma stem cells is also vastly different. In addition, the identification of a population of slow-cycling JARID1B positive cells that has stem-like properties in vivo suggests melanoma may not follow the classical hierarchy of stem cells and differentiated progeny, as JARID1B negative cells can give rise to JARID1B positive cells (Roesch et al., 2010). Further support for a dynamic melanoma cell phenotype comes from the phenotype switching model discussed previously. What is clear is that on a cell to cell basis, melanoma is a highly heterogeneous disease, however further investigation is required to determine the signalling pathways associated with, and regulating, heterogeneity and phenotype switching.

1.3 Metastasis and the microenvironment

As discussed previously, metastasis is the spread of cancer cells from the primary tumour to distant organs and is the main cause of death in cancer patients (Figure 1.3). It requires a number of steps and thankfully is an inefficient process, which likely demonstrates the wide range of behaviours required for a cancer cell to initiate distant metastases.

1.3.1 Exiting the primary tumour

Metastasis starts with the acquisition of motility in the primary tumour. A full discussion of cancer cell motility in vivo can be found in the next section, however, most of the cells in the primary tumour are non-motile and both extrinsic and intrinsic factors influence the acquisition of motility. Extrinsic factors include signals from the microenvironment that promote cancer cell motility such as LPA, which can activate SRF signalling (Descot et al., 2009), TGF-β and HGF (Hanahan and Coussens, 2012). Intrinsic factors may also influence the acquisition of motility, for example the mutations present or the differentiation state of the cell (Sahai, 2005). Furthermore, cancer cells have been observed to utilise a number of different modes of motility, including as single cells or as cohorts of cells (Friedl et al., 2012). To initiate distant metastases motile cancer cells must intravasate into either the lymphatics or blood vasculature and travel to secondary organs (Figure 1.3). The mode of motility utilised by cancer cells may dictate the route of travel as TGF-β-dependent single cell motility of breast cancer cells results in blood-borne metastasis whereas cells moving collectively only metastasise to local lymph-nodes, presumably through the lymphatics (Giampieri et al., 2009). Entry into the blood vasculature is likely to be more difficult than entry into lymphatics, as lymphatic vessels show pre-formed portals which can be used by dendritic cells for entry and may aid cancer cell intravasation (Pflicke and Sixt, 2009). Intravasation into blood vessels is dependent on N-WASP mediated invadopodia and involves cancer cells squeezing between endothelial cells in a process called trans-endothelial migration (Gligorijevic et al., 2012). Defective endothelial basement membranes, loose pericyte coverage and a decrease in endothelial tight junctions induced by VEGF-A in the tumour environment, reduce the barrier to cancer cells

and may facilitate entry into the bloodstream (Baluk et al., 2003) (Yonenaga et al., 2005) (Cooke et al., 2012). Stromal cells within the microenvironment can also aid intravasation. A subset of tumour-associated macrophages are found adjacent to blood vessels and using intra-vital imaging breast cancer cells were only found to intravasate adjacent to these peri-vascular macrophages (Wyckoff et al., 2007) (Figure 1.3). An EGF-CSF-1 paracrine loop between the breast cancer cells and macrophages (described later) helps to attract the breast cancer cells to peri-vascular macrophages and hence the vasculature. Furthermore, macrophages secrete VEGF-A, which can loosen endothelial cell contacts, and potentially aid cancer cell intravasation (Murdoch et al., 2008).

1.3.2 Survival in the circulation

Once in the lymphatics or blood vasculature, cancer cells must be able to survive the challenges of anchorage independence (Figure 1.3). The shear stress, found particularly in the blood vasculature, is an additional challenge to cancer cells. Analysis of metastatic versus non-metastatic variants of the same cell-line indicated that both could interact with blood vessels but the non-metastatic cells showed increased fragmentation when associated with the vasculature (Wyckoff et al., 2000). This suggests that the metastatic phenotype also provides protection from shear stress. Evidence for this comes from the fact that Vimentin, which is up-regulated during cancer cell epithelial-to-mesenchymal transition (EMT), helps maintain leukocyte cell shape in the circulation (Brown et al., 2001). Furthermore, cancer cells with high actomyosin contractility, associated with increased motility, show increased short-term survival after injection into the blood (Pinner and Sahai, 2008). In the blood stream cancer cells aggregate with platelets to form an embolus, which not only helps to protect against shear stress but also immune surveillance (Im et al., 2004) (Palumbo et al., 2007).

1.3.3 Arrival and survival at secondary sites

The location of cancer cell metastasis can in part be explained by cancer cells becoming lodged in the nearest capillary bed to the tumour. However many

cancers show preferential metastasis to certain sites, for example breast cancer to the bone and lungs (Nguyen et al., 2009). The long-standing "Seed and Soil" hypothesis proposes that successful organ colonisation depends on intrinsic properties of the cancer cell but also a permissive microenvironment for growth (Paget, 1989). The cancer cell intrinsic expression of chemokine receptors mediates cancer cell "homing" to tissues which show increased expression of the ligand. Bone metastases occur as a result of CXCR4 expression in breast cancer cells which attracts them to the bone marrow, a site rich in CXCL12, the CXCR4 ligand (Muller et al., 2001). Primary tumours also contain a heterogeneous population of cells with different intrinsic properties resulting in preferences for different secondary organs (Fidler, 1973). Work using the MDA MB 231 breast cancer cells generated sub-lines with a propensity to metastasise to the lungs, brain or bone and described their associated gene expression profiles (Minn et al., 2005) (Kang et al., 2003) (Bos et al., 2009). ST6GALNAC5, a sialyltransferase, is up-regulated only in the cells showing brain specific metastasis and it enables specific adhesion to brain endothelial cells and passage through the blood brain barrier (Bos et al., 2009). TGF-β enhances breast cancer metastasis to the bone and can act to increase expression of the genes highly expressed in cells which preferentially metastasise to the bone (Yin et al., 1999) (Kang et al., 2003).

Formation of metastases in distant organs requires the adhesion of cancer cells to the endothelium, survival, extravasation and invasion of the endothelium associated basement-membrane (Figure 1.3). A number of Integrins have been implicated in cancer cell adhesion to the vasculature including Integrin αVβ3, which binds PECAM-1, and Integrin α4β1 (Kikkawa et al., 2002) (Klemke et al., 2007). Both of these Integrins also increase trans-endothelial migration indicating a requirement for endothelial cell adhesion when traversing the vasculature wall. Cancer cells also release paracrine factors such as ANGPTL4 and CCL2 that disrupt endothelial cells cell-cell junctions and enhance trans-endothelial migration (Padua et al., 2008) (Wolf et al., 2012). Survival of cancer cells in the vasculature can be mediated by cell autonomous factors and interactions with stromal cells. The interaction of breast cancer cells and macrophages via VCAM-1 on the cancer cells and α4 Integrins on the macrophages enhances cancer cell survival by signalling through Ezrin and AKT (Chen et al., 2011). Increased Ezrin expression

in metastatic cells can also enhance survival in the lung through AKT-mTOR signalling (Krishnan et al., 2006).

1.3.4 Growth at secondary sites

Once within the parenchyma at secondary sites, many cancer cells remain dormant (Naumov et al., 2002) (Figure 1.3). Growth may be initiated either by a permissive microenvironment as suggested by the "soil and seed hypothesis" or through co-option of the stroma, although these two possibilities may not be mutually exclusive. Lung fibroblasts are induced to express Tenascin-C and VEGF-A, which promote the colonisation of breast cancer cells in the lungs (O'Connell et al., 2011). Additionally, breast cancer stem cells arriving at the lungs induce fibroblasts to secrete the matrix protein Periostin, which in turn recruits Wnt ligands to enhance cancer stem cell survival (Malanchi et al., 2012).

The effects of cancer cells on secondary organs may occur even before metastasis. Cancer cells in the primary tumour can direct recruitment of VEGFR-1 positive bone-marrow derived cells to future metastatic sites. The primary tumour induces expression of Fibronectin at future metastatic sites, enabling recruitment and adhesion of VEGFR-1 positive bone-marrow derived cells. Matrix-metalloproteases secreted by the bone-marrow derived cells subsequently induce release of active growth factors from the extracellular matrix (ECM) generating a pre-metastatic niche permissive for cancer cell growth (Kaplan et al., 2005). Bone-marrow derived cells are also attracted to the pre-metastatic niche through LOX dependent ECM remodelling (Erler et al., 2009). Hypoxic cells in the primary tumour secrete LOX, which accumulates in the pre-metastatic niche leading to Collagen cross-linking and increased adhesion of bone-marrow derived cells. In addition, the pre-metastatic niche may signal back to the cancer cells as up-regulation of the chemokine CXCL12 has been observed in the pre-metastatic niche, which can promote the chemotaxis of CXCR4 positive cancer cells (Kaplan et al., 2005).

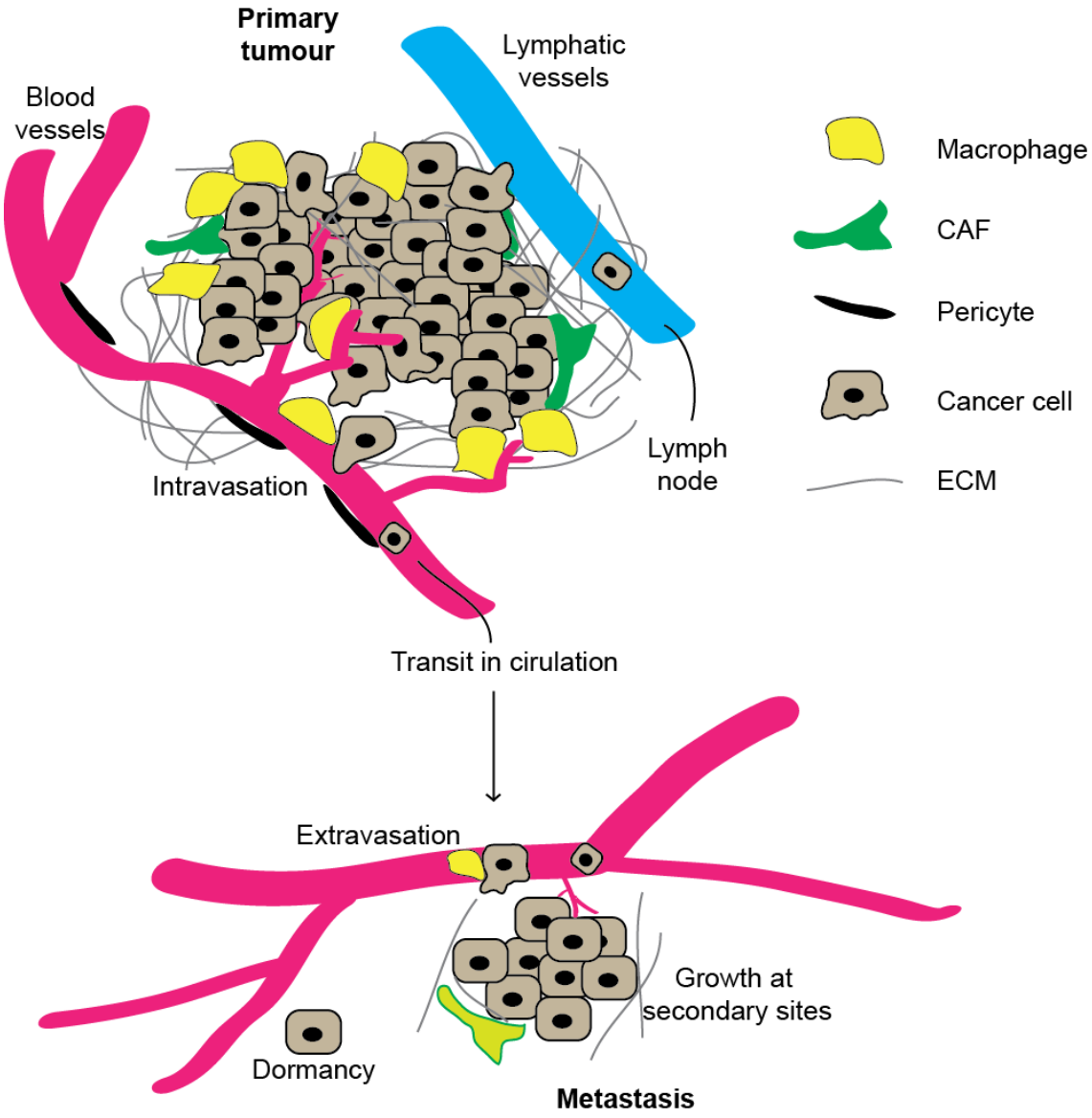

Figure 1.3 The metastatic process.

Metastasis is the spread of cancer to distant organs and involves a cancer cell invading the local environment of the primary tumour and intravasating into either blood or lymphatic vessels. On arrival at secondary sites, cancer cells adhere to the endothelial cell wall and extravasate. Formation of metastases requires the cells to survive and grow in the novel environment.

1.4 Cell motility

Cell motility is an important biological process that allows single-celled organisms to respond to differences in nutrient concentration and drives cell rearrangement and morphological changes in developing embryos. It helps the immune system to locate pathogens but also enables cancer cells to move and metastasise. The majority of research into cell motility has been carried out using cells on 2D surfaces, however, within the last decade the focus has shifted towards analysis of cells moving through 3D environments or tissues. It is clear that cells behave differently in different environments. Cells can move either as single cells or as groups or cohorts of cells (Friedl et al., 2012). There are multiple modes of single cell motility ranging from mesenchymal-like to amoeboid-like or blebbing motility (Figure 1.4).

Cell motility requires a cell to be able to make a protrusion in a forward direction, adhere to the surrounding matrix at the new position, and then retract the rear of the cell to turn the forward protrusion into bulk cell movement (Ridley et al., 2003). A pre-requisite for this set of processes is cellular polarity and the definition of a front and a back. The actin cytoskeleton is thought to provide the driving force for cell motility, however, microtubules also play a role (Etienne-Manneville, 2004).

1.4.1 The actin cytoskeleton

The actin cytoskeleton is composed of highly dynamic filamentous actin (F-actin) polymers, composed of globular actin (G-actin) monomers. G-actin can bind ATP in the cytoplasm and actin can hydrolyse ATP to ADP + Pi, although this reaction is faster when incorporated into F-actin filaments (Bugyi and Carlier, 2010). Following incorporation of G-actin-ATP into the barbed or plus end of the actin filament, ATP is hydrolysed leaving ADP + Pi. Actin depolymerisation, the loss of actin monomers from the pointed end is increased by loss of the phosphate group (Bugyi and Carlier, 2010). The rate of G-actin-ATP monomer addition and G-actin-ADP loss dictates the dynamics of the actin filament and actin treadmilling occurs when the rate of association of G-actin-ATP and the rate of loss of G-actin-ADP are balanced (Bugyi and Carlier, 2010).

Numerous processes control actin polymerisation (Nurnberg et al., 2011). G-actin can bind a number of proteins in the cytoplasm and binding to Profilin promotes ADP/ATP exchange and so increases the amount of G-actin-ATP (Wolven et al., 2000). Furthermore, binding to Thymosin β4 sequesters G-actin in the cytoplasm (Safer et al., 1991). Formins and Ena/VASP family members can increase the rate of actin monomer addition to barbed ends, whereas actin capping proteins prevent further actin monomer addition (Goode and Eck, 2007) (Chesarone and Goode, 2009). Actin filaments can also be branched and the Arp2/3 complex enables branching and the formation of new actin filaments, through mimicking the shape of actin dimers (Goley and Welch, 2006). Cofilin is an actin severing protein which can lead to actin depolymerisation, but also acts to increase the number of barbed ends available and can thereby enhance polymerisation (Wang et al., 2007).

Actin polymerisation can be stimulated downstream of the Rho family GTPases, a family of proteins regulated by binding to guanine nucleotides, that switch between an active GTP bound state and an inactive GDP bound state (Sahai and Marshall, 2002). Rho guanine nucleotide exchange factors (GEFs) are activated downstream of many receptors including receptor tyrosine kinases and G-protein-coupled receptors (Schiller, 2006). They promote the binding of Rho proteins to GTP, hence promoting an active state. Although most family members do have GTP hydrolysing activity, the reaction is slow, and binding of Rho GTPase activating proteins (GAPs) increases the rate of switching to the inactive state (Tcherkezian and Lamarche-Vane, 2007). Furthermore, Rho GDP dissociation inhibitors (GDIs) sequester GDP-bound Rho proteins in the cytoplasm, hence inactivating them (DerMardirossian and Bokoch, 2005). Many Rho proteins are subject to membrane targeting in a similar way to Ras proteins, through lipid modifications initiated by recognition of a C-terminal CAAX motif (Adamson et al., 1992). At the membrane, active GTP-bound proteins bind actin regulators leading to downstream actin polymerisation (DerMardirossian and Bokoch, 2005).

1.4.2 The microtubule cytoskeleton

The microtubule cytoskeleton is composed of polymers constructed from α and β-tubulin dimers and similar to the actin cytoskeleton, the polymers are highly dynamic (Watanabe et al., 2005). However, in contrast to the actin cytoskeleton, microtubules are nucleated and organised by a dedicated microtubule organising centre (MTOC). Microtubule polymers are polarised and polymerisation occurs at the plus end whilst the minus end anchors the microtubules to the MTOC (Watanabe et al., 2005). Microtubule disassembly also occurs at the plus end, so microtubules can switch between growing and shrinking phases dynamically, due to events at the plus end (Kirschner and Mitchison, 1986). Microtubule polymerisation can generate force and the microtubule cytoskeleton is found in some cell protrusions during cell motility (Watanabe et al., 2005). Furthermore, microtubules localise to focal adhesions and can regulate adhesion turnover (Stehbens and Wittmann, 2012). During polarised cell migration the MTOC is repositioned to the front of the nucleus in a mechanism dependent on microtubule dynamics (Magdalena et al., 2003).

The microtubule cytoskeleton also provides a platform for intra-cellular transport. Motor proteins such as Kinesins and Dyneins bind microtubules and convert chemical energy from ATP-hydrolysis into mechanical work to move along the microtubule polymers (Verhey et al., 2011). Most kinesins move towards the plus end of the microtubule and hence transport intracellular cargo towards the cell periphery (Verhey et al., 2011). During polarised cell migration, Kinesins may help transport protein complexes to the leading edge and by interacting with focal adhesions, they may bring molecules that promote adhesion turnover (Krylyshkina et al., 2002) (Stehbens and Wittmann, 2012). However, not all Kinesins act as motor proteins. KIF2C (also known as MCAK) is important for regulating microtubule dynamics and binds to the plus ends of microtubules causing microtubule depolymerisation (Hunter et al., 2003). Over-expression of KIF2C results in an almost total loss of microtubules in the cell (Maney et al., 2001).

1.4.3 Cell protrusions

Generation of protrusions is one of the first steps in cell motility (Ridley et al., 2003). Cells can generate a number of protrusions including filopodia, lamellipodia, invadopodia and blebs (Ridley, 2011). Most protrusions are generated through polymerisation of the actin cytoskeleton, which pushes the plasma membrane forward. However, cells can also generate forward motion through actomyosin contractility (Poincloux et al., 2011).

1.4.3.1 Filopodia

Filopodia are thin protrusions that contain parallel actin bundles. The main Rho GTPase involved in filopodia formation is Cdc42 and this is thought to induce localisation of its targets including the formin mDIA1, N-WASP and IRSp53 (Ridley, 2011). The I-BAR domain of IRSp53 bends the plasma membrane outwards and mDIA1 can induce the straight actin filaments (Ahmed et al., 2010) (Campellone and Welch, 2010). Fascin, an actin bundling protein, localises to filopodia and is important for their stability (Vignjevic et al., 2006) (Machesky and Li, 2010).

Filopodia are observed in a number of cell-types including endothelial tip cells during angiogenesis (Gerhardt et al., 2003) and epithelial cells in *Drosophila* dorsal closure (Millard and Martin, 2008). Furthermore, proteins important for filopodia, such as Fascin, are implicated in cancer cell invasion and metastasis (Machesky and Li, 2010).

1.4.3.2 Lamellipodia

Lamellipodia are broad protrusions and activation of the Rho GTPase Rac is sufficient to induce lamellipodium extension (Machacek et al., 2009). Downstream of Rac, the SCAR/WAVE complex binds Arp2/3 to induce the formation of a branched actin network (Kunda et al., 2003). However, there has been recent debate about the extent of branching within lamellipodia (Urban et al., 2010). The cell-type, conditions and the relative activity of the Arp2/3 complex and more linear

actin nucleators, such as the Formins, may dictate the extent of branching (Ridley, 2011). Lamellipodia are most abundant in mesenchymal-like cells migrating on rigid 2D substrates including the migration of neural crest cells during development (De Calisto et al., 2005).

1.4.3.3 Invadopodia

Invadopodia are protrusions that have matrix degrading properties and are thought to help cells cross basement membranes (Schoumacher et al., 2011). It is likely that invadopodia formation is initiated by co-ordination of Cdc42 and the tyrosine kinase, Src (Ridley, 2011). Both the Arp2/3 complex and Formins are required for invadopodia and Fascin also helps stabilise these protrusions (Buccione et al., 2009) (Lizarraga et al., 2009) (Li et al., 2010a). In addition to being actin-rich, invadopodia contain microtubules and intermediate filaments and the intermediate filaments can provide mechanical stability (Schoumacher et al., 2010). Matrix metalloproteases such as MT1-MMP are delivered to the ends of invadopodia by the Exocyst complex (Liu et al., 2009).

1.4.3.4 Blebs

Membrane blebs are not driven by actin polymerisation but instead through increases in hydrostatic pressure driven by actomyosin contraction (Charras et al., 2005). They are more often associated with cell motility in 3D environments rather than 2D surfaces and are utilised by migrating primordial germ cells in zebrafish, *Dictyostelium* and some cancer cell-lines (Blaser et al., 2006) (Langridge and Kay, 2006) (Sahai and Marshall, 2003). Blebs are thought to form at areas with weak attachments between the plasma membrane and actin cortex and once the bleb has extended the actin filaments polymerise to form a new actin cortex (Charras and Paluch, 2008).

The four types of protrusions are not necessarily mutually exclusive as both lamellipodia and blebs have been observed at different regions on migrating cells

during zebrafish gastrulation (Diz-Munoz et al., 2010). In addition, filopodia may emerge from the lamellipodial actin network (Gupton and Gertler, 2007).

Cells undergoing collective motility also produce protrusions, although they are often limited to the leading cells in the group. In 2D wound-healing models the front row of cells protrudes lamellipodia into the newly formed space (Vaughan and Trinkaus, 1966). *Drosophila* tracheogenesis involves collectively motility and the leading cells, closest to the chemotactic cue, produce filopodia in the direction of movement (Ribeiro et al., 2002).

1.4.4 Adhesions

Cell motility often requires adhesion to the surrounding matrix, particularly during motility on 2D substrates. This secures the new position of the membrane following protrusion and subsequently enables the generation of traction and force to move forwards (Ridley et al., 2003). Integrins are the main molecules that mediate adhesion to the ECM. They are trans-membrane heterodimers consisting of a large extracellular domain that binds to specific matrix components and a short cytoplasmic tail that links to the actin cytoskeleton (Huttenlocher and Horwitz, 2011). Activation of Integrins through binding to matrix ligands results in Integrin clustering and formation of multiprotein complexes. Nascent adhesions are small dynamic adhesions in the outer regions of protrusions that can mature into the larger focal adhesion complexes (Choi et al., 2008). Focal adhesions contain proteins such as Talin, Vinculin and Alpha-actinin which bind the intracellular tails of Integrins and help link the ECM to the actin cytoskeleton, hence providing traction for cell motility (Huttenlocher and Horwitz, 2011). Focal adhesions also contain the signalling molecules, Focal-adhesion kinase (FAK) and Src kinases, which control the turnover of focal adhesions and regulate cell motility (Webb et al., 2004) (Mitra et al., 2005). In order to move forward, cells must release the ECM attachments at the cell rear. This is in part mediated by contractile force, but Integrin endocytosis and Calpain dependent proteolytic cleavage of adhesion proteins may also play a role (Webb et al., 2004) (Lawson and Maxfield, 1995) (Franco and Huttenlocher, 2005).

The role of adhesions in vivo is less defined. Focal adhesions in cells on 3D substrates are more diffuse and have different molecular components, with fewer Integrins employed and less phosphorylated FAK (Cukierman et al., 2001). Furthermore, dendritic cells can migrate in vivo independently of Integrins and are thought to employ a mode of motility dependent on actomyosin contraction (Lammermann et al., 2008).

Collectively motile cells use similar mechanisms to cells on 2D substrates in order to bind the ECM. However, they must also maintain adhered to adjacent cells. Adherens junctions maintain cell-cell adhesions and are mediated by cadherins and catenins. Cells migrating collectively during mammary gland morphogenesis maintain E-cadherin at cell-cell contacts and loss of E-cadherin is associated with a more single-cell mode of motility and epithelial to mesenchymal transition (Ewald et al., 2008) (Thiery, 2003).

1.4.5 Contractile force

Contractile force is required for cell migration as it drives retraction of the rear of the cell to enable a net forward motion. The contractile machinery consists of the heavy and light chains of the motor protein Myosin II, together with actin filaments. Contractility is generated by multimeric Myosin II “walking” along multiple actin filaments in an ATP dependent process (Olson and Sahai, 2009). This causes the actin filaments to move relative to one another generating contraction. Contractility is regulated by the phosphorylation of Myosin light chain (MLC), which controls the conformation of the Myosin heads and hence increases ATPase activity (Vicente-Manzanares et al., 2009). MLC is phosphorylated by a number of kinases including ROCK1 and ROCK2 downstream of RhoA signalling and MRCK downstream of Cdc42 (Amano et al., 1996) (Wilkinson et al., 2005). MLC is also the target of Myosin phosphatase (MYPT), which is itself negatively regulated by ROCK1 (Ito et al., 2004). Hence RhoA signalling, leading to activation of ROCK, induces contractility through both MLC phosphorylation and inhibition of the MLC phosphatase. In cells on 2D substrates the activation of RhoA leads to the

formation of stress fibres and this requires both ROCK and the Formin mDIA1 (Watanabe et al., 1999).

Single cells moving in vivo are highly dependent on actomyosin contractility. As described earlier, some cell types can move independently of integrins instead using contractility to squeeze through gaps in the ECM. In a similar manner, some cancer cells utilise amoeboid-like modes of motility to move through 3D matrices and the tumour environment in vivo. During this form of motility, the contractile machinery is localised to the cell cortex and ROCK dependent contractility drives motility and local Collagen deformation (Wyckoff et al., 2006).

Collectively motile cells have a supra-cellular actomysoin organisation, with increased contractility around the edge of the group and decreased contractility at cell-cell junctions (Hidalgo-Carcedo et al., 2011). This enables the group to maintain cohesion, by stabilising cell-cell contacts. Some systems of collective cell motility, such as branching morphogenesis in the mammary gland, may utilise contraction as a method to drive motility, rather than cycles of protrusion and adhesion. Here, the leader cells are devoid of protrusions and the stiff stalk cells are thought to drive motility from the rear (Ewald et al., 2008).

1.4.6 Cell polarity and directional cell motility

Motile cells have a front, usually defined by active protrusions and the leading edge, and a rear, which is characterised by disassembly of adhesions and contraction. This polarisation can be spontaneous or arise from the external environment as a result of soluble chemokines, changes in the ECM, or changes in the position or presence of adjacent cells. The difference in localised cell behaviour in these regions is reflected by differences in the distribution or activation of signalling molecules. During leukocyte and *Dictyostelium* migration PI3K signalling is polarised so that there is an increase in the PI3K product PIP_3 at the leading edge (Ridley et al., 2003). PI3K products can activate Rac through GEFs leading to an increase in Rac activity and protrusions at the leading edge. PTEN, a

phosphatase that removes PIP_3, is restricted to the sides of migrating cells, which helps prevent the formation of protrusions in these areas (Merlot and Firtel, 2003).

The classical view of cell motility on 2D substrates involves increased Rac activity at the leading edge with RhoA activity restricted to the tail to promote tail retraction (Ridley et al., 2003). However, recent studies with Rho protein biosensors have revealed a much more complex situation with both Rac and RhoA activity at the leading edge and a spatial and temporal regulation of their activity (Pertz et al., 2006) (Machacek et al., 2009). RhoA is activated at the cell edge at the same time as leading edge advancement, however, Rac1 and Cdc42 are activated behind the leading edge with a slight delay (Pertz et al., 2006) (Machacek et al., 2009). Rac1 activity is low at the onset of protrusion, whereas RhoA activity is high suggesting that Rac1 may not be responsible for advancement of the leading edge in the system analysed. This is in contrast to reports showing that photo-activation of Rac is sufficient to drive protrusions (Wu et al., 2009).

As mentioned previously, the environment can affect cell polarity, but it can also induce a directionality to migration. Chemotaxis is the migration of cells towards a soluble factor such as the migration of *Dictyostelium* towards cAMP or leukocytes towards fMLP, a peptide derived from bacteria or damaged cells. These chemokines regulate directional migration, although exactly how they do so is not yet clear. Chemokine gradients may activate PI3K signalling to induce protrusional activity towards the source of the gradient. Alternatively, soluble chemokines may help to stabilise protrusions pointing in the direction of the source, thereby regulating direction. The chemokine CXCL12 is implicated in chemotaxis of primordial germ cells in zebrafish (Doitsidou et al., 2002). Chemokine receptors are also implicated in cancer metastasis and increased expression of CCR7 in melanoma cells can increase metastasis to the lymph-nodes (Wiley et al., 2001).

Cells moving collectively also have a polarity and move in a directed fashion. Usually there is a leader cell or cells, with distinct morphology, such as increased protrusions, but inputs must be integrated from the whole group of cells (Friedl and Gilmour, 2009). Collective migration of the zebrafish lateral line is directed by CXCL12 (David et al., 2002). In this system only the front cells respond to the

ligand but it is sufficient to drive directional migration of the group (Haas and Gilmour, 2006). However, the leader cell is not always fixed, as tip and stalk cells can switch position during angiogenesis and photo-activation of Rac in *Drosophila* border cells is sufficient to change the polarisation and direction of motility (Jakobsson et al., 2010) (Wang et al., 2010b). In some cases the leading cell is a different cell type. Fibroblasts found at the leading edge of collectively migrating cancer cells remodel and degrade the ECM making tracks for the cancer cells to follow (Gaggioli et al., 2007).

1.4.7 ERM proteins

Ezrin, Radixin and Moesin are a family of proteins that link the actin cytoskeleton with the plasma membrane. They contain a membrane associated FERM domain at their N-terminus and a C-terminal ERM-associated domain (C-ERMAD) (Fehon et al., 2010). The C-ERMAD can bind both the FERM domain and F-actin. In the inactive conformation, the C-ERMAD is bound tightly to the FERM domain, masking the F-actin binding site. On activation, the affinity between the C-ERMAD and the FERM domain is reduced, the molecule opens and the C-ERMAD binds F-actin (Simons et al., 1998). The FERM domain can bind to cytoplasmic tails of a number of membrane associated proteins, such as CD44 and ICAM2, hence linking the plasma membrane and the underlying actin cytoskeleton (Yonemura et al., 1998).

A number of signalling pathways contribute to ERM activation. The first step is through binding of PIP_2 enabling recruitment to the plasma membrane. This may lead to a slight conformational change revealing a conserved threonine residue (Fievet et al., 2004). Phosphorylation of the threonine results in the loss of intra-molecular association, and a subsequent conformational change releasing the C-ERMAD domain to bind F-actin (Simons et al., 1998). Numerous kinases can phosphorylate and activate the ERM proteins including ROCK, PKCα, PKCθ (Matsui et al., 1998) (Ng et al., 2001) (Simons et al., 1998).

ERM proteins have important roles in cell motility (Arpin et al., 2011). During amoeboid/bleb-like migration in 3D matrices, Ezrin accumulates at the cell rear together with actin and MLC. Blebbing is decreased at this area, possibly due to increased linkage between the actin cortex and plasma membrane, and this directs blebbing and protrusions in the forward direction, hence driving cell motility (Lorentzen et al., 2011). ERM proteins may act both upstream of RhoA by binding to Rho GEFs, GAPs and GDIs, and in addition they are activated by the RhoA substrate, ROCK (Fehon et al., 2010). ERM proteins are activated downstream of receptor tyrosine kinases and Ezrin promotes cell motility downstream of HGF (Crepaldi et al., 1997).

1.4.8 Different modes of single cancer cell motility in 3D

Singly motile cells can be classified on a continuum between mesenchymal-like and amoeboid-like modes of motility (Figure 1.4). Mesenchymal-like motility is slower and characterised by actin-rich protrusions such as filopodia or invadopodia (Friedl and Wolf, 2009). It is dependent on peri-cellular proteolysis to degrade the surrounding ECM and make a path for the cell-body (Friedl and Wolf, 2009). Amoeboid-like motility is faster and uses contractility to squeeze the cell through gaps and deform the local extra-cellular matrix (Wyckoff et al., 2006). This type of motility is more prominent in 3D environments. Cells with high contractility generate blebs that protrude into the local environment and can generate traction for forward movement (Charras and Paluch, 2008). Mesenchymal-like motility utilises adhesive structures such as focal-adhesions to generate traction, however, cells undergoing amoeboid-like motility may have weak or no attachment to the ECM (Schmidt and Friedl, 2010). The type of single cell motility utilised by a cell may be pre-determined and expression of adhesion molecules, such as Integrins, may play a role. Sarcoma and glioblastoma cells undergo a more mesenchymal-like motility whereas leukocytes, leukaemia and prostate cancer cells undergo an amoeboid-like mode of motility (Friedl, 2004).

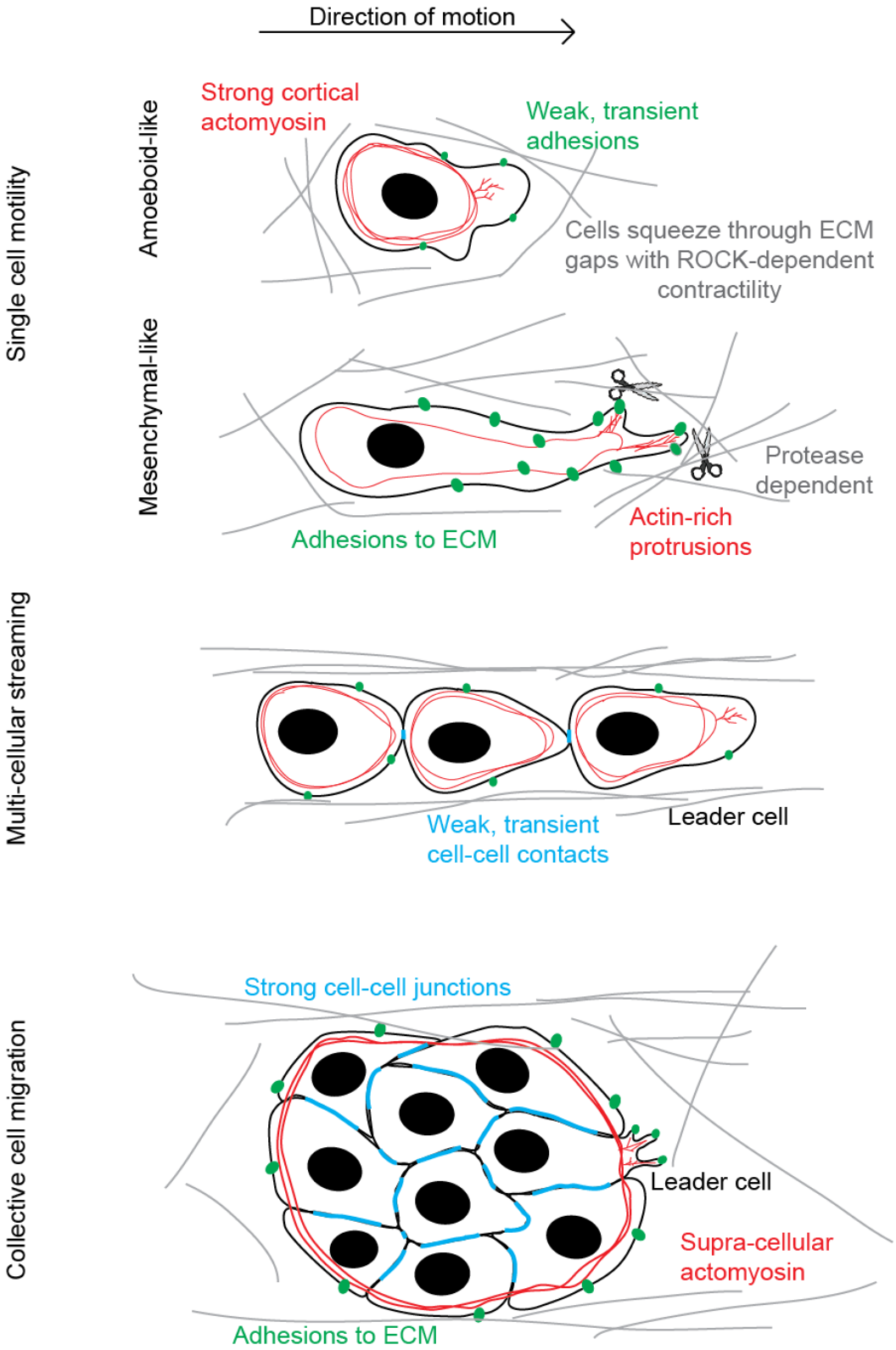

Figure 1.4. Modes of cell motility.

Cells can move either collectively or as single cells and single cell motility may be further represented by amoeboid-like or mesenchymal-like motility. Cells which move as a cohort but do not maintain strong cell-cell adhesions are considered to use a streaming form of motility.

Mesenchymal-like cell motility is utilised by many cell-types. For example, during development the cells of the neural crest undergo EMT and migrate as single cells throughout the embryo using a protrusion-based mesenchymal mode of motility (Thiery et al., 2009). EMT involves the loss of cell-cell adhesions through down-regulation of E-cadherin, acquisition of a motile phenotype and a gene-expression signature reminiscent of mesenchymal cells. It can be induced through soluble signals such as TGF-β and Wnts, which lead to a transcriptional response to up-regulate proteins such as MMPs, Fibronectin and Vimentin and repress E-cadherin (Thiery et al., 2009). EMT is thought to occur in cancer and there is a large body of evidence supporting EMT as a method of inducing motility of carcinoma cells in vitro (Thiery, 2003). Long-term exposure to signals such as TGF-β may not only induce EMT, but may also lead to the acquisition of stem-like properties (Mani et al., 2008). The role of EMT in vivo is less clear. Histological sections of human cancer have revealed an increase in EMT markers and a loss of E-cadherin at the invasive edge of tumours (Brabletz et al., 2001). However, these changes are not maintained in metastases, which could indicate EMT independent metastasis or rare and reversible EMT (Brabletz et al., 2001).

Cells are plastic in their modes of motility and can switch between mesenchymal-like and amoeboid-like modes of motility. This switching was first observed when cells using a mesenchymal-like mode of migration in a 3D Collagen matrix were treated with a protease inhibitor cocktail resulting in a switch to an amoeboid-like form of motility (Wolf et al., 2003). Furthermore, cells undergoing amoeboid-like motility switch to mesenchymal-like motility when treated with a ROCK inhibitor to inhibit contractility (Sahai and Marshall, 2003). This highlights the versatility of motile cells and helps to explain why protease inhibitors have not been a particularly effective anti-cancer treatment (Lah et al., 2006). However, total motility could be impaired by the joint use of protease and ROCK inhibitors, suggesting a combination of agents may be effective against invasion in vivo (Sahai and Marshall, 2003). Switching can also occur in physiological situations and the mode of motility may be dependent on ECM density, and elasticity (Wolf and Friedl, 2011).

Levels of Rac activity control the nature of single cell motility and so Rac regulation is likely involved in the switching mechanism. Rac activation by both NEDD9 and DOCK3 is required for mesenchymal-like motility and WAVE2 acts downstream of Rac to induce protrusions (Sanz-Moreno et al., 2008). Rac activation also reduces MLC phosphorylation hence reducing contractility and amoeboid-like characteristics (Sanz-Moreno et al., 2008). NEDD9 is another key regulator as it not only activates Rac, but also signals together with Integrin β3 and Src to promote mesenchymal-like motility whilst decreasing ROCK activity (Ahn et al., 2012).

During amoeboid-like motility ROCK signalling and contractility is high and Rac activation is low. RhoA-ROCK signalling is promoted by cytokine signalling through the JAK-STAT pathway. ROCK activation leads to an increase in STAT activation creating a positive feedback loop that may help to maintain amoeboid motility (Sanz-Moreno et al., 2011). Furthermore, ROCK activation leads to an ARHGAP22 dependent inhibition of Rac activity and so inhibits the mesenchymal phenotype (Sanz-Moreno et al., 2008).

A spatial localisation of RhoA signalling may also be important to regulate the mode of single cell motility. The E3 ubiquitin ligase SMURF1 degrades RhoA at the leading edge and SMURF1 depletion results in a mesenchymal to amoeboid transition due to the activation of RhoA at the cell cortex (Wang et al., 2003) (Sahai et al., 2007). $p27^{Kip1}$ inhibition of RhoA can also influence the mode of motility as loss of $p27^{Kip1}$ results in amoeboid-like motility (Besson et al., 2004) (Berton et al., 2009). Activation of Cdc42 through the GEF DOCK10 promotes amoeboid-like motility whereas inhibition of Cdc42 by RASGRF inhibits amoeboid-like characteristics (Gadea et al., 2008) (Calvo et al., 2011). Therefore the interplay between Rac, RhoA-ROCK and Cdc42 signalling helps to control the switch between mesenchymal- and amoeboid-like motility.

The cytokine regulation of amoeboid-like motility suggests that the mode of motility may depend on the microenvironment. However, many chemokines are known to activate Rac and so may lead to mesenchymal-like motility. Furthermore Vitronectin, the Integrin β3 ligand, is required for the NEDD9 dependent promotion

of mesenchymal-like motility (Ahn et al., 2012). This suggests that if cells with high NEDD9 encounter Vitronectin they may switch to a mesencymal-like mode of motility. The trans-membrane receptor EphA2 promotes an amoeboid-like mode of motility in melanoma and prostate cancer cells and so regions with high Ephrin A ligands may promote amoeboid motility (Taddei et al., 2011) (Parri et al., 2009).

1.5 Cancer cell motility in vivo

1.5.1 Imaging approaches to study cancer cell motility in vivo

There are a number of imaging based methods to study cancer cell motility and metastasis in vivo; from whole-body bioluminescence imaging to the sub-cellular resolution provided by intra-vital multi-photon microscopy. The work in this thesis utilises single-photon and two-photon intra-vital microscopy in mice so these techniques will be the focus of this section.

Single- and two-photon intra-vital microscopy use photons to excite a fluorophore into a higher energy state and collect the photons emitted on relaxation of the fluorophore. The requirement for fluorophores means that cancer cells need to stably express fluorescent proteins for visualisation. Two-photon microscopy excites fluorophores by simultaneous absorption of two low energy photons (Helmchen and Denk, 2005). This uses wavelengths in the infra-red range which has the advantage of being able to penetrate further into tissues (Oheim et al., 2001). The infra-red wavelengths also create second-harmonic generation signal from structures with highly ordered repeats, such as Collagen I fibres, which helps visualise aspects of the ECM together with labelled cancer cells (Zipfel et al., 2003). An additional advantage of multiphoton microscopy is that only fluorophores in the focal plane are excited. Outside of the focal plane the photon density is too low to allow simultaneous photon absorption (Helmchen and Denk, 2005). This is in contrast to single-photon microscopy, which excites fluorophores outside of the focal plane and so requires a pinhole to remove out-of focus light (Beerling et al., 2011). Therefore multi-photon excitation not only reduces photo-toxicity by exciting only the fluorophores in the plane of interest, but also more of the emitted light can

be collected as all emitted light can be assumed to originate from the focal plane without the need for a pinhole.

Exploring cancer cell motility using intra-vital imaging involves the generation of primary tumours with fluorescently labelled cancer cells. This thesis uses sub-cutaneous injection of fluorescent cell-lines into mice due to the ability to manipulate the cancer cells before injection. However, there are a number of spontaneous cancer models in which the cancer cells are fluorescently labelled. Furthermore, zebrafish can be used as a model to study cancer metastasis due to the ease of imaging and amenable genetics (Ignatius and Langenau, 2011).

Tumours can be imaged in different ways. The skin-flap method allows one-off short-term imaging, typically 3-4 hours, although up to 30 hours can be achieved (Egeblad et al., 2008). This method involves minor surgery immediately prior to imaging to expose the tumour, which may affect interstitial tissue flow and the tumour microenvironment. Longer-term imaging without immediate surgery can be achieved with the use of an imaging window. These were originally large, cumbersome structures surgically implanted on the back of the mouse (Lehr et al., 1993) (Alexander et al., 2008). However, recent refinement has resulted in a much smaller, lighter window that has been used for orthotopic imaging of mammary tumours in the mammary gland (Kedrin et al., 2008). A challenge for long-term imaging of cancer is the dynamic rearrangements within the microenvironment that make imaging the exact same position day after day quite difficult. Photo-switchable fluorescent proteins, such as Dendra2, a green-to-red photoswitchable protein, enable the long-term labelling of a population of cells or region of interest and can help to overcome this problem (Gligorijevic et al., 2009). This technique has also been used to determine the extent of cell motility by analysing the spread of the photo-switched cells after a defined time period (Canel et al., 2010).

Detection of additional components of the microenvironment can be achieved by using transgenic mice and fluorescently-labelled probes, dyes and antibodies. Intra-venous injection of high molecular weight fluorescent dextran indicates blood vessels with flow whilst injected lower molecular weight fluorescent dextrans are taken up by macrophages (Wyckoff et al., 2007). Intra-tumoural injection of

fluorescent dextran can also reveal the draining lymphatics (Giampieri et al., 2009). Transgenic mice with fluorescent protein expression under the control of a cell-specific promoter allow the imaging of stromal cells in the tumour. One example is the myeloid specific *c-fms:GFP* mice to visualise myeloid cells (Nakasone et al., 2012).

Intra-vital imaging can also be used to study the molecular processes associated with cell motility in vivo, such as signalling events and proteolytic cleavage. Probes to study the protease activity of MMPs include an injectable substrate that fluoresces after cleavage (Weissleder et al., 1999). Förster resonance energy transfer (FRET) based probes can report on the activity status of a signalling molecule, such as the GTPase Rac1 (Hirata et al., 2012), or can be used to indicate substrate cleavage, as in the FRET Caspase probe (Bins et al., 2007). Fluorescent proteins can be fused to a protein of interest and have been used to study E-cadherin dynamics and regulation in vivo (Canel et al., 2010). Alternatively, cells expressing a fluorescent protein under the control of a transcriptional based reporter can visualise cells with active signalling and have shown heterogeneity in TGF-β signalling in breast cancer in vivo (Giampieri et al., 2009).

1.5.2 Different modes of cancer cell motility in vivo

Intra-vital imaging has confirmed that cancer cells also use diverse mechanisms to move in vivo. Amoeboid-like cancer cell motility in vivo is fast, with speeds of up to 4 μm/min (Sahai, 2005). Cells in some tumours also display chaotic blebbing forms of motility (Sanz-Moreno et al., 2008). Similar to migration on 3D matrices, amoeboid-like migration is dependent on ROCK mediated contractility and imaging of MLC localisation revealed an accumulation at the cell cortex and behind the leading edge (Wyckoff et al., 2006). Consistent with in vitro studies showing MMP independent amoeboid-like motility, inhibition of MMP activity does not decrease the number of motile cells in A431 squamous cell carcinomas or MTLn3 breast tumours (Wyckoff et al., 2006) (Wolf et al., 2003). Mesenchymal-like cancer cell motility is also observed in vivo. Mesenchymal-like motility, however, may be

confined to the more central tumour regions whereas cells at the tumour margins use amoeboid-like motility (Sanz-Moreno et al., 2008). Although switching between modes of motility has not been addressed in vivo, the distinction between modes of motility based on location suggests that the microenvironment may play a part.

Ex-vivo imaging of glioblastoma cells in a brain slice culture system identified two different modes of invasion, invasion through the brain parenchyma, mediated by multiple pseudopodia, and peri-vascular invasion, in which cells had a single pseuodopod (Hirata et al., 2012). FRET probes revealed differences in Rho GTPase activation between cells. Cells undergoing invasion into the brain parenchyma had increased Rac1 and Cdc42 activity and lower RhoA activity than cells undergoing peri-vascular invasion. This shows that proteins known to be associated with motility have heterogeneous activity which correlates with heterogeneous motile behaviour of cancer cells. Indeed, the authors argue that inter-cell heterogeneity in Rho GTPase activity dictates the method of cell invasion (Hirata et al., 2012).

Cancer cells have been observed to move collectively in vivo in a number of different tumour types (Giampieri et al., 2009) (Alexander et al., 2008). This has revealed distinct types of collective motility depending on the cohesive-ness of the group and contacts maintained by the cells (Friedl et al., 2012). Streaming describes cells that are migrating in the same direction with weak cell contacts, perhaps following the same guidance cue, but each cell generates forward motion independently. An isoform of MENA, an Ena/VASP family member, promotes cell streaming through affecting paracrine signals in vivo (Roussos et al., 2011). Cohesive collective cell migration is slower than streaming and cells maintain cell-cell contacts over time (Giampieri et al., 2009) (Friedl et al., 2012).

A common theme reported by intra-vital imaging is that motile cancer cells are relatively rare, with less than 10 % of cells in the primary tumour being motile (Giampieri et al., 2009). Furthermore, some areas have no motile cancer cells whereas others have lots of motile cells (Condeelis and Segall, 2003). As discussed previously, both cancer cell intrinsic and extrinsic factors affect the acquisition of motility in the primary tumour. Purification of the motile cell

population in breast cancer using a microneedle of matrigel and EGF showed that motile cells have a distinct gene signature from the bulk of cancer cells. Motile cells had differential regulation of genes associated with the actin cytoskeleton and the cell-cycle (Wang et al., 2004) (Goswami et al., 2004). One explanation is that the motile cells may have intrinsic differences from the tumour mass and are a sub-population of the tumour. Alternatively, extrinsic signals from the local microenvironment could lead to a transient change in gene expression, resulting in the acquisition of motility and subsequent metastasis. Consistent with local effects of the microenvironment, photo-switching of fluorescently labelled breast cancer cells revealed that cells near to blood vessels disperse and migrate more than cells distant to blood vessels (Kedrin et al., 2008). This suggests that aspects of the microenvironment, such as blood vessels, may create a permissive environment and so affect the ability of cancer cells to migrate.

1.5.2.1 Interplay between the microenvironment and cancer cell motility

Extrinsic factors, such as signals in the microenvironment, can affect cancer cell motility. Macrophages influence cancer cell motility in vivo and have been observed to migrate in streams together with breast cancer cells (Condeelis and Weissleder, 2010). A paracrine loop between the two cell types operates to increase breast cancer cell motility and is an example of extrinsic factors regulating cancer cell gene expression and motility. Breast cancer cells release CSF-1 that induces tumour associated macrophages to express EGF. EGF then acts as a chemokine promoting the invasion of breast cancer cells, but also increasing CSF-1 production so maintaining the paracrine loop (Goswami et al., 2005). A subset tumour associated macrophages is found in peri-vascular regions, so this paracrine loop may be a reason for the increased motility near to blood vessels. The peri-vascular location of some macrophages also helps breast cancer cells to intravasate, as breast cancer cells are observed to migrate towards macrophages and only intravasate adjacent to peri-vascular macrophages (Wyckoff et al., 2007). This work starts to describe a permissive microenvironment for breast cancer cell motility, i.e close proximity to a blood vessel together with the presence of macrophages. Patient sections were analysed for the presence of a macrophage,

blood vessel and invasive cancer cell (marked by increased MENA expression) within the same region, designated a tumour microenvironment of metastasis. Patients who developed distant metastasis showed a significant increase in the number of tumour microenvironments of metastasis, indicating the clinical relevance of perivascular macrophages for cell motility and metastasis (Robinson et al., 2009).

Soluble signals from other cells in the microenvironment, such as CAFs, may also increase cancer cell motility in certain areas. Numerous in vitro studies describe CAFs as promoters of cancer cell motility through factors such as HGF and TGF-β (Hanahan and Coussens, 2012). TGF-β signalling is heterogeneous in breast cancer in vivo and correlates with single cell motility (Giampieri et al., 2009). Blocking TGF-β signalling in vivo blocks single cell motility suggesting that TGF-β mediates the induction of single cell motility. Furthermore, consistent with heterogeneous motile behaviour, TGF-β signalling only occurs in some cells. Although the source of TGF-β was not explored, localisation of TGF-β expressing CAFs may contribute to the heterogeneity in induction of single cell motility.

The ECM and physical environment of a tumour can also influence cancer cell motility. Motile cancer cells interact with Collagen fibres and are often observed traversing the Collagen network at high speed using an amoeboid-like mode of motility (Condeelis and Segall, 2003). Collectively invading strands of cancer cells associate with linear Collagen fibres suggesting that the ECM may help to provide a highway for migration (Alexander et al., 2008). In addition, ECM remodelling by stromal cells such as CAFs helps to promote cancer cell motility, as indicated in 3D models of collective invasion in vitro (Gaggioli et al., 2007). The different structures in the tumour microenvironment may affect whether cells are motile or which mode of motility they utilise. Long-term tracking of fibrosarcomas revealed that areas of the tumour adjacent to fat storage adipocytes had an increase in singly motile cells (Alexander et al., 2008). This correlates with in vitro reports that adipocytes promote cancer cell invasion and metastasis (Dirat et al., 2011) (Nieman et al., 2011).

1.5.2.2 Heterogeneous activation in vivo of pathways associated with motility

The varied behaviour of cancer cells in vivo probably reflects both internal and external differences, such as

1. Genetic differences
2. Differentiation or epigenetic changes
3. External signals

Motile melanoma cells in vivo were observed to be less pigmented and had higher activity of the promoter of the melanoblast transcription factor Brn2 (Pinner et al., 2009). This is suggestive of the motile cells being less differentiated, but whether this population represents the cancer stem cells is unknown. However, imaging of a zebrafish model for rhabdomyosarcoma identified a cell population with tumour propagating properties, but these were not motile and instead a distinct, more differentiated, myogenin positive cell population potentiated invasion and metastasis (Ignatius et al., 2012).

Heterogeneity in activation of signalling pathways associated with motility has been observed in human tumour slices, suggesting that intra-vital imaging of murine cancer models has relevance for the human disease. Colon cancer sections show β-catenin localised to cell-cell junctions in the tumour bulk, but accumulated in the nucleus at the invasive tumour margin (Brabletz et al., 2001). This pattern was also seen in the metastases. This indicates that cells may undergo a transient increase in Wnt signalling that drives invasion but this signalling is not retained in the bulk of cells on reaching the metastatic site. Further evidence for transient changes in signalling was revealed by intra-vital imaging of TGF-β reporter breast cancer cell-lines. As discussed previously, TGF-β signalling was heterogeneous and correlated with single cell motility (Giampieri et al., 2009). However, in lymph-node metastases the majority of cells were non-motile and TGF-β signalling was low, suggesting a transient induction of motility and TGF-β signalling in vivo. Furthermore, cells showed increased lung colonisation after a pulse of TGF-β, whereas cells with constitutive activation of TGF-β signalling had reduced capability for lung colonisation, indicating the requirement for down-regulation of the signal.

This report also showed heterogeneity in TGF-β signalling in human breast tumour sections providing support for signalling heterogeneity in human tumours (Giampieri et al., 2009).

In summary, intra-vital studies of cancer cell motility have shown that acquisition of motility is a rare and transient event that can be influenced by extrinsic factors in the microenvironment including macrophages and the presence of blood vessels. In addition, there are intrinsic differences between motile and non-motile cells in vivo such as differences in differentiation state and activation of certain proteins and signalling pathways.

The next section will cover some key mechanisms by which extrinsic cues can affect gene expression and how stable patterns of gene expression may be maintained.

1.6 Control of gene expression

A cell's phenotype and behaviour is dependent on the genes it expresses. External signals, for example from the tumour microenvironment, can lead to gene expression changes and subsequent changes in cell behaviour, such as the acquisition of motility. Gene expression can be controlled at many levels, including integration of external signals, transcription factor recruitment of RNA polymerase II complex components, remodelling of the higher order structure of DNA to increase polymerase access to genes, mRNA processing and mRNA stability. In the nucleus, DNA is associated with Histone proteins to form chromatin. For active gene transcription, the DNA must be accessible and RNA polymerase II complex must be recruited. This section will address these initial steps of gene expression control. There will be a focus on

1. Upstream pathways that initiate transcription factor dependent RNA polymerase II (RNA pol II) recruitment
2. Chromatin mediated control of gene expression, particularly gene silencing.

Transcription factors can be general factors, such as TFIIA, that help to recruit the RNA pol II complex to the promoter of a gene. Alternatively, specific transcription

factors mediate RNA pol II recruitment to a subset of genes through sequence specific DNA binding of key regulatory elements in gene promoters. The next few sub-sections will address some of the key pathways regulating specific transcription factors.

1.6.1 TGF-β signalling

TGF-β signalling is activated in response to extracellular signals and is involved in the regulation of many cellular processes such as growth, adhesion, migration and differentiation (Schmierer and Hill, 2007). It results in the nuclear accumulation of sequence specific transcription factors, called SMADS, that subsequently recruit other proteins and initiate transcription of target genes (Figure 1.5).

The core TGF-β pathway has a large number of ligands in mammals, including bone morphogenetic proteins (BMPs), growth and differentiation factors (GDFs), Activins, Nodal and 3 TGF-β isoforms. Some of the ligands, such as the TGF-βs, are secreted as latent forms and targeted to the ECM. They require subsequent proteolysis to release the active ligand (Annes et al., 2003). On release of active ligand, it binds to transmembrane serine-threonine kinase receptors to transfer the signal to inside the cell. There are two classes of receptor, type I and type II, and on binding to ligand, dimers of the two types of receptors are brought together to form heterotetramers. Type II receptors are constitutively active and so phosphorylate and activate the type I receptors. Phosphorylation of the type I receptors recruits the receptor-regulated SMADs (R-SMADs), SMAD1,2,3,5 and 8. R-SMADs are subsequently phosphorylated by the activated type I receptors and this enables binding to the common mediator SMAD (Co-SMAD), SMAD4. The receptor-R-SMAD interaction is specific due to differences in the amino-acid sequence of different type I receptors. The type I receptors ALK 4,5 and 7 activate SMAD2 and 3 whereas ALK1,2,3 and 6 activate SMAD1,5 and 8 (Schmierer and Hill, 2007). Active SMAD complexes accumulate in the nucleus and recruit other transcriptional regulators to activate transcription of target genes.

SMADs are continuously shuttling in and out of the nucleus, even in cells without receptor activation (Hill, 2009). On activation of the signal, phosphorylated R-SMADs, together with SMAD4, shuttle to the nucleus and activate transcription. The R-SMADs are also dephosphorylated in the nucleus leading to complex dissociation and R-SMAD nuclear export (Xu et al., 2002) (Inman et al., 2002). If the receptors are still active R-SMADS will be phosphorylated again and shuttle to the nucleus, leading to an overall accumulation of SMADs in the nucleus and activation of target gene transcription. TGF-β receptor activation can also lead to the SMAD independent activation of the MAPK, JNK, PI3K pathways and small Rho GTPases such as RhoA and Rac1 (Mu et al., 2012).

All R-SMADs (with the exception of SMAD2) and SMAD4 can bind directly to DNA. The SMAD3-SMAD4 binding site was characterised as a single 5'-AGAC-3' sequence known as a CAGA box, and promoters often consist of repeats of this sequence (Dennler et al., 1998). The SMADs are thought to regulate transcription through chromatin re-modelling and recruitment of the SWI-SNF chromatin remodelling complex, BRG and the histone acetyltransferases p300 and CBP (Ross et al., 2006) (Janknecht et al., 1998). This remodelling subsequently aids the recruitment of the general transcriptional machinery to activate transcription.

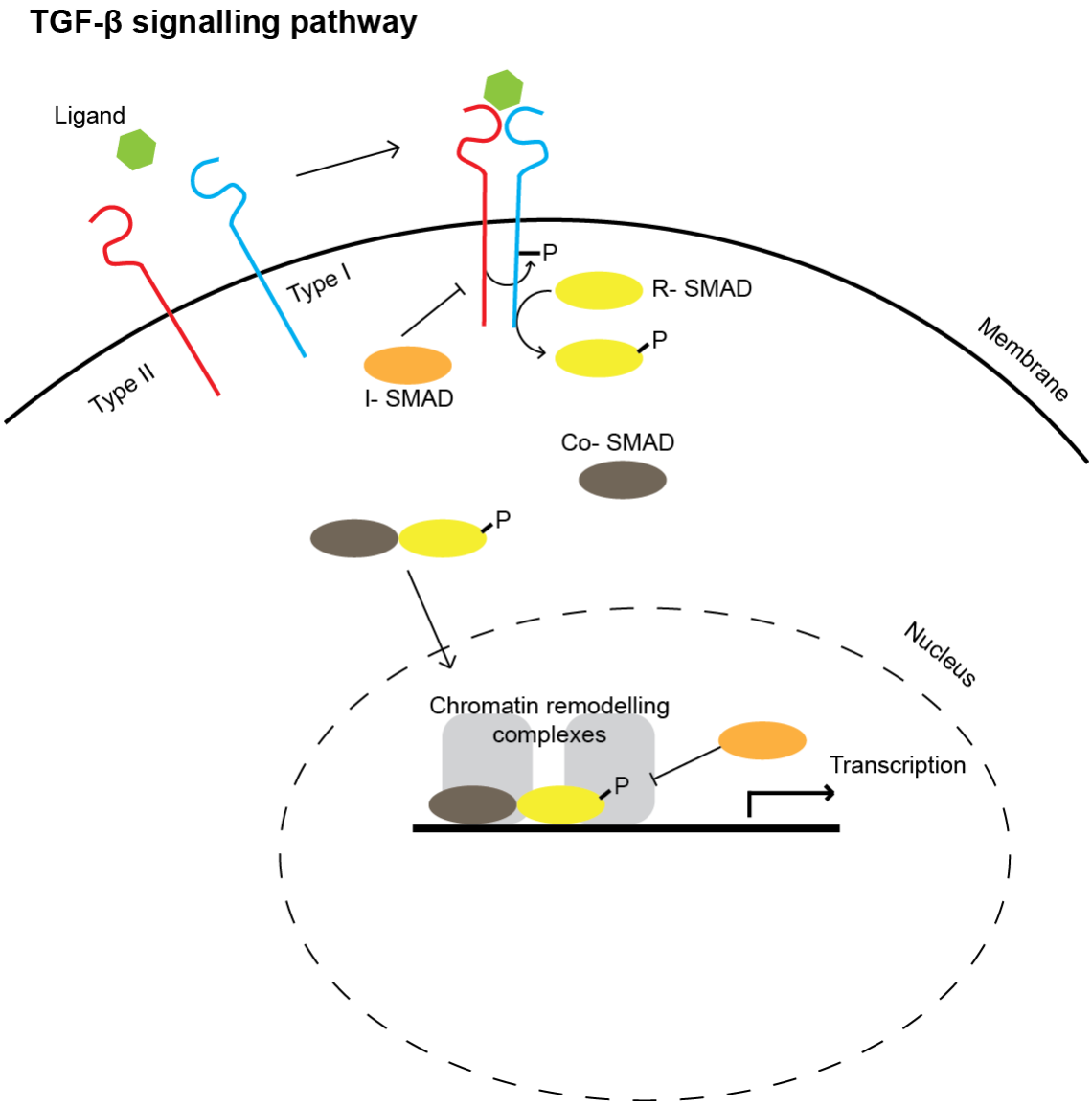

Figure 1.5 TGF-β signalling.

Extracellular TGF-β ligands bind to a heterotetramer of type I and type II receptors. The type I receptors are phosphorylated by type II receptors, which recruits R-SMADs. The R-SMADs are phosphorylated by the activated type I receptors and then bind to co-SMADs. The SMAD complexes accumulate in the nucleus resulting in transcription of TGF-β target genes. I-SMADs are transcriptional targets which can inhibit the pathway through direct inhibition of active SMAD complexes on DNA and by indirect inactivation of receptor complexes.

Further regulation of the pathway can be achieved in a number of ways and ubiquitination plays a major role. The inhibitor SMADs (I-SMADs), SMAD 6 and 7 are transcriptional targets of TGF-β signalling and can feedback to inhibit the pathway. SMAD7 is constitutively bound to the E3 ubiqutin ligases, SMURF1 and 2. Binding of SMAD-7 to receptor complexes targets the E3 ligases to the activated receptors leading to receptor degradation and signal inhibition (Kavsak et al., 2000). In opposition to this, the de-ubiquitinating enzyme USP4 removes ubiquitin from TGF-β receptors, thereby maintain active signalling (Zhang et al., 2012b). SMAD7 also recruits protein phosphatase 1 (PP1) to active receptors resulting in de-phosphorylation and signal inhibition. In addition, SMAD7 can directly inhibit binding of SMADs to DNA (Zhang et al., 2007). In the absence of signal, transcriptional repressors such a SKI and SNON, bind CAGA box sequences (Stroschein et al., 1999). TGF-β signalling results in degradation of SNON, which is dependent on the E3 ubiquitin ligase Arkadia, to allow transcriptional activation of target genes (Levy et al., 2007).

1.6.1.1 TGF-β signalling in melanoma

TGF-β signalling is implicated in many different cancers and has a complex role, acting as both a tumour supressor and invasion and metastasis promoter, even in the same cancer type. Melanocytes are subject to growth inhibition by TGF-β. However, melanoma cells are less sensitive to TGF-β dependent growth inhibition and this correlates with stage, as metastatic melanoma cells show the least growth inhibition (Krasagakis et al., 1994). Production of all 3 TGF-β isoforms is increased in melanoma compared to melanocytes (Krasagakis et al., 1999).

TGF-β signalling also promotes invasion and metastasis in melanoma as inhibition of the pathway through over-expression of the inhibitor-SMAD Smad7, decreased invasion through decreasing MMP2 and 9 expression (Javelaud et al., 2005). Small molecule inhibition of TGF-β signalling also decreased experimental bone metastasis of melanoma cells (Javelaud et al., 2008). Addition of TGF-β1 and 2 increases B16 melanoma cell motility in vitro and decreases pigment, a characteristic of motile B16 cells in vivo (Pinner et al., 2009). Other studies have

shown that TGF-β inhibits MITF expression through a decrease in PKA activation, and a subsequent loss of phosphorylated CREB and CREB dependent MITF expression (Pierrat et al., 2012). Given the role of TGF- β on MITF expression, TGF- β may promote switching to the more invasive MITF-/Brn2+ state. This is consistent with genome-wide studies of melanoma cell lines in vitro that indicate that the invasive phenotype gene-signature is reminiscent of TGF- β induced gene expression (Hoek et al., 2006).

TGF-β is known to drive a transcriptional program associated with melanoma invasion. TGF- β drives GLI2 expression, a transcription factor associated with sonic hedgehog signalling (Dennler et al., 2007). GLI2 can induce melanoma invasion through inhibition of E-cadherin and activation of MMP2 and 9 expression (Alexaki et al., 2010). GLI2 was found to be heterogeneous in human melanoma sections, with increased GLI2 associated with decreased E-cadherin expression at the invasive front (Alexaki et al., 2010).

Increased TGF- β in the melanoma microenvironment can also affect stromal cells. TGF-β activates normal fibroblasts and induces CAFs to produce ECM components, such as Fibronectin, Collagens and Tenascin-C (Xing et al., 2010). This can subsequently promote melanoma proliferation and invasion (Berking et al., 2001). TGF- β can induce angiogenesis by directly affecting endothelial cell migration and through stimulating the production of the pro-angiogenic factors VEGF-A and IL-8 (Javelaud et al., 2008). TGF- β can also influence immune cells in the microenvironment. It is a potent inhibitor of T cells and together with IL-2, can induce differentiation towards immune-suppressive regulatory T-cells (Yang et al., 2010). The high level of TGF- β found in melanoma likely increases invasion of melanoma cells, promotes tumour immunosuppression and angiogenesis and thereby promotes melanoma progression (Javelaud et al., 2008).

1.6.2 SRF signalling

SRF is a transcription factor that binds directly to DNA at 5'-CC(A/T_6)GG-3' sequences and associates with different co-factors to regulate transcription

(Treisman, 1986) (Olson and Nordheim, 2010). There are two main classes of SRF transcriptional co-activators, the ternary complex factor (TCF) family and the myocardin-related transcription factor (MRTF) family. These two families respond to different inputs and regulate distinct genes (Gineitis and Treisman, 2001). As work in this thesis uses a transcriptional reporter dependent on the MRTF family of transcription factors, the focus will be on regulation of this branch of SRF signalling and gene transcription.

MRTF-dependent SRF signalling links actin dynamics with gene transcription, thereby enabling cells to globally regulate transcription and cellular behaviour downstream of cytoskeletal rearrangement (Figure 1.6). Most of the MRTF family transcription factors bind G-actin, acting as cytoplasmic G-actin sensors (Olson and Nordheim, 2010). MRTF dependent SRF signalling is thus dependent on actin remodelling downstream of Rho GTPase activation (Sotiropoulos et al., 1999). Under conditions of low actin polymerisation, G-actin can bind MRTFs through 3 RPEL motifs in the N-terminus of the transcription factors. This leads to MRTF sequestration in the cytoplasm through obstruction of the nuclear localisation signal (Miralles et al., 2003) (Mouilleron et al., 2011). On F-actin polymerisation the availability of G-actin in the cytoplasm decreases, which liberates MRTFs, allowing nuclear import and activating SRF dependent transcription. Actin is also found within the nucleus and nuclear actin can further regulate the pathway. MRTF bound to nuclear actin cannot activate transcription and has enhanced nuclear export (Vartiainen et al., 2007).

Many external signals stimulate F-actin polymerisation from monomeric G-actin, leading either directly to Rho family GTPase activation, or activation of GEFs. Lysophosphatidic acid (LPA) and sphingosine-1 phosphate both activate RhoA leading to activation of SRF signalling (Descot et al., 2009) (Lockman et al., 2004). Multiple receptor tyrosine kinases activate GEFs and promote the switch to a GTP bound state of Rho proteins (Schiller, 2006). Consistent with this VEGFR signalling activates MRTF dependent SRF signalling in endothelial cells (Chai et al., 2004). SRF signalling can also be activated downstream of Integrin signalling via Integrin-linked kinase (ILK), FAK, Src and subsequent actin cytoskeleton remodelling (Huveneers and Danen, 2009) (Olson and Nordheim, 2010). Furthermore,

Integrins are mechanosensors that transduce external mechanical stress and MRTF-dependent SRF signalling can be activated downstream of mechanotransduction (Zhao et al., 2007b). This enables the cell to link gene transcription with external mechanical stress and tension.

MRTF-dependent SRF target genes include genes involved in actin dynamics, cell motility and contractile force production and actin itself is an SRF target (Olson and Nordheim, 2010). Therefore SRF signalling increases actin production leading to an increase in G-actin in the cell and an auto-regulatory negative feedback loop through G-actin dependent cytoplasmic sequestration of MRTF and MRTF nuclear exit (Olson and Nordheim, 2010).

As MRTF dependent SRF signalling requires actin remodelling, drugs that target the actin cytoskeleton also affect SRF transcription activation. Latrunculin B inhibits actin polymerisation and leads to an increase in SRF signalling. Alternatively, Cytochalasin D interacts with actin, disrupting the binding to MRTF and hence activates SRF signalling (Sotiropoulos et al., 1999).

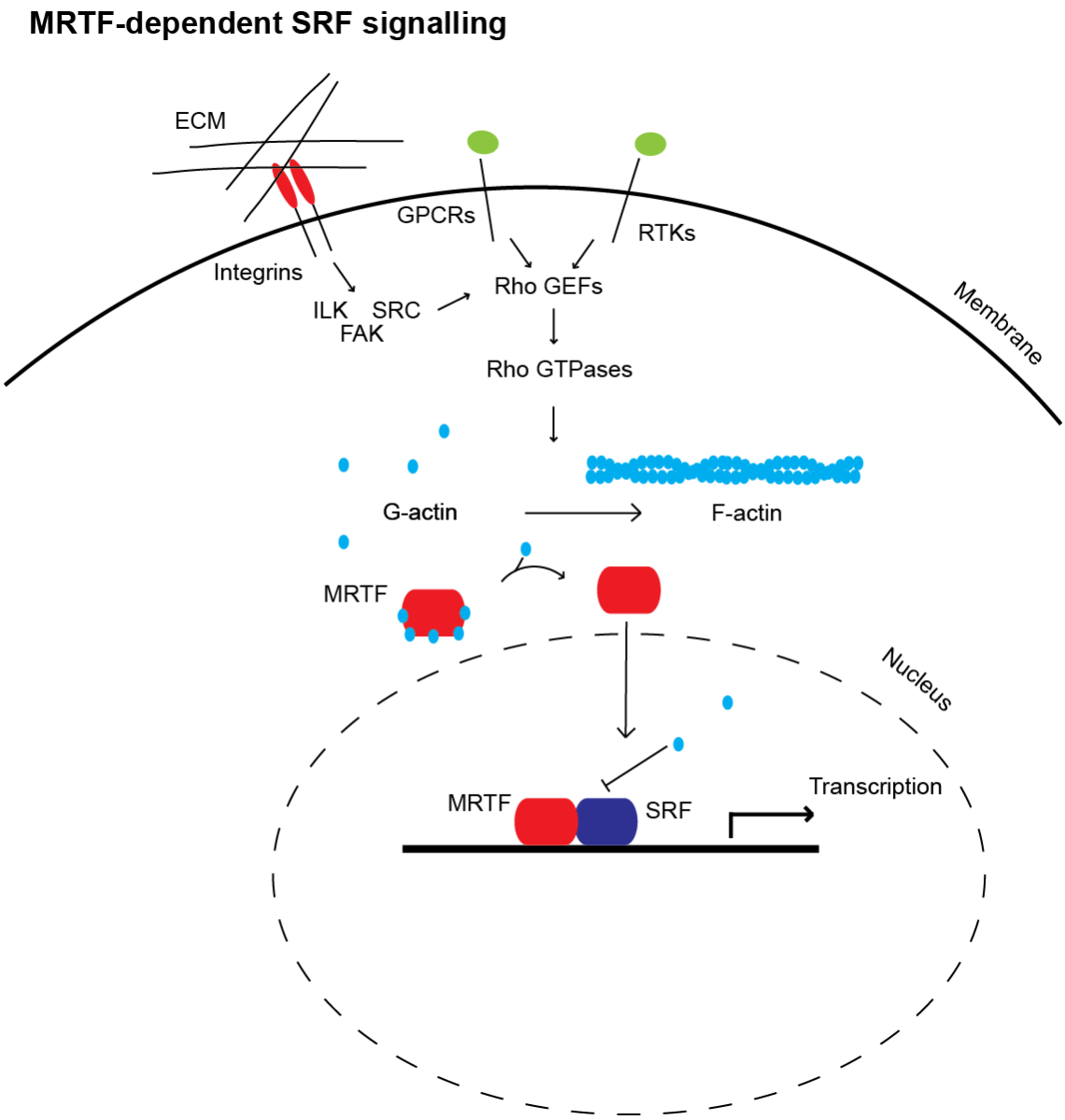

Figure 1.6 MRTF-dependent SRF signalling.

MRTF-dependent SRF signalling is activated downstream of F-actin polymerisation. A number of stimuli activate actin polymerisation including signalling downstream of receptor tyrosine kinases (RTKs), G-protein coupled receptors (GPCRs) and Integrins. Actin polymerisation decreases cellular G-actin releasing MRTF to accumulate in the nucleus and together with SRF activate transcription.

1.6.2.1 SRF signalling in melanoma

MRTF-dependent SRF signalling is required for melanoma invasion and metastasis. Loss of MRTF in B16 melanoma cells does not affect primary tumour growth but decreases the number of motile cells in vivo. MRTF depletion also decreases experimental metastasis to the lung (Medjkane et al., 2009). This may be mediated through altered adhesion as adhesion to ECM components is also reduced by loss of MRTF. Furthermore, expression of a constitutively active MRTF-A in poorly metastatic B16 F0 cells increased their metastastic potential by about 2-fold (Medjkane et al., 2009). Depletion of the SRF targets Myosin light chain and non-muscle Myosin heavy chain also reduced invasion and metastasis suggesting these targets may be important for SRF dependent regulation of metastasis in melanoma. Indeed, other studies have implicated myosin regulation in invasion and metastasis (Wyckoff et al., 2006).

Many proteins involved in actin regulation, up-stream of MRTF-dependent SRF signalling, have also been implicated in metastasis. Receptor tyrosine kinases are often over expressed in cancer, indeed increases in Receptor tyrosine kinase expression can lead to resistance to BRAF inhibitors (Nazarian et al., 2010). These receptors can lead to actin remodelling and activation of SRF signalling (Olson and Nordheim, 2010). A polymorphism in the *FGFR4* gene leads to prostate cancer progression and results in activation of SRF signalling and a subsequent increase in motility and invasion (Yu et al., 2011). The Rho GTPases have an important role in invasion and metastasis and many are over-expressed in cancer (Sahai and Marshall, 2002). RhoC is up-regulated in melanoma cells selected for increased metastatic potential (Clark et al., 2000). RhoC can regulate the formins mDIA1 and Fmnl2 to potentiate actin polymerisation and increase amoeboid-like invasion of melanoma cells (Kitzing et al., 2010). As RhoC induces actin polymerisation, its effects on metastasis may be in part through SRF signalling.

1.6.3 Notch signalling

The Notch pathway controls differentiation and proliferation decisions in a number of cell-types by activation of a sequence-specific transcription factor (Andersson et al., 2011). It has different roles in different cell-types and so the pathway must be able to respond in distinct ways in different cell contexts, possibly activating different sub-sets of target genes. The core components and transduction pathway of Notch signalling are relatively simple, with only a small number of components required for pathway dependent transcription.

Notch signalling is activated when a trans-membrane ligand binds a trans-membrane receptor on an adjacent cell (Figure 1.7). There are five canonical Notch ligands in mammals, Jagged 1,2 and Delta-like (Dll) 1,3 and 4, and four Notch ligands, Notch 1-4 (Andersson et al., 2011). Following trans-activation of a Notch receptor, it is cleaved twice, once at site 2 (S2) and subsequently at sites 3/4 (S3/4). S2 cleavage is a key regulatory step in receptor activation and is mediated by extracellular ADAM proteases (Brou et al., 2000) (van Tetering et al., 2009). S2 cleavage releases the Notch extracellular domain (NECD) still bound to ligand, which is trans-endocytosed into the ligand expressing cell (Parks et al., 2000). After S2 cleavage the Notch extracellular truncated domain (NEXT) is subject to further cleavage by the γ-secretase complex, either at the plasma membrane or in endocytic vesicles (Andersson et al., 2011). This releases the Notch intracellular domain (NICD), which translocates to the nucleus due to its nuclear localisation signals. NICD cannot bind directly to DNA but instead binds to CBF-1 (also known as RBPJ-κ) and together with the co-activator MAML-1, initiates expression of target genes (Borggrefe and Oswald, 2009). CBF-1 binds DNA via 5'-CGTGGGAA-3' motifs and is thought to act as a repressor of gene transcription in the absence of NICD (Hsieh et al., 1996). On Notch activation, NICD and MAML displace co-repressors of CBF-1 and recruit co-activators, thereby bringing about transcriptional activation (Borggrefe and Oswald, 2009). However, the DNA binding coefficient of CBF-1 has been found to be weaker than first thought and studies in *Drosopila* suggest CBF-1 is actively recruited to binding sites by NICD (Friedmann and Kovall, 2010) (Krejci and Bray, 2007). Therefore, the interaction of CBF-1 with its DNA binding sites may be more dynamic than anticipated. The

hairy/enhancer of split (HES) genes are Notch targets that have been identified in a number of cell contexts (Borggrefe and Oswald, 2009).

Layered on top of the simple core Notch pathway are additional mechanisms to regulate and finely tune Notch signalling. EGF repeats in Notch receptors can be glycosylated by Fringe proteins, which may affect the relative strength of ligand-receptor interactions (Hicks et al., 2000). Glycosylation has been shown to increase the levels of expression of Notch target genes, but not affect the set of genes activated (Andersson et al., 2011). The final cleavage of the Notch receptor may occur at either site 3 or 4, which results in NICD fragments with different N-terminal amino-acids. The different NICD fragments generated have different half-lives and so this could be a mechanism to regulate the duration of Notch signalling (Tagami et al., 2008). Notch signalling is also regulated by the ubiquitin signalling. Numb-like is a negative regulator of Notch signalling, which recruits the E3 ubiquitin ligase, Itch, to promote Notch receptor degradation (McGill and McGlade, 2003). Furthermore, ubiquitination of NICD by the E3 ubiquitin ligase Fbxw7, can lead to rapid degradation of NICD and loss of Notch signalling (Oberg et al., 2001). NICD is subject to other regulatory signals such as phosphorylation and acetylation. The PEST degradation domain within NICD contains many phosho-sites and these are important in determining NICD stability as they are triggers for subsequent ubiquitination (Andersson et al., 2011). The balance between acetlyation and de-acetylation of NICD regulates its half-life and SIRT1, a de-acetylase, decreases NICD stability in endothelial cells (Guarani et al., 2011). Notch target genes can also feedback to regulate the pathway. The Notch target Nrarp, can form a complex with NICD and CBF-1 and decrease NICD stability (Lamar et al., 2001).

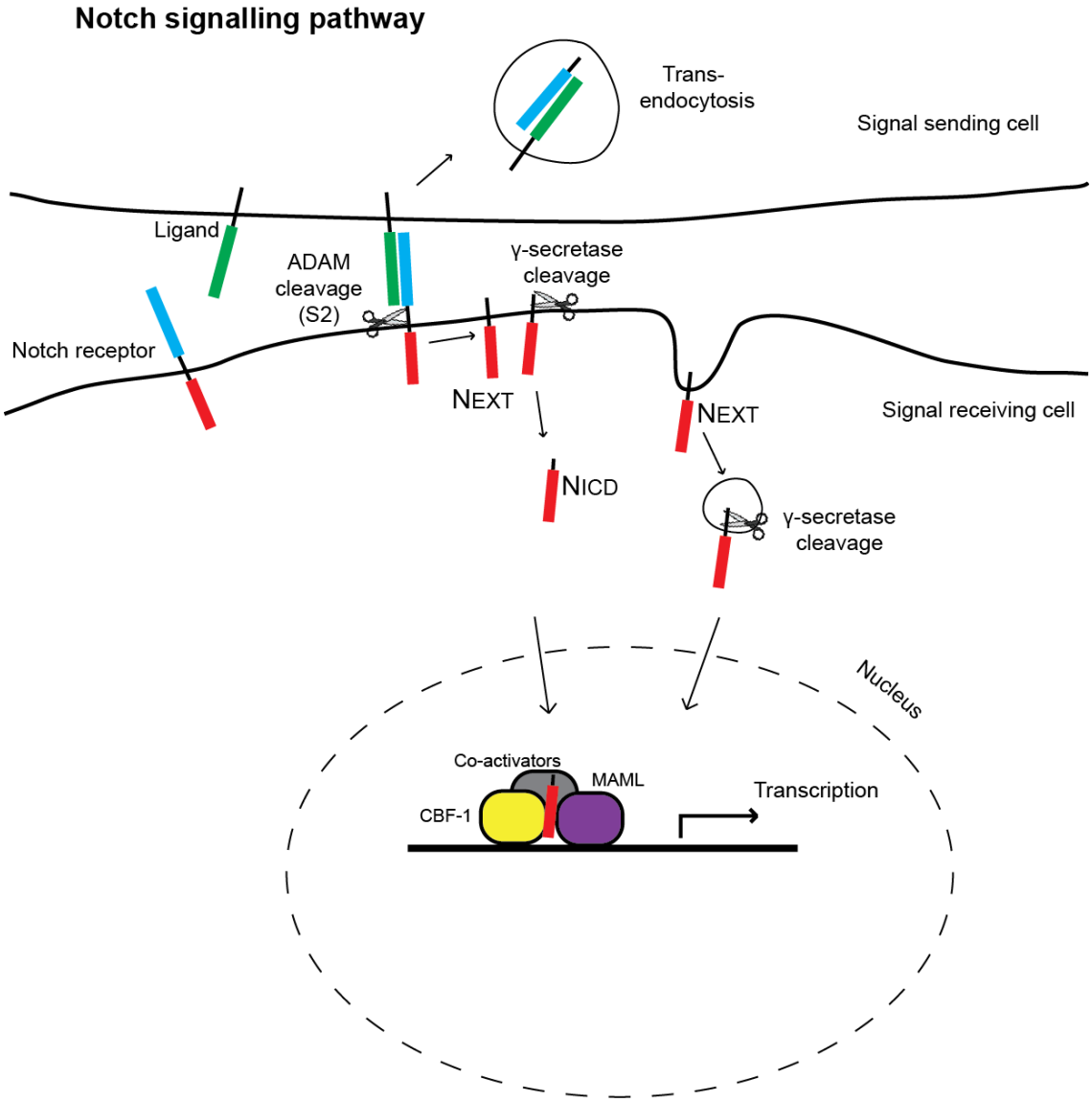

Figure 1.7 Notch signalling.

Notch ligands on the signal sending cell bind to Notch receptors on the signal receiving cell, leading to two separate cleavage steps. ADAM proteases first cleave at site S2 followed by γ-secretase cleavage to release the Notch intracellular domain (NICD). NICD translocates to the nucleus and together with CBF-1 and MAML, activates transcription of target genes.

1.6.3.1 Notch in melanocytic cells and melanoma

The Notch pathway has an important role in maintaining melanocyte stem cells and melanoblasts in vivo. Conditional deletion of CBF-1 (RBPJκ) in melanocyte lineage cells results in a loss of hair pigmentation, characteristic of an absence of melanocytes and a loss of melanocyte stem cells. In addition, treatment of mouse embryonic skin with the γ-secretase inhibitor DAPT, leads to melanoblast apoptosis and a loss of hair pigmentation (Moriyama et al., 2006). Notch activation in mature melanocytes is sufficient to induce re-programming and de-differentiation to neural crest stem cell–like cells (Zabierowski et al., 2011). This provides further evidence for the importance of Notch signalling in regulating the differentiation hierarchy of melanocytic cells.

Notch signalling is also implicated in melanoma progression. Notch1 and the Notch target, HEY1 are up-regulated in melanoma cells (Balint et al., 2005) (Pinnix et al., 2009) (Hoek et al., 2004). Constitutive activation of Notch signalling by expression of NICD in melanocytes confers a transformed phenotype with increased proliferation and migration (Pinnix et al., 2009). This suggests that Notch may be a driver of melanomagenesis. Notch up-regulation in melanocytes also induces MCAM expression and decreases E-cadherin expression leading to changes in adhesion of melanocytes (Pinnix et al., 2009).

Notch can drive proliferation of melanoma cells as γ-secretase inhibitors induce apoptosis in melanoma cells (Qin et al., 2004). Furthermore, constitutive activation of Notch signalling in melanoma cells increases cell proliferation in vitro and tumour growth in vivo (Balint et al., 2005). This Notch induced increase in tumour growth is dependent on β-catenin stability and β-catenin target gene expression, highlighting the importance of interactions between key signalling pathways in melanoma. Notch signalling in melanoma can also increase proliferation through activation of the MAPK and PI3K/AKT pathways (Liu et al., 2006). AKT is activated by the autocrine action of the Notch target NRG1, an ERBB3/4 ligand, resulting in increased proliferation (Zhang et al., 2012a).

Notch signalling has also been implicated in invasion and metastasis. Hypoxia induces Notch signalling in a number of different cancer cell-lines and Notch signalling induces EMT through directly up-regulating Snail expression (Sahlgren et al., 2008). Snail can also feedback to increase Notch4 expression (Kuphal et al., 2005). The EMT regulator Slug, is a Notch target, which represses E-cadherin and induces invasion and metastasis (Leong et al., 2007). Constitutive Notch signalling can also affect melanoma cell adhesion though increasing N-cadherin expression, which subsequently results in increased lung colonisation (Liu et al., 2006).

Given the role of the Notch pathway in differentiation decisions, Notch may be involved in the phenotype switching between MITF+/Brn2- and MITF-/Brn2+ populations. Brn2 can induce Notch signalling in neural progenitors and MITF down-regulation in melanoma cells increased Notch target genes (Castro et al., 2006) (Thurber et al., 2011). This suggests that Notch signalling may also be heterogeneous and increased in the potentially more motile MITF-/Brn2+ sub-population.

1.6.4 Interactions between signalling pathways

Many signalling pathways in the cell interact, overlap and impinge on each other so that overall cell behaviour is regulated by a signalling network with many nodes and points of interaction. The signalling pathways described above are no exception and this section will briefly discuss overlaps between Notch, TGF-β and SRF signalling.

Notch signalling can be functionally enhanced by TGF-β. NICD can bind to SMAD3 and this interaction increases expression downstream of both NICD and SMAD DNA binding sites (Blokzijl et al., 2003). In addition, expression of HES-1, a Notch target, up-regulated after TGF-β addition in an NICD dependent manner (Blokzijl et al., 2003). TGF-β also impacts on Notch signalling as TGF-β signalling induces HEY1 and Jagged1 expression during EMT and this is blocked if Notch signalling is inhibited (Zavadil et al., 2004). In addition, HEY1 expression is bi-phasic, showing an initial SMAD dependent peak, and a subsequent

Jagged1/Notch dependent transcriptional peak, highlighting the different levels of interaction between the Notch and TGF-β pathways (Zavadil et al., 2004).

TGF-β induced EMT involves actin cytoskeleton rearrangements and so may activate MRTF-dependent SRF signalling as a result, indeed TGF-β can induce MRTF nuclear translocation in a Rho dependent manner in epithelial cells (Morita et al., 2007). In a similar manner, hypoxia induced Notch-dependent EMT may also activate SRF signalling through changes in the G-/F-actin ratio. MRTF also directly interacts with SMAD3 downstream of TGF-β signalling to activate slug transcription and drive EMT (Morita et al., 2007). SMADs and MRTF share some of the same target genes such as *Cyr61* and *Ctgf* (Olson and Nordheim, 2010) (Bartholin et al., 2007). However, SMADs and MRTF can also have inhibitory interactions as SMAD3 is thought to inhibit MRTF dependent smooth muscle actin expression under certain conditions (Masszi et al., 2010).

1.6.5 Chromatin control of gene transcription

1.6.5.1 Chromatin

In the nucleus, DNA is packaged together with Histone proteins to form chromatin. The basic unit of chromatin is a nucleosome, which contains DNA wrapped around a Histone octamer (Kornberg and Lorch, 1999). Linker Histones associate with nucleosomes and form higher order chromatin structures to further increase packaging of the DNA (Kornberg and Lorch, 1999). However, the chromatin structure is highly dynamic and can unfold during transcription to allow easy access for RNA polymerases. Together with compacting DNA, Histones also provide a mechanism for regulation of gene transcription. Histone tails protrude from the nucelosome and are a target for multiple methods of modification. There are over 100 different sites recorded for Histone modification and numerous modifications including lysine methylation, acetylation, ubiquitination, arginine methylation and serine phosphorylation (Rando, 2012).

1.6.5.2 Histone modifications

Histone modifications not only alter chromatin structure, potentially regulating access to DNA, but also recruit different proteins and complexes (Rando, 2012). The number of Histone residues available for modification and wide range of modifications gives the possibility for a huge complexity in Histone modifications and combinations. However, studies report that patterns of modifications co-occur widely throughout the genome (Ernst et al., 2011). Analysis at the single nucleosome level of 18 different histone modifications in *Drosophila*,showed 9 distinct modification patterns, considerably smaller than the 2^{18} potential combinations (Kharchenko et al., 2011). The distinct patterns, or chromatin states typically describe genomic locations such as promoters, intron, exons, enhancers and insulators. Actively transcribed promoters are associated with tri-methylated lysine 4 of HistoneH3 (H3K4me3) and a range of acetylated modifications such as acetylated lysine 9 on Histone H3 (H3K9ac) (Mikkelsen et al., 2007). Repressed genes are associated with tri-methylated lysine 27 of HistoneH3 (H3K27me3) and methylated lysine 9 on Histone H3 (Mikkelsen et al., 2007). These distinct modification patterns enable or hinder RNA pol II recruitment, respectively. Given the distinct roles for these modifications, it is surprising that they can also be found together. Bivalent chromatin domains contain both repressive H3K27me3 marks and activating H3K4me3 marks. Genes in these regions are thought to be repressed, but poised for activation, such that key genes can remain silenced but ready for transcription when required (Bernstein et al., 2006).

1.6.5.3 Chromatin mediated gene silencing

The remainder of this section will focus on chromatin mediated gene silencing and the H3K27me3 mark. Around 15 % of Histone H3 is trimethylated at lysine 27 in ES cells and H3K27me3 enrichment is centred around the transcriptional start sites (TSS) of promoters (Zhao et al., 2007a). H3K27me3 is usually associated with gene silencing and the mark is lost in actively transcribed genes (Simon and Kingston, 2009). H3K27 tri-methylation is mediated by the polycomb repressor complex 2 (PRC2) (Margueron and Reinberg, 2011). The core PRC2 complex consists of the Histone methyltransferases EZH1 and EZH2 and two other

polycomb proteins, suppressor of zeste 12 (Suz12), which is essential for methyltransferase activity, and embryonic ectoderm development (EED) (Morey and Helin, 2010). The PRC2 complex works together with the polycomb repressor complex 1 (PRC1). PRC1 catalyses Histone H2A lysine 119 mono-ubiquitination (H2AK119Ub1), which is another repressive chromatin modification and is thought to compact chromatin (Morey and Helin, 2010). RING1A and RING1B are the catalytic subunits of PRC1 and their activity is stimulated by BMI-1, an additional PRC1 component (Li et al., 2006). PRC1 can bind H3K27me3, suggesting that PRC2 acts upstream to enable recruitment of PRC1 to repressed genes. However, not all PRC2 bound genes show H2AK119Ub1 and PRC1 can catalyse H2AK119 ubiquitination at polycomb target genes in the absence of PRC2 (Margueron and Reinberg, 2011) (Tavares et al., 2012). This seems to be the minority of repressed genes and for the most part PRC2 and PRC1 are required to maintain gene repression.

Exactly how PRC2 and H3K27me3 silence gene expression is under debate, it may be through regulation of chromatin structure or more likely recruitment of further regulatory factors (Simon and Kingston, 2009). H3K27me3 may prevent proteins binding to DNA through steric hindrance, although RNA pol II can be detected at a subset of H3K27me3 enriched promoters (Stock et al., 2007). RNA transcripts have been detected at low levels at these genes, suggesting that RNA pol II may be paused at H3K27me3 enriched genes (Zhao et al., 2007a) (Stock et al., 2007). Short transcripts generated from a paused RNA pol II may recruit PRC2 (Kanhere et al., 2010). Therefore PRC2 and H3K27me3 may regulate RNA pol II promoter escape and elongation rather than earlier steps such as recruitment and initiation (Margueron and Reinberg, 2011).

Jarid2 is also found together with the core PRC2 components (Pasini et al., 2010). It is a member of the Jumonji Histone demethylation family of proteins, but it is thought to lack demethylase activity due to a lack of the key residues for co-factor binding (Cloos et al., 2008). Jarid2 target genes overlap with 90 % of known PRC2 core component target genes and it aids PRC2 core complex recruitment to target genes and regulates PRC2 activity (Pasini et al., 2010). In addition, Jarid2 is

required for both PRC2 and RNA Pol II recruitment to bivalent genes in ES cells (Landeira et al., 2010).

The mechanism of PRC2 recruitment to genes is currently unclear. In *Drosophila* a specific DNA sequence named the polycomb response element targets polycomb proteins to chromatin (Margueron and Reinberg, 2011). Genome-wide studies in mammals have failed to find a similar sequence (Beisel and Paro, 2011). However, Jarid2 is able to bind DNA with a bias towards GC rich regions and CHIP-Seq of other PRC2 components also shows a bias towards binding to GC rich regions (Li et al., 2010b) (Margueron and Reinberg, 2011). Non-coding RNAs (ncRNAs) transcribed from the same DNA region (cis) or different DNA region (trans) may regulate H3K27me3 modifications and PRC2 recruitment. X-chromosome inactivation involves H3K27me3 modifications and an increase in the more compact heterochromatin. The ncRNA Xist is transcribed from the X-chromosome and is required for X-chromosome H3K27 methylation (Plath et al., 2003). Xist can bind to PRC2 in vitro suggesting it may recruit PRC2 to the X-chromosome (Zhao et al., 2008). Expression of the long ncRNA HOTAIR from the *Hoxc* locus leads to repression in trans of the *Hoxd* locus (Rinn et al., 2007). HOTAIR binds to the PRC2 complex, recruiting it to the locus to bring about H3K27 methylation (Tsai et al., 2010). PRC2 members can also bind to Histone modifications and EED has been shown to bind H3K27me3, increasing the enzymatic activity of EZH2 (Margueron et al., 2009). Therefore PRC2 recruitment may be through multiple interactions including Jarid2 binding to DNA, EED binding to H3K27me3 and other PRC2 components binding ncRNAs (Margueron and Reinberg, 2011).

Some PRC2 members may have non-chromatin-related activities. EZH2 has been shown to bind to Suz12 and EED to form a methyltransferase complex in the cytoplasm. This complex is thought to co-localise with F-actin and control actin polymerisation through regulation Cdc42 (Su et al., 2005). EZH2 can also bind and directly methylate a lysine residue within the transcription factor GATA4, resulting in a decrease in GATA4 dependent transcription (He et al., 2012). Therefore, EZH2 and other PRC2 complex members may have additional roles other than chromatin mediated transcriptional control.

1.6.6 PRC2 complex during development and differentiation

The PRC2 complex is important during differentiation and provides a memory function to maintain cellular identity and silence alternative transcriptional programs associated with other cell types (Prezioso and Orlando, 2011). This function must also be dynamic to respond to environmental cues that induce differentiation but also to maintain the memory through the cell cycle. In pluripotent ES cells, the PRC2 complex is thought to silence differentiation associated genes as loss of PRC2 components results in the up-regulation of differentiation associated genes (Boyer et al., 2006) (Lee et al., 2006). In addition, binding of PRC2 components and H3K27me3 levels decreased at these genes on induction of differentiation (Boyer et al., 2006). However, loss of Jarid2 in ES cells prevents differentiation and key differentiation associated genes are not primed for transcription (Landeira et al., 2010). This suggests that Jarid2 dependent priming of differentiation associated genes is required for the cell to differentiate correctly. Therefore, Jarid2 may have a different role to the core PRC2 components during differentiation. The requirement of core PRC2 components to silence differentiation associated genes and maintain cells in a less differentiated state is also highlighted in the epidermis, where EZH2 levels are high in epidermal progenitors but decrease with differentiation (Ezhkova et al., 2009). Furthermore, loss of EZH2 in the developing skin increases differentiation.

1.6.7 EZH2 in cancer

EZH2 is up-regulated in a number of cancers including melanoma and lymphoma and is associated with aggressive breast and prostate cancer (McHugh et al., 2007) (van Kemenade et al., 2001) (Kleer et al., 2003) (Varambally et al., 2002). Mutations in EZH2 are found in a number of cancers and a recent study identified EZH2 as a driver mutation in 3 % of melanomas (Chang and Hung, 2012) (Hodis et al., 2012). Up-regulation of EZH2 in prostate cancer has been shown to be a result of genomic loss of microRNA 101, which represses EZH2 transcription (Varambally et al., 2008). Additionally, EZH2 is regulated by the Rb-E2F pathway and increased expression is associated with cell proliferation (Bracken et al., 2003).

EZH2 can also affect cell proliferation acting as a typical oncogene, as loss of EZH2 in prostate and melanoma cells decreases proliferation (Varambally et al., 2002) (Fan et al., 2011). In melanoma, EZH2 expression increases from nevi to melanoma and is highest in metastatic disease. As discussed previously, benign nevi often harbour *Braf* mutations but are in a state of senescence. EZH2 up-regulation is thought to silence the cell cycle inhibitor p21 and bypass the senescent state, driving cancer progression (Fan et al., 2011). EZH2 is also involved in driving breast cancer progression as breast cancer initiating cells show high levels of EZH2. Hypoxia leads to an increase in EZH2 expression, which in turn decreases expression of the DNA damage protein RAD51 leading to increased DNA damage and subsequent activation of growth promoting pathways (Chang et al., 2011).

In addition to driving tumour growth, EZH2 can promote invasion and metastasis in some cancer types. An increase in EZH2 expression in prostate cancer results in silencing of the RasGAP, DAB2IP. DAB2IP acts as a signalling scaffold to co-ordinate both Ras and NF-κB signalling. Epigenetic silencing of this protein leads to activation of both of these pathways, increasing tumour growth, EMT and metastasis (Min et al., 2010). Increased levels of EZH2 in prostate cancer also lead to EMT and increased invasion through EZH2 silencing of the metastasis suppressor RKIP and direct silencing of E-cadherin (Ren et al., 2012) (Cao et al., 2008). In addition, EZH2 induces EMT in nasopharyngeal cancer by interacting with snail to repress E-cadherin expression (Tong et al., 2012). Further implication of the PRC2 complex in cancer metastasis comes from the role of the long ncRNA HOTAIR, a PRC2 interaction partner, which targets PRC2 to the genome. Metastatic breast cancer cells show increased levels of HOTAIR resulting in genome-wide re-targeting of PRC2 and increased invasion and metastasis (Gupta et al., 2010).

1.7 The tumour microenvironment and angiogenesis

Tumours are comprised of a range of cell-types including CAFs, macrophages, T cells, adipocytes, blood and lymphatic endothelial cells and pericytes. Interactions

between these different cell-types and cancer cells govern tumour progression and influence many of the hallmarks of cancer (Hanahan and Coussens, 2012). In addition, therapeutic treatments must consider the tumour microenvironment as a whole as interactions between stromal cells and cancer cells can affect response to therapy and lead to drug resistance (Straussman et al., 2012) (Nakasone et al., 2012). Work in this thesis explores the blood vasculature in vivo, its relationship with motility in the primary tumour and response to angiogenic therapy. This section will focus on the vasculature within the tumour microenvironment. The effects of the microenvironment on motility and metastasis are discussed elsewhere.

1.7.1 The tumour vasculature

Blood vessels are formed from a layer of endothelial cells surrounded by pericytes and a basement membrane. They provide tissues with oxygen and nutrients and help to remove carbon dioxide and waste metabolites (Potente et al., 2011). This is also true for tumours and the growth of blood vessels into tumours sustains tumour growth. Analysis of genetic mouse models of cancer revealed an "angiogenic switch", a distinct event relatively early in cancer progression that described an increase in blood vessel density and enabled further tumour growth (Hanahan and Folkman, 1996). The "angiogenic switch" was thought to be a rate-limiting step in tumour growth, leading to the idea that targeted therapy against blood vessels in human tumours could halt cancer progression.

The tumour vasculature is abnormal and compared to quiescent adult vessels, tumour vessels can be considered as in a state of hyper-activation. They are highly branched and often enlarged and convoluted. In addition, tumour vessels have uneven diameters, potentially as a result of pressure from tumour or stromal cells (Carmeliet and Jain, 2011b). Pericytes are usually only loosely associated with the endothelial cells and the endothelial basement membrane is disordered (Baluk et al., 2003). The result is leaky vessels that are poor at delivering oxygen and can hinder drug delivery to the tumour (McDonald and Baluk, 2002). The

loose pericyte association and vessel leakiness may also aid cancer cell intravasation (Yonenaga et al., 2005).

1.7.2 Induction of tumour angiogenesis

Tumours can become vascularised in a number of different ways. Vessels can sprout from existing ones and generate a new vascular network in a process called sprouting angiogenesis. Alternatively tumours can co-opt pre-exitisting blood vessels without initial sprouting. However, once the tumour outgrows the vascular network, hypoxia induces a sprouting angiogenic response (Potente et al., 2011). Vascular progenitor cells recruited to the tumour through paracrine signalling may form part of the tumour vasculature by intercalating with existing endothelial cells (Potente et al., 2011). In a similar manner, tumour cells can insert themselves into the tumour vasculature in a process called vascular mimicry (Wang et al., 2010a).

Sprouting angiogenesis is initiated by angiogenic factors in the environment, such as VEGF-A, PlGF, PDGF, FGF family members and Angiopoietins (Sakurai and Kudo, 2011). Both cancer cells and stromal cells can contribute to angiogenesis. VEGF-A expression is up-regulated in cancer cells by both hypoxic conditions and oncogenic signalling, leading to an increase in tumour angiogenesis (Shweiki et al., 1992) (Rak et al., 1995). Tie2 positive macrophages in the tumour environment express an array of pro-angiogenic molecules such as VEGF-A and bFGF and large numbers of macrophages correlates with increased vessel density in human tumours (Murdoch et al., 2008). Paracrine interactions between CAFs and cancer cells can induce CAFs to express VEGF-A leading to sprouting angiogenesis (Fukumura et al., 1998). Furthermore, CAFs can also promote angiogenesis through the CXCL12-dependent recruitment of endothelial progenitor cells (Orimo et al., 2005).

The *Vegfa* gene product is subject to alternative splicing and results in a number of different isoforms (Harper and Bates, 2008). Some isoforms contain a heparin binding domain enabling them to bind the ECM (Ferrara, 2010). Other angiogenic factors, such as PDGF-BB can also bind to the ECM. Stromal derived proteases

such as MMP9 release bio-active angiogenic ligands from the ECM hence promoting angiogenesis (Bergers et al., 2000) (Du et al., 2008). Soluble and ECM bound ligands may have different effects on the tumour vasculature. Soluble VEGF-A isoforms are thought to promote vessel enlargement whereas ECM bound VEGF-A isoforms induce vessel sprouting and branching (Lee et al., 2005).

1.7.3 Sprouting angiogenesis

VEGF-A stimulates endothelial sprouting and angiogenesis by binding to VEGFR-2 and inducing filopodia formation in endothelial cells. Cells responding in this way to angiogenic signals are labelled tip cells and these tip cells lead the nascent sprout (Gerhardt et al., 2003). Stalk cells make up the rest of the vessel and these cells lack filopodia. During developmental angiogenesis, further sprouting requires pericyte detachment and degradation of the basement membrane by MMPs (Potente et al., 2011). Tip cells are enriched in MT1-MMP, which helps breakdown the basement membrane and also liberates ECM bound angiogenic factors (Yana et al., 2007). As tumour vessels have weakly attached pericytes and an abnormal basement membrane, the importance of these steps in tumour angiogenesis is unknown.

During developmental angiogenesis, tip cells interact with their neighbouring endothelial cells to induce a stalk cell phenotype in the adjacent cell, and prevent multiple tip cells and excessive sprouting. VEGF signalling in tip cells, together with other external signals, such as Laminin α4 in the basement membrane, induces Dll4 expression (Phng and Gerhardt, 2009) (Stenzel et al., 2011). Dll4 expression on tip cells stimulates Notch signalling in adjacent cells. High Notch signalling inhibits VEGFR-2/3 signalling and prevents sprouting creating a stalk cell phenotype (Benedito et al., 2012) (Phng and Gerhardt, 2009). This situation is complicated by the switching of tip and stalk cell positions during sprouting (Jakobsson et al., 2010). Nascent sprout growth is induced by stalk cell proliferation and endothelial cell migration (Potente et al., 2011). High VEGF-A and other angiogenic molecules in the tumour environment are likely to stimulate multiple tip cells leading to increased vessel branching and increased vessel

density. Whether filopodial sprouting is restricted to tip cells, and if lateral inhibition of sprouting occurs in tumour endothelium is unknown.

During development, the vascular network grows through multiple cycles of sprouting and vessel fusion, forming new connections. Vessel fusion occurs when two tip cells meet in a process known as anastomosis. The tip cells make initial contact through filopodial extensions before forming new cell-cell contacts. The process is aided by macrophages at the site of fusion (Fantin et al., 2010). Vessels subsequently mature both at a cellular level and a network level. On a cellular level, pericytes are recruited by endothelial expression of PDGF-B, which stimulates their proliferation and migration (Gaengel et al., 2009). In addition, endothelial cells become quiescent and form cell-cell contacts to create a barrier between the blood and surrounding tissues. VE-Cadherin is up-regulated during quiescence and localises to adherens junctions to regulate cell-cell adhesion and intracellular signalling (Harris and Nelson, 2010). Mature endothelial cells also require survival signals and these include VEGF-A expressed by the endothelial cells themselves, and blood flow, which up-regulates the transcription factor KLF2 (Lee et al., 2007) (Dekker et al., 2002). Finally, the vascular network is subject to remodelling and pruning of vessels to generate an efficient network for blood flow (Potente et al., 2011).

During tumour angiogenesis, many of these stages are disrupted. High VEGF-A in the microenvironment means that growth factor gradients, which normally operate during developmental angiogenesis, are absent. Disruption of the stages of normal sprouting angiogenesis is highlighted by the abnormal tumour vessel architecture. Analysis of vessel structures induced by acute VEGF-A treatment in vivo together with vessels observed in tumours, revealed heterogeneity in vascular structures. VEGF-A initially stimulates the formation of large, thin-walled, hyperpermeable sinusoids called mother vessels (MV). These subsequently turn into capillary structures through sprouting, or vascular malformations (VMs) through proliferation of endothelial cells (Nagy and Dvorak, 2012). This suggests that merely the increase is VEGF-A can lead to abnormal vasculature structures through endothelial cell proliferation and sprouting.

High VEGF-A levels lead to VEGFR-2 dependent signalling in endothelial cells and phosphorylation of VE-Cadherin. This results in a loosening of endothelial cell-cell contacts and contributes to vascular leakage (Esser et al., 1998). Tumour vessels often have poor blood flow and this can lead to an up-regulation of inflammation associated genes contributing to the inflammatory tumour microenvironment (Tozer et al., 2005) (Chiu and Chien, 2011). As flow provides a survival signal to endothelial cells, presumably other mechanisms, potentially VEGF-A, provide adequate survival signals in the tumour context. As discussed earlier, the tumour endothelium has a loose connection with pericytes.

1.7.4 Targeting tumour angiogenesis

Given that blood vessels are required to bring vital nutrients and oxygen to the tumour, a number of agents have been developed to target the tumour vasculature with the aim to starve the tumour and prevent growth. The anti-VEGF-A antibody Bevacizumab, is approved in the US for combination treatment with chemotherapy for metastatic cancers. A number of pan-VEGFR tyrosine kinase inhibitors have also been developed including Sunitinib and Sorafenib. Sunitinib is approved in the US for treatment of metastatic renal cell carcinoma. Both Sunitinib and Sorafenib also target other receptor tyrosine kinases and Sunitinib can additionally inhibit PDFR, CSF-1R and RET. Clinical benefit of anti-angiogenic therapies is thought to be derived from both the inhibition of vascular expansion due to blockade of vessel branching, and vessel regression due to the inhibition of endothelial survival signals (Potente et al., 2011). The loss of survival signals may also sensitise endothelial cells to chemotherapy or irradiation therapy, potentially explaining why anti-angiogenic therapies are more effective in combination with other more traditional cancer therapies (Jain, 2005).

Despite positive pre-clinical results, there have been a number of unsuccessful clinical trials with anti-angiogenic therapies and many trials indicated no benefit for overall survival in patients, (Allegra et al., 2011). Some patients showed no response and other patients developed resistance later in disease progression. Furthermore, subsequent pre-clinical studies have suggested that anti-angiogenic

therapy creates a hypoxic environment that can act to increase cancer cell invasion and metastasis (Paez-Ribes et al., 2009) (Ebos et al., 2009).

Resistance to anti-angiogenic therapy may arise through a number of mechanisms. Following anti-angiogenic treatment of experimental tumours, vascular density decreases but normal looking vessels with tightly associated pericytes remain (Bergers et al., 2003). This suggests that pericyte coverage of tumour vessels may dictate the responsiveness to therapy. Pericytes could protect endothelial cells by secreting VEGF-A and other growth factors, hence providing survival signals (Bergers and Hanahan, 2008). It is likely that stromal cells have an important role in resistance to anti-angiogenic therapy. Stromal cells may produce endothelial survival signals or VEGF/VEGFR independent pro-angiogenic ligands. For example, CAFs from anti-angiogenic resistant tumours show an up-regulation of PDGF-C compared to non-resistant tumours (Crawford et al., 2009). Furthermore, blocking antibodies against ANG2, another pro-angiogenic factor, together with anti-VEGF-A therapies improved anti-tumour activity (Brown et al., 2010). Alternatively, the cancer cells may up-regulate these non-VEGF "rescue" ligands such as PlGF and FGFs as a result of hypoxia (Potente et al., 2011). Cancer cells may also recruit pro-angiogenic stromal cells. Recruitment of CD11b+ Gr-1+ myeloid cells aids tumour growth in the presence of anti-angiogenic therapy (Shojaei et al., 2007a). These cells have subsequently been shown to promote angiogenesis through secretion of Bv8, a G-protein receptor ligand that stimulates endothelial cells in a VEGFR independent manner (Shojaei et al., 2007b).

Few, if any, of the receptor tyrosine kinase inhibitors inhibit all VEGFRs. Sunitinib only inhibits VEGFR-1 and 2, whereas Sorafenib only inhibits VEGFR-2 and 3, and so pro-angiogenic signalling may occur through non-inhibited VEGF receptors (Azam et al., 2010). Hypoxia is a key factor in resistance to anti-cancer therapies (Azam et al., 2010). Generation of a hypoxic tumour environment after anti-angiogenic treatment can induce autophagy in cancer cells, which aids survival (Hu et al., 2012). Furthermore, investigation of the response of different tumour associated vessels, such as mother vessels or vascular malformations (described earlier) indicated that different vessels within the tumour may respond differently to anti-angiogenic therapy. Vessel structures formed early in the response to VEGF-

A, such as mother vessels, were sensitive to anti-VEGF therapy, whereas vessels formed later, such as vascular malformations, were resistant (Nagy and Dvorak, 2012). Therefore, different vessels in the same tumour may respond differently to anti-angiogenic therapy.

Given the lack of success of VEGF-A or VEGFR targeting agents, other methods are being developed to target the tumour vasculature. Vascular normalisation aims to reduce vasculature permeability and abnormalities, hence improving cytotoxic drug delivery and therapeutic response (Carmeliet and Jain, 2011b). This is in direct contrast to anti-VEGF and anti-VEGFR treatments which aim to reduce vascularisation and starve tumours of oxygen. Treatments that affect macrophage polarisation may enable vessel normalisation as loss of M2 skewed macrophages results in vessel normalisation (Rolny et al., 2011). M2 macrophages secrete a range of pro-angiogenic factors such as PlGF resulting in abnormal vessels. In addition vessel normalisation increased response to chemotherapy and decreased metastasis in this study, highlighting the potential of vascular normalisation as a therapy (Rolny et al., 2011).

In summary, the tumour vasculature is highly abnormal, with different mechanisms working together to increase tumour vasculature density and different vascular structures present in tumours. This leads to heterogeneous vascular organisation and regulation in the tumour environment. Anti-angiogenic therapies have not performed as well as predicted in the clinical setting and this may be due to the heterogeneous nature of the vasculature and adaptation in the tumour microenvironment.

Chapter 2. Materials and Methods

2.1 Reagents and chemicals

Potassium chloride (KCl), Tris base, Tris HCl, potassium phosphate (KH_2PO_4), sodium phosphate (Na_2HPO_4), ethylene diamine tetraacetic acid (EDTA), glycine, β-mercaptoethanol, sodium hydroxide (NaOH), hydrochloric acid (HCl), tetramethylethylenediamine (TEMED), ethanol (EtOH), methanol (MeOH), dimethyl sulfoxide (DMSO), Tween-20, TRITON X100, bromophenol blue, xylene cyanol FF, Ponceau S, bovine serum albumin (BSA), adenosine triphosphate (ATP), deoxynucleotides (dNTPs), paraformaldehyde (PFA), ethidium bromide, were all purchased from SIGMA. Acetic acid, glycerol, 40 % acrylamide solution, sodium dodecyl sulphate (SDS), sodium acetate, sodium chloride (NaCl), and magnesium chloride ($MgCl_2$) were purchased from Fisher Scientific. UltraPure agarose was purchased from Invitrogen.

2.1.1 Enzymes

Restriction enzymes were purchased from New England BioLabs (NEB) and were supplied and used with the appropriate buffers. PCR reactions were performed using Phusion polymerase from NEB in HighFidelity (HF) buffer. DNA polymerase 1 (Klenow fragment) was purchased from NEB and was used to blunt DNA ends. Ligation reactions were carried out using T4 DNA Ligase, also from NEB.

2.1.2 Buffers and solutions

Some common buffers and solutions are listed below.

Phosphate buffered saline (PBS)
1.5 mM KH_2PO_4, 8 mM Na_2HPO_4, 2.7 mM KCl, 137 mM NaCl, pH 7.4

Tris buffered saline (TBS)
137 mM NaCl, 2.7 mM KCl, 20 mM Tris HCl, pH 7.4

TE buffer
10 mM Tris HCl pH 7.5, 1 mM EDTA

50 x TAE
2 M Tris-acetate (242 g Tris base + 57.1 ml glacial acetic acid per litre), 0.05 M EDTA pH 8.0

10 x Protein buffer
1.92 M glycine, 0.25 M Tris Base

SDS running buffer
100 ml of 10 x protein buffer, 890 ml distilled water (dH_20), 10 ml 10 % SDS

Transfer buffer
100 ml of 10 x protein buffer, 699 ml distilled water (dH_20), 200 ml methanol, 1 ml 10 % SDS

Stripping buffer
0.15 M glycine pH 2.5, 0.4 % SDS

5 x SDS sample buffer
0.32 M Tris pH 6.8, 10 % SDS, 50 % glycerol, 0.5 M β-mercaptoethanol, 0.05 % bromophenol blue

6 x DNA loading buffer
0.25 % bromophenol blue, 0.25 % xylene cyanol FF, 30 % glycerol

2.1.3 Cell-culture reagents

Fetal calf serum (FCS) was purchased from PAA. Matrigel was purchased from BD Biosciences. DMEM, Opti-MEM and Penicillin-Streptomycin (Pen-Strep) were purchased from Gibco. Methyl cellulose was purchased from SIGMA. Common growth factors, inhibitors or drugs used include

TGF-β1	(Peprotech)
HGF	(SIGMA)
α-MSH	(SIGMA)
Cytochalasin D	(Tocris)
H89	(Tocris)
SB 431542	(Tocris)
Sunitinib	(LC Laboratories)

2.2 Cell culture manipulations

2.2.1 Cell-lines

Melanoma cell-lines used were the murine B16 F2 and F10 pigment producing lines and the 5555 and 4434 lines derived from the BRAF-V600E mouse melanoma model (Dhomen et al., 2009). B16 F2 cells had been previously transduced with a retro-viral vector for mRFPCAAX or GFPCAAX expression to label the plasma membrane. B16 F10 GFP and mCherry cells had been previously transfected and stably selected for constitutive GFP and mCherry expression. All melanoma cells were cultured in DMEM with 10 % FCS and 1 % penicillin-streptomycin in 10 % CO_2. Clonal B16 F2 reporter cell-lines, and the B16 F2 polyclonal cell-line expressing NICD-GFP were also cultured under these conditions after selection with antibiotics (see later). The more metastatic B16 F10 were used for motility assays and short-term lung metastasis experiments unless stated.

2.2.2 Cell culture

Cells were removed from cell culture dishes with 0.1 % trypsin and 0.02 % versene after washing with PBS. Trypsin was neutralised by addition of media containing 10 % FCS.

2.2.3 Generation of B16 melanoma spheroids

B16 F2 cells were removed from cell culture dishes with trypsin and resuspended in a sterile 0.25 % methyl cellulose solution in DMEM at 1 x10^6 cells per ml. 20 µl droplets were plated onto the underside of a 10 cm culture dish and allowed to form spheroids in a 37 °C incubator overnight.

2.2.4 Transient DNA transfections

B16 F2 cells were transfected with Fugene6 (Roche). 60 000 B16 F2 cells were plated in 6-well plates 24 hours before transfection and the media changed to Opti-MEM 30 minutes prior to transfection. 6 µl of Fugene6 was added to 100 µl of Opti-MEM followed by 1 µg DNA. The tube was mixed and incubated for 30 minutes before being added dropwise to the 6-well plate. After 6-8 hours the media was changed to DMEM + 10 % FCS. When cells were transfected with two or more plasmids, the constructs were mixed to give a total of 1 µg of DNA.

2.2.5 Transfection of siRNA oligos

siRNA oligos were ordered from Dharmacon and stock concentrations made up at 20 µM. Smart pools were generated by mixing an equal volume of each of the four siRNA oligos for a single gene. The Allstars non-targeting siRNA oligo (Qiagen) was used as a control. B16 F2 and F10 cells were transfected with Lipofectamine 2000 using a final siRNA concentration of 100 nM. For a 12-well plate, 35 000 B16 cells were plated 24 hours before transfection and the media changed to 400 µl Opti-MEM 30 minutes prior to transfection. On the day of transfection two tubes were prepared:

Tube 1. 50 µl Opti-MEM and 1 µl Lipofectamine 2000.
Tube 2. 50 µl Opti-MEM plus 2.5 µl of siRNA (20 µM stock).

Tubes 1 and 2 were incubated separately for 5 minutes and then mixed and incubated for a further 30 minutes. Finally the transfection complexes were added

dropwise to the cells. After 6-8 hours FCS was added to the cells to a final concentration of 10 %. The following day the cells were washed with PBS and transferred to DMEM + 10 % FCS. If required, the cells were trypsinised and plated onto glass-bottomed cell culture dishes (MatTek) 24 hours after transfection and fixed a further 24 hours later.

When cells were transfected with siRNA oligos and DNA plasmids, Lipofectamine 2000 was used with a similar protocol to above. The two tubes prepared for a 12-well plate transfection were:

Tube 1. 50 µl Opti-MEM and 0.5 µl Lipofectamine 2000.
Tube 2. 50 µl Opti-MEM, 1.25 µl of siRNA (20 µM stock) and 0.5 µg DNA.

The sequences used for transient knockdown experiments are shown below:

EZH2	EZH2 #1	D-040882-01	GGAAAGAACUGAAACCUUA
	EZH2 #2	D-040882-02	CAGAAGAGCUGAUGAAGUA
	EZH2 #4	D-040882-04	GGAGGGAGCUAAGGAGUUU
Jarid2	Jarid2 #1	D-054799-01	GCGGAAAGGUGGACACUAA
	Jarid2 #2	D-054799-02	CGGCUAGCCUGCAUAAAGA
	Jarid2 #4	D-054799-04	UAAGGUAAAUGGAGUCACU
Suz12	Suz12 #1	D-040180-01	GGACCUACAUUACAAUUUA
	Suz12 #2	D-040180-02	GAUGUAAGUUGUCCAAUAA
	Suz12 #4	D-040180-04	GCACAGAACUCUUACUUAC
BMI-1	BMI-1 #1	MU-065526-01	CAGCAAGUAUUGUCCUAUU
	BMI-1 #2	MU-065526-02	GUAUGAAGAGGAACCUUUA
	BMI-1 #3	MU-065526-03	GUAAAUAAAGAGAAGCCUA
	BMI-1 #4	MU-065526-04	GAUAAAAGGUACUUACGAU

P protein	P protein #1	MU-041297-01	GGACUUCGCUGGUUUCACA
	P protein #2	MU-041297-02	GCUCAAAGGUUGCACACUU
	P protein #3	MU-041297-03	AUACAGAGUUUGGCUCAUU
	P protein #4	MU-041297-04	UGUAAAGGCAUAUCAACUU
Control	Allstars	1027281	Sequence not specified

2.2.6 Generation of stable cell-lines

Clonal reporter cell-lines were generated by transient co-transfection of B16 F2 mRFPCAAX cells with the reporter plasmid together with a pbabe-hygro plasmid at a ratio of 3:1. pBabe hygro contains a hygromycin resistance cassette and so confers resistance to hygromycin. After 48 hours, cells were transferred to selection medium containing DMEM + 10 % FCS + 500 µg/ml hygromycin and maintained in selection medium for 2-3 weeks. Clones were derived by either

1. Stimulating the reporter cell-lines (10 % FCS after serum starvation for SRF reporter, 2 ng/ml TGF-β1 for TGF-β reporter), FACS sorting 12-18 hours later and collecting responsive cells in 96 well plates.
   or
2. Splitting the reporter cell-line sparsely and manually picking clones.

Further testing of clones was undertaken to ensure transcription of fluorescent protein in response to stimulus and loss of fluorescent protein expression on inhibition of the pathway of interest.

B16 F2 cells stably expressing NICDGFP were generated by transiently transfecting B16 F2 mRFPCAAX cells with a plasmid encoding Notch1-ICD-GFP. After 48 hours cells were transferred to selection medium containing DMEM + 10 % FCS + 1 mg/ml G418 and maintained in selection medium for 2-3 weeks. Cells were subsequently FACS sorted to ensure expression of the NICD-GFP fusion protein.

2.2.7 Flow cytometry analysis and sorting

Flow cytometry analysis and sorting was used to generate and test clonal reporter cell-lines, purify cells stably expressing fluorescent proteins, perform cell cycle analysis and collect reporter cell populations for microarray.

To prepare cells for flow cytometry analysis or sorting, cells were trypsinised, washed in PBS, resuspended in sterile PBS and filtered through a 70 µm sterile cell filter (BD Falcon). The filtered cells were then transferred to a polystyrene FACS tube (BD Falcon) and kept on ice. Sorted cells were collected in polypropylene FACS tubes (BD Falcon) or 96-well cell culture plates containing media + 10 % FCS. After sorting into FACS tubes, cells were re-plated and cultured as normal.

Reporter cell-lines were subject to cell sorting to collect the reporter high and reporter low populations for subsequent microarray analysis. Cells grown in vitro were prepared as described above. B16 F2 mRFPCAAX Brn2 reporter tumours were dissected and cut into small pieces. The tumour pieces were incubated in 1 mg/ml sterile Collagenase/dispase (Roche) in PBS (no Ca^{2+} or Mg^{2+}) for 40 minutes at 37 °C and were pipetted up and down at intervals to generate a single cell suspension. The cell suspension was filtered 2-3 times through 70 µm filters, once through a 40 µm filter and finally diluted with PBS. The tumours cells were identified by expression of mRFP and sorted according to GFP expression. As a control, B16 F2 mRFPCAAX cells grown in vitro were also analysed to help identify tumour cells and provide a GFP negative control. For microarray analysis, 100 000 cells were collected directly in 700 µl of RLT lysis buffer containing 1 % β-mercaptoethanol. Multiple tubes were collected to maximise yield and subsequently RNA was extracted using RNeasy micro kit (Qiagen).

Most cell cycle analysis was performed by the FACS Laboratory using propidium iodide. Cells were trypsinised, centrifuged and then fixed with 70 % ethanol before being taken to the FACS Lab. Live Notch reporter cells for cell cycle analysis were incubated with 10 µg/ml Hoechst 33342 at 37 °C for 45 minutes before being analysed for GFP expression and Hoechst 33342 staining.

2.3 Nucleic acid manipulations

2.3.1 Preparation of DNA

Plasmid DNA was prepared from small overnight bacterial cultures transformed with the plasmid of interest using the QIAfilter Plasmid Midi kit (Qiagen) and QIAprep Miniprep kit (Qiagen). Briefly, the bacteria were collected by centrifugation and subject to alkaline lysis. For mini preps, the lysates were neutralised and adjusted to high salt binding in a single step and subsequently cleared by centrifugation. Plasmid DNA was then purified on a silica membrane. For midi preps the lysates were applied to a QIAGEN Anion-Exchange Resin under low-salt and pH conditions. Subsequent washes removed RNA, proteins, and low-molecular-weight impurities. The plasmid DNA was then eluted, precipitated with propan-2-ol and centrifuged to pellet the DNA. The DNA pellet was washed with 70 % ethanol and resuspended in TE buffer.

2.3.2 Quantification of nucleic acids

The concentration of nucleic acids from minipreps, maxipreps or RNA extraction was quantified using a Nanodrop Spectrophotometer (Nanodrop) to measure the absorbance at 260 nm.

2.3.3 Polymerase chain reaction (PCR)

Polymerase chain reactions were carried out according to the reagent mix and temperature cycles below.

1 µl DNA template (10 ng)
10 µl 5 x HF buffer (supplied with Phusion polymerase)
2.5 µl Forward primer (25 pmol)
2.5 µl Reverse primer (25 pmol)
2 µl dNTPs (400 µM)
0.5 µl Phusion polymerase (NEB)
dH_2O to 50 µl

Temperature cycles

98 °C 5 mins		
98 °C 30 s	denaturing	
52 °C 30 s	annealing	
72 °C 30 -120 s	extension	return to denaturing x 18 - 25 cycles
72 °C 10 mins		
4 °C hold		

2.3.4 Agarose gels

Agarose was melted in 1 x TAE buffer in the microwave at concentrations of between 0.7 and 2 % depending on the DNA fragments to be separated. Ethidium bromide was added to a final concentration of 0.5 µg/ml before casting the gel. DNA samples were mixed with 6 x DNA loading buffer and loaded. A 1 kb ladder was also loaded to help identify DNA fragment sizes. Gel electrophoresis was performed in TAE buffer at 70-100V. DNA was visualised using a UV transilluminator and if required the band of interest was cut out from the gel.

2.3.5 Purification of DNA from agarose gels

DNA was purified from agarose gels using QIAquick Gel extraction kit (Qiagen). Briefly, the agarose band containing the DNA was dissolved at 65 °C in 3 volumes of Buffer QG. Then, one volume of isoproponal was added and the solution applied to a Qiaquick column. The column was subsequently washed, dried and the DNA eluted in dH_2O.

2.3.6 Restriction enzyme DNA digest

DNA was digested according to the enzyme used.

2 µg DNA
5 µl 10 x buffer
1 µl BSA (if required)
1 µl Restriction enzyme
dH_2O to 50 µl

2.3.7 Klenow blunting of DNA ends

If required, DNA ends were blunted using Klenow which has polymerization activity and 3'→ 5' exonuclease activity. Following restriction enzyme digestion of DNA, the restriction enzymes were heat inactivated. Subsequently 2 µl of dNTPs (400 µM) and 1 µl of Klenow were added and the reaction incubated at 37 °C for 20 minutes before a final heat inactivation at 75 °C for 5 minutes.

2.3.8 Calf intestinal alkaline phosphatase treatment of DNA ends

Following restriction enzyme digest of vectors intended for ligation reactions, the vectors were treated with calf intestinal alkaline phosphatase (CIP) to remove 5' phosphate groups. 1 µl of CIP was added to the digestion reaction and incubated at 37 °C for 20 minutes.

2.3.9 Ligation of DNA fragments

Small volumes of the DNA fragments were run out on an agarose gel to roughly determine the relative amounts of vector and insert. Ligation reactions were set up using a range of vector:insert ratios. Each 20 µl ligation reaction contained:
2 µl T4 ligase buffer,
x µl Vector DNA,
y µl Insert fragment DNA,
1 µl T4 ligase,
dH_2O up to 20 µl.

Reactions were left at room temperature for at least 2 hours. The ligation reaction was then used to transform competent E.coli.

2.3.10 DNA sequencing

DNA constructs were checked by sequencing before being used in cell-based assays. Big Dye terminator (BDT) kit (Applied Biosystems) was used and each sequencing reaction contained:

8 µl BDT reaction mix
1 µl DNA (100 ng)
1 µl Primer (4 pmol)
10 µl dH_2O

The temperature cycles were as follows:

96 °C 1 min
96 °C 10 sec -denaturing
50 °C 5 sec - annealing
60 °C 4 min - extension return to denaturing x 25 cycles
4 °C hold

DNA from sequencing reactions was purified using ethanol/EDTA/sodium acetate precipitation. Briefly, DNA was precipitated by adding 2 µl of 125 mM EDTA, 2 µl of 3M sodium acetate (pH 5.2) and subsequently 50 µl 100 % ethanol. The precipitated DNA was centrifuged, the pellet washed with 70 % ethanol and allowed to dry at room temperature. The purified DNA was then analysed by an in house research services laboratory.

2.3.11 RNA extraction

RNA was extracted from cells using the RNeasy mini and micro kits (Qiagen) in order to determine mRNA expression levels and to prepare samples for microarray. Briefly, cells were lysed in RLT buffer and the lysate homogenised by vortexing or by passing the lysate through a 21-gauge needle 5-10 times. After addition of 70 % ethanol, the sample was loaded onto a spin column. DNA digestion was carried out on the column and then the column was washed and the RNA eluted in RNAase free water.

2.3.12 Preparation of cDNA

Complementary DNA (cDNA) was prepared by reverse transcription of 1-2 µg of total RNA. The reagents below were mixed and heated to 70 °C for 5 minutes before being incubated on ice for 5 minutes.
1-2 µg total RNA
2 µl Random primer mix (Promega)
1 µl RNasin ribonuclease inhibitor (Promega)
Nuclease-free water up to 14 µl

Subsequently the reagents below were added and incubated at room temperature for 10 minutes before being incubated at 40 °C for 50 minutes.
5 µl M-MLV RT 5 x buffer (Promega)
2 µl dNTPs (400 µM)
1 µl M- MLV Reverse Transcriptase (Promega)
3 µl nuclease-free water

Finally nuclease-free water was added up to 100 µl for a starting amount of 2 µg RNA, or 50 µl for a starting amount of 1 µg of RNA. 1 µl of this cDNA was used in subsequent Q RT-PCR reactions.

2.3.13 Quantitative Real-Time PCR (Q RT-PCR)

Q RT-PCR was used to determine the expression of mRNAs of interest relative to a control mRNA. Platinum SYBR Green qPCR SuperMix-UDG with Rox (Invitrogen) was used in conjunction with a 7900HT Fast Real-Time PCR system (Applied Biosystems). Reactions were set-up on ice in a 96 well optical reaction plate (Applied Biosystems) as outlined below:
12.5 µl Platinum SYBR Green qPCR SuperMix-UDG with Rox
0.5 µl Forward primer (0.5 pmol)
0.5 µl Reverse primer (0.5 pmol)
1 µl cDNA
10.5 µl dH_2O

50 °C 20 s
95 °C 10 mins
95 °C 15 s Denaturing
60 °C 60 s Annealing/Extension return to denaturing x 40 cycles
4 °C hold

Commonly used DNA oligonucleotide primers are shown below:

Gapdh	Forward	GTGCAGTGCCAGCCTCGTCC
	Reverse	GCCACTGCAAATGGCAGCCC
Actin	Forward	CACCCGCGAGCACAGCTTCT
	Reverse	CGTTGTCGACGACCAGCGCA
Hes-1	Forward	TGGCTGCTACCCCAGCCAGT
	Reverse	CGCTGCAGGTTCCGGAGGTG
Dct	Forward	GCTTCAGGAATGCACTGGAAGGGT
	Reverse	TCGTTGGCTGCTGAGTGTGGC
Tyr	Forward	GCGATGGAACACCTGAGGGACC
	Reverse	GTGAGTGGACTGGCAAATCCTTCC
Tyrp1	Forward	GCGAAGCGCACAACTCACCC
	Reverse	CCTGCAGCATCTCCTGCATGTCT
Ezh2	Forward	ATTGCGCGGGACTAGGGAGTG
	Reverse	GCACCGAGGCGACTGCATTCA
Jarid2	Forward	GGCCGTCGAGGAAAAGGCCC
	Reverse	GGCAGCGCAGGAGAACCTCG
Oca2	Forward	GCCTGCCTGGGAGGTAATGGGA
	Reverse	TGCAAATGATGGCTGGCTGGCT

Sparc	Forward	GTGTGTGCCAGGACCCCACC
	Reverse	CCAGGCAGGGGGCGATGTATTT
Mcam	Forward	CTCACGCTGACCTGCGAGGC
	Reverse	TGGGGACCCAAAAATGCCCACG
Actn4	Forward	TCGCAGGGAAGCCTTGGAGAAAACA
	Reverse	GGCCAGGATGGCCTCACGCT

2.4 Plasmids

2.4.1 Mammalian expression constructs

The Notch reporter pCBFRE:GFP construct was a gift from Julian Lewis.

The Notch luciferase reporter pCBFRE:luciferase construct was purchased from Addgene.

The TGF-β reporter pCAGA:CFP (with linker) was generated by Silvia Giampieri and on cloning of CFP downstream of the CAGA sequence, a 46 bp linker sequence was also introduced. I subsequently removed this linker sequence by digestion with AgeI and HindIII, Klenow treatment and blunt-end ligation to generate pCAGA:CFP (no linker).

The SRF reporter p3DA:2eGFP and p3DA:2eGFP Fos 3'UTR constructs were a gift from Richard Treisman.

The pbabe Hygro construct was a gift from Gordon Peters.

The constitutive renilla expression construct was a gift from Axel Behrens.

The pNICD-GFP construct was a gift from Julian Lewis.

The peGFP C1 construct was purchased from Clontech.

The pmCherry C1 construct was made by Steven Hooper by cloning in the mCherry expression sequence into the peGFP C1 clontech vector backbone.

The full-length Ezrin-GFP and constitutively active mutant EzrinTD-GFP were generated by Erik Sahai.

2.5 Bacterial techniques

2.5.1 Bacterial media and plates

Competent E.coli were grown in suspension in LB containing the appropriate antibiotic. Transformations were plated onto 10 cm dishes containing Agar and either ampicillin (75 ug/ml) or kanamycin (50 ug/ml) as appropriate.

2.5.2 Bacterial strains

Subcloning Efficiency DH5α Chemically Competent Cells (Invitrogen) were used for transformation of plasmids for midipreps. One Shot TOP10 Chemically Competent Cells (Invitrogen) were used for transformation of ligation reactions.

2.5.3 Bacterial transformation

Bacteria were thawed on ice for 15 minutes. Bacterial suspension was mixed with plasmid DNA or ligated DNA fragments and incubated on ice for a further 20 minutes. The bacteria and DNA were then heated to 42 °C in a water bath for 45 s and returned to ice for 10 minutes. 250 µl of SOC media was added and the bacteria incubated for 45 min at 37 °C with shaking. The bacteria were then added to an agar plate containing the appropriate antibiotic resistance and spread over the surface. The plate was incubated overnight at 37 °C.

2.6 Protein manipulations

2.6.1 Preparation of cell protein lysates

Plates containing cells for lysis were washed with cold PBS before 1 x SDS sample buffer was added and the cells scraped and collected. The sample was boiled at 95 °C for 5 minutes before being used for western blotting.

2.6.2 SDS-Polyacrylamide gel electrophoresis (SDS-PAGE)

Poly-acrylamide gels were made with:
0.1 % SDS
375 mM TRIS HCl pH 8.8
8-15 % poly acrylamide depending on protein molecular weights to be separated
0.1 % APS
0.001 % TEMED

The gels were poured into mini-gel systems (BioRad) and over-laid with dH_20 to ensure the gels were flat. When set, the dH_20 was removed and stacking gel was overlaid:
0.1 % SDS
125 mM TRIS HCl pH 6.8
5 % acrylamide
0.1 % APS
0.001 % TEMED

A 1.5 mm comb (10-15 wells) was inserted and the stacking gel left to set. Set gels were inserted into a gel cassette in a running tank (BioRad) and the cassette and tank filled with SDS running buffer. A prestained protein ladder (Benchmark, Invitrogen) was run and the remaining wells loaded with up to 50 µl of sample. Gels were run at 100-125 V.

2.6.3 Western blotting

After SDS-PAGE, the proteins in the gel were transferred to PROTRAN nitrocellulose membrane (Whatmann). The gel was placed on top of 2 sheets of 3MM chromatography paper (Whatmann), the membrane, which had been pre-wet in transfer buffer, was then laid on top of the gel, followed by 2 more sheets of 3MM paper. This "tower" was placed inside two sponges in a transfer cassette (BioRad). The tank was filled with transfer buffer and the gel was transferred for 2-3 hours at 80-90 V on ice. After transfer the membrane was subject to Ponceau red staining, washed with dH_2O and blocked by incubating with TBS + 3 % milk (Marvel) + 2 % BSA for 1 hour. Primary antibodies were generally incubated with the membrane overnight at 4 °C at a dilution of 1:1000 in 3 % milk + 2 % BSA. Primary antibodies were washed off with 3 x 5 minute washes in TBS + 0.05 % Tween-20. HRP-labelled secondary antibodies (Fisher Scientific) were used at a dilution of 1:100 000 in TBS + 3 % milk + 2 % BSA and incubated with the membrane for 1 hour. Secondary antibodies were washed off the membrane in 3 x 5 min washes with TBS + 0.05 % Tween-20. The blot was then developed by rinsing for 1 minute in Luminata Western HRP Substrate (Millipore) before being exposed to chemoluminescent film (GE Healthcare).

Antibodies used:

Target	Source	Product number	Antibody type	Dilution
β-tubulin	Sigma	T7816	Mouse monoclonal	1:10000
Vinculin	Abcam	ab18058	Mouse monoclonal	1:2000
Notch1-ICD	Abcam	ab8925	Rabbit polyclonal	1:1000
EZH2	Cell Signalling	#5246	Rabbit polyclonal	1:1000
Suz12	Abcam	ab12073	Rabbit polyclonal	1:1000
BMI-1	Abcam	ab14389	Mouse monoclonal	1:1000
Phospho-MLC (Thr18/Ser19)	Cell Signalling	#3674	Rabbit polyclonal	1:1000
Phospo-ERM (Ezrin-Thr567, Radixin Thr564, Moesin Thr558)	Cell Signalling	#3141	Rabbit polyclonal	1:1000
Ezrin	Cell Signalling	#3145	Rabbit polyclonal	1:1000
Moesin	Cell Signalling	#3146	Rabbit polyclonal	1:1000

2.6.4 Luciferase assays

Luciferase assays were performed with the dual luciferase assay kit (Promega) in conjunction with an Envision Multilabel plate reader (Perkin Elmer). 12-well plates containing cells for lysis were washed with cold PBS before 100 µl passive lysis buffer (Promega) was added and the cells incubated with shaking for 15 minutes and collected. 30 µl of lysate was added to a white 96-well plate (Matrix Technologies), then 100 µl of luciferase assay reagent II (Promega) was added and a luminescence reading taken to measure luciferase activity. Subsequenly 100 µl of Stop and Glo reagent (Promega) was added and another luminescence reading taken to measure Renillla activity.

2.7 In vivo techniques

2.7.1 Injection of melanoma cells

To generate tumours for skin-flap imaging or analysis of lymph-node metastasis, mice were injected sub-cutaneously on the flank with 1 x10^6 B16 F2 cells or 2 x10^6 5555 cells in 100 µl of sterile PBS.

For short-term metastasis assays a 50:50 mix of 1.5 x 10^6 red and green labelled B16 cells in 100 µl of sterile PBS were injected into the tail-vein of mice. For metastasis assays lasting 10 days, a total of 1x 10^6 cells were injected.

2.7.2 Tumour measurements

Tumour measurements were performed by technicians in the Biological Resources Unit. Tumour volumes were calculated from the equation
Volume = ½(Length x width^2)

2.7.3 Implantation of imaging windows

Imaging windows were generated the day before implantation. A 12 mm coverslip was glued to the titanium imaging frame using superglue (UHU) and allowed to dry before being sterilised in 70 % ethanol overnight. Mice were also shaved on a small area on the lower back the day before window implantation. On the day of window implantation, mice were injected sub-cutaneously with 5 mg/kg Rimadyl 1 hour before being anaesthetised with isofluorane. The skin around the area of surgery was sterilised with Hibiscrub (VetTech) and a small incision made in the skin, sufficient to fit the imaging window. Mersilk sutures (VetTech) were used around the incision using a purse-string method, the imaging window was fitted and the sutures pulled tightly around the window and tied off. B16 spheroids resuspended in 100% matrigel were injected underneath the window using a 19-gauge needle. The mouse was allowed to recover on a heat-pad and maintained in isolation for the duration of the imaging window experiment.

2.7.4 Drug administration

Sunitinib was dissolved in DMSO to give a stock concentration of 40 mg/ml. 25 µl of the stock, together with 100 µl of sterile PBS, giving a final dose of 40 mg/kg, was administed to mice by oral gavage with the help of technicians from the Biological Resources Unit.

2.7.5 Tumour fixation and immunohistochemical staining

Following imaging or alternative tumour analysis the tumours were fixed either by snap freezing in OCT embedding matrix (Fisher Scientific) or by immersion in 10 % NBF (Experimental Histopathology Lab) overnight. Frozen tumour sections were analysed by immunofluorescence (described later) and NBF fixed tumours were paraffin embedded and subject to immunohistochemistry by the internal Experimental Histopathology Lab.

Antibodies used for immunohistochemistry:

Target	**Source**	**Product number**
Notch1-ICD	Abcam	ab8925
Endomucin	Santa Cruz	sc-65495
EZH2	Cell Signalling	#5246
NG-2	Millipore	AB5320
α-SMA	Dako	M0851
F4/80	eBioscience	14-4801
CD3	Dako	a0452
Cleaved Caspase-3	Cell signalling	#9664

2.8 Microscopy

2.8.1 Immunofluorescence

Samples were fixed using 4 % paraformaldehyde, washed with PBS and permeabilised using 0.2 % Triton X100. Samples were subsequently blocked for 1

hour with PBS + 5 % BSA before incubation with primary antibody in PBS + 5 % BSA overnight at 4 ° C. Primary antibody was washed off in 3 washes of 5 minutes with PBS containing 0.05 % Tween-20. Fluorescent secondary antibodies (Molecular probes and Jackson) were diluted 1:500 in PBS + 5 % BSA and incubated with the samples overnight, then washed off using 3 washes of PBS containing 0.05 % Tween-20. Samples only requiring staining for F-actin and nuclei were fixed and permeabilised as above but then treated with phalloidin and DAPI both at 1:500 dilution. Otherwise, phalloidin and DAPI were added at 1:500 at the secondary antibody stage. If required, the samples were mounted on microscope slides using Mowiol. Immunofluorescence of frozen tissue samples and cells in culture were carried out the same way. Images were taken using confocal microscopy.

Antibodies used in immunofluorescence

Target	**Source**	**Product number**	**Antibody type**	**Dilution**
EZH2	Cell Signalling	#5246	Rabbit polyclonal	1:100
H3K27me3	Abcam	Ab6002	Mouse monoclonal	1:50
Phospho-MLC (Thr18/Ser19)	Cell Signalling	#3674	Rabbit polyclonal	1:100

F-actin was visualised using FITC, TRITC, or 633- phalloidin (SIGMA). Nuclei were visualised with DAPI (SIGMA).

2.8.2 Phase contrast timelapse microscopy

24 hours before imaging, glass-bottomed cell culture plates (MatTek) were incubated with 10 µg/ml Fibronectin (SIGMA) in PBS for 30 minutes before the cells were plated on top. Cells were incubated at 37 °C with 10 % CO_2 in DMEM media contain 10 % FCS and stimulated with 5 ng/ml HGF 2 hours before imaging. Imaging was carried out on a Nikon microscope with a motorised stage for multiple positions (controlled by Metamorph software) using 20 x phase1 and 10 x phase1 lenses.

2.8.3 Skin flap tumour imaging

Sub-cutaneous tumours (described previously) were imaged when they reached between 6-10 mm in diameter. The mice were anaesthetised using isofluorane carried on oxygen, and anaesthetic was maintained during imaging using a mouthpiece. Minor surgery was performed to expose the tumour and the mice were placed on a heated stage and covered with a heated blanket maintained at 37 °C. The tumour was laid on a cover slip and imaged from underneath. Imaging lasted up to 3 hours, during which time either z-stack images or timelapse movies were captured with a 20 x Plan Apochromat lens. Timelapse movies involved capturing a z-stack image every 1-2 minutes. After imaging, the mouse was sacrificed. If needed, the tumour material was dissected and fixed as described previously.

Imaging was carried out using both single photon and two-photon lasers. A two-photon femto-second-pulsed Ti-Sapphire laser (Coherent) was used to image pigment and Collagen fibres at 825 nm and occasionally GFP at 872 nm. Second harmonic signal from Collagen was collected at half the wavelength of excitation. Pigment signal was collected between 500 and 550 nm. Single-photon 458 nm, 488 nm, 543 nm, 561 nm and 633 nm lasers were used to image CFP, GFP, mRFP, mCherry and injectable probes with fluorescence at 680 nm.

Blood vessels remained intact during imaging and blood flow could be monitored by intravenous injection of 100 µl Angiosense 680 (Perkin Elmer) immediately prior to imaging. MMP activity could be monitored by intravenous injection of 100 µl MMPsense 680 (Perkin Elmer) 6-8 hours before imaging. Healthy blood vessels for comparison with tumour vessels were imaged in the skin on the opposite flank to the tumour.

2.8.4 Window imaging

Mice with imaging windows were imaged everyday starting at 4 days subsequent to window implantation. The mice were anesthetised using isofluorane carried on oxygen, and anaesthetic was maintained during imaging using a mouthpiece. The mice were placed on a heated stage and the imaging window placed in a hole in the stage. Windows were subsequently imaged from underneath. Every imaging session a tile z-stack image of the whole window area was taken using a 10 x Plan Apochromat lens. Subsequently the lens was switched to a 20 x Plan Apochromat lens and regions of interest imaged. Lasers and injectable probes used were as described previously.

2.8.5 Imaging of lungs for experimental metastasis assays

Lungs were removed 48 hours or 10 days after injection of melanoma cells, washed in PBS and placed on a coverslip. Lungs removed 48 hours after injection were imaged using a 10 x Plan Apochromat lens and images taken using a large pinhole size. Images were taken randomly over the two lungs using single photon 488 nm and 561 nm lasers and subsequently analysed for area of mCherry vs GFP cells. At the time of injection, 10 µl of the injection mix containing mCherry and GFP melanoma cells was plated onto a cell culture dish with a glass bottom (MatTek), the cells allowed to adhere and subsequently fixed. This was imaged using the same settings and hence provided a control for the ratio of mCherry and GFP cells injected. Lungs removed 10 days after injection were analysed using the microscope eye-piece and 10 x lens and the number of colonies of each colour counted manually.

2.8.6 Imaging of lymph-nodes for spontaneous metastasis assays

Inguinal and axillary lymph-nodes on the same side of the tumour were removed when the tumour reached 1-1.2 cm in diameter. Excess fat was trimmed away and the lymph-node placed on a coverslip and imaged from underneath using a 20 x lens. Presence of fluorescent tumour cells indicated lymph-node metastasis.

2.9 Image and data analysis

2.9.1 Quantification of signalling reporter activity

Quantification of signalling reporter activity was performed using LSM510 Image Examiner (Carl Zeiss) and Zen (Carl Zeiss). Cellular reporter intensity was measured by drawing around a cell to create a region of interest and noting the fluorescence intensity. The background fluorescence intensity was measured by generating a region of interest in an area not covered by cells. The average intensity for the whole image was measured by making a region of interest the same size as the entire image. Cellular fluorescence intensity was corrected for background levels and then normalised to the average GFP intensity for the whole image to give reporter activity.

2.9.2 Quantification of pigment intensity

Pigment intensity was analysed in two ways. Pictures of cell pellets were taken with a digital camera (Canon) after trypsinising the cells, washing in PBS and centrifugation to collect the cells. Pigment intensity was quantified on a cell to cell basis by plating the cells on glass-bottomed cell culture dishes (MatTek), fixing and staining for F-actin. The pigment was then imaged using a two-photon femto-second-pulsed Ti-Sapphire laser (Coherent) tuned to 870 nm with fluorescence detection between 500 and 550 nm. The pigment intensity was measured using Zen software (Carl Zeiss) by drawing around a cell to generate a region of interest and noting the fluorescence intensity. Background fluorescent levels were measured by creating a region of interest in an area lacking cells and noting the fluorescence. Cellular pigment intensity was calculated by subtraction of the background fluorescence. Microscope settings were kept the same between imaging of control and siRNA depleted cells in the same experiment.

2.9.3 Quantification of EZH2 and Histone H3 lysine-27 tri-methyl (H3K27me3) staining intensity

Quantification of EZH2 and H3K27me3 staining was performed using Volocity image analysis software (Perkin Elmer) and Prism (GraphPad). Images stained for EZH2, H3K27me3, and nuclei were acquired on a confocal microscope. Nuclei were identified using automatic nuclei detection in Volocity and used to form objects. To calculate relative EZH2 intensity, the nuclear EZH2 intensity was normalised to DAPI intensity. The average H3K27me3 nuclear intensity was compared between conditions.

2.9.4 Quantification of immunohistochemical staining

Quantification of vessel density, morphology and Caspase 3 staining was performed with Volocity image analysis software (Perkin Elmer). RGB images were taken for analysis using a Nikon Eclipse light microscope. For the vessel analysis, endomucin positive objects were identified using intensity in the red channel and any holes in the objects filled in. The area of the objects was noted and for vessel density, total vessel area for an image was divided by the total area of the image. For vessel lumen area, the area of each object was noted and compared between tumour conditions. Analysis of cleaved Caspase-3 was similar, cleaved Caspase-3 positive objects were identified using intensity in the red channel. To measure apoptosis in the tumour centre versus tumour margin, a region of interest was generated to cover roughly the outer 200 μm of tumour. The total area of cleaved Caspase-3 positive objects was calculated in the region of interest and the remaining area (to give Caspase 3 activity in the centre of the tumour) for DMSO and Sunitinib treated tumours.

2.9.5 Cell area analysis

Measures of the cell area were obtained both manually and using Volocity (Perkin Elmer) image analysis software. Analysis of the cell area on P protein depletion was performed by manually drawing around the cell to create a region of interest in

Zen imaging software (Carl Zeiss) and the area noted. Volocity was used for the other analyses. Images of cells were thresholded based on F-actin staining, for analysis after siRNA depletion of PRC2 components, or GFP intensity, after siRNA depletion and rescue with Ezrin-GFP DNA constructs. Thresholding created objects and any holes in the objects were filled in to give the area covered by cells in the image. Nuclei were detected using DAPI staining and automatic nuclei detection. The area covered by cells was subsequently divided by the number of nuclei to give the average cell area. A minimum of 5 images were analysed per condition in each experiment.

2.9.6 Quantitative morphometric vessel analysis

Quantification of vessel morphology and dynamics was performed in LSM510 Image Examiner (Carl Zeiss) and Zen (Carl Zeiss). For characterisation of different tumour areas, representative vessels from each area were quantified. For correlation purposes morphological characteristics were determined per z-stack of images. Tortuosity indices, variation in width and branch point measurements, were calculated as averages of representative vessels in the z-stack. Tortuosity index was calculated as a ratio of the arc length and chord length for a vessel bend. Variation in vessel width was determined by measuring vessel width every 10 μm for a 150 μm stretch of vessel and calculating the coefficient of variance. Branch points were calculated by measuring vessel length and counting branch points in that length. Blunt ends were determined by counting the number of blunt ends per image plane, and dividing by the area of vessels in an image plane. Multiple planes were averaged over the z-stack. The vessel area was measured for a whole image plane by thresholding on the GFP intensity and noting the area of the thresholded region. Correlation of cell motility with vessel area was performed by counting the number of motile cells in the field of view averaged over the z-stack and measuring the vessel area also averaged over the z-stack.

2.9.7 Cell tracking in vitro

Tracking of B16 F10 cells plated on Fibronectin was carried out using data from phase contrast time-lapse movies captured using MetaMorph software (Molecular Devices). Timelapse movies underwent automatic cell tracking, again using MetaMorph software (Molecular Devices). Briefly, in the first frame the cells were selected with the mouse and an area around the cell identified. Through each frame the software determined the new position of each cell. If the software failed to identify the cell in the next frame, for example when a cell underwent division, or if the cell moved out of the frame, the user paused the analysis and instructed the program to the accurate position of the cell, or to terminate the track. The tracking data was stored as a log file and was inputted in to a template in Mathematica (Wolfram research) designed by the Light Microscopy Facility to calculate cell speed.

2.9.8 Motile cell analysis in vivo

The number of motile cells was calculated manually using LSM510 Image Examiner software (Carl Zeiss). Cells were classified as non-motile, moving singly, collectively or streaming and the number of cells in each category counted per field of view in a 20 minute timelapse movie. For correlation of signalling reporter activity and motility, cells were classified as non-motile, moving singly or streaming and the signalling reporter activity calculated as described previously.

2.9.9 Analysis of experimental lung metastasis assays

Lung images were analysed using Volocity (Perkin Elmer) image analysis software to measure the area of mCherry and GFP cells in the lung. Images were thresholded on either GFP or mCherry to generate objects and the area of thresholded objects measured in each image. A minimum of 7 images were analysed from each mouse and the total area of mCherry or GFP objects calculated per mouse. The ratio of mCherry and GFP areas was obtained. This was also performed for images of the injection mix plated on cell culture dishes.

The mCherry:GFP ratio from the lungs was normalised to the ratio from the plated injection mix. The relative colonisation ability of control to siRNA treated cells was finally normalised to the relative colonisation ability of control to control cells to account for differences in detection of mCherry and GFP cells.

2.9.10 Microarray analysis

Microarray analysis was carried out in collaboration with the Paterson institute using Affymetrix chips (MOE430 2.0) and The Genome Centre at Barts using Illumina chips (REF6V3). Both chips included probes of the whole mouse genome. Microarray results were analysed by Phil East in the Bioinformatics department. The ranges of values for each chip were normalised to each other and then points with very low intensity were excluded from the analysis. The fold change between conditions was then calculated and averaged for the replicates.

2.9.11 Geneset enrichment analysis (GSEA)

Geneset enrichment analysis was performed using free software from The Broad Institute (http://www.broadinstitute.org/gsea/index.jsp). Microarray data was adjusted to contain only the gene symbols, a description column and numerical expression values and saved in .txt format. A phenotype file was created to describe the columns in the expression data file and the layout of the experiment i.e number of repeats. Genesets were obtained from the MSigDB (The Molecular Signatures Database), curated by The Broad Institute and also generated from personal microarray analysis and publicly available microarray data. Briefly, the free software ranks the genes in the microarray data file according to expression changes between conditions. It subsequently tests how a list of genes (geneset) is distributed within the ranked data and calculates an enrichment score that represents the degree to which the geneset is represented at the top or bottom of the ranked list. The score is calculated by walking down the ranked list and measuring a running-sum statistic. The score is increased on encountering a gene within the geneset and decreased on encountering genes not in the geneset. The enrichment score is then the maximum deviation score achieved. An estimate of

statistical significance is obtained and if multiple genesets are used an adjustment for multiple hypothesis testing is applied. The data is displayed graphically by showing the running sum on the y-axis and the ranked list on the x-axis and black bars indicate the presence of genes in the geneset.

2.9.12 Overlap analysis

Free software available on the MSigDB website (Broad Institute) was used to calculate the degree of overlap between a list of genes generated from personal microarray analysis and the genesets in the MSigDB. The number of overlapping genes was compared to the number of expected overlaps based on the size of the geneset and an estimate of statistical significance derived.

The degree of overlap between two lists of genes both generated from personal microarray analysis was calculated in conjunction with Phil East in the Bioinformatics department. The analysis carried out was similar to that of the free software. The number of overlapping genes was compared to the number of expected overlaps based on the number of genes in the lists and the chip used in the microarrays. An estimate of statistical significance was also derived.

2.9.13 Cluster analysis

Hierarchical clustering was performed in conjunction with Robert Jenkins using the free software R (http://www.r-project.org). Z-stack images of tumour-associated vasculature were analysed to quantifiy the morphometric parameters as outlined previously. Hierarchical clustering was carried out by attempting to minimise the Euclidean distance between groups using Ward's linkage, whereby groups are clustered such that the total variance within the cluster is minimised at each step.

2.9.14 Statistical analysis

Most of the statistical testing including t-tests and analysis of variance (ANOVA) testing was performed using Prism software (GraphPad). Correlations between

melanoma cell motility values and vascular morphometric and dynamic data using Spearman's rank correlation co-efficient and linear regression were performed in conjunction with Robert Jenkins using R (http://www.r-project.org.

Chapter 3. Heterogeneous cell behaviour correlates with differences in Notch, TGF- β and SRF signalling

3.1 Chapter introduction

Previous intra-vital imaging studies of motility and invasion have revealed heterogeneous cancer cell behaviour in a number of different systems (Giampieri et al., 2009), (Pinner et al., 2009). The majority of cancer cells in a tumour are non-motile. However, there is a small population of motile cells that can move either as single cells, or using more cohesive modes of motility. The acquisition of motility is also likely to be reversible as even in lymph node metastases most cells are non-motile (Giampieri et al., 2009).

There could be many reasons for heterogeneous cell motility. Motile cells may have acquired additional mutations driving an invasive state or signals from the local environment may cause cells to become motile only in certain areas. Alternatively, differentiation state of the cell may influence whether or not the cell is motile. However, the above are most likely over simplified and it may be a combination of reasons, together with a permissive microenvironment, that enables motility.

Previous work in the B16 melanoma model suggests that the motile cells are less differentiated. Motile cells had lower pigment levels and higher Brn2 promoter activity, a transcription factor down-regulated during melanocyte differentiation (Pinner et al., 2009). *Tgfb2* mRNA was up-regulated in the less pigmented cells and TGF-β2 increased motility in vitro. However, little is known about which pathways are important in maintaining or driving these changes in differentiation in vivo.

Therefore a number of signalling pathways were investigated in vivo to try and determine whether differences in signalling correlated with differences in motility and which pathways may be involved in the acquisition of motility and a less differentiated state.

3.2 B16 F2 melanoma cells exhibit heterogeneous cell behaviour in vivo

To confirm that B16 F2 melanoma cells display heterogeneous motile behaviour in vivo, intra-vital imaging was performed on sub-cutaneous B16 F2 tumours. B16 F2 cells had stable expression of a red fluorescent membrane marker to enable visualisation. Z-stack images were taken every 1-2 minutes for 20 minutes and analysed for motile melanoma behaviour. This revealed that, similar to previous reports, melanoma cells utilised different modes of motility (Figure 3.1 and Supplementary movies 1-3). Cells were seen moving as single cells with a rounded amoeboid morphology (Figure 3.1). Cells utilising this mode of motility were seen interacting with Collagen fibres and changing morphology to squeeze through gaps in the ECM. Cells were also seen moving collectively, either as groups, that on a macro scale maintained cell-cell contacts, or in streams (Figure 3.1). Streaming cells were chains of cells moving in a similar direction but they did not always maintain connections with the adjacent cells. Unlabelled host cells, often termed ghost cells, were seen within the chains. These may correspond to the macrophage population that promote cancer cell motility through a paracrine feedback loop (Wyckoff et al., 2004).

Quantification of multiple movies revealed that less than 10 % of B16 F2 melanoma cells in the primary tumour are motile (Figure 3.2A). Out of the motile population 56 % of cells used a rounded single cell mode of motility, 30 % were found in streams and the rest moved collectively as groups.

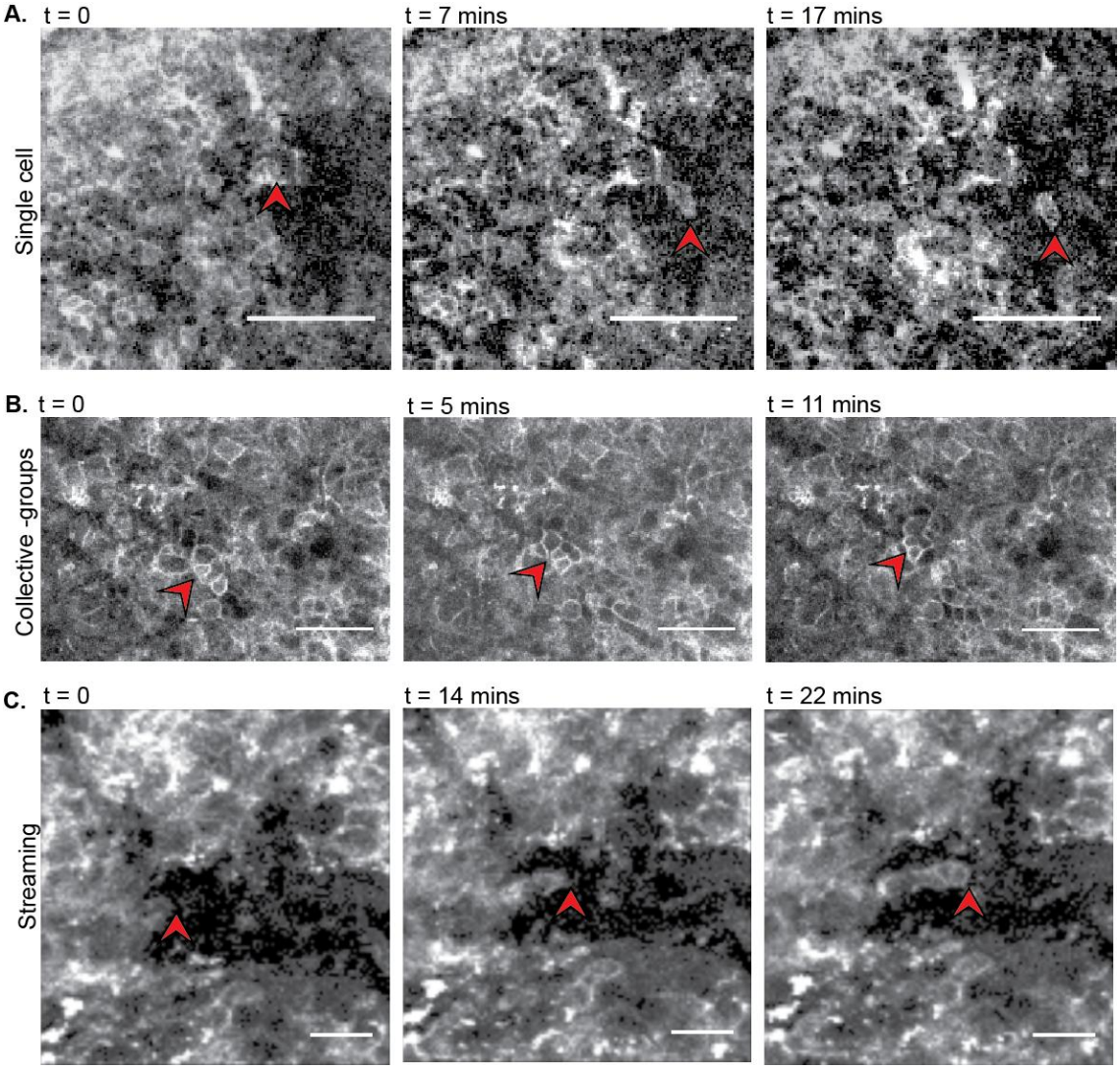

Figure 3.1 Examples of modes of motility used by B16 F2 melanoma cells in vivo.

Stills taken from intra-vital movies of B16 F2 melanoma showing A. Single cell motility. Scale bar 50 µm. B. Collective motility in groups. Scale bar 50 µm. and C. Streaming cells. Scale bar 100 µm. Cell membranes shown in white.

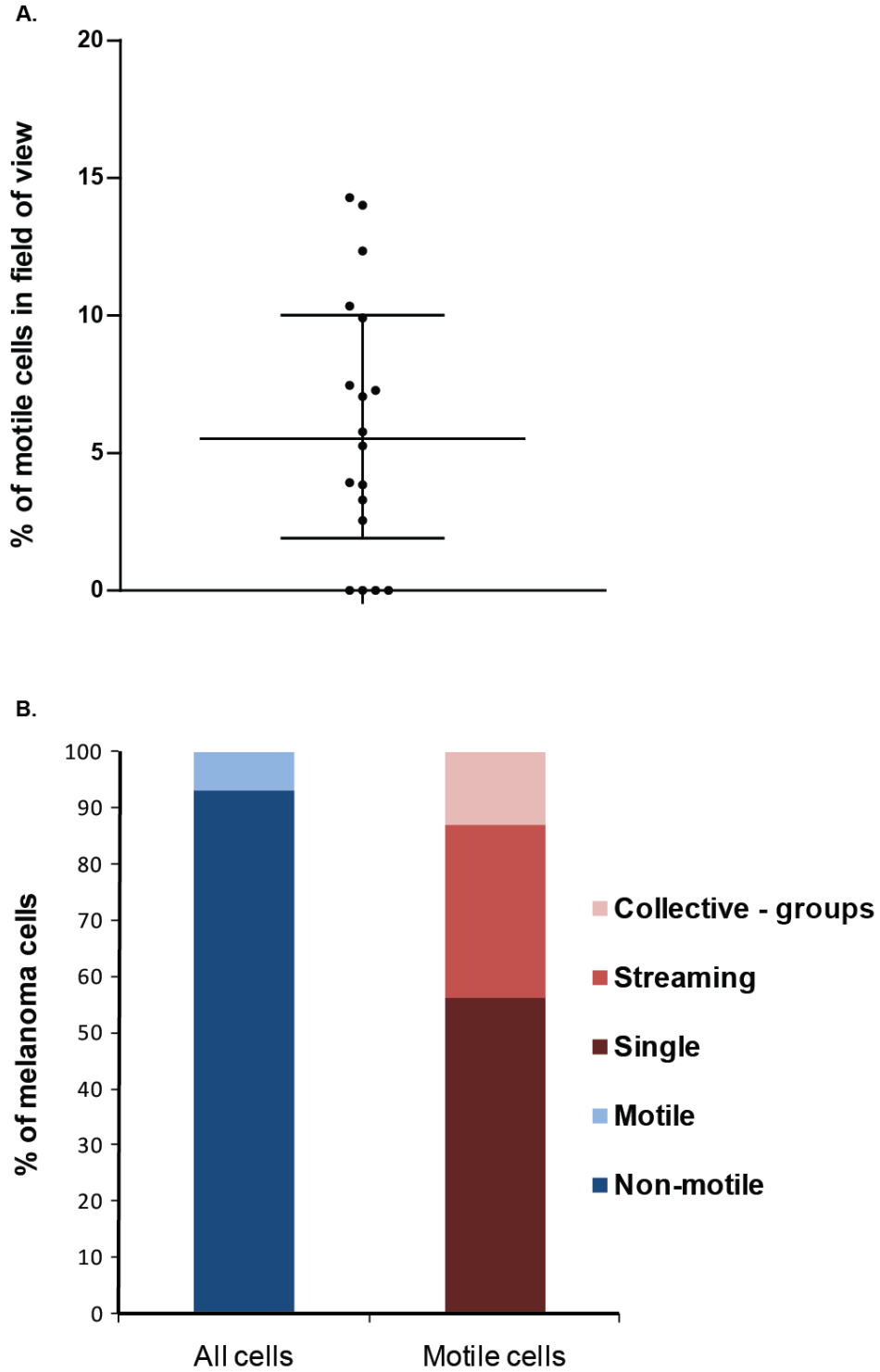

Figure 3.2 Quantification of B16 F2 melanoma cell motile behaviour in vivo.

A. Graph showing percentage of motile cells in each movie. Each point represents a single movie. Bar indicates median with interquartile range. B. Analysis of different modes of motility. Time-lapse movies of B16 F2 melanomas were analysed and the number of non-motile and motile melanoma cells counted. Motile cells were further classified in to using collective, streaming or single cell modes of motility. Data from 18 movies of 9 mice.

3.3 Clonal reporter cell-lines reveal heterogeneous signalling in B16 F2 melanoma in vivo

Differences in cell behaviour imply differences in the signalling status of the cells. To test the hypothesis that differences in cell behaviour correlated with differences in signalling, a number of clonal B16 F2 reporter cell-lines were generated. The Notch, TGF-β and SRF pathways were chosen for investigation due to the reasons outlined below. Transcription-based fluorescent protein reporter constructs were used to enable the visualisation of signalling status, as active signalling would drive fluorescent protein expression. However, as the half-life of the fluorescent proteins used is around 24 hours, the presence of fluorescent protein would indicate that the cell had received the signal within the last 24 hours or so and does not necessarily denote current active signalling. The reporter constructs were co-transfected with a hygromycin selection vector into B16 F2 cells with a red fluorescent membrane marker so all cells could be visualised by the membrane marker in vivo. Stable cell-lines were generated by selection in 500 µg/ml hygromycin. The stable cell-lines were then single-cell cloned and the clones tested for reporter sensitivity. Clones were generated to circumvent heterogeneity in signalling arising as a consequence of differences in mutational status.

3.3.1 Notch signalling is heterogeneous in B16 F2 melanoma in vivo

Notch signalling was chosen because it has been found to promote EMT and motility in numerous cancer types (Leong et al., 2007) (Sahlgren et al., 2008). Also, it is required for maintenance of the melanocyte stem cell population and is sufficient to confer neural crest stem cell-like properties on melanocytes (Moriyama et al., 2006) (Zabierowski et al., 2011). As motile B16 melanoma cells are thought to be less differentiated, the hypothesis was that Notch signalling may drive or maintain melanoma cells in a less differentiated state thereby promoting motility.

The Notch reporter construct consisted of 4 CBF responsive elements (CBFREs) and the minimal simian virus promoter upstream of eGFP (Figure 3.3A). CBFREs have been shown to bind the transcriptional repressor CBF-1 (Hsieh et al., 1996).

Binding of the intra-cellular domain of Notch to CBF-1 releases the repression and activates transcription downstream of the CBF-1 binding sites. Therefore activation of Notch signalling and cleavage of the receptor to generate the intra-cellular domain should promote transcription and translation of eGFP, allowing visualisation of cells with active Notch signalling.

The Notch reporter construct was tested in a transient transfection assay to confirm the response to NICD. The reporter construct was co-transfected with either a constitutive mCherry (Shaner et al., 2004) plasmid alone or in conjunction with NICD or the empty vector (E.V). The ratio of cells expressing GFP, driven by the CBFRE promoter, to mCherry positive cells was then calculated to give a measure of CBFRE response. The percentage of responsive cells was significantly higher in NICD transfected wells compared to both the empty vector and mCherry alone (Figure 3.3B), confirming the construct was a Notch reporter. A mutant construct containing mutant CBFREs was also tested. Both the empty vector and NICD increased the percentage of responsive cells compared to mCherry alone suggesting a non-specific response of the mutant reporter (Figure 3.3B).

After stable selection of the B16 reporter cells and single cell cloning, one clone was found to be responsive to Notch signalling. To test the clone's response to Notch signalling, NICD or the empty vector was co-transfected with a constitutive mCherry plasmid in a ratio of 2:1. The cells were then subjected to flow-cytometry analysis. Gates were set to analyse only the mCherry positive cells as these should have been transfected with either the empty vector or NICD due to the ratio of the plasmids transfected. Transfection of the clonal reporter cell-line with NICD caused a shift towards increased GFP intensity compared to transfection of the empty vector (Figure 3.3C). This confirms that the clonal reporter cell-line is responsive to Notch signalling.

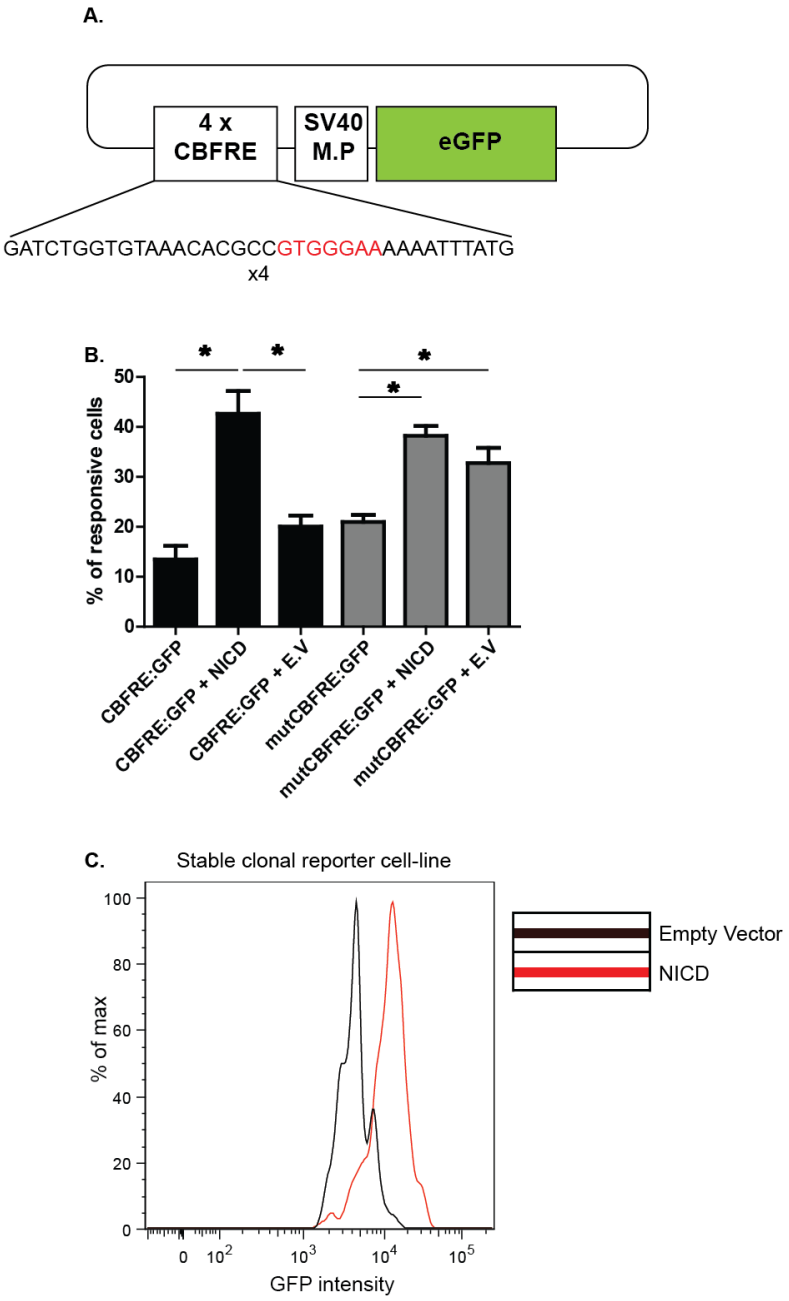

Figure 3.3 Generation and testing of a clonal Notch reporter cell-line.

A. Schematic of the Notch reporter construct and CBF responsive element. CBF-1 binding site shown in red. SV40 M.P denotes the simian virus 40 minimal promoter. B. Graph showing percentage of responsive cells in a transient transfection assay to test the Notch reporter (CBFRE:GFP). CBFRE:GFP or mutant CBFRE:GFP were co-transfected with mCherry and either NICD or the empty vector (E.V) in a ratio of 2:1. The ratio of GFP positive responsive cells to mCherry positive cells was calculated and converted to a percentage. Error bars show standard error. Stars indicate a p-value <0.05 in an ANOVA test. C. The clonal Notch reporter cell-line was transiently transfected with constitutive mCherry and NICD or empty vector and then subjected to FACS analysis gating only on the mCherry positive cells.

Flow-cytometry analysis of the Notch reporter clone grown in vitro revealed a broad distribution of GFP intensities spanning two orders of magnitude (Figure 3.4), implying that Notch signalling in B16 F2 cells is heterogeneous in vitro. To test whether endogenous Notch targets correlated with GFP expression of the reporter, Notch reporter high and Notch reporter low populations were purified by FACS and sorted directly into RLT lysis buffer (Qiagen RNAeasy minikit). Subsequent Q RT-PCR for *Hes-1* mRNA levels revealed that *Hes-1* transcript levels were higher in the Notch reporter high population than the reporter low population. This confirmed that GFP expression correlated with expression of endogenous Notch targets and helped validate the reporter cell-line.

Further validation of the clonal Notch reporter cell-line came following microarray analysis of the Notch reporter GFP high and Notch reporter GFP low populations and identification of Notch targets in B16 F2 melanoma cells (discussed further in chapters 4 and 5). Geneset enrichment analysis (Subramanian et al., 2005) (Mootha et al., 2003) using freeware from The Broad Institute (http://www.broadinstitute.org/gsea/index.jsp) indicated that the Notch reporter GFP high population was significantly enriched for Notch target genes (Figure 3.5). This provides more support for the reporter cell-line, as expression of endogenous Notch targets, identified in B16 melanoma cells, correlated with the GFP expression of the Notch reporter cell-line.

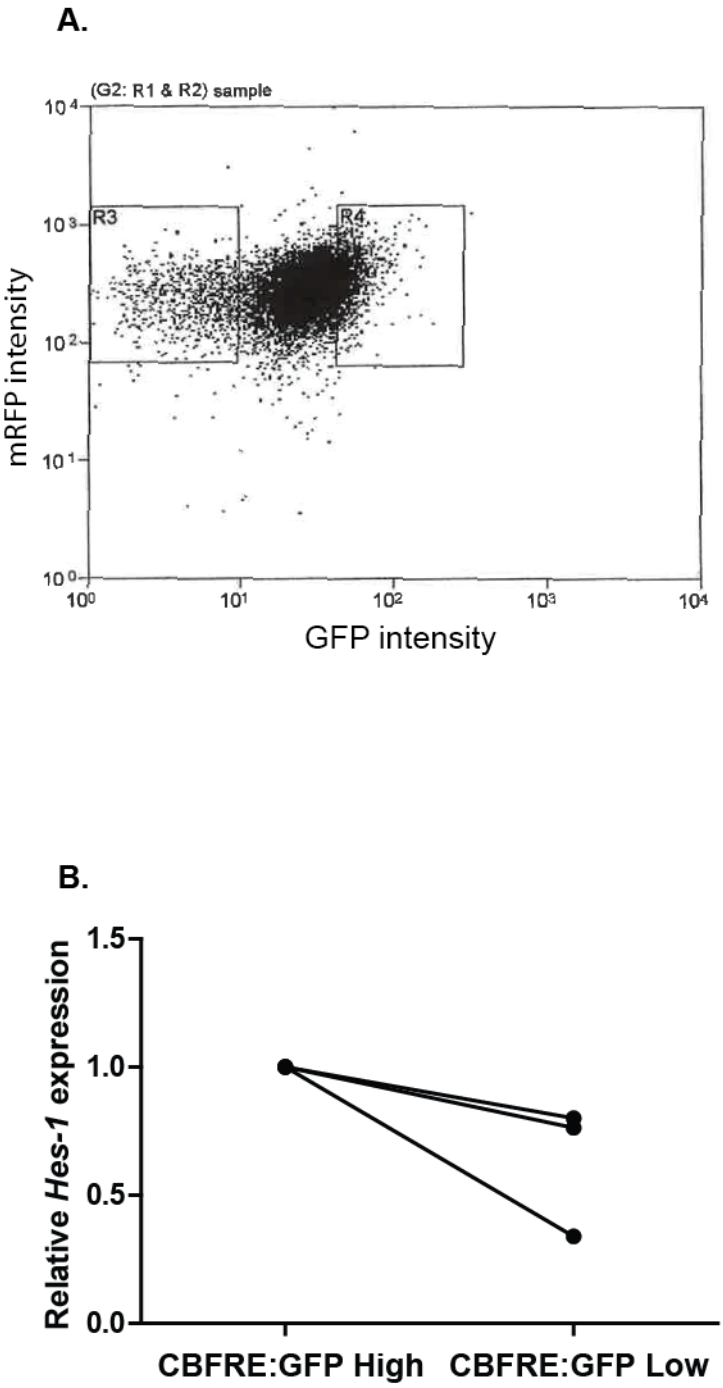

Figure 3.4 Notch signalling is heterogeneous in vitro.

A. FACS plot of the clonal Notch reporter cell-line indicating heterogeneity in Notch signalling in vitro. R3 and R4 represent the gates used to sort the Notch low and Notch high populations respectively. B. Q RT-PCR of *Hes-1* mRNA levels in the Notch high and Notch low populations in vitro. Graph shows 3 independent pairs.

Array data: Notch reporter

Geneset: Genes upregulated on average >1.2x in B16 F2 NICD-GFP cells compared to control B16 F2 cells.

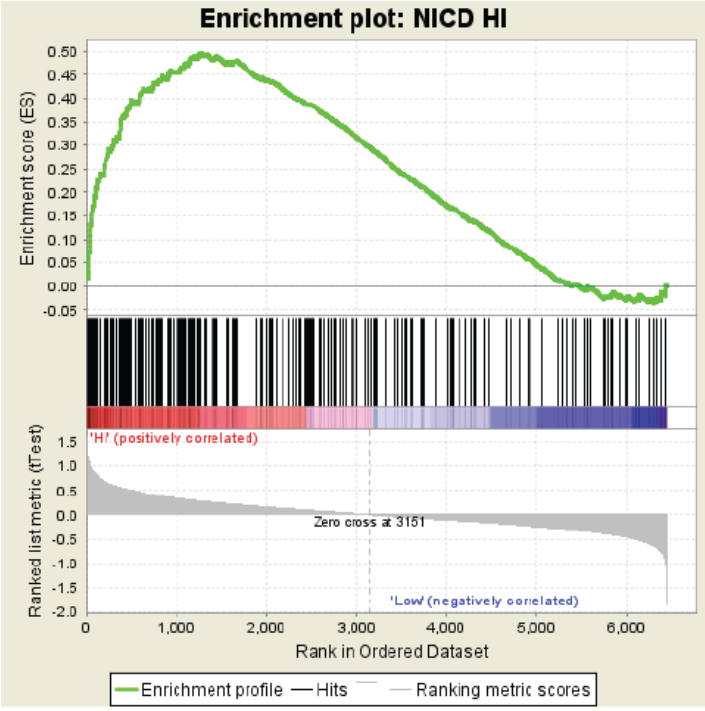

Enrichment of Notch targets in Notch reporter high population p-value = 0.

Figure 3.5. Notch target gene expression is enriched in the Notch reporter GFP high population.

Geneset enrichment analysis using free-ware from The Broad Institute. Genes up-regulated on average greater than 1.2 fold in B16 F2 NICD-GFP cells compared to B16 F2 control cells are significantly enriched in the Notch reporter GFP high population.

As less than 10 % of cells in vivo are motile, if Notch signalling promotes a motile state then activity through the Notch pathway should also be heterogeneous in vivo and correlate with motility. To investigate this, the clonal Notch reporter cell-line was injected sub-cutaneously into C57Bl6 mice. Intra-vital imaging of the Notch reporter tumours revealed a small population of GFP positive cells (Figure 3.6A) indicating that indeed Notch signalling was heterogeneous in vivo. This small percentage was in contrast to the in vitro data in which around 80 % of cells were GFP positive (Figure 3.4). However, this may have been as a result of the region of the tumours imaged because intra-vital imaging can only provide an idea of the outer 200 μm of the tumour. Collagenase-dispase digestion of the tumours and subsequent FACS analysis of the Notch reporter tumours allowed the whole tumour to be analysed. This confirmed that throughout the tumour only a small percentage of cells were GFP positive and had active Notch signalling (Figure 3.6B).

Immunohistochemical staining of B16 F2 tumours with an antibody against the intracellular domain of Notch1 provided further evidence of heterogeneous Notch signalling in vivo. It revealed cell populations with different staining patterns suggesting heterogeneous signalling activity (Figure 3.6C). Most cells had nuclear or sub-nuclear staining, but some cells had no staining or staining in both the nucleus and cytoplasm (Figure 3.6C). The frequency of cells stained in both the nucleus and cytoplasm was roughly similar to the frequency of GFP positive cells in the Notch reporter cell-line. The cells with staining in both the nucleus and cytoplasm may have higher levels of signalling compared to the cells with only nuclear staining. Perhaps the Notch reporter cell-line is only responsive to very high levels of Notch signalling.

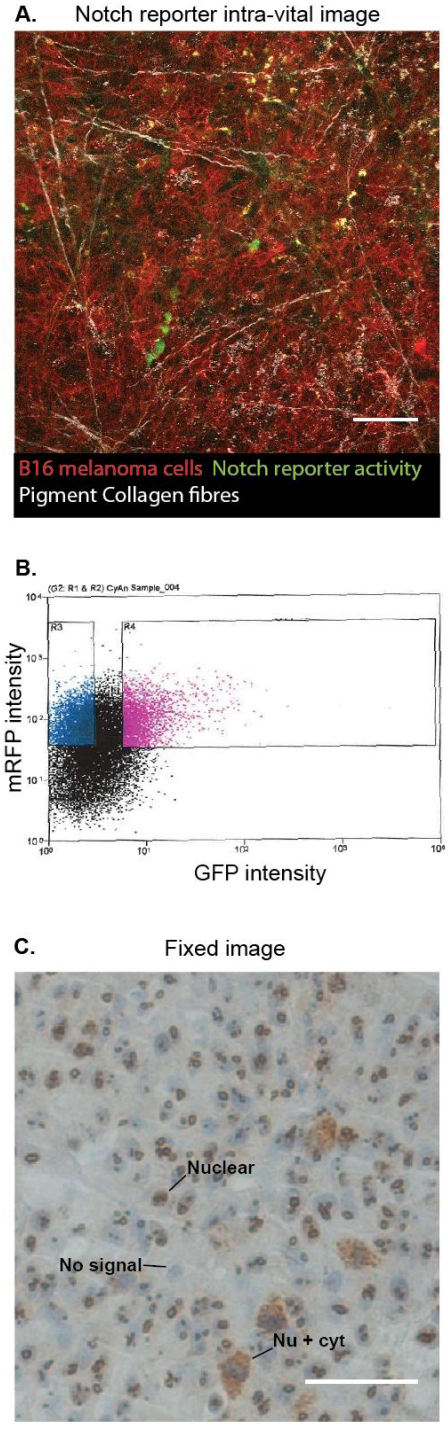

Figure 3.6 Notch signalling is heterogeneous in vivo.

A. Intra-vital still image of the clonal Notch reporter cell-line. B16 melanoma cells have a red membrane marker. Active Notch signalling is represented by GFP expression. Pigment and Collagen fibres in white. Scale bar indicates 100 μm. B. Flow-cytometry analysis of tumours derived from the clonal Notch reporter cell-line. Gates indicate Notch high and Notch low populations. C. Immunohistochemical staining of B16 tumour with anti NICD antibody. Labels show representative cells with different staining patterns. Scale bar indicates 50 μm.

3.3.1.1 Notch signalling is increased in the B16 F2 singly motile cell population

To try to determine whether Notch signalling correlated with motility, B16 Notch reporter tumours were subjected to intra-vital imaging (Supplementary movie 4). If the hypothesis was correct then the motile cells should be GFP positive or have increased GFP expression compared to the non-motile cells. The GFP intensity was measured in non-motile cells and cells using single cell and more collective modes of motility. As it is difficult to distinguish between streaming cells and cells moving collectively and the number of cells moving collectively in groups is very low, cells displaying cohesive modes of motility were labelled “streaming”. Cellular GFP intensity was corrected for background levels and then normalised to the average GFP intensity for the whole image. This allowed comparison across different tumours and tumour areas. Cells using the rounded single cell mode of motility had higher levels of GFP expression compared to non-motile or streaming cells indicating increased Notch signalling in singly motile cells (Figure 3.7A). Hence Notch signalling correlates with single cell motility in primary B16 melanoma. This provides support for the hypothesis that Notch promotes motility by maintaining cells in a less differentiated state. However, a small number of non-motile cells had active Notch signalling suggesting that Notch is not sufficient to initiate motility (Figure 3.7A).

To test the relationship between Notch and differentiation, pigment levels were used as a surrogate indicator of differentiation status. This is because pigment production in the melanocyte lineage is suggestive of differentiated cells. The GFP intensity, giving a measure of Notch activity, and pigment intensity of cells in vivo was measured. Notch reporter activity had a mutually exclusive relationship with pigment intensity (Figure 3.7). Cells with high Notch reporter activity had low pigment and cells with high pigment had low Notch reporter activity. The increase in Notch signalling in singly motile cells and the mutual exclusive relationship of Notch reporter activity and pigment agrees with the hypothesis that Notch signalling is associated with a less differentiated, more motile state. However, pigment levels are not the same as differentiation state and a more thorough analysis of differentiation markers is required (see next chapter).

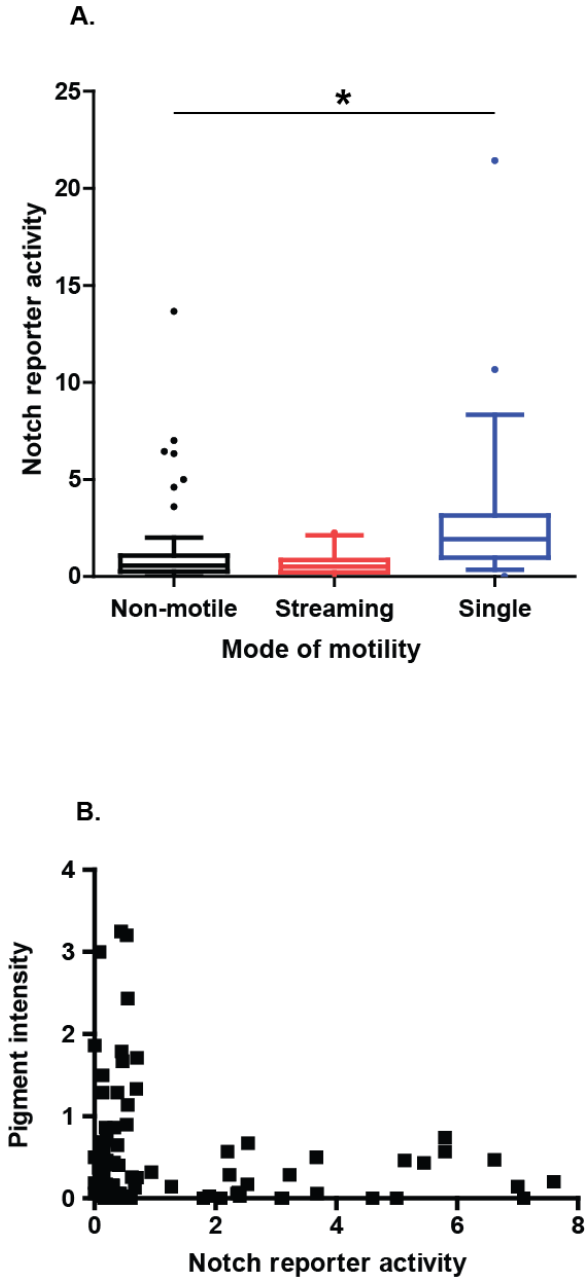

Figure 3.7 Notch signalling is increased in singly motile cells.

A. Box and whiskers plot showing GFP intensity and hence Notch reporter activity in non-motile, singly motile or streaming cells. Box indicates median and inter-quartile range. Whiskers indicate 10^{th}-90^{th} percentile. Outliers indicated by single points. 80 non-motile cells, 25 singly motile cells and 15 streaming cells analysed. Data from 9 movies of 4 mice. Background GFP intensity subtracted from cellular GFP intensity before normalising to the average GFP intensity for the image. B. Graph of pigment intensity vs GFP intensity and hence Notch reporter activity. Pigment and GFP intensities measured in the same cell. First background intensity was subtracted and then the values normalised to the average signal for the channel in the whole image.

3.3.2 TGF-β signalling is heterogeneous in B16 F2 melanoma in vivo

TGF-β signalling is interesting because it has been found to promote single cell motility in breast cancer (Giampieri et al., 2009) and it has a well-characterised role in EMT both in development and cancer (Nieto, 2011). *Tgfb2* mRNA levels were found to be up-regulated in the less pigmented B16 cell population in vivo and TGF- β2 could decrease pigment and increase motility in vitro (Pinner et al., 2009). As the motile cells in vivo are less pigmented, TGF- β may both promote motility and decrease pigment explaining why the motile cells are less pigmented.

To test whether TGF-β signalling is associated with motility, two clonal TGF-β reporter cell-lines were generated. The reporter constructs used were based on the well characterised $CAGA_{12}$ luciferase reporter which has 12 Smad binding sites upstream of a minimal promoter and luciferase. This reporter had been used previously in the lab to generate a fluorescence-based TGF-β reporter, with the 12 Smad binding sites and minimal promoter upstream of CFP (Figure 3.8A). However, during cloning, a 46 base-pair linker sequence was introduced (black bar in Figure 3.8A). Use of this reporter in zebrafish indicated that the linker sequence alone, without the Smad binding sites, may promote some CFP expression (Caroline Hill, personal communication). For comparison I generated a second CFP TGF-β reporter without the linker sequence (Figure 3.9A).

The two reporters were selected for stable expression in the B16 F2 melanoma cell-line with a red membrane marker. Single cell-cloning generated clonal TGF-β reporter cell-lines that were subsequently tested for response to TGF-β by flow cytometry. The clonal reporter cell-lines were treated overnight with either 1 ng/ml TGF-β, 10μM SB431542 the TGF-β receptor inhibitor, or vehicle control DMSO. Both reporter cell-lines had increased CFP expression in the TGF-β treated wells compared to the DMSO control (Figure 3.8B (+linker) and Figure 3.9B (no linker)) confirming that they did behave as TGF-β reporters. However, the reporter cell-line generated from the construct with the linker contained a fraction of cells that did not respond to TGF-β (Figure 3.8B). Therefore this reporter cell-line may slightly underestimate the extent of TGF-β signalling. This cell-line also showed a slightly larger increase in CFP expression, suggesting that the linker may increase the

sensitivity to TGF-β. There was little difference in CFP expression between the DMSO vehicle control and SB treated wells for either reporter cell-line (Figure 3.8B (+linker) and Figure 3.9B (no linker)). This implies that there is little basal TGF-β signalling in B16 F2 cells grown in vitro.

To investigate patterns of TGF-β signalling in B16 melanoma in vivo and to test whether it correlated with single cell motility, the two clonal TGF-β reporter cell-lines were injected sub-cutaneously into C57Bl6 mice and the resulting tumours subjected to intra-vital imaging. This revealed heterogeneous CFP expression in both reporter cell-lines (Figure 3.10 A and B) implying B16 F2 melanoma cells have heterogeneous TGF-β signalling in vivo. Both reporter cell-lines had a similar percentage of CFP positive cells suggesting that the linker did not adversely affect reporter response or promote non-specific CFP expression. The reporter cell-line generated from the construct without the linker required more laser power to visualise the CFP, suggesting that the linker may increase the sensitivity of the reporter.

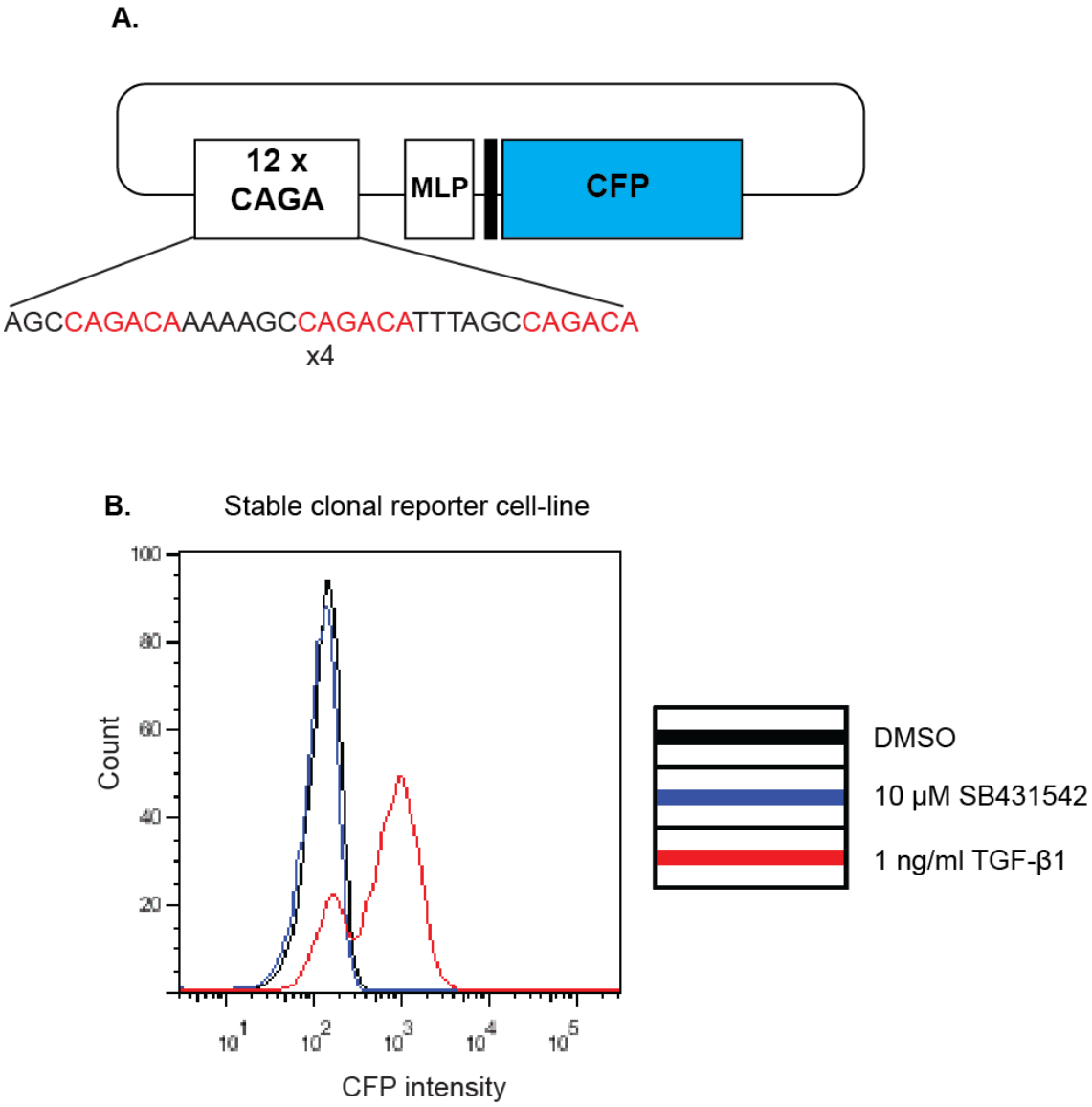

Figure 3.8 Generation of clonal TGF-β reporter cell-line from construct containing linker sequence.

A. Schematic showing TGF-β reporter construct used. Red indicates Smad binding sequences. MLP indicates minimal promoter and black bar indicates the 46 base-pair linker sequence introduced previously. B. FACS analysis of the clonal TGF-β reporter cell-line treated overnight with 1 ng/ml TGF-β, 10 µM SB431542, the TGF-β receptor inhibitor, or DMSO vehicle control.

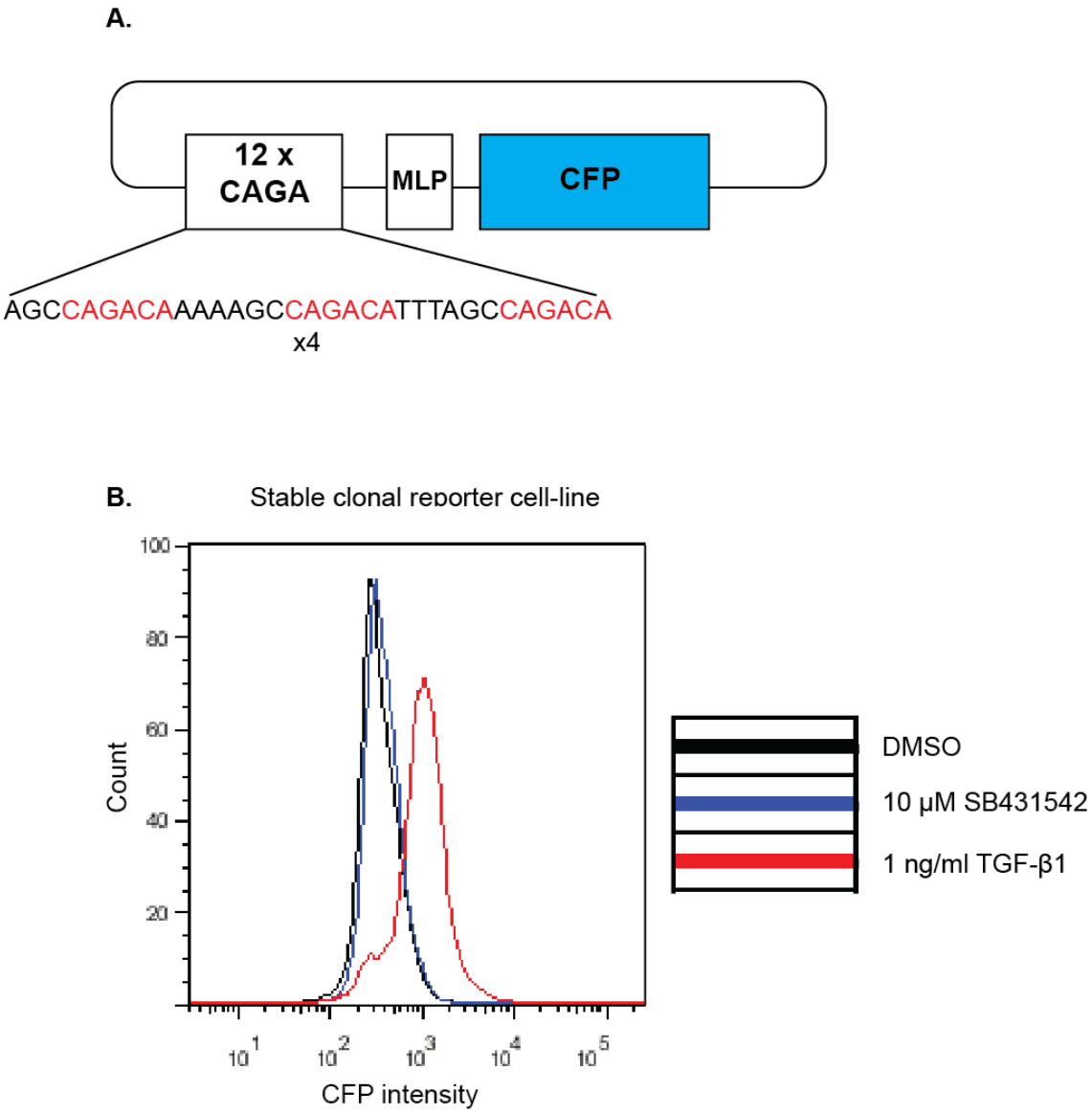

Figure 3.9 Generation of clonal TGF-β reporter cell-line from construct without linker sequence.

A. Schematic showing TGF-β reporter construct used. Red indicates Smad binding sequences. MLP indicates minimal promoter. No linker sequence present. B. FACS analysis of the clonal TGF-β reporter cell-line treated overnight with 1 ng/ml TGF-β, 10 µM SB431542, the TGF-β receptor inhibitor, or DMSO vehicle control.

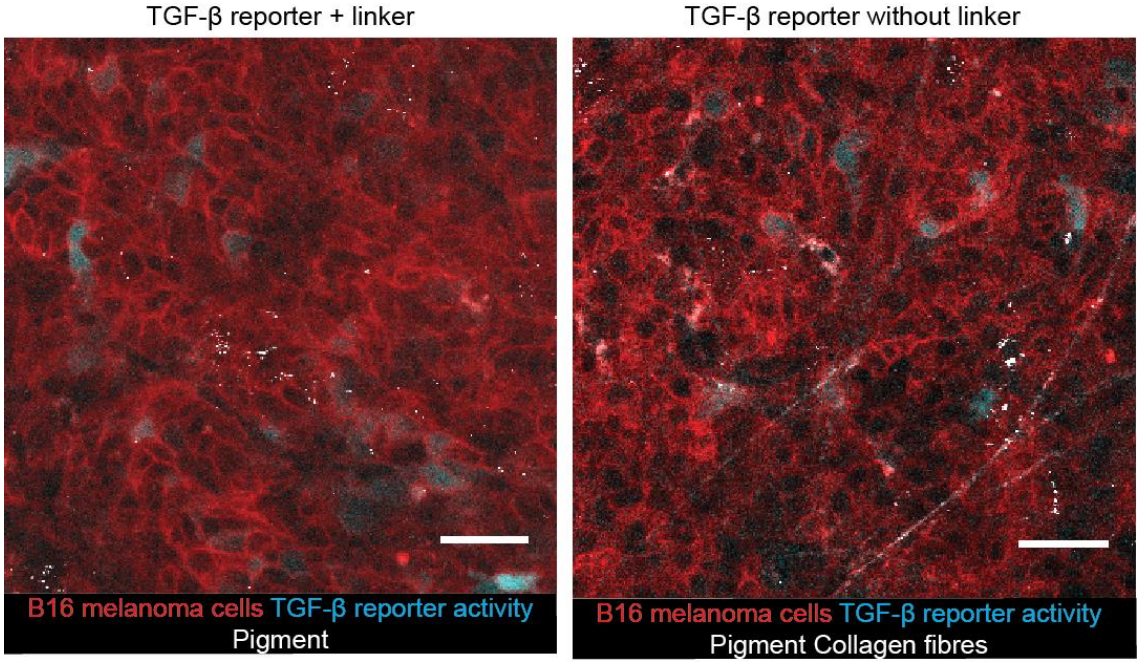

Figure 3.10 TGF-β reporters show heterogeneous TGF-β signalling in vivo.

Intra-vital still images from the two clonal TGF-β reporter cell-lines. B16 F2 melanoma cells have a red membrane marker. CFP expression indicates active TGF-β signalling. Pigment and Collagen fibres in white. Scale bar indicates 50 μm.

3.3.2.1 TGF-β signalling is increased in the B16 F2 singly motile cell population

Having confirmed heterogeneous TGF-β signalling in vivo, the relationship between TGF-β signalling and motility was investigated, to test if signalling correlates with motility. The CFP intensity of non-motile, singly motile and streaming cells was measured. In a similar way to analysis of the Notch reporter, the background CFP intensity was subtracted and then the values normalised to the average CFP intensity for the image. Both clonal TGF-β reporter cell-lines showed that singly motile cells had increased CFP expression compared to non-motile or cells using a streaming mode of motility (Figure 3.11 and Supplementary movie 5). The reporter cell-line generated from the construct without the linker did not have as big an increase in CFP intensity in singly motile cells as the other reporter cell-line; however it was still a significant difference. This correlates with the magnitude of response to TGF-β of the two reporter cell-lines in vitro. Therefore both reporter cell-lines showed that TGF-β signalling correlates with single cell motility.

The motile cells in the B16 melanoma model are less pigmented and TGF-β2 has been shown to decrease pigment in vitro (Pinner et al., 2009). As TGF-β signalling is increased in the singly motile cells the relationship between pigment and TGF-β reporter activity was examined to see whether TGF-β correlated with decreased pigment in vivo. Both clonal TGF-β reporter cell-lines showed a mutually exclusive relationship between pigment and TGF-β reporter activity (Figure 3.12). Cells with higher TGF-β reporter activity showed lower pigment levels indicating that TGF-β signalling correlates with decreased pigment. These results support the hypothesis that TGF-β signalling promotes single cell motility and decreases pigment, however, it is possible that the increased TGF-β signalling could be a downstream product of a different pathway that drives motility. Additionally the decreased pigment may also be result of other signalling pathways that are concurrent with TGF-β signalling. The reporters only suggest a correlation between TGF-β signalling, motility and decreased pigment.

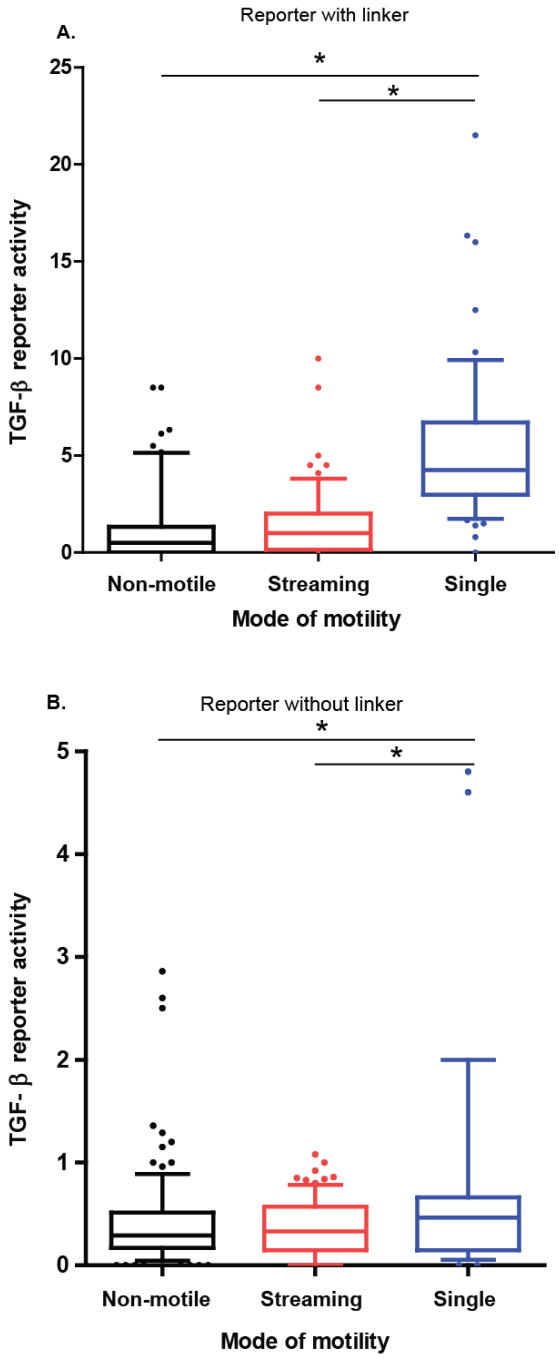

Figure 3.11. TGF-β signalling correlates with single cell motility.

Box and whiskers plot showing TGF-β reporter activity in non-motile, singly motile or streaming cells in B16 tumours generated from A. TGF-β reporter containing linker sequence. 67 non-motile cells, 54 singly motile cells and 64 streaming cells analysed. Data from 6 movies of 3 mice. B. TGF-β reporter without linker sequence. 118 non-motile cells, 36 singly motile cells and 88 streaming cells analysed. Data from 11 movies of 3 mice. Background CFP intensity subtracted from cellular CFP intensity before normalising to the average CFP for the image. Box indicates median and inter-quartile range. Whiskers indicate 10^{th}-90^{th} percentile. Outliers represented by individual points. Star indicates p value < 0.05 in ANOVA test.

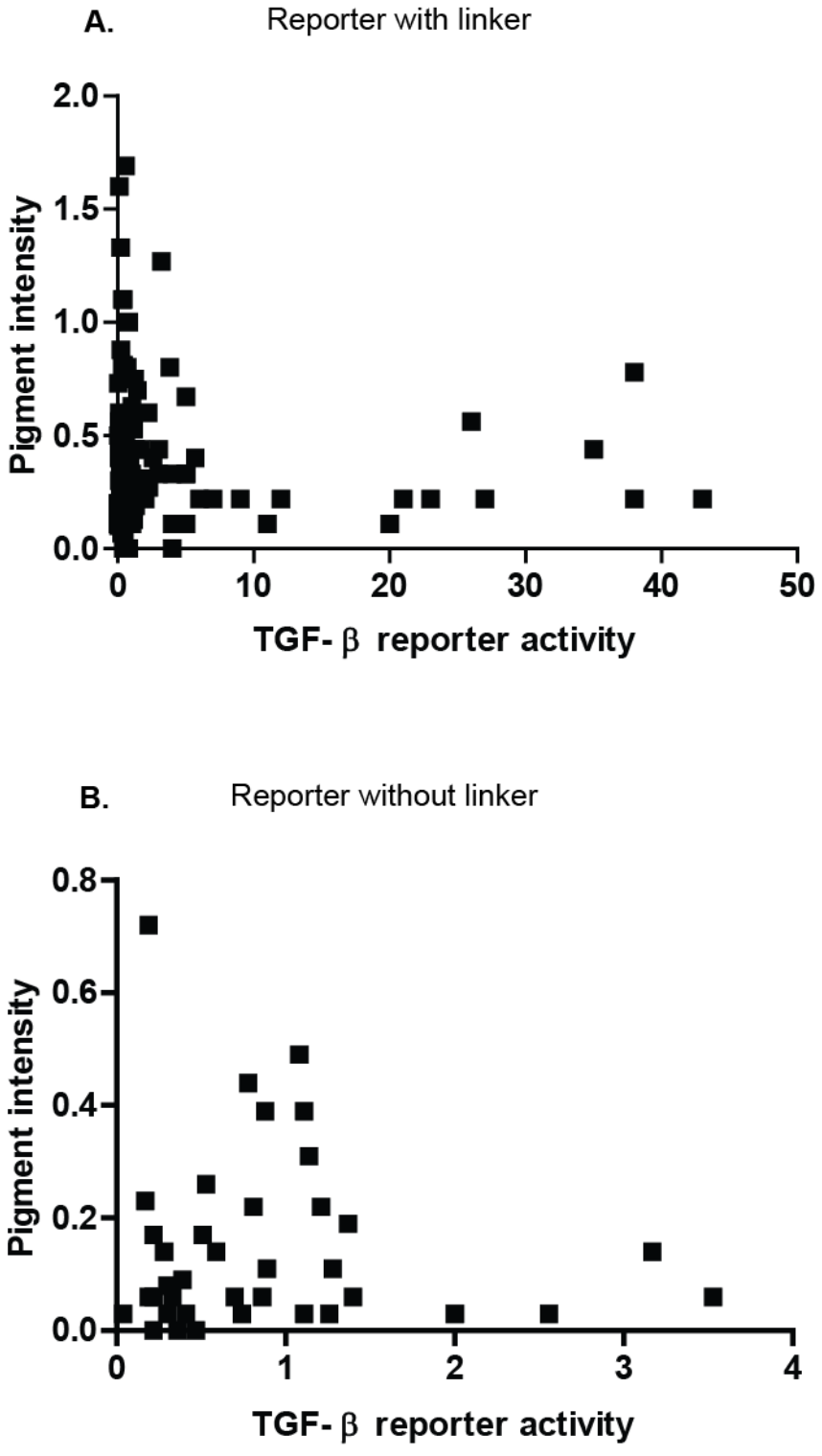

Figure 3.12. TGF-β signalling is mutually exclusive with pigment levels.

Graphs of pigment intensity vs CFP intensity and hence TGF-β reporter activity for A. TGF-β reporter containing linker sequence. B. TGF-β reporter without linker sequence. Pigment and CFP intensities measured in the same cell. First background intensity was subtracted and then the values normalised to the average signal for the channel in the whole image.

3.3.3 SRF signalling is heterogeneous in B16 melanoma in vivo

SRF signalling provides a link between actin cytoskeleton remodelling and gene transcription. It has been shown to regulate metastasis in the B16 model and loss of MRTF, a SRF co-factor, was shown to decrease the number of motile cells in vivo (Medjkane et al., 2009). Loss of MRTF may have decreased motility due to a lower basal level of MRTF targets such as Myosin light chain and Tropomyosin (Medjkane et al., 2009). Alternatively, SRF signalling may be activated during induction of motility and required to maintain the motile state. Based on this data, the prediction was that SRF signalling promotes motility and correlates with motile B16 cells.

To test whether SRF signalling correlates with motility in vivo, two clonal SRF reporter cell-lines were generated from two different reporter constructs. Both constructs were based on the 3D.A reporter, which contains three serum response elements (SREs) from the *c-Fos* promoter (Mohun et al., 1987). The reporter only responds to the Rho-actin arm of the SRF pathway and not the MAPK arm (Hill et al., 1995). One construct contained the three SREs upstream of two eGFP copies (Figure 3.13A). The other construct had the 3' UTR sequence of the *c-Fos* gene downstream of eGFP to try and couple the stability of eGFP mRNA to the mRNA stability of SRF targets (Figure 3.14A).

The constructs were tested for responsiveness to SRF signalling by transient co-transfection with a constitutive CFP plasmid in B16 F2 cells. The cells were then serum starved and treated with either 15 % FCS or 5 μM cytochalasin D before being subjected to flow-cytometry analysis. Cytochalasin D activates SRF signalling by preventing MRTF binding to monomeric actin, MRTF then accumulates in the nucleus and together with SRF, activates transcription (Vartiainen et al., 2007). Flow-cytometry analysis was restricted to the CFP positive cells because those were the cells to receive the reporter constructs. Treatment of both reporters with 5 μM cytochalasin D increased the GFP positive population in a time-dependent manner; cells treated with cytochalasin D for 10 hours had a larger GFP positive population, with increased GFP intensity compared to cells treated for 5 hours (Figure 3.13B and Figure 3.14B (with *c-Fos*

3'UTR). There was a slight increase in the GFP positive population on treatment with 15 % FCS. This confirmed that both reporters responded to SRF signalling.

Co-transfection of the reporter plasmids together with a hygromycin selection plasmid and subsequent selection in hygromycin generated stable SRF reporter cell-lines. These were then subjected to single cell cloning to generate clonal SRF reporter cell-lines. The clonal reporter cell-lines were tested for response to both 15 % FCS and 5 μM cytochalasin D. Flow-cytometry analysis showed an increase in the GFP intensity of clonal reporter cell-lines generated from both constructs, confirming the cells were indeed SRF reporter cell-lines (Figure 3.13C and Figure 3.14C (with *c-Fos* 3' UTR)). However, the reporter cell-line generated from the standard SRF reporter construct contained a proportion of cells that did not respond to cytochalasin D. Therefore this cell-line may underestimate SRF signalling.

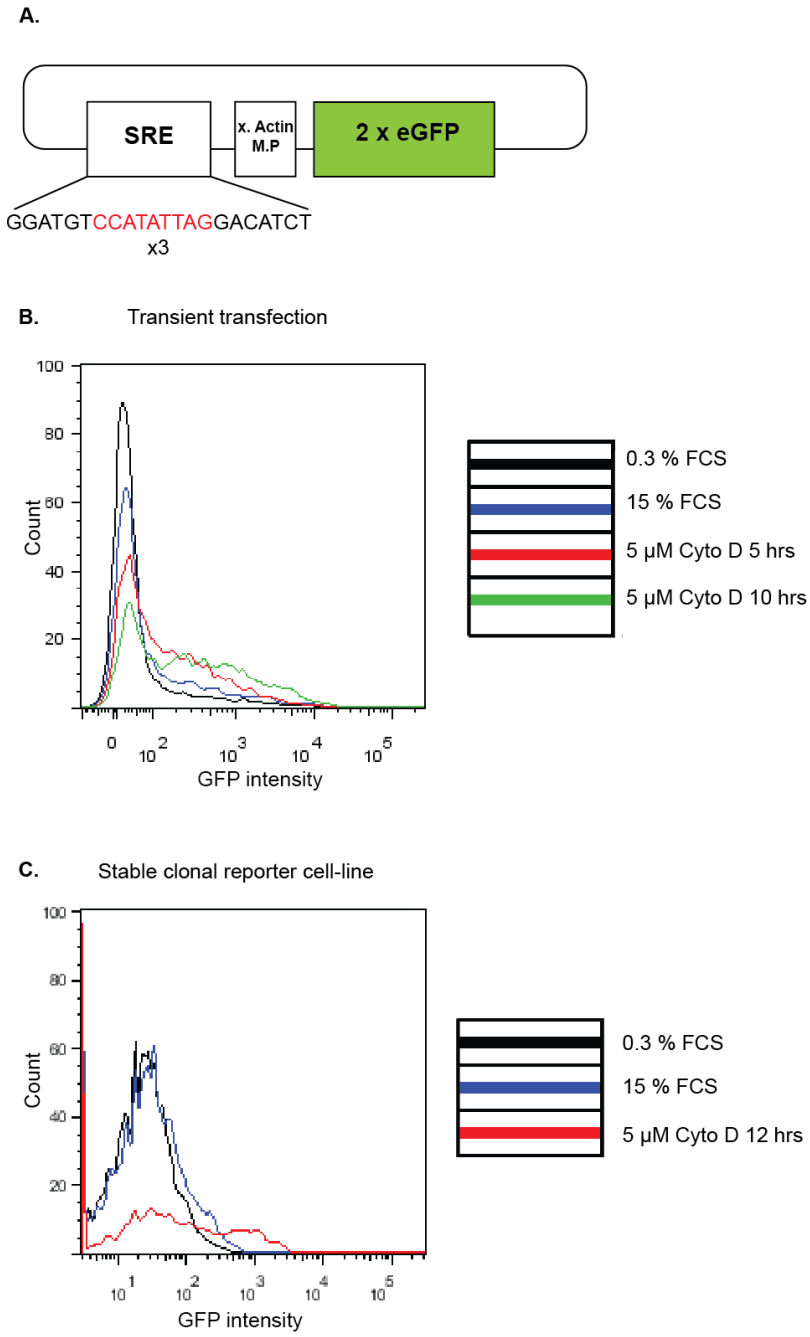

Figure 3.13 Generation of a clonal SRF reporter cell-line.

A. Schematic showing SRF reporter construct used. Red indicates SRF binding sequences. xActin M.P denotes Xenopus type 5 Actin minimal promoter containing the TATA box and transcription start site. B. Flow-cytometry analysis after transient transfection assay to test the SRF reporter. The SRF reporter construct was co-transfected with a constitutive CFP plasmid. The cells were serum starved and then stimulated with either 15 % FCS or 5 µM cytochalasin D for 5 or 10 hours. Gates were set to analyse only the CFP positive cells. C. Flow-cytometry analysis of the clonal SRF reporter cell-line after serum starvation and treatment with 15 % FCS or 5 µM cytochalasin D for 12 hours.

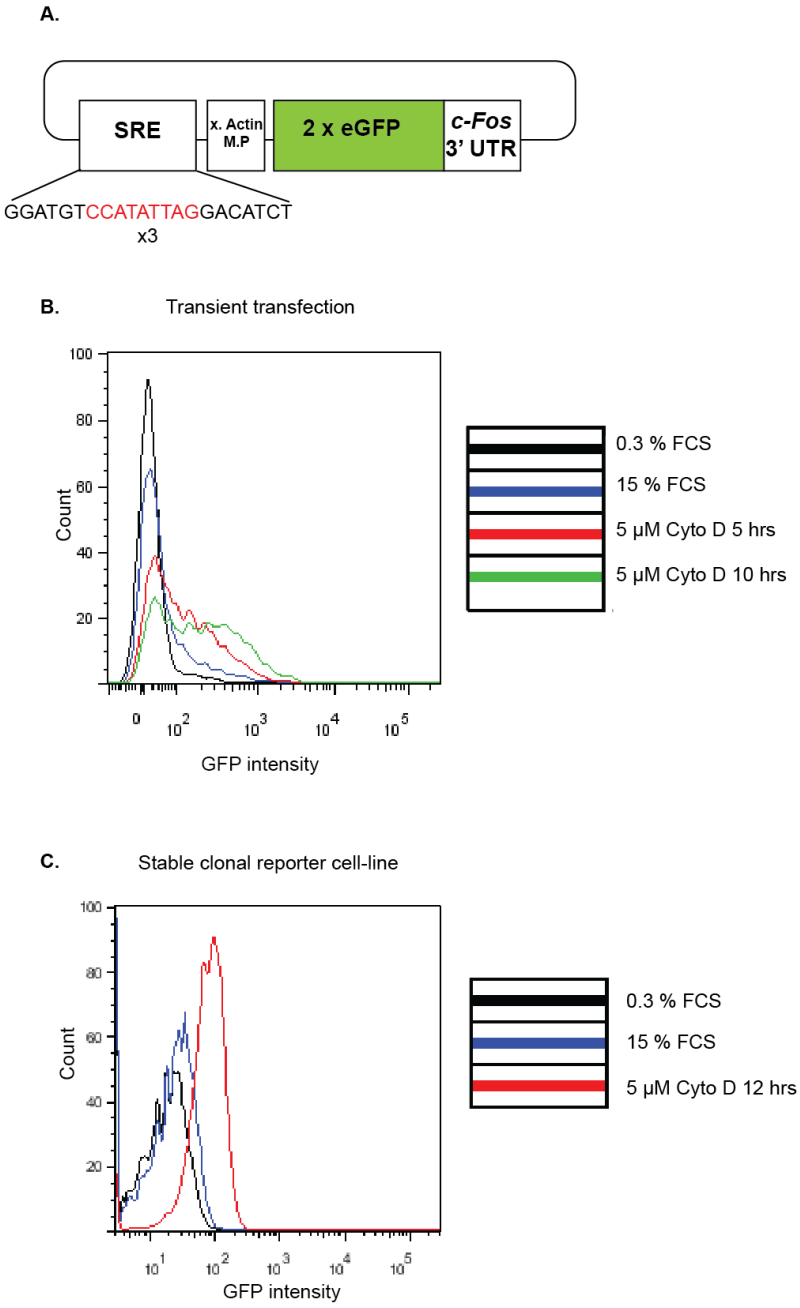

Figure 3.14 Generation of a clonal SRF reporter cell-line with a construct containing the 3' UTR of the *c-Fos* gene.

A. Schematic showing SRF reporter construct. Red indicates SRF binding sequences. xActin M.P denotes Xenopus type 5 Actin TATA box and transcription start site. Construct contains 3'UTR of *c-Fos* downstream of eGFP. B. Flow-cytometry analysis after transient transfection assay to test the SRF reporter. The SRF reporter construct was co-transfected with a constitutive CFP plasmid. The cells were serum starved and then stimulated with either 15 % FCS or 5 µM cytochalasin D for 5 or 10 hours. Gates were set to analyse only the CFP positive cells. C. Flow-cytometry analysis of the clonal SRF reporter cell-line after serum starvation and treatment with 15 % FCS or 5 µM cytochalasin D for 12 hours.

3.3.3.1 SRF signalling is increased in the B16 F2 motile cell population

To try to establish whether SRF signalling correlated with motility, the clonal SRF reporter cell-lines were injected sub-cutaneously into C57Black6 mice and the tumours subjected to intra-vital imaging (Supplementary movie 6). Still images revealed that GFP intensity was heterogeneous, indicating heterogeneous SRF signalling in vivo (Figure 3.15). The GFP intensity of non-motile, singly motile and streaming cells was measured. The intensity was corrected for background levels and normalised to the average GFP intensity for the whole image. This showed that in both SRF reporter cell-lines both singly motile cells and streaming cells had higher GFP intensity than non-motile cells, indicating SRF signalling correlates with overall motility (Figure 3.16). These data support the hypothesis that SRF signalling drives motility, however, as there were some non-motile GFP positive and so SRF active cells, further gain of function experiments need to be performed to confirm that SRF signalling is sufficient to induce motility.

As motile cells in the B16 melanoma model are less pigmented and SRF signalling is increased in motile cells, the expectation was that cells with high SRF signalling should have low pigment. Pigment and GFP intensity were measured simultaneously and plotted against each other. Both SRF reporter cell-lines exhibited a mutually exclusive relationship between pigment and reporter activity (Figure 3.17). Cells with active SRF signalling had low pigment and vice-versa. This also suggests that the cells with active SRF signalling are more motile since cells with less pigment are more likely to be motile (Pinner et al., 2009).

Previous data in a breast cancer model had suggested that acquisition of motility was a reversible process because cells in lymph-node metastases were non-motile. In line with this, TGF-β signalling, shown to be increased in motile cells, was low or inactive in breast cancer cells in the lymph node (Giampieri et al., 2009). To examine whether SRF signalling was also transiently activated, the GFP intensity of cells in the lymph-node was compared to both non-motile and motile cells in the primary tumour. The reporter cell-line generated using the standard SRF reporter construct was used as it was the brightest in vivo. Comparison of histograms of cellular GFP intensity showed that cells in the lymph-node had higher

GFP intensity than non-motile cells in the primary tumour (Figure 3.18). Lymph-node metastases also had higher GFP intensity than motile cells in the primary tumour. This suggests that SRF signalling is increased in motile cells of the primary tumour and once these cells arrive at the lymph-node, SRF remains active, potentially even increasing. This is a different pattern to activity of TGF-β signalling seen in the breast cancer model, but it may be a result of the different ways of activating the two pathways. TGF-β signalling is sensitive to the environment however SRF signalling is sensitive to changes in the actin cytoskeleton. It is possible that the lymph-node has low levels of TGF-β signalling, explaining the decrease seen in the breast cancer model, but once cells reach the lymph node they still require actin cytoskeleton remodelling, hence SRF signalling, to cope with arriving at a site with different ECM geometries.

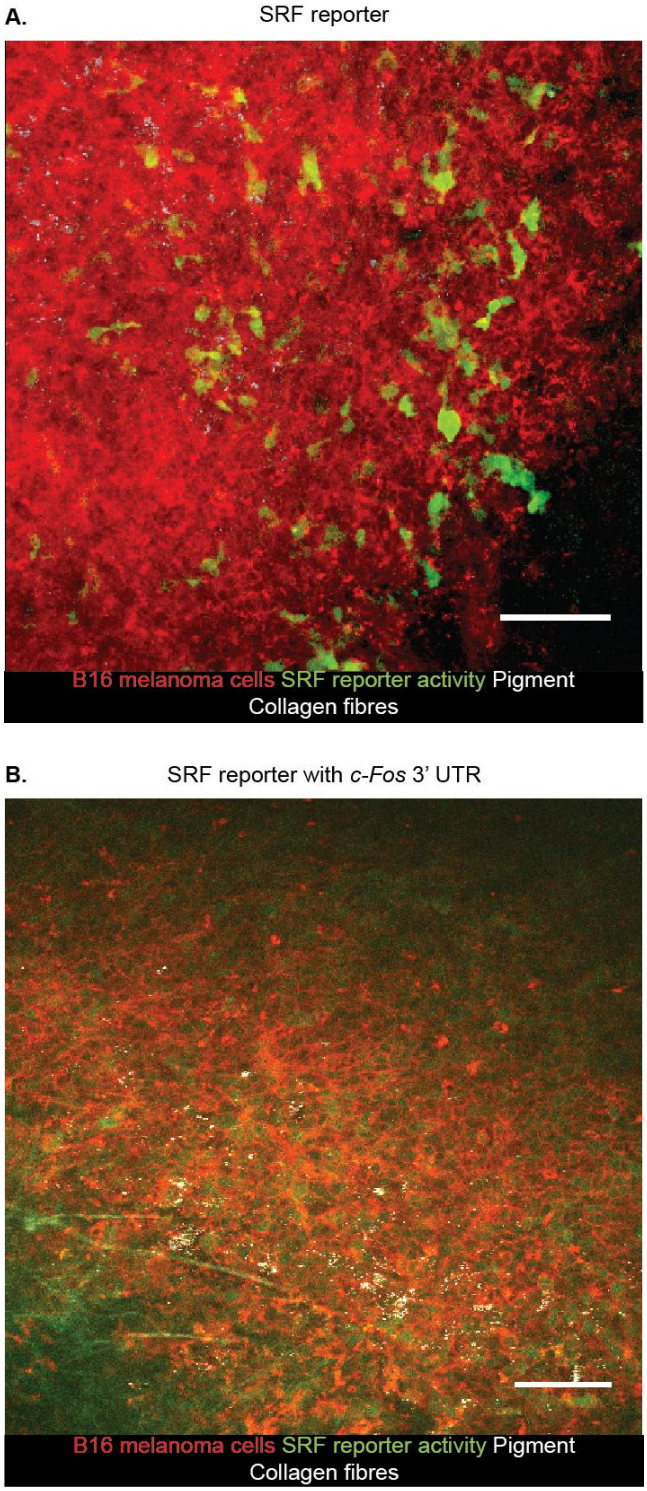

Figure 3.15 SRF signalling is heterogeneous in vivo.

Intra-vital still images from clonal B16 F2 melanoma SRF reporter cell-lines. Reporter cell-line generated from A. Construct with no additional 3'UTR. B. Construct with *c-Fos* 3'UTR. B16 F2 cells have a red membrane marker. GFP expression indicates active SRF signalling. Pigment and Collagen fibres in white. Scale bar indicates 100 µm.

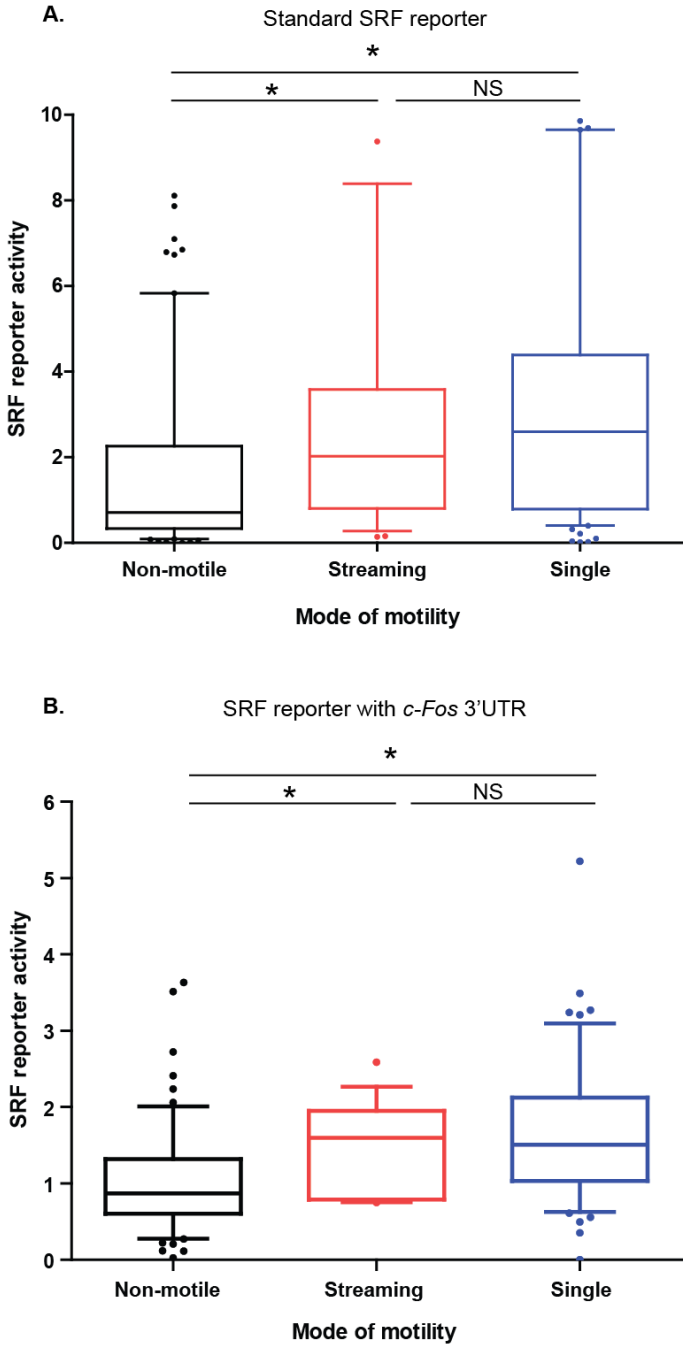

Figure 3.16 SRF signalling correlates with motile melanoma behaviour in vivo.

Box and whiskers plots showing GFP intensity and hence SRF reporter activity in non-motile, singly motile or streaming cells in B16 F2 tumours generated from A. Standard SRF reporter. 79 non-motile cells, 79 singly motile cells and 27 streaming cells analysed. Data from 8 movies of 4 mice. B. SRF reporter with *c-Fos* 3'UTR. 61 non-motile cells, 51 singly motile cells and 17 streaming cells analysed. Data from 9 movies of 3 mice. Background GFP intensity subtracted from cellular GFP intensity before normalising to the average GFP intensity for the image. Box indicates median and inter-quartile range. Whiskers indicate 10^{th}-90^{th} percentile. Outliers indicated by single points. Star indicates p value < 0.05 in ANOVA test. NS denotes not significant.

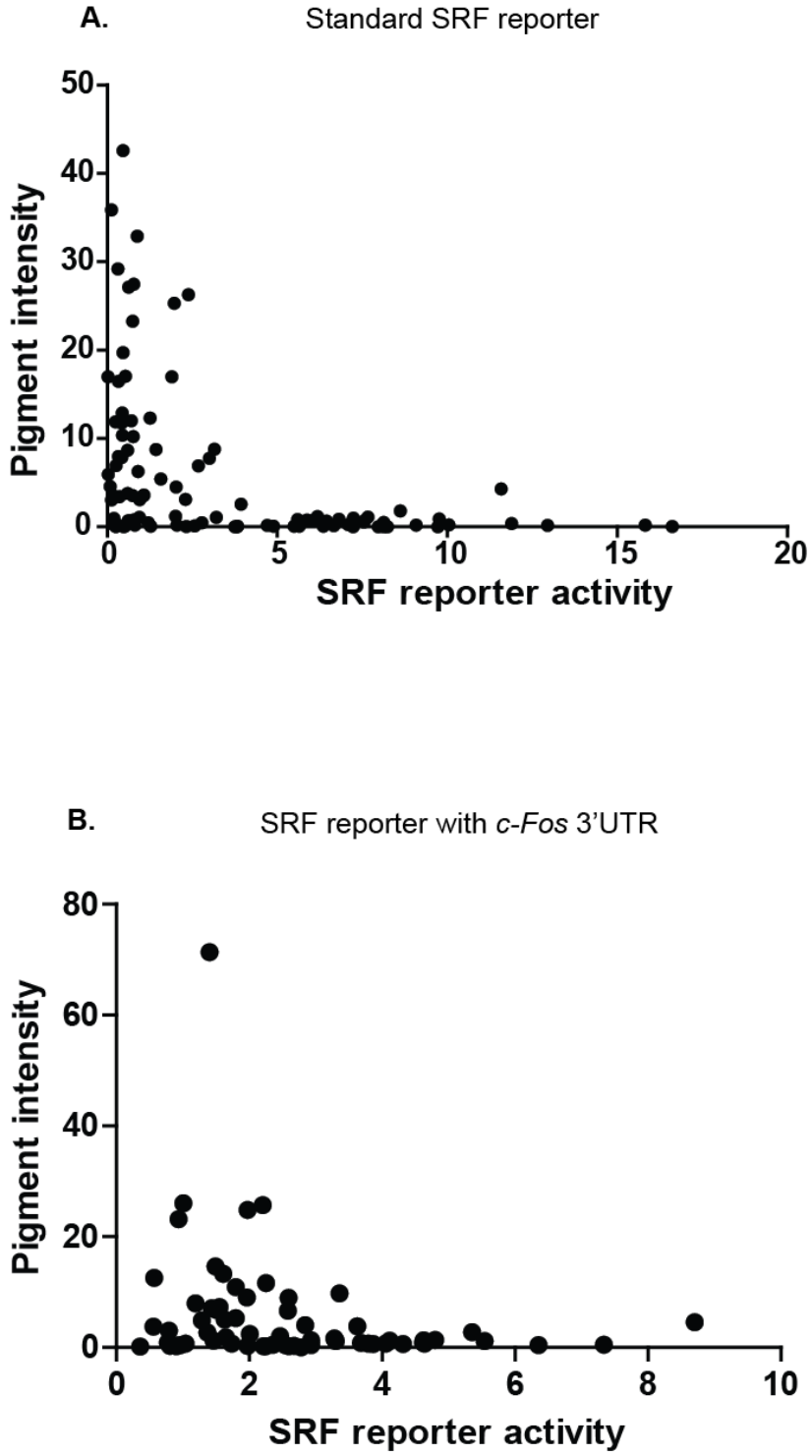

Figure 3.17 SRF signalling correlates with decreased pigment production.

Graphs of pigment intensity vs GFP intensity and hence SRF reporter activity for A. Standard SRF reporter. B. SRF reporter with *c-Fos* 3'UTR. Pigment and GFP intensities measured in the same cell. First background intensity was subtracted and then the values normalised to the average signal for the channel in the whole image.

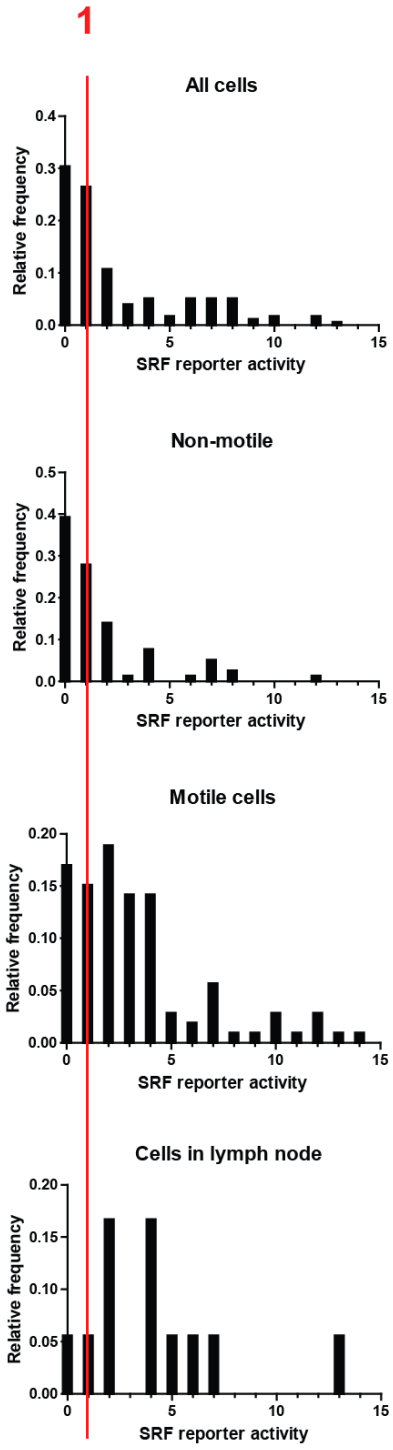

Figure 3.18 SRF signalling is increased in motile cells and cells in lymph node metastases.

Histograms of GFP intensity and hence SRF reporter activity for different populations of cells in the primary tumour and lymph-node metastases. Cellular GFP intensities were corrected for background GFP intensity and then normalised to the average GFP for the image. SRF reporter activity is categorised into bins of width 1.

3.4 Chapter summary

Intra-vital imaging of B16 F2 melanoma confirmed heterogeneous cell behaviour in vivo as less than 10 % of cells were motile and of this 10 % more than 50 % used a rounded single cell mode of motility. Generation of clonal reporter cell-lines showed heterogeneous activity of the Notch, TGF-β and SRF signalling pathways. Time-lapse analysis of the reporter cell-lines in vivo showed that the singly motile cells had higher levels of Notch and TGF-β signalling than non-motile or streaming cells. This was in contrast to SRF signalling which was increased in all motile cells. Notch, TGF-β and SRF signalling all showed a mutually exclusive relationship with pigment, providing more evidence that these pathways were associated with motility since motile cells have lower pigment. In addition, because pigment may be considered a surrogate readout for differentiation, these pathways may be involved in maintaining or promoting a less differentiated state. The reporter analysis showed non-motile cells that had high levels of Notch, TGF-β and SRF signalling, suggesting that none of the pathways alone are sufficient for motility.

Chapter 4. Notch signalling is insufficient to drive motility but promotes metastasis through both cell-autonomous and non cell-autonomous mechanisms

4.1 Chapter introduction

The results outlined in chapter three indicated that singly motile cells in the B16 F2 melanoma model had increased levels of Notch, TGF-β and SRF signalling compared to non-motile cells. Previous data also showed that motile cells have less pigment and have increased Brn2 promoter activity, which suggested that motile cells were less differentiated (Pinner et al., 2009). Notch is required for maintenance of the melanocyte stem cell (Moriyama et al., 2006) and is sufficient to confer neural-crest stem cell-like properties on melanocytes (Zabierowski et al., 2011). Therefore the role of Notch signalling in melanoma motility and differentiation was investigated further. The aim was to determine whether Notch signalling could drive or maintain melanoma cells in a less differentiated state, thereby promoting motility. The data in chapter three only showed a correlation between Notch signalling, single cell motility and decreased pigment. The plan was to generate B16 F2 cells with constitutive Notch signalling to ask whether Notch signalling alone was sufficient to drive motility in vivo and also to promote a less differentiated state.

4.2 Generation of a B16 F2 cell-line with constitutive Notch signalling

Canonical Notch signalling proceeds through engagement of the membrane spanning Notch receptor with a membrane bound Notch ligand on an adjacent cell (D'Souza et al., 2008). The Notch receptor is subsequently cleaved twice to generate an intra-cellular domain (NICD) which translocates to the nucleus and activates transcription together with co-factors such as CBF-1 (Schroeter et al., 1998). A B16 F2 cell-line with constitutive Notch signalling was generated by transfection of a plasmid containing the Notch1 intracellular domain (NICD) fused

to GFP (Figure 4.1A) into B16 F2 melanoma cells with a red membrane marker. Subsequent growth of the cells in 1 mg/ml G418 for 2-3 weeks selected for cells which had stably inserted the construct into the genome. These were then FACS sorted to collect the double-positive mRFP and GFP cell population to generate a pool of cells expressing both a red membrane tag and the NICD-GFP fusion protein. This B16 F2 NICD-GFP cell-line enabled gain of function experiments to ascertain the sufficiency of Notch signalling in melanoma motility and metastasis.

A number of experiments were performed to confirm that the B16 F2 NICD-GFP cells had increased Notch signalling compared to a control cell-line expressing GFP alone. Western blot using an anti-NICD antibody confirmed that the B16 F2 NICD-GFP cell-line had higher levels of NICD than the control (Figure 4.1B). To test that NICD-GFP was driving Notch dependent transcription a CBFRE dependent Notch luciferase reporter was used. The reporter was similar to the one used in chapter 1, but with expression of luciferase, not GFP, dependent on Notch pathway activation. The B16 F2 NICD-GFP and B16 F2 control cell-lines were co-transfected with the CBFRE:luciferase reporter and a constitutive renilla plasmid. Lysates were made two days after transfection and subjected to analysis of luciferase and renilla activity. The CBFRE dependent luciferase signal was normalised to renilla to account for differences in transfection efficiency. This showed that the B16 F2 NICD-GFP cell-line had more than twice the CBFRE dependent luciferase activity of the control cell-line, indicating increased Notch dependent transcription in the B16 F2 NICD-GFP cell-line (Figure 4.1C). The cell-lines were also tested for expression of the endogeneous Notch target, HES-1. Q RT-PCR showed that the B16 F2 NICD-GFP cell-line had higher levels of *Hes-1* mRNA than the control cell-line (Figure 4.1D). Together this indicates that the B16 F2 NICD-GFP has increased Notch signalling.

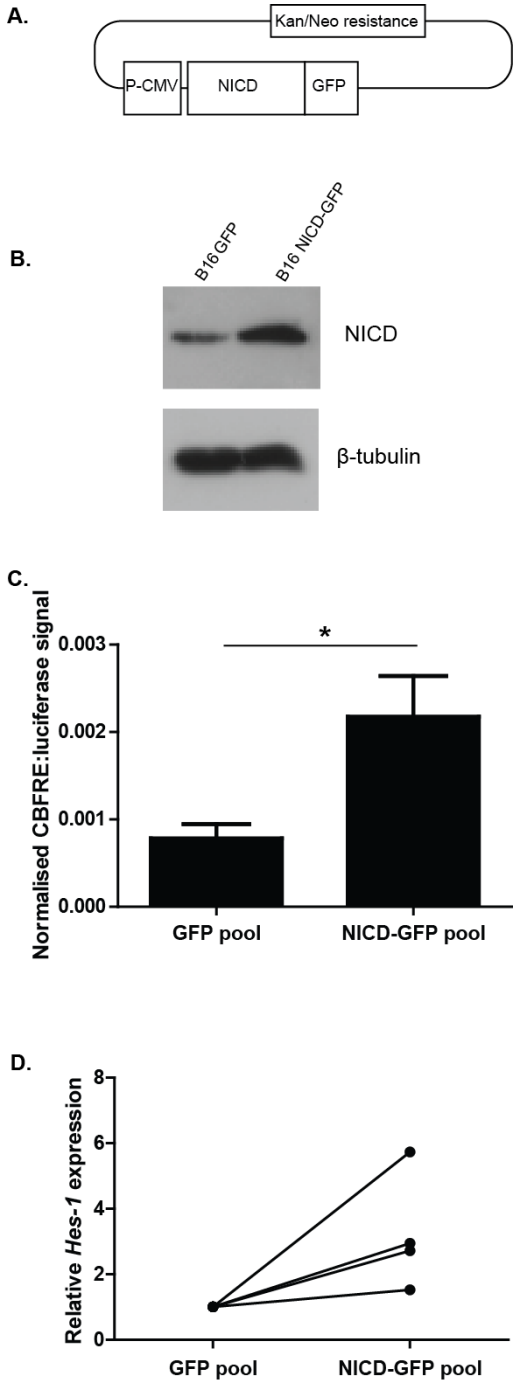

Figure 4.1 Generation of a B16 F2 cell-line with constitutive Notch signalling.

A. Plasmid encoding NICD-GFP fusion protein downstream of CMV promoter (denoted P-CMV). B. Western blot showing NICD levels in B16 F2 cell-lines generated from GFP (control plasmid) or NICD-GFP plasmid. C. Graph showing normalised luciferase signal in B16 F2 GFP (control) or B16 F2 NICD-GFP cell-lines. B16 F2 GFP and B16 F2 NICD-GFP cell-lines were co-transfected with a CBFRE:luciferase plasmid and a plasmid encoding constitutive renilla at a ratio of 5:1. Lysates were made 48 hours after transfection and assayed for luciferase and renilla activity. Luciferase signal was normalised to the renilla signal. Data from 3 independent experiments. Star indicates significance in t-test. Error bars show standard error. D. Graph showing relative *Hes-1* mRNA levels as measured by Q RT-PCR. Each pair indicates a single experiment.

4.3 Driving Notch signalling decreases pigment but may increase differentiation

To test whether Notch signalling can drive cells towards a less differentiated state, pigment intensity, used as a surrogate for differentiation status, was measured in the B16 F2 NICD-GFP and control B16 F2 cell-line in vivo. Tumours were generated from a 50:50 mix of B16 F2 NICD-GFP and control cells to enable analysis of the two different cell-lines in the same tumour environment. Pigment intensity was measured, the background levels subtracted and finally values were normalised to the average pigment intensity for the image. This allowed comparison of pigment levels between numerous tumours. B16 F2 NICD-GFP cells had lower pigment levels than control cells in vivo, potentially implying that the NICD-GFP cells are less differentiated (Figure 4.2).

To more thoroughly test whether Notch can promote a less differentiated state, expression of the melanoma differentiation markers, DCT, TYR and TYRP1 was analysed by Q RT-PCR. These markers are transcriptional targets of MITF, and MITF is an important transcription factor in the melanocyte lineage whose increased expression is associated with differentiation (Cheli et al., 2011) (Carreira et al., 2006). mRNA was extracted from B16 F2 NICD-GFP and control cells growing in vitro. Q RT-PCR showed that B16 F2 NICD-GFP cells had higher mRNA levels of all three differentiation markers (Figure 4.3). However, this was not statistically significant in a paired t-test. This implies that according to the known markers, driving Notch signalling may actually slightly increase the differentiation state, and is in contradiction to the pigment data. Therefore pigment is probably not a good surrogate for differentiation. The proposition that Notch signalling maintains cells in a less differentiated state, thereby promoting motility, is now unlikely since Notch signalling does not decrease melanoma differentiation markers. However, Notch signalling may promote melanoma motility by other means, potentially by transcriptional control of genes that regulate motility. As Notch signalling can decrease pigment in vivo and correlates with motility, the decrease in pigment seen in motile cells may be as a result of Notch signalling and unrelated to changes in differentiation.

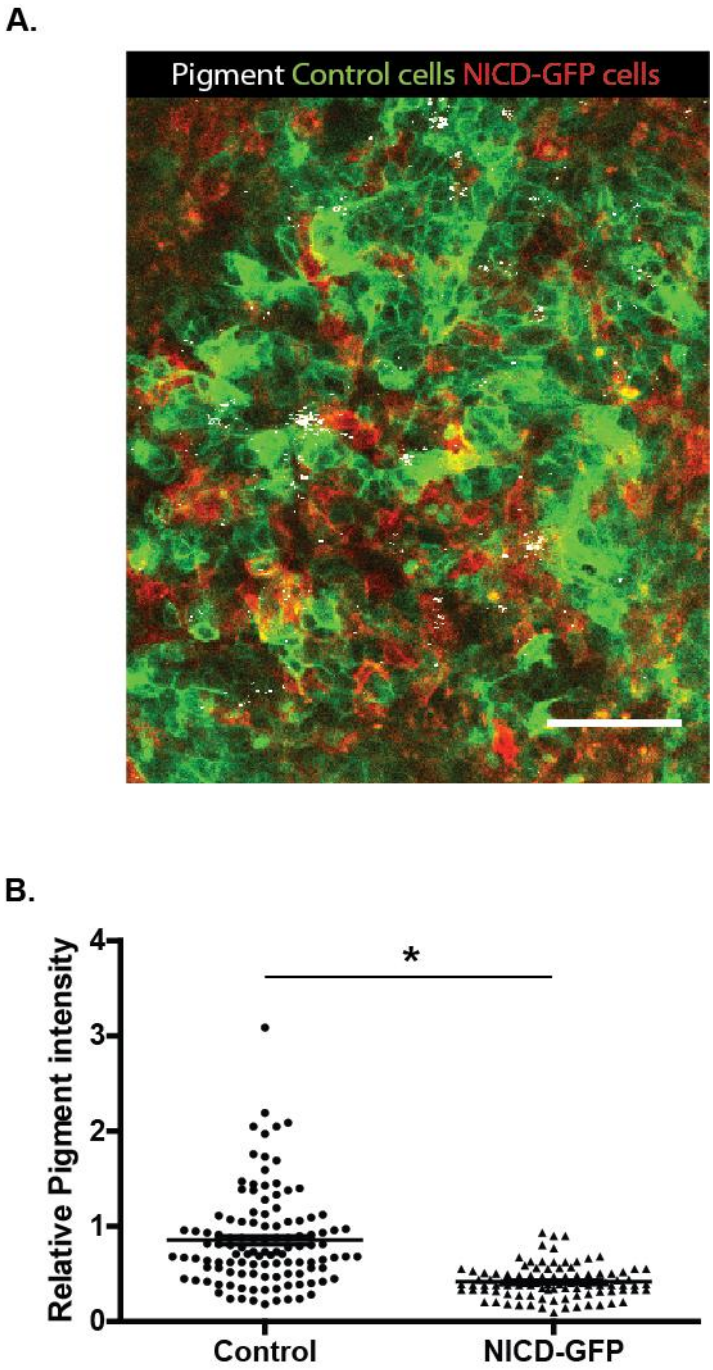

Figure 4.2 Driving Notch signalling decreases pigment in vivo.

A. Image of a mixed tumour with B16 F2 NICD-GFP with red membrane and B16 control cells with green membrane. Some B16 F2 NICD-GFP cells have lost the NICD-GFP expression. Pigment shown in white. Scale bar indicates 100 μm. B. Graph showing pigment intensity in vivo for B16 F2 NICD-GFP and B16 F2 control cell-lines. Pigment intensity measured on a cell by cell basis. Background intensity was subtracted from the cellular pigment intensity and then the values normalised to the average pigment intensity for the whole image. Each data point represents a single cell. Quantification of at least 100 cells from 4 mice. Star indicates significance in statistical t-test.

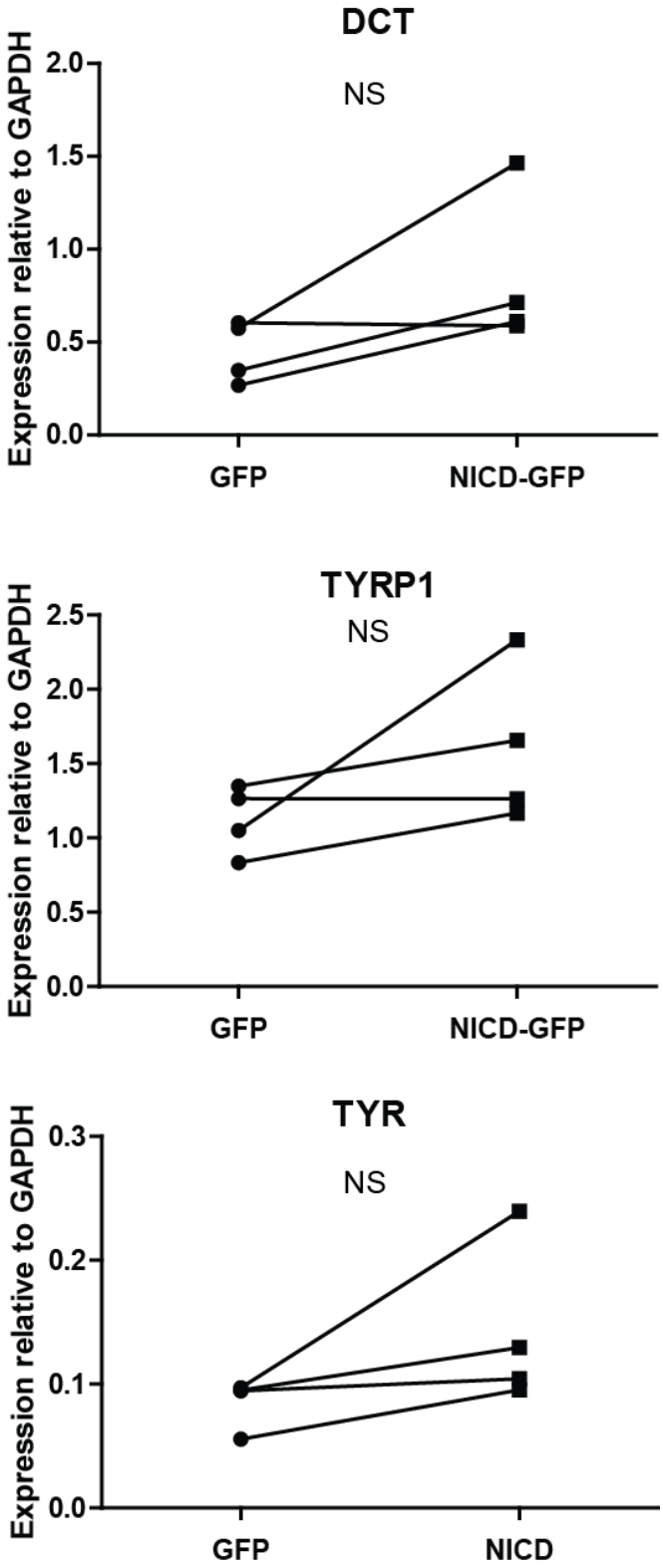

Figure 4.3 Driving Notch signalling may increase differentiation in vitro.

mRNA levels of the melanoma differentiation markers DCT, TYR and TYRP1 relative to GAPDH in B16 F2 NICD-GFP and control B16 F2 cells grown in vitro. 4 independent experiments. NS indicates no significance in paired statistical t-test.

4.4 Notch signalling is insufficient to drive melanoma motility in vivo

Although Notch did not drive cells into a less differentiated state it may still promote melanoma motility by other means. To test if this was the case, a 50:50 mix of B16 F2 NICD-GFP and control cells were injected sub-cutaneously into C57Bl6 mice. The tumours were subjected to intra-vital imaging and the number of motile cells per area of tumour was quantified. The NICD-GFP and control cells could be distinguished because the control cells had a green membrane marker and the NICD-GFP cells had a red membrane marker and nuclear NICD-GFP expression. Tumours generated from a mix of the two cell-lines enabled comparison of the cells in the same tumour environment. There was no difference in the number of cells moving either singly or using more collective modes of motility between the B16 F2 control and B16 F2 NICD-GFP cell-lines in the mixed tumours (Figure 4.4). This indicated that Notch signalling is insufficient to drive motility in the B16 melanoma model in vivo and invalidated the original hypothesis. The previous chapter however, showed that Notch signalling correlated with melanoma motility in vivo. Therefore it is most likely that pathways driving acquisition of motility in vivo also activate Notch signalling and although this is unlikely to influence the motile behaviour it can still be used to mark the singly motile population.

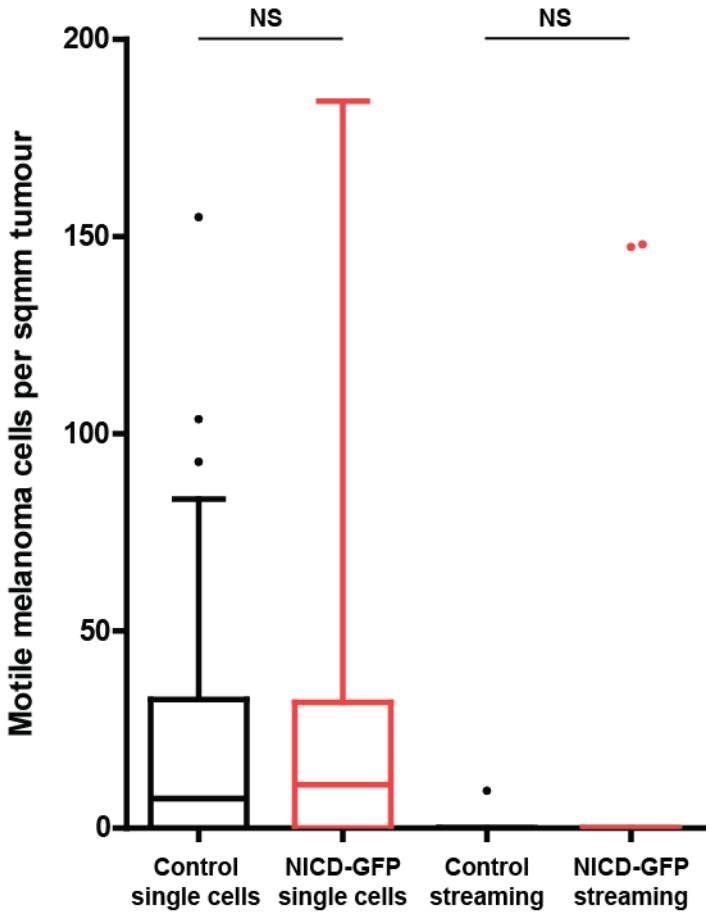

Figure 4.4 Notch signalling is insufficient to drive melanoma motility in vivo.

Box and whiskers plot showing the number of cells using different modes of motility per sq mm of tumour. Tumours were generated from a 50:50 mix of GFP membrane labelled B16 F2 control and mRFP membrane labelled B16 F2 NICD-GFP cells. Box indicates median and inter-quartile range. Whiskers indicate 10^{th}-90^{th} percentile. Outliers represented by single points. Atleast 25 cells analysed for each condition. Data from 12 movies of 6 mice. N.S indicates not significant in statistical t-test.

4.5 Cells with active Notch signalling can promote lymph-node metastasis in a non cell-autonomous manner

Although Notch signalling is not sufficient to promote melanoma motility, Notch may have a role in other aspects of metastasis. The B16 F2 melanoma cells can spontaneously metastasise to the lymph-node and fluorescently labelled melanoma cells can be visualised within the lymph-node using either confocal or epifluorescent microscopy. Primary tumours were generated from B16 F2 control cells alone, B16 F2 NICD-GFP cells alone or a 50:50 mix of the two cell-lines. Each mouse was scored as either positive or negative for lymph node metastases. Single cells could be visualised in the lymph-node and so the presence of just a single cell counted as positive for lymph-node metastases. Tumours generated from a 50:50 mix of B16 F2 control and B16 F2 NICD-GFP cells had the greatest percentage of mice with lymph-node metastases (Figure 4.5). B16 F2 NICD-GFP tumours also showed increased lymph node metastasis compared to control however this was not statistically significant (Figure 4.5). As previous data had shown no difference in motility between control and NICD-GFP cells (Figure 4.4), this hinted that cells with active Notch signalling in the tumour may promote metastasis in a non-cell autonomous manner.

To further probe the potential non-cell autonomous role for Notch signalling in melanoma, the cells in metastases from the mixed tumours were examined to see if they were predominantly B16 F2 NICD-GFP, control or a mixture of both. If cells with active Notch signalling promote metastasis in a non-cell autonomous manner, then the expected ratio of B16 F2 control to B16 F2 NICD-GFP cells in the lymph-node would be the same ratio as the primary tumour, 50:50. Indeed lymph-node metastases from mixed tumours contained about 50:50 B16 F2 control and B16 F2 NICD-GFP cells (Figure 4.6A). Still images of these tumours confirmed that they had maintained roughly the 50:50 ratio of control to NICD-GFP cells used at the time of injection (Figure 4.6B). Tumour volume measurements showed no difference in tumour growth between B16 F2 control, NICD-GFP and mixed tumours indicating the increased metastasis was not from increased tumour size (Figure 4.7). Therefore cells in the primary tumour with active Notch signalling promote metastasis to the lymph-node in a non-cell autonomous manner.

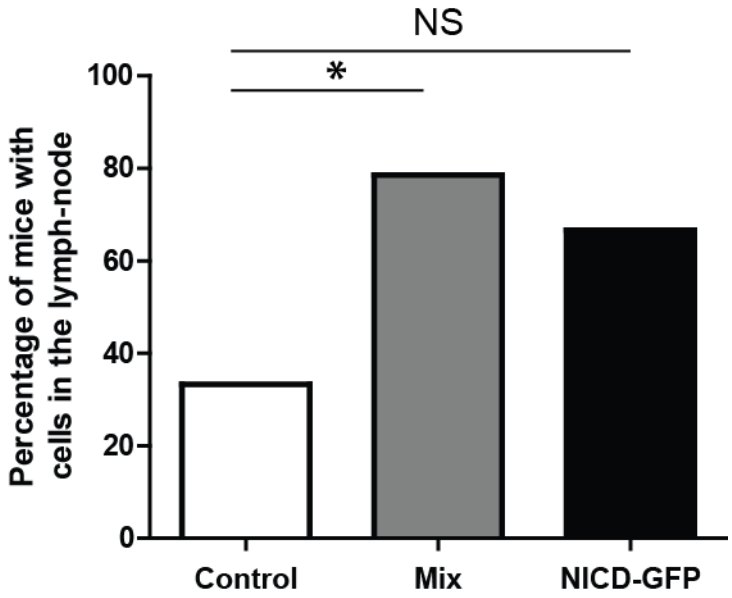

Figure 4.5 Notch signalling increases metastasis to the lymph node.

Graph showing percentage of mice with B16 F2 control, B16 F2 NICD-GFP or B16 F2 control plus NICD-GFP tumours with lymph-node metastases. Mixed tumours were generated from injection of a 50:50 mix of both B16 F2 cell types. 12 mice in B16 F2 control and B16 F2 NICDGFP cohorts, 14 mice in mixed tumour cohort. Star indicates significance in Fishers exact test, NS indicates non significance.

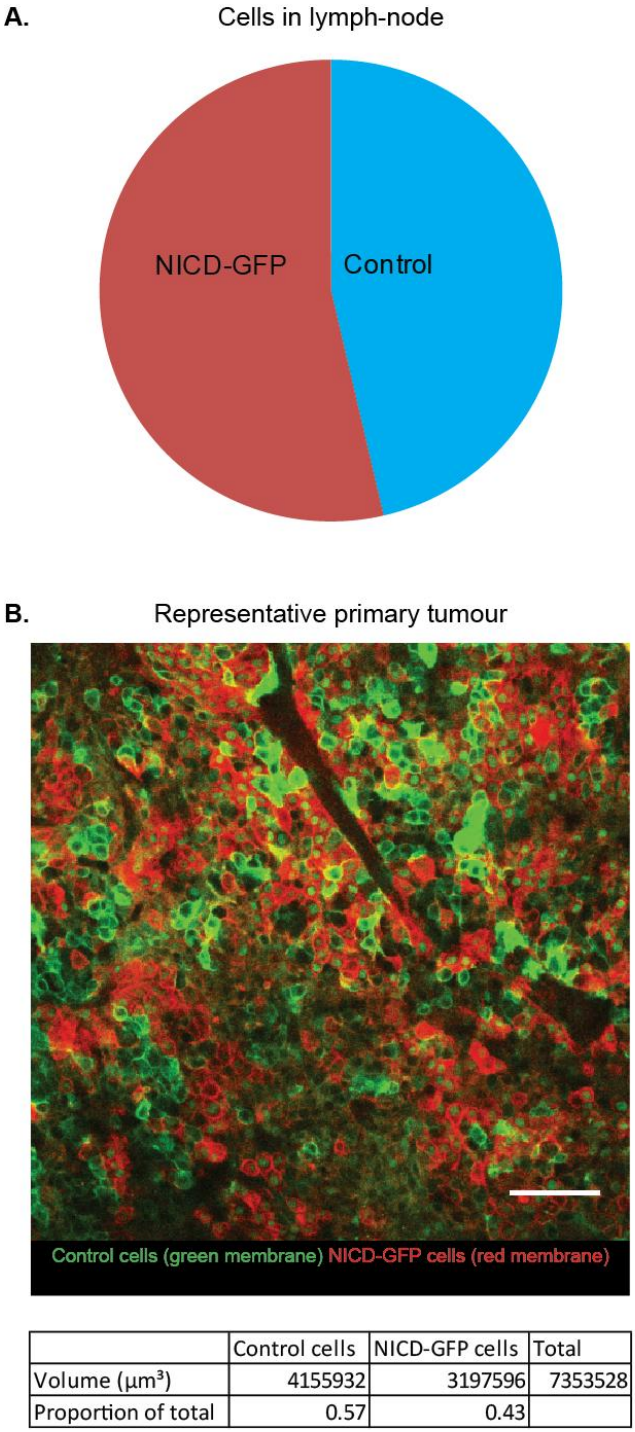

	Control cells	NICD-GFP cells	Total
Volume (μm³)	4155932	3197596	7353528
Proportion of total	0.57	0.43	

Figure 4.6 Notch signalling promotes lymph-node metastasis in a non-cell autonomous manner.

A. Pie-chart showing proportion of B16 F2 control and B16 F2 NICD-GFP cells in lymph-node metastases from mice with mixed B16 F2 control and B16 F2 NICD-GFP tumours (The same tumours analysed as those in Figure 4.5). B. Still image of a mixed tumour generated from 50:50 mix of B16 F2 control (green membrane) and B16 F2 NICD-GFP (red membrane). Scale bar indicates 100 μm. Quantification of volume of B16 F2 control and NICD-GFP cells in this image using Volocity image analysis software (Perkin Elmer).

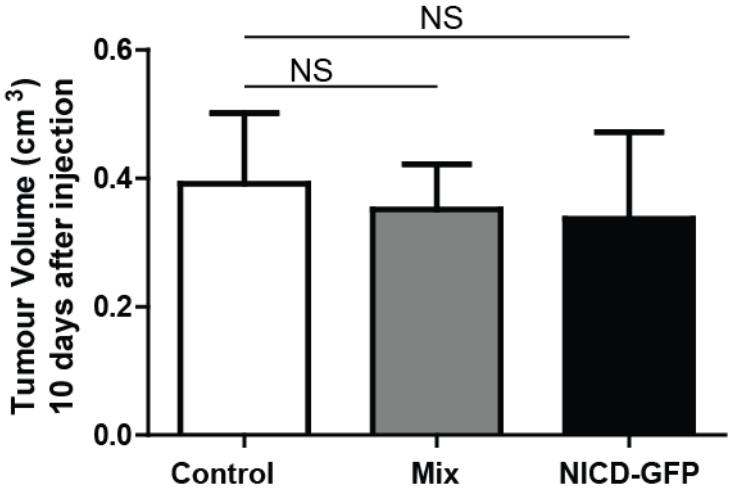

Figure 4.7. Notch signalling does not affect B16 F2 melanoma growth in vivo.

Graph showing tumour volume 10 days after injection of 1 x 10^6 B16 F2 melanoma cells for control, NICD-GFP and tumours containing a 50:50 mix of control and NICD-GFP cells. (The same tumours analysed as those in Figure 4.5). Tumour volume calculated from ½(length x width^2) with 8 mice in each cohort. Error bars show standard error and NS denotes no significance in ANOVA statistical test.

Melanoma cells with active Notch signalling in the primary tumour could promote metastasis in a non-cell autonomous manner through a variety of mechanisms. They may increase the motility of other melanoma cells through secretion of chemokines, or affect aspects of the microenvironment such as the blood or lymphatic vessels, thereby increasing the spread of all cells in the tumour. To try and address the first point regarding cells with active Notch signalling promoting motility in general, the number of motile control cells per mm^2 in mixed tumours was compared to tumours generated from control cells alone. The number of control cells using a single cell mode of motility was the same in control tumours and tumours generated from a 50:50 mix of B16 F2 control and B16 F2 NICD-GFP cells (Figure 4.8). This indicates that cells with active Notch signalling do not promote metastasis through increasing the single cell motility of other melanoma cells in the tumour. The number of control cells using more collective modes of motility was actually decreased in the mixed tumours compared to control only tumours (Figure 4.8). This was unexpected and potentially counter-intuitive as in a breast cancer model collective motility enabled metastasis to the lymph-node (Giampieri et al., 2009), and here in tumours where metastasis to the lymph-node was increased, there was a decrease in collective modes of motility. Overall the data suggested that melanoma cells with active Notch signalling do not promote metastasis in a non-cell autonomous manner through the induction of motility of other melanoma cells.

An alternative explanation for the non-cell autonomous promotion of metastasis, is that the cells with active Notch signalling affect the microenvironment and thereby increase metastasis without influencing acquisition of motility in the primary tumour. Examples of this could include altering the endothelial cells resulting in increased extravasation, or signalling to the pre-metastatic niche to increase survival of melanoma cells at secondary sites. To investigate the effects of cells with active Notch signalling on the microenvironment, B16 F2 control, NICD-GFP or mixed tumours were removed, fixed and subjected to immunohistochemical analysis of various stromal markers. Analysis of the endothelial vessels using an anti-Endomucin antibody revealed changes to the vessels in B16 F2 NICD-GFP and mixed tumours (Figure 4.9). These were most likely blood vessels as staining with lymphatic markers revealed very few lymphatic vessels within the tumour bulk.

Volocity image analysis software was used to identify the vessels based on Endomucin staining. Objects found by Volocity were subsequently "filled in" to include the vessel lumen and the area of each individual object or vessel calculated. Analysis of the vessel density by calculating the percentage of tumour area covered by vessels indicated the B16 F2 NICD-GFP tumours had a higher density of vessels (Figure 4.9B). However, B16 F2 NICD-GFP tumours also had larger vessel lumens than either mixed or B16 F2 control tumours (Figure 4.9C). It is likely that the increased vessel coverage of the tumour is due to the increased lumen size of individual vessels. The lumen size of vessels in tumours with a 50:50 mix of B16 F2 control and NICD-GFP cells was also significantly larger than control, but significantly smaller than in B16 F2 NICD-GFP alone tumours. This suggests that the more cells with active Notch signalling in the tumour, the larger the vessel lumen size, therefore implying that cells with active Notch signalling affect components of the tumour microenvironment.

Metastasis to the lymph-node most likely occurs through lymphatic vessels, however, analysis of the lymphatics was complicated by technical issues. A number of antibodies specific for LYVE-1, a lymphatic marker (Jackson et al., 2001), were tested without success. In addition, Podoplanin, an established marker for lymphatic vessels (Breiteneder-Geleff et al., 1999), gave potentially non-specific lymphatic staining in the margins. This was similar to published data in the B16 melanoma model describing a lymphoid-like stroma at B16 melanoma margins (Shields et al., 2010). Therefore analysis of lymphatic vessel density or size was not possible.

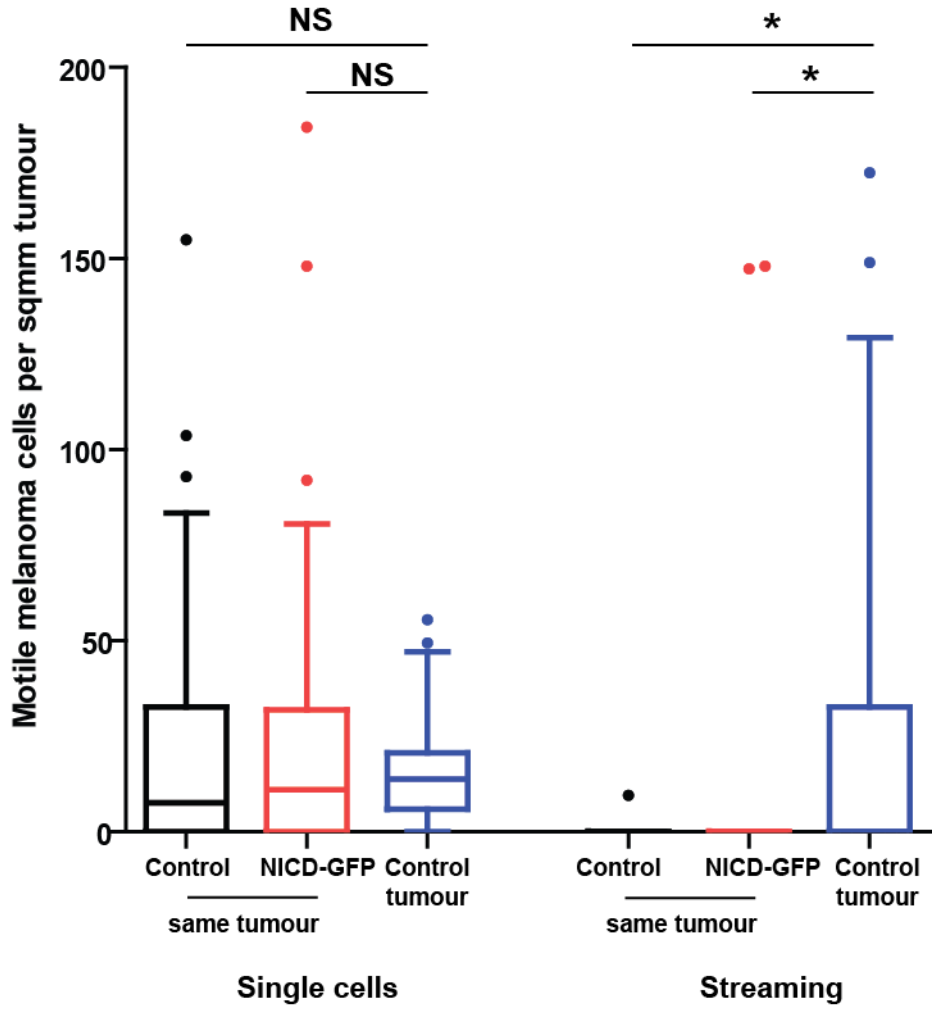

Figure 4.8 Melanoma cells with active Notch signalling in the primary tumour do not promote a general increase in motility.

Box and whiskers plot showing the number of motile cells per sq mm of tumour in mixed B16 F2 control plus B16 F2 NICD-GFP and B16 control alone tumours. Same tumour denotes cells in mixed tumours generated from a 50:50 mix of B16 F2 control and B16 F2 NICD-GFP cells. Control tumour denotes tumours made up of 100 % control cells Box indicates median and inter-quartile range. Whiskers indicate 10^{th}-90^{th} percentile. Outliers represented by single points. 6 mixed tumours analysed and 4 control tumours. Stars indicate p value < 0.05 in ANOVA statistical test and N.S indicates non-significance.

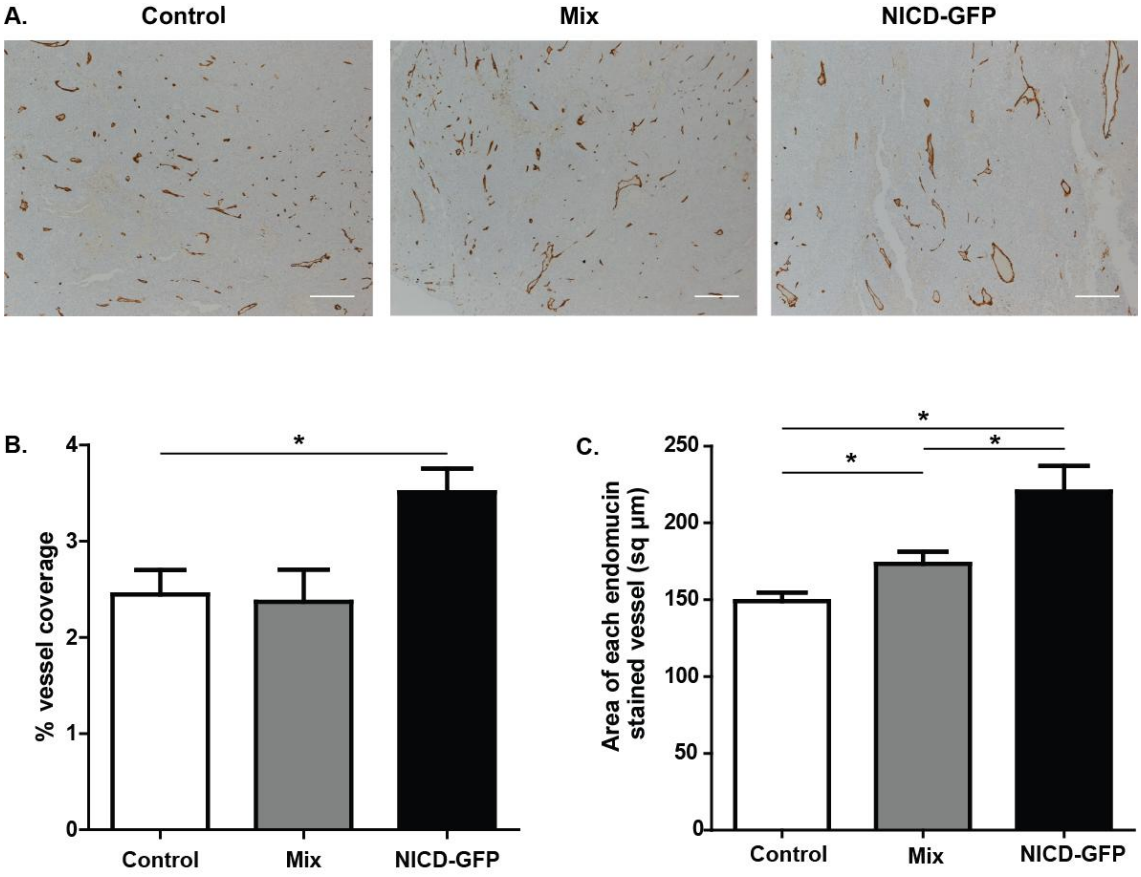

Figure 4.9 Cells with active Notch signalling promote an increase in vessel lumen size.

A. Immunohistochemical analysis of endothelial vessels in a subset of the tumours analysed in Figure 4.5 using anti-Endomucin antibody. Scale bar indicates 150 µm. B. Quantification of percentage area of tumour covered by vessels vessel in B16 F2 control, NICD-GFP and mixed tumours. C. Quantification of the area of each individual vessel in B16 F2 control, NICD-GFP and mixed tumours. Volocity image analysis software was used to identify vessel objects based on the Endomucin staining. The objects were filled in and the area of each object or vessel measured. Analysis of 3 images from 4 tumours for each condition. Star indicates statistical significance in an ANOVA statistical test.

4.6 Notch signalling in B16 F2 melanoma cells increases experimental lung metastasis

Although Notch signalling is insufficient to drive melanoma motility in vivo, the Notch reporter indicated that motile cells had increased Notch signalling and hence Notch correlated with motility. As the motile cells in the primary tumour are believed to be those that metastasise to secondary sites, the effects of increased Notch signalling were investigated on lung colonisation. The F2 sub-line of B16 cells do not spontaneously metastasise to the lungs before the mouse needs to be sacrificed, so an experimental lung metastasis assay was used. A 50:50 mix of B16 F2 control and NICD-GFP cells was injected into the mouse tail-vein and the ratio of cells in the lung examined by confocal microscopy after 48 hours or 10 days. The cells were distinguished by different fluorescent protein labelling of the plasma membrane. A separate cohort of control mice received a 50:50 mix of control cells (red membrane) and control cells (green membrane). The ratio of NICD-GFP (red membrane) to control cells (green membrane) was normalised to the ratio of red:green cells from control mice. Mixing the cell-types accounted for differences in injection efficiency between mice. This showed that both after 48 hours and 10 days, NICD-GFP cells were more successful at colonising the lung than control cells (Figure 4.10). Given that there are many steps involved in lung colonisation, such as survival in the bloodstream, adherence to vessel walls, intravasation and survival in the lung parenchyma, it is difficult to pinpoint the step at which Notch exerts its effects. However, since Notch signalling promotes lung colonisation after only 48 hours it is likely to influence the initial steps of survival in the bloodstream, adhering to blood vessels or intravasation. Therefore, although Notch signalling does not directly influence the motility of cells in the primary tumour, if motile cells have increased Notch signalling (as suggested by the reporter), they are then more able to colonise the lungs.

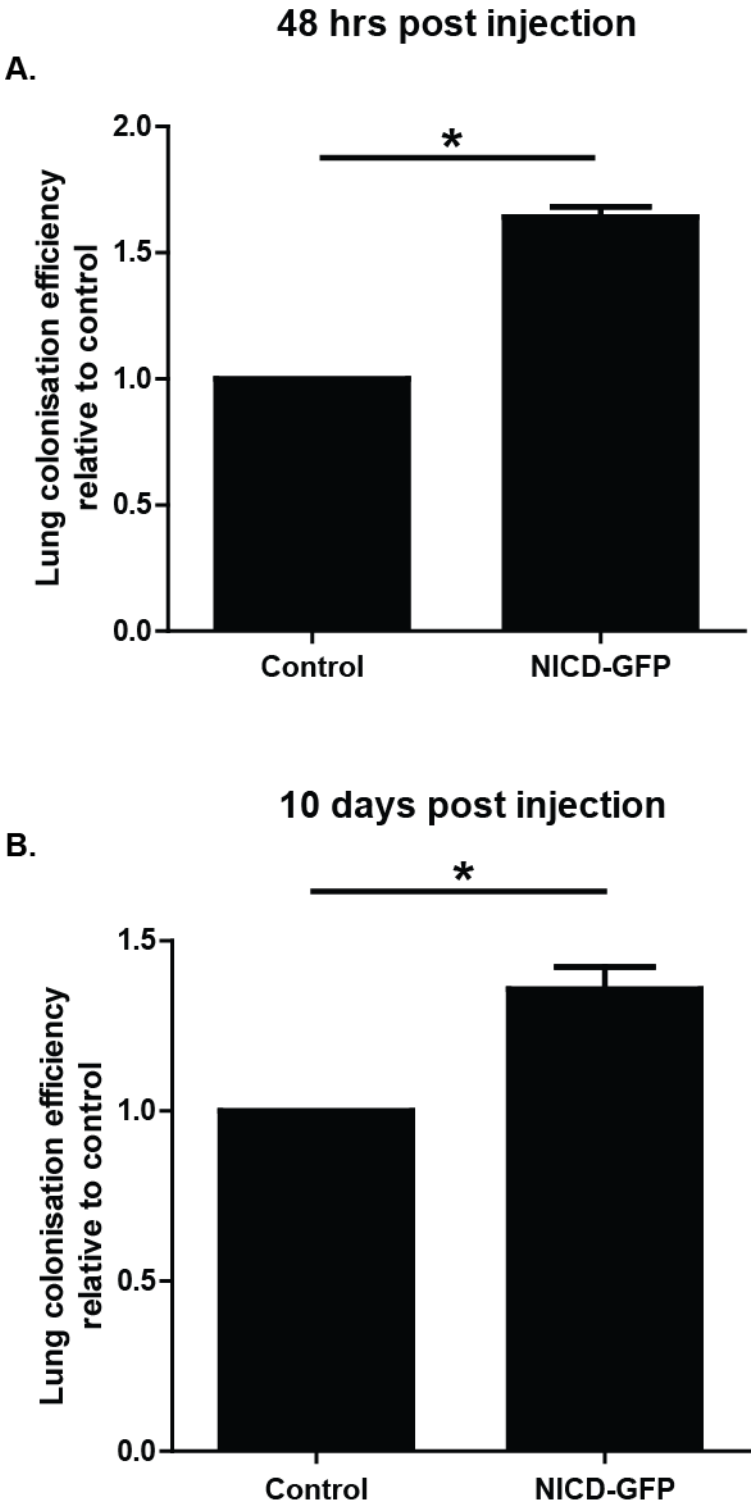

Figure 4.10 Notch signalling increases lung colonisation ability of B16 F2 cells.

Graphs showing relative efficiency of lung colonisation for B16 F2 control and NICD-GFP cells after A. 48 hours (5 mice per condition) and B. 10 days (9 mice per condition). Star indicates statistical significance in t-test.

4.7 Microarray to identify Notch targets in B16 F2 melanoma

To try and identify Notch targets in B16 F2 melanoma cells and to look for potential regulators of the increased lung and lymph-node metastasis, B16 F2 control and B16 F2 NICD-GFP cells were subjected to microarray analysis. Biological triplicates of RNA extracted from cells grown in vitro revealed a number of genes up-regulated on NICD-GFP expression. The list of these Notch targets can be found in the appendix. Geneset enrichment analysis (Mootha et al., 2003; Subramanian et al., 2005), using software from The Broad Institute, was used to try and identify pathways and processes enriched in the Notch targets. The list of Notch targets was compared with over 3000 genesets in the Molecular Signatures Database (MSigDB) C2 category (compiled by The Broad Institute). The C2 collection contains curated genesets from online pathway databases, PubMed publications and knowledge of domain experts. This showed an enrichment for interferon regulated genes in the Notch targets (Table 1). *Stat1*, *Ifitm3*, *Ifit3*, *Irf9 and Ifi35* mRNA levels were all up-regulated greater than 1.5 times in the B16 F2 NICD-GFP cells. MYLK, a kinase that phosphorylates myosin light chain leading to increased actomysoin contractility, was also identified to be a putative Notch target by microarray. Actomysoin contractility is important for extravasation and lung colonisation (Wyckoff et al., 2006) (Pinner and Sahai, 2008). *Vegfb* mRNA is up-regulated about 1.3 times in the B16 F2 NICD-GFP cell-line relative to control. VEGF-B is a vascular endothelial growth factor member and can promote endothelial survival (Zhang et al., 2009). Further consideration of how these Notch targets may influence metastasis can be found in the discussion.

Gene Set Name	# Genes in Gene Set (K)	Description	# Genes in Overlap (k)	k/K	p value
BROWNE_INTERFERON_RESPONSIVE_GENES	68	Genes up-regulated in primary fibroblast culture after treatment with interferon alpha for 6 h.	8	0.1176	2.39E-09
CASTELLANO_NRAS_TARGETS_UP	83	Genes up-regulated in MEF cells (embryonic fibroblast) isolated from NRAS [Gene ID=4893] knockout mice.	8	0.0964	1.19E-08
TAKEDA_TARGETS_OF_NUP98_HOXA9_FUSION_3D_UP	181	Genes up-regulated in CD34+ [Gene ID=947] hematopoetic cells by expression of NUP98-HOXA9 fusion [Gene ID=4928, 3205] off a retroviral vector at 3 days after transduction.	10	0.0552	3.74E-08
BENNETT_SYSTEMIC_LUPUS_ERYTHEMATOSUS	23	Genes significantly up-regulated in the blood mononuclear cells from patients with systemic lupus erythematosus compared to those from healthy persons.	5	0.2174	1.09E-07
MARTORIATI_MDM4_TARGETS_FETAL_LIVER_UP	120	Genes up-regulated in non-apoptotic tissues (fetal liver) after MDM4 [Gene ID=4194] knockout.	8	0.0667	2.17E-07
EINAV_INTERFERON_SIGNATURE_IN_CANCER	27	A gene expression signature found in a subset of cancer patients suggestive of a deregulated immune or inflammatory response.	5	0.1852	2.57E-07
MOSERLE_IFNA_RESPONSE	30	Top 50 genes up-regulated in ovarian cancer progenitor cells (also known as side population, SP, cells) in response to interferon alpha (IFNA).	5	0.1667	4.47E-07
TSAI_DNAJB4_TARGETS_UP	13	Genes up-regulated in CL1-5 cells (lung cancer) overexpressing DNAJB4 [Gene ID=11080] off a plasmid vector.	4	0.3077	4.78E-07
JISON_SICKLE_CELL_DISEASE_UP	183	Genes up-regulated in peripheral blood mononuclear cells (PBMC) from sickle cell disease patients compared to those from healthy subjects.	9	0.0492	4.95E-07
NUYTTEN_EZH2_TARGETS_UP	974	Genes up-regulated in PC3 cells (prostate cancer) after knockdown of EZH2 [Gene ID=2146] by RNAi.	19	0.0195	6.44E-07

Table 1 Top 10 genesets of the MSigDB C2 category showing enrichment in Notch targets.

4.8 Chapter summary

Contrary to the initial hypothesis, Notch signalling does not promote a less differentiated state, although it does reduce pigment levels in vivo. In addition, driving Notch signalling is not sufficient to increase motility in the B16 melanoma model. This implies that Notch does not maintain cells in a less differentiated state to promote motility. As Notch has been found to correlate with motility, it is possible that the signalling/state that induces motility in vivo also increases Notch signalling. The decrease in pigment observed in motile cells (Pinner et al., 2009) may be driven by the co-increase in Notch signalling.

Cells with active Notch signalling increase metastasis to the lymph node in a non-cell autonomous manner. Primary tumours containing a mix of NICD and control cells showed increased metastasis and the cells that arrived in the lymph node were both NICD and control cells. Analysis of the microenvironment confirmed that NICD cells could influence vascular phenotype and therefore potentially increase metastasis through effects on the endothelium. Experimental lung metastasis assays showed that cells with active Notch signalling were favoured in lung colonisation. An increase in Notch signalling may not affect the motility of cells in the primary tumour, but it is beneficial for later stages of the metastatic cascade.

Notch target genes in B16 F2 melanoma cells were identified by microarray analysis. This provided a number of potential regulators of the increased lung colonisation displayed by B16 F2 NICD-GFP cells, including Stat signalling, MYLK and VEGF-B. Increased VEGF-B production by B16 F2 NICD-GFP cells may also explain the vascular phenotype seen in tumours containing these cells.

Chapter 5. Gene expression analysis to identify novel genes associated with B16 F2 melanoma motility

5.1 Chapter introduction

The metastatic cascade begins with the acquisition of motility and local cancer cell invasion in the primary tumour. The motile cells as observed by intra-vital imaging are thought to be those that subsequently leave the primary tumour and form metastases. To try to identify novel genes associated with melanoma motility, cells with high levels of Brn2 promoter activity and Notch signalling, both pathways associated with motility, were purified and their patterns of gene expression analysed. Genes identified in this way may provide fresh ways of targeting cancer cell invasion and metastasis.

5.2 Identification of genes up-regulated in populations enriched for motile cells

Data in chapter 3 and previous data showed that the clonal B16 Notch reporter and Brn2 promoter activity in a Brn2 reporter cell-line (Pinner et al., 2009) correlated with B16 F2 melanoma motility in vivo. The Brn2 promoter reporter was generated using the sequence between about -2.5 kb and -520 upstream of the ATG initiator codon of the human *Brn2* gene, upstream of eGFP (Goodall et al., 2004). Therefore eGFP expression in the Brn2 reporter cells indicated cells with active Brn2 promoter expression. Re-analysis of the Notch reporter data showed that cells in the top quartile of Notch reporter intensity were significantly enriched for motile cells compared to cells in the lowest quartile of Notch reporter intensity (Figure 5.1A). The data collected from the Brn2 reporter cell-line presented in Pinner et al (Pinner et al., 2009) was also re-analysed and showed a significant enrichment of motile cells in the top quartile of Brn2 promoter reporter intensity (Figure 5.1A). Therefore, FACS sorting of these reporters to purify the GFP high population in each case, i.e Notch high and Brn2 promoter high, should purify a

population enriched for motile cells. To try to identify novel genes that regulate motility, the GFP high and GFP low populations from the two reporter cell-lines were subjected to microarray analysis.

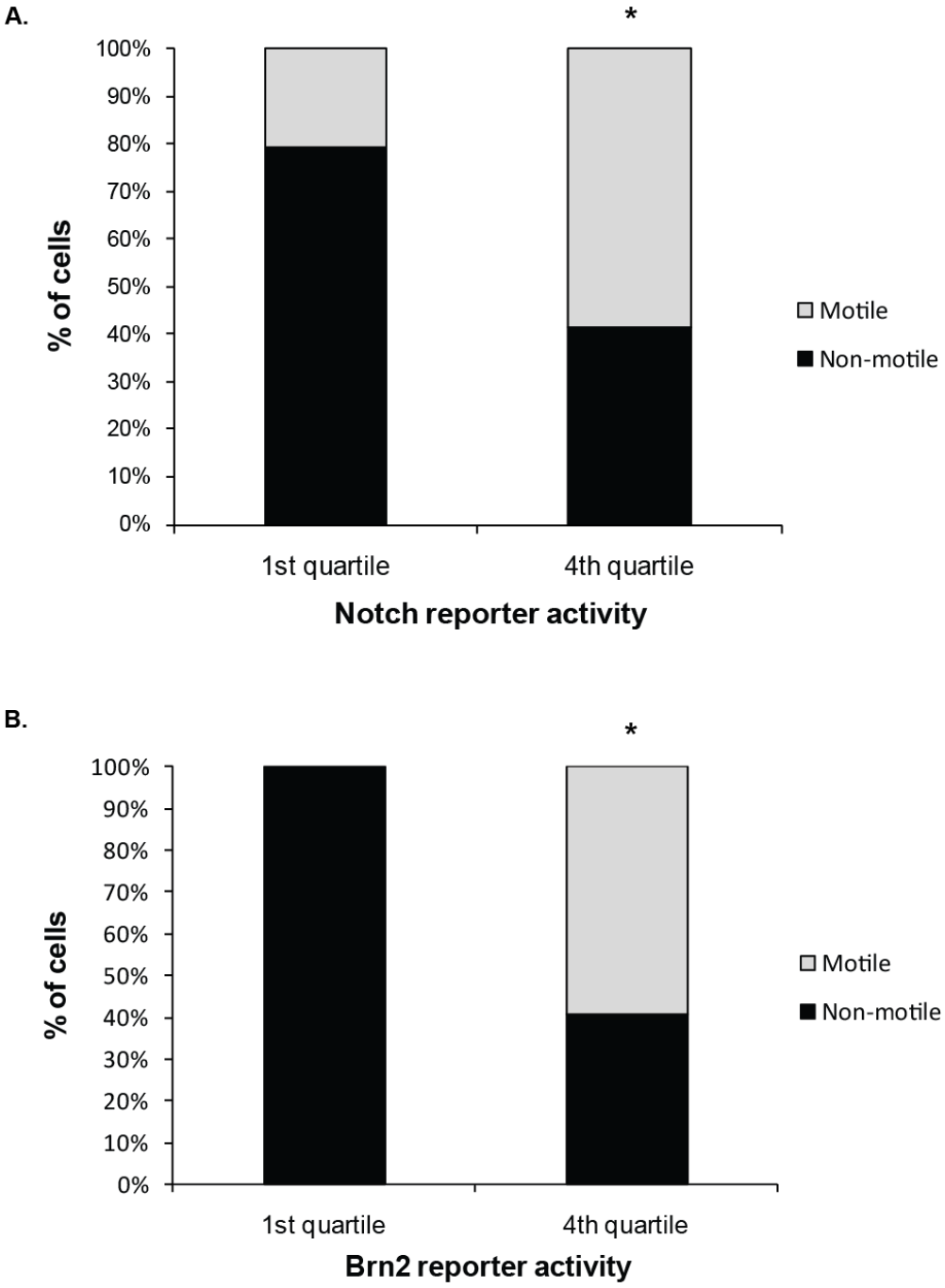

Figure 5.1. Notch reporter high and Brn2 promoter reporter high cells are enriched for motile cells.

Graph showing percentage of non-motile and motile cells in the top and bottom quartile of cells based on A. Notch reporter activity. Re-analysis of data in Figure 3.7. (Data from 9 movies of 4 mice) and B. Brn2 promoter reporter activity. Data from Pinner et al. Cells were categorised as motile or non-motile and their Notch reporter GFP intensity measured. Background GFP intensity subtracted from cellular GFP intensity before normalising to the average GFP for the image. Star indicates statistical difference in Fischer's exact test.

5.2.1 Purification and microarray analysis of B16 F2 melanoma cells with high Brn2 promoter reporter activity

The B16 Brn2 promoter reporter cell-line (Pinner et al., 2009) was injected sub-cutaneously into C57Black6 mice. When the tumours reached around 0.8 cm in diameter, the mouse was sacrificed, the tumour excised and fully digested in a Collagenase dispase solution. The tumour digest was prepared into a single cell suspension and filtered numerous times before FACS sorting to purify the GFP high, high Brn2 promoter activity and GFP low, low Brn2 promoter activity populations (Figure 5.2). The melanoma cells were distinguished from the stromal cells by a red fluorescent membrane marker. RNA purified from two tumour samples was sent off for microarray to analyse gene expression differences between the high Brn2 promoter activity and low Brn2 promoter activity populations.

Genes up-regulated in the high Brn2 promoter activity population were identified and can be found in the appendix. To analyse these genes, geneset enrichment analysis was performed. This utilised free software from The Broad Institute and a public database of genesets (MSigDB). Over 3000 genesets from the C2 collection of the MSigDB were queried against the Brn2 reporter microarray. The C2 collection contains curated genesets from online pathway databases, PubMed publications and knowledge of domain experts.

The top 20 genesets overlapping with the high Brn2 promoter activity gene list are shown in Table 2. Within the top 10 were 2 genesets that correlated with the grade or outcome of cancer. The second most significant geneset was genes up-regulated in the more aggressive and metastatic grade 3 breast cancer versus grade 1 (Table 2). Geneset 8 comprised of genes that were up-regulated in melanoma patients that went on to develop metastases within 4 years compared to patients whose melanoma did not spread (Table 2). A number of other genesets outside of the top 20, but still showing significant overlap, were also associated with disease recurrence or metastasis. This supports the notion that the high Brn2 promoter activity population of cells is enriched for the more motile, more metastatic cells and also suggests that the genes up-regulated in this population

may have relevance outside of melanoma. The geneset showing the most significant overlap was that containing genes associated with proliferation in cervical cancer. In addition, a geneset containing genes associated with pro-metaphase showed significant overlap with genes up-regulated in the high Brn2 promoter activity population. On examination of the genes up-regulated in the high Brn2 promoter activity population, a number of cell-cycle regulators and genes involved in mitotic progression and cytokinesis were identified. This may suggest a link between the cell cycle and cell motility.

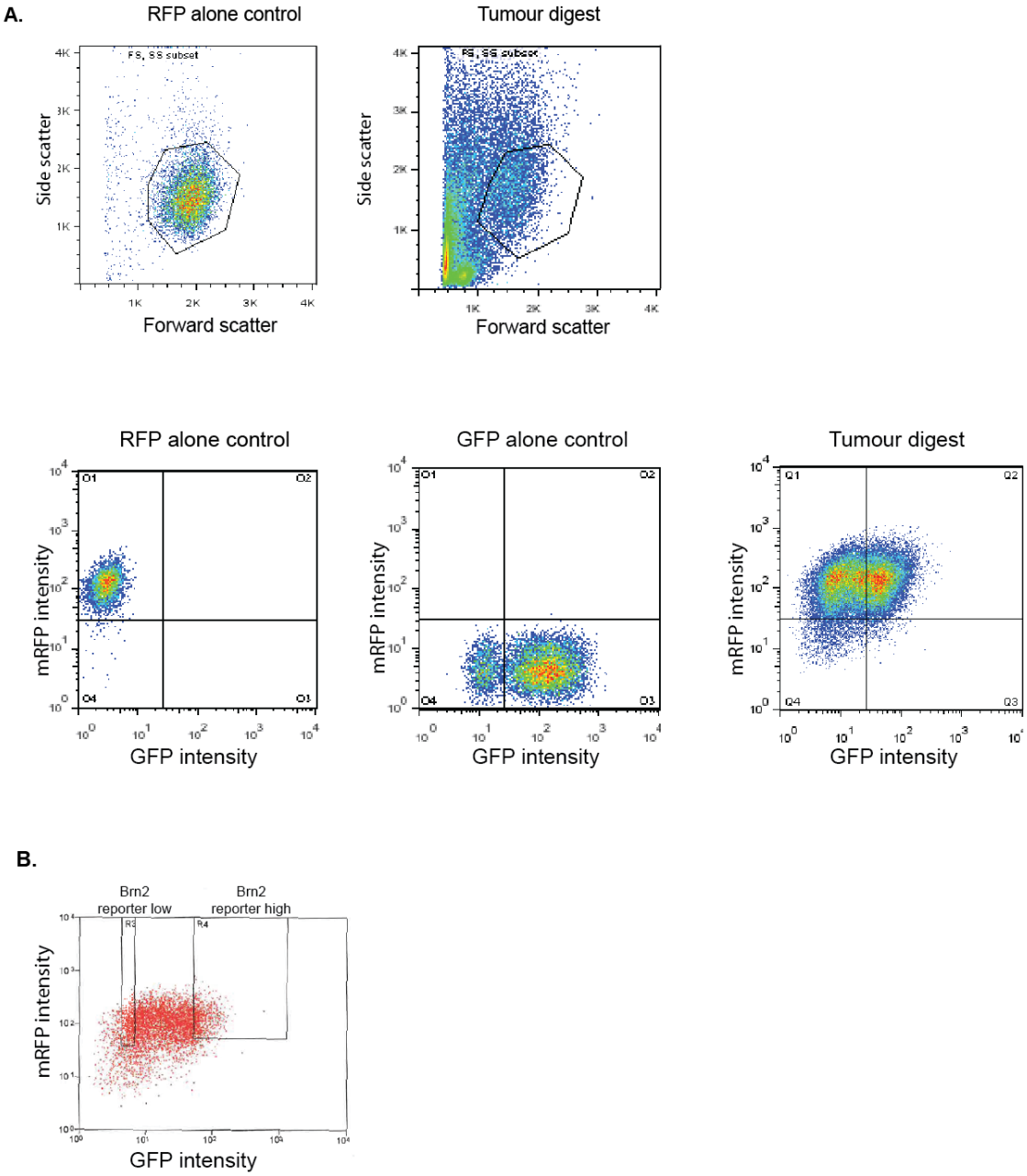

Figure 5.2. Purification of the high Brn2 promoter activity population in B16 F2 melanoma.

B16 Brn2 promoter reporter tumours were digested into a single cell suspension and subjected to FACS sorting. FACS plots were generated after sorting. A. B16 melanoma cells with a mRFP membrane label grown in vitro were used to gate around cells in the tumour with forward and side scatter characteristics of B16 cells. mRFP and GFP labelled B16 melanoma cells were used to identify mRFP positive cells from the tumours and identify the Brn2:GFP high and low populations. B. FACS plot showing the gates used to purify the Brn2:GFP high and low populations.

NAME	Number of genes in geneset	Enrichment score	Normalised enrichment score	p-value	FDR
ROSTY_CERVICAL_CANCER_PROLIFERATION_CLUSTER	118	0.71	3.11	0	0
SOTIRIOU_BREAST_CANCER_GRADE_1_VS_3_UP	115	0.69	2.93	0	0
KOBAYASHI_EGFR_SIGNALING_24HR_DN	217	0.62	2.88	0	0
MORI_IMMATURE_B_LYMPHOCYTE_DN	45	0.79	2.83	0	0
HOFFMANN_LARGE_TO_SMALL_PRE_BII_LYMPHOCYTE_UP	89	0.69	2.81	0	0
CROONQUIST_NRAS_SIGNALING_DN	56	0.74	2.80	0	0
WINNEPENNINCKX_MELANOMA_METASTASIS_UP	130	0.64	2.80	0	0
MORI_LARGE_PRE_BII_LYMPHOCYTE_UP	46	0.76	2.77	0	0
KANG_DOXORUBICIN_RESISTANCE_UP	41	0.77	2.73	0	0
LEE_EARLY_T_LYMPHOCYTE_UP	61	0.72	2.70	0	0
PUJANA_XPRSS_INT_NETWORK	135	0.60	2.67	0	0
REACTOME_MITOTIC_PROMETAPHASE	80	0.66	2.66	0	0
FURUKAWA_DUSP6_TARGETS_PCI35_DN	57	0.69	2.61	0	0
MOLENAAR_TARGETS_OF_CCND1_AND_CDK4_DN	44	0.73	2.56	0	0
CROONQUIST_IL6_DEPRIVATION_DN	69	0.65	2.55	0	0
ZHAN_MULTIPLE_MYELOMA_PR_UP	35	0.76	2.55	0	0
WHITEFORD_PEDIATRIC_CANCER_MARKERS	80	0.63	2.55	0	0
CHANG_CYCLING_GENES	38	0.73	2.54	0	0
FARMER_BREAST_CANCER_CLUSTER_2	31	0.76	2.52	0	0

Table 2. Top 20 genesets from the MSigDB C2 collection showing significant overlap with genes up-regulated in high Brn2 promoter activity population.

5.2.2 Purification and microarray analysis of B16 F2 melanoma cells with high Notch reporter activity

The Notch reporter high population, which is enriched for motile cells, is small in vivo (Figure 3.6). Therefore the B16 clonal Notch reporter cells were grown in vitro before FACS sorting to collect the GFP high, Notch reporter high cells and GFP low, Notch reporter low cells (Figure 5.3). RNA purified from one sample was sent off for microarray to analyse gene expression differences between the Notch reporter high and Notch reporter low populations. Genes up-regulated in the Notch reporter high population were identified and can be found in the appendix.

In a similar manner to analysis of the high Brn2 promoter activity population, geneset enrichment analysis was used to analyse the genes up-regulated in the Notch reporter high population. The top 20 genesets overlapping with the Notch reporter high list are shown in Table 3. Within the top 20 were a number of genesets containing genes associated with proliferation or genes encoding for cell cycle regulators and components. This included the "REACTOME MITOTIC PROMETAPHASE" geneset which contains genes encoding for components required for pro-metaphase and also showed significant overlap with genes up-regulated in the Brn2 reporter high population. However, to test whether the Notch reporter high cells had a different cell-cycle profile to the Notch reporter low population, which may influence the expression analysis, the Notch reporter cell-line was subject to DNA content analysis by flow cytometry. Gating on the Notch reporter high and low populations showed little difference in the DNA profiles between the two populations (Figure 5.4). Therefore the enrichment of cell cycle associated genes in the Notch reporter high population is unlikely due to differences in cell cycle status between the high and low populations.

The geneset containing genes up-regulated in the more aggressive grade 3 breast cancer versus grade 1 breast cancer, which overlapped with the high Brn2 promoter activity population, also showed significant overlap with the genes up-regulated in the Notch reporter high population (Table 3). In addition, genes up-regulated in invasive breast cancer compared to normal tissue were also enriched in the Notch reporter high population. These genes were not enriched in the high

Brn2 promoter activity population suggesting they may show specific co-regulation with Notch signalling rather than co-regulation with motility.

Other genesets, not in the top 20 but also showing significant overlap, included genes up-regulated on breast cancer cell EMT and genes up-regulated in melanoma patients that had distant metastasis within 4 years compared to patients that did not. Both of these genesets also showed significant overlap with genes up-regulated in the high Brn2 promoter activity population. This supports the notion that the Notch reporter high population is enriched for more motile, more metastatic cells. Other interesting genesets that overlapped with genes up-regulated in the Notch high population included EGR2 targets and B-Myb targets. Both of these genesets showed significant overlap with genes up-regulated in the high Brn2 promoter activity population suggesting that these signalling pathways may regulate or be co-regulated with motility in melanoma.

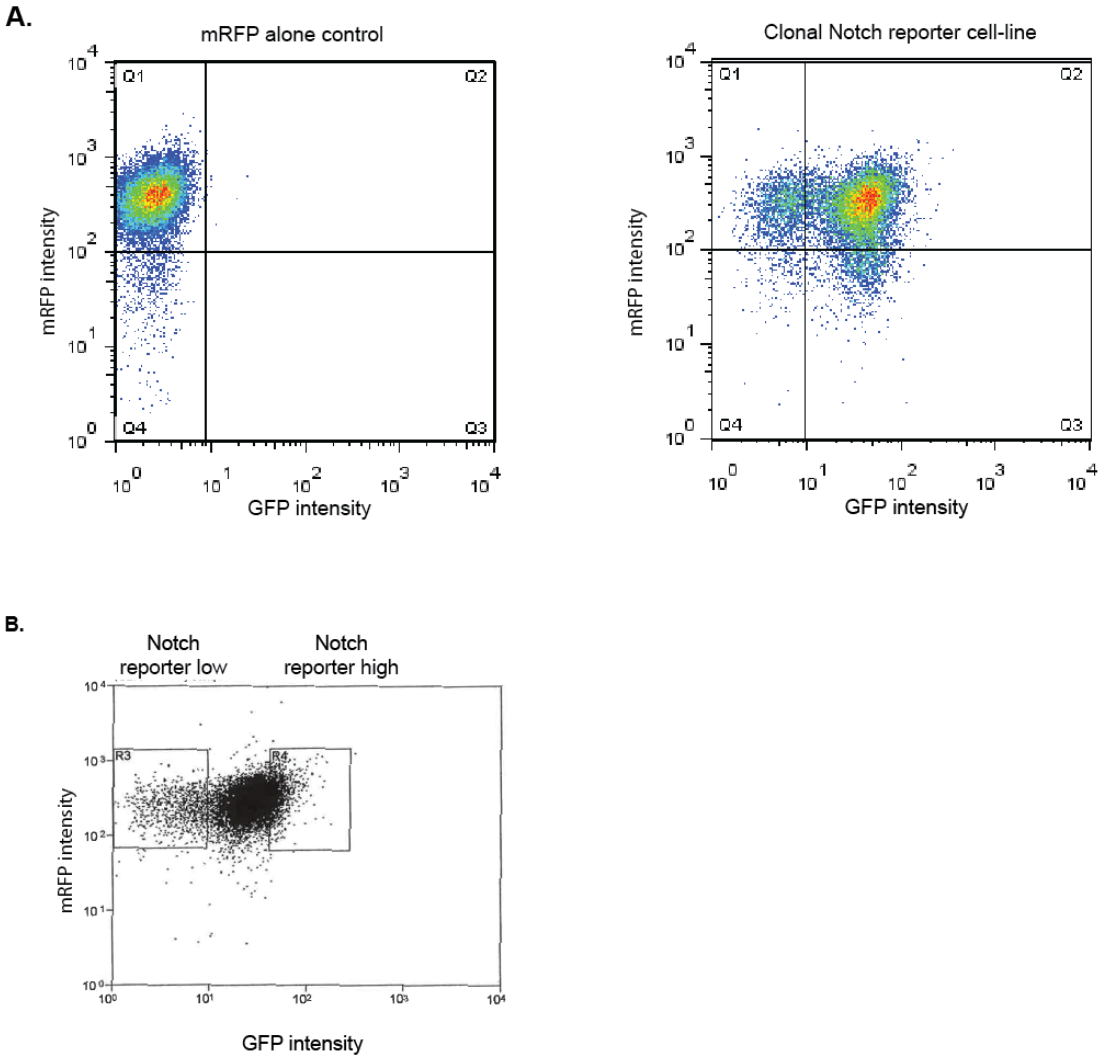

Figure 5.3. Purification of the Notch reporter high population in B16 F2 melanoma.

B16 F2 Notch reporter cells were grown in vitro and subjected to FACS sorting. FACS plots were generated after sorting. A. B16 melanoma cells with a mRFP membrane label were used to identify the mRFP positive cells and helped indicate the GFP negative population. B. FACS plot showing the gates used to purify the Notch reporter high and low populations.

NAME	Number of genes in geneset	Enrichment score	Normalised enrichment score	p-value	FDR
HOFFMANN_LARGE_TO_SMALL_PRE_BII_LYMPHOCYTE_UP	63	0.69	2.73	0	0
ROSTY_CERVICAL_CANCER_PROLIFERATION_CLUSTER	76	0.61	2.44	0	0
CROONQUIST_NRAS_SIGNALING_DN	39	0.69	2.43	0	0
ZHAN_MULTIPLE_MYELOMA_PR_UP	20	0.80	2.40	0	0
SHEPARD_CRUSH_AND_BURN_MUTANT_DN	49	0.63	2.36	0	2.22E-04
CROONQUIST_IL6_DEPRIVATION_DN	43	0.65	2.32	0	3.64E-04
REACTOME_MITOTIC_PROMETAPHASE	55	0.62	2.32	0	3.12E-04
NAKAYAMA_SOFT_TISSUE_TUMORS_PCA2_UP	27	0.71	2.30	0	2.73E-04
FRASOR_RESPONSE_TO_SERM_OR_FULVESTRANT_DN	28	0.70	2.30	0	2.43E-04
LE_EGR2_TARGETS_UP	58	0.60	2.26	0	2.19E-04
CROONQUIST_NRAS_VS_STROMAL_STIMULATION_DN	31	0.66	2.26	0	1.99E-04
MORI_IMMATURE_B_LYMPHOCYTE_DN	35	0.65	2.24	0	1.82E-04
SCIAN_CELL_CYCLE_TARGETS_OF_TP53_AND_TP73_DN	16	0.78	2.21	0	4.22E-04
SOTIRIOU_BREAST_CANCER_GRADE_1_VS_3_UP	72	0.54	2.21	0	4.72E-04
MOLENAAR_TARGETS_OF_CCND1_AND_CDK4_DN	23	0.70	2.21	0	4.41E-04
GRAHAM_CML_QUIESCENT_VS_NORMAL_QUIESCENT_UP	28	0.67	2.20	0	4.83E-04
AMUNDSON_GAMMA_RADIATION_RESPONSE	15	0.79	2.19	0	4.55E-04
LY_AGING_MIDDLE_DN	12	0.86	2.18	0	4.29E-04
POOLA_INVASIVE_BREAST_CANCER_UP	63	0.56	2.17	0	5.24E-04

Table 3. Top 20 genesets from the MSigDB C2 collection showing significant overlap with genes up-regulated in the Notch reporter high population.

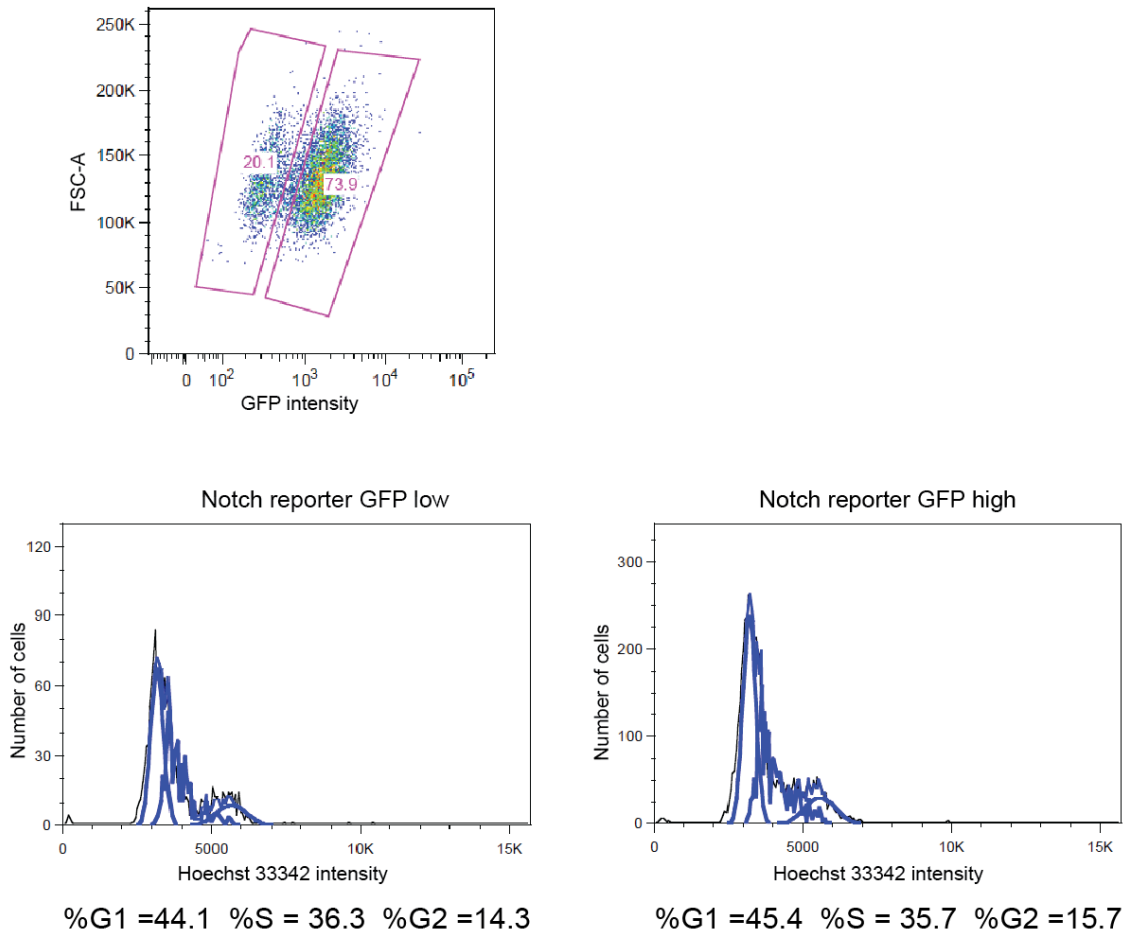

Figure 5.4. Notch reporter high and low populations have similar cell cycle profiles.

B16 F2 clonal Notch reporter cell-line was grown in vitro and stained with 10 µg/ml Hoechst 33342 for 45 minutes at 37 °C. Cells were subject to flow cytometry analysis and gated based on the GFP intensity of the Notch reporter as shown in the upper plot. Lower plots show raw DNA staining intensity data in the black line. Overlaid blue lines show FlowJo predictions for G0/G1, S and G2/M phases of cell cycle.

5.2.3 Genes up-regulated in the Notch high and high Brn2 promoter activity populations show significant overlap

There were a number of genesets that showed significant overlap with both the high Brn2 promoter activity population and the Notch reporter high population. As both populations should be enriched for motile cells, a certain degree of overlap between the two populations is expected. Geneset enrichment analysis was used to test if the genes up-regulated in the Notch reporter high population were significantly enriched in the high Brn2 promoter activity population and vice versa. This indeed showed that genes up-regulated by greater than 1.2 fold in the Notch reporter high population were significantly enriched in the high Brn2 promoter activity population, with a p-value of 0 (Figure 5.5A). Genes up-regulated on average greater than 1.2 fold in the high Brn2 promoter activity population were also significantly enriched in the Notch reporter high population again with a p-value of 0 (Figure 5.5B). This indicates a very high degree of overlap between the two populations consistent with the fact that they are both enriched for motile cells. However, it may be that the high Brn2 promoter activity population also shows high Notch signalling or vice versa. To try and address this, geneset enrichment analysis was used to test whether Notch target genes, as determined in the previous chapter, were enriched in the high Brn2 promoter activity population. There was no significant enrichment of Notch targets in the high Brn2 promoter activity population (Figure 5.6) signifying that the high Brn2 promoter activity population does not show high Notch signalling. Therefore, the overlap in gene expression between the two populations is likely to suggest a similar phenotype between the two populations and is consistent with them both being enriched for motile cells. Although the Notch reporter high cell population was purified in vitro and only one sample was used, the considerable overlap between the two populations increases my confidence in using this approach to identify novel genes associated with melanoma motility. Another sample is being prepared for the Notch reporter high and low populations to further increase the robustness of the approach.

A. Array data: Brn2 promoter reporter

Geneset: Genes upregulated >1.2 x in Notch reporter high population

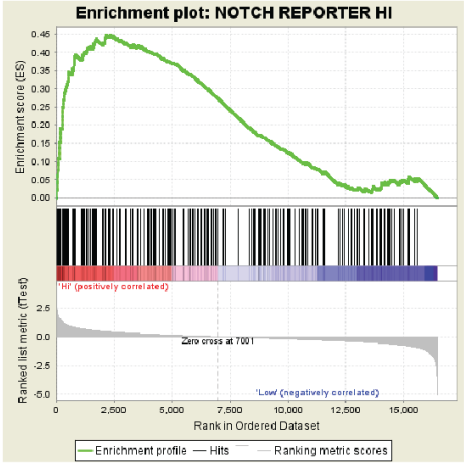

Enrichment of Notch reporter high genes in high Brn2 promoter activity population p-value = 0

B. Array data: Notch reporter

Geneset: Genes upregulated on average >1.2 x in high Brn2 promoter activity population

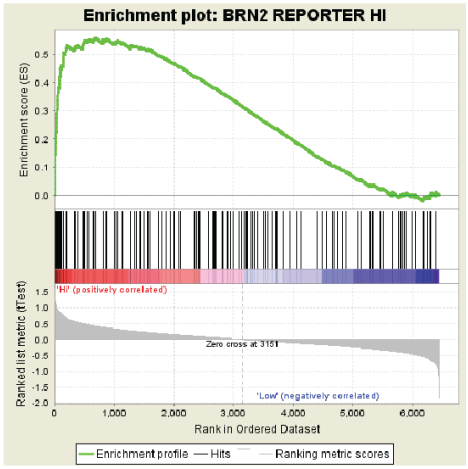

Enrichment of Brn2 promoter reporter high genes in the Notch reporter high population p-value = 0

Figure 5.5. Geneset enrichment analysis shows significant overlap between the Brn2 reporter high and Notch reporter high populations.

Geneset enrichment analysis using free-ware from The Broad Institute. A. Genes up-regulated in the Notch reporter high population by greater than 1.2 fold are significantly enriched in the high Brn2 promoter activity population. B. Genes up-regulated in the high Brn2 promoter activity population on average by greater than 1.2 fold are significantly enriched in the Notch reporter high population.

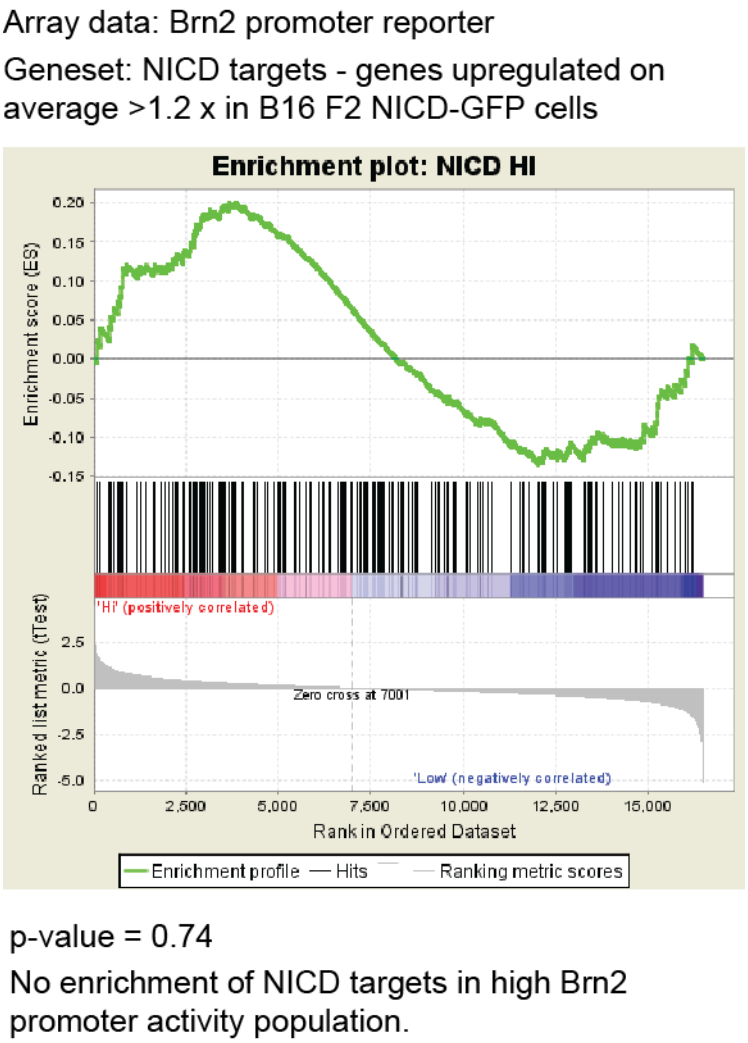

Figure 5.6. No enrichment of Notch targets in high Brn2 promoter activity population.

Geneset enrichment analysis using free-ware from The Broad Institute. Notch targets, as determined by an average 1.2 fold increase or greater on expression of NICD-GFP, are not enriched in the high Brn2 promoter activity population.

5.2.4 Identification of common genes up-regulated in the populations enriched for motile cells

Genes up-regulated in both the Notch reporter high and high Brn2 promoter activity populations are likely to be associated with motility as both populations are enriched for motile cells. Lists of genes up-regulated in these two populations were compared and overlapping genes identified (Figure 5.7). These overlapping genes, up-regulated in both the Notch high and high Brn2 promoter activity populations, were postulated to be bona fide genes up-regulated in the motile cell population in B16 melanoma (Table 4). For simplicity these genes will now be referred to as genes up-regulated in the motile B16 population, although formally are up-regulated in the B16 population enriched for motile cells.

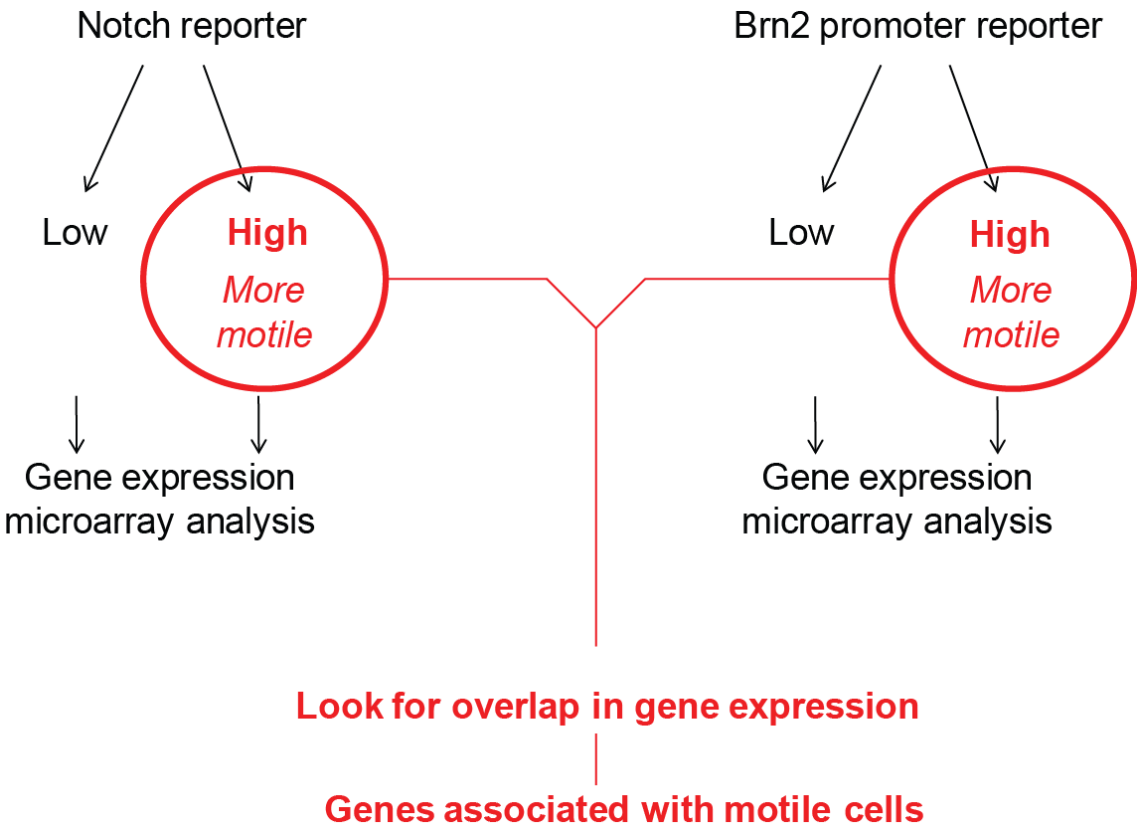

Figure 5.7. Approach to identify novel genes associated with motile cells in B16 F2 melanoma.

Schematic showing experimental approach to purify B16 F2 population enriched for motile cells and to identify novel genes associated with motility.

Symbol	Genename
2610039C10RIK	*RIKEN cDNA 2610039C10 gene*
4930432O21RIK	*NA*
6330503K22RIK	*RIKEN cDNA 6330503K22 gene*
Ada	*Adenosine deaminase*
Adh7	*Alcohol dehydrogenase 7 (class IV), mu or sigma polypeptide*
Anln	*Anillin, actin binding protein*
Aurka	*Aurora kinase A*
Blm	*Bloom syndrome homolog (human)*
Bub1b	*Budding uninhibited by benzimidazoles 1 homolog, beta (S. cerevisiae)*
Bub3	*Budding uninhibited by benzimidazoles 3 homolog (S. cerevisiae)*
Cacnb4	*Calcium channel, voltage-dependent, beta 4 subunit*
Casp7	*Caspase 7*
Ccl5	*Chemokine (C-C motif) ligand 5*
Ccnb1	*Cyclin B1*
Ccng1	*Cyclin G1*
Cdc20	*Cell division cycle 20 homolog (S. cerevisiae)*
Cdca2	*Cell division cycle associated 2*
Cdca4	*Cell division cycle associated 4*
Cdca5	*Cell division cycle associated 5*
Cdca8	*Cell division cycle associated 8*
Cdkn2c	*Cyclin-dependent kinase inhibitor 2C (p18, inhibits CDK4)*
Cetn4	*Centrin 4*
Chkb	*Choline kinase beta*
Clspn	*Claspin homolog (Xenopus laevis)*
Dbf4	*DBF4 homolog (S. cerevisiae)*
Dcxr	*Dicarbonyl L-xylulose reductase*

Table .4

Symbol	Genename
Ddit4l	*DNA-damage-inducible transcript 4-like*
Depdc1b	*DEP domain containing 1B*
Depdc6	*DEP domain containing 6*
E130306d19rik	*RIKEN cDNA E130306D19 gene*
E2f2	*E2F transcription factor 2*
Ecm1	*Extracellular matrix protein 1*
Esco2	*Establishment of cohesion 1 homolog 2 (S. cerevisiae)*
Espl1	*Extra spindle poles-like 1 (S. cerevisiae)*
Fen1	*Flap structure specific endonuclease 1*
Gbp2	*Guanylate binding protein 2*
Gpatch2	*G patch domain containing 2*
Gsg2	*Germ cell-specific gene 2*
Gtse1	*G two S phase expressed protein 1*
Ifit2	*Interferon-induced protein with tetratricopeptide repeats 2*
Incenp	*Inner centromere protein*
Irf1	*Interferon regulatory factor 1*
Kif11	*Kinesin family member 11*
Kif22	*Kinesin family member 22*
Kif23	*Kinesin family member 23*
Kif2c	*Kinesin family member 2C*
Kif4	*Kinesin family member 4*
Mlf1	*Myeloid leukemia factor 1*
Mpp5	*Membrane protein, palmitoylated 5 (MAGUK p55 subfamily member 5)*
Mtap2	*Microtubule-associated protein 2*
Mxd3	*Max dimerization protein 3*
Ncapd3	*Non-SMC condensin II complex, subunit D3*
Ncaph	*Non-SMC condensin I complex, subunit H*

Table 4.

Symbol	Genename
Ndc80	*NDC80 homolog, kinetochore complex component (S. cerevisiae)*
Nde1	*Nuclear distribution gene E homolog 1 (A nidulans)*
Nup107	*Nucleoporin 107*
Nusap1	*Nucleolar and spindle associated protein 1*
Parp3	*Poly (ADP-ribose) polymerase family, member 3*
Polh	*Polymerase (DNA directed), eta (RAD 30 related)*
Prc1	*Protein regulator of cytokinesis 1*
Ptplad2	*Protein tyrosine phosphatase-like A domain containing 2*
Rad51ap1	*RAD51 associated protein 1*
Rad54l	*RAD54 like (S. cerevisiae)*
Rbms1	*RNA binding motif, single stranded interacting protein 1*
Rdh5	*Retinol dehydrogenase 5*
Rfwd3	*Ring finger and WD repeat domain 3*
Serf2	*Small EDRK-rich factor 2*
Sfrs3	*Splicing factor, arginine/serine-rich 3 (SRp20)*
Sgol1	*Shugoshin-like 1 (S. pombe)*
Slc22a18	*Solute carrier family 22 (organic cation transporter), member 18*
Stk17b	*Serine/threonine kinase 17b (apoptosis-inducing)*
Tk1	*Thymidine kinase 1*
Top2a	*Topoisomerase (DNA) II alpha*
Zcchc8	*Zinc finger, CCHC domain containing 8*
Zfp41	*Zinc finger protein 41*

Table 4. Genes up-regulated by >1.2 fold in both the B16 Notch reporter high and high Brn2 promoter activity populations.

5.3 Bioinformatic analysis to identify potential regulators of the genes up-regulated in the motile B16 F2 population

Gene ontology (GO) analysis of the genes up-regulated in the B16 F2 population enriched for motile cells was performed using The Broad Institute's MSig Database. The overlap between known genesets of GO biological processes, cellular components and molecular function, was calculated with the geneset consisting of genes up-regulated in the motile B16 population. This revealed a striking association with the cell-cycle (Table 5) which had also been suggested by the genes up-regulated in the Notch reporter high population and also to a certain extent the high Brn2 promoter activity population. The genesets were sorted according to statistical significance of the overlap and the top 7 genesets were all cell cycle processes. The remainder of genesets in the top 20 were a mix of more cell cycle processes and components required for the cell-cycle. This included the two cellular component genesets "microtubule_cytoskeleton" and "cytoskeleton_part", indicating that, as you might expect, cytoskeletal components are up-regulated in motile cells. The genes from these genesets that were up-regulated in the motile B16 population included *Anln*, an actin binding protein, and a number of *kinesins*, including *Kif2c*. The human homologs, of *Kif2c* and *Anln*, have been found to correlate with poor survival in breast cancer (Sadi et al., 2011) suggesting that these genes might have a wider relevance to cancer metastasis.

The list of genes up-regulated in the motile B16 population was surprising and did not reveal any obvious pathways associated with cell motility. To try and address this, geneset enrichment analysis was used to query a public database of over 3000 genesets for significant overlap with the genes up-regulated in the motile B16 population. The aim was to identify potential regulators of B16 melanoma cell motility. The 30 genesets with the most significant overlap are shown in Table 6.

Gene set name	# of genes in geneset	# of genes in overlap	Fraction overlap	p-value
Cell_Cycle_Process	188	16	0.0851	1.24E-12
Cell_Cycle_Go_0007049	306	19	0.0621	1.99E-12
Mitotic_Cell_Cycle	148	14	0.0946	9.02E-12
Cell_Cycle_Phase	168	13	0.0774	6.85E-10
Mitosis	81	10	0.1235	7.91E-10
M_Phase_Of_Mitotic_Cell_Cycle	83	10	0.1205	1.01E-09
M_Phase	112	11	0.0982	1.28E-09
Spindle	37	7	0.1892	1.51E-08
Chromosome_Segregation	31	6	0.1935	1.49E-07
Microtubule_Cytoskeleton	148	10	0.0676	2.80E-07
Chromosome_Condensation	10	4	0.4	8.28E-07
Cytoskeletal_Part	231	11	0.0476	2.25E-06
Microtubule_Motor_Activity	16	4	0.25	6.92E-06
Mitotic_Sister_Chromatid_Segregation	16	4	0.25	6.92E-06
Microtubule_Cytoskeleton_Organization_And_Biogenesis	34	5	0.1471	7.29E-06
Sister_Chromatid_Segregation	17	4	0.2353	8.99E-06
Cytokinesis	19	4	0.2105	1.45E-05
Cell_Division	21	4	0.1905	2.21E-05
Mitotic_Spindle_Organization_And_Biogenesis	9	3	0.3333	4.25E-05
Spindle_Organization_And_Biogenesis	10	3	0.3	6.03E-05

Table 5. GO analysis of genes up-regulated in the motile B16 population.

Top 20 GO genesets showing overlap with genes up-regulated in the motile B16 F2 population. Genesets sorted based on statistical significance of the overlap (see last column).

Rank	Geneset Name	# total Genes (K)	Description	# Genes in Overlap (k)	k/K	p value
1	DODD_NASOPHARYNGEAL_CARCINOMA_DN	1375	Genes down-regulated in nasopharyngeal carcinoma (NPC) compared to the normal tissue.	28	0.0204	0.00E+00
2	KINSEY_TARGETS_OF_EWSR1_FLI1_FUSION_UP	1281	Genes up-regulated in TC71 and EWS502 cells (Ewing's sarcoma) upon knockdown of the EWSR1-FLI1 fusion [Gene ID=2130, 2314].	30	0.0234	0.00E+00
3	NUYTTEN_EZH2_TARGETS_DN	915	Genes down-regulated in PC3 cells (prostate cancer) after knockdown of EZH2 [Gene ID=2146] by RNAi.	24	0.0262	0.00E+00
4	BENPORATH_CYCLING_GENES	648	Genes showing cell-cycle stage-specific expression [PMID=12058064].	26	0.0401	0.00E+00
5	SHEDDEN_LUNG_CANCER_POOR_SURVIVAL_A6	459	Cluster 6 of method A: up-regulation of these genes in patients with non??small cell lung cancer (NSCLC) predicts poor survival outcome.	20	0.0436	0.00E+00
6	BERENJENO_TRANSFORMED_BY_RHOA_UP	568	Genes up-regulated in NIH3T3 cells (fibroblasts) transformed by expression of contitutively active (Q63L) form of RHOA [Gene ID=387] off plasmid vector.	25	0.044	0.00E+00
7	PUJANA_BRCA2_PCC_NETWORK	432	Genes constituting the BRCA2-PCC network of transcripts whose expression positively correlated (Pearson correlation coefficient, PCC >= 0.4) with that of BRCA2 [Gene ID=675] across a compendium of normal tissues.	21	0.0486	0.00E+00
8	GOLDRATH_ANTIGEN_RESPONSE	405	Genes up-regulated at the peak of an antigen response of naive CD8+ [Gene ID=925, 926] T-cells.	21	0.0519	0.00E+00
9	BLUM_RESPONSE_TO_SALIRASIB_DN	343	Selected genes down-regulated in response to the Ras inhibitor salirasib [PubChem=54693318] in a panel of cancer cell lines with constantly active HRAS [Gene ID=3265].	18	0.0525	0.00E+00
10	HORIUCHI_WTAP_TARGETS_DN	308	Genes down-regulated in primary endothelial cells (HUVEC) after knockdown of WTAP [Gene ID=9589] by RNAi.	20	0.0649	0.00E+00
11	KOBAYASHI_EGFR_SIGNALING_24HR_DN	252	Genes down-regulated in H1975 cells (non-small cell lung cancer, NSCLC) resistant to gefitinib [PubChem=123631] after treatment with EGFR inhibitor CL-387785 [PubChem=2776] for 24h.	22	0.0873	0.00E+00
12	SOTIRIOU_BREAST_CANCER_GRADE_1_VS_3_UP	153	Up-regulated genes whose expression correlated with histologic grade of invasive breast cancer tumors: comparison of grade 1 vs grade 3.	15	0.098	0.00E+00
13	CHIANG_LIVER_CANCER_SUBCLASS_PROLIFERATION_UP	137	Top 200 marker genes up-regulated in the 'proliferation' subclass of hepatocellular carcinoma (HCC); characterized by increased proliferation, high levels of serum AFP [Gene ID=174], and chromosomal instability.	14	0.1022	0.00E+00
14	ROSTY_CERVICAL_CANCER_PROLIFERATION_CLUSTER	140	The 'Cervical Cancer Proliferation Cluster' (CCPC): genes whose expression in cervical carcinoma positively correlates with that of the HPV E6 and E7 oncogenes; they are also differentially expressed according to disease outcome.	18	0.1286	0.00E+00
15	HOFFMANN_LARGE_TO_SMALL_PRE_BII_LYMPHOCYTE_UP	107	Genes up-regulated during differentiation from large pre-BII to small pre-BII lymphocyte.	15	0.1402	0.00E+00
16	VECCHI_GASTRIC_CANCER_EARLY_UP	434	Up-regulated genes distinguishing between early gastric cancer (EGC) and normal tissue samples.	18	0.0415	3.33E-16
17	SHEPARD_CRUSH_AND_BURN_MUTANT_DN	147	Human orthologs of genes down-regulated in the crb ('crash and burn') zebrafish mutant that represents a loss-of-function mutation in BMYB [Gene ID=4605].	13	0.0884	3.33E-16
18	LE_EGR2_TARGETS_UP	113	Genes up-regulated in P14 nerves of transgenic mice having hypomorphic (reduced function) allele of EGR2 [Gene ID=1959].	12	0.1062	5.55E-16
19	SHEPARD_BMYB_TARGETS	60	Human orthologs of BMYB [Gene ID=4605] target genes in zebra fish, identified as commonly changed in the BMYB loss of function mutant crb ('crush and burn') and after knockdown of BMYB by morpholino.	10	0.1667	1.55E-15
20	WONG_EMBRYONIC_STEM_CELL_CORE	335	The 'core ESC-like gene module' genes coordinately up-regulated in a compendium of mouse embryonic stem cells (ESC) which are shared with the human ESC-like module.	16	0.0478	1.78E-15
21	CROONQUIST_NRAS_SIGNALING_DN	62	Genes down-regulated in ANBL-6 cell line (multiple myeloma, MM) expressing a constantly active form of NRAS [Gene ID=4893] off a plasmid vector compared to those grown in the presence of IL6 [Gene ID=3569].	10	0.1613	2.22E-15
22	BASAKI_YBX1_TARGETS_UP	293	Genes up-regulated in SKOC-3 cells (ovarian cancer) after YB-1 (YBX1) [Gene ID=4904] knockdown by RNAi.	15	0.0512	5.44E-15
23	ODONNELL_TFRC_TARGETS_DN	138	Genes dpwn-regulated in P493-6 cells (B lymphocyte) upon knockdown of TFRC [Gene ID=7037] by RNAi.	12	0.087	6.44E-15
24	GRAHAM_CML_DIVIDING_VS_NORMAL_QUIESCENT_UP	187	Genes up-regulated in quiescent CD34+ [Gene ID=8842] cells isolated from peripheral blood of normal donors compared to the dividing cells from CML (chronic myeloid leukemia) patients.	13	0.0695	8.22E-15
25	REACTOME_CELL_CYCLE_MITOTIC	306	Genes involved in Cell Cycle, Mitotic	15	0.049	1.02E-14
26	KIM_WT1_TARGETS_DN	471	Genes down-regulated in UB27 cells (osteosarcoma) at any time point after inducing the expression of a mutant form of WT1 [Gene ID=7490].	17	0.0361	2.09E-14
27	CROONQUIST_IL6_DEPRIVATION_DN	80	Genes down-regulated in the ANBL-6 cell line (multiple myeloma, MM) after withdrawal of IL6 [Gene ID=3569].	10	0.125	3.23E-14
28	CASORELLI_ACUTE_PROMYELOCYTIC_LEUKEMIA_DN	670	Genes down-regulated in APL (acute promyeolocytic leukemia) blasts expressing PML-RARA fusion [Gene ID=5371, 5914] compared to normal promyeloblasts.	19	0.0284	3.65E-14
29	LEE_EARLY_T_LYMPHOCYTE_UP	82	Genes up-regulated at early stages of progenitor T lymphocyte maturation compared to the late stages.	10	0.122	4.17E-14
30	WINNEPENNINCKX_MELANOMA_METASTASIS_UP	161	Genes from the 254-gene classifier which were up-regulated in melanoma patients with a reported distant metastasis within 4 years.	12	0.0745	4.19E-14

Table 6. Top 30 genesets from MSigDB C2 showing overlap with genes up-regulated in the B16 motile population.

The geneset enrichment analysis, similar to the GO analysis, also found genesets associated with the cell cycle. However, there were also some transcriptional-based genesets identified. Interestingly, the third most significant geneset was genes regulated by EZH2 (Table 6). EZH2 is a member of the polycomb repressor 2 complex and is involved in gene silencing (Margueron and Reinberg, 2011). In embryonic stem cells it is involved in silencing genes associated with differentiation (Ezhkova et al., 2009) (Lee et al., 2006) (Boyer et al., 2006), so it may maintain B16 cells in a less differentiated, more motile state. In a similar vein, genes associated with both human and mouse embryonic stem cells were found to be enriched in the genes up-regulated in the motile B16 population (Geneset entitled "WONG EMBRYONIC STEM CELL CORE at rank 20). This provides further support for the idea that the motile cells are less differentiated.

Similar to the analysis of the Notch high and high Brn2 promoter activity populations individually, there were a number of genesets associated with poor prognosis within the top 30. This included a geneset containing genes up-regulated in melanoma patients that developed metastasis within 4 years compared to patients that did not. This provides further support for the genes up-regulated in the B16 melanoma population enriched for motile cells being associated with distant metastasis in melanoma.

Two genesets within the top 30 were B-Myb target genes (SHEPARD CRUSH AND BURN MUTANT DN and SHEPARD BMYB TARGETS). B-Myb is a transcription factor involved in cell proliferation and survival (Sala, 2005) and this analysis suggests it may also play a role in regulating B16 melanoma motility. Genes co-regulated with *Brca2* are also significantly enriched in the B16 motile cell population. Although BRCA2 is classically thought of as involved in the DNA damage response it is also known to have transcriptional activities (Scully, 2000) and so may regulate motility through transcriptional changes. *Brca2* germline mutation is also associated with increased risk of malignant melanoma (1999).

Genes up-regulated on transformation with a constitutively active RhoA Q63L plasmid were the sixth most significant geneset. RhoA is important to initiate cytoskeletal changes and the induction of contractility required for motility (Ridley

and Hall, 1992) (Takaishi et al., 1994). Although less is known about the transcriptional role of RhoA in motility, SRF, a transcription factor activated as a result of RhoA induced F-actin polymerisation, is involved in B16 melanoma motility and metastasis (Medjkane et al., 2009) (chapter 3.3.3). The publication in which the RhoA regulated geneset was identified, shows that E2F is required for RhoA induced transcriptional changes (Berenjeno et al., 2007). This is consistent with the up-regulation of E2F2 in the motile B16 cell population (Table 4).

Data in chapter three showed that SRF signalling correlates with B16 melanoma motility and in addition loss of SRF has previously been shown to decrease B16 melanoma motility in vivo (Medjkane et al., 2009). If SRF signalling is a key driver of motility in this model, then SRF target genes would be expected to show overlap with the genes up-regulated in the B16 melanoma population enriched for motile cells. To test this hypothesis, genesets were generated from genes up-regulated or down-regulated by MRTF loss in B16 F2 cells as published in Medjkane et al (Medjkane et al., 2009). Overlap analysis showed that MRTF dependent SRF targets, i.e genes down-regulated on MRTF loss, showed significant overlap with the genes up-regulated in the B16 melanoma population enriched for motile cells (Table 7). This is consistent with the data in chapter three showing that SRF signalling correlated with motility. Also, by using an independent array dataset, it provided more evidence that the list of genes generated by FACS purification of the reporter cell-lines is representative of the genes up-regulated in the motile cell population.

Geneset	Observed overlap	Expected overlap	p-value	FDR
Genes downregulated on MRTF loss	15	1.05	3.87E-014	3.61E-013
Genes upregulated on MRTF loss	0	0.38625	0.320402	0.35885

Table 7. MRTF-dependent SRF targets significantly overlap with genes up-regulated in the B16 F2 melanoma population enriched for motile cells.

5.4 Chapter summary

To identify novel genes associated with melanoma motility and metastasis, the B16 high Brn2 promoter activity and Notch reporter high populations were purified as they are enriched for motile cells. The gene expression profiles of the reporter high and low populations were compared. Genes up-regulated in either the high Brn2 promoter activity and Notch reporter high populations showed significant overlap with a number of genesets associated with disease progression and metastasis. This included a geneset containing genes up-regulated in melanoma patients that developed distant metastasis in 4 years compared to patients that did not. Genes up-regulated in the high Brn2 promoter activity and Notch reporter high populations showed significant overlap with each other, consistent with them both being enriched for genes up-regulated in the motile cell population. The individual genes overlapping between the high Brn2 promoter activity and Notch reporter high populations were identified and considered to be genes up-regulated in the B16 F2 population enriched for motile cells. Gene ontology analysis of these genes revealed a link with mitotic machinery. A non-biased geneset enrichment analysis approach revealed potential regulators of the transcriptional program associated with B16 cell motility including the polycomb protein EZH2. Further bioinformatic analysis confirmed that SRF targets showed significant overlap with genes up-regulated in the B16 F2 melanoma population enriched for motile cells. This is consistent with the data in chapter three and previous data that showed SRF regulates B16 F2 motility.

Chapter 6. PRC2 components regulate the actin cytoskeleton and metastasis

6.1 Chapter introduction

Geneset enrichment analysis of the genes up-regulated in the B16 F2 population enriched for motile cells suggested that EZH2 may regulate B16 motility, as genes positively regulated by EZH2 in prostate cancer cells were significantly enriched in genes up-regulated in the motile B16 population. EZH2 is a member of the Polycomb repressor complex 2 (PRC2) and the other core members include EZH1, Suz12 and EED. The PRC2 complex mediates gene silencing through regulation of chromatin modifications (Margueron and Reinberg, 2011) and during development it silences differentiation associated genes (Boyer et al., 2006) (Landeira et al., 2010) (Ezhkova et al., 2009). Jarid2 is a more recently identified member of the PRC2 complex and is thought to regulate PRC2 activity and gene occupancy (Li et al., 2010b) (Peng et al., 2009) (Shen et al., 2009). EZH2 is up-regulated in melanoma (McHugh et al., 2007) and promotes metastasis in prostate, breast and squamous cell carcinoma (Min et al., 2010) (Wang et al., 2011). Therefore the hypothesis was that EZH2 may promote cell motility by silencing differentiation associated genes to maintain cells in a less-differentiated, more motile state.

6.2 EZH2 levels are heterogeneous in melanoma

The microarray analysis suggested that *Ezh2* mRNA was up-regulated in the Notch reporter high population, a population enriched in motile cells. To further explore heterogeneity in EZH2 levels and to confirm the microarray data, the levels of *Ezh2* mRNA were examined in the Notch reporter cell populations. This confirmed the array analysis and showed that *Ezh2* mRNA was increased in the Notch reporter high population, a population enriched for motile cells (Figure 6.1).

Given that less than 10 % of melanoma cells are motile (Figure 3.2) and *Ezh2* mRNA is up-regulated in the B16 F2 motile cell population (Figure 6.1), if EZH2

regulates cell motility the levels should be heterogeneous in vivo. To address this, tumours of the syngeneic Black6 melanoma models, B16, 4434 and 5555 were stained for EZH2 using immunohistochemistry and immunofluorescence. EZH2 immunohistochemistry of paraffin embedded B16, 4434 and 5555 tumours revealed heterogeneity of EZH2 staining on a cell to cell basis (Figure 6.2 A). 4434 and 5555 tumours also showed increased EZH2 staining at the tumour margin, an area enriched for invasive cells (Figure 6.2). This is consistent with increased EZH2 being associated with motility and invasion. Immunofluorescent staining of frozen B16 tumours allowed quantification of the EZH2 staining intensity. This showed that the majority of cells have similar levels of nuclear EZH2 but a shoulder of the frequency histogram extended to higher EZH2 levels (Figure 6.2 B and C). The skewness of the distribution was calculated to be 0.97, indicating a positive skew and suggesting more cells than expected from a normal distribution, have high EZH2 staining. The shoulder of cells with high EZH2 staining contained about 7 % of cells, similar to the percentage of motile cells.

Two frozen tissue samples of human melanoma metastases were also tested for heterogeneity in EZH2 expression using immunofluorescence. EZH2 levels were also heterogeneous in human melanoma, and again the distributions had a positive skew. The skewness value was 1.33 for human melanoma metastasis 1 and 2.02 for human melanoma metastasis 2. This suggests that an EZH2 high population of cells may also exist outside of murine melanoma (Figure 6.3).

EZH2 catalyses the tri-methylation of histone H3 at lysine 27 (H3K27me3). If EZH2 regulates cell motility through histone modification and gene regulation then levels of H3K27me3 should also be heterogeneous. The second human melanoma metastasis was co-stained for global levels of H3K27me3 together with EZH2. This showed heterogeneity in the global levels of the tri-methyl mark catalysed by PRC2 (Figure 6.3). Image analysis software to measure the staining intensity of EZH2 and H3K27me3, showed a significant correlation between the two, with a Spearman correlation coefficient of 0.34 (Figure 6.3 B). This was consistent with data showing a significant decrease in global levels of H3K27me3 on PRC2 component depletion (Figure 6.4 C).

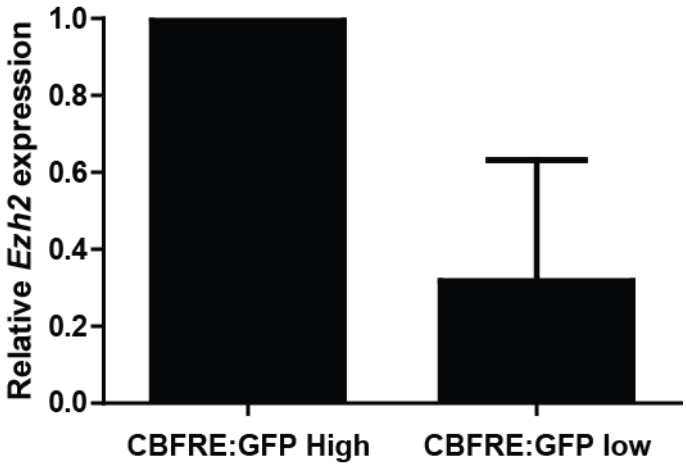

Figure 6.1. *Ezh2* mRNA is up-regulated in the Notch reporter high population.

Q RT-PCR confirmation of *Ezh2* transcript levels in the Notch reporter high and low populations of the clonal Notch reporter cell-line grown in vitro. Data from 2 samples and error bars show the standard error. FACS plots showing controls and the gates for collection of the Notch reporter high and low populations are presented in Figure 5.3.

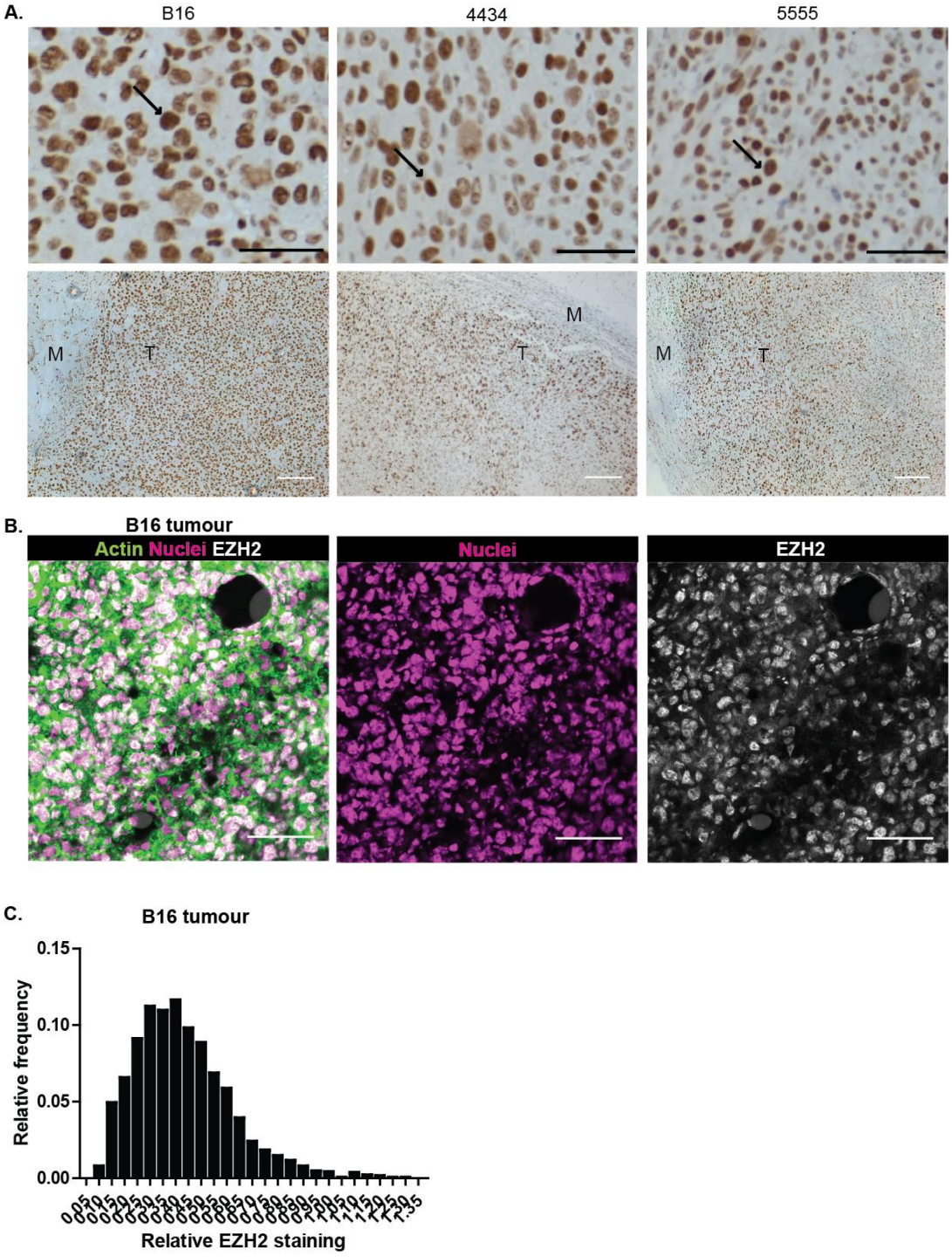

Figure 6.2. EZH2 levels are heterogeneous in syngeneic mouse melanoma.

A. Immunohistochemical staining for EZH2 in B16 F2, 4434 and 5555 melanoma grown in syngeneic C57Black6 mice. Tumours were excised and fixed at 0.7 cm diameter. Top row images have scale bar indicating 50μm, bottom row images have scale bar indicating 150 μm. Arrows indicate nuclei with high EZH2 staining. T indicates the tumour and M indicates the margin. B. Immunofluorecence staining of B16 frozen tumour sections for actin (green), nuclei (pink) and EZH2 (white). Scale bar indicates 50 μm. C. Histogram showing the relative frequency of relative EZH2 staining intensity in individual nuclei in B16 tumour sections.

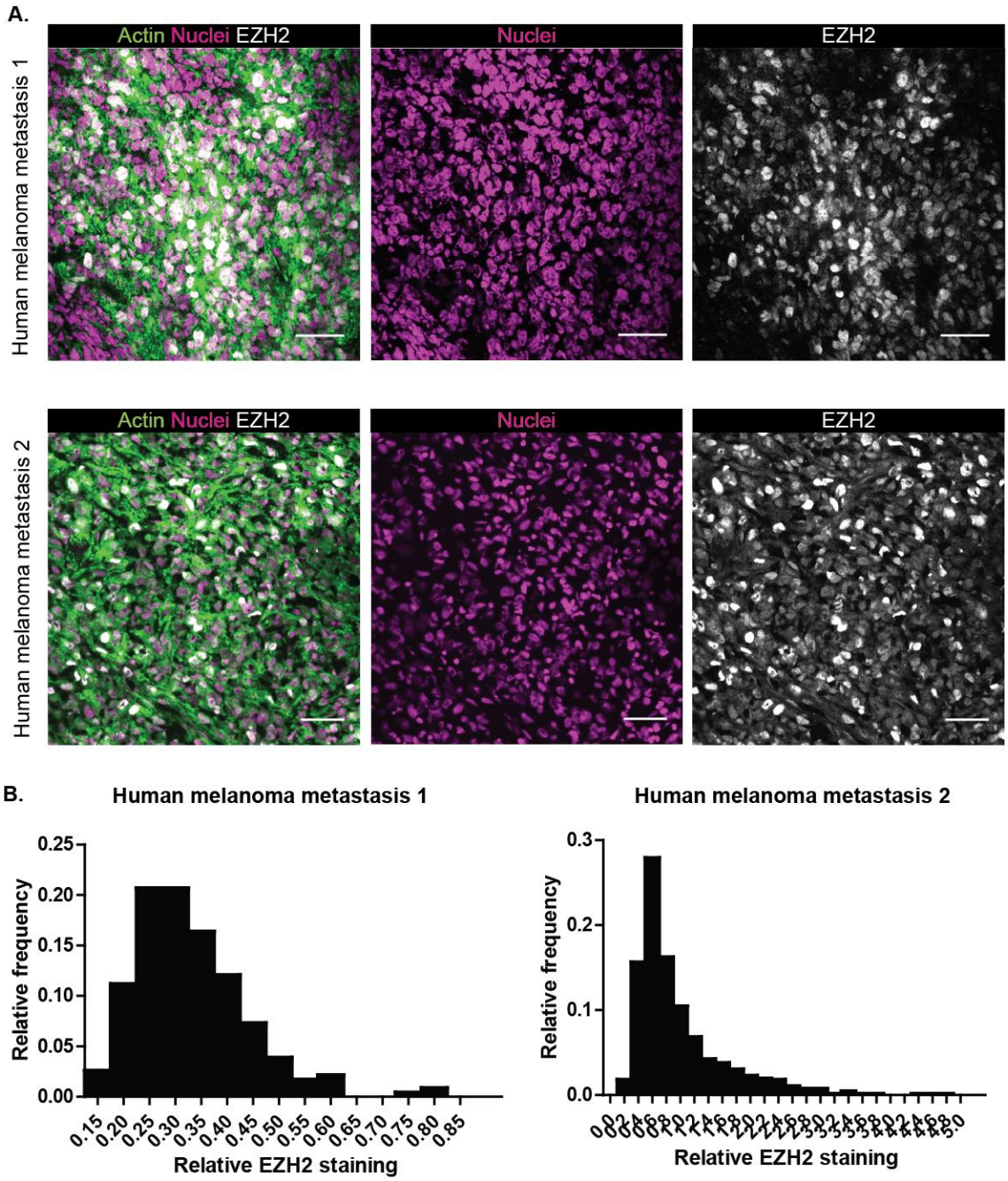

Figure 6.3. EZH2 levels are heterogeneous in human melanoma metastases.

Immunofluorecence staining of frozen sections from 2 human melanoma metastases for actin (green), nuclei (pink) and EZH2 (white). Scale bar indicates 50 μm. B. Histograms showing the relative frequency of relative EZH2 staining intensity in individual nuclei in sections from human melanoma metastases.

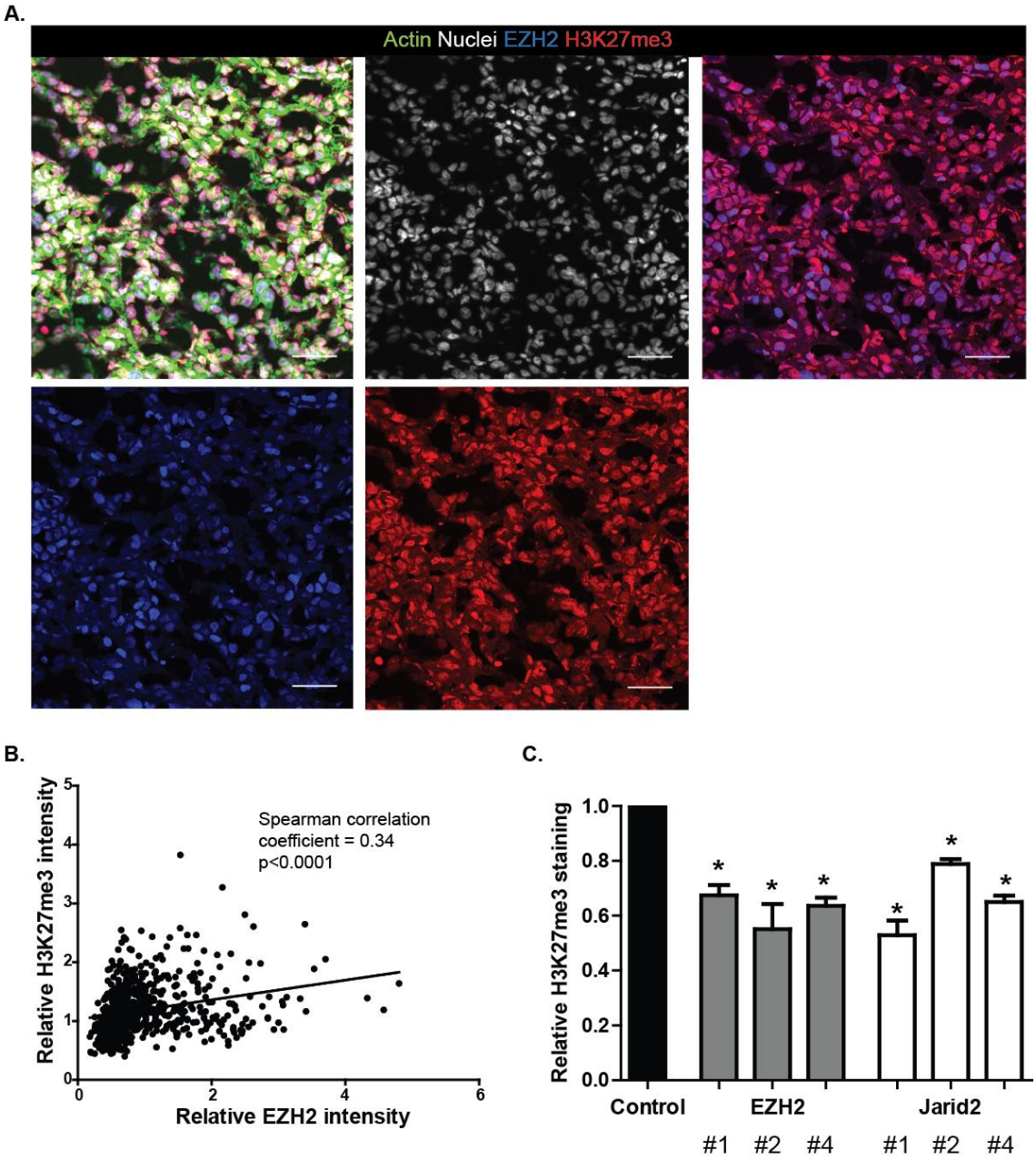

Figure 6.4. Levels of tri-methylated lysine 27 on histone H3 are heterogeneous in vivo.

A. Immunofluorecence staining of frozen sections of human melanoma metastasis 2 for actin (green), nuclei (white) and EZH2 (blue) and tri-methylated lysine 27 on histone H3 (H3K27me3) (red). Scale bar indicates 50 μm. B. Graph showing correlation between relative nuclear EZH2 and H3K27me3 intensities. p-value indicates statistically significant correlation using Spearmans rank test. C. Graph showing a decrease in global H3K27me3 levels on PRC2 component depletion. B16 F2 cells were transfected with control or PRC2 targeted siRNA and fixed for immunofluorescent staining of H3K27me3 48 hours after transfection. Data from at least 5 images of 3 independent experiments. Error bars show the standard error and stars indicate significant decrease in H3K27me3 staining by ANOVA statistical test.

6.3 PRC2 components regulate cell morphology

6.3.1 Loss of EZH2 leads to an increase in cell area

To determine whether EZH2 may promote motility, cell morphology was examined following knockdown of EZH2 with targeted siRNA. The idea was that regulators of motility should also regulate the actin cytoskeleton and hence cell morphology. B16 F2 cells were transfected with either control or EZH2 targeted siRNAs, plated on glass and fixed after 48 hours. Three different EZH2 siRNAs gave a similar flat cell phenotype with an increased cell area (Figure 6.5). EZH2 knockdown was confirmed using both Q RT-PCR and western blot (Figure 6.6). Although all siRNAs increased the cell area, siRNA #2 had a slightly different phenotype to the other two siRNA. siRNA #1 and 4 increased the cell area and many cells had long tails indicative of tail retraction problems (Figure 6.5), however, siRNA #2 resulted in very large and flat cells with F-actin cables at the cell edge.

.

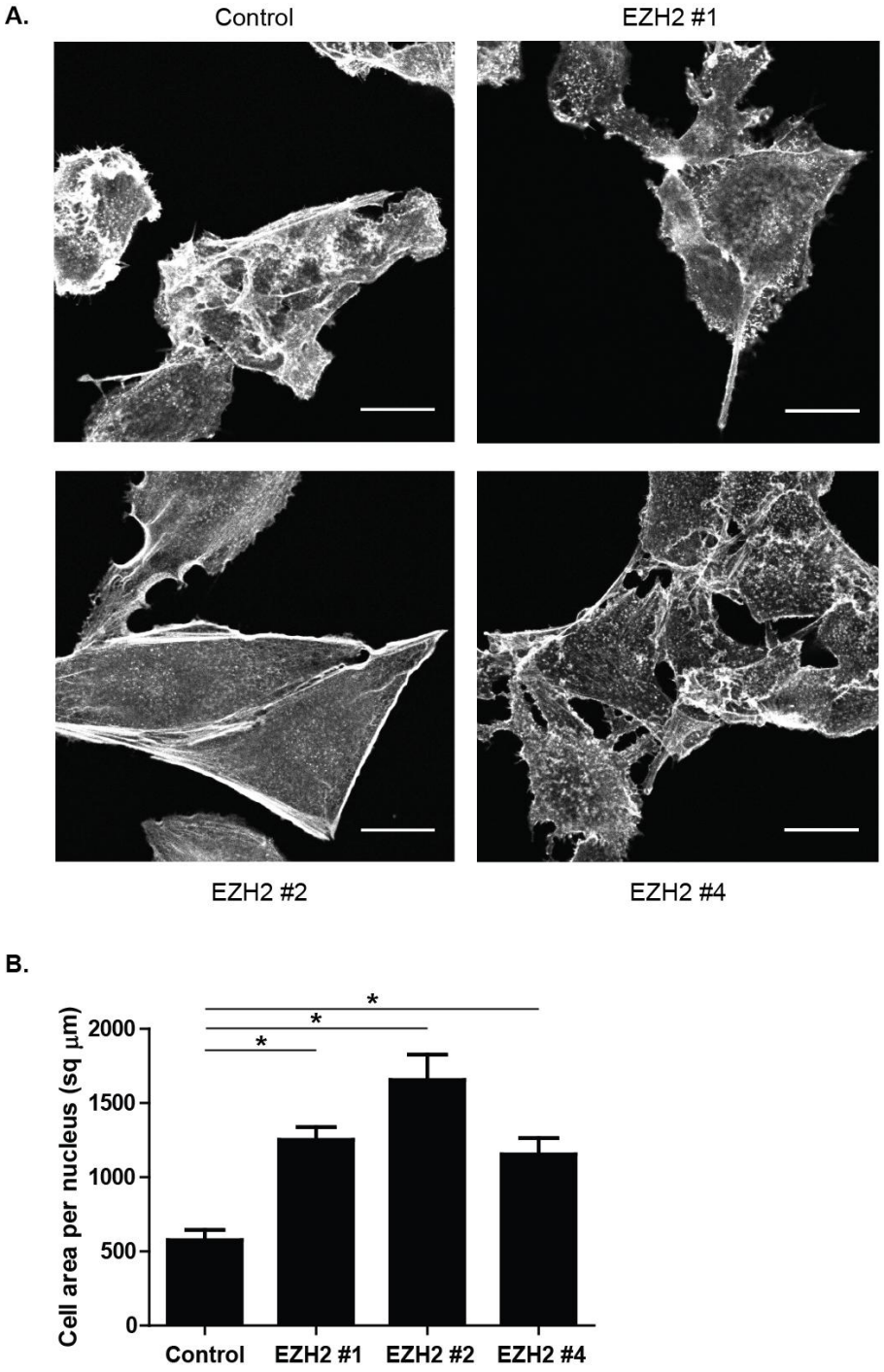

Figure 6.5. Loss of EZH2 leads to an increase in cell area.

A. B16 F2 cells were transfected with control or EZH2 siRNA and plated on glass. Cells were fixed 48 hours after knockdown. Image shows cells with labelled plasma-membrane. Scale bar indicates 25 µm. B. Cells used for measuring cell area were first stained with DAPI and then imaged. The cell area per image, measured with Volocity image analysis software, was divided by the number of nuclei. Data from at least 5 individual images of 2 different experiments. Stars indicate significance in ANOVA statistical test.

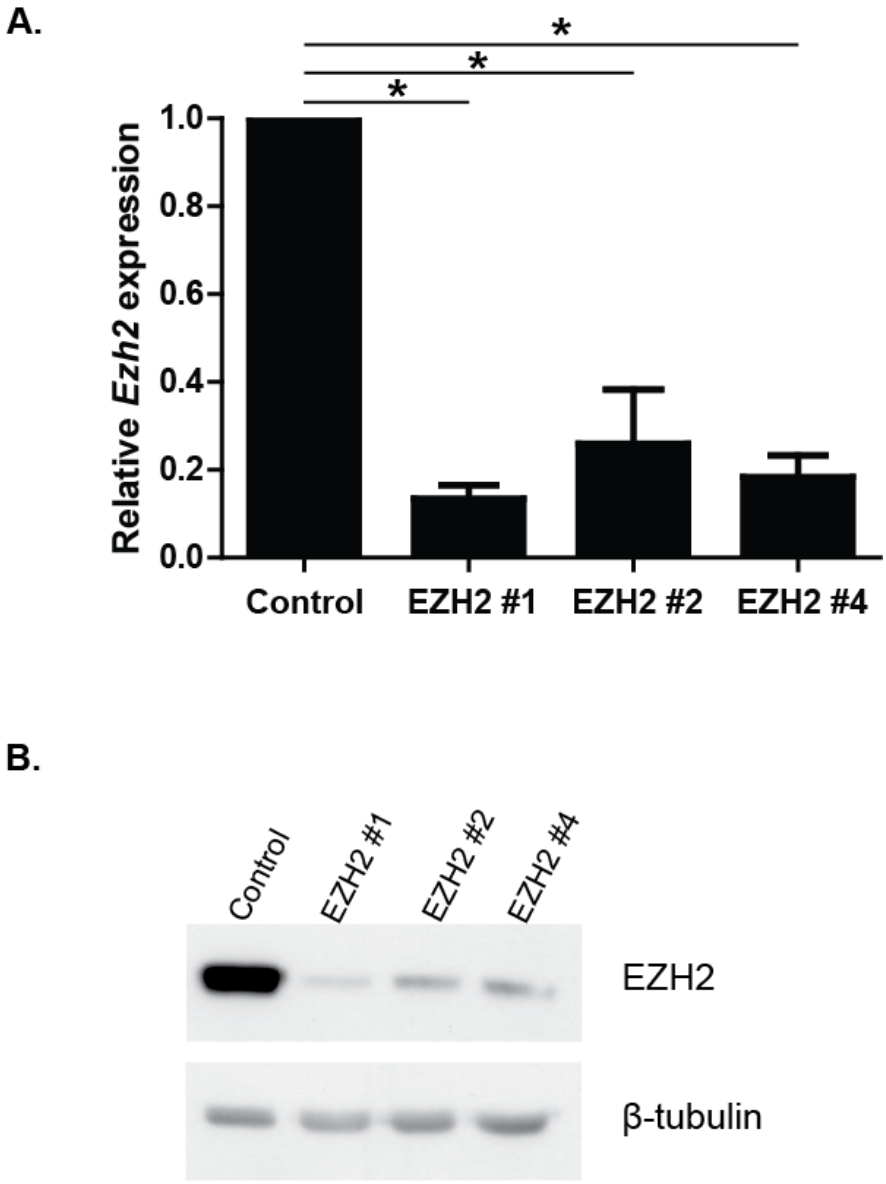

Figure 6.6 Confirmation of EZH2 knockdown.

A. Q RT-PCR analysis of *Ezh2* mRNA levels 48 hours after knockdown with control or EZH2 targeted siRNA in B16 F2 cells. Error bars show the standard error from 3 independent experiments and stars indicate significance in ANOVA statistical test. B. Western blot of EZH2 protein levels 48 hours after knockdown with control or EZH2 targeted siRNA in B16 F2 cells.

6.3.2 Loss of the PRC2 components, Suz12, and Jarid2 also leads to an increased cell area

To try and determine whether the change in cell morphology on loss of EZH2 was a PRC2 dependent or independent phenomenon, other members of the PRC2 complex were subject to siRNA knockdown and the cell morphology phenotype analysed. Depletion of the PRC2 core complex member, Suz12, led to an increase in cell area, although siRNA #2 also resulted in an increase in actin ruffles. This was not seen with other Suz12 siRNA and so may be an off-target effect (Figure 6.7). Depletion of Jarid2 also resulted in a similar cell morphology phenotype to EZH2 loss, with a concurrent increase in cell area. However, the increase in cell area with Jarid2 siRNA #2 did not reach significance compared to control (Figure 6.7). As knockdown of the PRC2 components EZH2, Suz12 and Jarid2 all gave an increase in cell area, this suggests that the PRC2 complex can regulate cell morphology and the actin cytoskeleton.

The PRC2 complex works together with the PRC1 complex to mediate gene silencing (Simon and Kingston, 2009). If the effects on cell morphology on PRC2 component knockdown are through changes in gene regulation then loss of PRC1 components should give a similar phenotype. Loss of BMI-1 only resulted in a significant increase in cell area in 1 out of the 3 siRNAs that depleted BMI-1 levels (Figure 6.8). This suggests that BMI-1 and the PRC1 complex does not regulate cell morphology, although analysis of further PRC1 components would help to confirm this.

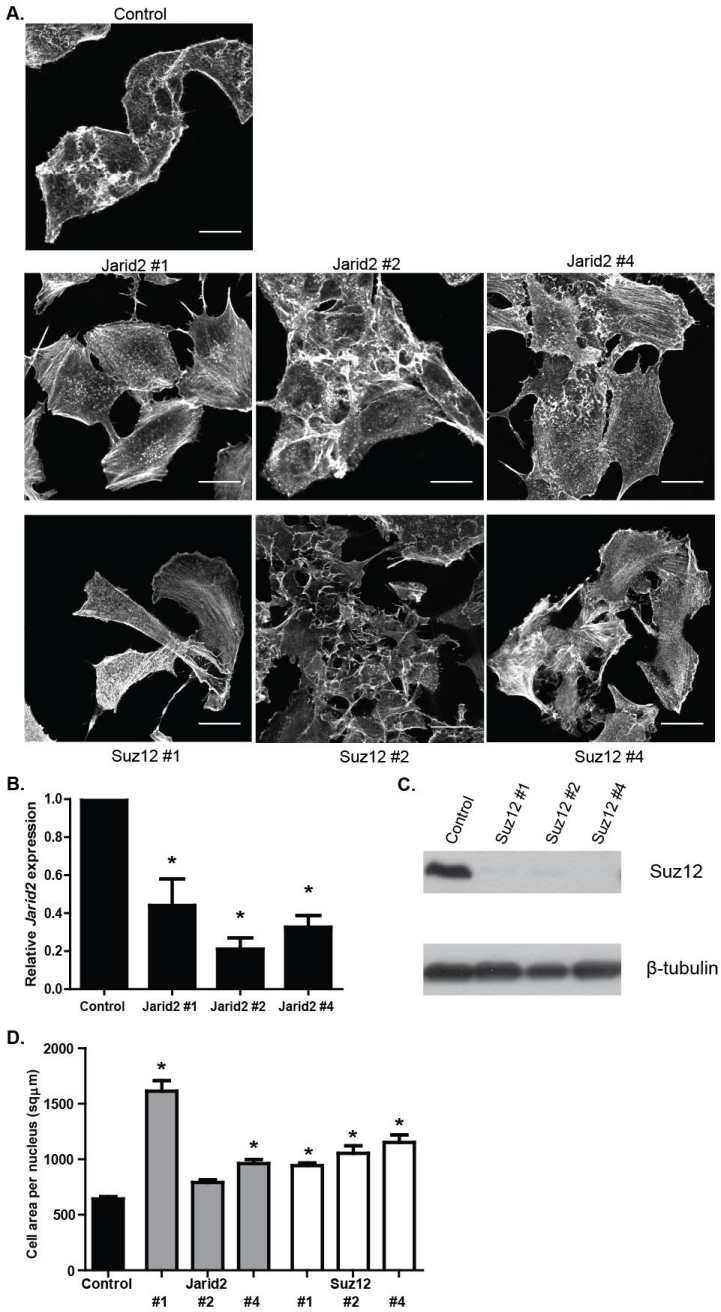

Figure 6.7. Loss of PRC2 components leads to an increase in cell area.

A. B16 F2 cells were transfected with control, Suz12 or Jarid2 siRNA and plated on glass. Cells were fixed 48 hours after knockdown and stained with phalloidin. Scale bar indicates 25 μm. B. Q RT-PCR analysis of *Jarid2* mRNA levels 48 hours after transfection in B16 F2 cells. Data from 3 independent experiments. C. Western blot of Suz12 protein levels 48 hours after transfection in B16 F2 cells. D. Graph of cell area on Jarid2 and Suz12 knockdown. Cells were stained with DAPI and phalloidin. The cell area per image, measured with Volocity image analysis software, was divided by the number of nuclei. Data from at least 5 individual images of 2 different experiments. Error bars show the standard error and stars indicate significance in ANOVA statistical test.

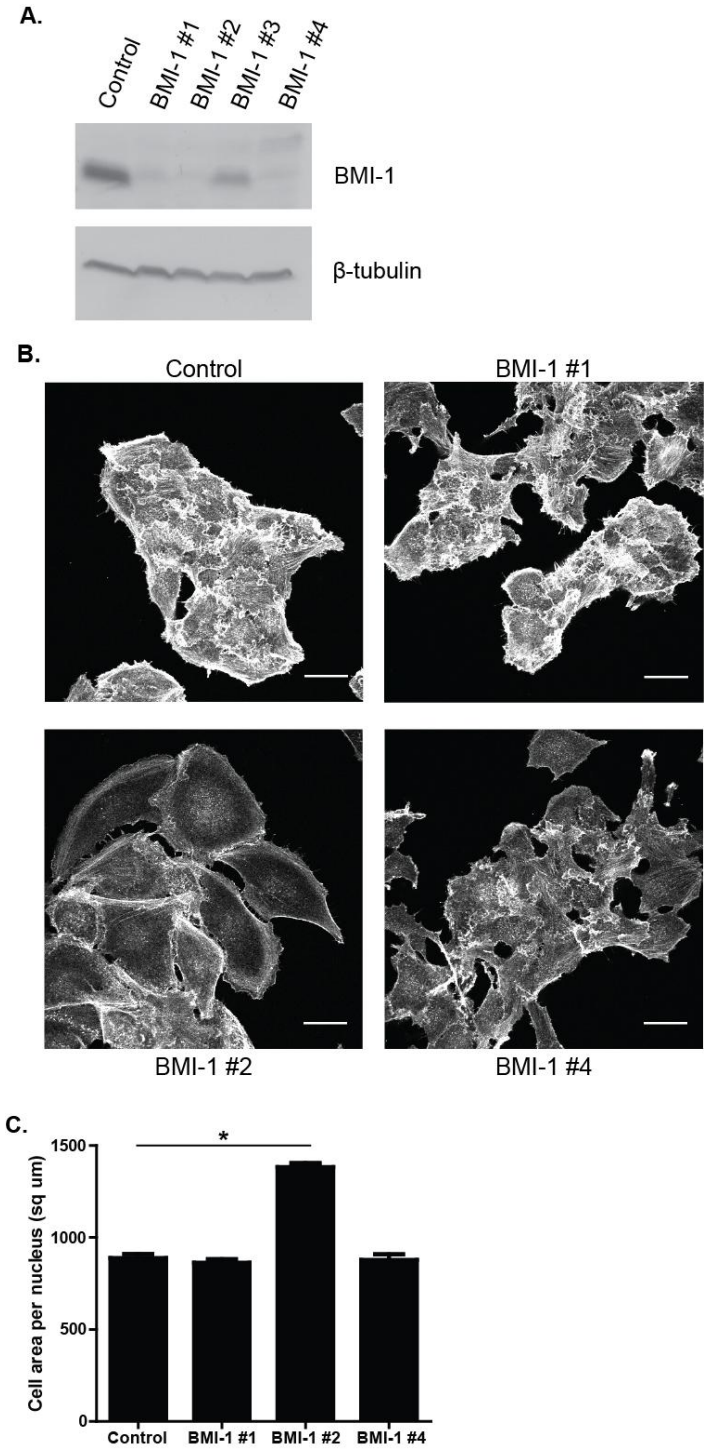

Figure 6.8. Loss of the PRC1 component BMI-1 does not increase cell area.

A. Western blot of BMI-1 protein levels 48 hours after knockdown with control or BMI-1 targeted siRNA in B16 F2 cells. B. B16 F2 cells were fixed 48 hours after transfection with control or BMI-1 siRNA and stained with phalloidin. Scale bar indicates 30 μm. C. Graph of cell area on BMI-1 depletion. The cell area per image, measured with Volocity image analysis software, was divided by the number of nuclei. Data from at least 5 individual images of 2 different experiments. Error bars show the standard error and stars indicate significance in ANOVA statistical test.

6.4 PRC2 regulates cell morphology through ERM protein activation

6.4.1 PRC2 depletion does not decrease actomyosin contraction

Cells depleted for EZH2 and other PRC2 components are flatter with an increased cell area and possible tail retraction problems (section 6.3). This phenotype could be indicative of a loss of actomyosin contractility, as contraction is required to retract the rear of the cell during cell motility on a 2D surface and for maintenance of cell morphology (Levayer and Lecuit, 2012). However, neither western blot nor immunofluorescence revealed a decrease in phospho-MLC levels on EZH2 depletion (Figure 6.9 and Figure 6.10). In fact, EZH2 siRNA #2 resulted in a slight increase in phospho-MLC by western blot and this could be visualised in the strong actin cables at the cell periphery using immunofluorescence. Therefore the flat cell phenotype and increase in cell area is not as a result of a decrease in actomyosin contractility.

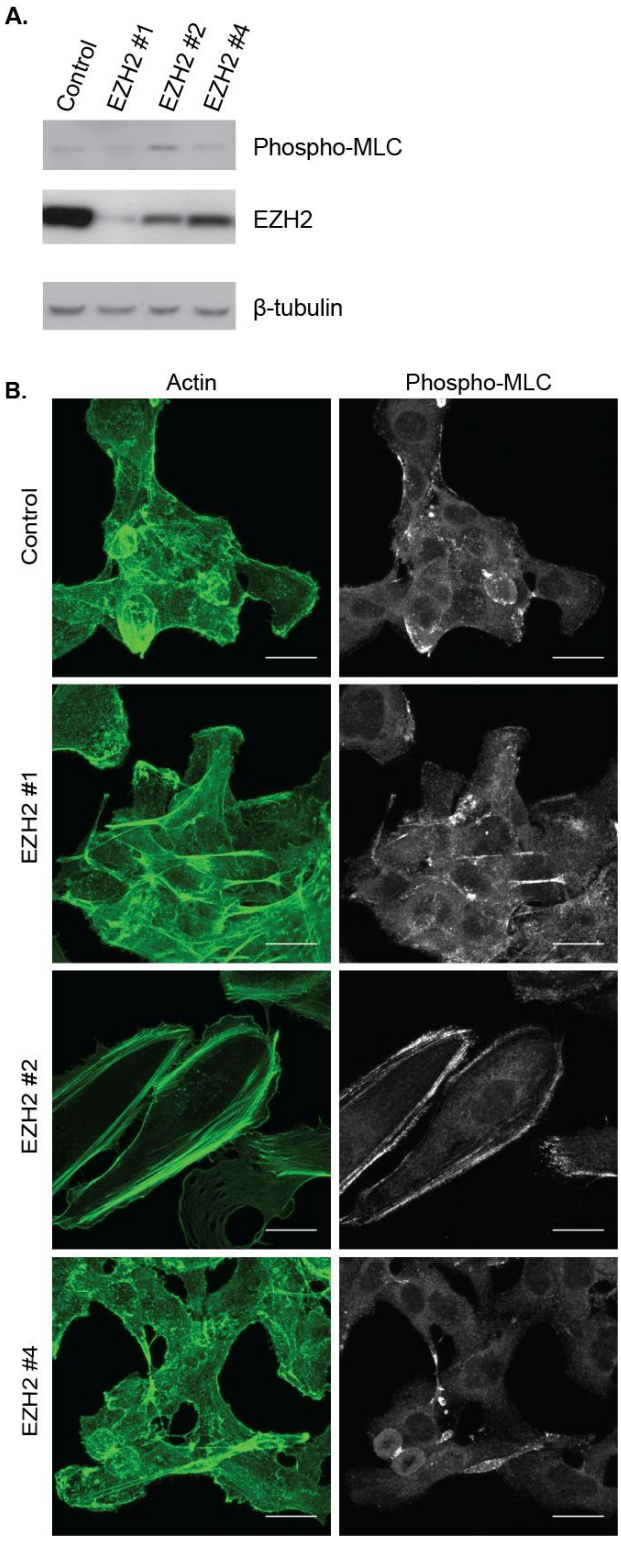

Figure 6.9. Loss of EZH2 does not decrease total phospho-MLC levels.

A. Western blot of B16 F2 cells 48 hours after transfection with control or EZH2 targeted siRNA. B. Immunofluorescent staining for phospho-MLC. B16 F2 cells were transfected with control or EZH2 targeted siRNA and plated on glass. 48 hours after transfection cells were fixed and stained with phalloidin and a phospho-MLC antibody. Scale bar indicates 25 μm.

6.4.2 Loss of PRC2 leads to a decrease in Ezrin and Radixin phosphorylation and activation

Ezrin, Radixin and Moesin are a family of proteins that link the actin cytoskeleton to the plasma membrane and are involved in maintaining cell shape and polarity and regulating migration (Fehon et al., 2010). Phosphorylation of ERM proteins by kinases such as ROCK, PKCα and PKCθ, leads to a conformational change and activation (Matsui et al., 1998) (Ng et al., 2001) (Simons et al., 1998). This allows ERM proteins to bind both F-actin and membrane proteins, acting to link the two cellular components. To investigate whether PRC2 components may exert their effects on cell morphology through regulation of ERM proteins, western blotting was performed for phosphorylated ERM proteins after PRC2 knockdown.

Loss of EZH2 resulted in a decrease of a subset of phosphorylated ERM proteins (Figure 6.10), suggesting that EZH2 can regulate ERM activation. The ERM proteins are closely related and the activating phosphorylation occurs on a conserved threonine residue (Mangeat et al., 1999). The antibody recognises the phosho-site on all three proteins, however, the molecular weight of Moesin is 75 kDa and Ezrin and Radixin are both around 80 kDa. As Ezrin and Moesin have a very similar molecular weight, it is difficult to resolve the three bands on a gel. Figure 6.10A shows a loss in the upper phospo-band (indicated by an arrow) on EZH2 knockdown. If the bands represent the individual ERM proteins according to molecular weight, this suggests a loss of phosphorylated Ezrin, Radixin or both. To check that regulation of ERM activation is a PRC2 dependent mechanism phospho-ERM levels were also analysed after Suz12 and Jarid2 depletion. In Figure 6.10B, 3 bands can just about be determined and loss of Suz12 and Jarid2 leads to a loss of the two upper bands, indicative of a decrease in activity of both Radixin and Ezrin. Suz12 siRNA #2 reproducibly resulted in a total loss of all phosphorylated ERM proteins, which correlates with it resulting in a slightly different cell morphology phenotype due to possible off-target effects (Figure 6.7).

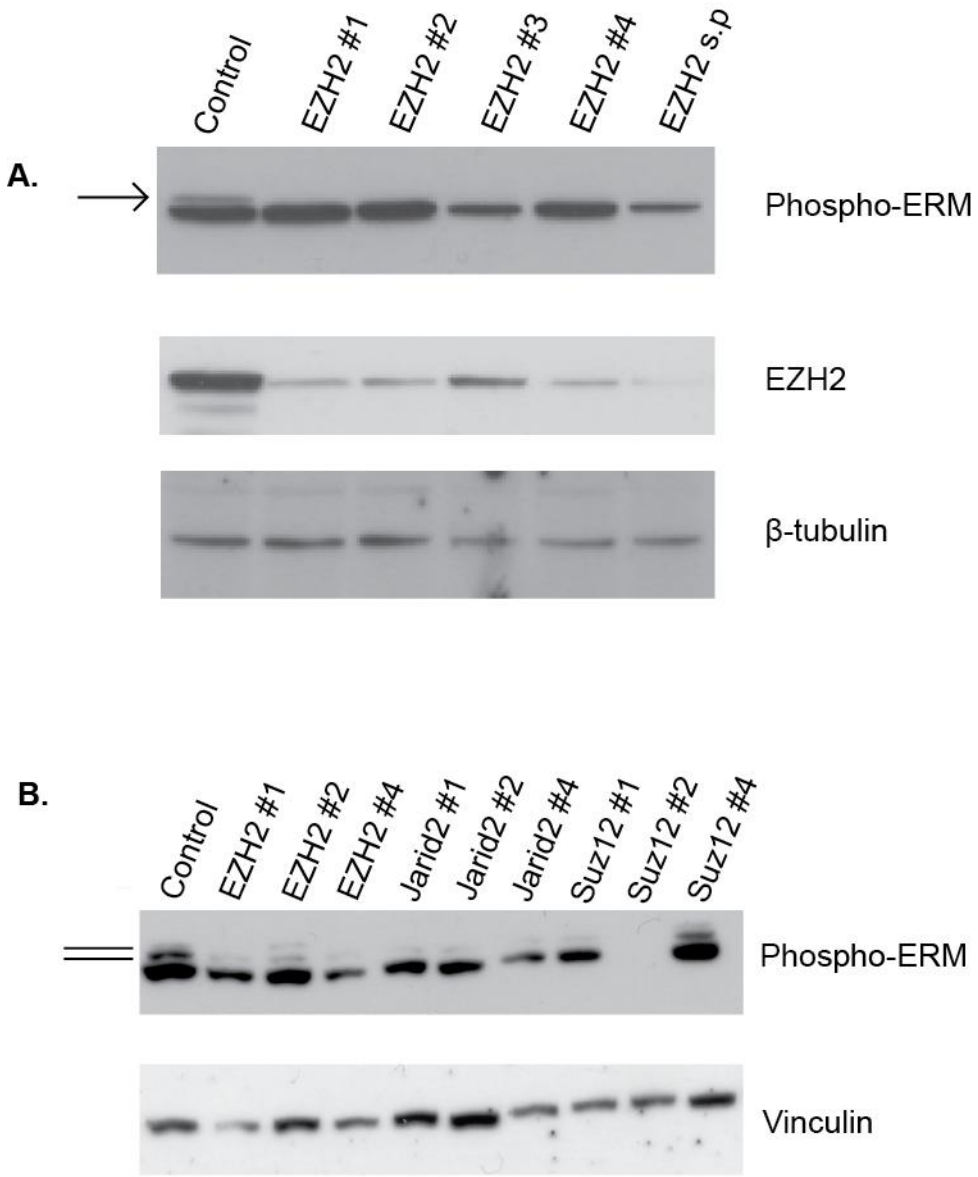

Figure 6.10 Loss of PRC2 leads to a decrease in ERM phosphorylation.

A. Western blot of phospo-ERM levels 48 hours after transfection with control or EZH2 targeting siRNAs. Arrow indicates the upper phospho-ERM band lost on EZH2 depletion. EZH2 blot shows the efficiency of knockdown with each individual siRNA and β-tubulin is a loading control. B. Western blot of phospo-ERM levels 48 hours after transfection with control, EZH2, Jarid2 or Suz12 targeting siRNAs. Lines show the two upper phospho-ERM bands decreased on PRC2 depletion. Vinculin used as a loading control.

To further dissect which member or members of the ERM family were affected on loss of PRC2, lysates of control cells were run on the same gel, transferred together and then the membrane was cut to blot for total Ezrin, total Moesin and phospho-ERM. The membranes were lined up before exposure to help identify which bands in the phospho-ERM blot corresponded to which ERM proteins. The individual bands represented the individual phospho-proteins and were in order according to molecular weight (Figure 6.11). The upper most band being Ezrin, followed by Radixin and the lowest band Moesin. This suggests that loss of PRC2 components leads to a decrease in activation of Ezrin and Radixin.

To check that loss of PRC2 components lead to a decrease in activation of ERM proteins rather than a decrease in the total levels, western blots of total Ezrin were performed after knockdown of EZH2 and Jarid2. This showed no change in total levels of Ezrin after PRC2 component depletion, indicating that PRC2 regulates Ezrin and Radixin phosphorylation and activation (Figure 6.12).

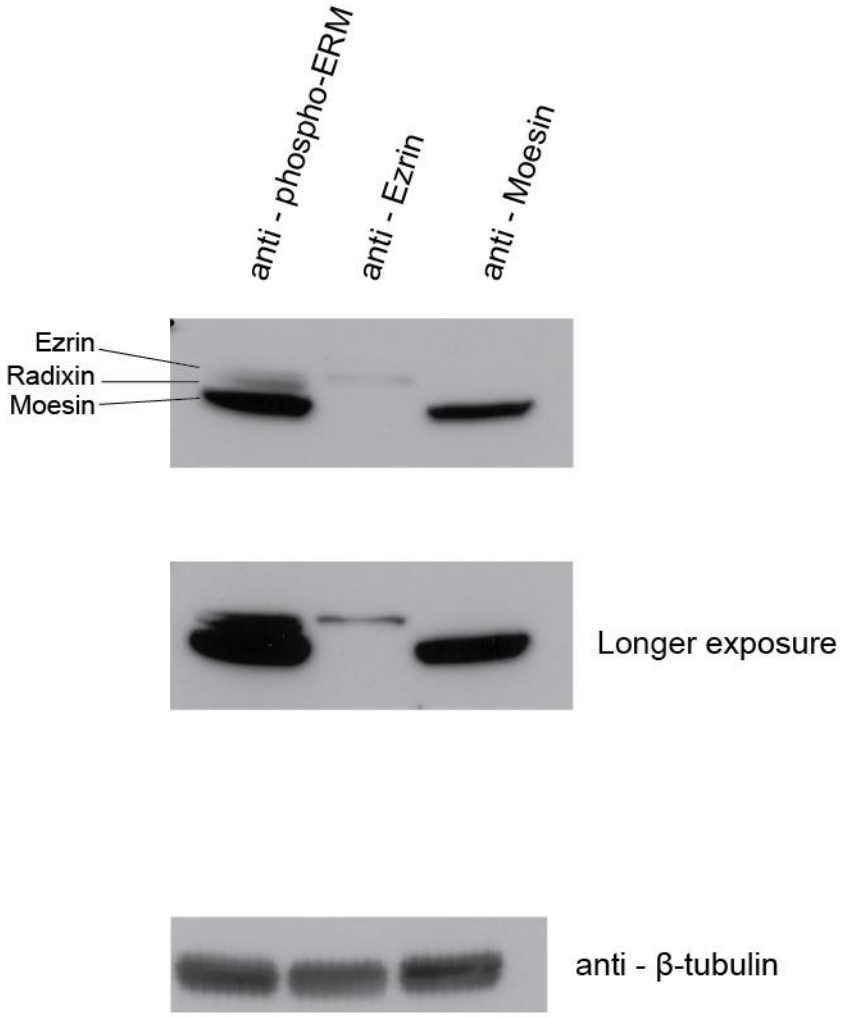

Figure 6.11. Confirmation of the identity of phospho-ERM bands on a western blot.

Control cell lysates were run on the same gel and then the membrane cut before blotting for phospho-ERM, total Ezrin and total Moesin on separate membranes. The membranes were lined up again before exposure. β-tubulin acts as a control to check the efficiency of membrane line-up before exposure.

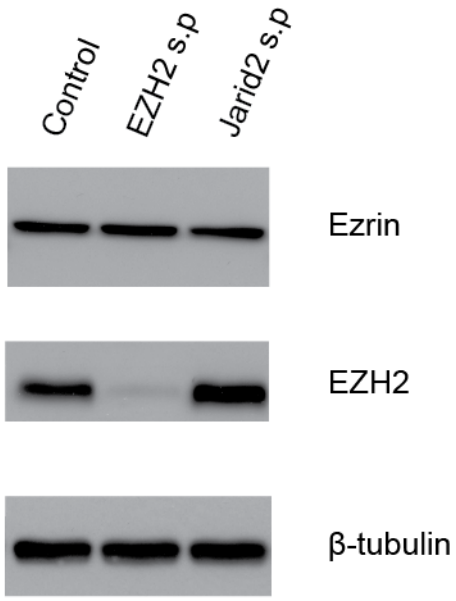

Figure 6.12 PRC2 component loss does not change total Ezrin levels.

Western blot of total Ezrin levels 48 hours after transfection with control, EZH2 or Jarid2 smartpool siRNAs. EZH2 blot shows the efficiency of knockdown and β-tubulin is a loading control.

6.4.3 Constitutively active Ezrin is sufficient to rescue the increase in cell area on PRC2 depletion

Loss of PRC2 components causes an increase in cell area and a decrease in activation of ERM proteins (section 6.3 and 6.4.2). As ERM proteins are known to regulate cell morphology, the hypothesis was that the increase in cell area on PRC2 depletion was due to a decrease in ERM protein activation and a subsequent decrease in the connection between the plasma membrane and underlying actin cytoskeleton. To test this hypothesis, plasmids encoding Ezrin-GFP and constitutively active Ezrin-GFP (EzrinTD-GFP) were used to try and rescue the cell area phenotype seen on PRC2 depletion. The consitutively active Ezrin construct contained full-length Ezrin fused to GFP with a threonine to aspartate point mutation at Ezrin residue 567 to mimic phosphorylation.

B16 F2 cells were co-transfected with either control or EZH2 targeted siRNA together with a plasmid encoding either Ezrin-GFP, EzrinTD-GFP or membrane targeted GFP (GFPCAAX). Ezrin-GFP and GFPCAAX were used as controls for the increased Ezrin and GFP in the cells respectively. Cells transfected with EZH2 targeted siRNA showed an increase in cell area as expected, however, cells co-transfected with EZH2 siRNA and EzrinTD-GFP had a similar morphology to control cells, indicating that constitutively active EzrinTD-GFP can rescue the phenotype (Figure 6.13 A). No rescue was observed with the Ezrin-GFP or GFPCAAX constructs, confirming that the increase in cell area is a result of loss of ERM activation rather than loss of ERM levels (Figure 6.13A). Quantification of the cell area using Volocity image analysis software confirmed that only the constitutively active Ezrin construct significantly rescued the EZH2 depletion phenotype (Figure 6.13 B). The cell area after co-transfection of EZH2 targeted siRNA #2 and EzrinTD-GFP did not return to control levels but was significantly reduced compared to co-transfection with Ezrin-GFP.

The experiment was repeated for depletion of Jarid2. Constitutively active EzrinTD-GFP also significantly rescued the cell area phenotype seen on Jarid2 depletion (Figure 6.14). This indicates the increase in cell area seen on PRC2 component depletion is most likely a result of decreased ERM protein activation.

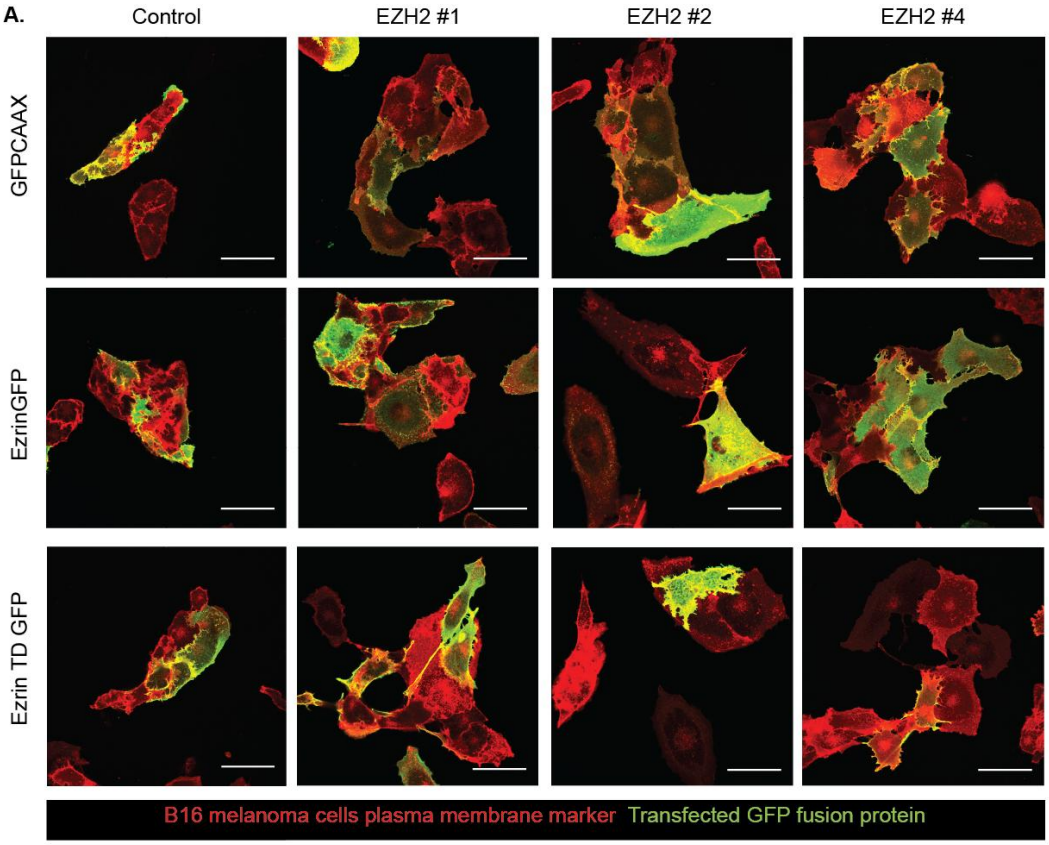

Figure 6.13 Constitutively active Ezrin-GFP rescues the increase in cell area seen on EZH2 depletion.

A. Single confocal images of B16 F2 cells plated on glass 48 hours after co-transfection with EZH2 targeted siRNA and either a GFPCAAX, Ezrin-GFP or EzrinTD-GFP plasmid. B16 F2 cells have a red plasma membrane marker and green indicates transfected cells. B. Quantification of B16 F2 cell area after co-transfection with EZH2 targeted siRNA and GFPCAAX, Ezrin-GFP or EzrinTD-GFP plasmids. Cell area was measured from at least 4 individual images of 3 different experiments using Volocity image analysis software. Error bars show standard error and stars indicate significant reduction in cell area compared to GFPCAAX and Ezrin-GFP transfected cells.

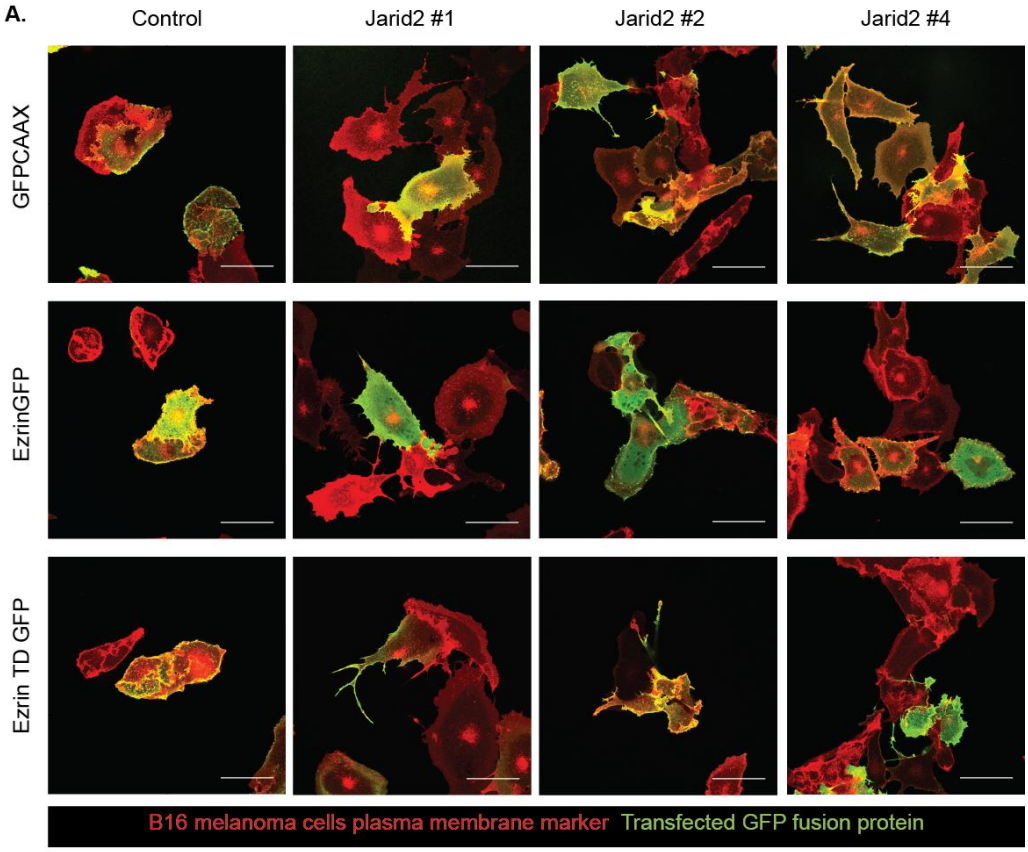

Figure 6.14. Constitutively active Ezrin-GFP rescues the increase in cell area seen on Jarid2 depletion.

A. Single confocal images of B16 F2 cells plated on glass 48 hours after co-transfection with Jarid2 targeted siRNA and either a GFPCAAX, Ezrin-GFP or EzrinTD-GFP plasmid. B16 F2 cells have a red plasma membrane marker and green indicates transfected cells. B. Quantification of B16 F2 cell area after co-transfection with Jarid2 targeted siRNA and GFPCAAX, Ezrin-GFP or EzrinTD-GFP plasmids. Cell area was measured from at least 4 individual images of 3 different experiments using Volocity image analysis software. Error bars show standard error and stars indicate significant reduction in cell area compared to GFPCAAX and Ezrin-GFP transfected cells.

6.5 EZH2 positively regulates motility in vitro and metastasis

As PRC2 components regulate cell morphology through ERM protein activation and Ezrin positively regulates metastasis (Hunter, 2004), the hypothesis was that EZH2 regulates melanoma cell motility and metastasis. To test this hypothesis, the more metastatic sub-line B16 F10 was plated on Fibronectin in vitro to examine cell motility and also used in experimental metastasis assays.

6.5.1 EZH2 depletion slightly decreases cell speed in vitro

As an initial investigation into the role of EZH2 in regulating cell motility, B16 F10 cells treated with control or EZH2 targeted siRNA were plated on Fibronectin coated glass plates and imaged following stimulation with 5 ng/ml HGF (Supplementary movie 7). This indicated that EZH2 depletion resulted in cells having tail retraction problems, consistent with the increase in cell tails observed in fixed cells. Cell tracking showed that cells depleted for EZH2 were also slower than control cells, although this only reached significance after 2 experiments for EZH2 siRNA #2.

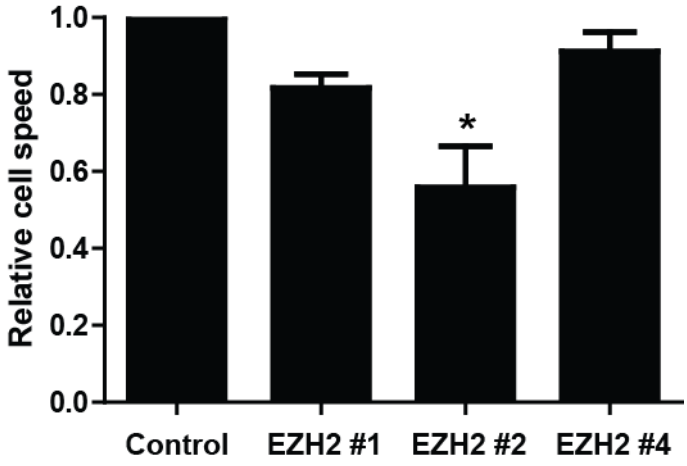

Figure 6.15. EZH2 depletion decreases cell speed in vitro.

B16 F10 cells were transfected with control or EZH2 targeted siRNA and plated on Fibronectin coated glass. Cells were stimulated with 5 ng/ml HGF for 2 hours before imaging with a Nikon lowlight microscope. Cells were tracked using Metamorph software and cell speeds calculated. Error bars show standard error of the mean for the average cell speeds from two experiments. Star indicates significance in ANOVA statistical test.

6.5.2 EZH2 positively regulates metastasis

Given that PRC2 components regulate Ezrin and Radixin activation and EZH2 depletion resulted in altered cell motility, the role of EZH2 in metastasis was investigated using short term lung metastasis assays. B16 F10 cells constitutively expressing mCherry or GFP were transfected with control or EZH2 targeted siRNA. A 50:50 mix of GFP expressing B16 F10 cells transfected with control siRNA and mCherry expressing B16 F10 cells transfected with EZH2 targeted siRNA was injected into the mouse tail-vein. The ratio of green:red cells in the lung was examined by confocal microscopy after 48 hours. A separate cohort of control mice received a 50:50 mix of B16 F10 GFP and B16 F10 mCherry cells both transfected with control siRNA. The ratio of control transfected B16 F10 GFP to EZH2 siRNA transfected B16 F10 mCherry cells was normalised to the ratio of red:green cells from control mice. Mixing the cell-types accounted for differences in injection efficiency between mice. The control transfected B16 F10 cells were alternated between GFP and mCherry expressing to ensure that the cell-line or colour was not creating bias in the analysis.

Loss of EZH2 in the metastatic B16 F10 sub-line decreased the lung colonisation efficiency in 2 out of the 3 siRNAs tested (Figure 6.16 A). EZH2 siRNA #2, which gave the largest increase in cell area, dramatically increased the lung colonisation efficiency of B16 F10 cells. As 2 out of 3 of the siRNAs tested decreased lung colonisation this suggests that EZH2 positively regulates metastasis and correlates with the increased EZH2 levels in the motile cell population of B16 melanoma. However, analysis of more siRNAs are required to be more confident of the data.

To test whether the positive regulation of metastasis was a general PRC2 mechanism the experimental metastasis assays were repeated for Jarid2 depletion. Depletion of Jarid2 with 2 out of the 3 siRNAs tested had no effect on the lung colonisation efficiency of the metastatic B16 F10 sub-line (Figure 6.16). However, siRNA #1 considerably increased lung colonisation efficiency. This was surprisingly similar to EZH2 siRNA #2 as again the siRNA that induced the greatest increase in cell area promoted metastasis. The fact that Jarid2 depletion in 2 of the siRNA had no effect on metastasis was also surprising because Jarid2 depletion

results in a change in cell morphology mediated by the loss of ERM protein activation, yet this had no effect on metastasis. Ezrin has well characterised roles in different steps during metastasis (Hunter, 2004), yet it appears in B16 melanoma loss of Radixin and Ezrin activation does not affect metastasis. As 1 out of 3 siRNAs for both EZH2 and Jarid2 gave contradictory results, more siRNAs are required to confirm these observations.

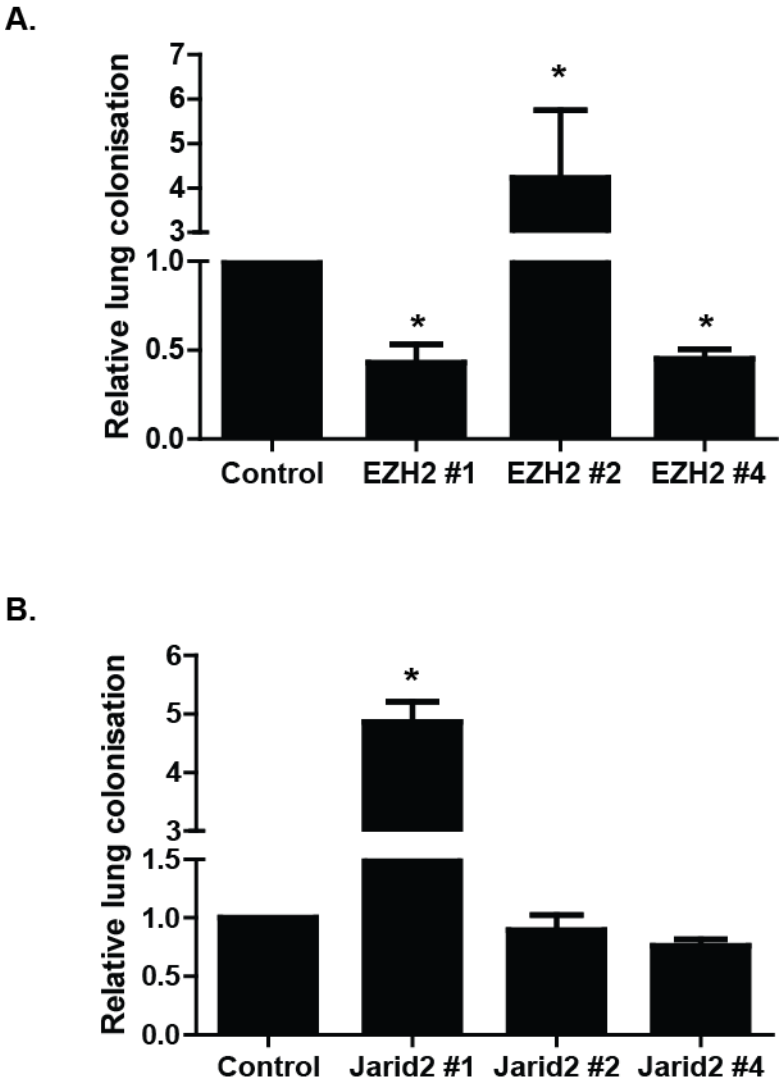

Figure 6.16. Analysis of PRC2 regulation of metastasis.

Graphs showing relative efficiency of lung colonisation 48 hours after injection of B16 F10 cells depleted for A. EZH2 and B. Jarid2 using 3 different siRNAs for each gene. Data from at least 5 mice over at least 2 experiments for each point. Error bars show standard error and star indicates a statistically significant difference to control cells in ANOVA test.

6.6 PRC2 components regulate pigment production but do not significantly affect melanoma differentiation marker expression

During development, the core PRC2 component EZH2, mediates silencing of differentiation associated genes and loss of EZH2 induces premature expression of differentiation markers (Boyer et al., 2006) (Lee et al., 2006) (Ezhkova et al., 2009). However, Jarid2 has a different role. Jarid2 is essential for differentiation and depletion of Jarid2 leaves ES cells unable to differentiate in vitro (Landeira et al., 2010) and leads to an arrest in gastrulation of xenopus embryos (Peng et al., 2009).

EZH2 levels decrease during murine epidermal differentiation (Ezhkova et al., 2009), so to determine whether EZH2 levels correlate with differentiation in B16 F2 melanoma, the cells were subject to α-MSH treatment for 48 hours, as α-MSH is known to induce differentiation in this cell-type (Hunt et al., 1994) (Bennett et al., 1994). Treatment with 10 μM α-MSH significantly reduced *Ezh2* mRNA levels and *Jarid2* mRNA also showed a slight decrease (Figure 6.17). This suggests that *Ezh2* mRNA levels correlate with differentiation status in B16 melanoma.

As motile cells in B16 melanoma are thought to be less differentiated (Pinner et al., 2009) and EZH2 correlates with differentiation state, EZH2 may maintain cells in a less differentiated state to promote motility. To test this hypothesis, pigment levels and expression of differentiation markers were assessed in cells depleted for EZH2 and other PRC2 components. Although discussion in previous chapters notes that pigment is not a good substitute for differentiation markers, decreased pigment correlates with motility in vivo and it is a simple assay to perform.

Depletion of EZH2 in B16 F2 cells led to an increase in pigment levels as determined by both the colour of the B16 F2 cell pellet and quantification of pigment intensity on a cell by cell basis following imaging with a two-photon microscope (Figure 6.18). To further explore the role of PRC2 in regulation of pigment levels, depletion of Jarid2 and Suz12 was performed. Pigment levels on

loss of Jarid2 were dependent on the individual siRNA (Figure 6.18). siRNA #1 consistently decreased pigment levels as determined by the colour of the cell pellet. siRNA #2 slightly increased pigment and siRNA #4 consistently increased pigment levels. Due to the differences between siRNA oligos, a reliable conclusion of the effects of Jarid2 depletion on pigment levels could not be reached. Depletion of Suz12 lead to a significant increase in pigment in 2 out of the three siRNAs tested (Figure 6.18). This suggests that loss of PRC2 activity increases pigment production in B16 F2 cells, but this may or may not be Jarid2 dependent. An increase in pigment after PRC2 loss implies that PRC2 activity maintains cells in a less pigmented state.

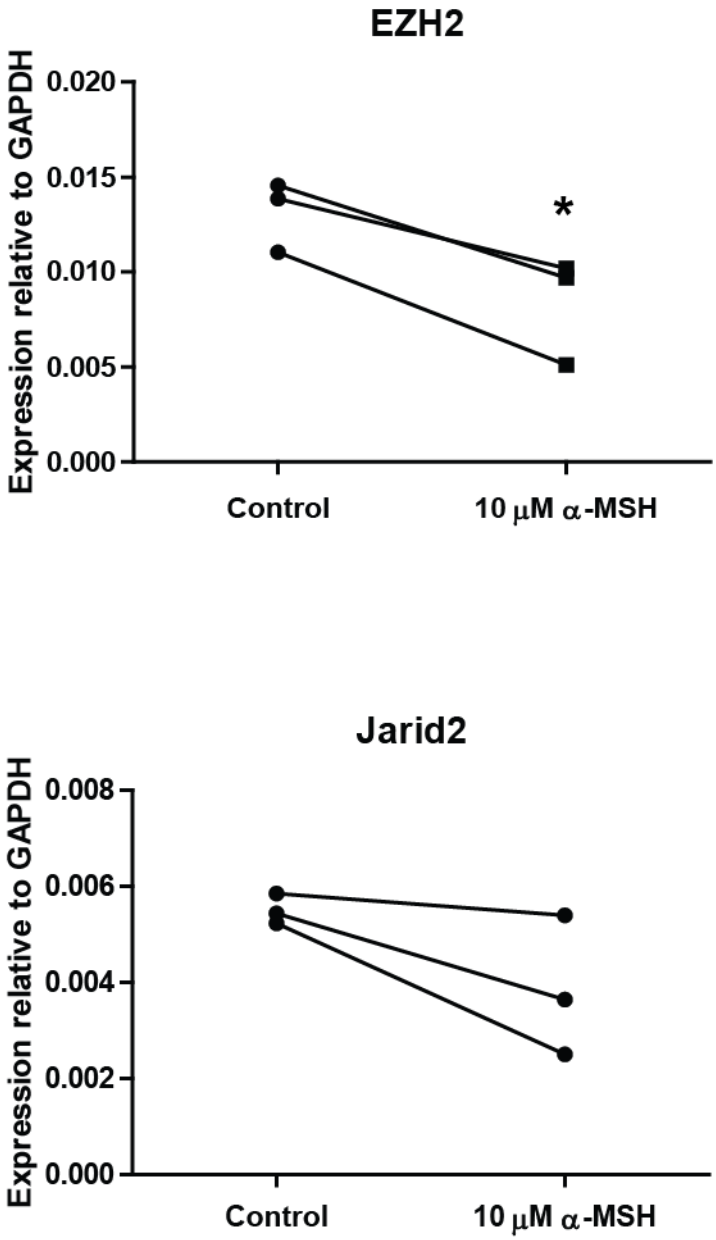

Figure 6.17. *Ezh2* mRNA levels decrease on differentiation of B16 melanoma cells.

B16 F2 cells were treated with 10 μM α-MSH or PBS control for 48 hours before Q RT-PCR analysis of *Ezh2* and *Jarid2* mRNA levels. Data points show 3 independent experiments. Star indicates statistical significance in a paired t-test.

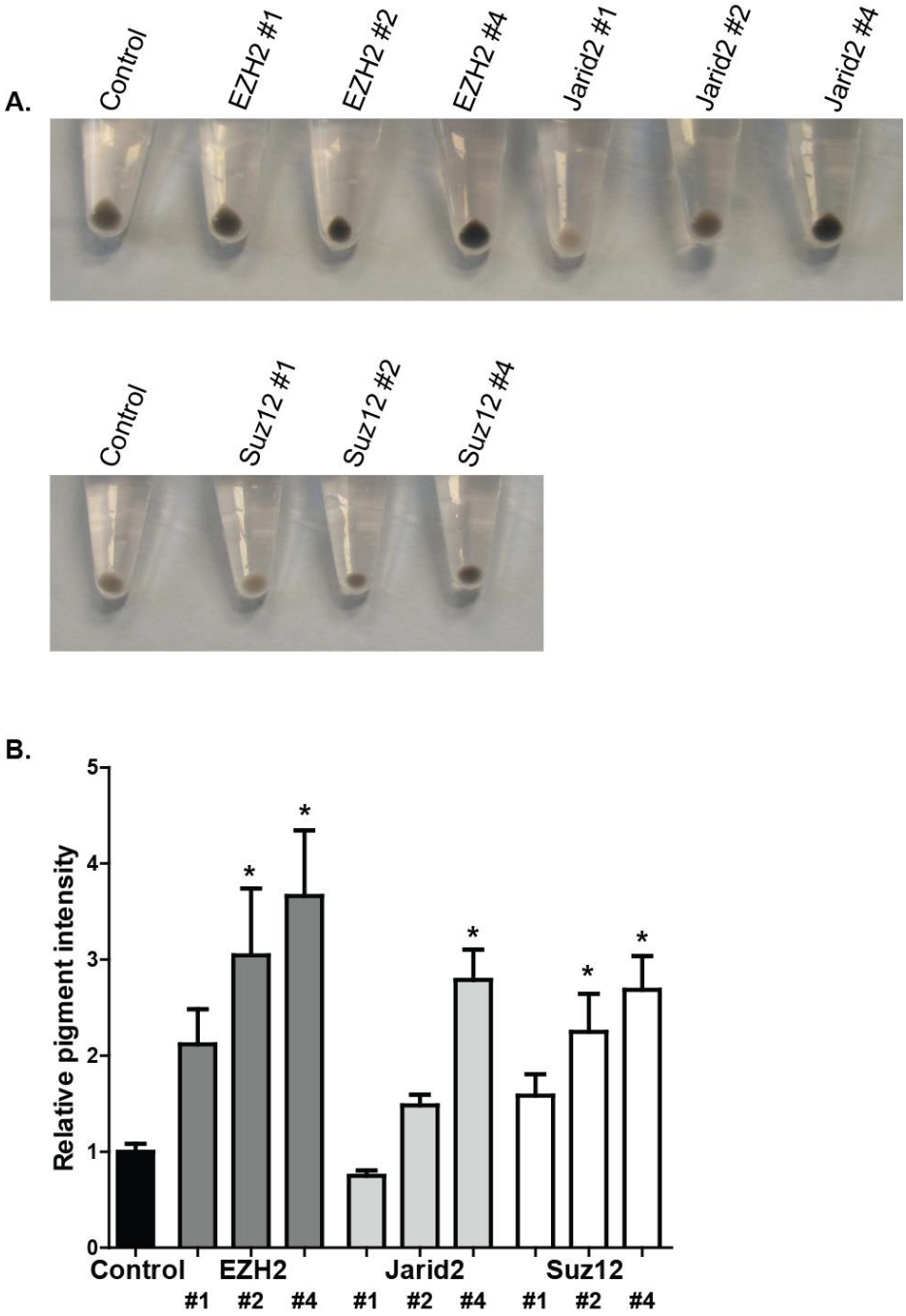

Figure 6.18. PRC2 complex regulates pigment levels in vitro.

A. B16 F2 cells were transfected with control, EZH2, Jarid2 or Suz12 targeted siRNA and collected by centrifugation 48 hours after transfection. B. Quantification of pigment levels on a cell by cell basis following depletion of EZH2, Jarid2 and Suz12. B16 F2 cells were transfected with control, EZH2, Jarid2 or Suz12 targeted siRNA and plated on glass. Cells were fixed 48 hours after transfection and imaged using a two-photon microscope to detect pigment. Cellular pigment intensity was measured and background levels subtracted. At least 50 cells quantified from at least 2 experiments. Error bars show standard error and stars indicate significance in ANOVA statistical test.

To investigate the interplay between known regulators of pigment and differentiation and EZH2, B16 F2 cells depleted of EZH2 were treated with α-MSH or H89. α-MSH results in an increase in B16 cell differentiation and pigment through stimulating MC1R (Hunt et al., 1994) (Kondo and Hearing, 2011). H89 is a PKA inhibitor and decreases pigment levels through inhibition of the signal downstream of MC1R (Kondo and Hearing, 2011). Stimulation of EZH2 depleted cells with α-MSH did not increase pigment levels further (Figure 6.19). However, H89 treatment of EZH2 depleted cells prevented the increase in pigment normally seen on the loss of EZH2 (Figure 6.19). This indicates that the increase in pigment on loss of EZH2 is dependent on PKA signalling.

To test the requirements for EZH2 and Jarid2 in differentiation of B16 melanoma, cells were transfected with EZH2 or Jarid2 targeted siRNA and the mRNA levels of melanoma differentiation markers assessed by Q RT-PCR. Basal levels of *Tyrp1*, *Tyr* and *Dct* mRNA did not change dramatically on EZH2 and Jarid2 loss (Figure 6.20). However, there was a trend towards increased mRNA levels of differentiation markers on EZH2 depletion and decreased mRNA levels of differentiation markers on Jarid2 depletion (Figure 6.20). This trend is consistent with data from ES cells regarding PRC2 regulation of differentiation, however, given the small changes in differentiation markers there is not sufficient evidence to confirm a role for PRC2 in regulating B16 melanoma differentiation state.

Overall, the data suggest that EZH2 regulates pigment independently of the differentiation associated MITF targets DCT, TYR, and TYRP1 as the increase of the MITF target genes on EZH2 depletion is not significant. In addition, the changes in *Dct*, *Tyr*, and *Tyrp1* mRNA levels between EZH2 siRNAs do not correlate with changes in pigment. This is consistent with data discussed later in this chapter regarding a role for the P protein in EZH2 pigment regulation. Therefore, it is unlikely that EZH2 maintains cells in a less differentiated state to promote motility.

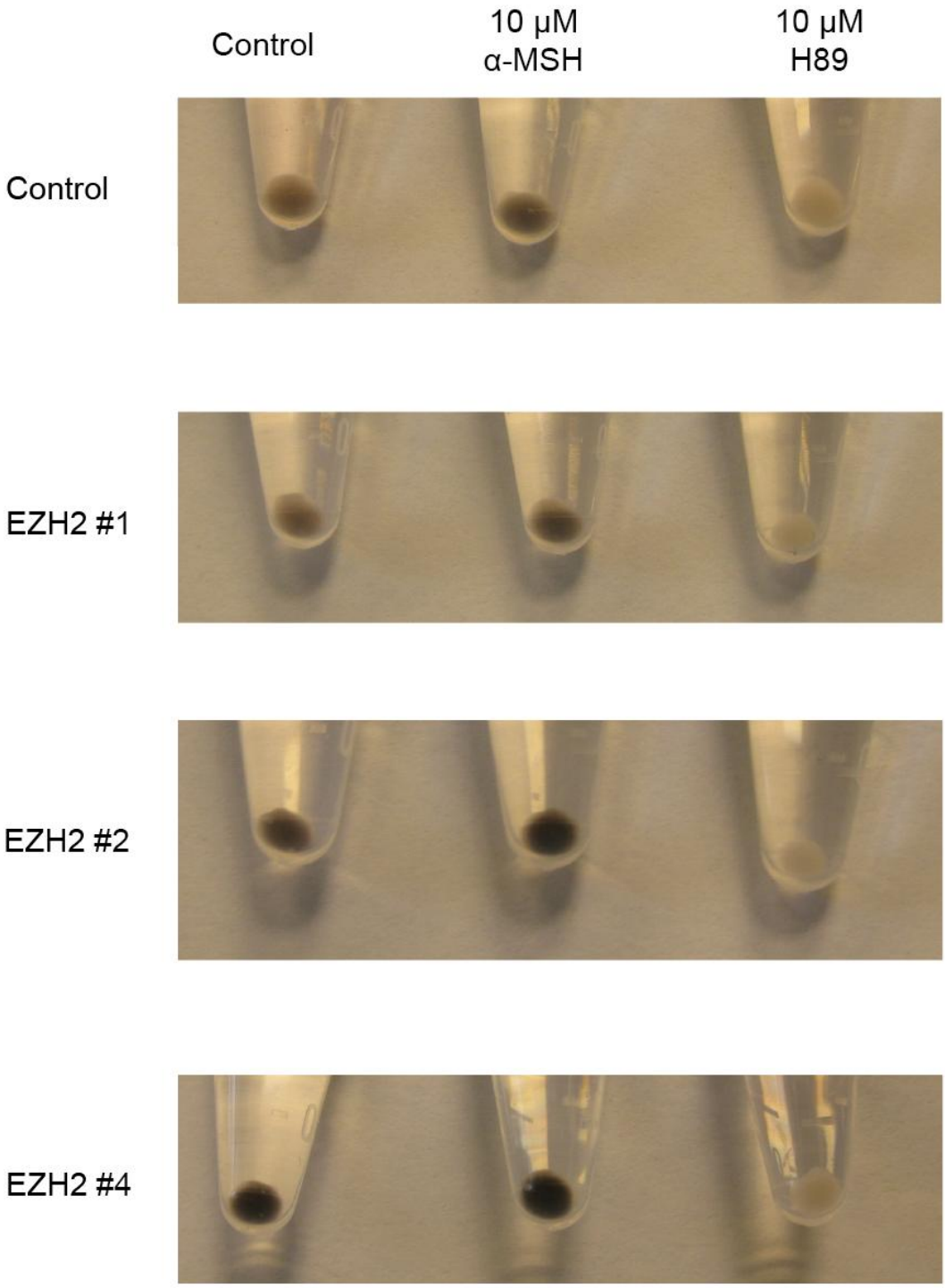

Figure 6.19. The increase in pigment observed on EZH2 depletion is dependent on PKA signalling.

B16 F2 cells were transfected with control or EZH2 targeted siRNA. 24 hours after transfection PBS, 10 μM α-MSH or 10 μM H89 was added for a further 48 hours, before centrifugation to pellet the cells.

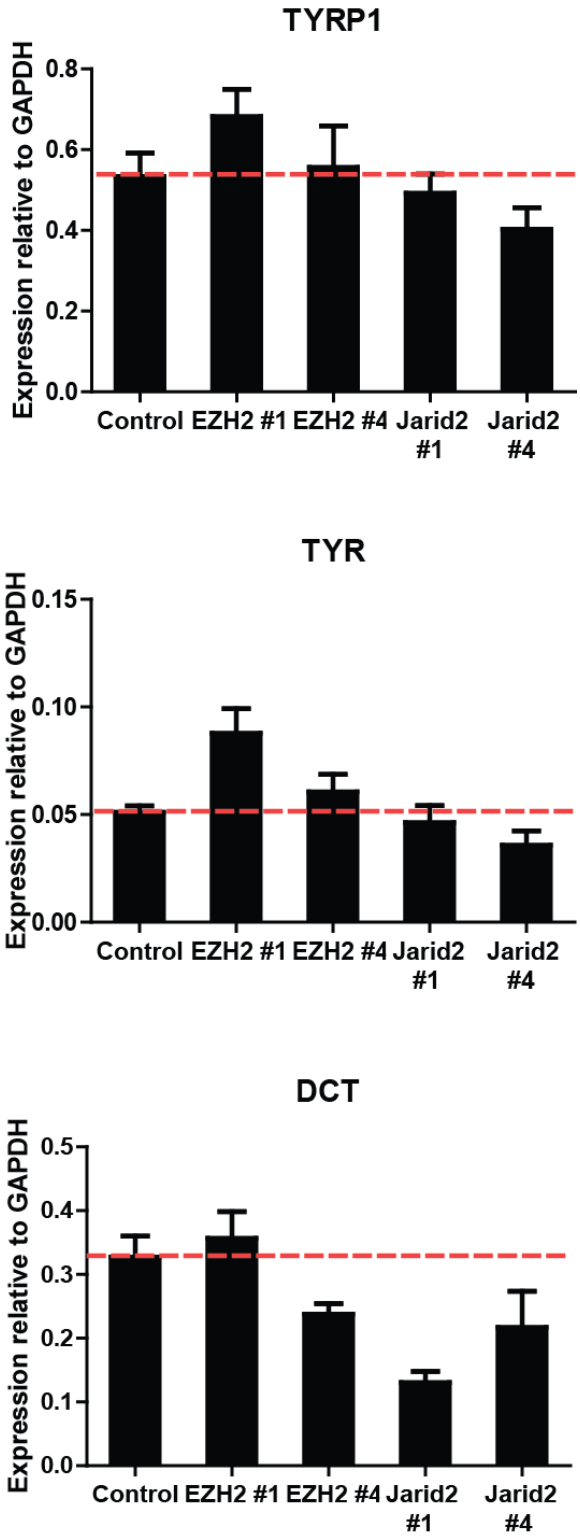

Figure 6.20. Depletion of EZH2 and Jarid2 may have different effects on melanoma differentiation markers.

Q RT-PCR analysis of the melanoma differentiation markers TYPR1, TYR and DCT in B16 cells 48 hours after transfection with control, EZH2 or Jarid2 targeted siRNA. Error bars show standard error.

6.7 PRC2 depletion decreases the number of cells in mitosis

EZH2 up-regulation in melanoma is thought to suppress oncogene-induced senescence, a state associated with benign nevi, hence allowing the progression from benign nevi to melanoma (Fan et al., 2011) (Michaloglou et al., 2005). Senescence is usually associated with an up-regulation of cell-cycle inhibitors including p16, however B16 cells have lost the *Ink4/ARF* locus and so are p16 null (Campisi and d'Adda di Fagagna, 2007) (Melnikova et al., 2004). EZH2 has been shown to regulate senescence in melanoma through suppression of the cell cycle inhibitor p21 (Fan et al., 2011) and microarray analysis discussed later (chapter 6.8), identified p21 as an EZH2 target in B16 F2 cells. Furthermore, senescent cells change morphology in vitro and have a large cell area (Campisi and d'Adda di Fagagna, 2007) so the change in cell morphology on PRC2 depletion may be as a result of senescence. To test whether EZH2 and PRC2 suppresses senescence in B16 F2 cells, cell cycle profile analysis was carried out on cells depleted for PRC2 components. Loss of EZH2 and Jarid2 led to a decrease in the percentage of cells in S and G2 phase, however in all siRNAs tested there was a significant percentage of cells in mitosis (Figure 6.21). This suggests that PRC2 depleted cells are not senescent, however, β-galactosidase staining would help to confirm this. The siRNAs that induce the largest increase in cell area, EZH2 #2 and Jarid2 #1, also decrease the mitotic population the most, suggesting a link between cell morphology and cell growth.

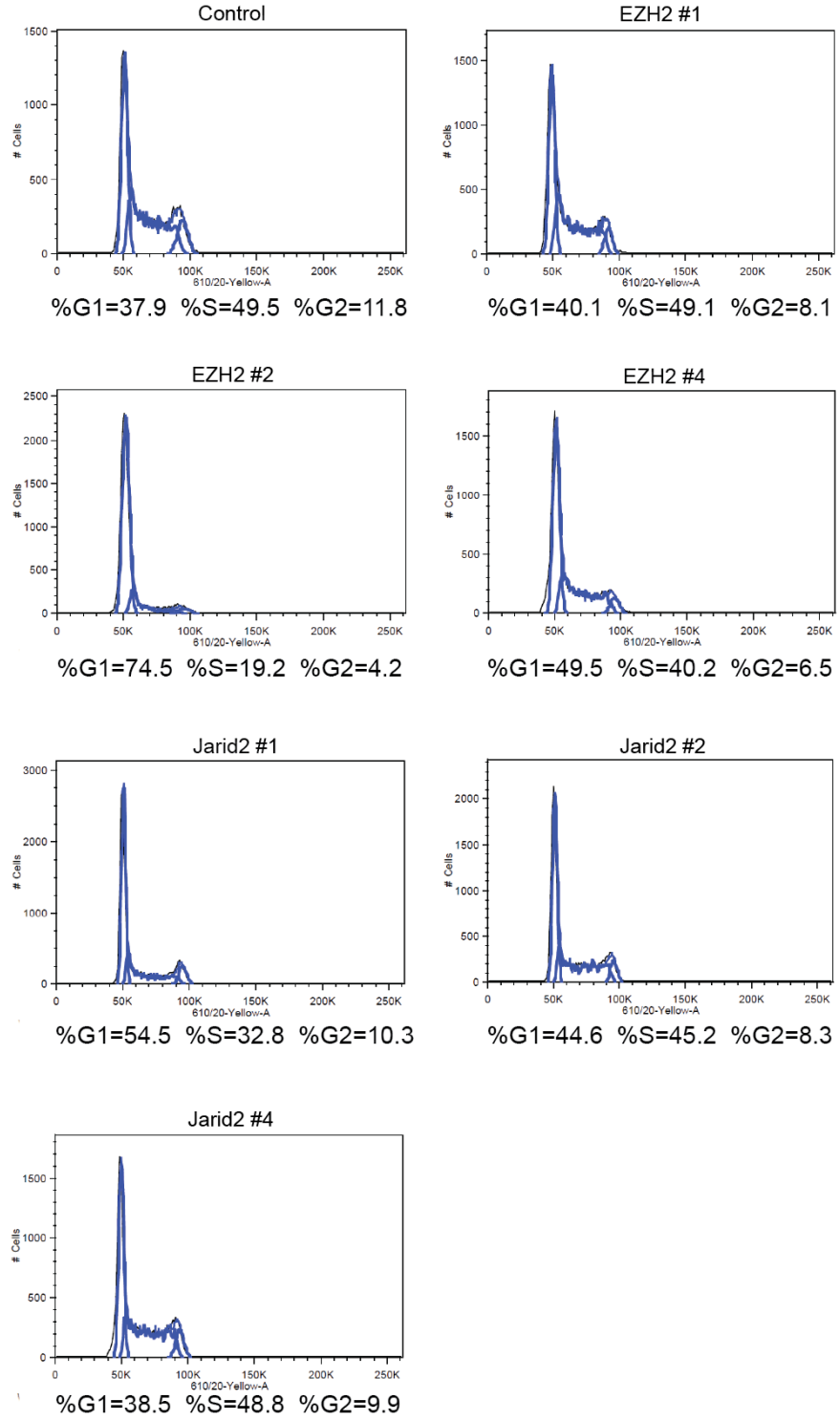

Figure 6.21. PRC2 depletion reduces the percentage of cells in S and G2 phases of the cell cycle.

B16 F2 cells were fixed in 70 % Ethanol 48 hours after transfection with control or EZH2 targeted siRNA. Cells were then stained with propidium iodide and subject to flow cytometry and cell cycle profile analysis using FlowJo software. Plots show raw DNA staining intensity data in the black line. Overlaid blue lines show FlowJo predictions for G0/G1, S and G2/M phases of cell cycle.

6.8 Genome-wide analysis of EZH2 and Jarid2 gene regulation

6.8.1 Microarray analysis of EZH2 and Jarid2 depleted cells

To try and establish how the PRC2 complex regulates ERM protein activation and how EZH2 may regulate cell motility and metastasis, microarrays were performed on depletion of EZH2 and Jarid2. B16 F2 cells were transfected with EZH2 siRNA #1 and 4 and Jarid2 #1 and 4 as these showed the greatest similarity to each other in terms of cell morphology phenotype.

To try and identify genes mediating the decrease in Ezrin and Radixin activation on PRC2 component depletion, genes showing a fold reduction of greater than 1.2 in all EZH2 and Jarid2 siRNAs were filtered from the microarray (found in appendix). This included *Fscn1*, and if the filters were relaxed to a reduction in 3 out of 4 siRNAs, *Rhoc*. Fascin is an actin cross-linking protein and RhoC is a small Rho-GTPase protein with high sequence similarity to RhoA (Hashimoto et al., 2011) (Wheeler and Ridley, 2004). However, western blot for both of these proteins did not reveal a loss in expression on EZH2 or Jarid2 depletion. In addition, siRNA targeting Fascin and RhoC did not greatly decrease levels of phosphorylated ERM proteins. A suitable candidate for loss of ERM protein activation on EZH2 and Jarid2 loss could not easily be found.

6.8.2 EZH2 and Jarid2 can regulate genes up-regulated in motile B16 population

As work in chapter 5 had determined a list of genes up-regulated in the motile B16 population, it would be interesting to test if EZH2 or Jarid2 could regulate these genes. This may help to determine if either EZH2 or Jarid2 are chief components regulating B16 melanoma motility. Overlap analysis was performed between genes up- or down-regulated on EZH2 or Jarid2 depletion and the genes up-regulated in the motile B16 population. In addition, genes that co-regulated with EZH2 in public datasets (oncomine) were analysed (all gene lists can be found on accompanying CD). These genes co-regulated with EZH2 were shown to have the greatest overlap with the genes up-regulated in the motile B16 population (Table

8). This suggests that EZH2 may control expression of the genes up-regulated in B16 motile cells. To further support this notion, genes that are down-regulated on EZH2 loss in B16 F2 cells show significant overlap with genes up-regulated in the B16 motile cell population (Table 8) (genes found in appendix). As *Ezh2* mRNA is increased in the motile cell population (Figure 6.1), this is consistent with EZH2 positively regulating motility through positive regulation of the genes up-regulated in the motile cell population. However, EZH2 is normally considered to silence genes, so these genes down-regulated on EZH2 loss may be indirect targets.

To test if Jarid2 could regulate the transcriptional program associated with B16 melanoma motility, Jarid2 target genes were analysed for overlap. Genes up-regulated after Jarid2 knockdown significantly overlapped with the genes up-regulated in the motile B16 cell population (Table 8) (genes found in appendix). This may suggest that Jarid2 activity is low in the motile cell population. Taken together this correlates with data from experimental metastasis assays in which loss of EZH2 decreased metastasis yet loss of Jarid2 had no effect. If the gene expression pattern associated with motility is similar for metastasis, then genes positively regulated by EZH2 but Jarid2 independent should overlap with genes increased in motile B16 cells (gene lists found in Supplementary file 1). Indeed, these genes show significant overlap (Table 8). Therefore it is likely that control of the genes up-regulated in the motile cell population in B16 melanoma correlates with ability to regulate metastasis.

Geneset	Observed overlap	Expected overlap	p-value	FDR
Genes that co-vary with *Ezh2* (oncomine)	16	0.42	3.96×10^{-20}	3.96×10^{-19}
Genes up-reg. by Jarid2	7	1.09	0.00014	0.00065
Genes down-reg by EZH2 and Jarid2 independent (only oligo 4)	7	1.19	0.00024	0.00065
Genes down-reg by EZH2	8	1.65	0.00031	0.00065
Genes down-reg by EZH2 and Jarid2 independent (both Jarid2 oligos)	5	0.78	0.00129	0.00215

Table 8. Overlap analysis of EZH2 and Jarid2 regulated genes with genes up-regulated in the B16 motile cell population.

6.8.3 Identification of PRC2 regulated genes that correlate with pigment

EZH2 depletion resulted in an increase in pigment production and Jarid2 depletion gave mixed results, with siRNA #1 resulting in a decrease in pigment and siRNA #4 resulting in an increase in pigment levels. The microarray data was used to try and identify genes regulated by the PRC2 complex that control pigment production. Genes that correlated with changes in pigment levels were selected, i.e genes that were both up-regulated on EZH2 siRNA #1, 4 and Jarid2 siRNA #4 and down-regulated on Jarid2 siRNA #1 depletion. This resulted in a list of 31 genes that correlated with changes in pigment (Table 9). One of the genes was *Oca2* and mutations in this gene in humans are known to result in a form of albinism called oculocutaneous albinism type 2 (Donnelly et al., 2012). In addition, polymorphisms in *Oca2* result in most of the variation in human eye colour (Duffy et al., 2007) and can account for differences in skin and hair pigmentation (Han et al., 2008). *Oca2* encodes a melanosomal membrane protein known as the P protein, which is thought to be involved in tyrosine transport and processing (Rosemblat et al., 1994) (Chen et al., 2002) (Toyofuku et al., 2002). Therefore, changes in expression of this gene may affect pigment production.

To confirm that PRC2 components could regulate *Oca2* mRNA levels, B16 F2 cells depleted for EZH2 and Jarid2 were subject to Q RT-PCR for *Oca2*. This validated the array results and showed an increase in *Oca2* mRNA levels on depletion of EZH2 (Figure 6.22), in parallel with the increased pigment observed on EZH2 depletion. *Oca2* mRNA levels decreased on knockdown of Jarid2 siRNA #1 (Figure 6.22), correlating with a decrease in pigment levels in cells treated with this siRNA. Depletion of Jarid2 with siRNA #2 and 4 increased *Oca2* mRNA (Figure 6.22). This correlated with the quantification of pigment levels on a cell to cell basis as both these siRNA increased pigment levels in this assay.

Gene symbol	Fold change			
	EZH2 #1	EZH2 #4	Jarid2 #1	Jarid2 #4
1810014f10rik	1.23	1.44	-1.22	1.26
1810058m03rik	1.33	1.40	-1.50	1.52
Trnp1	1.53	2.38	-2.29	1.25
A530050n04rik	2.10	2.48	-1.28	2.03
Bace2	1.75	1.45	-1.88	1.34
Capzb	1.60	1.34	-1.29	1.49
Ccl5	1.69	1.39	-1.66	1.77
E430003j01rik	1.42	1.28	-1.28	1.24
Esrra	1.26	1.20	-1.75	1.42
Gsta1	1.66	1.54	-3.66	1.37
Hist1h1c	1.87	2.37	-1.39	2.57
Hist1h2bc	1.30	1.53	-1.38	1.88
Hist1h2be	1.23	1.64	-1.28	1.57
Hist1h2bf	1.23	1.92	-1.30	1.75
Hist2h2aa1	1.38	1.26	-1.36	1.24
Irf9	1.31	1.53	-1.35	1.84
L3mbtl2	1.47	1.98	-1.53	1.46
Loc100038882	1.71	1.64	-1.69	1.87
Loc100048346	1.55	1.63	-1.49	2.46
Loc634731	1.31	1.56	-1.64	2.00
Lrrc8a	1.25	1.22	-1.68	1.21
Mpv17l	1.44	1.26	-1.29	1.30
Oas1g	1.20	1.58	-1.35	1.93
Oca2	2.38	2.08	-1.32	2.25
Rab1	1.31	1.35	-1.92	1.23
Rbks	1.26	1.25	-1.27	1.68
Samd9l	1.28	1.67	-1.44	1.25
Sepw1	1.30	1.43	-1.25	1.52
St6galnac2	1.55	1.21	-1.41	1.37
Tbrg4	1.24	1.25	-1.28	1.34
Usp18	1.65	1.74	-1.77	3.13

Table 9. Genes correlating with changes in pigment levels.

Genes selected showed a fold change of greater than 1.2 in EZH2 siRNA #1, 4 and Jarid2 #4 and a change of less than -1.2 in Jarid2 siRNA #1.

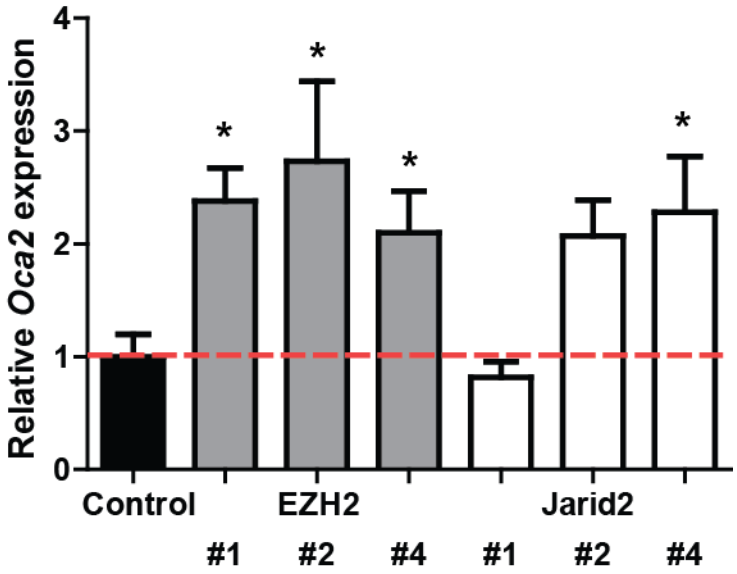

Figure 6.22. *Oca2* mRNA expression on EZH2 and Jarid2 depletion.

B16 F2 cells were transfected with control, EZH2 or Jarid2 targeted siRNA. 48 hours after transfection the cells were lysed and the total RNA extracted for Q RT-PCR analysis. Error bars show the standard error of the mean. Data from at least four experiments. Stars indicate statistical significance in ANOVA test.

To test whether the P protein could regulate pigment levels in B16 F2 melanoma, cells were depleted of P protein and the colour of the cell pellet analysed. This showed a dramatic loss of pigment levels on loss of P protein expression (Figure 6.23) Even treatment with siRNA #3 and 4, which only slightly reduced mRNA levels, resulted in very little pigment in the cell pellets .

As *Oca2* mRNA levels are regulated by PRC2 components and P protein regulates pigment, the hypothesis was that PRC2 regulates P protein resulting in changes in pigment levels. To investigate this hypothesis, P protein and PRC2 components were simultaneously depleted and the pigment levels of cell pellets examined. B16 F2 cells were transfected with equal amounts of control and EZH2 siRNA or P protein smart pool and EZH2 siRNA. Control cells received control siRNA alone. The total amount of siRNA was kept constant. EZH2 depletion resulted in an increase in pigment levels as expected, however concurrent loss of EZH2 and P protein decreased pigment compared to control cells (Figure 6.24). This indicates that P protein is required for the increase in pigment observed on EZH2 depletion.

Surprisingly, on depletion of P protein, changes to the cell morphology were observed. P protein depleted cells appeared flatter and had a larger cell area (Figure 6.25). Although the increase in cell area was similar to the EZH2 depletion phenotype, the actin phenotype was slightly different, as depletion of P protein resulted in an increase in actin cables in the cell. The change in cell morphology was unexpected because although the motile cell population has less pigment, a direct link between pigment regulation and the actin cytoskeleton was not expected. However, as P protein is involved in regulating pigment levels and depletion results in altered cell morphology, there may be a role for pigment associated proteins in control of the actin cytoskeleton.

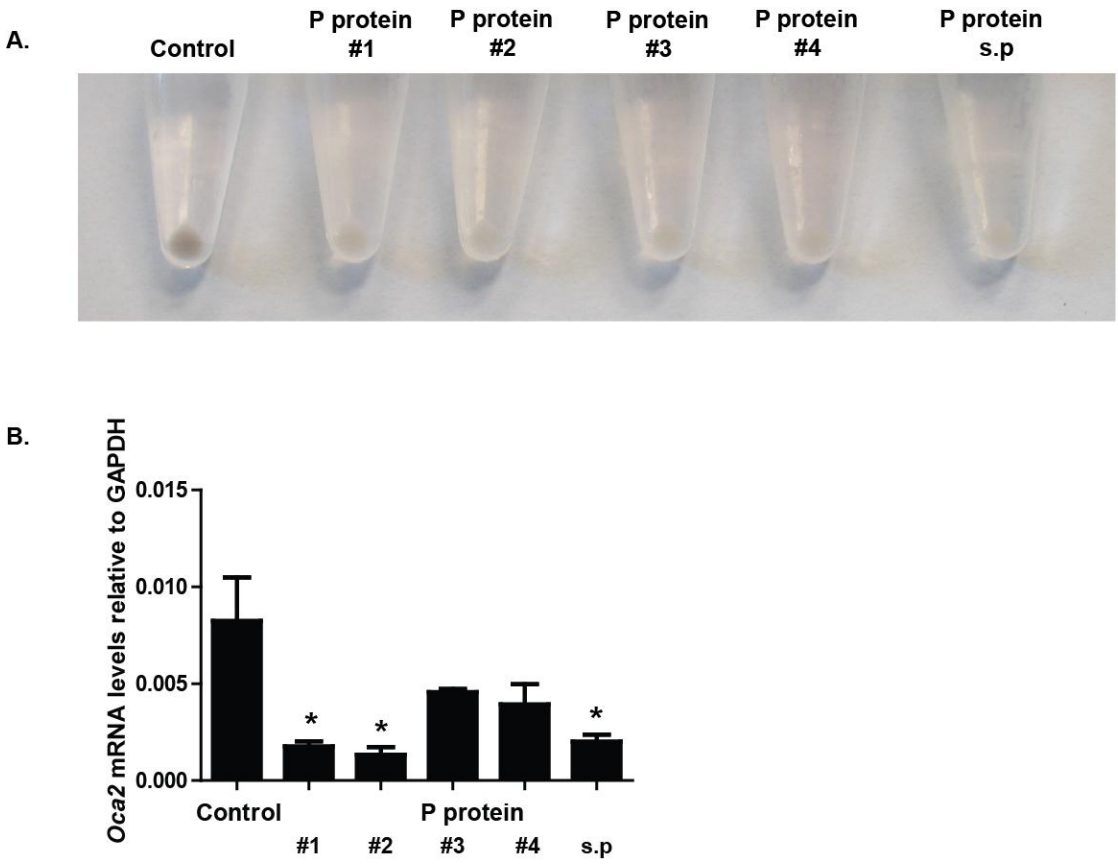

Figure 6.23. P protein regulates pigment levels in B16 F2 melanoma cells.

A. Image showing pigment levels in B16 F2 cell pellets after transfection with control or P protein targeted siRNA. 48 hours after transfection the cells were pelleted and imaged. B. Graph showing *Oca2* mRNA levels (encoding for P protein) in B16 F2 cells 48 hours after transfection with control or P protein targeted siRNA as determined by Q RT-PCR. Error bars show the standard error for three experiments. Stars indicate statistical significance in ANOVA test.

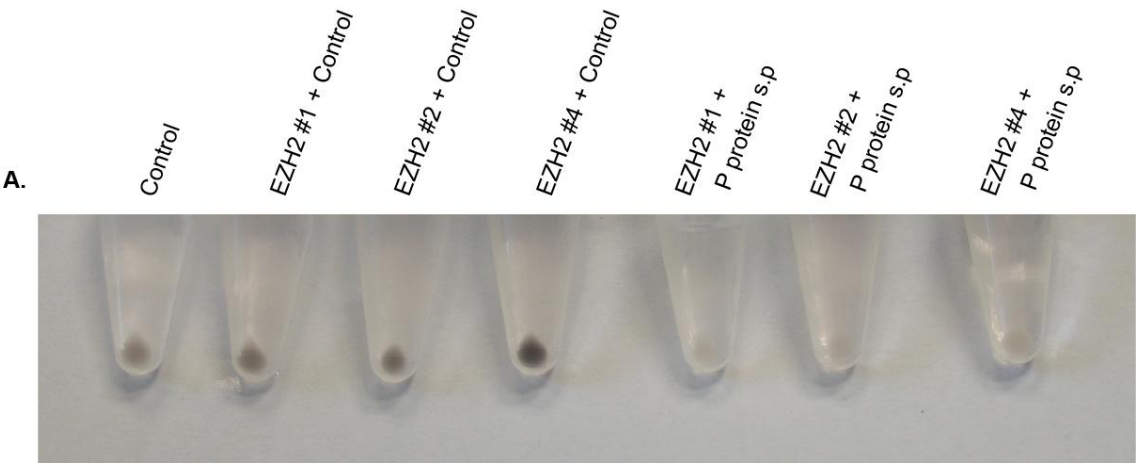

Figure 6.24. P protein is required for EZH2 pigment regulation in B16 melanoma cells.

A. Image showing pigment levels in B16 F2 cell pellets after transfection with individual or combinations of control, EZH2 or P protein targeted siRNAs. Total siRNA was kept constant at 100 nmols. 48 hours after transfection the cells were pelleted and imaged.

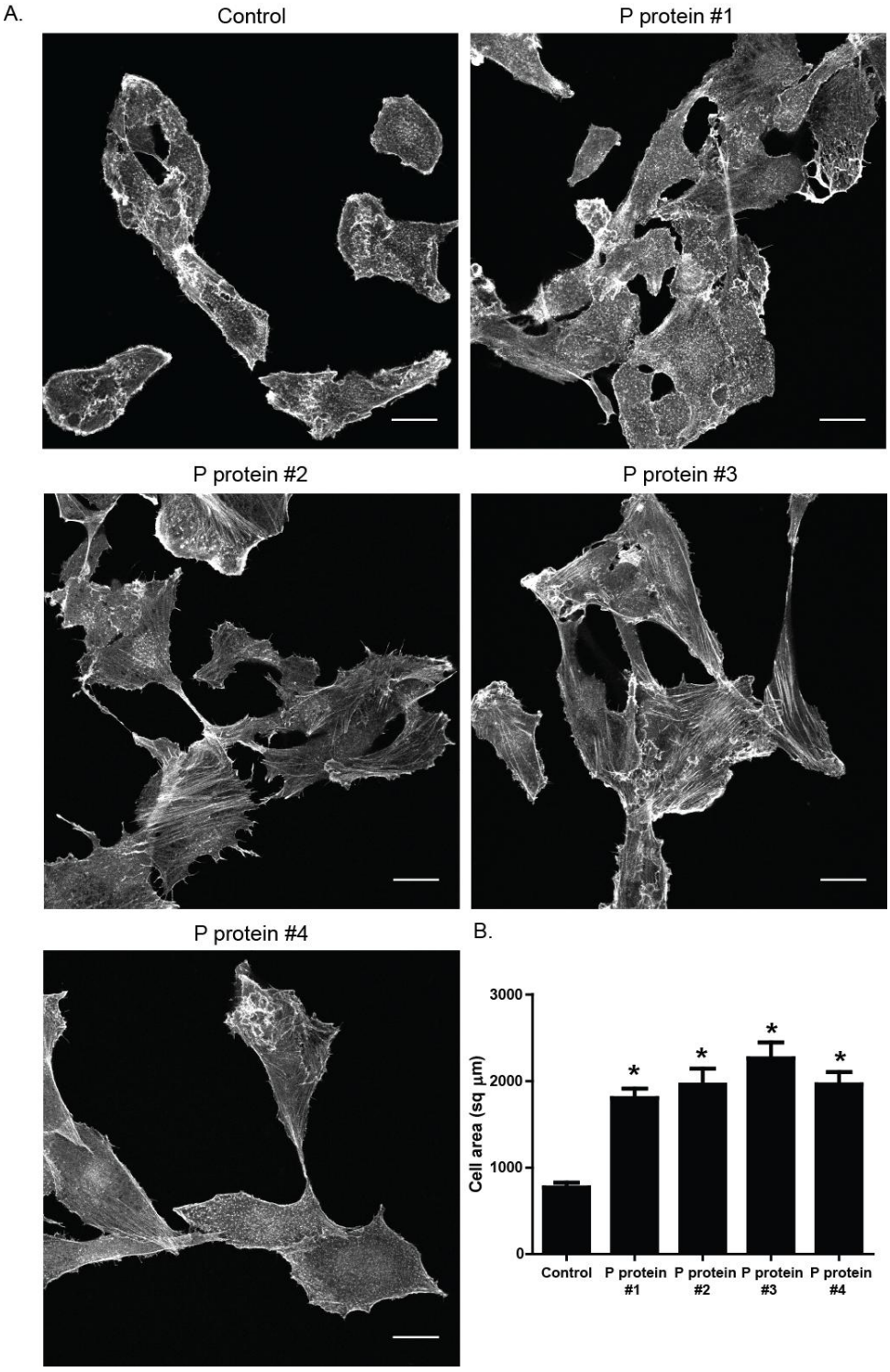

Figure 6.25. P protein depletion results in a change of cell morphology.

A. Images of B16 F2 cells transfected with control or P protein siRNA and plated on glass. Cells were fixed 48 hours after knockdown and stained with phalloidin. Scale bar indicates 25 µm. B. Quantification of B16 F2 cell area after P protein or control knockdown. Area was quantified manually by drawing around 20 cells in Zen imaging software.

6.8.4 Identification of PRC2 regulated genes that correlate with metastasis

To try and identify which EZH2 target genes regulate metastasis, the microarray data was queried to identify genes that correlated with metastasis. EZH2 depletion with siRNA #1 and 4 in B16 F10 cells resulted in decreased metastasis and Jarid2 depletion with siRNA #2 and 4 had no effect on metastasis. However Jarid2 siRNA#1 resulted in a dramatic increase in metastasis. Therefore, genes up-regulated on Jarid2 siRNA #1 depletion and down-regulated on EZH2 siRNA #1 and 4 depletion were filtered out from the microarray. The microarray analysis was performed in the F2 sub-line and the metastasis assays with the F10 sub-line, but this analysis assumes that EZH2 targets will be maintained between the two lines.

The expression of 40 genes correlated with metastasis (Table 10). Out of these 40 genes, *Actn4, Mcam, Mybl2, Myl12b, Smarce1, Sparc* and *Srf* were chosen because they were known cytoskeletal regulators or had previously been associated with metastasis. Their expression levels after EZH2 and Jarid2 depletion were analysed by Q RT-PCR to confirm the microarray results. SPARC, Alpha actinin-4 and MCAM expression most closely correlated with metastatic potential of B16 F10 cells on knockdown of EZH2 and Jarid2 with the individual siRNAs (Figure 6.26). Although the genes were initially chosen based on the expression after knockdown with EZH2 siRNA #1, 4 and Jarid2 #1, all genes showed an increase in expression after knockdown with EZH2 #2. As shown previously, (Figure 6.16) this siRNA dramatically increases metastasis showing good correlation between regulation of these genes and metastasis. However, only MCAM showed a significant reduction in expression on knockdown with EZH2 siRNA #1 and 4 (Figure 6.26). As both of these siRNA decrease metastasis, MCAM is the most likely candidate to regulate metastasis on PRC2 component depletion.

Gene symbol	Fold change			
	EZH2	EZH2 #4	Jarid2	Jarid2
Fam76b	-1.26	-1.21	1.26	-1.34
9430080k19rik	-1.41	-1.30	1.26	-1.36
9830001h06rik	-1.24	-1.21	1.43	-1.13
Actn4	-1.49	-1.21	1.24	-1.04
Anp32a	-1.52	-1.44	1.36	-1.44
Ddx39b	-1.35	-1.38	1.21	-1.02
Casp2	-1.58	-1.38	1.32	-1.09
Cdca4	-1.32	-1.24	1.23	-1.03
Celf2	-1.30	-1.21	1.23	-1.54
Dennd2a	-1.29	-1.28	1.31	-1.30
E030026i10rik	-1.35	-1.32	1.40	-1.12
Ehbp1l1	-1.22	-1.45	1.37	-1.02
G3bp1	-1.33	-1.20	1.23	-1.00
Gm22	-1.37	-1.32	1.44	-1.45
Hmgb2	-1.24	-1.34	1.25	1.13
Igfbp4	-1.41	-1.23	1.24	-1.30
Loc381889	-1.34	-1.25	1.21	-1.02
Mapre2	-1.41	-1.28	1.32	-1.45
Mbnl1	-1.28	-1.24	1.58	-1.18
Mcam	-1.58	-1.53	3.66	-1.00
Mybl2	-1.43	-1.24	1.25	-1.33
Myl12b	-1.30	-1.28	1.40	-1.06
Ncapd2	-1.38	-1.41	1.24	-1.09
Nfib	-1.29	-1.36	1.80	1.04
Nrm	-1.47	-1.48	1.49	-1.08
Hmgn5	-1.38	-1.20	1.22	-1.30
Pabpc1	-1.72	-1.21	1.23	-1.12
Pias1	-1.32	-1.25	1.30	-1.62
Polr2a	-1.22	-1.31	1.31	-1.02
Zmynd8	-1.21	-1.21	1.55	-1.27
Raly	-1.26	-1.25	1.25	1.15
Skp2	-1.50	-1.28	1.50	1.01
Smarce1	-1.36	-1.43	1.25	-1.06
Sparc	-1.69	-1.28	2.41	-1.51
Srf	-1.41	-1.68	1.50	-1.29
Suds3	-1.47	-1.49	1.25	-1.42
Tmsb10	-1.20	-1.57	1.26	-1.06
Tpm1	-1.35	-1.22	1.29	1.06
Vgll4	-1.32	-1.56	1.53	-1.02
Wnk1	-1.33	-1.20	1.23	1.04

Table 10. PRC2 regulated genes that correlate with metastasis.

Genes selected showed a fold change of less than -1.2 in EZH2 siRNA #1, 4 and a change of greater than 1.2 in Jarid2 siRNA #1.

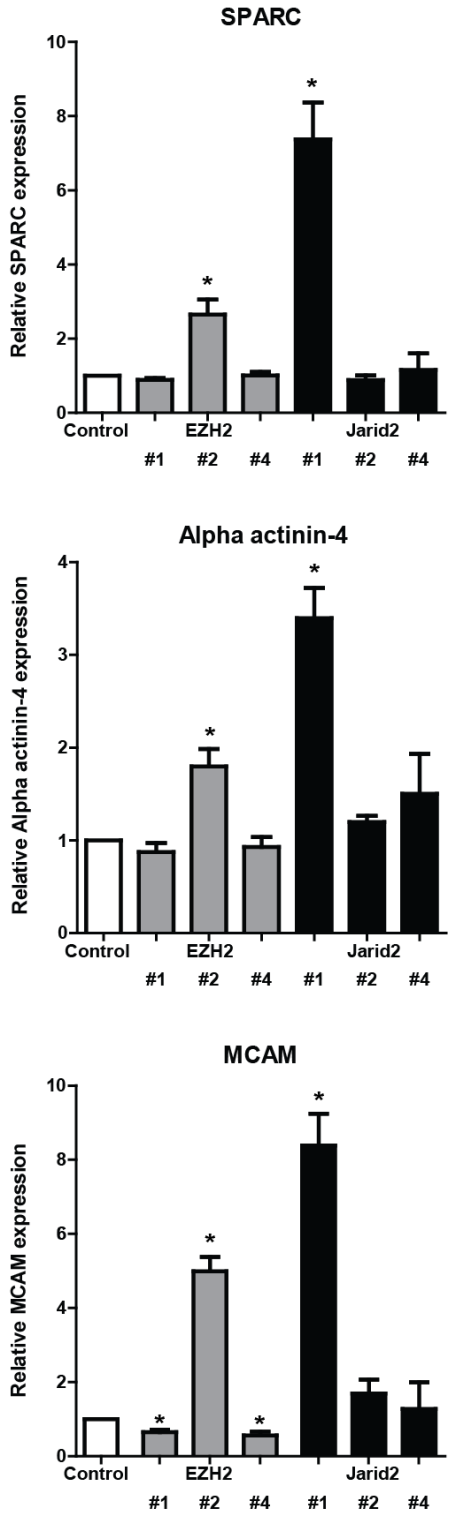

Figure 6.26. SPARC, Alpha-actinin-4 and MCAM expression closely correlates with individual EZH2 and Jarid2 siRNA effects on metastasis.

Graphs showing *Sparc*, *Actn4* and *Mcam* mRNA levels in B16 F2 cells 48 hours after transfection with control, EZH2 or Jarid2 targeted siRNA as determined by Q RT-PCR. Data from at least three experiments. Error bars show the standard error and stars indicate statistical significance in ANOVA test.

6.9 Chapter summary

Bioinformatic analysis of the genes up-regulated in the motile B16 F2 population identified EZH2 as a potential regulator of motility. Consistent with EZH2 having a role in regulating the motile B16 F2 population, *Ezh2* mRNA was up-regulated in the Notch reporter high population, a population enriched for motile cells. EZH2 levels were also heterogeneous in a number of syngeneic mouse melanoma models and in two human melanoma metastases. EZH2 and other PRC2 components including Jarid2 regulate B16 F2 cell morphology and the actin cytoskeleton through activation of the ERM proteins Ezrin and Radixin (Figure 6.27). To test whether EZH2 regulates cell motility and metastasis, the more metastatic B16 F10 sub-line was used. Cells depleted in EZH2 showed tail retraction problems and a reduction in cell speed when migrating on Fibronectin in vitro. EZH2 depletion also decreased metastasis although depletion of Jarid2 had no effect (Figure 6.27). This indicates that the PRC2 dependent regulation of ERM proteins does not influence metastasis since Jarid2 depletion could decrease ERM activation yet had no effect on metastasis. Microarray analysis suggested that EZH2 regulation of MCAM may influence the metastatic ability of B16 F10 cells. Further support for EZH2's role in regulating motility and metastasis came from overlap analysis of the genes up-regulated in the motile B16 F2 population. Genes positively regulated by EZH2 showed significant overlap with the genes up-regulated in the motile B16 F2 population. As EZH2 is currently believed to suppress gene expression, EZH2 regulation of these genes may be indirect. CHIPSeq analysis is currently underway to differentiate between direct and indirect EZH2 targets. EZH2 depletion resulted in an increase in pigment levels in B16 F2 cells and this was mediated by an increase in P protein (Figure 6.27). However, the role of the PRC2 component, Jarid2, in regulation of pigment levels was unclear. Consistent with data from ES cells, loss of EZH2 slightly increased differentiation markers and loss of Jarid2 slightly decreased differentiation markers in B16 F2 cells, although the changes were not significant.

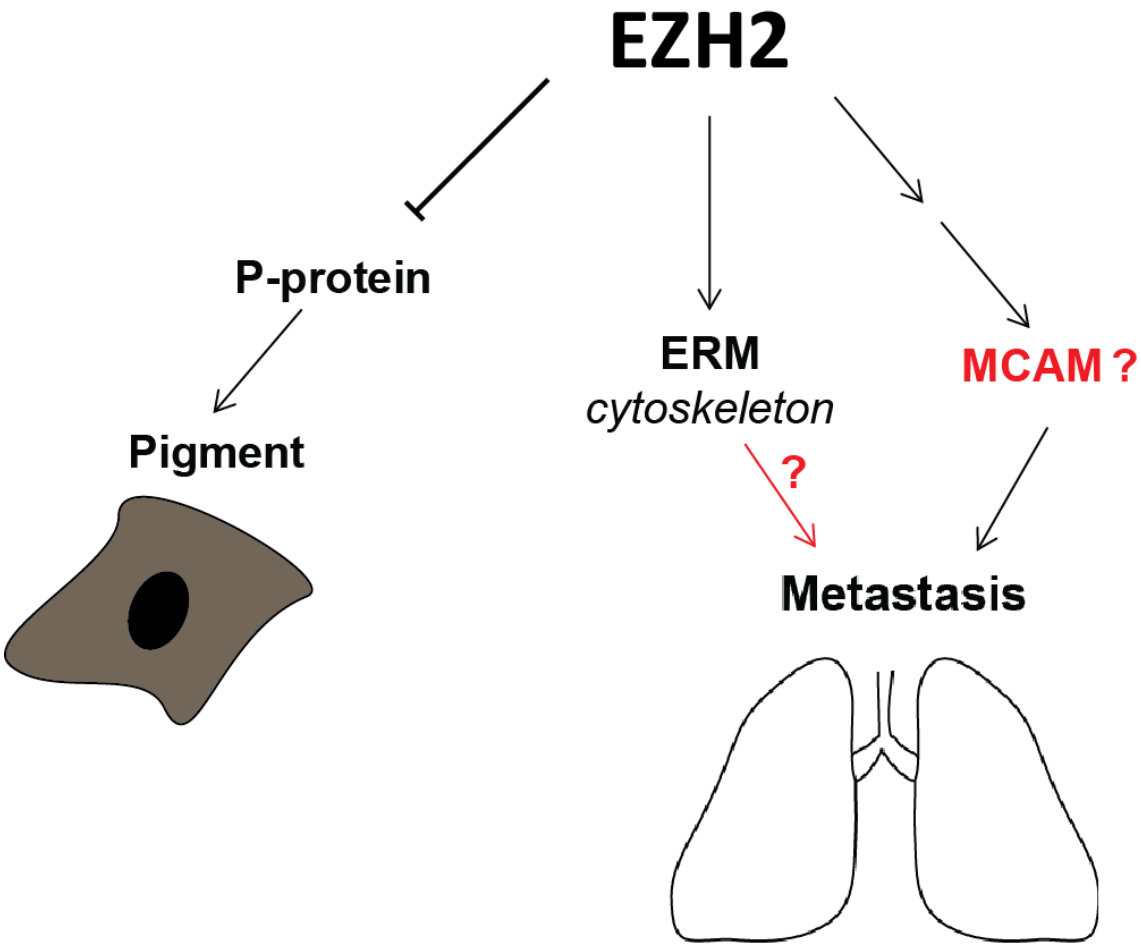

Figure 6.27. Summary.

Schematic showing a summary of the role of EZH2 in B16 melanoma cells. Details in black supported by data in chapter 6 and details in red remain speculative. EZH2 silences P-protein expression resulting in reduced pigment levels in EZH2 high cells. EZH2 regulates the cytoskeleton and cell morphology through regulation of Ezrin and Radixin activation. EZH2 also positively regulates metastasis, possibly through positive regulation of MCAM expression or through regulation of the cytoskeleton.

Chapter 7. Intra-vital imaging reveals distinct tumour vascular zones with different responses to Sunitinib

7.1 Chapter introduction

The previous chapters have considered heterogeneous melanoma behaviour, in particular motility, and melanoma cell properties associated with it. However, stromal components can also influence cancer cell invasion and metastasis (Gaggioli et al., 2007; Wyckoff et al., 2004). The vasculature is an important component of the tumour microenvironment, and provides a route for cells to metastasise (Zetter, 1998). It provides oxygen, metabolites and growth factors to the tumour and access to these may affect tumour cell behaviour (Folkman, 1971). Data from intra-vital imaging suggests breast cancer cells are more motile in regions with increased blood vessel density (Wang et al., 2005). In addition the blood vasculature is a novel target for cancer therapy. Mono-clonal antibodies targeting VEGF-A, such as Bevacizumab, or VEGFR-2 inhibitors, such as Sorafenib and Sunitinib, have been developed and licensed to treat a variety of cancers. However, treatments have not performed as well as expected and numerous clinical trials have indicated no benefit for overall survival (Allegra et al., 2011). Furthermore, pre-clinical testing has indicated that anti-angiogenic treatments may cause tumours to relapse into a more aggressive state, increasing metastasis (Ebos et al., 2009; Paez-Ribes et al., 2009). Therefore the relationship between blood vessels and cancer cell motility was investigated further. The aim was to determine whether cancer cell motility is associated with certain vascular morphologies or behaviours and whether anti-angiogenic treatments may perturb the relationship. A transgenic mouse with GFP-labelled endothelial cells was used to analyse the tumour vasculature of the syngeneic B16 and 5555 models of melanoma.

7.2 Tumour vascular morphology and dynamic behaviour is heterogeneous in vivo

7.2.1 Intra-vital imaging using VE-Cadherin:GFPCAAX mice provides a high resolution dynamic picture of the tumour vasculature

Current methods to analyse the tumour vasculature include immunohistochemistry (Figure 7.1A) and injecting labelled probes into the blood. Immunohistochemistry involves fixing the tumour and cutting thin slices. Due to fixation any dynamic information is lost and artefacts may be introduced during the fixation process. In addition, the technique does not easily allow 3-D analysis of the vasculature. Injectable probes, whether fluorescent or radiolabelled, only give information about perfused vessels and information about the endothelial cells themselves is not easily available. To circumvent these issues, intra-vital imaging was used to analyse the tumour vasculature. Intra-vital imaging allows serial z-sections to be imaged to form a 3-D reconstruction. Additionally time-lapse imaging enables dynamic information to be recorded.

VE-Cadherin:GFPCAAX mice were used to visualise the vasculature. These mice were generated by Ralf Adams and have GFP with a membrane targeting CAAX box under the control of the VE-Cadherin promoter. Briefly, cDNA encoding for enhanced green fluorescent protein fused to a C-terminal CAAX box was introduced by recombineering into the start codon of VE-Cadherin in a PAC clone. The resulting construct was used in a circular form for pronuclear injection into fertilised mouse oocytes. Founders, identified by PCR genotyping, were screened and, following successful validation, bred into a C57BL/6J background. VE-Cadherin expression is limited to endothelial cells and so only the vasculature is labelled with membrane GFP. Sub-cutaneous injection of either B16 F2 or 5555 melanoma cells with a red fluorescent membrane marker into VE-Cadherin:GFPCAAX mice allowed visualisation of both the melanoma cells and the vasculature using either two-photon or single photon intra-vital microscopy. This enabled analysis ranging from a large scale overview of the tumour microenvironment (Figure 7.1 B) to a high magnification look at individual sprouting vessels interacting with the ECM (Figure 7.1F). However, due to the penetration

capabilities of single and two-photon lasers, the depth into the tumour that could be imaged was limited to around 200µm with a two-photon laser. This is indicated in Figure 7.1A by the dashed box showing the limit of intra-vital imaging on a immunohistochemical staining.

Injection of the fluorescent probe Angiosense 680 immediately prior to imaging tumours in VE-Cadherin:GFPCAAX mice indicated that many of the nascent sprouting vessels in the tumour are not perfused. (Compare Figure 7.1C,D and E). This highlights the fact that injectable probes do not provide information about the entire tumour vasculature network.

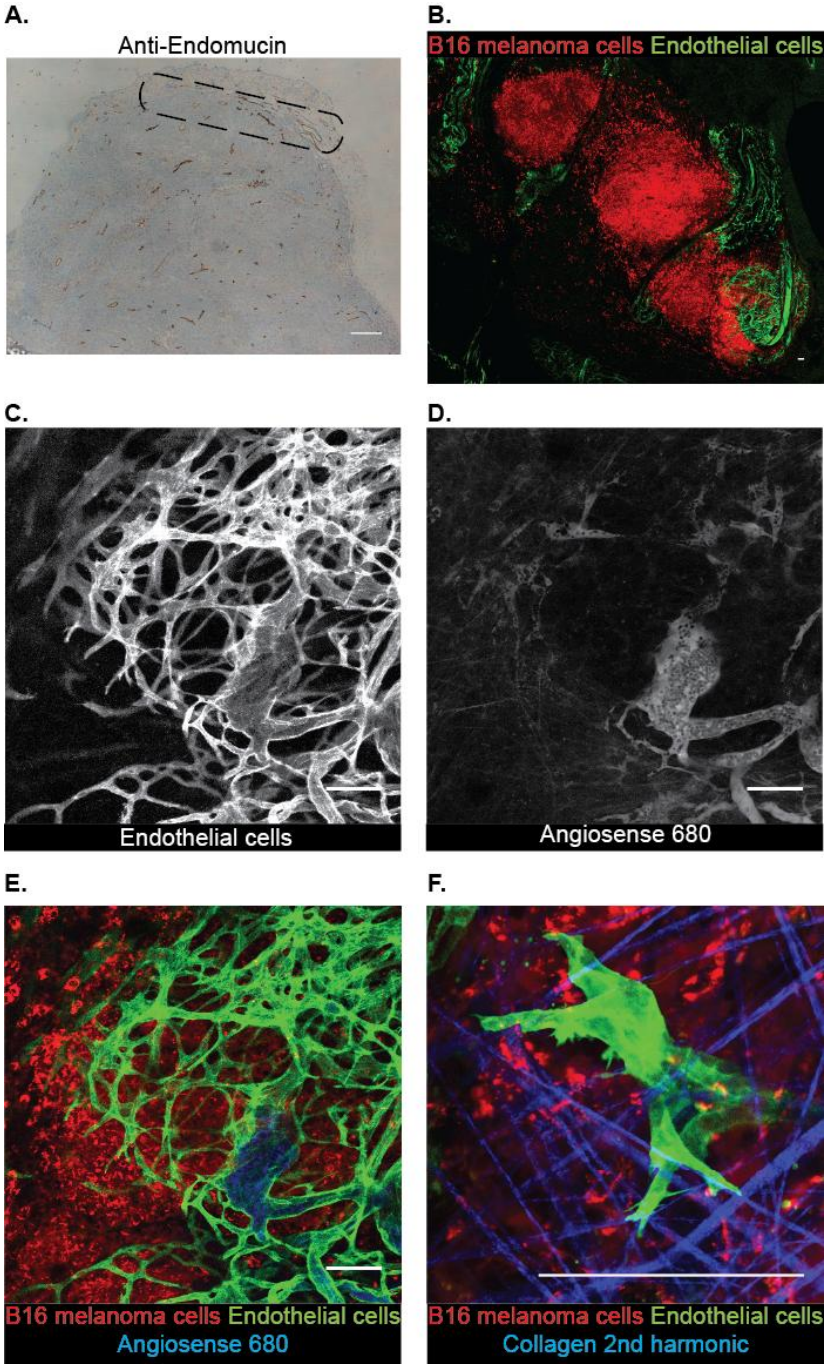

Figure 7.1 Imaging the tumour vasculature.

A. Immuno-histochemical staining of B16 F2 tumours using anti-Endomucin antibody to identify blood vessels. Dashed area roughly represents the area possible to image with multi-photon intra-vital microscopy. B. Intra-vital confocal tile image showing whole tumour and margin. C-E. Intra-vital confocal image of angiogenic sprouting towards tumour. C. GFP channel showing only vasculature. D. Infra-red channel showing extent of blood flow using Angiosense 680. E. Merge of red melanoma cells, green vasculature and Angiosense 680. F. Two-photon intra-vital image of a sprouting blood vessel with Collagen second harmonic in blue. Intra-vital images show B16 F2 melanoma cells with red membrane marker in VE-Cadherin:GFPCAAX mice. Endothelial cells have green membrane marker. Scale bar indicates 100μm.

7.2.2 Quantification of vascular morphologies reveals distinct zones in the tumour environment

Tile images spanning several hundred microns of B16 F2 melanomas in VE-Cadherin:GFPCAAX mice suggested that different vessels in the same tumour had different morphologies (Figure 7.1). To further characterise the vessel morphologies, images of numerous vessel areas in several tumours were taken using a 20x objective (3D reconstructions shown in Supplementary movies 8 and 9). Images were characterised into tumour or margin depending on the presence or absence of tumour cells. Healthy vessels were analysed on the alternative flank to the tumour as a control. A number of morphometric parameters were analysed for each image. The parameters chosen were based on conventional parameters used to define vascular morphology with a focus on aspects of morphology known to be abnormal in the tumour vasculature. Tortuosity was calculated by measuring the arc length and chord length of a vessel and dividing the arc length by chord length (Figure 7.2A). Branch points were measured by counting the number of branch points and dividing by the vessel length to get a number of branch points per vessel length (Figure 7.2A). Blunt ends were measured by counting the number and dividing by the vessel area (Figure 7.2A). Vessel area was calculated by thresholding on the GFP signal for the image and using image analysis software to measure the area. Variation in vessel width was calculated by measuring the vessel width every 15μm along a 150μm vessel section. The mean and standard deviation of vessel width were determined for the 150μm section and variation in vessel width was calculated by dividing the standard deviation by the mean (Figure 7.2A).

The morphological data for individual vascular networks was then subject to hierarchical clustering to create a cluster dendrogram (Figure 7.2 B). The distance along the arms in the dendrogram represents the degree of similarity in morphology between vascular networks, with smaller distances indicating increased similarity. This analysis revealed three predominant classes of vascular organisation: one class was dominated by healthy tissue (Figure 7.2 B cluster 1), the second by vessels from the tumour margin (Figure 7.2 B cluster 2), and the third included both tumour vessels and some tumour marginal vessels (Figure 7.2 B cluster 3). The

margin vascular networks fell into two distinct clusters (cluster 2 and 3), which shows that there are two distinct types of vascular networks found at the tumour margin. The vascular networks at the tumour margin in cluster 2, were the least similar to any other group and were characterised by increased tortuosity and variation in vessel width. The margin networks in cluster 3 were characterised by increased branch points and vessel ends.

Further analysis of tile images of B16 F2 tumours indicated that the distinct margin regions may be related to distance to tumour (Figure 7.3 and Supplementary movie 10). However, it is difficult to conclusively show the relationship between distance to tumour and vascular morphology due to the curvature of the tumour and the distance limit of imaging. The distinct vascular zones were thereby labelled immediate margin and peripheral margin. The peripheral margin refers to the most morphometrically abnormal zone (cluster 2 in Figure 7.2) and the immediate margin (cluster 3 in Figure 7.2) refers to the zone with similar morphology to tumour vasculature.

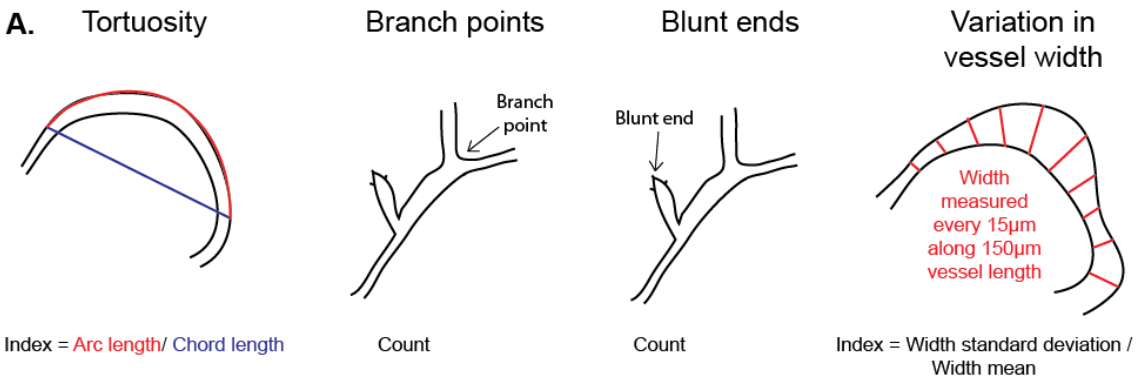

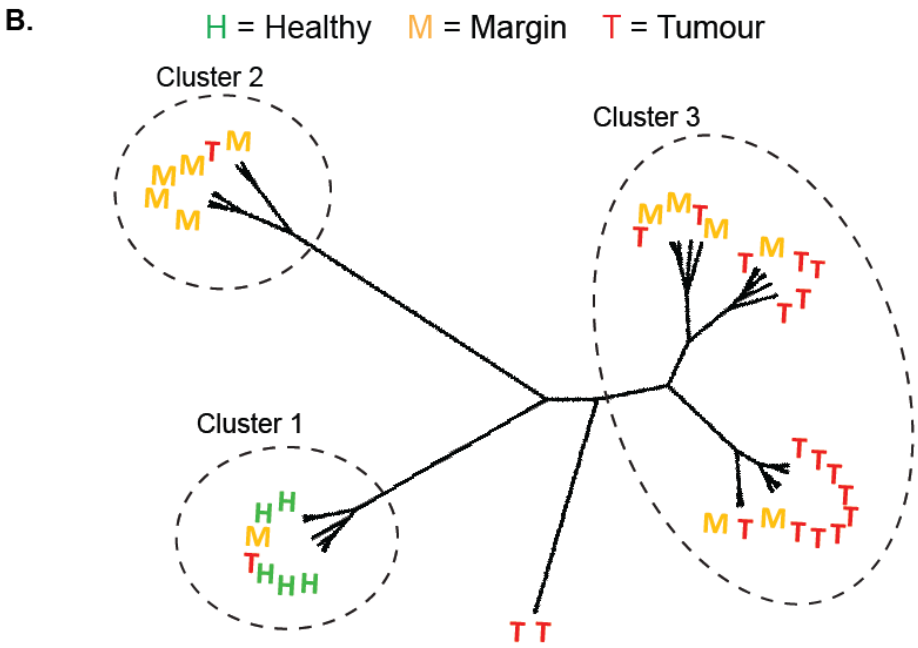

Figure 7.2 Quantification of vascular morphology reveals distinct margin regions.

A. Schematic showing parameters quantified; tortuosity, number of branch points per vessel length, number of blunt ended vessels (tip cells), variation in vessel width. B. Hierarchical cluster dendrogram of vessels based on the four morphometric parameters. 3 individual clusters are designated by the dashed lines. Clustering using Ward's criterion and Euclidean distance. Multiple images for each region are shown by coloured letters, tumour regions with a red "T", margin regions with an orange "M" and healthy regions with a green "H". Numerous representative vessels were quantified in each image and images from at least 3 mice used for each region. Healthy regions were imaged in skin on opposite flank to tumour growth.

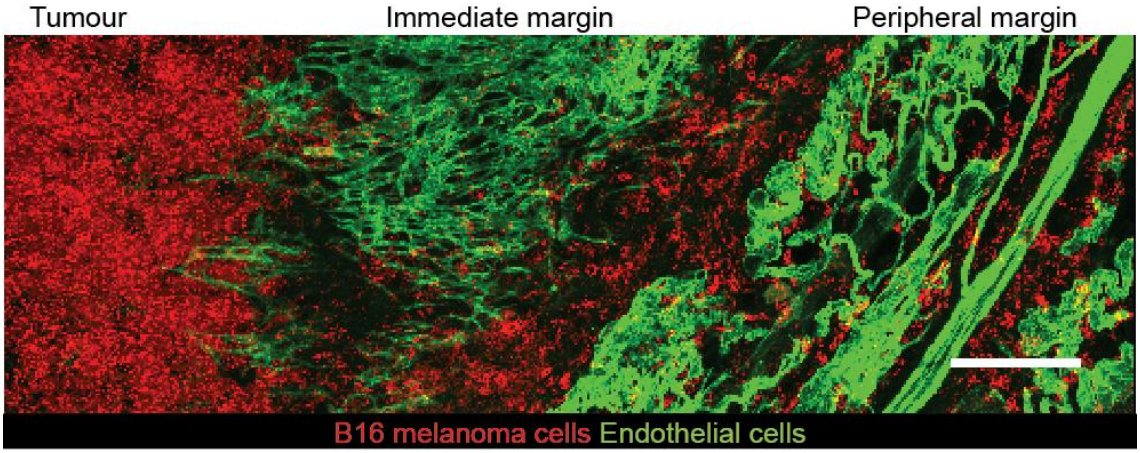

Figure 7.3 Two zones with distinct vascular morphology exist within the tumour margin.

Intra-vital tile image of B16 F2 melanoma in VE-Cadherin:GFPCAAX mouse. B16 F2 melanoma cells have red membrane marker. Additional auto-fluorescent cells, potentially phagocytic macrophages, can be seen in the red channel in both margin zones. Endothelial cells have green membrane marker. Scale bar indicates 50μm.

Images illustrating vascular morphology in the different zones are shown in Figure 7.4. The main characteristics of the peripheral margin are high tortuosity and a large variation in vessel width. The immediate margin has the most branch points and a high density of blunt ends, very similar to the tumour (Figure 7.5).

To test if the vascular morphologies observed in B16 F2 melanoma were a more general phenomenon, vascular morphology was also quantified in different areas of sub-cutaneous 5555 melanomas. This also indicated that there were differences in morphology in different margin areas, again highlighting the increased tortuosity and variation in vessel width in the peripheral margin (Figure 7.5). However values for tortuosity and variation in vessel width were not as high as in the B16 model. The 5555 model also had a high number of branch points and blunt ends in the intermediate margin and tumour (Figure 7.5). In the 5555 model the intermediate margin had the most blunt ends whereas in the B16 model the tumour had the most blunt ends, potentially indicating a slower angiogenic response in 5555 tumours.

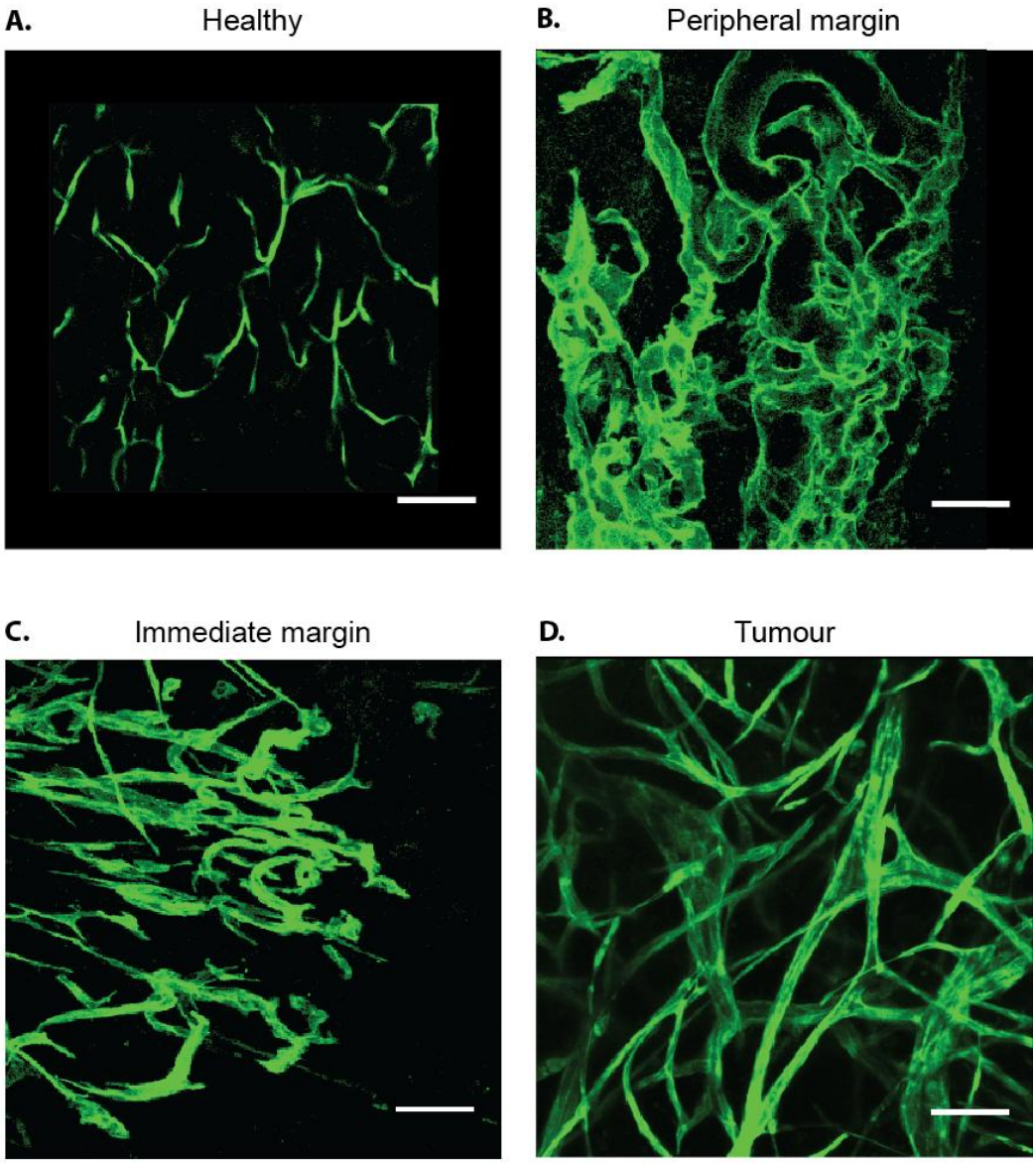

Figure 7.4 Heterogeneity in vascular morphology in different tumour environments.

Intra-vital images of vasculature from VE-Cadherin:GFPCAAX mice with sub-cutaneous B16 F2 melanoma tumours. A. Healthy skin was imaged on adjacent flank to the tumour. B. Peripheral margin. C. Immediate margin. D. Tumour. Endothelial cells have green membrane marker. Scale bar indicates 50μm.

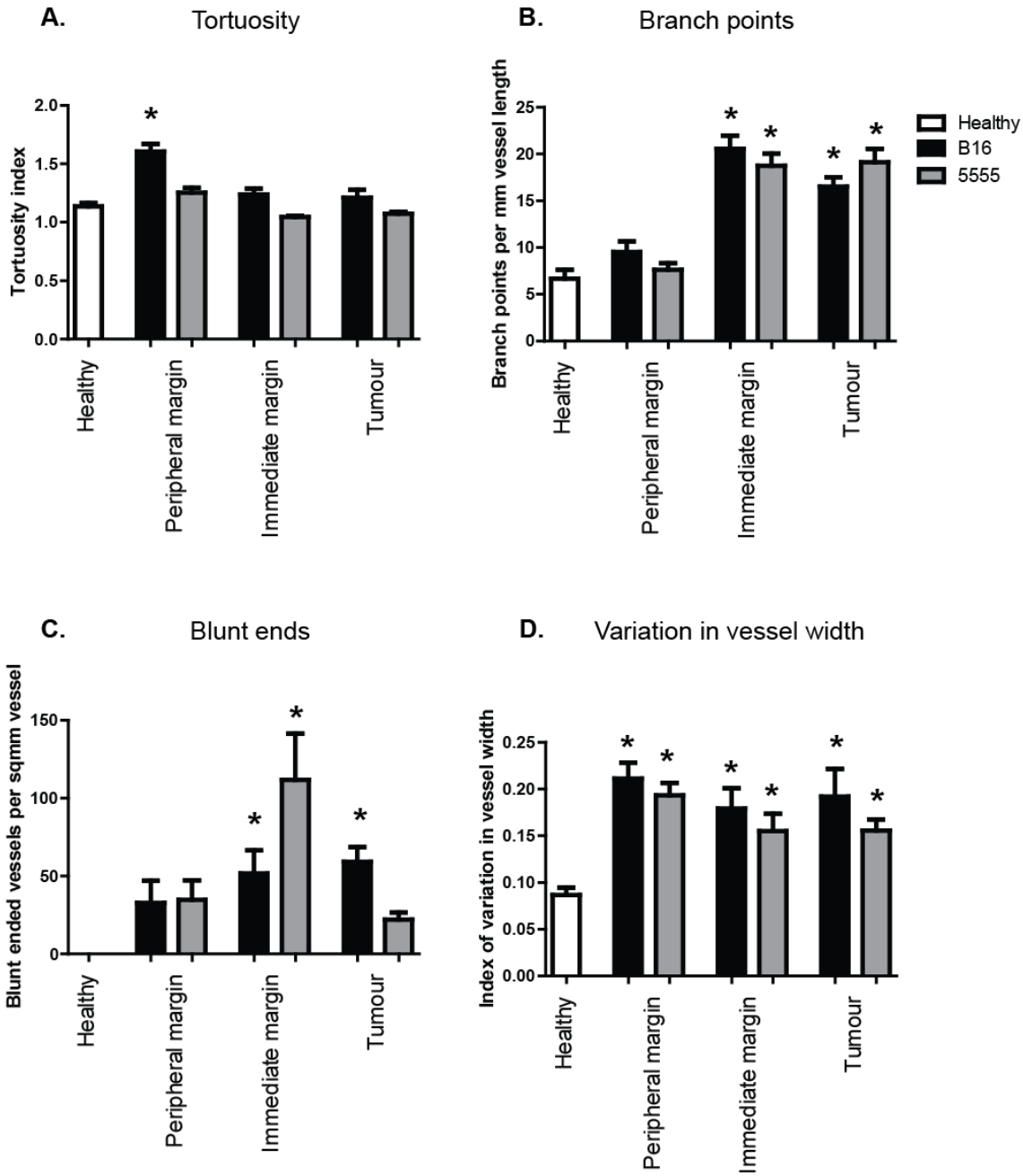

Figure 7.5 Quantifcation of vascular morphometric parameters in two melanoma models.

Graphs of morphometric variables A. Tortuosity, B. Branch points, C. Blunt ends and D. Variation in vessel width. Vessels were quantified in the four distinct vascular zones in both B16 and 5555 BRAFV600E melanomas grown in syngeneic C57Black6 mice. Numerous representative vessels were quantified in each image and images from at least 3 mice used for each region. Error bars show standard errors. Stars indicate a p-value <0.05 in a one-way ANOVA with a post-test to compare against Healthy vessels.

7.2.3 Intra-vital imaging reveals heterogeneous dynamic endothelial cell behaviour

To analyse the dynamic behaviour of tumour associated endothelial cells 3-D z-stacks of the vasculature were taken every minute for a period of 20-30 minutes. Movies of healthy, peripheral margin, immediate margin and tumour vasculature were analysed. This indicated a number of dynamic cellular behaviours (Figure 7.6). Two different types of protrusions were observed; filopodia-like (Supplementary movie 11) and bleb-like (Supplementary movie 12), and these could be either intra- or extra-luminal. Endothelial cells were observed moving within the vessel walls (Supplementary movie 13). Unexpectedly, they were also observed using a rounded mode of motility (Supplementary movie 14), reminiscent of amoeboid cancer cell motility, to move within the tumour distant to vessels at speeds of about 35 μm/hour.

Quantification of dynamic behaviour by counting the number of events and normalising to the vessel area revealed that, as expected, the healthy vessels were relatively quiescent with little dynamic behaviour. The peripheral margin was the most dynamic (Figure 7.7A). This correlates with the peripheral margin also having the most abnormal morphology. Dynamic activity in the peripheral margin was characterised by cell protrusions (Figure 7.7). The immediate margin and tumour had similar levels of dynamic activity, although the types of behaviours differed slightly. Vessels in the immediate margin had more protrusions where as tumour vessels had increased motility both within the vessel and distant to it (Figure 7.7). The dynamic information confirms that vessels in distinct vascular zones based on morphology, also have distinct dynamic behaviour.

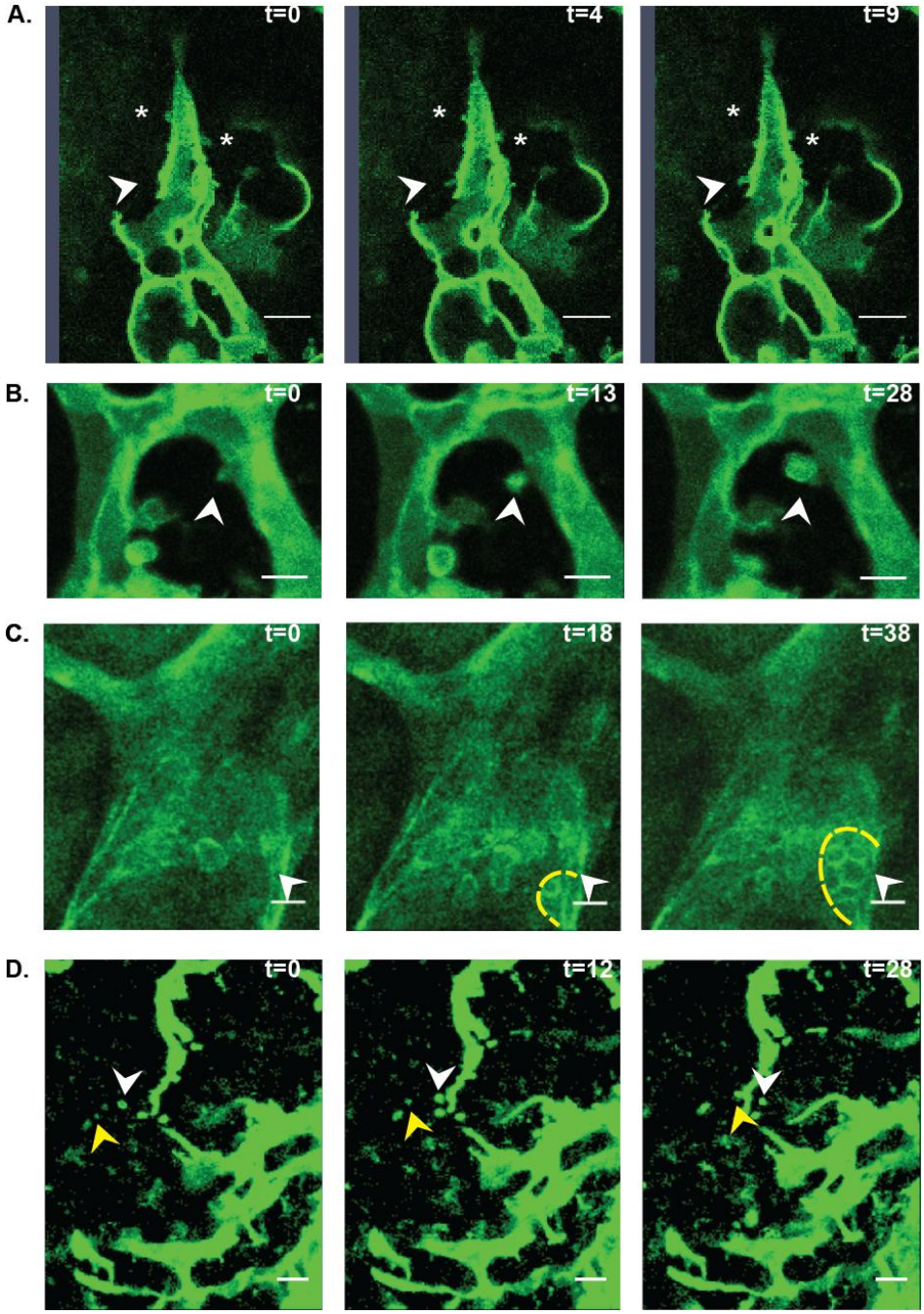

Figure 7.6 Dynamic endothelial cell behaviour in vivo.

A Filopodia-like protrusions. Stills taken from a movie at time 0, 4 and 9 minutes. Arrowheads indicate filopodia-like protrusion from tip cell and stars indicate filopodia retraction. Scale bar indicates 20 μm. B. Bleb-like protrusions. Stills taken from a movie at time 0, 13 and 25 minutes. Arrowhead indicates a bleb-like protrusion from a vessel. Scale bar indicates 20 μm. C. Intra-vessel wall motility. Stills taken from a movie at time 0, 18 and 38 minutes. Arrow indicates collective movement of endothelial cells within the vessel wall and yellow dashed line indicates extent of movement. Scale bar indicates 20 μm. D. Endothelial cell motility distant to vessels. Stills taken from a movie at time 0, 12 and 28 minutes. Arrowheads indicate two different motile endothelial cells. Scale bar indicates 50 μm. Endothelial cells have green membrane marker.

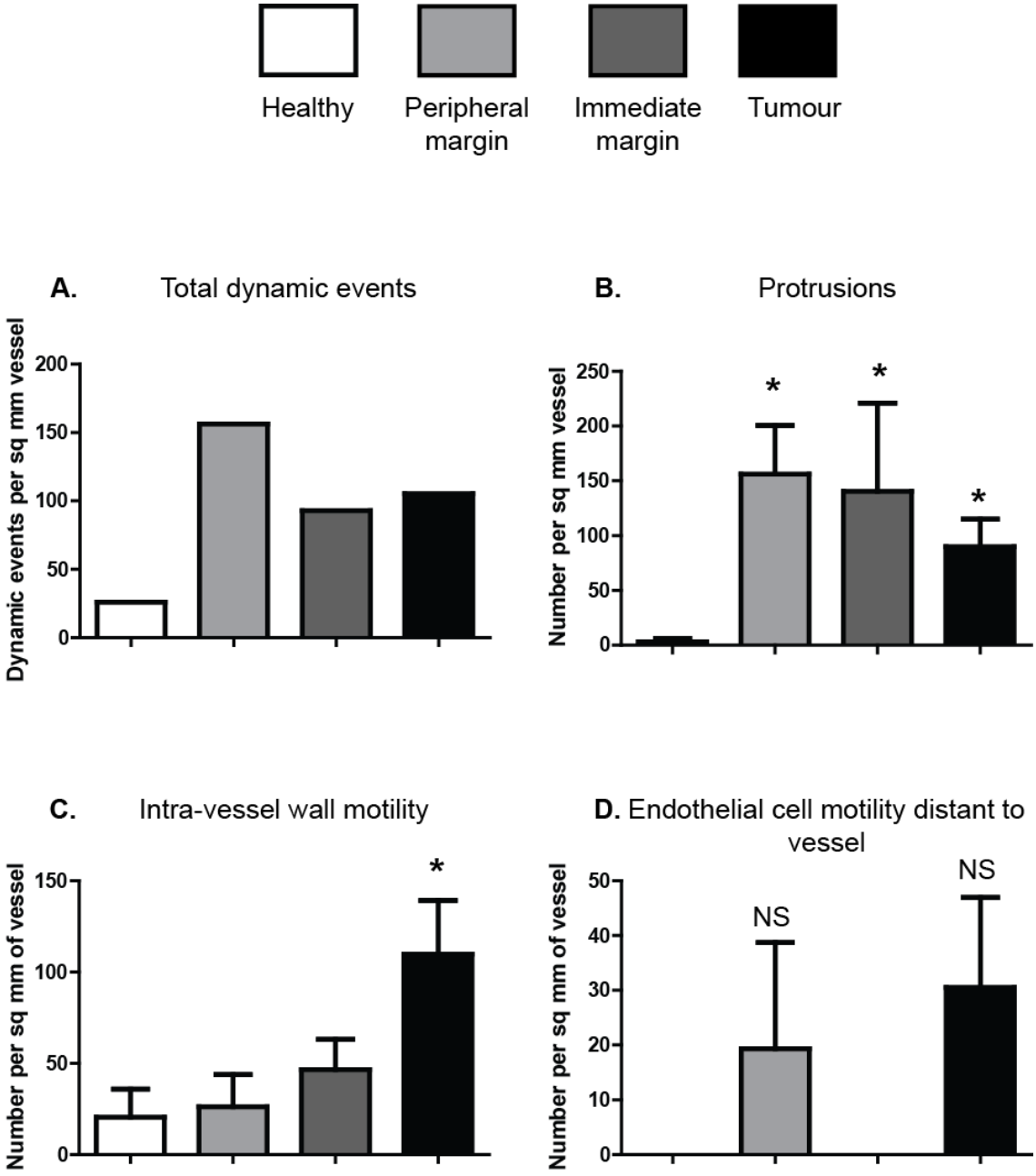

Figure 7.7 Quantification of dynamic behaviours in different vascular zones.

A.Graph showing total number of dynamic events in distinct vessel regions. Dynamic events measured by intra-vital time-lapse imaging and given as an average over the z-stack. Graphs showing prevalence of different dynamic events; B. Protrusions, C. Intra-vessel wall motility, D. Endothelial cell motility distant to vessel, in distinct vessel regions. At least 8 movies analysed from 4 mice for each region. Error bars show standard errors. Stars indicate a p-value < 0.05 in ANOVA statistical tests and ns is not significant.

7.3 Melanoma cell motility correlates with aspects of vascular morphology and dynamics

Chapter three discussed the heterogeneity in melanoma motility in vivo. Differences in motile behaviour could be a result of the microenvironment and after determining heterogeneity in morphology and dynamics of the vasculature in vivo, the correlation between vasculature and melanoma cell motility was investigated. Melanoma cell motility, vessel density and the previously described morphological and dynamic parameters were measured simultaneously in twenty different tumour time-lapse movies. Parameters were averaged to get a value for the whole volume of the z-stack movie. Z-stacks were typically 20µm deep. Initially cancer cell motility was plotted against vessel area to determine if there was a simple correlation between the extent of vascularisation and melanoma motility. Statistical tests did not reveal a significant correlation between melanoma cell motility and vessel area (Figure 7.8).

To determine if melanoma cell motility correlated with morphological features of the vasculature, levels of cell motility was arbitrarily divided into six groups from no cancer cell motility to high (>120 cells moving per sqmm tumour) and given a colour from white, through pink to red for high melanoma cell motility. This was then overlaid onto the dendrogram generated through hierarchical clustering of vascular morphology. Tumour areas in the dendrogram were thereby represented by a measure for melanoma cell motility in the same region. This revealed that even though the clustering was performed using morphological parameters, tumour regions with high melanoma cell motility were within the same cluster (Figure 7.9). Furthermore, tumour vascular networks fell into two main sub-clusters based on morphology, sub-cluster A and B (shown in Figure 7.9) and sub-cluster A had statistically higher melanoma motility than sub-cluster B. This suggests that there is a link between overall vascular morphology and levels of melanoma cell motility.

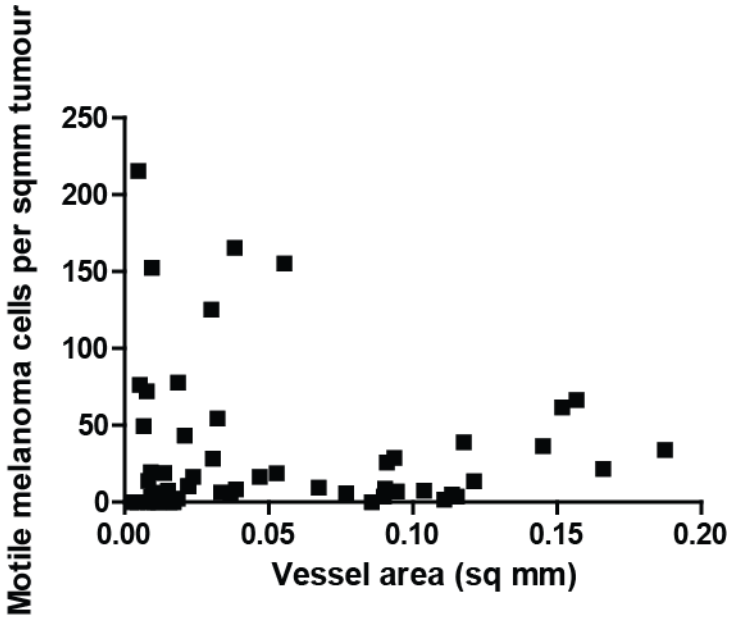

Figure 7.8 Melanoma cell motility does not correlate with vessel area

Plot of cancer cell motility vs vessel area. Cancer cell motility and vessel area measured in the same intra-vital z-stack time-lapse movie. Cancer cell motility given as an average over the z-stack. Vessel density measured by thresholding green endothelial cell channel and given as an average over the z-stack. Time-lapse movies from 7 mice analysed.

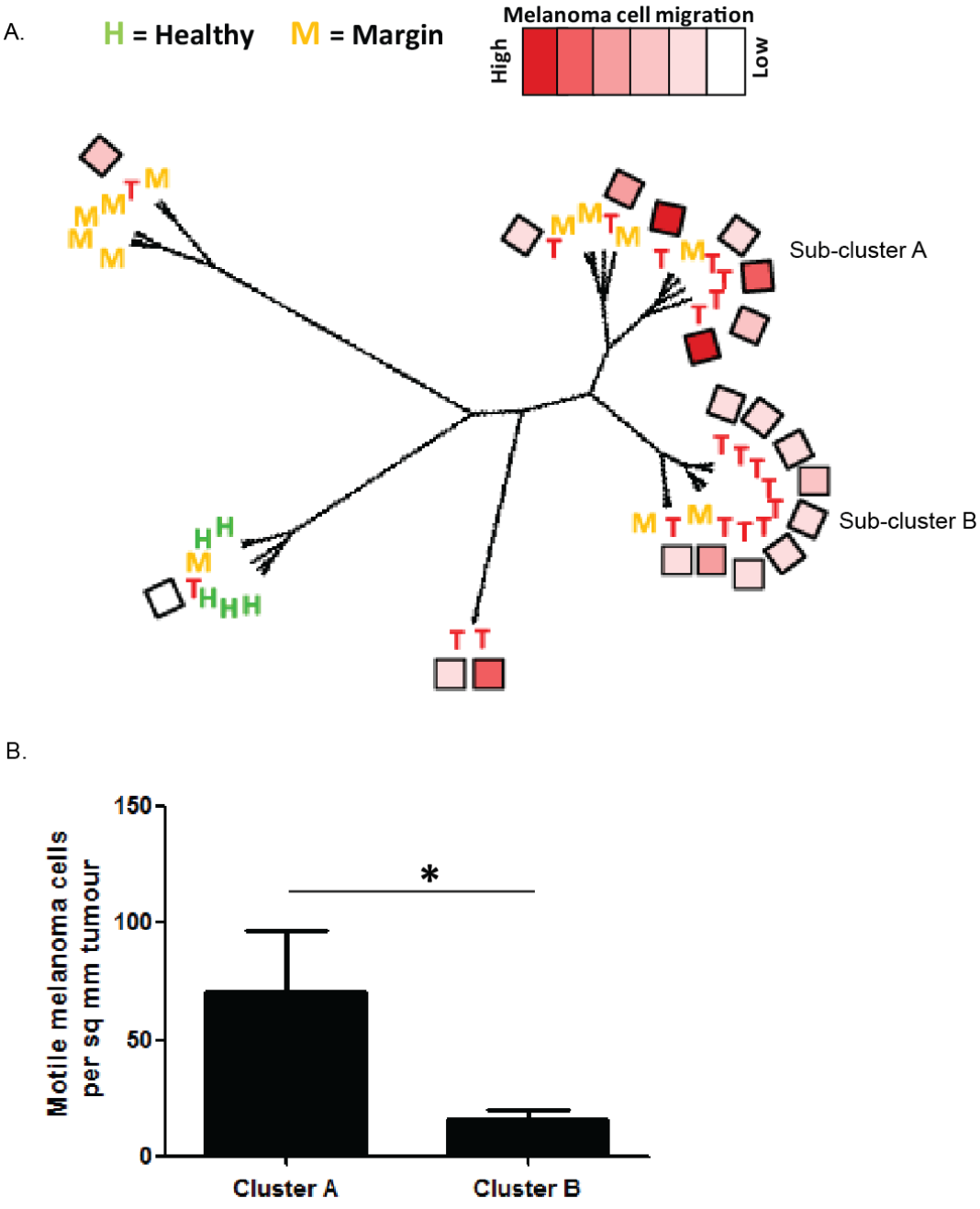

Figure 7.9 Melanoma cell motility correlates with vascular morphology.

A. Hierarchical cluster dendrogram of vessel morphology. Tumour regions have been replaced with relative cancer cell motility metric on a white to red scale. White represents no motile cancer cells and red represents high cancer cell motility with > 120 motile cancer cells per sqmm of tumour. Melanoma cell motility measured by counting the number of motile cells from a 20 minute intra-vital timelapse movie and averaging over the z-stack. 20 timelapse movies from 7 mice analysed. B. Graph showing average motile melanoma cells for tumour areas in sub-clusters A and B. Star indicates p-value <0.05 in t-test.

To determine which morphological, and in addition whether dynamic characteristics of the vasculature correlated with high melanoma cell motility, each parameter was correlated to melanoma cell motility using data from 20 tumour areas. In addition, each morphometric and dynamic parameter was correlated with each other to look for interesting correlations between the characteristics. The correlations used the Spearman co-efficient which is robust to non-parametric parameters. The correlations showed potential links between melanoma cell motility and endothelial cell intra-vessel wall motility, endothelial bleb-like extra-luminal protrusions and variation in vessel width (

Table 11). The correlation p-values are not corrected for the large number of correlations and due to the small sample size (20 data points) the correlations can only be considered as potential links between the two variables. Interesting relationships from the matrix were subsequently plotted against each other (Figure 7.10). Endothelial intra-vessel wall motility and endothelial bleb-like extra-luminal protrusions both show correlation with melanoma cell motility, but also with each other. To determine if there was a relationship between endothelial intra-vessel wall motility and endothelial bleb-like extra-luminal protrusions to melanoma cell motility, model fitting was carried out using both standard linear regression and robust linear regression, which is more robust to outliers. Models that included various combinations of linear terms and quadratic and cubic interaction terms were considered. Interaction terms suggest that the relationship between one interacting variable and the dependent variable is reliant on the second interacting variable. Hypothesis tests using ANOVA were carried out to deduce which model is the most significant. The model that fitted the data best is given by

$$M = \beta_0 + \beta_1 I + \beta_2 B + \beta_3 I^2 B$$

where M is the melanoma cell motility, I is the intra-vessel wall motility and B is the bleb-like extra-luminal protrusions. βs are fitted parameters. The fitted model indicates that the effects between the two independent variables on melanoma cell motility are not additive, but that there is a cubic interaction between them. Hence these two variables may describe a permissive environment for melanoma motility.

The correlations suggested a link between endothelial cell intra-vessel wall motility and extra-luminal bleb-like protrusions (
Table 12). Both protrusions and endothelial cell motility are driven by VEGF-A (Rousseau et al., 2000) (Gerhardt et al., 2003) and as both of these parameters correlate with melanoma cell motility, melanoma motility may be increased in regions of high VEGF-A (see Discussion for alternative hypotheses). A further interesting point is that bleb-like and filopodia-like protrusions are negatively correlated. This suggests that these distinct protrusions form in different microenvironments potentially as a result of different growth factor stimulation.

Variable One	Variable Two	Spearman Correlation Coefficient (Robust to non-Gaussian)	Spearman Correlation p-value
Melanoma Cell Motility	Intra-vessel Wall Motility	0.59	0.006545
Melanoma Cell Motility	Extra Luminal Protrusions (Bleb-like)	0.55	0.01200
Melanoma Cell Motility	Variation in vessel width	0.46	0.04423

Table 11 Correlations between dynamic and morphological parameters and melanoma cell motility.

Spearman correlations were performed for each variable against melanoma motility. Correlations with p-value <0.05 are shown. No p-value correction for the number of correlations performed.

Variable One	Variable Two	Spearman Correlation Coefficient (Robust to non-Gaussian)	Spearman Correlation p-value
Intra-vessel Wall Motility	Extra Luminal Protrusions (Bleb-like)	0.65	0.001942
Extra Luminal Protrusions (Filopodia)	Extra Luminal Protrusions (Bleb-like)	-0.56	0.009441
Blunt Ends	Sum of Extra Luminal Protrusions	0.54	0.01384
Extra Luminal Protrusions (Filopodia)	Branch Points	0.51	0.02280
Variation in vessel width	Sum of Intra Luminal Protrusions	0.49	0.02713

Table 12 Correlation matrix for morphometric and dynamic parameters.

Spearman correlations were performed for each dynamic and morphological variable against each other. Correlations with p-value <0.05 are shown. No p-value correction for the number of correlations performed.

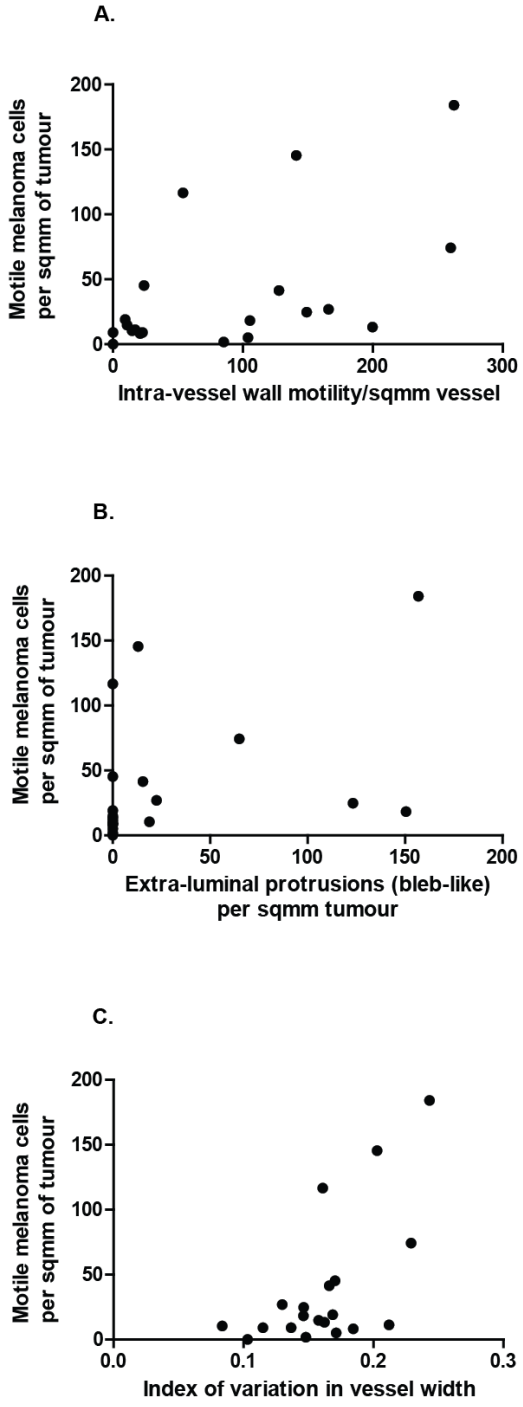

Figure 7.10 Melanoma cell motility correlates with specific endothelial dynamic behaviour

Graphs showing motile melanoma cells vs A. Endothelial cell intra-vessel wall motility, B. Endothelial cell bleb-like extra-luminal protrusions and C. Index of variation in vessel width. Melanoma cell motility and dynamic behaviours measured in the same intra-vital z-stack time-lapse movie and given as an average over the z-stack. 20 time-lapse movies from 7 mice analysed.

7.4 Sunitinib anti-angiogenic therapy decreases tumour growth but vascular response is heterogeneous in vivo

7.4.1 Sunitinib decreases vascular density and tumour growth in the B16 melanoma model

Results outlined in the previous section indicated a correlation between vascular morphology and dynamics and melanoma cell motility. Therefore Sunitinib, an anti-angiogenic drug, was used to try and perturb the vasculature and look at the effects on melanoma cell motility. B16 F2 melanoma cells were injected sub-cutaneously. When the tumour was palpable, 40 mg/kg of Sunitinib or DMSO vehicle control was administered daily by oral gavage. During this time tumour length and width were measured using callipers and tumour volume was calculated. Mice were treated for three to four days and then imaged immediately following a Sunitinib/DMSO injection. After imaging, tumours were fixed in 10 % neutral buffered saline overnight and subjected to immunohistochemical staining to analyse vessel density.

Treatment with 40 mg/kg Sunitinib treatment significantly decreased the vessel density of B16 F2 melanoma (Figure 7.11) confirming the anti-angiogenic capabilities of the drug. Treatment also slowed the growth of sub-cutaneous B16 melanomas and significantly reduced the increase in tumour volume during the treatment period (Figure 7.12).

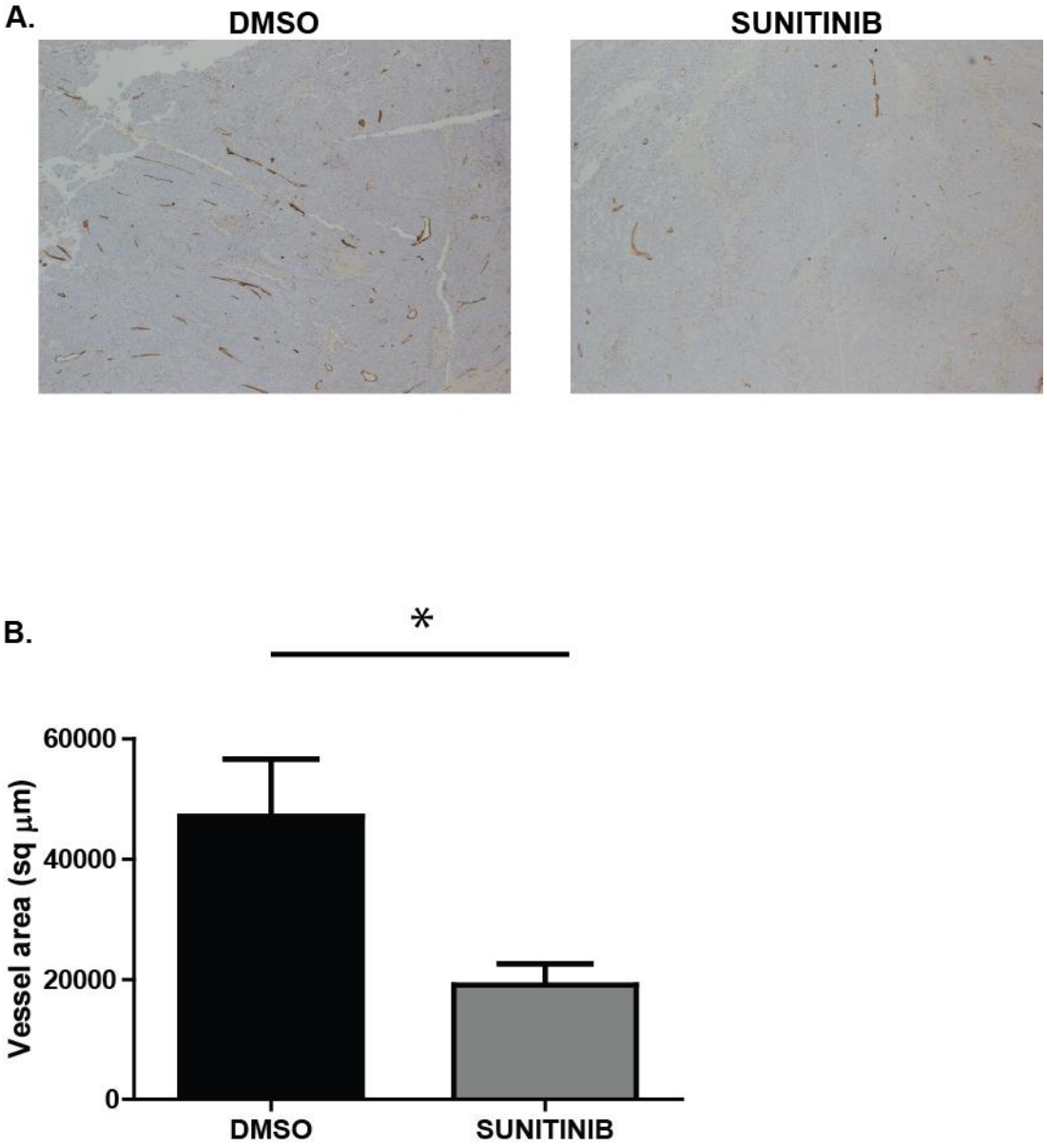

Figure 7.11 Sunitinib decreases vessel density in B16 F2 melanoma.

A. Representative immunohistochemical staining of vessels in DMSO vehicle control or 40 mg/kg Sunitinib treated tumours. A subset of the tumours analysed in Figure 7.12 B. Graph showing tumour vessel area after 4 days treatment. Vessel area measured by immunohistochemical staining of paraffin fixed tumour sections using anti-Endomucin and subsequent area analysis using Volocity software. 3 separate images analysed per tumour section and 4 tumours used for each treatment. Star indicates p-value of <0.05 in statistical t-test. Error bars show standard errors.

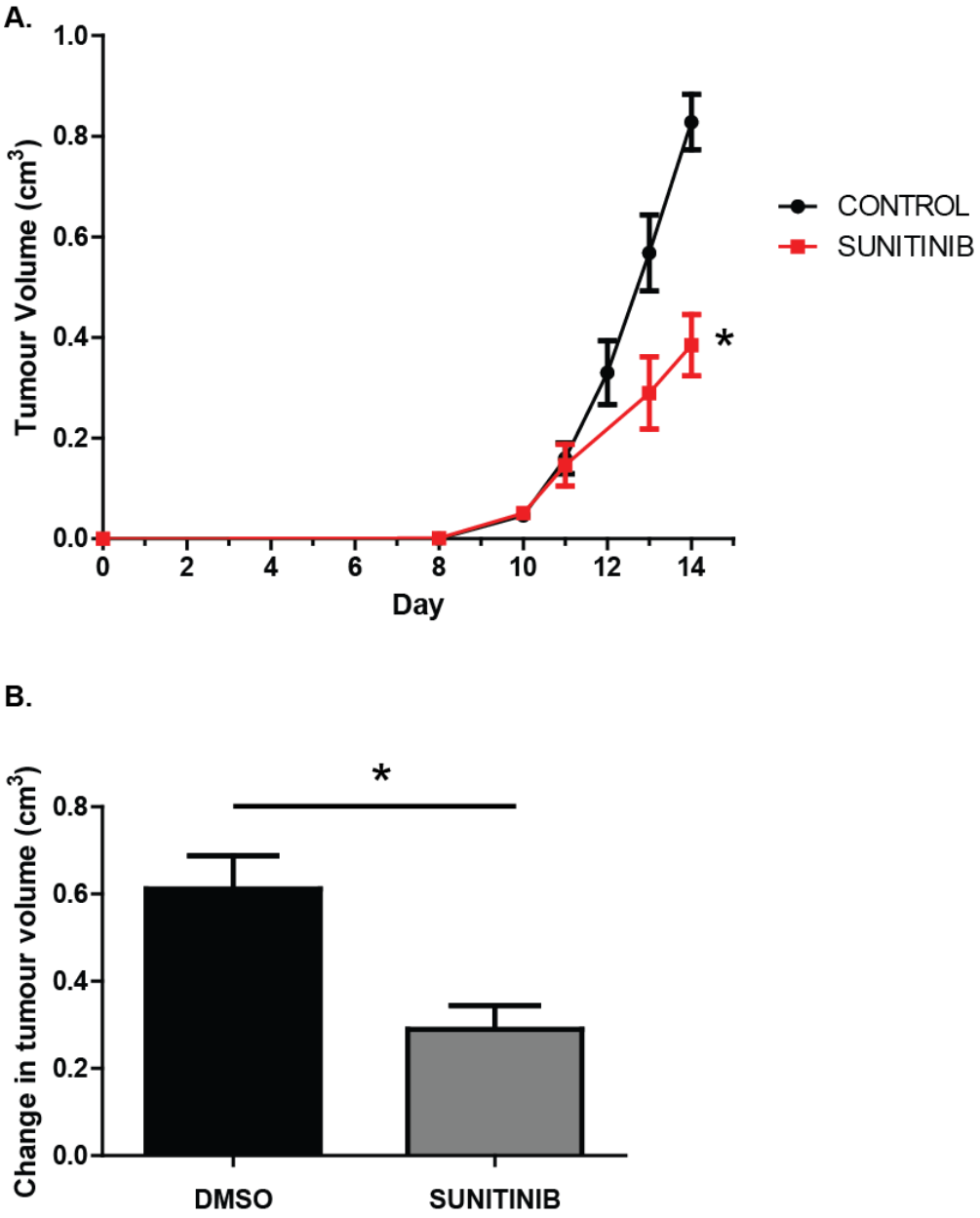

Figure 7.12 Sunitinib decreases B16 melanoma growth in vivo.

A. Tumour growth for DMSO vehicle control tumours (black line) and Sunitinib treated tumours (red-line). Tumours were treated from Day 10 when the tumour became palpable. B. Change in tumour volume over the treatment period for DMSO vehicle control and Sunitinib treated tumours. Tumour volume calculated from ½(length x width^2) with 7 mice in each cohort. Star indicates p-value of <0.05. Error bars show the standard error.

7.4.2 Sunitinib treatment does not affect B16 F2 melanoma cell motility in vivo

To try to determine if there is a causal relationship between the vasculature and melanoma cell motility, the number of motile cells was determined in DMSO or Sunitinib treated tumours. The number of motile cells in Sunitinib treated tumours was not significantly different to DMSO vehicle control tumours. In addition the relationship between number of motile melanoma cells and vessel area did not differ between the treatments. This suggests that at least in the relatively short-term (three to four days) Sunitinib does not affect melanoma cell motility. However, as discussed in the forthcoming sections, the response of the vasculature in regions image-able by intra-vital microscopy was not as expected. Therefore it is difficult to comment on the link between vascular morphology and dynamics and melanoma cell motility.

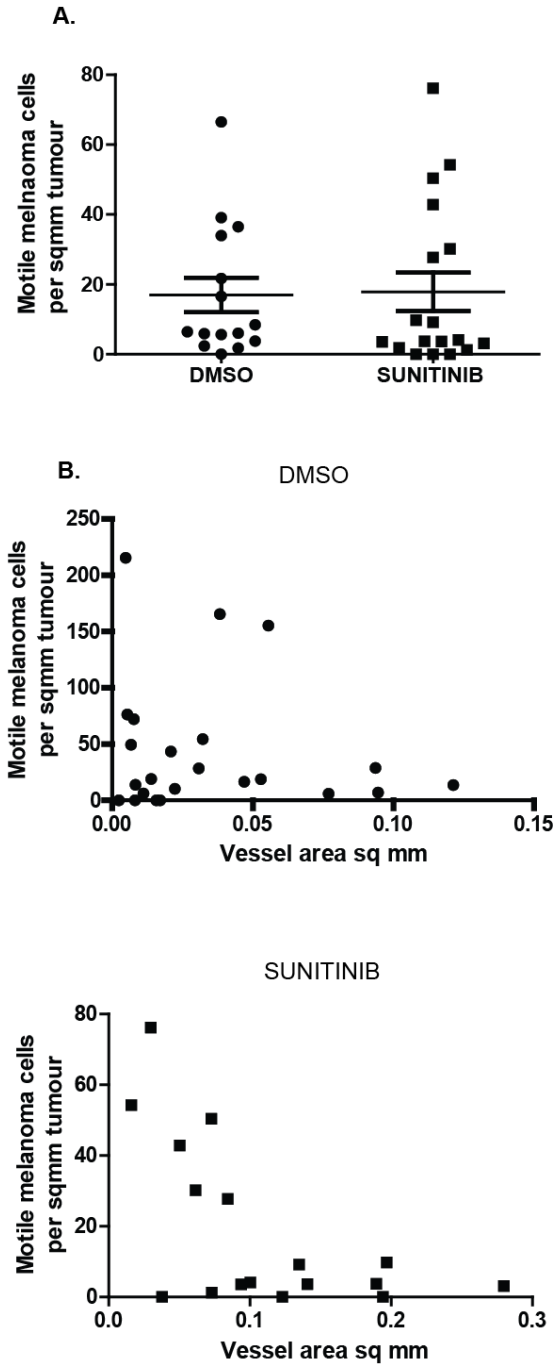

Figure 7.13 Sunitinib does not affect melanoma cell motility.

A. Number of motile cancer cells measured by intra-vital time-lapse imaging in DMSO vehicle control or Sunitinib treated tumours using a subset of the tumours analysed in Figure 7.12. Tumours treated for 3-4 days prior to imaging and immediately before imaging. Each data point indicates a single movie. NS indicates no significant difference in statistical t-test. Error bars show standard errors. B. Plots of vessel density vs cancer cell motility for DMSO vehicle control tumours and Sunitinib treated tumours. Cancer cell motility and vessel density measured in the same intra-vital z-stack time-lapse movie. Cancer cell motility is given as an average over the z-stack. Vessel density was measured by thresholding green endothelial cell channel and is given as an average over the z-stack.

7.4.3 Vessels in the tumour margin are resistant to Sunitinib anti-angiogenic therapy

Time-lapse intra-vital movies of the vasculature after DMSO vehicle control or Sunitinib treatment enabled analysis of the response of tumour associated vasculture to anti-angiogenic treatment. Although Sunitinib treatment significantly decreased vessel area and tumour growth, there was not a significant difference in dynamic behaviour on Sunitinib treatment. However, there was a trend towards fewer protrusions, and less endothelial cell motility, whether within the vessels or distant to it (Figure 7.14).

Previous data had shown distinct vasculature zones based on dynamics and morphology. The response of the different zones to Sunitinib was assessed based on the number of endothelial cell protrusions. This was used as a read-out of the angiogenic response because angiogenic factors are known to promote filopodia and tip-cell sprouting (Gerhardt et al., 2003). Vessels in the tumour showed a significant decrease in endothelial cell protrusions on Sunitinib treatment (Figure 7.15). However, vessels in the two tumour margin zones, as well as vessels in the margin as a whole, did not show a significant difference in number of protrusions on Sunitinib treatment. This suggests that vessels in the margin are still responding to angiogenic factors and exhibiting an angiogenic response, even in the presence of the anti-angiogenic drub Sunitinib. It also explains why that when considering all vessels together there is no significant difference in the number of protrusions between DMSO and Sunitinib treated tumours.

Immunohistochemistry revealed a decrease in tumour vessel area after Sunitinib treatment and this correlates with the decrease in protrusions in tumour vessels seen by intra-vital imaging. A closer look at the immunohistochemical staining revealed similar Endomucin staining at the margins of both DMSO and Sunitinib treated tumours confirming these vessels may be resistant to Sunitinib (Figure 7.16).

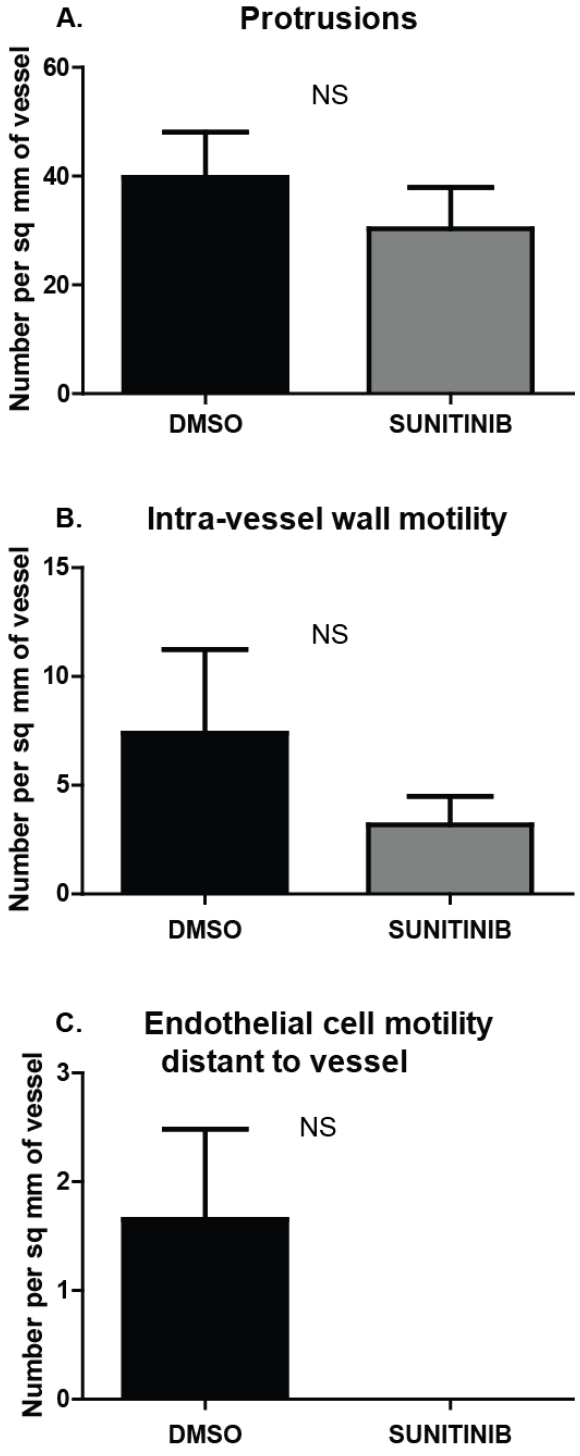

Figure 7.14 Quantification of endothelial cell dynamics in DMSO and Sunitinib treated tumours.

A. Extra and intra-lumenal protrusions, B. Endothelial cell intra-vessel wall motility C. Endothelial cell motility distant to vessels. NS indicates no significant difference in statistical t-test. Endothelial cell dynamics measured using intra-vital timelapse imaging. Quantification of at least 7 movies from 4 mice. Error bars show standard errors.

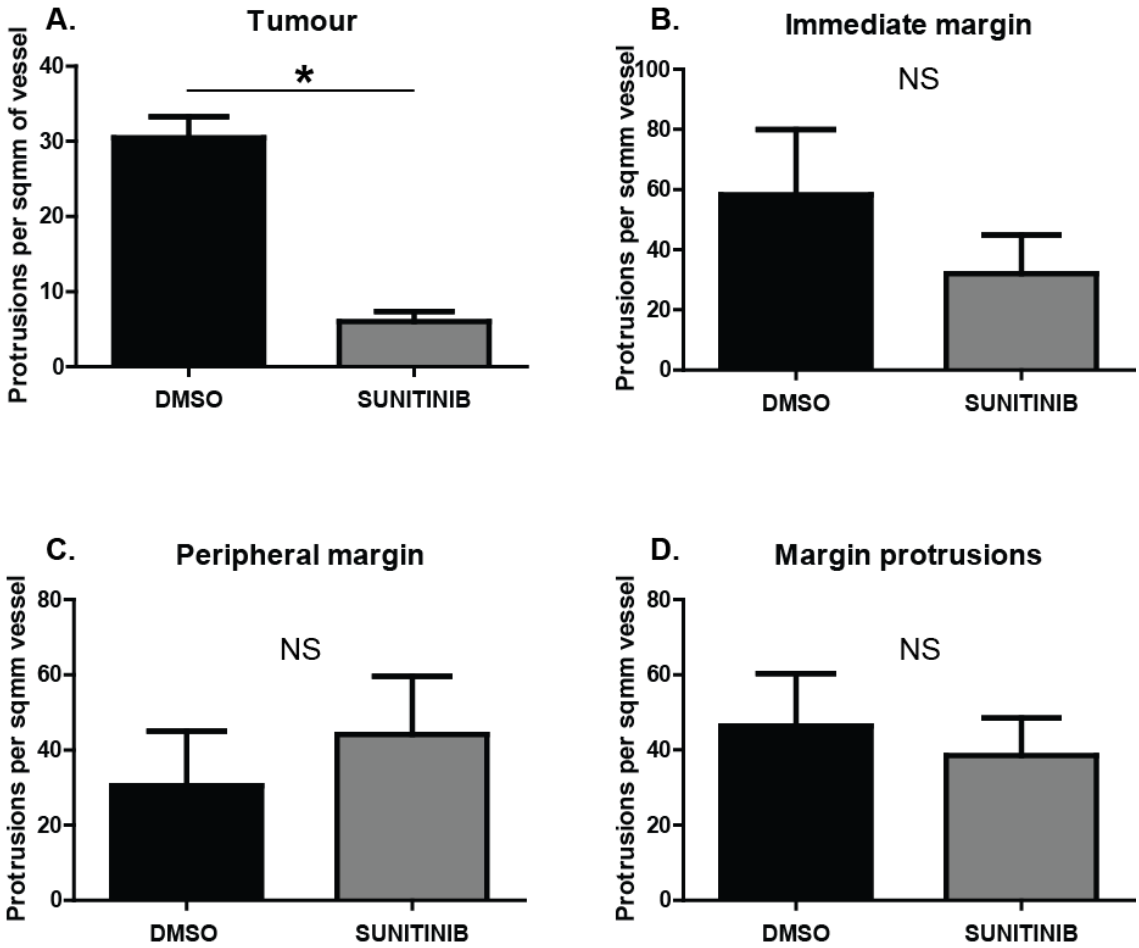

Figure 7.15 The tumour margin is resistant to Sunitinib anti-angiogenic therapy.

Breakdown of endothelial cell protrusions based on vessel region. A Tumour regions, B immediate margin C. peripheral margin and D. Collation of margins. Star indicates p-value of <0.05 in statistical t-test and ns indicates no significant difference. Quantification of atleast 7 movies from 4 mice. Error bars show standard errors

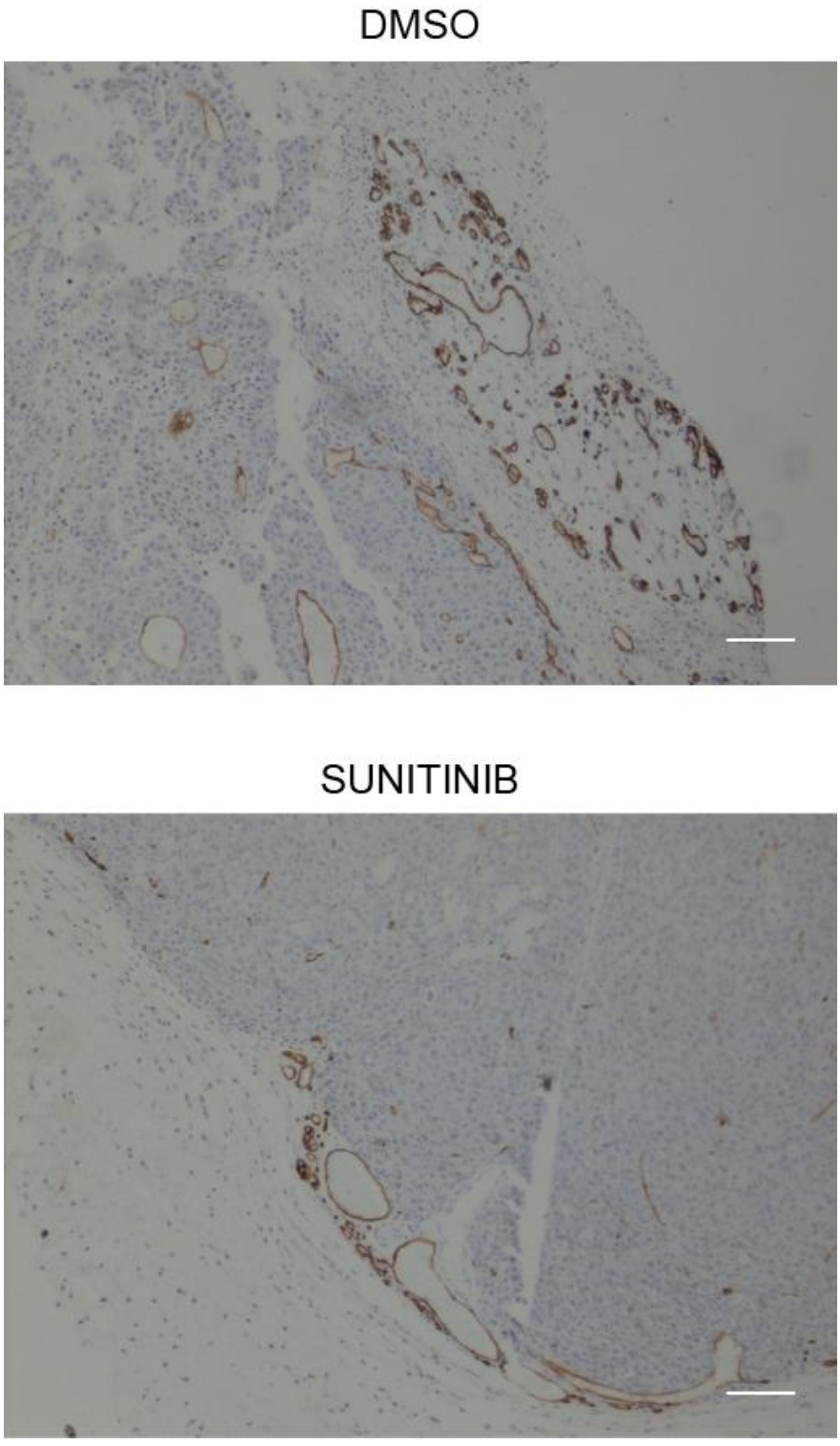

Figure 7.16 Tumour margin vessels persist during Sunitinib treatment.

Immunohistochemical staining of vessels in the margin using anti-Endomucin in DMSO vehicle control and Sunitinib treated tumours. Scale bar indicates 100 μm.

One prediction of the heterogeneous vascular response to Sunitinib is that the tumour cell response would also be heterogeneous. Melanoma cells at the edge of the tumour may still be receiving oxygen and nutrients due to the resistant vessels in the margin. To test this prediction, DMSO vehicle control and Sunitinib treated tumours were stained for cleaved Caspase-3 to show melanoma cells undergoing apoptosis. Quantification of the area of cleaved Caspase-3 staining demonstrated a decrease in melanoma cell apoptosis at the tumour edge in both DMSO and Sunitinib treated tumours. However this was only significant in Sunitinib tumours (Figure 7.17). In addition Sunitinib treated tumours showed a slight increase in apoptosis in the tumour centre when compared to DMSO vehicle control tumours, but apoptosis at the tumour edge was actually decreased in Sunitinib tumours (Figure 7.17). This demonstrates that in Sunitinib treated tumours melanoma cells at the edge of the tumour are protected from apoptosis potentially due to the Sunitinib resistant vessels that are still able to provide oxygen and nutrients to the very outer parts of the tumour.

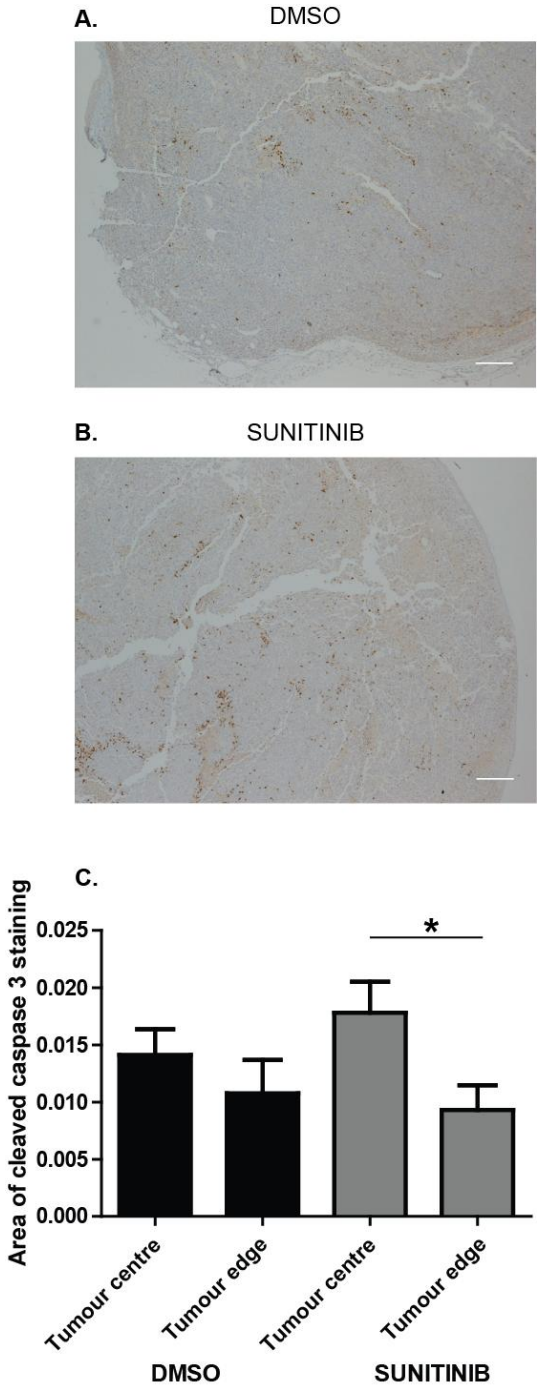

Figure 7.17 Heterogeneous melanoma response to Sunitinib.

Immunohistichemical staining of cleaved Caspase 3 in A. DMSO vehicle control and B. Sunitinib treated tumours using a subset of the tumours analysed in Figure 7.12. Scale bar indicates 250μm. C. Caspase 3 signal area in tumour centre and tumour margin for DMSO vehicle control and Sunitinib treated tumours. Immuno-histochemical staining of paraffin fixed tumour sections using anti-cleaved Caspase-3 and subsequent area analysis using Velocity software. Tumour edge defined as outer 200μm of tumour area as visible by hematoxylin and eosin staining. Caspase 3 staining area normalised to area of margin or tumour centre for individual section. 3 separate images analysed per tumour section and 4 tumours used for each treatment. Star indicates p-value of <0.05 in statistical t-test. Error bars show standard errors.

7.4.4 Tumour margins are enriched for stromal cells and have increased MMP activity

Previous reports indicate that response to anti-angiogenic therapy may depend on the pericyte coverage of vessels (Bergers et al., 2003). To investigate whether vessels in the margin had different pericyte coverage, tumours were stained for the pericyte markers NG2 and α-SMA. There was little difference between pericyte staining in the tumour margin and tumour interior (Figure 7.18) suggesting that differences in response to Sunitinib were not as a result of pericyte coverage.

Many different cell-types in the tumour can promote angiogenesis and a heterogeneous distribution may provide a reason for the heterogeneous vascular response to Sunitinib. To test whether there was an increase in stromal cells at the tumour margins, B16 melanoma tumours were stained for a variety of stromal cell markers using immunohistochemistry. Endomucin staining helped to highlight the tumour margin due to the increase in vessels at the very edge of the tumour. F4/80 staining showed a concurrent increase in macrophages at the tumour margin (Figure 7.19). Additionally, the tumour margin was enriched for both CAFs indicated by α-SMA positive cells not associated with vessels, and T-lymphocytes (Figure 7.19). Both CAFs and macrophages are known to be pro-angiogenic and so these stromal cells in the tumour margin may provide VEGFR-2 independent pro-angiogenic signals. Alternatively, the sheer number of cells pro-angiogenic cells in the margin may result in a less effectual inhibition of angiogenesis by Sunitinib.

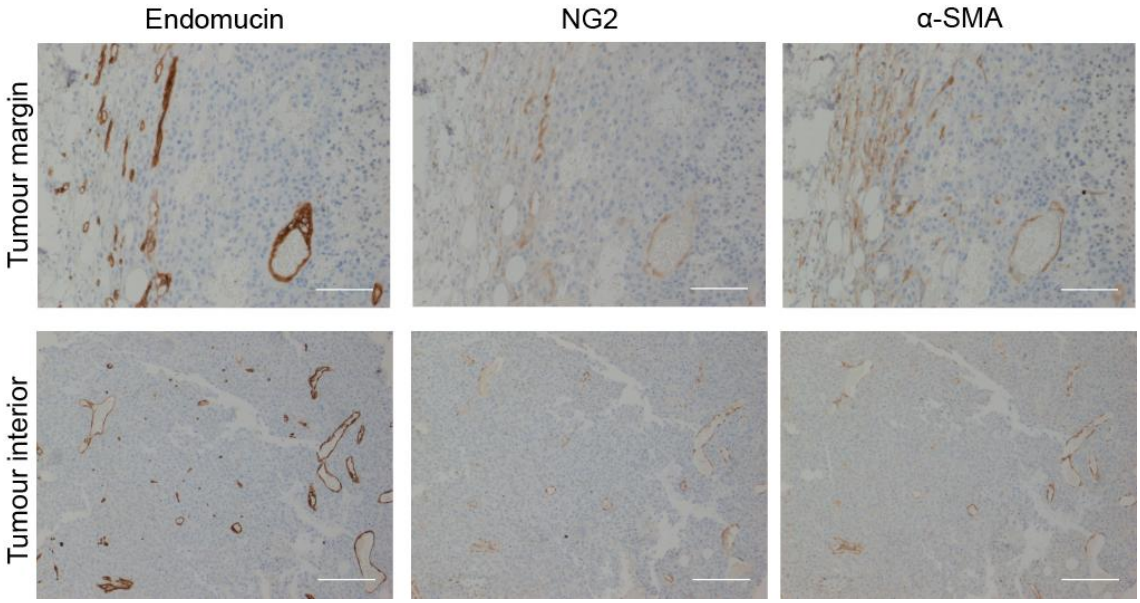

Figure 7.18 Vessels in the tumour margin and tumour interior have similar pericyte coverage.

Immunohistochemical staining of vessels in tumour margin and interior. Endomucin indicates presence of vessels and NG2 and α-SMA indicate extent of pericyte coverage. Scale bar indicates 100μm.

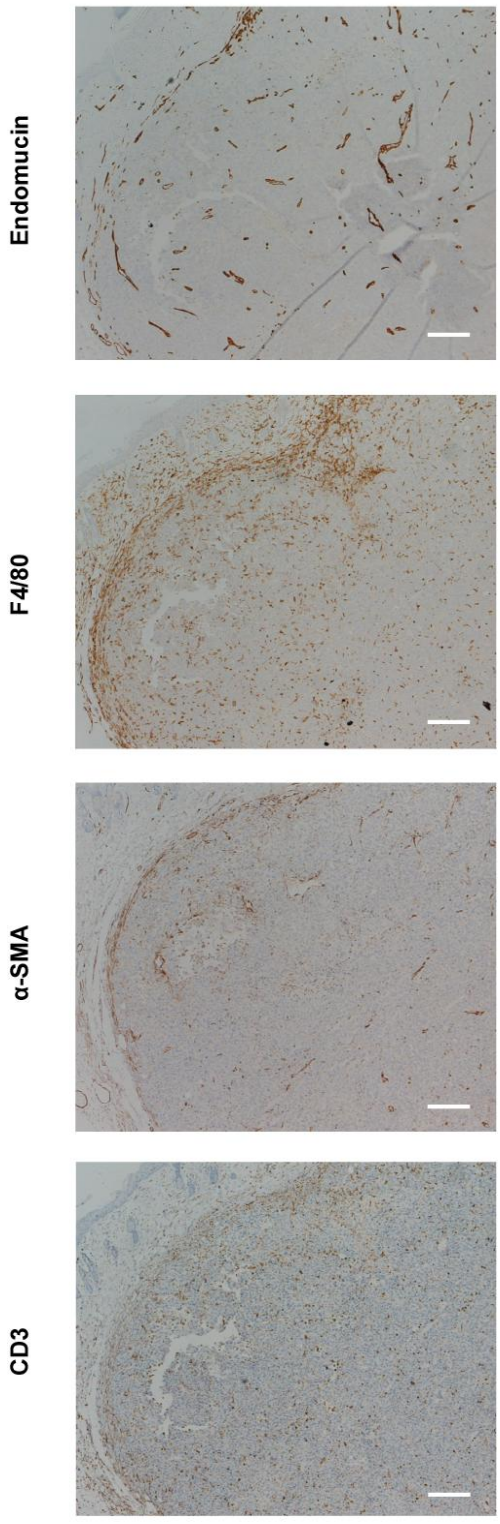

Figure 7.19 Stromal cells are enriched at the tumour margin.

Immunohistochemical staining of B16 melanomas for various stromal cells. Endomucin indicates blood vessels. F4/80 is a marker for macrophages. α-SMA is a marker for both pericytes and cancer-associated fibroblasts. CD3 is a marker for T-lymphocytes. Scale bar represents 250 μm.

In vivo pro-angiogenic growth-factors, such as VEGF-A, bind the ECM and a common mechanism of activation is cleavage by proteases (Lee et al., 2005). Stromal cells, including CAFs and macrophages, secrete proteases and for this reason the level of protease activity was investigated in the different vascular zones in vivo. Protease activity was determined with MMPsense 680, an injectable probe that is only activated after protease cleavage. MMPsense 680 was injected 6-8 hours before imaging and activity in different vascular zones was compared with healthy vessels on the alternate flank to the tumour. Very little fluorescence was detected in and around healthy vessels (Figure 7.20). However, high levels of fluorescence were found around the tumour, particularly in the peripheral margin zone and to a lesser extent in the intermediate margin. Some signal in the peripheral margin looked to be coming from phagocytic macrophages. Fluorescence signal dropped off in the tumour itself (Figure 7.20). This suggests that there is increased protease activity in the margins and supports the notion that stromal cells in the margin provide angiogenic signals, potentially by activating ECM bound factors through protease function, to enable an angiogenic response even in the presence of Sunitinib.

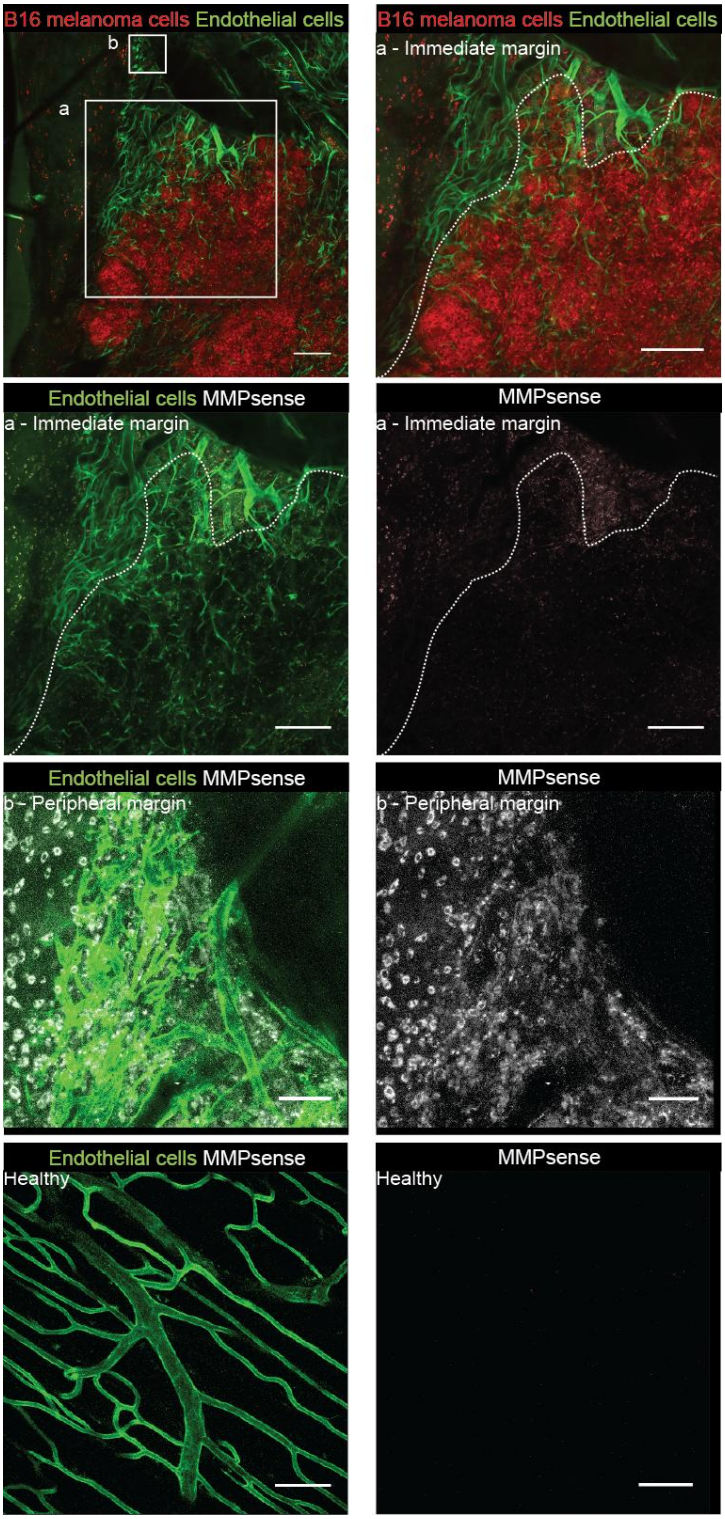

Figure 7.20 Tumour margins have increased protease activity.

Confocal images of different vascular zones showing protease activity. Endothelial cells have green membrane marker, B16 F2 melanoma cells with red membrane marker and protease activity shown in purple using MMPsense 680. Extent of the tumour indicated by white dashed line. First tile and immediate margin images the scale bar represents 250 μm. Peripheral margin and healthy vessel images the scale bar represents 30 μm.

7.5 Longitudinal analysis of the tumour vasculature

Intra-vital imaging of sub-cutaneous tumours using the skin-flap method is limited to one imaging session per tumour. For that reason, information regarding the development of the tumour vasculature over a number of days is lost. Imaging windows enable day-after day imaging of the tumour microenvironment and may help to provide temporal links between the different vascular zones. In collaboration with Dr Jacco van Rheenen in Utrecht, I set-up the use of imaging windows for repeated imaging of sub-sutaneous melanoma.

Imaging windows were made of titanium, a lightweight yet strong metal that is biologically inert. Coverslips were glued on to the window frame the day before implantation (Figure 7.21). After the glue had set the window was placed in 70 % ethanol overnight for sterilisation. On the day of surgery, mice were given an analgesic and anaesthetised. A small incision was made lengthways in the skin of the animal, large enough to accommodate the window. Sutures were made around the outside of the incision, similar to a running stitch, so that when the ends were pulled tight the skin was drawn into a groove on the outside of the window. This left the skin snug to the window. Immediately following the surgery, B16 F2 melanoma spheroids in 100 % matrigel were injected underneath the window. 4-5 days after surgery the tumour environment underneath the window was imaged every day until the tumour became too large.

Immunohistochemical staining for stromal cell markers revealed a similar microenvironment in tumours grown under the window and those grown sub-cutuaneously (Figure 7.22). There was a slight increase in the F4/80 staining in window tumours but this may be due to the initial surgical procedure. The staining showed fewer Endomucin positive vessels in the tumour bulk, however, window tumours were smaller than sub-cutaneous tumours when removed. It is likely that this difference in tumour size accounted for the decrease in tumour vessels as endomucin staining was seen around the margins of window tumours.

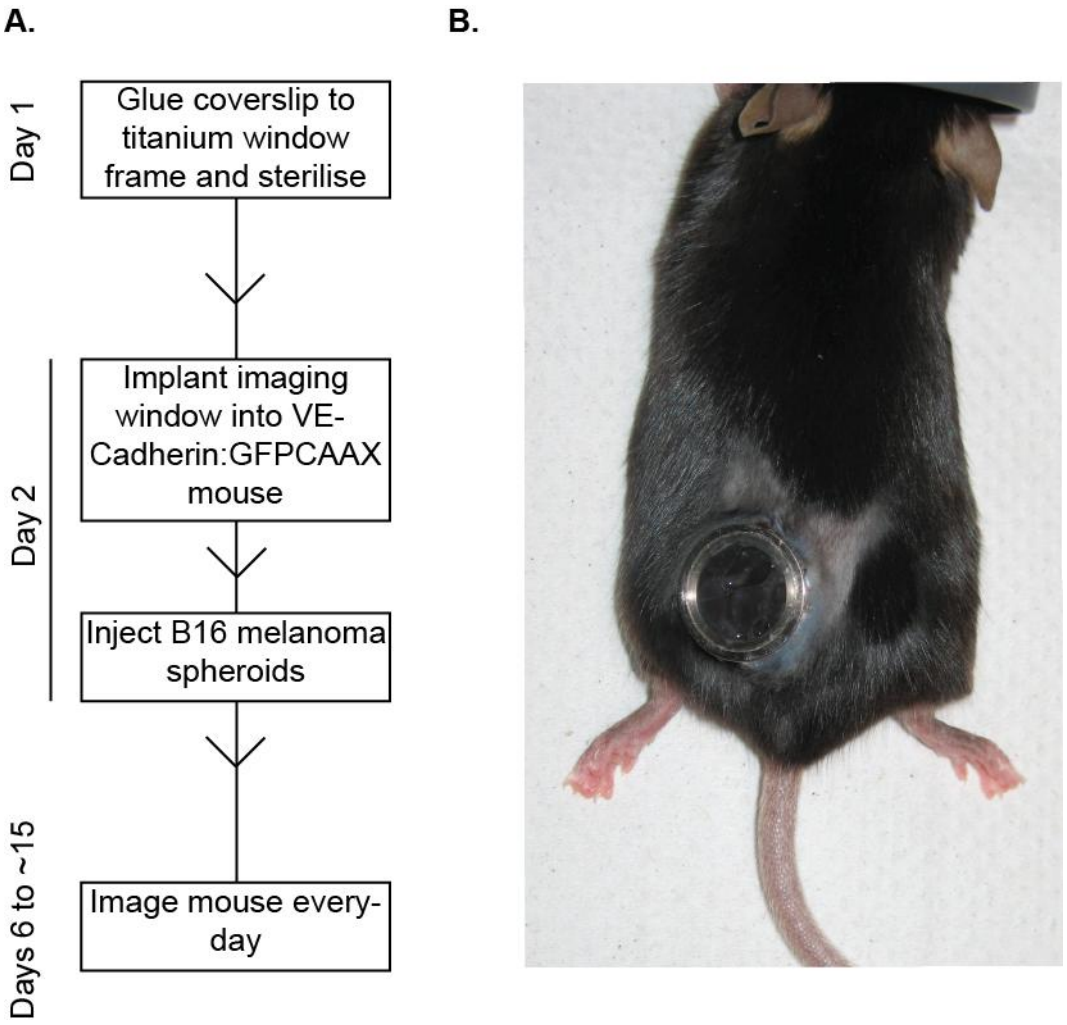

Figure 7.21 Imaging window experimental outline.

A. Schematic of experimental approach for window imaging experiments. B. Image showing window implanted in VE-CADherin:GFPCAAX mouse with B16 melanoma growing under window.

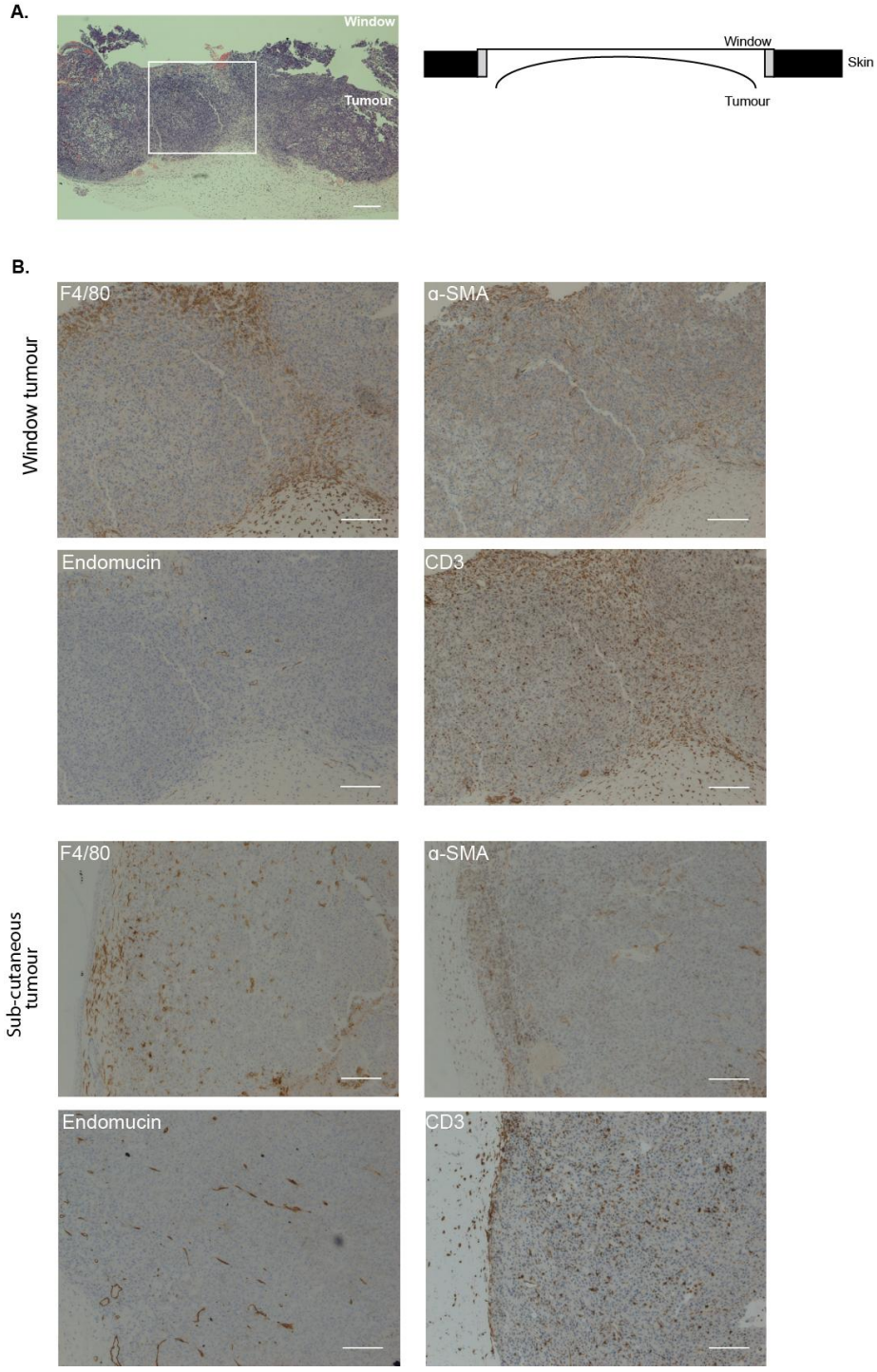

Figure 7.22 Sub-cutaneous tumours and tumours grown under imaging windows have similar stromal components.

A. Haemotoxylin and eosin staining of a window tumour to show orientation. White box indicates area represented in B. Scale bar represents 200 μm. B. Immunohistochemical staining of a sub-cutaneous tumour or tumour grown under imaging window for various stromal cell markers. F4/80 stains macrophages. α-SMA marks cancer associated fibroblasts and pericytes. Endomucin stains endothelial cells and CD3 marks T cells. Scale bar indicates 150 μm.

7.5.1 Tumour angiogenesis in the B16 model occurs through a similar mechanism to developmental sprouting angiogenesis

The tumour vasculature is thought to arise through at least two possible mechanisms, sprouting of new vessels from existing ones, or co-option of existing vessels in to tumour vessels (Carmeliet and Jain, 2011a). Although intra-vital imaging using the skin-flap method revealed blunt-ended vessels pointing in the direction of the tumour suggestive of vascular sprouting, this was not conclusive. To further investigate whether tumour vessels in the B16 melanoma model arise from sprouting angiogenesis, window analysis of B16 melanoma in VE-Cadherin:GFPCAAX, involving repeated imaging of the same tumour area, was performed. The same vessels could be tracked over time and this showed a clear angiogenic front, consisting of tip cells, growing towards the tumour and eventually totally surrounding the tumour (Figure 7.23). This indicates that sprouting angiogenesis is the main source of tumour-associated vasculature in B16 melanoma.

A more detailed analysis of angiogenic front progression and sprouting angiogenesis in B16 melanoma revealed striking similarities to developmental sprouting angiogenesis. Sprouting vessels were seen to extend and grow and were frequently seen to branch (sprouts a,b and f in Figure 7.24). Individual sprouts were measured and the rate of extension was calculated to be 186 μm per day (Figure 7.25). Vessel branching is a response to angiogenic factors such as VEGF or FGF family members and helps to increase the vascular network (Carmeliet and Jain, 2011a). Therefore vessel branching in the tumour environment increases the tumour volume receiving oxygen and other factors from the blood. Anastomosis is the process of connection between two branches of the vascular network (Fantin et al., 2010). It helps to form a functional vascular network by forming new circuits. Anastomosis was also observed between two neighbouring nascent sprouts during tumour angiogenesis (Figure 7.26). Similar to developmental anastomosis (Fantin et al., 2010), the tip cells protruded filopodia towards each other before fusion (
Figure 7.27).

Later steps in developmental vascular patterning include vessel remodelling and pruning. Branch point migration, a form of vessel remodelling, was observed in the B16 melanoma tumour vasculature (Figure 7.28). Vascular remodelling is thought to be dependent on blood flow (Lucitti et al., 2007) and the vessels undergoing remodelling were large vessels within the tumour. Therefore it is likely that blood flow was present in these vessels. The process of vessel pruning was difficult to observe and the evidence for it was not clear. This was due to the fast growth of B16 melanoma cells and the fact that it occurs later during vascular patterning. After just a day in the late stages of tumour development, it was not clear whether the same z-sections were being imaged. However, a noticeable decrease in vessel density, suggestive of vessel pruning, was observed.

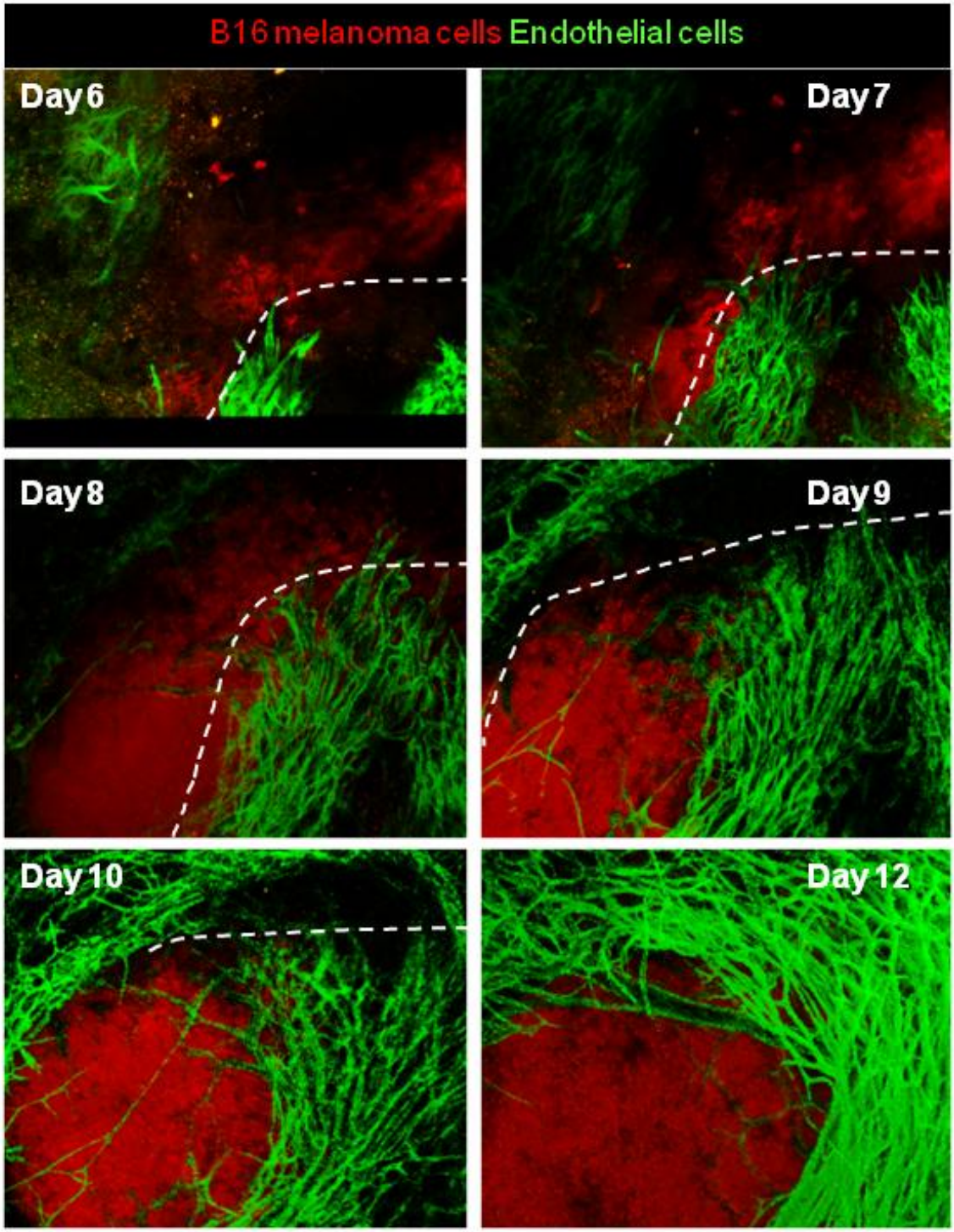

Figure 7.23 Advance of the tip-cell rich angiogenic front towards the tumour.

Image series of tumour-associated vasculature from days 6 to 12 after injection of melanoma cells. The dotted line indicates the angiogenic front, note the advancement towards the tumour over time. B16 F2 melanoma cells in red and endothelial cells shown in green. Images show a region 1000 μm by 800 μm.

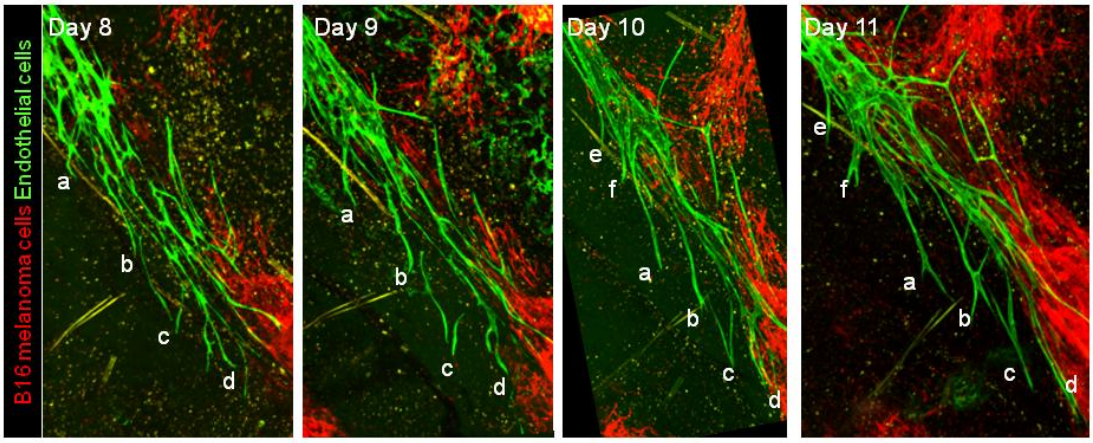

Figure 7.24 Sprout extension and branching during angiogenesis in B16 melanoma.

Image series of tumour-associated vasculature from days 8 to 11 after injection of melanoma cells. Letters indicate the same sprout in sequential images. Note the increasing length of sprouts over time and branching behaviour of sprouts a,b and f. B16 F2 melanoma cells in red and endothelial cells shown in green. Images show an area 1.3 mm by 2 mm.

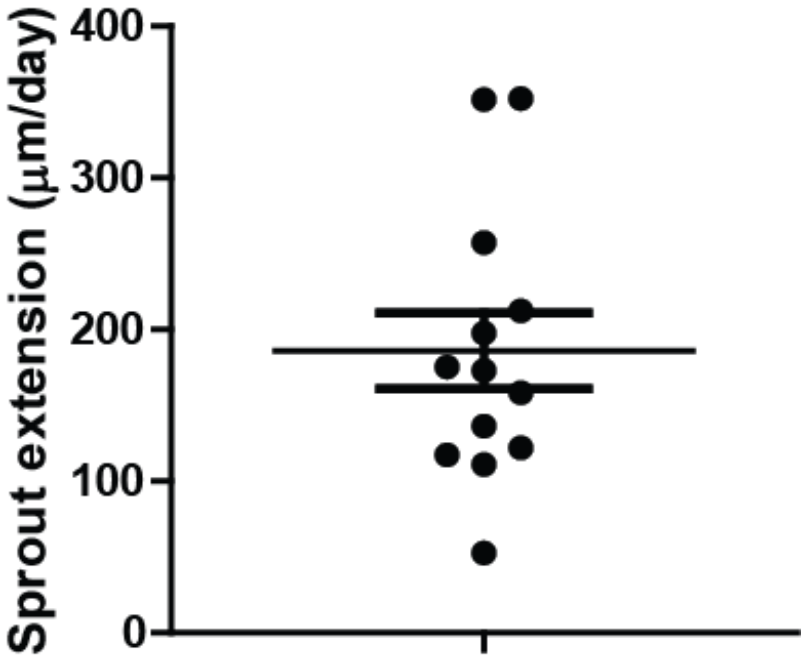

Figure 7.25. Quantification of the rate of sprout extension.

6 individual sprouts were tracked between 2 and 4 days and their length measured every day. Individual data points show daily extension rate. Error bars show the standard error of the mean.

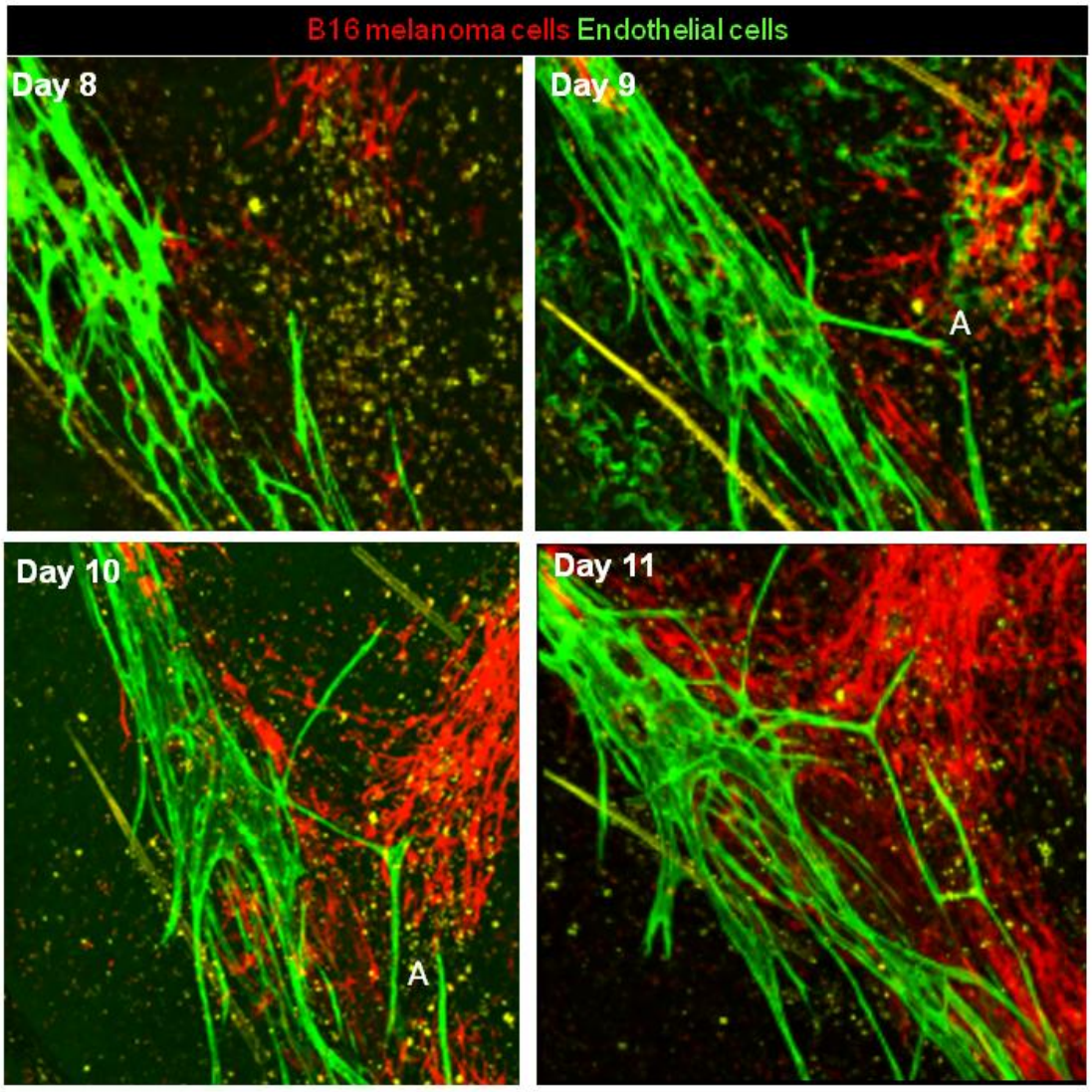

Figure 7.26 Anastomosis between two neighbouring vessels.

Image series of tumour-associated vasculature from days 8 to 11 after injection of melanoma cells. "A" marks sites of vessel anastomosis. B16 F2 melanoma cells in red and endothelial cells shown in green. Images show an area 1 mm by 1 mm.

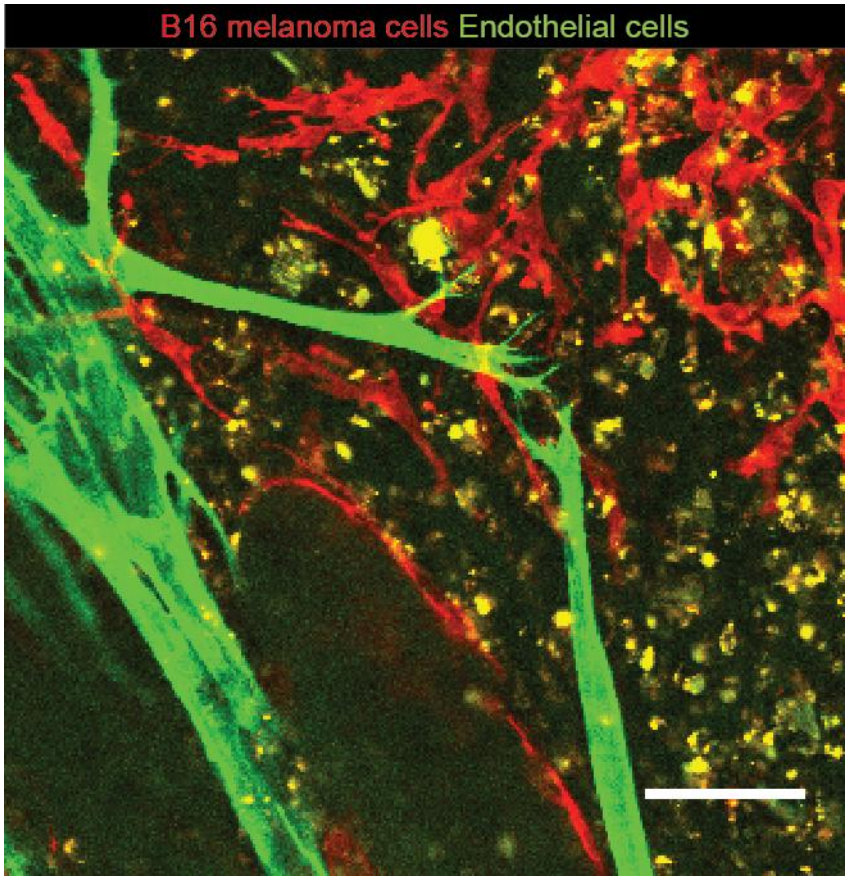

Figure 7.27 Tip cells protrude filopodia towards each other before anastamosis.

Confocal image of B16 F2 melanoma spheroids in a VE-Cadherin:GFPCAAX mouse. B16 F2 melanoma cells have red membrane marker. Endothelial cells have green membrane marker. Yellow is overlap of two channels and most likely represents auto-fluorescent phagocytic cells. Scale bar indicates 100 μm.

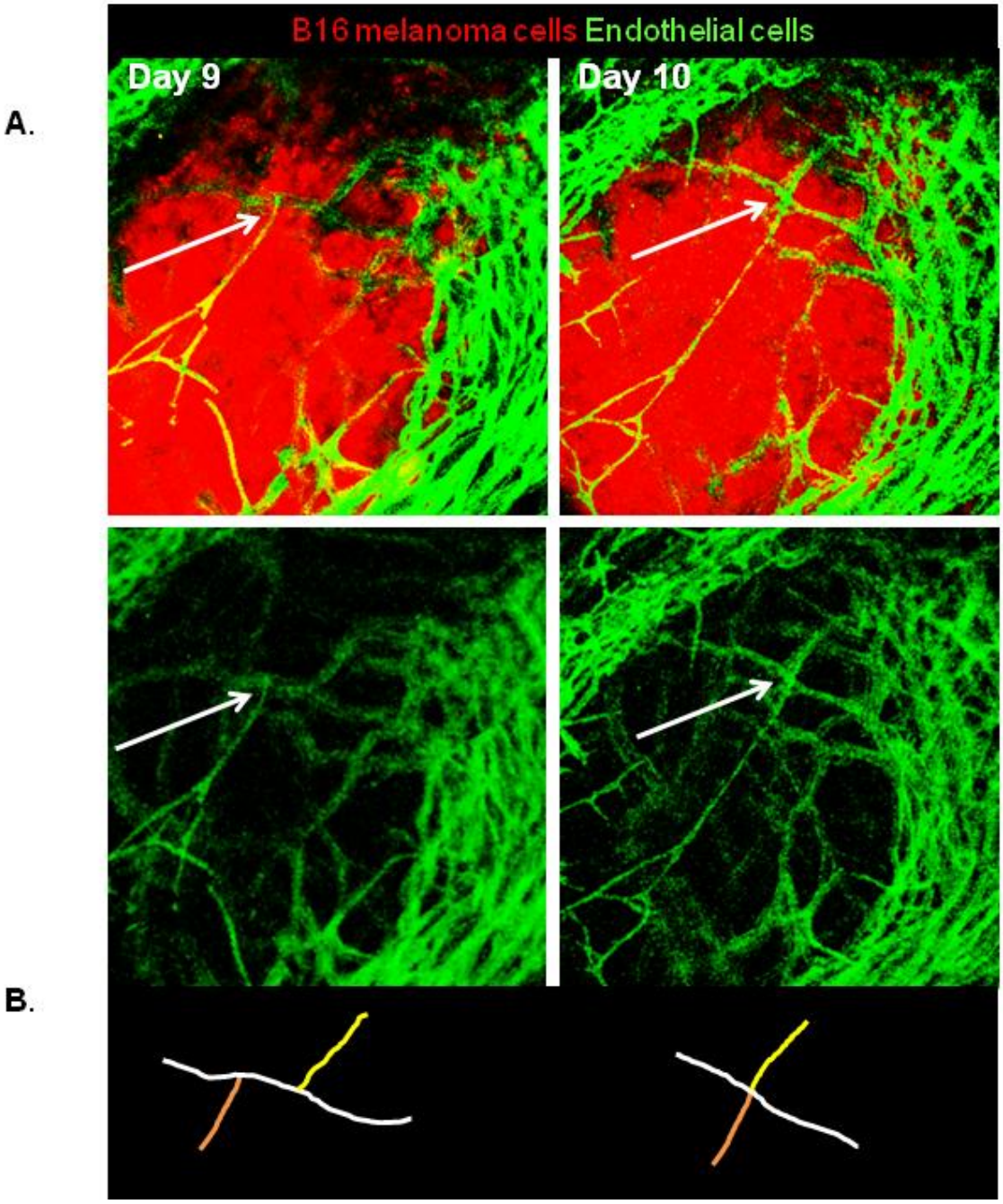

Figure 7.28 Vessel remodelling during tumour angiogenesis.

A. Image series of tumour-associated vasculature on days 9 and 10 after injection of melanoma cells. Arrow marks vessel branch that migrates during remodelling. B16 F2 melanoma cells in red and endothelial cells shown in green. B. Schematic of vessel remodelling shown in A. Each vessel marked in separate colour.

7.5.2 Analysis of the temporal relationship between the immediate and peripheral margins

Although skin-flap imaging of sub-cutaneous B16 melanoma revealed two distinct vascular zones in the margin, how they develop and the relationship between the two is unknown. Window imaging of B16 melanoma was used to try and address these points. It revealed the development of the immediate margin from existing vessels, a process that involved the emergence of tip cells, or blunt ended vessels, and extension of these nascent sprouts to form similar vascular morphologies to those seen in the immediate margin (Figure 7.29).

A key characteristic of the peripheral margin is increased vessel tortuosity. Analysis of similar areas day after day revealed that tortuous vessels arose in areas that had previously exhibited a more sprouting morphology, similar to the immediate margin (Figure 7.30). This suggested a progression from an immediate margin phenotype to a peripheral margin phenotype, implying that the peripheral margin may arise out of the immediate margin. To further analyse this, the number of blunt ends and vessel tortuosity was quantified in the same area of marginal vessels for a number of days. An increase in blunt ends was observed over time in the tumour margins (Figure 7.31) indicating the development of the immediate margin. This was then followed by a decrease in blunt ends, potentially as the angiogenic response stabilised and sprouts extended. However, the number of blunt ends was still comparable to those measured using the skin-flap method of imaging. Vessel tortuosity also increased over time (Figure 7.31), although this increase was delayed by 1 or 2 days in comparison to the increase in blunt ends. This shows that characteristics of the peripheral margin develop later than characteristics of the immediate margin and hints that the peripheral margin may develop from areas that had once been immediate margins. It is possible that as the angiogenic front progresses regions further from the front develop increased tortuosity and characteristics of the peripheral margin.

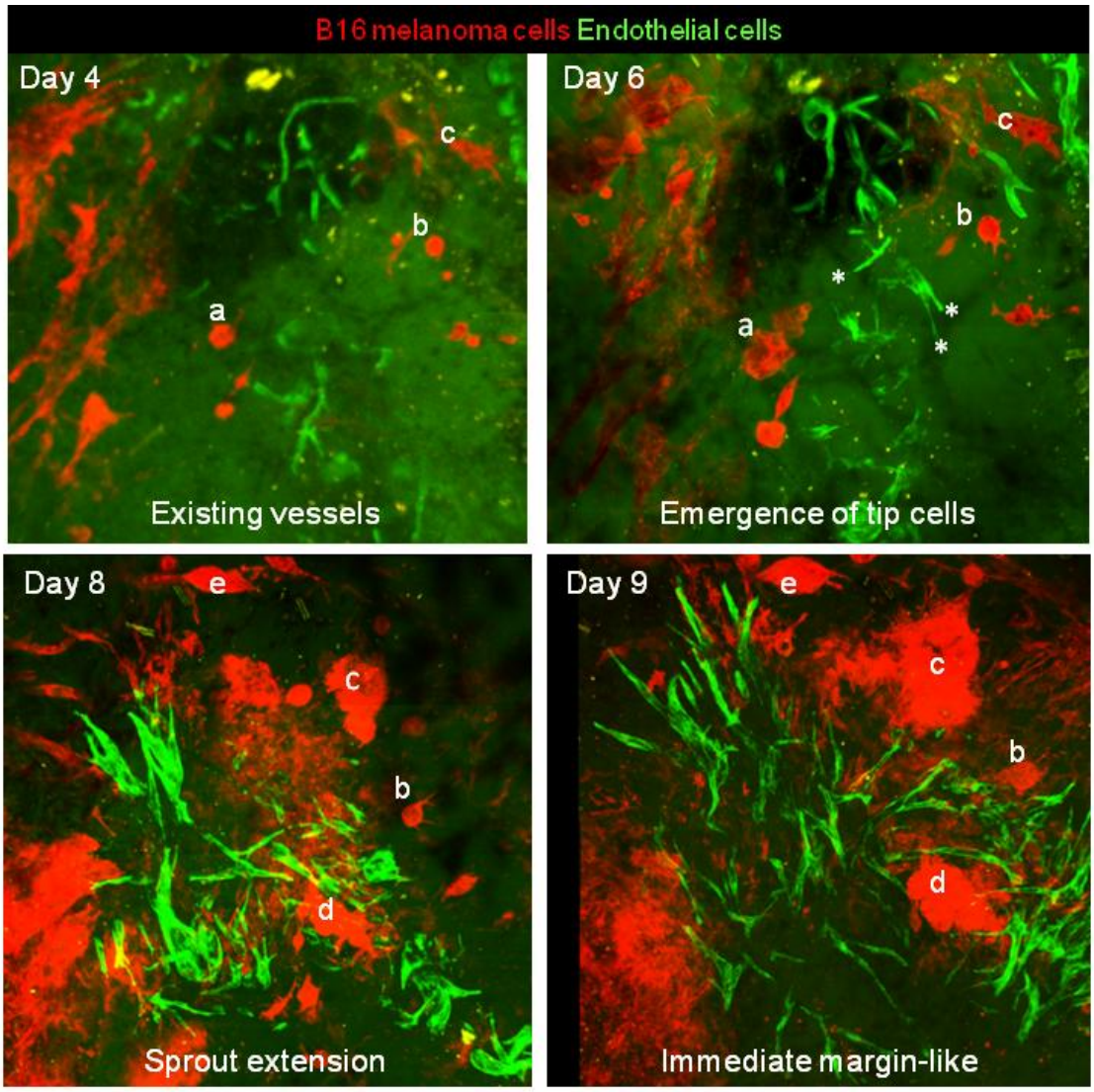

Figure 7.29 Emergence of the immediate margin.

A. Image series of tumour-associated vasculature between days 4 and 9 after injection of melanoma cells. Letters indicate the same B16 F2 melanoma spheroid in sequential images. Note the increasing number of tip cells over time. B16 F2 melanoma cells in red and endothelial cells shown in green. Images show an area 1.5 mm by 1.6 mm.

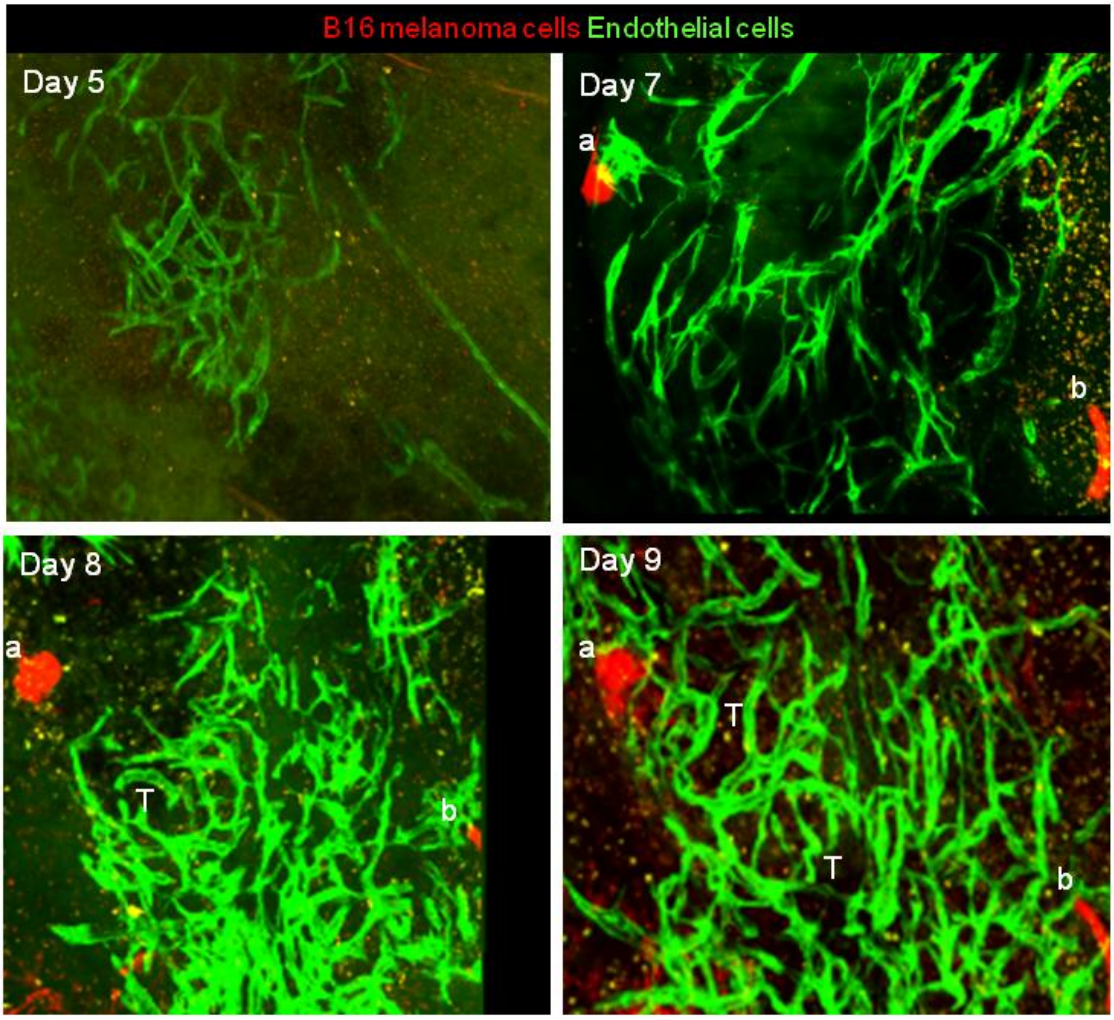

Figure 7.30 Margin vessels show an increase in tortuosity over time.

A. Image series of tumour-associated vasculature between days 5 and 9 after injection of melanoma cells. Letters indicate the same object in sequential images. T indicates vessels with medium to high tortuosity. B16 F2 melanoma cells in red and endothelial cells shown in green. Images show an area 850 μm by 750 μm.

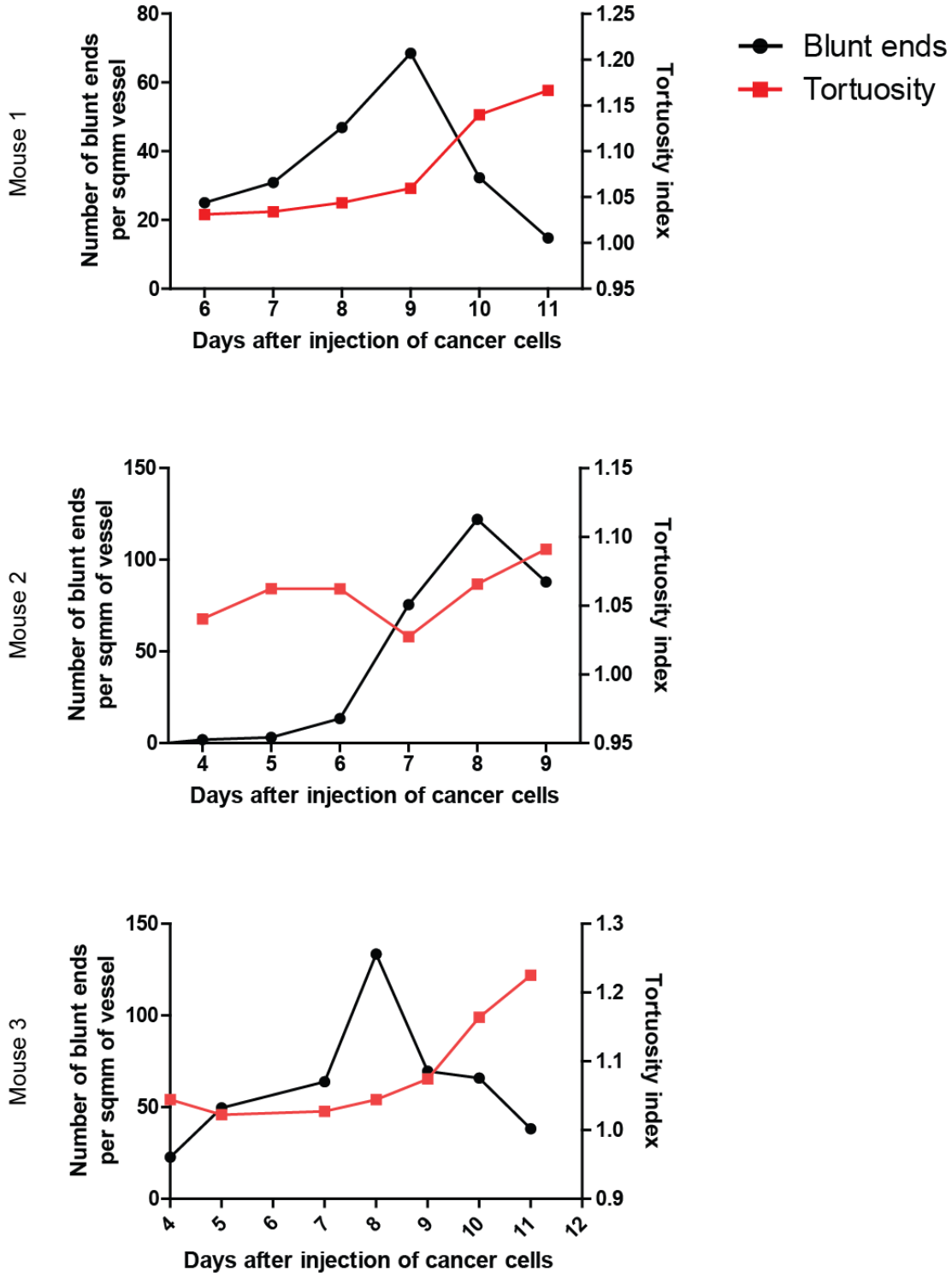

Figure 7.31 Increase in margin vessel tortuosity is delayed compared to the increase in number of blunt ends.

Graphs showing number of blunt ends per vessel area and tortuosity of vessels in the tumour margins over time. Each graph from a different tumour. Individual data points are an average over the image stack for the day.

7.6 Chapter summary

Intra-vital imaging of the tumour vasculature revealed heterogeneous vascular morphology and dynamics. Two distinct vascular zones in the margin, named immediate margin and peripheral margin, were defined based on morphology and this also correlated with distinct dynamic endothelial cell behaviour. Longitudinal analysis of the tumour vasculature using imaging windows revealed that the tumour vasculature in B16 melanoma stems from sprouting angiogenesis of existing vessels and proceeds with similar steps to developmental angiogenesis. Furthermore, day after day imaging of the same tumour environment suggested that the peripheral margin may arise from areas which previously had immediate margin characteristics, suggesting the two distinct vascular zones in the margin are temporally linked. Melanoma cell motility, previously shown to be heterogeneous, correlated with aspects of vascular morphology and endothelial dynamics, in particular extra-lumenal bleb-like protrusions and endothelial intra-vessel wall motility. The anti-angiogenic drug Sunitinib did not affect melanoma cell motility. However endothelial cell response to Sunitinib was heterogeneous and vessels in the tumour margin displayed resistance to Sunitinib anti-angiogenic therapy. This correlated with an increase in stromal cells and protease activity in the margin.

Chapter 8. Discussion

8.1 Chapter overview

Many factors, intrinsic and extrinsic, influence melanoma motility in vivo. Induction of motility in melanoma may be coupled to changes in gene expression, resulting in specific signalling pathways and gene expression patterns in motile melanoma cells. The main section of this discussion will first address modes of motility in vivo and the contribution of the microenvironment on motility. It will then address the regulation of gene expression in motile cells including the Notch, TGF-β and SRF pathways and chromatin mediated control of gene expression. Later steps in the metastatic cascade and the vasculature in melanoma will then be discussed. The final sections will discuss the broader relevance of this work to melanoma and clinical treatment.

8.2 Melanoma motility and metastasis

8.2.1 Melanoma behaviour is heterogeneous in vivo

A benefit of intra-vital imaging is the possibility for analysis of cell to cell variation in behaviour and signalling. Work in chapter 3 illustrates that motile behaviour of B16 F2 melanoma is heterogeneous in vivo and that motility correlates with differences in signalling pathway activation. Less than 10 % of B16 F2 melanoma cells are motile in vivo (Figure 3.2), a similar percentage to that found in murine breast cancer models (Giampieri et al., 2009). B16 F2 cells also use similar modes of motility in vivo to those described previously. More than 50 % of the motile cells use an amoeboid-like single cell mode of motility. However, a significant fraction, 30 %, use a streaming mode of motility. The caveat to this quantification is that it is often difficult to categorise the mode of motility. Singly motile cells often use the same path and, depending on their proximity, it can be difficult to determine if they are streaming or moving independently as single cells. This can be compounded if non-labelled host cells, such as macrophages, are also present in the stream. The difference between streaming cells and collectively motile cells is even more difficult to interpret as the main difference is the level of adhesion between cells.

Use of membrane-labelled cells, as in chapter 3, helps to ascertain whether the cells are in contact, however, the nature of the contacts is unknown. Therefore work in this thesis to investigate signalling in different modes of motility considers streaming and collective motility together.

Despite the difficulties in determing between modes of motility, streaming most likely represents a distinct mechanism of motility as the work in chapter 3 shows differences in the activation of TGF-β and Notch signalling pathways between single and streaming cells (discussed later). Streaming cells also appear faster than singly motile cells and may be following pre-generated tracks in the ECM, potentially made by fibroblasts, as illustrated by in vitro studies (Gaggioli et al., 2007). Occasionally multiple streams of cells were observed travelling in the same direction, possibly as a result of interstitial flow. Indeed, interstitial flow can increase the metastatic potential of melanoma cells and can direct cancer cell motility in a CCR7 dependent manner (Shields et al., 2007).

8.2.1.1 Microenvironment contribution to melanoma motility

The microenvironment may contribute to cancer cell motility and heterogeneity in motility through paracrine signalling, stromal cell ECM remodelling and other mechanisms to create a permissive environment for motility. Imaging of melanoma cells together with the blood vasculature enabled analysis of morphological and dynamic features of endothelial cells that correlate with melanoma cell motility. Unlike previous reports, data in chapter 7 shows that cancer cell motility is not increased in areas with increased vessel density (Figure 7.8). However, my work hints that melanoma cell motility is high in areas where endothelial cells show dynamic bleb-like protrusions, migrate within vessel walls and the vessels have increased variation in width (Figure 7.10). In some cases of endothelial bleb-like protrusions, I found autofluorescent signal, believed to be from macrophages, adjacent to the vessel. Previous reports have shown that peri-vascular macrophages attract cancer cells and are associated with sites of intravasation (Wyckoff et al., 2007). As I observed increased melanoma motility in areas with endothelial bleb-like protrusions, this is consistent with a link between increased

melanoma motility, endothelial bleb-like protrusions and peri-vascular macrophages.

The endothelial behaviours associated with melanoma motility, described in chapter 7, may indicate low pericyte coverage, as pericytes act to maintain endothelial cell quiescence and may impose a structure and hence limit the vessel width. Therefore, areas with low vessel pericyte coverage may have increased melanoma motility. The quantitative analysis of stromal components and cancer cell motility, such as described in this thesis, should help to describe a permissive environment for cancer cell motility.

8.2.2 Regulation of gene expression in motile melanoma cells

8.2.2.1 TGF-β, SRF and Notch signalling is heterogeneous and associated with motility

In addition to a general description of motility, I took a more targeted approach to investigate the regulation of gene expression in motile cells. Work in chapter 3 shows that singly motile B16 F2 melanoma cells in vivo have increased activation of Notch, TGF-β and SRF signalling as assessed by transcriptional reporters. Consistent with previous work showing that the motile cells in B16 melanoma have decreased pigment (Pinner et al., 2009), Notch, TGF-β and SRF signalling are mutually exclusive with pigment levels (Chapter 3). Streaming cells have increased activation of SRF signalling but do not show increased TGF-β or Notch signalling (Chapter 3). This is interesting as it suggests that different pathways control the different modes of motility. In addition, it implies that there may be mechanistic differences between single cell motility and streaming and that streaming cells are not just adjacent single cells following a similar track or chemokine gradient. SRF signalling may be increased in both singly motile and streaming cells as a response to changes in the G-/F-actin ratio. Actin polymerisation is likely to occur in both forms of motility, which would subsequently reduce the G-actin concentration releasing MRTF to accumulate in the nucleus and activate SRF dependent transcription.

The data in chapter 3, showing that TGF-β signalling is increased in singly motile but not streaming cells, is consistent with previous work in the B16 model. Pinner et al showed that TGF-β2 induces motility in vitro and hypothesised that TGF-β induces motility and decreases pigment of cells in vivo (Pinner et al., 2009). The work by Pinner et al showed that the less pigmented cells, which are enriched for motile cells, had increased TGF-β2 expression, suggesting an autocrine mechanism for TGF-β induced motility (Pinner et al., 2009). A similar study using intra-vital imaging of TGF-β reporters in breast cancer showed that TGF-β induces single cell motility in vivo (Giampieri et al., 2009). This, together with my work, suggests that TGF-β may have a wider role in promoting single cell motility of cancer cells.

In contrast to TGF-β signalling, work in chapter 3 shows that SRF signalling is increased in both the singly motile and streaming cells. SRF has previously been shown to be required for B16 motility in vivo (Medjkane et al., 2009). The earlier experiments required long-term MRTF-A depletion, which decreases expression of important actin regulators including actin itself. Therefore there are two possibilities for the role of SRF in motility:

1. Cells with high SRF signalling may be motile because SRF signalling is required for sufficient expression of actin regulators.
2. SRF signalling may be activated during the induction of motility, due to the changes in the G-/F-actin ratio, and SRF signalling may be needed for maintenance of motility.

Chapter 3 shows that some non-motile cells have high SRF-dependent transcription suggesting SRF signalling is not a consequence of motility. However, given the half-life of GFP (~24 hours) it is not possible to rule out that these non-motile, SRF high cells were motile previous to imaging (the kinetic limitations of reporters are discussed later). Therefore it is difficult to determine whether SRF signalling is activated during or prior to motility.

Although Notch is up-regulated in singly motile cells (Figure 3.7), further analysis in chapter 4 suggested that Notch is not sufficient for motility, as driving Notch signalling through expression of NICD does not increase the number of motile cells

in vivo (Figure 4.4). This is in contrast to previous in vitro studies showing that Notch signalling increases motility of melanocytes (Pinnix et al., 2009). Perhaps Notch signalling in melanoma does not increase motility because expression of the relevant target genes is already increased compared to melanocytes. However, my analysis of motile cells after NICD expression does not address whether Notch signalling is required for motility. Further loss of function analysis, for example using γ-secretase inhibitors or expression of dominant-negative MAML, could address this point. If Notch signalling is not required for motility in vivo it may be co-activated with motility, indeed TGF-β has been shown to induce HES-1 expression in a NICD dependent manner (Blokzijl et al., 2003). This may explain the decrease in pigment observed in motile cells as expression of NICD was sufficient to decrease pigment in vivo (Figure 4.2).

Chapter 3 showed using individual clonal reporters that Notch, TGF-β and SRF signalling is increased in motile cells. However, it did not address whether the signalling pathways were co-activated or the relationship between cells with active Notch, TGF-β or SRF signalling. Combinatorial reporter cell-lines, showing activation of more than one pathway, for example both TGF-β and SRF signalling, would help to address if activation of more than one of these pathways is required for motility.

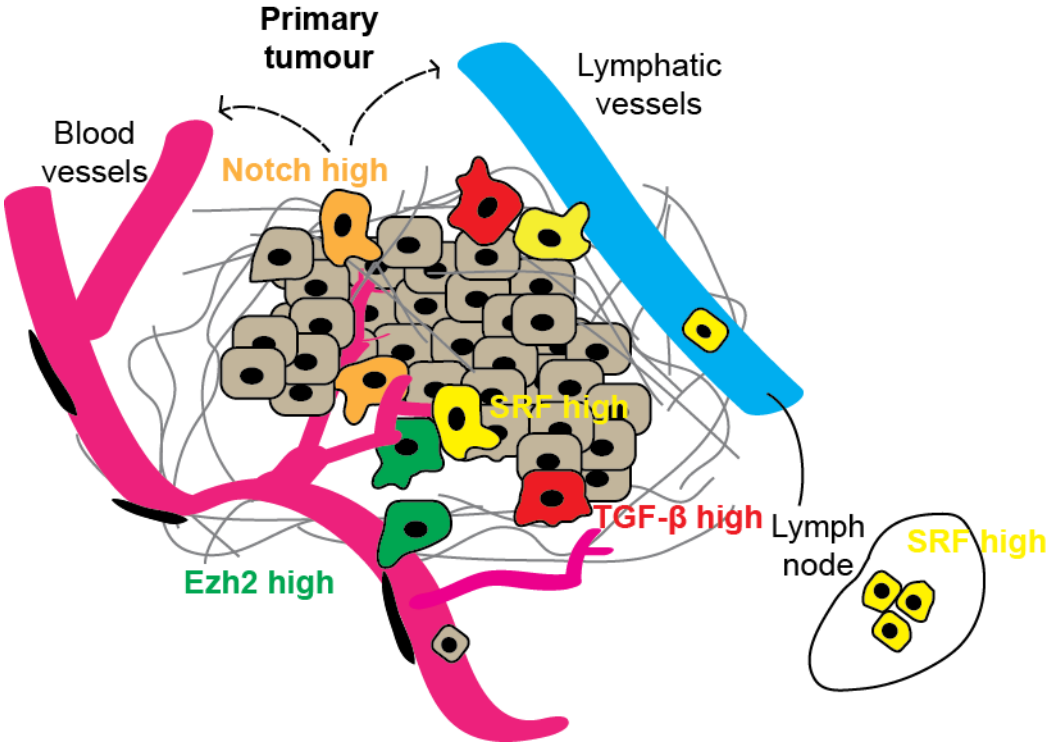

Figure 8.1 Model of heterogeneity in melanoma in vivo.

Notch, TGF-β and SRF signalling is heterogeneous in vivo and increased in the motile cell population. The Notch high population can promote metastasis in a non-cell autonomous manner potentially through effects on tumour endothelium. EZH2 expression levels are also heterogeneous in vivo and EZH2 positively regulates metastasis.

8.2.2.2 EZH2 expression is heterogeneous in vivo and increased EZH2 expression may be associated with the motile state

Work described in chapter 6 shows that expression of EZH2, a PRC2 Histone methyltransferase, is heterogeneous in both murine and human melanoma (Figure 6.2 and 6.3). The proportion of EZH2 high cells is similar to the proportion of motile cells perhaps indicating an overlap of the two populations. Bioinformatic analysis in chapter 5 (discussed later) provides further support that EZH2 may be associated with the motile state as EZH2 is co-regulated with Notch signalling and it may positively regulate the genes associated with the motile B16 population.

Heterogeneity in chromatin modifying enzymes has previously been described in melanoma. Reports have shown that expression of the JARID1B histone demethylase is heterogeneous with around 10 % of cells showing high JARID1B expression (Roesch et al., 2005) (Roesch et al., 2010). The JARID1B positive cells were shown to proliferate slowly and be important for maintainance of melanoma growth (Roesch et al., 2010). The work in chapter 6 describes an EZH2 high population of cells also around 10 % of the total, so it is interesting to speculate whether JARID1B levels would also be elevated in these cells. I propose that the EZH2 high population in melanoma is more motile, however JARID1B was not up-regulated in the motile cell population, and JARID1B siRNA knockdown had no effect on B16 F2 cell morphology. This suggests that JARID1B is not implicated in motility and perhaps that the EZH2 and JARID1B population do not overlap. It is interesting to note that the slow-cycling JARID1B positive population that maintains melanoma growth is reported to have increased expression of Notch targets (Roesch et al., 2010). Therefore the sub-populations of cells in melanoma may be overlapping.

EZH2 and motility have not been formally linked in melanoma, but a number of reports in other cancer types indicate a role for EZH2 in promoting cancer cell invasion and EMT (Ren et al., 2012) (Tong et al., 2012). The next sections will discuss the links between EZH2 and melanoma cell motility.

8.2.2.2.1 PRC2 complex regulates cell morphology and motility in vitro

Previously, a single publication had shown that EZH2 may control actin polymerisation (Su et al., 2005). Work in chapter 6 shows that depletion of EZH2 and other PRC2 components, such as Jarid2, in B16 F2 cells induces a flat cell phenotype with an increase in cell area (Figure 6.5 and 6.7). Changes in cell morphology are likely to require changes in the actin cytoskeleton and so this provides additional evidence for EZH2-dependent regulation of the actin cytoskeleton. Further investigation into the cytoskeletal associated changes showed that PRC2 components regulate cell morphology through regulating phosphorylation of the ERM proteins Ezrin and Radixin (Figure 6.10 and Figure 6.13). Intriguingly, depletion of the PRC1 complex member BMI-1, does not have consistent effects on cell morphology, suggesting a PRC1 independent role for PRC2 in regulating cell morphology (Figure 6.8). However, analysis of further PRC1 components would confirm this. How PRC2 may regulate Ezrin and Radixin phosphorylation is unclear. The microarray analysis outlined in chapter 6 did not show a change in any of the well established ERM kinases. However, it did suggest a decrease in expression of Fascin, an actin bundling protein, on EZH2 and Jarid2 depletion. This could lead to effects on actin binding of the ERM proteins. However, decreases in Fascin expression could not be detected at the protein level. As PRC2 regulation of Ezrin and Radixin activation may be PRC1 independent, this may suggest PRC1 independent control of gene expression or a cytoplasmic protein methylation mechanism similar to that suggested by Su et al. Given the important roles for the actin cytoskleleton and ERM proteins in cell motility, this suggests that EZH2 may regulate melanoma motility. Indeed, timelapse analysis of B16 cells in vitro showed a decrease in cell speed on EZH2 depletion and an increase in tail retraction problems (Figure 6.15). The presence of tail retraction problems is consistent with an increase in cell tails observed in fixed cells after EZH2 depletion (Figure 6.5). It would be interesting to perform timelapse analysis of EZH2 depleted cells rescued with constitutively active EzrinTD-GFP to test whether the tail retraction problem is associated with a loss of ERM protein activation.

8.2.2.2.2 EZH2 and Jarid2 regulate the genes associated with B16 motility

In chapter 3, the heterogeneous activation of transcriptional-based reporters correlating with motility indicates different patterns of gene expression in the motile population compared to the tumour bulk. The genes up-regulated in the B16 population enriched for motile cells, were identified using the Brn2 promoter and Notch reporters (discussed later). Overlap analysis described in chapter 6 suggests that EZH2 positively regulates genes associated with motility whereas Jarid2 negatively regulates the genes associated with motility (Table 8). Therefore, EZH2 may have a positive role in motility, in opposition to Jarid2. This is consistent with the effects of EZH2 and Jarid2 on short-term lung colonisation as determined in an experimental lung metastasis assay (Figure 6.16). How EZH2 positively regulates the genes associated with melanoma motility is unknown as EZH2 and PRC2 are classically considered to silence gene expression. Perhaps EZH2 indirectly regulates these genes through silencing a transcriptional repressor. Further experiments involving long-term silencing of EZH2 and Jarid2 are required to test their roles in motility in the primary tumour in vivo. In addition, genome-wide CHIP experiments could establish if EZH2 is directly regulating the genes associated with motility and could explore the contrasting effects of EZH2 and Jarid2 in this system.

8.2.2.2.3 EZH2 regulates changes in pigment associated with motility

Previous work has shown that the motile cells in B16 melanoma are less pigmented than non-motile cells (Pinner et al., 2009). Work in chapter 6 shows that EZH2 can control this phenotype change associated with motility, potentially through regulation of P protein expression, as loss of EZH2 increases pigment in an P protein dependent manner (Figure 6.24). EZH2 depletion results in increased *Oca2* mRNA levels (Figure 6.22) and previous reports have shown an increase in pigmentation with increased P protein expression (Sitaram et al., 2009). To confirm the role of P protein in EZH2 dependent pigment regulation, CHIP could be performed to test if EZH2 directly binds the *Oca2* promoter and inhibits expression. The role of Jarid2 in pigment regulation is unclear due to different results from different siRNA tested. Further siRNA oligos are required to determine if Jarid2 also regulates P protein expression and hence pigment.

8.2.2.3 Overlapping heterogeneity in signalling activation

Analysis of the reporter cell-lines in chapter 3 shows that a small proportion of non-motile cells exhibit activation of TGF-β, SRF or Notch signalling, implying that none of these pathways alone are sufficient for motility. Perhaps, activation of more than one signalling pathway is required for motility and interplay between all three pathways and additional ones, e.g Brn2 expression, together with a permissive microenvironment, is required for motility. Combinatorial reporter cell-lines which show activation status of more than one pathway would help to address this point.

I propose that EZH2 high cells are more motile, and we know that TGF-β, Notch, SRF dependent transcription and Brn2 promoter activity are increased in the motile cell population, but how do they all interact? The epigenetic status of a cell may dictate how responsive it is to external signals such as TGF-β or indeed it may dictate the target genes transcribed. Alternatively, an increase in EZH2 may sensitise the cells to activity through the TGF-β, Notch, SRF and Brn-2 pathways hence promoting motility, or an altered cytoskeleton, due to changes in EZH2 expression, may activate SRF and potentially Notch signalling.

Given the heterogeneity in Notch, TGF-β and SRF signalling described in chapter 3, it is interesting to think about how these populations with active signalling of various pathways overlap. The use of combinatorial reporter cell-lines showing the signalling status of multiple pathways would help and may enable the characterisation of further sub-populations within melanoma

8.2.2.4 Sources of heterogeneity in vivo

The reporter cell-lines outlined in chapter 3 indicate heterogeneity in Notch, TGF-β and SRF signalling activation in vivo and immunohistochemistry shown in chapter 6 indicates heterogeneous expression of EZH2. As the cell-lines are clonal in origin, the heterogeneity does not result from genetic differences but potentially from the local microenvironment or differences in the differentiation hierarchy. Another

possibility is heterogeneity in gene expression as a result of noise in gene transcription (Marusyk et al., 2012).

Heterogeneity in TGF-β signalling has also been reported in murine breast cancer in vivo (Giampieri et al., 2009). TGF-β is secreted by many cell-types in the tumour microenvironment, such as fibroblasts and macrophages, so proximity to stromal cells may dictate levels of TGF-β signalling. It would be interesting to image the TGF-β reporter cell-line together with other stromal components in the microenvironment to look for a correlation between the stroma and signalling status of melanoma cells. Attempts early in my PhD to GFP-tag TGF-β failed, but may have enabled visualisation of paracrine signalling in the tumour microenvironment. SRF signalling is responsive to external physical tension (Zhao et al., 2007b) and so the heterogeneity in SRF signalling observed in chapter 3 may reflect local differences in ECM stiffness and tension.

Chapter 3 shows that Notch signalling is heterogeneously active in melanoma in vivo (Figure 3.6). This may be a result of differences in differentiation state between cells as Notch is known to regulate differentiation (Andersson et al., 2011) and is required for maintainance of melanocyte stem cells (Moriyama et al., 2006). Notch signalling is also sufficient to confer a neural-crest like state on melanocytes suggesting that cells with active Notch in melanoma may be less differentiated (Zabierowski et al., 2011). However, work in chapter 4 showed that driving Notch signalling by expression of NICD slightly increased the differentiation associated genes TYR, TYRP and DCT, indicating that Notch did not promote a less differentiated state of B16 F2 cells (Figure 4.3). Therefore it is unlikely that heterogeneity in Notch signalling is a result of differences in differentiation.

Notch signalling is activated through cell-cell interactions (Andersson et al., 2011) so heterogeneous Notch activation may arise from heterogeneous expression of Notch ligands. Alternatively, Notch ligands are expressed by different stromal cell types, such as endothelial cells, so for example, melanoma cells adjacent to blood vessels cells could have increased Notch signalling. However, imaging of the Notch reporter cell-line in the VE-Cadherin:GFPCAAX mice did not reveal an obvious relationship between the vasculature and cells with active Notch signalling.

Notch signalling is also activated by hypoxia (Sahlgren et al., 2008), so regions of hypoxic tumour cells may have increased Notch signalling. However, the pattern of Notch reporter high cells in vivo does not seem to match this hypothesis. Therefore the origin of Notch heterogeneity is unclear. It is also interesting that the proportion of GFP positive cells in the Notch reporter cell-line changed vastly between in vitro and in vivo cultures (Chapter 3). It suggests that Notch signalling is high in vitro but low in vivo, this highlights the difference between cells in vitro and cells in the tumour microenvironment and the importance of in vivo studies.

Work in chapter 6 shows that EZH2 expression is heterogeneous in both murine and human melanoma and that it is increased at the invasive tumour margins in murine melanoma (Figure 6.2 and Figure 6.3). Previous work in an arthritis model has shown that EZH2 is up-regulated by the inflammatory cytokine, TNF-α, in synovial fibroblasts (Trenkmann et al., 2011). TNF-α is expressed by both melanoma cells and stromal cells in the microenvironment (Balkwill, 2002) and work in chapter 7 shows that the tumour margins are enriched for stromal cells (Figure 7.19). Therefore, areas such as the tumour margin, with increased stromal cells and TNF-α, may have increased melanoma EZH2 expression leading to heterogeneity in EZH2 levels. If EZH2 promotes motility and TNF-α induces increased EZH2 expression, then TNF-α should promote melanoma cell motility. Indeed TNF-α been reported to promote melanoma invasion in vitro (Katerinaki et al., 2003).

Alternatively, EZH2 is an E2F transcriptional target (Bracken et al., 2003), so cells with high E2F activity may drive high EZH2 expression. Chapter 4 indicates that E2F2 is up-regulated in the B16 motile cell population (Table 4), which correlates with a high E2F, high EZH2 motile population. E2F activity is cell-cycle state dependent and so the cell cycle may be an additional source of heterogeneity (Verona et al., 1997).

8.2.2.5 Approach to analyse signalling in motile melanoma cells in vivo

The approach to characterise signalling pathways associated with melanoma motility uses transcription-based reporter cell-lines, which depends heavily on the reliability of the reporter construct and subsequent cell-lines. It is difficult to absolutely exclude that reporter promoters respond to other signals. Preferably, multiple clones would be tested for each reporter cell-line, however, I only obtained one responsive Notch reporter clone. A drawback of the fluorescent transcriptional based reporters is the kinetics of response. Ideally, the fluorescent protein of the reporter should have a similar half-life to endogenous transcriptional targets of the pathway, so that expression of the fluorescent protein mirrors expression of relevant targets. GFP has quite a long half-life of about 24 hours, so its expression may not closely follow targets of the relevant pathways. How well GFP expression mirrored transcriptional target expression was not addressed for any of the reporters in this thesis. Therefore we cannot be certain that a cell with GFP reporter expression has pathway dependent transcription at that exact moment, but potentially the pathway has been active within the last 24 hours. To further validate heterogeneity in signalling of the SRF and TGF-β pathways I would perform immunohistochemical staining of the endogeneous transcription factors, in a similar manner to the NICD staining in Figure 3.6. In addition, imaging fusion proteins of SMAD2 and MAL (MRTF-A) with fluorescent proteins in vivo would improve the kinetics of the reporter and would allow determination of transcription factor localisation and hence activity, in motile versus non-motile cells.

8.2.3 Investigating the gene signature of motile cells

Although the transcriptional reporters used in chapter 3 suggest a different transcriptional program of motile cells, they only report on a single signalling pathway. Chapter 5 describes the genome-wide approach to analyse gene transcriptional programs associated with melanoma motility and will be discussed in this section. The Notch reporter from chapter 3 and a Brn2 promoter reporter developed in Pinner et al were used to purify the B16 F2 population enriched for motile cells. Subsequent microarray analysis enabled the derivation of a gene signature associated with motile cells (Chapter 5).

Analysis of the Brn2 promoter and Notch reporter microarrays revealed significant overlap between the high Brn2 promoter activity population and Notch high population, resulting in around 70 genes up-regulated in both populations. Having confirmed that the high Brn2 promoter activity population did not have an increase in Notch signalling and Notch targets, these genes were assumed to overlap due to similar cell phenotypes and hence were used to define a gene signature associated with motile cells. The geneset enrichment analysis also showed a number of genesets enriched in both the high Brn2 promoter activity population and Notch reporter high population, such as genes up-regulated in melanoma patients that had distant metastasis within 4 years compared to patients that did not. Although there was statistically significant overlap, the genes up-regulated in the high Brn2 promoter activity population and Notch reporter high population were not identical. This could be because the Notch reporter cells were purified in vitro and so the cells were under different conditions to the Brn2 promoter reporter cells purified from the tumour environment. In addition, data in chapter 3 shows that the proportion of cells in the Notch reporter high population is much larger in vitro and so the population in vivo may only be a subset and hence only have certain genes of the Notch reporter high list up-regulated. Additionally, although these populations are enriched for motile cells, chapter 3 shows the presence of non-motile Notch reporter high cells. These cells contribute to the analysed population and may result in the identification of genes that are not co-regulated with motility and hence not present in both lists. The acquisition of motility may not require the same gene expression changes each time. Instead, activation of a core gene expression network may be required together with additional inputs, which may differ. These additional inputs may come from the microenvironment and depend upon the local composition.

Surprisingly, a number of genes regulating the cell-cycle, especially cytokinesis and spindle assembly were up-regulated in motile cells (Table 4). However, this is not too dissimilar to previous expression analysis of the motile cell population of breast cancer cells collected by an in vivo chemotactic assay. In motile breast cancer cells more than half of the differentially regulated genes were associated with the cell-cycle (Goswami et al., 2004).

There are a number of similarities between the genes up-regulated in the motile B16 F2 cells outlined in chapter 5 and previously identified genes up-regulated in the motile breast cancer cell population. Geneset enrichment analysis in chapter 5 revealed that B-Myb targets are enriched in the genes up-regulated in motile melanoma cells (Table 6). B-Myb is also up-regulated in the motile cell population of breast cancer (Goswami et al., 2004). Geneset enrichment analysis also revealed that genes positively regulated by EZH2 in prostate cancer are enriched in the B16 motile cell population. Further analysis in melanoma described in chapter 6 also points to EZH2 having a positive role in promoting motility (discussed earlier). This is consistent with the other PRC2 components EZH1 and EED being up-regulated in the motile cell population of breast cancer (Goswami et al., 2004). Genes co-regulated with BRCA2 are enriched in the motile B16 population (Table 6) and BRCA2 is itself up-regulated in the breast cancer motile cell population (Goswami et al., 2004).

Kinesins are up-regulated in the motile population of both B16 F2 melanoma and breast cancer. KIF2C (also known as MCAK) and KIF23 (also known as MKLP1) are up-regulated in the motile B16 population (Table 4). Interestingly previous reports show that KIF2C is over-expressed in a number of human tumours and is associated with lymph-node metastasis and poor prognosis in colorectal cancer (Ishikawa et al., 2008). Furthermore, overexpression of KIF2C in gastric cancer cells increases motility (Nakamura et al., 2007). Therefore the reporter cell-line approach described in chapter 5 to identify genes up-regulated in motile cells in melanoma seems to have similar results to both previous reports identifying genes up-regulated in motile breast cancer cells and wider analyses of metastasis. This helps to validate the approach taken in this thesis to identify novel genes associated with motility and metastasis.

Due to the large proportion of genes involved in cell cycle control in the B16 F2 motile cell gene signature (Table 4 and Table 5), it is interesting to speculate that melanoma cell motility is dependent on the cell cycle. During development, neural crest cells synchronously delaminate and migrate in S-phase and migration can be blocked by blocking the G1/S transition (Burstyn-Cohen and Kalcheim, 2002). As

melanocytes arise from the neural crest, aspects of neural crest migration regulation may still remain in melanoma cells. A number of the genes increased in the motile cell population identified in chapter 5 regulate cytokinesis (Table 4). As cytokinesis requires Kinesins and localised control of the actomyosin network, regulators of cytokinesis may also be controlling actomyosin during amoeboid-like motility in vivo.

8.2.3.1 Approach to derive a gene signature associated with melanoma motility

The gene signature associated with the B16 motile cell population described in chapter 5 was derived from the overlap of genes up-regulated in the high Brn2 promoter activity population and Notch reporter high population. The Notch high population was purified from in vitro culture, which is not ideal but in vivo purification did not yield enough cells. Also only one sample of the Notch reporter was subject to microarray, compared to two samples of the Brn2 promoter reporter populations. Work is ongoing to repeat the Notch reporter microarray and increase the strength of the analysis. Despite these caveats, there was a surprising degree of overlap between the Notch and Brn2 promoter reporter cells. Having shown the high Brn2 promoter activity population is not enriched in NICD targets (Figure 5.6), one can assume that the high Brn2 promoter activity and Notch high populations share a similar phenotype (increased motility) and subsequently gene expression pattern. To further support the gene signature associated with the B16 F2 motile cell population, there is considerable overlap with a totally independent array performed in a different laboratory identifying MRTF-A targets (Table 7) (Medjkane et al., 2009). Chapter 3 shows that MRTF dependent SRF signalling is increased in singly motile B16 cells and so the overlap between the gene signature associated with the B16 motile cell population and MRTF targets further validates the relevance of the approach.

The majority of genes up-regulated in the B16 population enriched for motile cells have not been functionally validated. Knockdown of the genes in an invasion assay would determine if they contributed to melanoma cell motility and invasion.

The kinesins CENPE and KIF2C are drug targets, some of which are in clinical trials (Rath and Kozielski, 2012). These drugs could be tested in vivo to determine if they reduce the number of motile B16 melanoma cells. Furthermore, the potential regulators of the gene signature, such as B-Myb, identified by geneset enrichment analysis in chapter 5, should also be tested in invasion assays. As the genes are up-regulated in the B16 motile cell population the protein expression should be heterogeneous. Immunohistochemical staining of both mouse and human tumours would be able determine heterogeneity in expression and potentially highlight the relevance for human melanoma.

8.2.4 SRF, TGF-β and EZH2 are associated with motility and metastasis in other melanoma models

The work in this thesis characterising gene expression changes and signalling pathways associated with motile melanoma cells is confined to B16 F2 cells. To investigate the relevance of the findings of this thesis to human melanoma motility and metastasis I have used publicly available microarray data and subsequent geneset enrichment analysis. I will now present and discuss this analysis but stress that the original data is not my own.

The A375 cell-line is derived from human melanoma and multiple sub-lines have been generated from the parental A375 P cells including the A375 M2 sub-line that is enriched for the more motile and metastatic cell population. Geneset enrichment analysis indicates that TGF- β and MRTF-dependent SRF targets are enriched in the A375 M2 sub-line, compared to the parental line (Figure 8.2). This is consistent with my data in chapter 3 showing an increase in activity of these pathways in motile murine melanoma cells. Furthermore, similar to the results in murine melanoma presented in chapter 6, genes positively regulated by EZH2 and genes that co-vary with EZH2 are up-regulated in the A375 M2 sub-line compared to the parental population (Figure 8.2). The consistency with my data from murine B16 F2 cells suggests that SRF, TGF-β and EZH2 may have relevance for human melanoma. This is also supported by my analysis of both murine and human

melanoma samples showing heterogeneous EZH2 expression (Figure 6.2 and Figure 6.3).

The derivation of more metastatic sub-lines and subsequent gene expression analysis, as performed with the A375 P and M2 lines, documents stable changes associated with motility and metastasis. Imaging of the SRF reporter cell-line in lymph-node metastases suggests that SRF signalling is up-regulated in motile cells and furthermore, is maintained in cells in metastases. This maintenance of SRF signalling is consistent with the stable up-regulation of MRTF-dependent SRF targets in the more metastatic sub-line of A375 cells. Geneset enrichment analysis indicated that Notch target genes are not up-regulated in the more motile and metastatic sub-line of A375 cells. In addition, the genes up-regulated in the B16 population enriched for motile cells are not up-regulated in the more motile and metastatic sub-line of A375 cells. This could be because Notch signalling and regulation of the genes associated with motility is transient during induction of motility and metastasis.

Array data: A375 parental line vs M2 metastatic line grown on deformable collagen gels

Geneset: MRTF dependent SRF target genes in B16

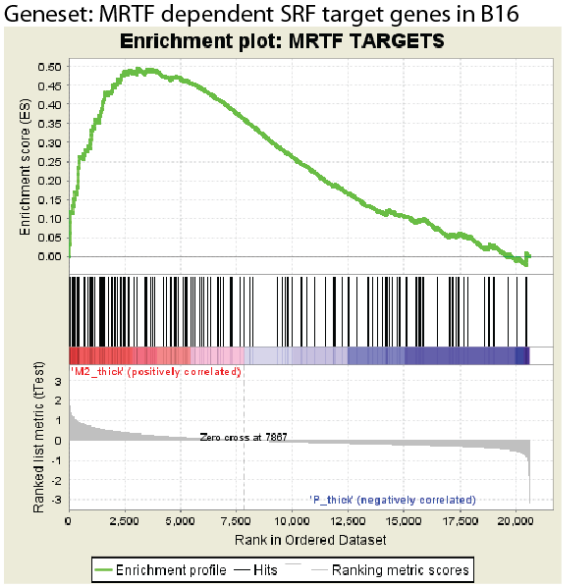

Geneset: TGF-β target genes

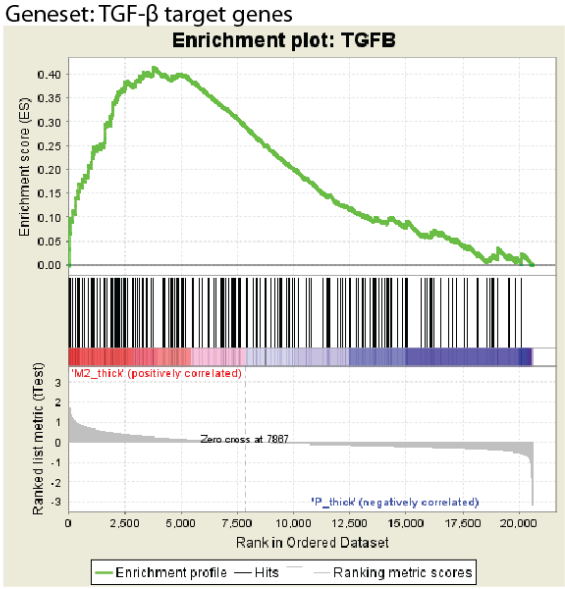

Geneset: Genes positively regulated by Ezh2 in B16

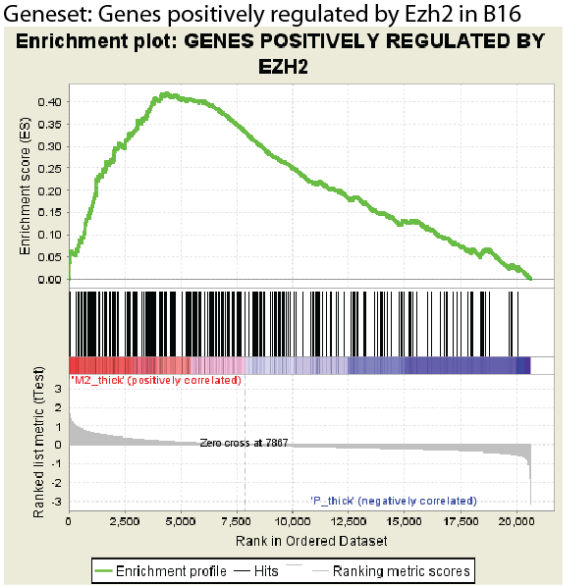

Genesets: Genes that co-vary with Ezh2

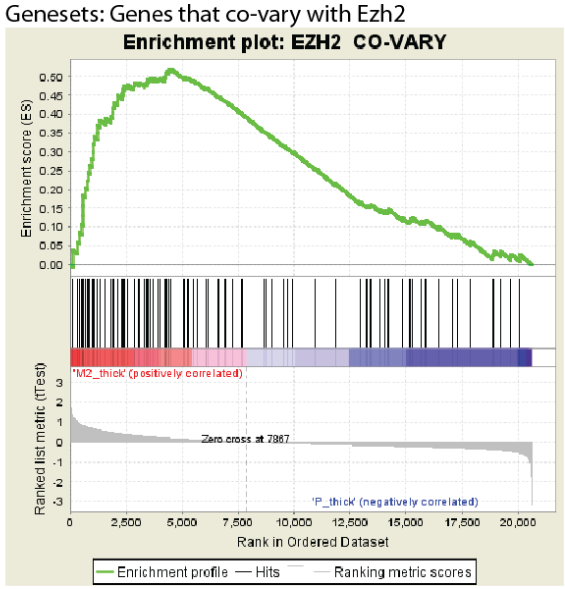

Figure 8.2. SRF, TGF-β and EZH2 regulated genes are enriched in the more motile and metastatic sub-line of A375 human melanoma cells.

Geneset enrichment analysis using free-ware from The Broad Institute, using publicly available array data from A375 P and A375 M2 cell-lines grown on deformable Collagen gels (Sanz-Moreno et al., 2011). The genesets used are MRTF dependent SRF targets in B16 cells, common TGF-β target genes, genes positively regulated by EZH2 in B16 cells (listed in appendix) and genes that co-vary with EZH2 in melanoma.

8.2.5 Differentiation state and melanoma motility

Previous reports suggest that B16 melanoma motility and metastasis is associated with a less differentiated state (Gupta et al., 2005; Kameyama et al., 1990; Pinner et al., 2009). Although the idea of a less differentiated, more motile state was very much at the forefront of my mind, my investigations do not reveal any further links between differentiation and melanoma cell motility. Microarray analysis of the Brn2 promoter reporter used in Pinner et al revealed that it is not a true differentiation reporter as there was little difference in differentiation markers between the reporter high and low populations. However, it reports on some signalling pathways associated with differentiation.

As Notch signalling is increased in the motile melanoma population and maintains melanocyte stem cells, I hypothesised that Notch maintains a less differentiated state and promotes motility. However, as Notch neither increases motility nor decreases differentiation associated genes, this hypothesis was disproved. Despite this, Notch is sufficient to decrease pigment, suggesting that Notch may promote a less pigmented state unrelated to differentiation status.

PRC2 silences differentiation associated genes in ES cells so I also hypothesised that EZH2 maintains cells in a less differentiated state to promote motility. Work in chapter 6 shows that EZH2 transcript levels decrease on α-MSH mediated differentiation of B16 melanoma cells (Figure 6.17), consistent with data from the developing epidermis where EZH2 expression decreases with differentiation (Ezhkova et al., 2009). Despite this, neither EZH2 nor Jarid2 depletion have significant effects on expression of the differentiation markers TYR, TYRP1 and DCT (Figure 6.20), suggesting that PRC2 levels do not dictate differentiation status of B16 melanoma cells. Nonetheless, EZH2-mediated suppression of *Oca2* maintains EZH2 high cells in a less pigmented state.

In chapter 5, geneset enrichment analysis supports the hypothesis that the motile cells are less differentiated, as genes associated with human and mouse ES cells were up-regulated in the B16 population enriched for motile cells (Table 6). However, genes associated with differentiation in melanoma did not change in

expression between populations enriched for motile or non-motile cells. Furthermore, geneset enrichment analysis suggested that transcription factors known to co-ordinate melanocyte differentiation, such as Pax-3, SOX-10 and MITF, did not regulate the genes associated with motile melanoma cells (data not shown). This potentially argues that there is little difference in the differentiation state of motile and non-motile melanoma cells.

My work suggests that the motile cells in the B16 F2 melanoma model cannot simply be considered as a less differentiated melanocytic or melanoblast-like state. However, it is possible that increased EZH2 levels drive the cells into an altered differentiation state with some similarities to ES cells.

8.2.6 The phenotype switching model to induce melanoma motility

The phenotype switching model proposed by Hoek and Goding suggests that "phenotypic heterogeneity is driven by specific gene expression programs which are imposed by the cellular microenvironment rather than by the accumulation of genetic events" (Hoek and Goding, 2010). Furthermore, it suggests the microenvironment potentiates switching (in either direction) between a proliferative MITF+/Brn2-, and migratory MITF-/Brn-2+, state. My work highlights the importance of the microenvironment to gene expression and signalling heterogeneity as the reporter cell-lines used in chapter 3, which although clonal in origin, show heterogeneity in signalling and motile behaviour. Therefore the work presented here supports the initial aspects of the phenotype switching model.

The increased TGF-β signalling in singly motile cells observed in chapter 3 is also consistent with switching between proliferative and motile states as previous data from genome-wide melanoma cell-line analysis shows an increase in TGF-β targets associated with the motile phenotype (Hoek et al., 2006). The role of Notch in phenotype switching is currently hypothetical and postulates that Notch signalling is increased in the motile state as Brn-2 has been shown to induce Notch signalling in neural progenitors (Castro et al., 2006). Work in chapter 3 shows an increase in Notch signalling in motile B16 melanoma cells, which is consistent with a

concurrent increase in Notch signalling in the motile phenotype, although my work indicates that this is not sufficient for motility (Figure 4.4). However, the relative abundance of cells with Brn-2 and Notch promoter activity is quite different as the Notch active population is small in vivo. Co-staining of tumours for NICD, Brn2 and MITF would help to determine if Notch signalling was a characteristic of the Brn2+/MITF- phenotype.

Geneset enrichment analysis of both the Brn2 promoter reporter and Notch reporter shows that MITF targets are not enriched in the populations enriched for non-motile cells or motile cells. This is not consistent with the MITF+/Brn2- MITF-/Brn2+ switching model (Hoek and Goding, 2010), which argues that MITF is a main regulator of the switch and that the non-invasive population should have increased MITF targets.

Switching between the two states, Brn2+ and Brn2-, is thought to be quite stable and have a hierarchy. Previous results have shown that Brn2+ cells are capable of producing Brn2+ and Brn2- cells in vivo but that Brn2- cells very rarely produce Brn2+ cells (Pinner et al., 2009). The stability in phenotypes may be epigenetically regulated by EZH2 and PRC2, as EZH2 controls cell plasticity in a number of situations and epigenetic regulation is maintained over many cell generations (Prezioso and Orlando, 2011). In the developing heart, EZH2 loss leads to hypoplasticity and impairment of EMT (Chen et al., 2012). EZH2 may maintain cells in their current phenotypic state and I would hypothesise that increased EZH2 maintains cells in the motile phenotype. Overall, my work supports the role of the microenvironment in contributing to changes in phenotype and switching to a motile state. It also raises interesting questions about the involvement of Notch and EZH2 in the different phenotypes and switching between states.

8.2.7 Other stages of the metastatic process

8.2.7.1 Notch signalling promotes metastasis through cell autonomous and non-cell autonomous mechanisms

Subsequent to motility in the primary tumour, cancer cells intravasate into endothelial vessels, travel to secondary sites, extravasate and must survive and proliferate to form metastases. In chapter 4, I investigated the role of Notch signalling in B16 melanoma metastasis as I had found it is increased in the motile cell population and previous reports had suggested Notch could increase metastasis (Liu et al., 2006).

Data in chapter 4 shows that Notch signalling is not sufficient to promote motility in vivo but it increases the metastatic potential of B16 F2 cells. Notch promotes spontaneous lymph-node metastasis in a non-cell autonomous manner as mice with tumours containing a mix of NICD and control cells had increased lymph-node metastases and the cells in the lymph-node were a 50:50 mix of control and NICD cells (Figure 4.6). As the number of motile cells in mixed tumours was similar to control or NICD tumours, this suggests that changes to the microenvironment increase the ability of motile cells to metastasise. Indeed, tumours containing NICD cells had an increase in blood vessel lumen size (Figure 4.9). However, lymphatic metastasis likely occurs through the lymphatic system. Unfortunately, staining of lymphatics using anti-podoplanin and LYVE-1 antibodies was not very successful. Few lymphatic vessels were observed in the tumour mass, but there was increased staining around the tumour margins. The margin staining looked to be non-specific, but was similar to the lymphoid-like stroma described previously for the B16 model (Shields et al., 2010). Therefore I was unable to determine whether cells with active Notch signalling impacted the lymphatic endothelium. Given that tumours containing NICD cells had increased blood vessel lumen size, it is interesting to consider that if left longer, these tumours may show increased spontaneous lung metastasis.

Consistent with previous data in other melanoma cell-lines, B16 F2 experimental lung metastasis was increased by active Notch signalling (Figure 4.10). As Notch

signalling is increased in motile cells in vivo (Figure 3.7), active signalling in motile cells can also impact other steps in the metastatic process, even though it may not be sufficient for motility. Microarray analysis of control versus NICD cells, described in chapter 4, suggests a number of possible reasons for the increase in metastasis. Transcripts of the interferon regulated genes, *Stat1*, *Ifitm3*, *Ifit3*, *Irf9 and Ifi35* are all up-regulated greater than 1.5 times in the B16 F2 NICD-GFP cells. Interferon leads to an activation of Stat proteins by JAK kinases and a subsequent increase in Stat target genes (Stark and Darnell, 2012). Previous studies have shown that B16 F1 cells have heterogeneous activation of Stat1 and cells with high Stat1 signalling have increased ability to colonise the lung (Khodarev et al., 2009). Furthermore, JAK kinases have been shown to induce actomyosin contractility in melanoma cells (Sanz-Moreno et al., 2011), which is important for short-term survival in the circulation and lung colonisation (Pinner and Sahai, 2008). Therefore the increase in Stat1 and interferon regulated genes on expression of NICD-GFP may explain the increase in lung colonisation seen in the B16 F2 NICD-GFP cell-line in chapter 4.

Mylk transcript levels were was also identified in chapter 4 as up-regulated in cells with increased Notch signalling. Actomyosin contractility is important for amoeboid cancer cell migration in vivo, extravasation and lung colonisation (Wyckoff et al., 2006) (Pinner and Sahai, 2008). Increased MYLK expression in the B16 F2 NICD-GFP cells may lead to increased actomyosin contractility and help explain the increased ability to extravasate and colonise the lungs. However, the increased MYLK would also be expected to increase amoeboid motility in the primary tumour, but this was not observed.

The microarray analysis also indicated that *Vegfb* mRNA is up-regulated about 1.3 times in the B16 F2 NICD-GFP cell-line relative to control. VEGF-B is a ligand of VEGFR-1, a receptor expressed on endothelial cells, monocytes, and tumour associated macrophages (Fischer et al., 2008). VEGFR-1 positive bone-marrow cells have been shown to initiate the pre-metastatic niche and promote metastasis (Kaplan et al., 2005). Therefore increased VEGF-B secretion from the B16 F2 NICD-GFP cells may increase the recruitment of VEGFR-1 positive bone-marrow cells to pre-metastatic sites, including the lymph-node, hence promoting

metastasis. The increase in lung colonisation seen by B16 F2 NICD-GFP cells in chapter 4 could be a result of a similar mechanism of recruitment of bone-marrow cells to the lung, which subsequently aid melanoma cell growth through paracrine interactions. However, VEGFR-1 staining of sub-cutaneous tumours and lungs containing either B16 F2 control or NICD-GFP metastases did not reveal a difference in VEGFR-1 positive cell recruitment (data not shown). This suggests that increased VEGF-B production by B16 F2 NICD-GFP cells does not act in a systemic way to increase metastasis, however, it does not rule out a paracrine effect on the vasculature. VEGF-B is a member of the vascular endothelial growth factor family, however, it is unusual in that it has no activity under normal conditions and any activity it does have, is context dependent (Li et al., 2012). It has a survival effect on both endothelial and neuronal cells (Li et al., 2008; Zhang et al., 2009), so it is possible that increased VEGF-B expression in the B16 F2 NICD-GFP cells increases cell survival during lung colonisation. Alternatively, VEGF-B may signal to the vasculature and, potentially through increased angiogenesis or paracrine interactions, lead to increased lung colonisation of B16 F2 NICD-GFP cells. In addition the increase in vascular lumen size seen in tumours containing the B16 F2 NICD-GFP cells in chapter 4 may be a result of increased VEGF-B signalling.

To determine if VEGF-B, MYLK or STAT promote lung metastasis, these proteins could be knocked down by siRNA and the cells used in short-term experimental lung colonisation assays. Furthermore, to determine if they are required for Notch induced increase in lung metastasis, VEGF-B, MYLK or STAT could be knocked down in NICD cells and subject to experimental metastasis assays. To further investigate the effect of NICD cells on the endothelium, sprouting angiogenesis and lymphangiogenesis assays could be performed in vitro in the presence of NICD or control cells. This would determine if NICD cells had direct effects on endothelial sprouting or morphology.

8.2.7.2 EZH2 positively regulates metastasis

Much of the hypothesis that EZH2 positively regulates melanoma motility is based on it's role in lung colonisation and also it's effects on motility in vitro. Work in chapter 6 shows that loss of EZH2 decreases experimental metastasis whereas loss of Jarid2 has no effect (Figure 6.16). This was surprising given that depletion of both EZH2 and Jarid2 results in a loss of Ezrin and Radixin phosporylation (Figure 6.10) and that Ezrin promotes metastasis (Hunter, 2004). Therefore, ERM protein phosphorylation does not seem to affect metastatic potential of B16 F10 cells. However, phosphorylation of Moesin is not affected on PRC2 depletion and so Moesin may be compensating for loss of activation of the other ERM proteins. The observation that Jarid2 depletion does not affect metastasis suggests that PRC2 and EZH2 regulated genes but Jarid2 independent genes are the most likely to regulate metastatic potential of B16 melanoma cells. EZH2 may promote metastasis through positive regulation of MCAM expression, as MCAM expression is decreased concurrent with decreased metastasis on EZH2 depletion (Figure 6.26). MCAM is an adhesion molecule whose increased expression is associated with metastasis in melanoma cells (Xie et al., 1997). Decreased MCAM expression on EZH2 depletion may decrease B16 cell adhesion to endothelial cells on arrival to the lungs and hence decrease metastasis. However, the mechanism of EZH2-dependent MCAM regulation is unclear, as EZH2 is classically associated with gene silencing. EZH2 may regulate MCAM indirectly by silencing a repressor of MCAM expression.

8.2.8 Problems with siRNA mediated gene silencing

Investigating the role of PRC2 components in melanoma motility, differentiation and metastasis relied heavily on siRNA mediated depletion of key PRC2 components. However, siRNA studies are sensitive to off-target effects of the siRNA. This study encounters a number of problems associated with siRNA mediated depletion. Depletion of EZH2 with 3 different siRNA did not lead to the exact same phenotype with all three oligos. Cells depleted with EZH2 siRNA #2 were much flatter, had a larger surface area and had actin cables at the cell periphery compared to cells depleted with EZH2 siRNA #1 and 4 which also had increased cell area, but to a

lesser extent, and had long tails (Figure 6.5). This was a common problem as oligos silencing Suz12 and Jarid2 also resulted in slightly different phenotypes. The problem was accentuated in the analysis of the effects of Jarid2 on pigment to such a degree that no conclusion could be found (Figure 6.18). In addition, one out of three oligos for both EZH2 and Jarid2 resulted in a vast increase in metastasis in contrast to the effects of the other two oligos (Figure 6.16). In sections 6.8.3 and 6.8.4 I attempted to utilise these problems, together with microarray analysis after different siRNA knockdown, to identify genes that correlated with various phenotypes such as pigment and metastasis. This highlighted the role of P protein in the regulation of pigment and hinted that MCAM may regulate metastasis. Overall, the siRNA oligos which consistently gave the majority phenotype, such as EZH2 #1 and 4, were considered when drawing conclusions from the data. Ideally, more siRNA oligos are required to test the role of Jarid2 in pigment and to confirm the roles of both EZH2 and Jarid2 in metastasis. In addition, re-expression of siRNA resistant cDNA would help to confirm the roles of EZH2 and Jarid2 in the relevant phenotypes.

8.3 Heterogeneity in the tumour vasculature

In addition to analysis of the motile cell population in melanoma, this thesis describes investigations into the vasculature in the melanoma microenvironment, which will be discussed further in this section. Intra-vital imaging of the tumour vasculature in melanoma, presented in chapter 7, revealed heterogeneity in vascular morphology and response to Sunitinib anti-angiogenic therapy. Two morphologically and dynamically distinct vascular zones in the tumour margin were identified, the immediate margin, a region with increased branch points and blunt ends, and the peripheral margin, a region with increased tortuosity and variation in vessel width (section 7.2). Chapter 7 also describes the use of imaging windows for long-term tracking of the tumour vasculature. Vascularisation of the B16 melanoma model was shown to mainly arise through sprouting angiogenesis, and involved many of the same steps as developmental angiogenesis, such as sprout formation, sprout elongation, anastomosis and potentially vascular remodelling (section 7.5.1). Sprout formation in the tumour environment showed the greatest

differences to developmental angiogenesis as protrusions were not limited to the tip cell leading the sprout. Interestingly, although the tumour was vascularised, there was higher vascular density around the tumour. This has also been observed with B16 melanoma spheroids in vitro (personal communication, Holger Gerhardt). Perhaps the B16 melanoma is a dense environment that is difficult for endothelial cells to penetrate. Long-term tracking also indicated that the peripheral tortuous margin may arise from immediate sprouting margin areas, as margin vessels initially showed an increase in blunt ends, followed by increased tortuosity (Figure 7.31). This suggests that the immediate and peripheral margins are temporally linked.

The overall morphologies of tumour vessels described in chapter 7 are similar to previous reports showing that tumour vessels are tortuous, chaotic, often with large lumens and increased branching (Carmeliet and Jain, 2011b). Heterogeneity in the tumour vasculature has been previously reported, however the analysis of vascular phenotypes was based on immunohistochemical sections (Nagy et al., 2010). Therefore comparison with the vascular morphologies described in chapter 7 is difficult. The previous reports indicate that large, thin walled mother vessels are the first vessels to appear in tumours and that they arise from existing vessels by degradation of the basement membrane, pericyte detachment and vascular expansion. However, my longitudinal imaging studies point towards the first tumour vessels arising from nascent spout growth. Furthermore, the morphological analysis of the vessels described in chapter 7 suggests these vessels, created by nascent sprouting and characteristic of the immediate margin, are relatively “normal” (more so than the vessels in the peripheral margin) narrow vessels with a number of blunt ends and branch points. This disputes the idea of large mother vessels as the first tumour associated vessels and highlights the power of imaging studies. However, the differences could be dependent on the tumour type analysed.

The previous analysis of tumour vessel heterogeneity also indicates that the initial mother vessels are transient and then evolve into various types of daughter vessels including capillaries, glomeruloid microvascular proliferations (GMPs) and vascular malformations (VMs) (Nagy et al., 2010). The longitudinal analysis of tumour

vasculature in chapter 7 indicates that phenotypes associated with the peripheral margin vessels, such as vessel tortuosity, develop after phenotypes associated with the immediate margin. Therefore the peripheral margin vessels may be somewhat similar to daughter vessels. However, due to the different methods used to analyse the vasculature; intravital imaging vs immunohistochemistry, it is quite difficult to determine which type of daughter vessel the peripheral margin corresponds to. Due to the increased tortuosity and chaotic nature of peripheral margin vessels, they most closely resemble GMPs.

Although the different vessel morphologies and vascular zones described in chapter 7 do not easily correspond to previous reports of tumour vascular heterogeneity, the different vascular zones do correspond to previous reports describing vascular phenotypes dependent on availability and processing of VEGF-A. VEGF-A can bind the ECM and be cleaved by a subset of MMPs (Lee et al., 2005). Previous studies have indicated that expression of MMP cleavage resistant VEGF-A in tumours leads to highly branched narrow vessels, whereas expression of the cleaved form of VEGF-A leads to an enlargement of vessels (Lee et al., 2005). The enlarged vessel phenotype is similar to vessels found in the tortuous peripheral margin of melanomas and the increased branching and narrow vessels are reminiscent of vessels in the tumour and immediate melanoma margin. Work in chapter 7 confirms that there is increased MMP activity in the margins indicating that the heterogeneity in vessel architecture may be as a result of differential VEGF-A cleavage.

Time-lapse imaging of the tumour vasculature revealed interesting endothelial cell behaviour. Endothelial cells were observed extruding bleb-like protrusions, however, typically endothelial cells are considered to respond to growth factors by producing filopodia (Gerhardt et al., 2003). Interestingly, filopodia and bleb-like protrusions were both observed in vivo and correlation analysis suggested a negative correlation between the two behaviours (Figure 7.10). Perhaps different environments or growth factors induce the different protrusions. Bleb-like protrusions may be the initial events in another interesting tumour associated endothelial cell behaviour observed in vivo. Endothelial cells were observed undergoing a rounded, amoeboid-like form of motility distant to tumour vessels

(Figure 7.6). This may be similar to the Endothelial to mesenchymal transitions (EndMT) described during development and pathology (van Meeteren and ten Dijke, 2012). In one movie (Supplemental movie 12), an endothelial cell extruded a bleb-like protrusion from the vessel wall and subsequently escaped the vessel using rounded amoeboid-like motility. This is similar to events observed during zebrafish development when aortic endothelial cells contract to bend out of the aorta and subsequently migrate away from the vessel (Kissa and Herbomel, 2010). TGF-β has been shown to drive EndMT and as TGF-β signalling is increased in motile melanoma cells, endothelial and melanoma cells may be responding to the same signal to induce motility (van Meeteren and ten Dijke, 2012)

Due to the links between endothelial behaviour, vessel morphology and melanoma cell motility (discussed earlier) tumours were treated with Sunitinib, a relatively broad receptor tyrosine kinase inhibitor with anti-angiogenic properties, in an attempt to perturb the vasculature (section 7.4). However, the vasculature was not perturbed as expected. Although vessel density and tumour growth was decreased, vessels in the tumour margin were resistant to Sunitinib and still displayed angiogenic protrusions (section 7.4). This was concurrent with lower melanoma cell apoptosis in the margins compared to the tumour bulk (Figure 7.17). Although previous studies suggest that pericyte coverage may affect response to Sunitinib, there was no indication of differences in pericyte coverage between tumour and margin vessels (Figure 7.18). Instead, margins had a higher density of stromal cells, such as macrophages and CAFs, compared to the tumour bulk (Figure 7.19). These stromal cells may provide VEGFR independent pro-angiogenic signals suggesting that the microenvironment may be a cause of the lack of response to anti-angiogenic therapies. In vitro sprouting angiogenesis assays did not provide evidence for paracrine VEGFR independent pro-angiogenic signals between CAFs, macrophages and B16 melanoma cells (data not shown) However, they do not accurately recapitulate the tumour environment, for example, many angiogenic ligands bind the ECM and are released after MMP activity. Indeed MMP activity is increased in the tumour margins compared to the tumour bulk (Figure 7.20). This suggests that increased MMP activity, together with increased stromal cells, may lead to increased availability of pro-angiogenic ligands at the margins resulting in vessel resistance to Sunitinib.

Interestingly, heterogeneity in response to anti-angiogenic therapy has been reported previously in a system to reproduce tumour-associated vasculature by over-expression of VEGF-A in vivo (Sitohy et al., 2011). In this case, the later forming vessels such as vascular malformations, feeding arteries and draining veins were resistant to anti-VEGF therapy and the authors argue that a decrease in VEGFR-2 levels in these vessel types explains the independence to VEGF-A. I tested this hypothesis by staining of B16 tumour sections for VEGFR-2, but found no difference in expression between vessels in the margin and tumour bulk, indicating that this is unlikely to be the reason for Sunitinib resistance in the margin.

8.4 Tumour heterogeneity and implications

My work has revealed signalling heterogeneity in murine melanoma in vivo. Intra-tumoural heterogeneity can result from intrinsic factors such as genetic differences. However, the clonal nature of the reporter cell-lines suggests that the heterogeneity may arise from the microenvironment, differences in differentiation state and noise in gene expression (Marusyk et al., 2012). In human tumours it is likely that a mix of all of these factors results in a complex heterogeneity in gene expression patterns over space and time.

The implications of intra-tumour heterogeneity are readily observed in patient response to therapy. Human tumours often have a small population of cells that are resistant to therapy and cancer stem cells have been reported to be resistant to standard therapies (Reya et al., 2001). In addition, the different microenvironments within the same cancer may lead to different selective pressures within the same tumour and multiple resistant cell populations (Marusyk et al., 2012). A further compounding factor with cancer therapy is that the drug needs to reach the cancer at an effective dose. However, heterogeneity of the tumour vasculature, as described in this thesis, may result in poor drug delivery or heterogeneous drug delivery to the tumour.

Some of the genes identified in this study as up-regulated in the motile melanoma population are linked to drug resistance, suggesting that the motile state may also represent a more drug-resistant state (Eyler and Rich, 2008). For example, *Kif2c* mRNA is up-regulated in motile B16 cells and its expression mediates resistance to the chemotherapeutic, paclitaxel (Ganguly et al., 2011). Many other Kinesins are up-regulated in the B16 population enriched for motile cells and their increased expression is associated with docetaxel resistance (De et al., 2009). Increased EZH2 expression is also associated with drug resistance and ovarian cancer cells resistant to cisplatin show EZH2 over-expression (Hu et al., 2010). In addition, loss of EZH2 in pancreatic cancer cells sensitises the cells to the chemotherapeutics, doxorubicin and gemcitabine (Ougolkov et al., 2008). Furthermore, heterogeneity in chromatin state and expression of the Histone demethylase JARID1A results in heterogeneity in drug response in non-small cell lung cancer (Sharma et al., 2010).

Intra-tumour heterogeneity leads to interactions between the different populations in the tumour, which may further promote growth and metastasis (Marusyk and Polyak, 2010). The work in this thesis describes heterogeneity in Notch signalling in B16 melanoma and further shows that heterogeneity in the status of the Notch pathway promotes lymph-node metastasis. Although this is likely due to effects on the microenvironment, phenotypic heterogeneity in small cell lung cancer leads to increased metastasis through paracrine interactions between cell populations (Calbo et al., 2011).

Heterogeneity is likely to be dynamic, with patterns of gene expression changing over time. My work does not address dynamic heterogeneity in the primary tumour, however the combination of transcriptional reporter cell-lines and long-term imaging using imaging windows would start to address these issues.

8.5 Concluding remarks

This thesis covers investigation of gene expression regulation during melanoma motility in vivo and a study of the tumour vasculature in melanoma. It finds that Notch, SRF and TGF-β signalling is heterogeneous in vivo and is increased in the

motile B16 F2 cell population. Although Notch signalling is not sufficient for motility in vivo, it promotes metastasis through cell autonomous and non cell autonomous mechanisms. Derivation of a gene-signature of the B16 F2 melanoma population enriched for motile cells suggests a role for the chromatin modifier EZH2, in regulation of motility. Further analysis indicates that EZH2 also positively regulates melanoma metastasis. Imaging of the vasculature in melanoma revealed morphological and dynamic heterogeneity, with the identification of two distinct vascular zones within the tumour margin. Endothelial behaviours and vascular morphology were found to correlate with melanoma motility. Endothelial bleb-like protrusions, endothelial cell motility and increased variation in vessel width correlate with melanoma motility and help to describe a permissive microenvironment for motility.

This work highlights the involvement of cancer cell and microenvironmental heterogeneity in the clinically relevant problem of metastasis. More investigation of genes in the gene-signature of the B16 F2 motile cell population may identify novel genes associated with motility and metastasis in vivo. Furthermore, EZH2 and some of the genes up-regulated in the B16 population enriched for motile cells may provide therapeutic anti-invasion and metastasis targets for melanoma in the clinic.

Chapter 9. Appendix

9.1 Notch targets

Genes up-regulated >1.2 fold in B16 F2 NICD vs B16 F2 control cells

Cck	*Ctsa*	*Ncald*
Mgll	*Rpl7a*	*Trappc6a*
Usp18	*Oas1g*	*Pkia*
Ifitm3	*Mylk*	*Mgat4b*
Gsta4	*Pqlc3*	*Gnpda1*
Loc100038882	*Sytl2*	*S100a1*
Ifit3	*Ddx24*	*Pgpep1*
D12ertd647e	*Phlda3*	*Eif2ak2*
Rsad2	*Scotin*	*Tead2*
Lgals3bp	*Adh7*	*Loc100048721*
Loc100048346	*Dennd2a*	*Mrps12*
Sgk2	*Ptgds*	*1810030n24rik*
Irf9	*Trim21*	*E330034g19rik*
Fez1	*B2m*	*Bst2*
Cdkn1a	*Cpne4*	*Pi4k2b*
Hs3st1	*Hes1*	*Ssbp3*
Slc22a18	*Pcbd2*	*Tmsb4x*
Sspn	*Ccng1*	*1500010j02rik*
Anxa11	*Apobec1*	*Rpl22*
Dcxr	*Ephx1*	*Ecm1*
Iigp2	*Col4a1*	*Ddah1*
Irgm	*Entpd2*	*Smpd1*
Stat1	*Egfl7*	*Aaas*
Ptp4a3	*Insig2*	*Arl2*
Samd9l	*Scly*	*Timp2*
Ifi35	*Ubl7*	*1110008p14rik*
Parp14	*Pmm1*	*Agrn*
Mgst1	*C230021p08rik*	*Itm2b*

Nme4	*Mras*	*Apoa1bp*
Flrt3	*Pex2*	*Psme1*
Mcts1	*Cuedc2*	*Atp5d*
Capg	*Sac3d1*	*Mknk2*
Stx8	*Acot1*	*Gpr137b*
Mrps6	*Stx3*	*Cdc42ep4*
Ccdc53	*Smpdl3a*	*Slc25a20*
1500011h22rik	*1190007f08rik*	*Uchl3*
Loc100045617	*Gstm2*	*Haghl*
Tmem9	*Mlkl*	*Oca2*
Pigp	*Leprel2*	*Tcfap2a*
Sept8	*Tceb1*	*Mrpl43*
Rhox5	*Ei24*	*Asna1*
0610006i08rik	*2810417h13rik*	*Mrpl14*
Sumo1	*Enc1*	*Reep5*
Vegfb	*Csrp1*	*Impa2*
Ndufs4	*2310016c16rik*	*Ddx25*
Nckipsd	*Phpt1*	*Ndufc1*
Prickle4	*Txnip*	*Tulp2*
Col4a2	*Endod1*	*Xrcc1*
Tomm7	*Dstn*	*Kdelr3*
Slc25a1	*Bid*	*Tbc1d2*
Gsta2	*Gsta1*	*Stx7*
Cox6a2	*Trp53*	*Eg436240*
Mc1r	*Atp6v1h*	*Loc100044298*
Lmna	*Cyba*	*Map3k11*
Paqr6	*Actr3*	*Psip1*
Rgl1	*Dci*	*Gtse1*
Nol5a	*Cebpb*	*Bckdk*
Prkaca	*Mrpl30*	*H2afx*
Lhfpl2	*X99384*	*Laptm4a*
Fxyd5	*Ctsb*	*Agpat2*
Mcoln2	*1110058l19rik*	*Cd274*
Sepw1	*Josd2*	*Cetn4*

Atp5l	*Gnai2*	*Rdh14*
Loc100041500	*Sc4mol*	*Rbck1*
Tspan3	*C230093n12rik*	*Ubl3*
Vps16	*1810049h13rik*	*Atp6v0d1*
Scand1	*Taldo1*	*Tmem179b*
1700023m03rik	*Atp5g2*	*Ndufb3*
Ube2m	*Timp1*	*Tst*
Bace2	*5330431n19rik*	*Cdca5*
Prelp	*Marcks*	*Tpm3*
C1qbp	*Cdk2*	*Mrps23*
Pold4	*Sumo2*	*Tspo*
Cd59a	*Ddx58*	*Aldh3b1*
Tk1	*Nagk*	*Tyrp1*
Hist1h2bj	*Arsb*	
Bcs1l	*Tmem25*	

9.2 Brn2 promoter reporter high genes

Genes up-regulated >1.2 fold in B16 mRFPCAAX population with high Brn2 promoter activity.

Lce3b	*Olfr749*	*Olfr1252*
Olfr441	*Apol10a*	*Olfr1154*
Olfr151	*Rnf148*	*Olfr945*
Slc8a1	*Magea9*	*Olfr111*
Gm12669	*Olfr295*	*Ednrb*
Bc003266	*Olfr784*	*Olfr776*
Olfr676	*Klk1b1*	*Ccl8*
Olfr1238	*Psmb11*	*Olfr231*
Eml5	*Olfr952*	*Lyve1*
Vmn1r72	*Olfr38*	*Tas2r140*
Gal3st2	*Slbp*	*Ifna13*
Tcstv3	*Vmn1r47*	*Olfr733*
Olfr435	*Hsd3b3*	*Il22*

Olfr1255	*9630013d21rik*	*Vmn1r62*
Gbp4	*Neil3*	*Cp*
Olfr995	*Gpr1*	*Olfr68*
Olfr97	*Tmsb15b1-Tmsb15b2*	*Zfp658*
Otos	*Olfr99*	*Olfr433*
D930046h04rik	*Cstad*	*Fbxo5*
Olfr729	*Olfr1030*	*Psat1*
Olfr519	*Tuba8*	*Speer3*
Olfr462	*H2-Q6*	*Magea4*
Olfr285	*Olfr918*	*Prc1*
Olfr1165	*1700019m22rik*	*Zfp738*
Olfr968	*Casp4*	*Olfr895*
Krtap16-8	*Olfr458*	*Olfr103*
Cetn1	*Casp12*	*Olfr530*
9030203c11rik	*Gm8979*	*Rdh7*
Taf9	*Sh3bp1*	*Olfr702*
Olfr1188	*Klk1b11*	*Gp5*
Olfr118	*Zfp474*	*Stil*
Hist1h4h	*3110052m02rik*	*Gcsh*
Gpr182	*Rab11b*	*Mrfap1*
Txn1	*Olfr282*	*Vmn1r216*
Npl	*Olfr1302*	*Hist1h2ac*
Oog2	*Mrgpra3*	*Slc18a3*
Tas2r129	*Kif11*	*Ak5*
D3ertd751e	*Olfr474*	*Fam54a*
Il11ra2	*Olfr136*	*Tubb2a*
Nusap1	*Tgtp1*	*Olfr829*
1700029p11rik	*C79407*	*Ifit1*
Pdgfrb	*Olfr659*	*Olfr1383*
Hyls1	*H2-T10*	*Klk1b9*
Lmbr1	*5330416c01rik*	*Il17rd*
1700010m22rik	*Olfr1396*	*Akr1b7*
Olfr553	*Klhl38*	*Foxl1*
Pdgfd	*Tdg*	*Kir3dl2*

Olfr361
Vmn1r18
Aoc2
Cdkn2c
A930006j02rik
6030452d12rik
Olfr1339
Gm3604
Olfr657
Hoxd3
B3galt1
Gm11428
Esco2
Gbp3
Nhsl1
Slc40a1
Phxr4
Olfr564
Nfxl1
Cdca5
Fut2
Olfr196
Olfr13
Hist1h2bp
Defb20
A630033h20rik
Clec4d
Pde7b
Cetn4
Vmn1r75
Olfr684
Spdya
Prl7a2
Gbp2
Myoc
Fgf21
Olfr875
F13a1
Sln
Mup21
Ssx9
Tas2r105
Chek1
Aurkb
Cyct
Hspb8
Hist1h1t
1500015o10rik
B830004h01rik
Top2a
6720463m24rik
Kif20b
Olfr686
8030498b09rik
Plscr2
Rad54l
Olfr921
Sult5a1
Neto2
Tex13a
Trp53rk
Sgol2
A4galt
Npff
Lgals2
Sp100
Rdh5
Cdca2
Rab27b
Fam71f1
Raet1e
Kir3dl1
Fcna
Olfr1208
Fkbpl
Gm4455
Ankrd58
Oas1a
Olfr108
Ncaph
Olfr1009
4631416l12rik
Olfr1412
Cep55
Kbtbd3
Adam34
Wdr86
Fbxo48
Oasl2
Ccne2
Kif18a
Olfr635
Olfr849
Ppp1r14a
Spc25
4930504o13rik
5730577i03rik
Calm5
1700008p20rik
Cdo1
Dnajb7
Zfp59

Rnasel
Brip1
Olfr297
Af366264
Nrgn
Ocm
Zfp74
A130004g07rik
Xpo7
Uts2r
Spdye4
Atp6v0d2
Incenp
Gm4841
Fam110c
Hsd3b5
Gstm6
Igtp
Ifi44
Ccdc163
Olfr776
Mogat1
Mrgprb4
Olfr90
Gm5111
4921509c19rik
1810019j16rik
Rxfp3
Gdap1l1
Lbx1
Gnat1
Oasl1
Serp2
1700001g17rik
Reps2
Adam6a
Klhl25
Mrgprx1
Obox5
Igf1
Defb50
Vmn1r172
Serpinb9d
Lypd4
Mx2
Tk1
Gk2
Gm5105
Ctf1
Ube2t
Wdr25
Mybl1
Kif23
Tmem74
Fcer1a
Olfr792
Marco
Tuba1a
Il9
Olfr1163
Smad9
Sod3
Msx1
Abcc2
H2-M1
Mef2d
Zfp101
Diras2
Pcdhb5
Ucn3
Ai836003
Wdr65
Dbil5
Hist2h3c1
4921517d21rik
Dimt1
Serpinb9f
Olfr554
Elfn2
Fsd1l
Gnrh1
Folr2
Zfp7
Eif2c3
Ubc
Olfr1112
Dyrk3
Ensmust00000057700
Il17d
Olfr1323
Mcts2
Olfr194
Prss23
Gm3579
C230066g23rik
Pde4dip
Lcat
Ramp1
Kif18b
Opn1mw
4930599n23rik
Gsg2

Zfa
Tas2r117
A130066n16rik
E130306d19rik
Cdk1
Mixl1
Akr1c14
Olfr1480
Scgb3a1
Larp7
Hmox1
Ccnb1
Olfr347
Gpr45
Sgol1
G2e3
Cdc45
Kctd12b
2010111i01rik
D17h6s56e-5
Ncapd3
F730047e07rik
Olfr1202
Hsd3b6
9330175e14rik
Ak033775
Kif4
Il25
Nmbr
Cenpe
Rxfp4
Cenpj
5730590g19rik
Folr4
Slc7a9
8430431k14rik
Ubqlnl
Olfr653
Olfr235
Vmn1r228
Clec4g
Tagap1
Phospho1
Prl5a1
Tcfap2d
Slc10a5
E2f8
9330175e14rik
Casc5
Zfp354b
Hoxa11
Fam83d
Rad54b
Gm9734
5830403l16rik
Lcn4
Olfr486
Cacnb4
Actg2
Fabp3
Bc147361
1700120k04rik
Gm128
Fam111a
Prkg1
Olfr669
Dlx1
Melk
Ska1
Adrb3
Trim12
Vmn2r60
Foxc2
Mlf1ip
Amigo3
1700001c19rik
6030445d17rik
Taf5
Arf1
Pmp22
Pcdhb9
Ear6
Ercc6l
Olfr801
Olfr961
2010003k11rik
P2rx3
Aurka
Olfr493
Grin3a
A330049m08rik
Trim59
Gucy1b3
Gas6
9430031j16rik
Hsfy2
Ptgr1
Kif2c
Irf1
Olfr821
Gm5434
Ppnr

Skint10	*Tusc5*	*Rps18*
Npr2	*Olfr208*	*Hnrnpul2*
Ndc80	*Fkbp7*	*Kcna5*
2610039c10rik	*Spata9*	*Ankrd33b*
Mastl	*Phlda2*	*A330008l17rik*
Aspm	*Gen1*	*Cyp3a41b*
Gsta3	*A230052g05rik*	*Dyrk2*
Epha5	*Ckap2*	*H2-T9*
Rdh16	*Zfp868*	*Rbm11*
4930422g04rik	*1700007k13rik*	*Morn4*
Olfr1214	*Ifi203*	*Lrrtm1*
Cox8b	*Olfr649*	*Ttk*
Cenph	*Nxt1*	*Cap2*
H2afv	*Zfp846*	*Nck1*
Olfr1102	*Rap1a*	*Dnajc2*
Vmn1r35	*Efna2*	*Crh*
Serpina12	*Osbpl7*	*Prim1*
Kif26b	*Ptplad2*	*Olfr247*
Ppil5	*Olfr199*	*Rtp4*
Rhox11	*9330119m13rik*	*D130058e03*
Rdh14	*Vsx1*	*Smc2*
Hist1h2be	*Chrm5*	*Cyp8b1*
Wdr20b	*Ccl5*	*Prr11*
Dnajb3	*Cenpi*	*Pxt1*
Cxcl17	*Camk2n1*	*Olfr463*
Cga	*4930432o21rik*	*Clec2g*
Eu234013	*Rbm8a*	*Psg22*
Pnliprp2	*Olfr56*	*Apbh*
Fam81a	*Ctsg*	*Enpep*
Olfr183	*Paqr7*	*Fut1*
Ubd	*Cenpc1*	*Gcfc1*
Hsp90aa1	*B230340j04rik*	*Tbcc*
A530079e22rik	*Ugt2b35*	*Lrrc4c*
Best1	*Smarce1*	*Rbbp5*

Sord	*2210012g02rik*	*Kcna4*
Prph	*4833444g19rik*	*Mageb3*
Ckap2l	*Iqgap3*	*Rab3c*
Sac3d1	*Dscc1*	*Ccdc28a*
Prdm15	*Kif15*	*Pbk*
Gast	*Sfrs8*	*Cdca8*
Olfr1467	*Ube2c*	*Olfr102*
Sftpc	*Eri3*	*Glt28d2*
Zfp69	*Dbf4*	*Casp7*
Trpv3	*Pou3f2*	*Zcchc7*
Morn5	*Olfr1104*	*Atpaf1*
Gngt1	*Flt3l*	*Rab33a*
Ccne1	*Olfr938*	*Ifnz*
Gm4876	*Gch1*	*Bc147505*
9930104l06rik	*4932415g12rik*	*Rpl39l*
Semg1	*Olfr1499*	*Lin9*
Olfr677	*Wnt5b*	*Txndc12*
Bub1b	*Saa4*	*Snai1*
Fam123a	*Serpina7*	*Copg2*
Bc150970	*Htr6*	*Pcdhb21*
Lce1f	*Cenpq*	*Zfp783*
Chrna3	*Gpr84*	*Vmn1r45*
Unc13a	*Adh7*	*Vamp5*
Got1l1	*Bub3*	*Ngf*
1700055d18rik	*5031438a03rik*	*Chkb*
Kcnc3	*Hist1h1a*	*Cyp2c44*
Manbal	*A730037c10rik*	*Cyp4a12b*
Drd1a	*Nlk*	*Batf2*
Kazald1	*9530091c08rik*	*Slc22a13*
Lingo4	*Tas2r134*	*Rad51*
Gip	*Gins1*	*Olfr652*
Ubl4b	*C130046b21rik*	*Tbrg3*
Fam55b	*Kif22*	*Magea2*
Xkr7	*4931417g12rik*	*Hormad1*

Rfwd3
Cpsf4l
Kdm4d
Hsd11b1
Haus6
9330176c04rik
Ankrd61
Rapgef5
Cit
Gm5420
Hes1
Bc025446
Fam178a
Krt34
Dclre1c
Ppp2r3a
Bcdin3d
Gemin4
Htr3a
Pex11a
Tctex1d1
Nuf2
Wdfy3
Fbxw15
A430057m04rik
Apba1
Myl4
Gpr63
Bnipl
Kcnv2
Pea15b
Atad2
Nostrin
Zfp85-Rs1
Olfr1459
Vmn1r66
Olfr1270
Sucnr1
Gbp6
Rmnd1
Aa415398
Ctsq
Bc089491
Hmgb3
Prim2
Gpr158
Rep15
Tpx2
Kcna6
Rad51ap1
Pnma3
4632434i11rik
5930403n24rik
Olfr1099
Bc049715
Wnt1
Sgms1
Cd274
Tnp2
Fen1
Socs2
Chst8
Anln
Fkbp1b
Emx2
Npffr2
Cd59a
Slc1a6
Mcam
Hspb6
Camk4
Txndc9
Tmem69
Olfr446
Hmmr
Hells
Ddit4l
Vmn1r26
Ankrd9
Gimap3
Olfr74
Zdhhc16
1110058l19rik
Mnx1
B3galt2
Slc25a2
Fsd2
Mafb
Avp
Olfr160
Mki67
Gm5424
Cts6
B3galt6
Lrrc49
Ttc9b
C87436
Dlgap5
Fam110a
Zcchc7
Olfr284
Sost

Clspn	*Gtse1*	*Olfr1364*
Serpina5	*6330407j23rik*	*Zfp605*
Vpreb3	*Vasn*	*Ddx58*
Dopey1	*Ifit2*	*Hpvc-Ps*
Gemin6	*Tspan1*	
F630043a04rik	*D330045a20rik*	

9.3 Notch reporter high genes

Genes up-regulated >1.2 fold in B16 mRFPCAAX Notch reporter high population.

Cdkn1a	*Chka*	*Mllt3*
H2afx	*Ptp4a3*	*Adh7*
Rpo1-4	*Ncaph*	*Gsg2*
Fzr1	*Ezh2*	*Fen1*
E130306d19rik	*Tk1*	*Phlda1*
D10bwg1379e	*Slc22a18*	*Cdca8*
9430015g10rik	*Ddx24*	*Mmab*
Smtn	*Lrp11*	*Ifitm3*
Cenpl	*Pigt*	*A730008h23rik*
Prkcbp1	*Hist1h1c*	*Tbx2*
Aurka	*Pif1*	*Nfib*
3000004c01rik	*Slc25a10*	*Eif4ebp2*
Incenp	*Stard8*	*Isg20l2*
Kif23	*Rpl23*	*Kif22*
Sgol1	*Nup160*	*Snrp70*
Cdca2	*Taf15*	*Tbrg4*
Kif11	*5830457o10rik*	*Rad54l*
Depdc1b	*Gtse1*	*Nedd4*
Vps16	*Ncor1*	*Cck*
Top2a	*Dcxr*	*Zfp36l1*
Ccnb1	*5430432m24rik*	*Espl1*

Caprin1	*Stim1*	*Clk3*
Cetn4	*Pfkl*	*Dynll2*
Dbf4	*Tcf25*	*Rbms1*
Samd9l	*Ncapd3*	*Samd4b*
Cdc2a	*Taf11*	*Scand1*
Gpatch2	*Ncapd2*	*Sypl*
6430706d22rik	*3300001p08rik*	*Polh*
Nedd1	*Myst4*	*Slc41a3*
Kif4	*Prc1*	*Nup107*
Capns1	*Gna13*	*Ubac1*
Zcchc8	*Rnf26*	*Impdh1*
Ckap5	*Lsm2*	*C030011o14rik*
Mcm6	*4931406p16rik*	*Prkx*
Ifit3	*Cdkn2c*	*Wdr6*
Loc667609	*Ppp4r1*	*Tspo*
Cib1	*Mysm1*	*Vps37b*
Tmem176a	*1500010j02rik*	*Sfrs3*
Rad23a	*Lmna*	*6330503k22rik*
Nusap1	*Cdc42ep5*	*Bscl2*
Vezf1	*Dennd2a*	*Usp52*
Bc030476	*Foxm1*	*Mterfd1*
Psg23	*Mbd1*	*Tmod1*
Ccdc77	*Zfp41*	*Phf17*
Nde1	*Gtf3c1*	*Mid1ip1*
Gsta4	*Trmt1*	*Zfp326*
4933439c20rik	*Pcyt2*	*4833446k15rik*
2610039c10rik	*Sfrs5*	*Dpm2*
Nr1h2	*Rbm5*	*Anapc5*
Csrp1	*Kif2c*	*Ogdh*
Gbp2	*Timp1*	*Xrcc1*
Aldoa	*Prf1*	*Supt5h*
Dok1	*1500003o03rik*	*Bub3*
Cstf3	*Mpp5*	*Cacnb4*
Rnf14	*Cenpn*	*Cenpp*

Pip4k2a	*Sox5*	*Mrps21*
Lrba	*Rapgef4*	*Loc100038882*
Chkb	*Mlf1*	*Nrbp2*
Cdca5	*Gtf3c2*	*Ccng1*
Sfrs1	*Col5a3*	*D12ertd647e*
Npm1	*4933407p14rik*	*Asb6*
Stk17b	*Extl1*	*Mxd3*
1500001m20rik	*Smad3*	*Lace1*
D14ertd231e	*Bud13*	*Ppp1r11*
Bcas3	*Syngr2*	*Fadd*
Birc5	*Fastk*	*Sh3rf1*
Wdr51b	*Slc38a2*	*6030443o07rik*
Blm	*Mdm2*	*Paqr6*
Csnk1d	*Ada*	*Ccl5*
Actn4	*E2f2*	*Mtap2*
0610012g03rik	*Alg10b*	*Cdc20*
Akap9	*Tigd2*	*3010026o09rik*
Fez1	*Mrps25*	*Rhbdd3*
Tex9	*Rfwd3*	*Klhl30*
Spc24	*2310005n01rik*	*Ars2*
Atp6v0a1	*Ihpk1*	*Nadk*
Rbm38	*Tmem49*	*Hsf4*
Cugbp1	*Fbxo21*	*9630058j23rik*
Ganab	*Wiz*	*Wdr54*
Ruvbl2	*Nipbl*	*Cryz*
Irgm	*Clspn*	*Stat1*
Rfc2	*Crocc*	*Hmgb2*
Pcyox1l	*Tsga14*	*Tmsb10*
Suclg2	*2010003j03rik*	*Dgkz*
Tssc1	*Elf2*	*1700027j05rik*
Rhbdl2	*Phf12*	*Cdca4*
Depdc6	*Ecm1*	*Serf2*
Loc675228	*Mcph1*	*Phlda3*
Xrcc6	*Ei24*	*2610021k21rik*

Pofut2	*6430510m02rik*	*Tex264*
Clk2	*Adssl1*	*Prpf19*
Parp3	*Mapre2*	*Srebf1*
Srxn1	*Bbs4*	*Rbm43*
Riok3	*Scamp5*	

9.4 EZH2 and Jarid2 regulated genes

Genes down-regulated by <-1.2 on EZH2 k.d using oligos 1 and 4.

Ezh2	*Anp32a*	*Tmcc2*
Fscn1	*Nt5dc2*	*Ptpn6*
Tpp1	*Agrn*	*Loc100042405*
Igfbp4	*Cd8b*	*Hdgf*
H2afx	*Loc633016*	*Rnps1*
Rnf6	*Skp2*	*1110007a13rik*
C230021p08rik	*Alg8*	*Mybl2*
Tead2	*Isy1*	*Loc100044779*
Rnf6	*Ddx5*	*Zcchc8*
Pabpc1	*Anapc5*	*Lmnb1*
Usp1	*Top2a*	*Ets1*
Csda	*Actn4*	*Ptbp1*
Sparc	*C230067o06rik*	*Bcl2l2*
Ezh2	*9830169e20rik*	*Slc6a6*
Gnai2	*Nrm*	*Loc100045677*
Cdca4	*Kntc1*	*Mrps33*
2310040a07rik	*B130015m16rik*	*E130016e03rik*
Mcam	*Suds3*	*Setd8*
Casp2	*Ttyh3*	*Acat2*
Mum1	*Gtf3c2*	*Marcksl1*
Pabpc4	*Cdca4*	*6230401i02rik*
Gdi1	*C230021p08rik*	*Rpa3*
2810417h13rik	*Timp1*	*B230333e16rik*

Srf	*D17h6s56e-5*	*Mcm3*
Igfbp4	*Zfp746*	*Gdi1*
Mapre2	*Gm22*	*Gdi1*
9430080k19rik	*0610037l13rik*	*Tmed10*
5830434p21rik	*Rpl4*	*Nap1l1*
Loc280487	*Phf2*	*2410014a08rik*
Fubp3	*Gtf3c2*	*G3bp1*
Eg666609	*Thoc3*	*Parp2*
Ppapdc1b	*Icmt*	*Wnk1*
Pabpc4	*Odz4*	*Tpm4*
Tmsb10	*Taf15*	*Sf3b4*
2810417k24rik	*1810055e12rik*	*H2afy*
Rnps1	*Smarce1*	*Eg667190*
3110001o07rik	*E030026i10rik*	*Vgll4*
Hdlbp	*Loc671878*	*Mfap3*
Zmiz2	*Magoh*	*Rbmx*
C79267	*Tpm1*	*Hist1h2af*
Ncapd2	*Pcyt2*	*Dhcr7*
Nsbp1	*Bat1a*	*Ppm1g*
4833426j09rik	*Rnasen*	*Rapgef1*
1110001n06rik	*3930401e15rik*	*Magoh*
Prpf4	*Senp3*	*Prmt6*
Tsc22d4	*Zmynd11*	*2410014a08rik*
9430088n01rik	*Hdac3*	*Bc085271*
Cad	*Dek*	*Pias1*
Dpp9	*Pdia3*	*Wipi2*
Luc7l2	*Smarcc1*	*Hdgf*
Mbtps1	*2610036l11rik*	*Ilf3*
Npepl1	*Loc100046343*	*Pbx2*
Hsp90ab1	*Odc1*	*Tmed10*
Rhbdd3	*Loc381889*	*Fus*
Nasp	*Txn1*	*4121402d02rik*
Chek2	*Ttll4*	*Mcm6*
Hirip3	*Wiz*	*Cdca4*

Whsc1
Afg3l1
Hist1h2ao
Nup205
Ube2e3
Hnrpa0
Supt16h
Atxn1l
Kif22
Itpripl2
2310040a07rik
Bcas2
Bat1a
2310021p13rik
Cugbp2
Emp1
Top2a
Hist1h2an
Wdr76
Pfas
Cdc25a
Ubtf
Igsf3
Riok1
Zfp162
Loc100046136
Mta1
Wipi2
Mylc2b
Kif23
Smyd2
Dennd2a
Khdrbs1
Smarce1
Dlg3
Dusp19
Smek2
Dus4l
Loc380927
Thoc4
2410008k03rik
Loc100043126
Cnot3
Sfrs11
Nfib
Llph
Tmem110
Fance
Cbx3
Mbnl1
Ruvbl1
Hn1l
1190002h23rik
Bat2
Rnf4
Nup210
Camk1
Loc545866
Rbm5
Bc031781
Txndc11
U2af2
Hist1h2ad
Rbm38
Nup107
Loc100046081
Wbp5
Sorbs1
Snrpd3
4933424b01rik
Ncl
Mtdna_Nd4l
Snrpf
Clspn
Myst2
Thra
Nasp
Ai481316
Sf1
Nola3
Tcof1
Inppl1
Kif15
Mapk1
Sf1
Rhoc
Psmd11
Rnpep
Cdkn1b
Wiz
Dazap1
2810485i05rik
1110011c06rik
Raly
1110001n06rik
Nsdhl
Hnrnpf
Cul4a
Hmgn2
Ing4
Arpc5l
2310005n03rik

Pacs2	*Scn3b*	*Trim27*
1110003o08rik	*1110054h05rik*	*Bc025076*
Loc100046298	*Mmab*	*Loc100047012*
6720463m24rik	*9830001h06rik*	*Sgol2*
Med23	*Hsp105*	*Rpl31*
Calr	*Sf3b3*	*Dhcr24*
Usp1	*Ccnb1*	*Dhcr24*
Tmed7	*Lsm2*	*Megf8*
Mex3a	*Dut*	*Nadk*
Copg	*Nacc1*	*Tfdp1*
Unc119	*Chaf1a*	*Atic*
Loc100044557	*Rell1*	*Mcm10*
Nol5	*Mex3a*	*Nup85*
Whsc2	*D0h4s114*	*Ehbp1l1*
Dcps	*B9d1*	*Ears2*
Smc1a	*Fabp5*	*Rnf4*
Hcfc1	*Snrp70*	*Nup50*
Top1	*Eif4a3*	*Gdi1*
Nuak1	*Tmpo*	*Zfp553*
Purb	*6720469n11rik*	*Gnaq*
Sox11	*Cep57*	*Nmral1*
B130065g19rik	*Bc031781*	*Abi1*
Ensa	*Setd8*	*Ncaph2*
Nfib	*Fam129b*	*Uhrf1*
Cops6	*Loc100047834*	*Ubqln4*
Acadm	*Mysm1*	*Ddx1*
Lonp1	*4833420g11rik*	*Setd6*
Gstk1	*Mmp28*	*A730042j05rik*
Orai3	*Mlp*	*Polr2a*
Lig1	*Maea*	*Ncbp2*
Aph1a	*Kpnb1*	*Vezf1*
Irf2bp1	*Hnrpdl*	*D030056l22rik*
Trim27	*Ilf3*	*Prelp*
Hmgb2	*2610207i05rik*	*Timp1*

Gdi1	*Hnrpdl*	*Xpnpep3*
Smc6	*Timeless*	*Rap2a*
Tmem97	*Rbm12*	*Rbm8a*
Elavl1	*Ubap2l*	*Mafg*
Actb	*Gnl2*	*Pdzrn3*
Ide	*Tipin*	*Zswim6*
2210016l21rik	*Prkcbp1*	*Metap2*
Ppapdc1	*Pols*	*Exosc10*
Nup50	*C730029f17rik*	*Plaur*
Nob1	*Bc004012*	*Mcm7*
Olfr996	*Loc666036*	*Tmsb10*
Prmt5	*Catns*	*Ahcy*
Osgep	*Hdgf*	*Polr2f*
Prpf40b	*Dhcr24*	

Genes up-regulated by >1.2 fold on k.d with EZH2 oligos 1 and 4.

Mgll	*E130112e08rik*	*Sat2*
9930004g02rik	*Gjb2*	*Rhob*
Oca2	*Mvp*	*Capzb*
5730588l14rik	*Tmem53*	*Aa467197*
A530050n04rik	*Loc100038882*	*Atp6v0a1*
St3gal1	*Pla2g2e*	*Araf*
Tulp2	*Spp1*	*Siat7b*
Gsta4	*Fbxo36*	*Angpt2*
Ddx26	*Loc668631*	*Nus1*
Hist1h1c	*Ccl5*	*Loc100048346*
Loc380706	*Pi4k2b*	*Loc381770*
Copg	*Bst2*	*Rad50*
Cd72	*Rsph1*	*4931422a14rik*
Asb2	*Usp18*	*Bb128963*
Eg232599	*Scl0001849.1_2273*	*Cyp4f13*
Gpr158	*Ppargc1a*	*Slc36a1*
Bace2	*Scamp5*	*Loc212390*

Mapk8ip1
2700046g09rik
Gsta2
Terf2ip
L3mbtl2
Slc2a6
Stt3b
Cmpk
Creb3
Loc100047261
Rnf5
Sspn
Ptpre
Axin2
Tgfbr2
5031436o03rik
2300002d11rik
Mtap2
Arfgef2
Mocos
Spsb2
Slc11a1
Tnip1
Txndc13
Pold4
D19wsu162e
Pigt
Iigp2
Igtp
E430003j01rik
Prnp
Rab7l1
Fkbp14
Myo5a
Rcsd1
Hisppd2a
Gsta1
2810032e02rik
Wdr68
Vwf
Gyg
Lrrc51
Ctsz
Tmem42
Emp3
Ahnak
Slc4a8
Bc029214
Snx27
Cttnbp2
Dpm2
Cetn4
H2-Q5
Rn18s
Rgl1
Tcn2
Gm1446
Def6
Ccdc92
Vamp5
Gm26
Nagk
Dusp11
Optn
Akr1b8
Nudt7
Msi2
Alg3
Dph4
Ramp2
Camk2n2
Irgm1
Cd63
Adh7
Fbxo2
Myo1e
Aip
Gstm2
Myl4
Dusp16
Egfl7
St6gal1
Car13
Wisp1
Klf7
Ephx1
Il11ra1
B230209c24rik
Tuft1
Cdc42
Dhrsx
2510002j07rik
Hyi
Cryl1
Ufc1
Myd88
Cpne4
Mapt
Pomt2
Snta1
Zfp579
Isoc2a

4732458o05rik
Tpi1
1810058m03rik
Zfp238
Stau2
2410003p15rik
1110070o15rik
Abcc5
Ppap2a
Dkk3
Cryab
Lgals9
Ctsh
Mettl11a
Gtrgeo22
Scotin
Scrg1
Hmg20a
Rbm15
Etv1
1700088e04rik
Loc634731
Sepn1
Rab1
Lrp10
Efcab1
Cox5b
Loc100048622
1700009p17rik
Eg433865
Mcoln1
Adamtsl5
Pole3
S100a1
1110008p14rik
Cc2d1a
Mpv17l
Peci
Serpinf1
H2-T23
Kif1c
Irf9
Psmb10
Slc22a18
Rusc2
Pdpk1
Pigo
Mylk
Hist1h2bc
Ascc2
Loc100043555
Padi2
Ndufaf1
Nox4
Sepw1
Haghl
Slc35b2
Hist1h2bm
Col4a2
Wbp2
Gbl
Evi5l
Loc100044298
Loc331595
Lonp2
Sel1l
Aven
Sdf2
Mrpl12
Bfsp2
Adssl1
Tubb2c
Kdelr3
Hist1h2bn
Gpr89
Zfp672
Large
Gcs1
Gramd1b
Gcap14
Loc100044159
Tnfrsf19
Tmem120a
Slc19a2
Sgcb
Gpr108
Pdcd5
Atp5sl
Dbp
Ttc3
Samd9l
B930007l02rik
Nfic
Slc25a38
Elovl1
Wfdc12
Smpd1
Kctd1
Commd9
Loc100044103
1190007f08rik
Dnajc15

Smpdl3b
Zfp691
1110012o05rik
Mrap
Otud3
Cml4
Hist2h2aa1
2010001h16rik
Loc100045780
Bpnt1
Os9
Med16
Nat6
Pex11a
Creg1
Agpat2
Glrb
Rbks
Atp13a2
Loc212556
Grina
Pgp
Galnt10
Por
Acot1
Cdkn1a
9330186a19rik
Entpd5
Scarb2
Ubl7
Esrra
Slc4a2
Nr1h4
Cutc
Tyki
5730472n09rik
Exosc5
Tmem192
Lrrc8a
Abcd3
Mkln1
A730086l23rik
Aw212394
Sh3bgrl
Ptprd
Sft2d2
Cpt2
Dtna
Coq9
Tmem120b
1200003c05rik
Tmem9b
Kctd17
C030027h14rik
Stat3
Pbx4
Lman2l
Aig1
Mgst1
2310047d13rik
Eg623230
4921507p07rik
Prpsap1
Golga2
Fam108a
Tk2
Rhod
5930434b04rik
Wapal
Sord
Au040320
Trpv2
Dapk3
1600002k03rik
Tbrg4
Med11
Btbd6
Bc022224
Oxsr1
Lamc1
Gnptg
Chpf
Bace1
Mboat2
Gstt3
D16h22s680e
Tle2
Scd2
Klhl22
Osbpl2
Hist1h2be
1810014f10rik
Gpr155
Hist1h2bf
Loc100040525
Tmem115
Fut8
Gng12
Tec
Mfge8
Commd1
Rap1gap

Apol9b	*Smurf1*	*6720456h20rik*
Serhl	*Nod1*	*Nkiras2*
Fabp3	*Arl6ip5*	*1700021f05rik*
Commd6	*Rnf213*	*Gp38*
Mras	*Acp1*	*9330175b01rik*
Tbc1d15	*Phospho2*	*Muted*
C78339	*Ly6g5c*	*Cox19*
Slco3a1	*1500003o03rik*	*Thap7*
Ap4b1	*Tex264*	*5730469m10rik*
Tacc1	*Rcor1*	*Stat1*
Atp6v1b2	*Acadvl*	*Eg433224*
Slc44a3	*Loc100045864*	*C030002b11rik*
Stim2	*Eif4e2*	*Pik3ip1*
Lmf1	*Asb1*	*Tcfap2a*
Vti1a	*3830402i07rik*	*Tmed1*
Rhobtb2	*Dgcr6*	*Armc8*
Spg20	*Arf2*	*D4ertd22e*
D16bwg1494e	*Slc39a13*	*Oas1g*
Maged2	*Mtap6*	*Cript*
Glrx1	*Hist1h2bk*	*Chchd10*
Polr1b	*Pvr*	*C530044n13rik*
Stx8	*Crat*	*Tmem126b*
Ak3	*Hmg20b*	*Ndor1*
Au022252	*Klf6*	

Genes down-regulated by <-1.2 fold on k.d with Jarid2 oligos 1 and 4

Mgll	*Aebp1*	*Azgp1*
5730588l14rik	*Fez1*	*Scrg1*
Tulp2	*Rn18s*	*Mylk*
Gsta4	*Gm1446*	*Gbx2*
6430548m08rik	*Vamp5*	*Wfdc12*
Hgsnat	*Hpse*	*1110012o05rik*
Sspn	*Rsad2*	*D10bwg1379e*

Syt9	*Specc1*	*2900037o03rik*
1110059g02rik	*Psg23*	*S100b*
Gcat	*B230343a10rik*	*Slc35b1*
Xbp1	*Bcat1*	*Gas7*
Tbcd	*Ids*	*Edem2*
Timp3	*Cck*	*Galnt2*
V1rd21	*A830080h07rik*	*Acot7*
Entpd4	*Gjb2*	*Brp17*
Gstp2	*Golm1*	*1700021k14rik*
Loc638935	*Ldha*	*Loc100046996*
Grhpr	*Mic2l1*	*1810063b05rik*
1700003f12rik	*3830612m24*	*Klhl30*
Ptdss2	*Tex2*	*Tbc1d7*
Erlin2	*Bc019806*	*2700038c09rik*
Dkk3	*Ppib*	*Fbxo10*
Gpr125	*Tyr*	*Gins1*
Arpc1a	*Car9*	*Nubp1*
Cort	*5031439g07rik*	*A630053n20rik*
4930455g09rik	*Mgst3*	*Zdhhc15*
Elovl4	*Neo1*	*A630054l15rik*
4930402h24rik	*3110001p07rik*	*Aldh1a3*
St3gal3	*Wdfy1*	*Emb*
D14ertd449e	*Fam134b*	*Xpr1*
Aph1a	*Casp6*	*Abi2*
Slc2a1	*Myo5a*	*Glrx5*
4930583h14rik	*Gipc1*	*Unc84a*
Ano10	*Pdxdc1*	*Tmem50b*
Tmem180	*6720458d17rik*	*Cmtm5*
Pkib	*P4hb*	*Pfkm*
Armcx2	*Scn1a*	*Fam125a*
Metrn	*C630013b14rik*	*Papss1*
Cyp3a13	*Loc100047619*	*Odf3l1*
1810013d10rik	*Tubg1*	*Surf4*
Tpcn1	*Commd8*	*4930524j08rik*

1110001c20rik
Gcdh
Idh2
Scl0002507.1_236
Rab18
Gmds
Dag1
Tmc6
Txndc5
Wnk4
Pja2
Ptprm
Pak4
Ddx19b
Itpk1
Plp1
Cenpb
Phactr1
E2f5
Dynlt3
C1qtnf5
Fam134a
Abca3
Mycbp
Cldnd1
Ai595366
Reck
Mmd
Loc245892
Tmem56
Vps24
5630401d24rik
Fnta
Scd1
Dgkz
Slc31a1
Npc1
1500032d16rik
Herpud1
Extl1
Sybl1
Mbp
Hspg2
Srd5a3
Pdss2
Cyp7b1
Imp4
Rhox5
Dnajc16
Lman1
Epb4.1l4b
Loc381140
Tmem150
Bc023829
Hspb8
Il10rb
Zw10
Loc100045522
Ppme1
Ccdc56
Bc018371
Ssr1
1700052o22rik
Loc100044475
Cstf2
Ppard
Araf
Fkbp4
Zdhhc21
Rnu6
Tex261
Cdc40
Igf2bp3
Hs2st1
Si
Aw549877
5430417l22rik
Loc100048083
1500009l16rik
Gng7
Sort1
Rabgap1
Aldh3b1
Cotl1
Smtnl2
Arsb
Pacsin3
Kif3a
Prdm16
Mrpl3
Insig1
A630084d02rik
Mrps15
Insc
Wrb
Sec23ip
Loc100045280
1810008a18rik
Nxt2
Lbh
Agps
Cse1l

Lrp4
Mrpl37
5133400g04rik
Tnfaip1
Scamp5
Elovl6
Selk
Eg638695
Pi4ka
Bag3
Irak1
Tgfbr1
2310061j03rik
Acbd3
Tsen34
Tom1l2
Pfkl
C78339
Rab11fip4
Wipi1
Dlx6
Klhl21
1110012d08rik
Loc677317
Zdhhc12
Tspan14
Atp2a2
Rnf26
Stx12
Igsf11
Gprc5b
Slpi
4930564d15rik
Sidt2
Il1rl1l
Rnf10
2410042d21rik
Afg3l1
Tm7sf3
Rab34
Fin15
Bet1
Col9a1
Suclg2
Slc25a26
Ctsc
3110082i17rik
2310022m17rik
Hsp90b1
Loc385461
Cyb5
Gamt
Sfrs6
4833439l19rik
Ube2l3
Map3k11
Cdr2
Cmtm7
Pcna
Loc381386
Tyrp1
Loc234882
Tmc8
Hist1h3c
Dpysl2
Pdia6
Nipsnap1
Neto2
Pkd1
Wdr45l
Apba3
Hist1h2ah
Ahcy
Letmd1
Hsd17b11
Wsb2
Akt3
Lman2
Prelp
Tmem51
Mrpl51
Sec31a
Megf8
Dhcr24
Mod1
Celsr2
Gtf2h1
D0h4s114
Rell1
Hsp105
B230380d07rik
Loc675899
Gstk1
Ugcg
Idh1
Plod2
Loc100045882
Ptgds
Copg
2610035d17rik
Tmed7
Mast2

Pacs2	*Arl2bp*	*Cyp51*
Psmd11	*Nsdhl*	*Loc280487*
Napa	*Josd2*	*5830434p21rik*
Fbln1	*Tpm4*	*Hist1h3e*
1810043g02rik	*Asah3l*	*Acat2*
Bc031781	*Wwp2*	*2900041a11rik*
Tmem86a	*Tmed10*	*Lmnb1*
1190002h23rik	*Hist1h3d*	*Ptpn6*
Mapk11	*6230416j20rik*	*Cd8b*
Mest	*4432405b04rik*	*Nt5dc2*
Reep3	*Dek*	*Pabpc4*
Odz4	*Snx13*	*Arl10c*
Traf4	*Peli1*	*Pfn2*
Pdia4	*Hist1h3f*	*Tpp1*
Hus1	*Gtf3c2*	*Fscn1*
Iars	*Gm2a*	
Hexim1	*Hdlbp*	

Genes up-regulated >1.2 fold on k.d with Jarid2 oligos 1 and 4.

Ccl25	*5031436o03rik*	*Marcks*
Mvp	*Ccnd1*	*Ass1*
Fbxo36	*Txndc13*	*Loc100046232*
Pi4k2b	*Nppb*	*Cdc42*
Tmod1	*2810032e02rik*	*Dhrsx*
Ppargc1a	*Ncald*	*Gja1*
Rhob	*Dpm2*	*Myd88*
Araf	*Rgl1*	*Dusp16*
Angpt2	*Def6*	*Abcc5*
Tnfrsf12a	*Ppm1k*	*Lgals9*
Hs3st1	*Dph4*	*1700009p17rik*
Creb3	*Cd63*	*Eg433865*
Loc100047261	*Adh7*	*Adamtsl5*
Rnf5	*Myo1e*	*Gadd45a*

2410016f01rik
Nrp1
Carhsp1
Zfp672
Pdpk1
Slc19a2
Gpr108
B930007l02rik
Nfic
Dscr1
Dusp8
Rhobtb2
Med16
Anapc7
Exosc5
Ddit4l
A730086l23rik
Eg623230
Rhod
Upp1
Klrg2
Serhl
Epha3
Scl0002785.1_49
2510012j08rik
Spg20
2810474o19rik
Ly6g5c
1500003o03rik
Hist1h2be
Loc100045864
Arf2
Slc39a13
Klf6
Hmgn3
Gbl
Loc280205
Loc385825
Use1
Dusp3
Slc25a29
Apobec1
4832420l08rik
Ppp1r10
1810032o08rik
Eif2ak2
2310005l22rik
Bc031353
Eg624124
Cyhr1
Adss
Fam13b
Glrx2
Urb2
Sipa1l1
C430004e15rik
Rhou
1500001e21rik
Ube2b
Mttp
Pmm2
Suclg1
Tbx2
Slc25a38
Loc100039346
Ttc13
Znrf1
Syf2
Triap1
Loc100047093
1110032e23rik
Eg630499
Zfp91-Cntf
Bckdha
2410006h16rik
Loc100047419
Psrc1
Mrpl49
R74862
Pdlim1
Tmem166
Ccnd3
Bloc1s2
1810020d17rik
C430002d13rik
2410003k15rik
1110057k04rik
Ssbp2
Iqgap3
Wbp7
Loc381212
Pdcd10
Pdrg1
Uvrag
Crem
Nagk
C230075m21rik
Cdkn1a
Atp5j
Bc010462
Bc032203
Snx12

Id3
Mdm2
Peo1
Tcf4
Mat2a
Cox18
Polr2h
H2-D1
Bid
Cox7a2l
Smn1
Trp53inp1
Mrpl54
Rabac1
Luzp1
Loc641366
1110018j23rik
Loc665181
Six1
Thap11
Tigd2
Fosl2
Gabarap
1500012f01rik
Tprkb
Xpc
Cdkn2c
Bc024537
Vapb
6030458c11rik
Eed
Bud13
0610038f07rik
Fam178a
Ddx21
Ifit2
Aldh4a1
Mrpl9
Arl16
2010015p12rik
Dynlrb1
Gmip
Rap2c
Amotl1
Irf3
Bc017612
Plk2
Cenpp
Dhx9
Dab2
Rapgef2
Ncapd2
Sesn2
6430706d22rik
Cdc20
Tarbp2
Bbc3
1700040i03rik
Loc100046393
Ccnd2
Rassf1
Loc100048445
Mllt4
Iah1
Vkorc1
Trio
2010321i05rik
E130309d02rik
Mtf2
Tg
N6amt1
Frmd6
Pax3
Rnaset2
Btbd3
Ndrl
Polk
Akap8
Foxc1
Pip5k1b
Lhfp
Aw548124
Zfp367
D4bwg0951e
E2f6
Adh5
Dus3l
Mrpl24
Phgdh
Loc100040243
Tgs1
Sox4
Rnu65
Gbp2
Htra2
2810026p18rik
Eef2
1810026b05rik
5830457o10rik
Loc100048436
Snora65
Gtse1

B230369l08rik	*Prkcq*	*Vgll3*
Nola1	*Pptc7*	*Ifi30*
Trp53	*9430029l20rik*	

Genes down-regulated <-1.2 fold both on k.d with Jarid2 oligos 1 and 4 and EZH2 oligos 1 and 4.

	Hsp105
Dhcr24	
Ptpn6	*Megf8*
Dhcr24	*Loc280487*
Prelp	*Tmed10*
5830434p21rik	*Psmd11*
Dhcr24	*Tpm4*
Nt5dc2	*Bc031781*
Fscn1	
Rell1	
Gstk1	
Nsdhl	
Acat2	
Bc031781	
1190002h23rik	
Hdlbp	
Lmnb1	
Tpp1	
Pabpc4	
D0h4s114	
Cd8b	
Pacs2	
Dek	
Tmed10	
Gtf3c2	
Tmed7	
Ahcy	
Copg	

Reference List

(1999). Cancer risks in BRCA2 mutation carriers. The Breast Cancer Linkage Consortium. Journal of the National Cancer Institute *91*, 1310-1316.

Adameyko, I., Lallemend, F., Aquino, J.B., Pereira, J.A., Topilko, P., Muller, T., Fritz, N., Beljajeva, A., Mochii, M., Liste, I.*, et al.* (2009). Schwann cell precursors from nerve innervation are a cellular origin of melanocytes in skin. Cell *139*, 366-379.

Adamson, P., Paterson, H.F., and Hall, A. (1992). Intracellular localization of the P21rho proteins. The Journal of cell biology *119*, 617-627.

Ahmed, S., Goh, W.I., and Bu, W. (2010). I-BAR domains, IRSp53 and filopodium formation. Seminars in cell & developmental biology *21*, 350-356.

Ahn, J., Sanz-Moreno, V., and Marshall, C.J. (2012). The metastasis gene NEDD9 product acts through integrin beta3 and Src to promote mesenchymal motility and inhibit amoeboid motility. Journal of cell science *125*, 1814-1826.

Alexaki, V.I., Javelaud, D., Van Kempen, L.C., Mohammad, K.S., Dennler, S., Luciani, F., Hoek, K.S., Juarez, P., Goydos, J.S., Fournier, P.J.*, et al.* (2010). GLI2-mediated melanoma invasion and metastasis. Journal of the National Cancer Institute *102*, 1148-1159.

Alexander, S., Koehl, G.E., Hirschberg, M., Geissler, E.K., and Friedl, P. (2008). Dynamic imaging of cancer growth and invasion: a modified skin-fold chamber model. Histochemistry and cell biology *130*, 1147-1154.

Allegra, C.J., Yothers, G., O'Connell, M.J., Sharif, S., Petrelli, N.J., Colangelo, L.H., Atkins, J.N., Seay, T.E., Fehrenbacher, L., Goldberg, R.M.*, et al.* (2011). Phase III trial assessing bevacizumab in stages II and III carcinoma of the colon: results of NSABP protocol C-08. Journal of clinical oncology : official journal of the American Society of Clinical Oncology *29*, 11-16.

Amano, M., Ito, M., Kimura, K., Fukata, Y., Chihara, K., Nakano, T., Matsuura, Y., and Kaibuchi, K. (1996). Phosphorylation and activation of myosin by Rho-associated kinase (Rho-kinase). The Journal of biological chemistry *271*, 20246-20249.

Andersson, E.R., Sandberg, R., and Lendahl, U. (2011). Notch signaling: simplicity in design, versatility in function. Development *138*, 3593-3612.

Annes, J.P., Munger, J.S., and Rifkin, D.B. (2003). Making sense of latent TGFbeta activation. Journal of cell science *116*, 217-224.

Arozarena, I., Sanchez-Laorden, B., Packer, L., Hidalgo-Carcedo, C., Hayward, R., Viros, A., Sahai, E., and Marais, R. (2011). Oncogenic BRAF induces melanoma cell invasion by downregulating the cGMP-specific phosphodiesterase PDE5A. Cancer cell *19*, 45-57.

Arpin, M., Chirivino, D., Naba, A., and Zwaenepoel, I. (2011). Emerging role for ERM proteins in cell adhesion and migration. Cell adhesion & migration *5*, 199-206.

Azam, F., Mehta, S., and Harris, A.L. (2010). Mechanisms of resistance to antiangiogenesis therapy. Eur J Cancer *46*, 1323-1332.

Balint, K., Xiao, M., Pinnix, C.C., Soma, A., Veres, I., Juhasz, I., Brown, E.J., Capobianco, A.J., Herlyn, M., and Liu, Z.J. (2005). Activation of Notch1 signaling is required for beta-catenin-mediated human primary melanoma progression. The Journal of clinical investigation *115*, 3166-3176.

Balkwill, F. (2002). Tumor necrosis factor or tumor promoting factor? Cytokine & growth factor reviews *13*, 135-141.

Baluk, P., Morikawa, S., Haskell, A., Mancuso, M., and McDonald, D.M. (2003). Abnormalities of basement membrane on blood vessels and endothelial sprouts in tumors. The American journal of pathology *163*, 1801-1815.

Bartholin, L., Wessner, L.L., Chirgwin, J.M., and Guise, T.A. (2007). The human Cyr61 gene is a transcriptional target of transforming growth factor beta in cancer cells. Cancer letters *246*, 230-236.

Beaumont, K.A., Newton, R.A., Smit, D.J., Leonard, J.H., Stow, J.L., and Sturm, R.A. (2005). Altered cell surface expression of human MC1R variant receptor alleles associated with red hair and skin cancer risk. Human molecular genetics *14*, 2145-2154.

Beerling, E., Ritsma, L., Vrisekoop, N., Derksen, P.W., and van Rheenen, J. (2011). Intravital microscopy: new insights into metastasis of tumors. Journal of cell science *124*, 299-310.

Beisel, C., and Paro, R. (2011). Silencing chromatin: comparing modes and mechanisms. Nature reviews Genetics *12*, 123-135.

Benedito, R., Rocha, S.F., Woeste, M., Zamykal, M., Radtke, F., Casanovas, O., Duarte, A., Pytowski, B., and Adams, R.H. (2012). Notch-dependent VEGFR3 upregulation allows angiogenesis without VEGF-VEGFR2 signalling. Nature *484*, 110-114.

Bennett, D.C., Holmes, A., Devlin, L., and Hart, I.R. (1994). Experimental metastasis and differentiation of murine melanoma cells: actions and interactions of factors affecting different intracellular signalling pathways. Clinical & experimental metastasis *12*, 385-397.

Bentley, N.J., Eisen, T., and Goding, C.R. (1994). Melanocyte-specific expression of the human tyrosinase promoter: activation by the microphthalmia gene product and role of the initiator. Molecular and cellular biology *14*, 7996-8006.

Berenjeno, I.M., Nunez, F., and Bustelo, X.R. (2007). Transcriptomal profiling of the cellular transformation induced by Rho subfamily GTPases. Oncogene *26*, 4295-4305.

Bergers, G., Brekken, R., McMahon, G., Vu, T.H., Itoh, T., Tamaki, K., Tanzawa, K., Thorpe, P., Itohara, S., Werb, Z.*, et al.* (2000). Matrix metalloproteinase-9 triggers the angiogenic switch during carcinogenesis. Nature cell biology *2*, 737-744.

Bergers, G., and Hanahan, D. (2008). Modes of resistance to anti-angiogenic therapy. Nature reviews Cancer *8*, 592-603.

Bergers, G., Song, S., Meyer-Morse, N., Bergsland, E., and Hanahan, D. (2003). Benefits of targeting both pericytes and endothelial cells in the tumor vasculature with kinase inhibitors. The Journal of clinical investigation *111*, 1287-1295.

Berking, C., Takemoto, R., Schaider, H., Showe, L., Satyamoorthy, K., Robbins, P., and Herlyn, M. (2001). Transforming growth factor-beta1 increases survival of human melanoma through stroma remodeling. Cancer research *61*, 8306-8316.

Bernstein, B.E., Mikkelsen, T.S., Xie, X., Kamal, M., Huebert, D.J., Cuff, J., Fry, B., Meissner, A., Wernig, M., Plath, K.*, et al.* (2006). A bivalent chromatin structure marks key developmental genes in embryonic stem cells. Cell *125*, 315-326.

Bertolotto, C., Busca, R., Abbe, P., Bille, K., Aberdam, E., Ortonne, J.P., and Ballotti, R. (1998). Different cis-acting elements are involved in the regulation of TRP1 and TRP2 promoter activities by cyclic AMP: pivotal role of M boxes (GTCATGTGCT) and of microphthalmia. Molecular and cellular biology *18*, 694-702.

Berton, S., Belletti, B., Wolf, K., Canzonieri, V., Lovat, F., Vecchione, A., Colombatti, A., Friedl, P., and Baldassarre, G. (2009). The tumor suppressor functions of p27(kip1) include control of the mesenchymal/amoeboid transition. Molecular and cellular biology *29*, 5031-5045.
Besson, A., Gurian-West, M., Schmidt, A., Hall, A., and Roberts, J.M. (2004). p27Kip1 modulates cell migration through the regulation of RhoA activation. Genes & development *18*, 862-876.

Bins, A.D., van Rheenen, J., Jalink, K., Halstead, J.R., Divecha, N., Spencer, D.M., Haanen, J.B., and Schumacher, T.N. (2007). Intravital imaging of fluorescent markers and FRET probes by DNA tattooing. BMC biotechnology *7*, 2.

Blaser, H., Reichman-Fried, M., Castanon, I., Dumstrei, K., Marlow, F.L., Kawakami, K., Solnica-Krezel, L., Heisenberg, C.P., and Raz, E. (2006). Migration of zebrafish primordial germ cells: a role for myosin contraction and cytoplasmic flow. Developmental cell *11*, 613-627.

Blokzijl, A., Dahlqvist, C., Reissmann, E., Falk, A., Moliner, A., Lendahl, U., and Ibanez, C.F. (2003). Cross-talk between the Notch and TGF-beta signaling pathways mediated by interaction of the Notch intracellular domain with Smad3. The Journal of cell biology *163*, 723-728.

Borggrefe, T., and Oswald, F. (2009). The Notch signaling pathway: transcriptional regulation at Notch target genes. Cellular and molecular life sciences : CMLS *66*, 1631-1646.

Bos, P.D., Zhang, X.H., Nadal, C., Shu, W., Gomis, R.R., Nguyen, D.X., Minn, A.J., van de Vijver, M.J., Gerald, W.L., Foekens, J.A.*, et al.* (2009). Genes that mediate breast cancer metastasis to the brain. Nature *459*, 1005-1009.

Boyer, L.A., Plath, K., Zeitlinger, J., Brambrink, T., Medeiros, L.A., Lee, T.I., Levine, S.S., Wernig, M., Tajonar, A., Ray, M.K.*, et al.* (2006). Polycomb complexes repress developmental regulators in murine embryonic stem cells. Nature *441*, 349-353.

Brabletz, T., Jung, A., Reu, S., Porzner, M., Hlubek, F., Kunz-Schughart, L.A., Knuechel, R., and Kirchner, T. (2001). Variable beta-catenin expression in colorectal cancers indicates tumor progression driven by the tumor environment. Proceedings of the National Academy of Sciences of the United States of America *98*, 10356-10361.

Bracken, A.P., Pasini, D., Capra, M., Prosperini, E., Colli, E., and Helin, K. (2003). EZH2 is downstream of the pRB-E2F pathway, essential for proliferation and amplified in cancer. The EMBO journal *22*, 5323-5335.

Breiteneder-Geleff, S., Soleiman, A., Kowalski, H., Horvat, R., Amann, G., Kriehuber, E., Diem, K., Weninger, W., Tschachler, E., Alitalo, K.*, et al.* (1999). Angiosarcomas express mixed endothelial phenotypes of blood and lymphatic capillaries: podoplanin as a specific marker for lymphatic endothelium. The American journal of pathology *154*, 385-394.

Brou, C., Logeat, F., Gupta, N., Bessia, C., LeBail, O., Doedens, J.R., Cumano, A., Roux, P., Black, R.A., and Israel, A. (2000). A novel proteolytic cleavage involved in Notch signaling: the role of the disintegrin-metalloprotease TACE. Molecular cell *5*, 207-216.

Brown, J.L., Cao, Z.A., Pinzon-Ortiz, M., Kendrew, J., Reimer, C., Wen, S., Zhou, J.Q., Tabrizi, M., Emery, S., McDermott, B.*, et al.* (2010). A human monoclonal anti-ANG2 antibody leads to broad antitumor activity in combination with VEGF inhibitors and chemotherapy agents in preclinical models. Molecular cancer therapeutics *9*, 145-156.

Brown, M.J., Hallam, J.A., Colucci-Guyon, E., and Shaw, S. (2001). Rigidity of circulating lymphocytes is primarily conferred by vimentin intermediate filaments. J Immunol *166*, 6640-6646.

Buccione, R., Caldieri, G., and Ayala, I. (2009). Invadopodia: specialized tumor cell structures for the focal degradation of the extracellular matrix. Cancer metastasis reviews *28*, 137-149.

Bugyi, B., and Carlier, M.F. (2010). Control of actin filament treadmilling in cell motility. Annual review of biophysics *39*, 449-470.

Burstyn-Cohen, T., and Kalcheim, C. (2002). Association between the cell cycle and neural crest delamination through specific regulation of G1/S transition. Developmental cell *3*, 383-395.

Busca, R., Bertolotto, C., Abbe, P., Englaro, W., Ishizaki, T., Narumiya, S., Boquet, P., Ortonne, J.P., and Ballotti, R. (1998). Inhibition of Rho is required for cAMP-induced melanoma cell differentiation. Molecular biology of the cell *9*, 1367-1378.

Calbo, J., van Montfort, E., Proost, N., van Drunen, E., Beverloo, H.B., Meuwissen, R., and Berns, A. (2011). A functional role for tumor cell heterogeneity in a mouse model of small cell lung cancer. Cancer cell *19*, 244-256.

Calvo, F., Sanz-Moreno, V., Agudo-Ibanez, L., Wallberg, F., Sahai, E., Marshall, C.J., and Crespo, P. (2011). RasGRF suppresses Cdc42-mediated tumour cell movement, cytoskeletal dynamics and transformation. Nature cell biology *13*, 819-826.

Campellone, K.G., and Welch, M.D. (2010). A nucleator arms race: cellular control of actin assembly. Nature reviews Molecular cell biology *11*, 237-251.

Campisi, J., and d'Adda di Fagagna, F. (2007). Cellular senescence: when bad things happen to good cells. Nature reviews Molecular cell biology *8*, 729-740.

Canel, M., Serrels, A., Miller, D., Timpson, P., Serrels, B., Frame, M.C., and Brunton, V.G. (2010). Quantitative in vivo imaging of the effects of inhibiting integrin signaling via Src and FAK on cancer cell movement: effects on E-cadherin dynamics. Cancer research *70*, 9413-9422.

Cao, Q., Yu, J., Dhanasekaran, S.M., Kim, J.H., Mani, R.S., Tomlins, S.A., Mehra, R., Laxman, B., Cao, X., Kleer, C.G.*, et al.* (2008). Repression of E-cadherin by the polycomb group protein EZH2 in cancer. Oncogene *27*, 7274-7284.

Carmeliet, P., and Jain, R.K. (2011a). Molecular mechanisms and clinical applications of angiogenesis. Nature *473*, 298-307.
Carmeliet, P., and Jain, R.K. (2011b). Principles and mechanisms of vessel normalization for cancer and other angiogenic diseases. Nature reviews Drug discovery *10*, 417-427.

Carreira, S., Goodall, J., Denat, L., Rodriguez, M., Nuciforo, P., Hoek, K.S., Testori, A., Larue, L., and Goding, C.R. (2006). Mitf regulation of Dia1 controls melanoma proliferation and invasiveness. Genes & development *20*, 3426-3439.

Cartlidge, R.A., Thomas, G.R., Cagnol, S., Jong, K.A., Molton, S.A., Finch, A.J., and McMahon, M. (2008). Oncogenic BRAF(V600E) inhibits BIM expression to promote melanoma cell survival. Pigment cell & melanoma research *21*, 534-544.

Castro, D.S., Skowronska-Krawczyk, D., Armant, O., Donaldson, I.J., Parras, C., Hunt, C., Critchley, J.A., Nguyen, L., Gossler, A., Gottgens, B.*, et al.* (2006). Proneural bHLH and Brn proteins coregulate a neurogenic program through cooperative binding to a conserved DNA motif. Developmental cell *11*, 831-844.

Chai, J., Jones, M.K., and Tarnawski, A.S. (2004). Serum response factor is a critical requirement for VEGF signaling in endothelial cells and VEGF-induced angiogenesis. FASEB journal : official publication of the Federation of American Societies for Experimental Biology *18*, 1264-1266.

Chang, C.J., and Hung, M.C. (2012). The role of EZH2 in tumour progression. British journal of cancer *106*, 243-247.

Chang, C.J., Yang, J.Y., Xia, W., Chen, C.T., Xie, X., Chao, C.H., Woodward, W.A., Hsu, J.M., Hortobagyi, G.N., and Hung, M.C. (2011). EZH2 promotes expansion of breast tumor initiating cells through activation of RAF1-beta-catenin signaling. Cancer cell *19*, 86-100.

Chapman, P.B., Hauschild, A., Robert, C., Haanen, J.B., Ascierto, P., Larkin, J., Dummer, R., Garbe, C., Testori, A., Maio, M.*, et al.* (2011). Improved survival with vemurafenib in melanoma with BRAF V600E mutation. The New England journal of medicine *364*, 2507-2516.

Charras, G., and Paluch, E. (2008). Blebs lead the way: how to migrate without lamellipodia. Nature reviews Molecular cell biology *9*, 730-736.

Charras, G.T., Yarrow, J.C., Horton, M.A., Mahadevan, L., and Mitchison, T.J. (2005). Non-equilibration of hydrostatic pressure in blebbing cells. Nature *435*, 365-369.

Cheli, Y., Giuliano, S., Botton, T., Rocchi, S., Hofman, V., Hofman, P., Bahadoran, P., Bertolotto, C., and Ballotti, R. (2011). Mitf is the key molecular switch between mouse or human melanoma initiating cells and their differentiated progeny. Oncogene *30*, 2307-2318.

Cheli, Y., Giuliano, S., Fenouille, N., Allegra, M., Hofman, V., Hofman, P., Bahadoran, P., Lacour, J.P., Tartare-Deckert, S., Bertolotto, C.*, et al.* (2012). Hypoxia and MITF control metastatic behaviour in mouse and human melanoma cells. Oncogene *31*, 2461-2470.

Chen, K., Manga, P., and Orlow, S.J. (2002). Pink-eyed dilution protein controls the processing of tyrosinase. Molecular biology of the cell *13*, 1953-1964.

Chen, L., Ma, Y., Kim, E.Y., Yu, W., Schwartz, R.J., Qian, L., and Wang, J. (2012). Conditional ablation of Ezh2 in murine hearts reveals its essential roles in endocardial cushion formation, cardiomyocyte proliferation and survival. PloS one *7*, e31005.

Chen, Q., Zhang, X.H., and Massague, J. (2011). Macrophage binding to receptor VCAM-1 transmits survival signals in breast cancer cells that invade the lungs. Cancer cell *20*, 538-549.

Chesarone, M.A., and Goode, B.L. (2009). Actin nucleation and elongation factors: mechanisms and interplay. Current opinion in cell biology *21*, 28-37.

Chiaverini, C., Beuret, L., Flori, E., Busca, R., Abbe, P., Bille, K., Bahadoran, P., Ortonne, J.P., Bertolotto, C., and Ballotti, R. (2008). Microphthalmia-associated transcription factor regulates RAB27A gene expression and controls melanosome transport. The Journal of biological chemistry *283*, 12635-12642.

Chiu, J.J., and Chien, S. (2011). Effects of disturbed flow on vascular endothelium: pathophysiological basis and clinical perspectives. Physiological reviews *91*, 327-387.

Choi, C.K., Vicente-Manzanares, M., Zareno, J., Whitmore, L.A., Mogilner, A., and Horwitz, A.R. (2008). Actin and alpha-actinin orchestrate the assembly and maturation of nascent adhesions in a myosin II motor-independent manner. Nature cell biology *10*, 1039-1050.

Clark, E.A., Golub, T.R., Lander, E.S., and Hynes, R.O. (2000). Genomic analysis of metastasis reveals an essential role for RhoC. Nature *406*, 532-535.

Cloos, P.A., Christensen, J., Agger, K., and Helin, K. (2008). Erasing the methyl mark: histone demethylases at the center of cellular differentiation and disease. Genes & development *22*, 1115-1140.

Condeelis, J., and Segall, J.E. (2003). Intravital imaging of cell movement in tumours. Nature reviews Cancer *3*, 921-930.

Condeelis, J., and Weissleder, R. (2010). In vivo imaging in cancer. Cold Spring Harbor perspectives in biology *2*, a003848.

Cooke, V.G., LeBleu, V.S., Keskin, D., Khan, Z., O'Connell, J.T., Teng, Y., Duncan, M.B., Xie, L., Maeda, G., Vong, S.*, et al.* (2012). Pericyte depletion results in hypoxia-associated epithelial-to-mesenchymal transition and metastasis mediated by met signaling pathway. Cancer cell *21*, 66-81.

Cooper, C.D., and Raible, D.W. (2009). Mechanisms for reaching the differentiated state: Insights from neural crest-derived melanocytes. Seminars in cell & developmental biology *20*, 105-110.

Crawford, Y., Kasman, I., Yu, L., Zhong, C., Wu, X., Modrusan, Z., Kaminker, J., and Ferrara, N. (2009). PDGF-C mediates the angiogenic and tumorigenic properties of fibroblasts associated with tumors refractory to anti-VEGF treatment. Cancer cell *15*, 21-34.

Crepaldi, T., Gautreau, A., Comoglio, P.M., Louvard, D., and Arpin, M. (1997). Ezrin is an effector of hepatocyte growth factor-mediated migration and morphogenesis in epithelial cells. The Journal of cell biology *138*, 423-434.

Cukierman, E., Pankov, R., Stevens, D.R., and Yamada, K.M. (2001). Taking cell-matrix adhesions to the third dimension. Science *294*, 1708-1712.

Curtin, J.A., Fridlyand, J., Kageshita, T., Patel, H.N., Busam, K.J., Kutzner, H., Cho, K.H., Aiba, S., Brocker, E.B., LeBoit, P.E.*, et al.* (2005). Distinct sets of

genetic alterations in melanoma. The New England journal of medicine *353*, 2135-2147.

D'Souza, B., Miyamoto, A., and Weinmaster, G. (2008). The many facets of Notch ligands. Oncogene *27*, 5148-5167.

David, N.B., Sapede, D., Saint-Etienne, L., Thisse, C., Thisse, B., Dambly-Chaudiere, C., Rosa, F.M., and Ghysen, A. (2002). Molecular basis of cell migration in the fish lateral line: role of the chemokine receptor CXCR4 and of its ligand, SDF1. Proceedings of the National Academy of Sciences of the United States of America *99*, 16297-16302.

Davies, H., Bignell, G.R., Cox, C., Stephens, P., Edkins, S., Clegg, S., Teague, J., Woffendin, H., Garnett, M.J., Bottomley, W*., et al.* (2002). Mutations of the BRAF gene in human cancer. Nature *417*, 949-954.

De Calisto, J., Araya, C., Marchant, L., Riaz, C.F., and Mayor, R. (2005). Essential role of non-canonical Wnt signalling in neural crest migration. Development *132*, 2587-2597.

De, S., Cipriano, R., Jackson, M.W., and Stark, G.R. (2009). Overexpression of kinesins mediates docetaxel resistance in breast cancer cells. Cancer research *69*, 8035-8042.

Dekker, R.J., van Soest, S., Fontijn, R.D., Salamanca, S., de Groot, P.G., VanBavel, E., Pannekoek, H., and Horrevoets, A.J. (2002). Prolonged fluid shear stress induces a distinct set of endothelial cell genes, most specifically lung Kruppel-like factor (KLF2). Blood *100*, 1689-1698.

Dennler, S., Andre, J., Alexaki, I., Li, A., Magnaldo, T., ten Dijke, P., Wang, X.J., Verrecchia, F., and Mauviel, A. (2007). Induction of sonic hedgehog mediators by transforming growth factor-beta: Smad3-dependent activation of Gli2 and Gli1 expression in vitro and in vivo. Cancer research *67*, 6981-6986.

Dennler, S., Itoh, S., Vivien, D., ten Dijke, P., Huet, S., and Gauthier, J.M. (1998). Direct binding of Smad3 and Smad4 to critical TGF beta-inducible elements in the promoter of human plasminogen activator inhibitor-type 1 gene. The EMBO journal *17*, 3091-3100.

DerMardirossian, C., and Bokoch, G.M. (2005). GDIs: central regulatory molecules in Rho GTPase activation. Trends in cell biology *15*, 356-363.

Descot, A., Hoffmann, R., Shaposhnikov, D., Reschke, M., Ullrich, A., and Posern, G. (2009). Negative regulation of the EGFR-MAPK cascade by actin-MAL-mediated Mig6/Errfi-1 induction. Molecular cell *35*, 291-304.

Dhomen, N., Reis-Filho, J.S., da Rocha Dias, S., Hayward, R., Savage, K., Delmas, V., Larue, L., Pritchard, C., and Marais, R. (2009). Oncogenic Braf induces melanocyte senescence and melanoma in mice. Cancer cell *15*, 294-303.

Dirat, B., Bochet, L., Dabek, M., Daviaud, D., Dauvillier, S., Majed, B., Wang, Y.Y., Meulle, A., Salles, B., Le Gonidec, S.*, et al.* (2011). Cancer-associated adipocytes exhibit an activated phenotype and contribute to breast cancer invasion. Cancer research *71*, 2455-2465.
Diz-Munoz, A., Krieg, M., Bergert, M., Ibarlucea-Benitez, I., Muller, D.J., Paluch, E., and Heisenberg, C.P. (2010). Control of directed cell migration in vivo by membrane-to-cortex attachment. PLoS biology *8*, e1000544.

Doitsidou, M., Reichman-Fried, M., Stebler, J., Koprunner, M., Dorries, J., Meyer, D., Esguerra, C.V., Leung, T., and Raz, E. (2002). Guidance of primordial germ cell migration by the chemokine SDF-1. Cell *111*, 647-659.

Donnelly, M.P., Paschou, P., Grigorenko, E., Gurwitz, D., Barta, C., Lu, R.B., Zhukova, O.V., Kim, J.J., Siniscalco, M., New, M.*, et al.* (2012). A global view of the OCA2-HERC2 region and pigmentation. Human genetics *131*, 683-696.

Du, R., Lu, K.V., Petritsch, C., Liu, P., Ganss, R., Passegue, E., Song, H., Vandenberg, S., Johnson, R.S., Werb, Z.*, et al.* (2008). HIF1alpha induces the recruitment of bone marrow-derived vascular modulatory cells to regulate tumor angiogenesis and invasion. Cancer cell *13*, 206-220.

Duffy, D.L., Montgomery, G.W., Chen, W., Zhao, Z.Z., Le, L., James, M.R., Hayward, N.K., Martin, N.G., and Sturm, R.A. (2007). A three-single-nucleotide polymorphism haplotype in intron 1 of OCA2 explains most human eye-color variation. American journal of human genetics *80*, 241-252.

Ebos, J.M., Lee, C.R., Cruz-Munoz, W., Bjarnason, G.A., Christensen, J.G., and Kerbel, R.S. (2009). Accelerated metastasis after short-term treatment with a potent inhibitor of tumor angiogenesis. Cancer cell *15*, 232-239.

Egeblad, M., Ewald, A.J., Askautrud, H.A., Truitt, M.L., Welm, B.E., Bainbridge, E., Peeters, G., Krummel, M.F., and Werb, Z. (2008). Visualizing stromal cell dynamics in different tumor microenvironments by spinning disk confocal microscopy. Disease models & mechanisms *1*, 155-167; discussion 165.

Erler, J.T., Bennewith, K.L., Cox, T.R., Lang, G., Bird, D., Koong, A., Le, Q.T., and Giaccia, A.J. (2009). Hypoxia-induced lysyl oxidase is a critical mediator of bone marrow cell recruitment to form the premetastatic niche. Cancer cell *15*, 35-44.
Ernst, J., Kheradpour, P., Mikkelsen, T.S., Shoresh, N., Ward, L.D., Epstein, C.B., Zhang, X., Wang, L., Issner, R., Coyne, M.*, et al.* (2011). Mapping and analysis of chromatin state dynamics in nine human cell types. Nature *473*, 43-49.

Esser, S., Lampugnani, M.G., Corada, M., Dejana, E., and Risau, W. (1998). Vascular endothelial growth factor induces VE-cadherin tyrosine phosphorylation in endothelial cells. Journal of cell science *111 (Pt 13)*, 1853-1865.

Etienne-Manneville, S. (2004). Actin and microtubules in cell motility: which one is in control? Traffic *5*, 470-477.

Ewald, A.J., Brenot, A., Duong, M., Chan, B.S., and Werb, Z. (2008). Collective epithelial migration and cell rearrangements drive mammary branching morphogenesis. Developmental cell *14*, 570-581.

Eyler, C.E., and Rich, J.N. (2008). Survival of the fittest: cancer stem cells in therapeutic resistance and angiogenesis. Journal of clinical oncology : official journal of the American Society of Clinical Oncology *26*, 2839-2845.

Ezhkova, E., Pasolli, H.A., Parker, J.S., Stokes, N., Su, I.H., Hannon, G., Tarakhovsky, A., and Fuchs, E. (2009). Ezh2 orchestrates gene expression for the stepwise differentiation of tissue-specific stem cells. Cell *136*, 1122-1135.

Fan, T., Jiang, S., Chung, N., Alikhan, A., Ni, C., Lee, C.C., and Hornyak, T.J. (2011). EZH2-dependent suppression of a cellular senescence phenotype in melanoma cells by inhibition of p21/CDKN1A expression. Molecular cancer research : MCR *9*, 418-429.

Fantin, A., Vieira, J.M., Gestri, G., Denti, L., Schwarz, Q., Prykhozhij, S., Peri, F., Wilson, S.W., and Ruhrberg, C. (2010). Tissue macrophages act as cellular chaperones for vascular anastomosis downstream of VEGF-mediated endothelial tip cell induction. Blood *116*, 829-840.

Fedorenko, I.V., Paraiso, K.H., and Smalley, K.S. (2011). Acquired and intrinsic BRAF inhibitor resistance in BRAF V600E mutant melanoma. Biochemical pharmacology *82*, 201-209.

Fehon, R.G., McClatchey, A.I., and Bretscher, A. (2010). Organizing the cell cortex: the role of ERM proteins. Nature reviews Molecular cell biology *11*, 276-287.

Ferrara, N. (2010). Binding to the extracellular matrix and proteolytic processing: two key mechanisms regulating vascular endothelial growth factor action. Molecular biology of the cell *21*, 687-690.

Fidler, I.J. (1973). Selection of successive tumour lines for metastasis. Nature: New biology *242*, 148-149.

Fievet, B.T., Gautreau, A., Roy, C., Del Maestro, L., Mangeat, P., Louvard, D., and Arpin, M. (2004). Phosphoinositide binding and phosphorylation act sequentially in the activation mechanism of ezrin. The Journal of cell biology *164*, 653-659.

Fischer, C., Mazzone, M., Jonckx, B., and Carmeliet, P. (2008). FLT1 and its ligands VEGFB and PlGF: drug targets for anti-angiogenic therapy? Nature reviews Cancer *8*, 942-956.

Folkman, J. (1971). Tumor angiogenesis: therapeutic implications. The New England journal of medicine *285*, 1182-1186.

Franco, S.J., and Huttenlocher, A. (2005). Regulating cell migration: calpains make the cut. Journal of cell science *118*, 3829-3838.

Friedl, P. (2004). Prespecification and plasticity: shifting mechanisms of cell migration. Current opinion in cell biology *16*, 14-23.

Friedl, P., and Gilmour, D. (2009). Collective cell migration in morphogenesis, regeneration and cancer. Nature reviews Molecular cell biology *10*, 445-457.
Friedl, P., Locker, J., Sahai, E., and Segall, J.E. (2012). Classifying collective cancer cell invasion. Nature cell biology *14*, 777-783.

Friedl, P., and Wolf, K. (2009). Proteolytic interstitial cell migration: a five-step process. Cancer metastasis reviews *28*, 129-135.

Friedmann, D.R., and Kovall, R.A. (2010). Thermodynamic and structural insights into CSL-DNA complexes. Protein science : a publication of the Protein Society *19*, 34-46.

Fukumura, D., Xavier, R., Sugiura, T., Chen, Y., Park, E.C., Lu, N., Selig, M., Nielsen, G., Taksir, T., Jain, R.K.*, et al.* (1998). Tumor induction of VEGF promoter activity in stromal cells. Cell *94*, 715-725.

Fukunaga-Kalabis, M., Roesch, A., and Herlyn, M. (2011). From cancer stem cells to tumor maintenance in melanoma. The Journal of investigative dermatology *131*, 1600-1604.

Gadea, G., Sanz-Moreno, V., Self, A., Godi, A., and Marshall, C.J. (2008). DOCK10-mediated Cdc42 activation is necessary for amoeboid invasion of melanoma cells. Current biology : CB *18*, 1456-1465.

Gaengel, K., Genove, G., Armulik, A., and Betsholtz, C. (2009). Endothelial-mural cell signaling in vascular development and angiogenesis. Arteriosclerosis, thrombosis, and vascular biology *29*, 630-638.

Gaggioli, C., Hooper, S., Hidalgo-Carcedo, C., Grosse, R., Marshall, J.F., Harrington, K., and Sahai, E. (2007). Fibroblast-led collective invasion of carcinoma cells with differing roles for RhoGTPases in leading and following cells. Nature cell biology *9*, 1392-1400.

Ganguly, A., Yang, H., and Cabral, F. (2011). Overexpression of mitotic centromere-associated Kinesin stimulates microtubule detachment and confers resistance to paclitaxel. Molecular cancer therapeutics *10*, 929-937.
Gerhardt, H., Golding, M., Fruttiger, M., Ruhrberg, C., Lundkvist, A., Abramsson, A., Jeltsch, M., Mitchell, C., Alitalo, K., Shima, D.*, et al.* (2003). VEGF guides angiogenic sprouting utilizing endothelial tip cell filopodia. The Journal of cell biology *161*, 1163-1177.

Giampieri, S., Manning, C., Hooper, S., Jones, L., Hill, C.S., and Sahai, E. (2009). Localized and reversible TGFbeta signalling switches breast cancer cells from cohesive to single cell motility. Nature cell biology *11*, 1287-1296.

Gineitis, D., and Treisman, R. (2001). Differential usage of signal transduction pathways defines two types of serum response factor target gene. The Journal of biological chemistry *276*, 24531-24539.

Gligorijevic, B., Kedrin, D., Segall, J.E., Condeelis, J., and van Rheenen, J. (2009). Dendra2 photoswitching through the Mammary Imaging Window. Journal of visualized experiments : JoVE.

Gligorijevic, B., Wyckoff, J., Yamaguchi, H., Wang, Y., Roussos, E.T., and Condeelis, J. (2012). N-WASP-mediated invadopodium formation is involved in intravasation and lung metastasis of mammary tumors. Journal of cell science *125*, 724-734.

Goley, E.D., and Welch, M.D. (2006). The ARP2/3 complex: an actin nucleator comes of age. Nature reviews Molecular cell biology *7*, 713-726.

Goodall, J., Carreira, S., Denat, L., Kobi, D., Davidson, I., Nuciforo, P., Sturm, R.A., Larue, L., and Goding, C.R. (2008). Brn-2 represses microphthalmia-associated transcription factor expression and marks a distinct subpopulation of microphthalmia-associated transcription factor-negative melanoma cells. Cancer research *68*, 7788-7794.

Goodall, J., Wellbrock, C., Dexter, T.J., Roberts, K., Marais, R., and Goding, C.R. (2004). The Brn-2 transcription factor links activated BRAF to melanoma proliferation. Molecular and cellular biology *24*, 2923-2931.
Goode, B.L., and Eck, M.J. (2007). Mechanism and function of formins in the control of actin assembly. Annual review of biochemistry *76*, 593-627.

Goswami, S., Sahai, E., Wyckoff, J.B., Cammer, M., Cox, D., Pixley, F.J., Stanley, E.R., Segall, J.E., and Condeelis, J.S. (2005). Macrophages promote the invasion of breast carcinoma cells via a colony-stimulating factor-1/epidermal growth factor paracrine loop. Cancer research *65*, 5278-5283.

Goswami, S., Wang, W., Wyckoff, J.B., and Condeelis, J.S. (2004). Breast cancer cells isolated by chemotaxis from primary tumors show increased survival and resistance to chemotherapy. Cancer research *64*, 7664-7667.

Gray-Schopfer, V.C., da Rocha Dias, S., and Marais, R. (2005). The role of B-RAF in melanoma. Cancer metastasis reviews *24*, 165-183.

Greger, J.G., Eastman, S.D., Zhang, V., Bleam, M.R., Hughes, A.M., Smitheman, K.N., Dickerson, S.H., Laquerre, S.G., Liu, L., and Gilmer, T.M. (2012). Combinations of BRAF, MEK, and PI3K/mTOR inhibitors overcome acquired resistance to the BRAF inhibitor GSK2118436 dabrafenib, mediated by NRAS or MEK mutations. Molecular cancer therapeutics *11*, 909-920.

Guarani, V., Deflorian, G., Franco, C.A., Kruger, M., Phng, L.K., Bentley, K., Toussaint, L., Dequiedt, F., Mostoslavsky, R., Schmidt, M.H.*, et al.* (2011). Acetylation-dependent regulation of endothelial Notch signalling by the SIRT1 deacetylase. Nature *473*, 234-238.

Gupta, P.B., Kuperwasser, C., Brunet, J.P., Ramaswamy, S., Kuo, W.L., Gray, J.W., Naber, S.P., and Weinberg, R.A. (2005). The melanocyte differentiation program predisposes to metastasis after neoplastic transformation. Nature genetics *37*, 1047-1054.

Gupta, R.A., Shah, N., Wang, K.C., Kim, J., Horlings, H.M., Wong, D.J., Tsai, M.C., Hung, T., Argani, P., Rinn, J.L.*, et al.* (2010). Long non-coding RNA HOTAIR reprograms chromatin state to promote cancer metastasis. Nature *464*, 1071-1076.
Gupton, S.L., and Gertler, F.B. (2007). Filopodia: the fingers that do the walking. Science's STKE : signal transduction knowledge environment *2007*, re5.

Haas, P., and Gilmour, D. (2006). Chemokine signaling mediates self-organizing tissue migration in the zebrafish lateral line. Developmental cell *10*, 673-680.

Han, J., Kraft, P., Nan, H., Guo, Q., Chen, C., Qureshi, A., Hankinson, S.E., Hu, F.B., Duffy, D.L., Zhao, Z.Z.*, et al.* (2008). A genome-wide association study identifies novel alleles associated with hair color and skin pigmentation. PLoS genetics *4*, e1000074.

Hanahan, D., and Coussens, L.M. (2012). Accessories to the crime: functions of cells recruited to the tumor microenvironment. Cancer cell *21*, 309-322.

Hanahan, D., and Folkman, J. (1996). Patterns and emerging mechanisms of the angiogenic switch during tumorigenesis. Cell *86*, 353-364.

Hara, M., Yaar, M., Byers, H.R., Goukassian, D., Fine, R.E., Gonsalves, J., and Gilchrest, B.A. (2000). Kinesin participates in melanosomal movement along melanocyte dendrites. The Journal of investigative dermatology *114*, 438-443.

Harper, S.J., and Bates, D.O. (2008). VEGF-A splicing: the key to anti-angiogenic therapeutics? Nature reviews Cancer *8*, 880-887.

Harris, E.S., and Nelson, W.J. (2010). VE-cadherin: at the front, center, and sides of endothelial cell organization and function. Current opinion in cell biology *22*, 651-658.

Hashimoto, Y., Kim, D.J., and Adams, J.C. (2011). The roles of fascins in health and disease. The Journal of pathology *224*, 289-300.

He, A., Shen, X., Ma, Q., Cao, J., von Gise, A., Zhou, P., Wang, G., Marquez, V.E., Orkin, S.H., and Pu, W.T. (2012). PRC2 directly methylates GATA4 and represses its transcriptional activity. Genes & development *26*, 37-42.
Helmchen, F., and Denk, W. (2005). Deep tissue two-photon microscopy. Nature methods *2*, 932-940.

Hicks, C., Johnston, S.H., diSibio, G., Collazo, A., Vogt, T.F., and Weinmaster, G. (2000). Fringe differentially modulates Jagged1 and Delta1 signalling through Notch1 and Notch2. Nature cell biology *2*, 515-520.

Hidalgo-Carcedo, C., Hooper, S., Chaudhry, S.I., Williamson, P., Harrington, K., Leitinger, B., and Sahai, E. (2011). Collective cell migration requires suppression of actomyosin at cell-cell contacts mediated by DDR1 and the cell polarity regulators Par3 and Par6. Nature cell biology *13*, 49-58.

Hill, C.S. (2009). Nucleocytoplasmic shuttling of Smad proteins. Cell research *19*, 36-46.

Hill, C.S., Wynne, J., and Treisman, R. (1995). The Rho family GTPases RhoA, Rac1, and CDC42Hs regulate transcriptional activation by SRF. Cell *81*, 1159-1170.

Hirata, E., Yukinaga, H., Kamioka, Y., Arakawa, Y., Miyamoto, S., Okada, T., Sahai, E., and Matsuda, M. (2012). In vivo fluorescence resonance energy transfer imaging reveals differential activation of Rho-family GTPases in glioblastoma cell invasion. Journal of cell science *125*, 858-868.

Hodis, E., Watson, I.R., Kryukov, G.V., Arold, S.T., Imielinski, M., Theurillat, J.P., Nickerson, E., Auclair, D., Li, L., Place, C.*, et al.* (2012). A landscape of driver mutations in melanoma. Cell *150*, 251-263.

Hoek, K., Rimm, D.L., Williams, K.R., Zhao, H., Ariyan, S., Lin, A., Kluger, H.M., Berger, A.J., Cheng, E., Trombetta, E.S.*, et al.* (2004). Expression profiling reveals novel pathways in the transformation of melanocytes to melanomas. Cancer research *64*, 5270-5282.
Hoek, K.S., Eichhoff, O.M., Schlegel, N.C., Dobbeling, U., Kobert, N., Schaerer, L., Hemmi, S., and Dummer, R. (2008). In vivo switching of human melanoma cells between proliferative and invasive states. Cancer research *68*, 650-656.

Hoek, K.S., and Goding, C.R. (2010). Cancer stem cells versus phenotype-switching in melanoma. Pigment cell & melanoma research *23*, 746-759.

Hoek, K.S., Schlegel, N.C., Brafford, P., Sucker, A., Ugurel, S., Kumar, R., Weber, B.L., Nathanson, K.L., Phillips, D.J., Herlyn, M.*, et al.* (2006). Metastatic potential of melanomas defined by specific gene expression profiles with no BRAF signature. Pigment cell research / sponsored by the European Society for Pigment Cell Research and the International Pigment Cell Society *19*, 290-302.

Hornyak, T.J., Hayes, D.J., Chiu, L.Y., and Ziff, E.B. (2001). Transcription factors in melanocyte development: distinct roles for Pax-3 and Mitf. Mechanisms of development *101*, 47-59.

Hsieh, J.J., Henkel, T., Salmon, P., Robey, E., Peterson, M.G., and Hayward, S.D. (1996). Truncated mammalian Notch1 activates CBF1/RBPJk-repressed genes by a mechanism resembling that of Epstein-Barr virus EBNA2. Molecular and cellular biology *16*, 952-959.

Hu, S., Yu, L., Li, Z., Shen, Y., Wang, J., Cai, J., Xiao, L., and Wang, Z. (2010). Overexpression of EZH2 contributes to acquired cisplatin resistance in ovarian cancer cells in vitro and in vivo. Cancer biology & therapy *10*, 788-795.

Hu, Y.L., DeLay, M., Jahangiri, A., Molinaro, A.M., Rose, S.D., Carbonell, W.S., and Aghi, M.K. (2012). Hypoxia-induced autophagy promotes tumor cell survival and adaptation to antiangiogenic treatment in glioblastoma. Cancer research *72*, 1773-1783.

Hunt, G., Todd, C., Cresswell, J.E., and Thody, A.J. (1994). Alpha-melanocyte stimulating hormone and its analogue Nle4DPhe7 alpha-MSH affect morphology, tyrosinase activity and melanogenesis in cultured human melanocytes. Journal of cell science *107 (Pt 1)*, 205-211.

Hunter, A.W., Caplow, M., Coy, D.L., Hancock, W.O., Diez, S., Wordeman, L., and Howard, J. (2003). The kinesin-related protein MCAK is a microtubule depolymerase that forms an ATP-hydrolyzing complex at microtubule ends. Molecular cell *11*, 445-457.

Hunter, K.W. (2004). Ezrin, a key component in tumor metastasis. Trends in molecular medicine *10*, 201-204.

Hussussian, C.J., Struewing, J.P., Goldstein, A.M., Higgins, P.A., Ally, D.S., Sheahan, M.D., Clark, W.H., Jr., Tucker, M.A., and Dracopoli, N.C. (1994). Germline p16 mutations in familial melanoma. Nature genetics *8*, 15-21.

Huttenlocher, A., and Horwitz, A.R. (2011). Integrins in cell migration. Cold Spring Harbor perspectives in biology *3*, a005074.

Huveneers, S., and Danen, E.H. (2009). Adhesion signaling - crosstalk between integrins, Src and Rho. Journal of cell science *122*, 1059-1069.

Ignatius, M.S., Chen, E., Elpek, N.M., Fuller, A.Z., Tenente, I.M., Clagg, R., Liu, S., Blackburn, J.S., Linardic, C.M., Rosenberg, A.E.*, et al.* (2012). In vivo imaging of tumor-propagating cells, regional tumor heterogeneity, and dynamic cell movements in embryonal rhabdomyosarcoma. Cancer cell *21*, 680-693.
Ignatius, M.S., and Langenau, D.M. (2011). Fluorescent imaging of cancer in zebrafish. Methods in cell biology *105*, 437-459.

Im, J.H., Fu, W., Wang, H., Bhatia, S.K., Hammer, D.A., Kowalska, M.A., and Muschel, R.J. (2004). Coagulation facilitates tumor cell spreading in the pulmonary vasculature during early metastatic colony formation. Cancer research *64*, 8613-8619.
Inman, G.J., Nicolas, F.J., and Hill, C.S. (2002). Nucleocytoplasmic shuttling of Smads 2, 3, and 4 permits sensing of TGF-beta receptor activity. Molecular cell *10*, 283-294.

Ishikawa, K., Kamohara, Y., Tanaka, F., Haraguchi, N., Mimori, K., Inoue, H., and Mori, M. (2008). Mitotic centromere-associated kinesin is a novel marker for prognosis and lymph node metastasis in colorectal cancer. British journal of cancer *98*, 1824-1829.

Ito, M., Nakano, T., Erdodi, F., and Hartshorne, D.J. (2004). Myosin phosphatase: structure, regulation and function. Molecular and cellular biochemistry *259*, 197-209.

Jackson, D.G., Prevo, R., Clasper, S., and Banerji, S. (2001). LYVE-1, the lymphatic system and tumor lymphangiogenesis. Trends in immunology *22*, 317-321.

Jain, R.K. (2005). Normalization of tumor vasculature: an emerging concept in antiangiogenic therapy. Science *307*, 58-62.

Jakobsson, L., Franco, C.A., Bentley, K., Collins, R.T., Ponsioen, B., Aspalter, I.M., Rosewell, I., Busse, M., Thurston, G., Medvinsky, A.*, et al.* (2010). Endothelial cells dynamically compete for the tip cell position during angiogenic sprouting. Nature cell biology *12*, 943-953.

Janknecht, R., Wells, N.J., and Hunter, T. (1998). TGF-beta-stimulated cooperation of smad proteins with the coactivators CBP/p300. Genes & development *12*, 2114-2119.

Javelaud, D., Alexaki, V.I., and Mauviel, A. (2008). Transforming growth factor-beta in cutaneous melanoma. Pigment cell & melanoma research *21*, 123-132.

Javelaud, D., Delmas, V., Moller, M., Sextius, P., Andre, J., Menashi, S., Larue, L., and Mauviel, A. (2005). Stable overexpression of Smad7 in human melanoma cells inhibits their tumorigenicity in vitro and in vivo. Oncogene *24*, 7624-7629.

Kameyama, K., Vieira, W.D., Tsukamoto, K., Law, L.W., and Hearing, V.J. (1990). Differentiation and the tumorigenic and metastatic phenotype of murine melanoma cells. International journal of cancer Journal international du cancer *45*, 1151-1158.

Kang, Y., Siegel, P.M., Shu, W., Drobnjak, M., Kakonen, S.M., Cordon-Cardo, C., Guise, T.A., and Massague, J. (2003). A multigenic program mediating breast cancer metastasis to bone. Cancer cell *3*, 537-549.

Kanhere, A., Viiri, K., Araujo, C.C., Rasaiyaah, J., Bouwman, R.D., Whyte, W.A., Pereira, C.F., Brookes, E., Walker, K., Bell, G.W.*, et al.* (2010). Short RNAs are transcribed from repressed polycomb target genes and interact with polycomb repressive complex-2. Molecular cell *38*, 675-688.

Kaplan, R.N., Riba, R.D., Zacharoulis, S., Bramley, A.H., Vincent, L., Costa, C., MacDonald, D.D., Jin, D.K., Shido, K., Kerns, S.A.*, et al.* (2005). VEGFR1-positive haematopoietic bone marrow progenitors initiate the pre-metastatic niche. Nature *438*, 820-827.

Katerinaki, E., Evans, G.S., Lorigan, P.C., and MacNeil, S. (2003). TNF-alpha increases human melanoma cell invasion and migration in vitro: the role of proteolytic enzymes. British journal of cancer *89*, 1123-1129.

Kavsak, P., Rasmussen, R.K., Causing, C.G., Bonni, S., Zhu, H., Thomsen, G.H., and Wrana, J.L. (2000). Smad7 binds to Smurf2 to form an E3 ubiquitin ligase that targets the TGF beta receptor for degradation. Molecular cell *6*, 1365-1375.

Kedrin, D., Gligorijevic, B., Wyckoff, J., Verkhusha, V.V., Condeelis, J., Segall, J.E., and van Rheenen, J. (2008). Intravital imaging of metastatic behavior through a mammary imaging window. Nature methods *5*, 1019-1021.

Kharchenko, P.V., Alekseyenko, A.A., Schwartz, Y.B., Minoda, A., Riddle, N.C., Ernst, J., Sabo, P.J., Larschan, E., Gorchakov, A.A., Gu, T.*, et al.* (2011). Comprehensive analysis of the chromatin landscape in Drosophila melanogaster. Nature *471*, 480-485.

Khodarev, N.N., Roach, P., Pitroda, S.P., Golden, D.W., Bhayani, M., Shao, M.Y., Darga, T.E., Beveridge, M.G., Sood, R.F., Sutton, H.G.*, et al.* (2009). STAT1 pathway mediates amplification of metastatic potential and resistance to therapy. PloS one *4*, e5821.

Kikkawa, H., Kaihou, M., Horaguchi, N., Uchida, T., Imafuku, H., Takiguchi, A., Yamazaki, Y., Koike, C., Kuruto, R., Kakiuchi, T.*, et al.* (2002). Role of integrin alpha(v)beta3 in the early phase of liver metastasis: PET and IVM analyses. Clinical & experimental metastasis *19*, 717-725.

Kirschner, M., and Mitchison, T. (1986). Beyond self-assembly: from microtubules to morphogenesis. Cell *45*, 329-342.

Kissa, K., and Herbomel, P. (2010). Blood stem cells emerge from aortic endothelium by a novel type of cell transition. Nature *464*, 112-115.

Kitzing, T.M., Wang, Y., Pertz, O., Copeland, J.W., and Grosse, R. (2010). Formin-like 2 drives amoeboid invasive cell motility downstream of RhoC. Oncogene *29*, 2441-2448.

Kleer, C.G., Cao, Q., Varambally, S., Shen, R., Ota, I., Tomlins, S.A., Ghosh, D., Sewalt, R.G., Otte, A.P., Hayes, D.F.*, et al.* (2003). EZH2 is a marker of aggressive breast cancer and promotes neoplastic transformation of breast epithelial cells. Proceedings of the National Academy of Sciences of the United States of America *100*, 11606-11611.

Klemke, M., Weschenfelder, T., Konstandin, M.H., and Samstag, Y. (2007). High affinity interaction of integrin alpha4beta1 (VLA-4) and vascular cell adhesion molecule 1 (VCAM-1) enhances migration of human melanoma cells across activated endothelial cell layers. Journal of cellular physiology *212*, 368-374.

Kondo, T., and Hearing, V.J. (2011). Update on the regulation of mammalian melanocyte function and skin pigmentation. Expert review of dermatology *6*, 97-108.

Kornberg, R.D., and Lorch, Y. (1999). Twenty-five years of the nucleosome, fundamental particle of the eukaryote chromosome. Cell *98*, 285-294.

Krasagakis, K., Garbe, C., Schrier, P.I., and Orfanos, C.E. (1994). Paracrine and autocrine regulation of human melanocyte and melanoma cell growth by transforming growth factor beta in vitro. Anticancer research *14*, 2565-2571.

Krasagakis, K., Kruger-Krasagakes, S., Fimmel, S., Eberle, J., Tholke, D., von der Ohe, M., Mansmann, U., and Orfanos, C.E. (1999). Desensitization of melanoma cells to autocrine TGF-beta isoforms. Journal of cellular physiology *178*, 179-187.

Krejci, A., and Bray, S. (2007). Notch activation stimulates transient and selective binding of Su(H)/CSL to target enhancers. Genes & development *21*, 1322-1327.

Krishnan, K., Bruce, B., Hewitt, S., Thomas, D., Khanna, C., and Helman, L.J. (2006). Ezrin mediates growth and survival in Ewing's sarcoma through the AKT/mTOR, but not the MAPK, signaling pathway. Clinical & experimental metastasis *23*, 227-236.

Krylyshkina, O., Kaverina, I., Kranewitter, W., Steffen, W., Alonso, M.C., Cross, R.A., and Small, J.V. (2002). Modulation of substrate adhesion dynamics via microtubule targeting requires kinesin-1. The Journal of cell biology *156*, 349-359.

Kunda, P., Craig, G., Dominguez, V., and Baum, B. (2003). Abi, Sra1, and Kette control the stability and localization of SCAR/WAVE to regulate the formation of actin-based protrusions. Current biology : CB *13*, 1867-1875.

Kuphal, S., Palm, H.G., Poser, I., and Bosserhoff, A.K. (2005). Snail-regulated genes in malignant melanoma. Melanoma research *15*, 305-313.

Kuroda, T.S., and Fukuda, M. (2004). Rab27A-binding protein Slp2-a is required for peripheral melanosome distribution and elongated cell shape in melanocytes. Nature cell biology *6*, 1195-1203.

Lah, T.T., Duran Alonso, M.B., and Van Noorden, C.J. (2006). Antiprotease therapy in cancer: hot or not? Expert opinion on biological therapy *6*, 257-279.

Lamar, E., Deblandre, G., Wettstein, D., Gawantka, V., Pollet, N., Niehrs, C., and Kintner, C. (2001). Nrarp is a novel intracellular component of the Notch signaling pathway. Genes & development *15*, 1885-1899.

Lammermann, T., Bader, B.L., Monkley, S.J., Worbs, T., Wedlich-Soldner, R., Hirsch, K., Keller, M., Forster, R., Critchley, D.R., Fassler, R.*, et al.* (2008). Rapid leukocyte migration by integrin-independent flowing and squeezing. Nature *453*, 51-55.

Landeira, D., Sauer, S., Poot, R., Dvorkina, M., Mazzarella, L., Jorgensen, H.F., Pereira, C.F., Leleu, M., Piccolo, F.M., Spivakov, M.*, et al.* (2010). Jarid2 is a PRC2 component in embryonic stem cells required for multi-lineage differentiation and recruitment of PRC1 and RNA Polymerase II to developmental regulators. Nature cell biology *12*, 618-624.

Lang, D., Lu, M.M., Huang, L., Engleka, K.A., Zhang, M., Chu, E.Y., Lipner, S., Skoultchi, A., Millar, S.E., and Epstein, J.A. (2005). Pax3 functions at a nodal point in melanocyte stem cell differentiation. Nature *433*, 884-887.

Langridge, P.D., and Kay, R.R. (2006). Blebbing of Dictyostelium cells in response to chemoattractant. Experimental cell research *312*, 2009-2017.

Lawson, M.A., and Maxfield, F.R. (1995). Ca(2+)- and calcineurin-dependent recycling of an integrin to the front of migrating neutrophils. Nature *377*, 75-79.

Lee, S., Chen, T.T., Barber, C.L., Jordan, M.C., Murdock, J., Desai, S., Ferrara, N., Nagy, A., Roos, K.P., and Iruela-Arispe, M.L. (2007). Autocrine VEGF signaling is required for vascular homeostasis. Cell *130*, 691-703.

Lee, S., Jilani, S.M., Nikolova, G.V., Carpizo, D., and Iruela-Arispe, M.L. (2005). Processing of VEGF-A by matrix metalloproteinases regulates bioavailability and vascular patterning in tumors. The Journal of cell biology *169*, 681-691.

Lee, T.I., Jenner, R.G., Boyer, L.A., Guenther, M.G., Levine, S.S., Kumar, R.M., Chevalier, B., Johnstone, S.E., Cole, M.F., Isono, K.*, et al.* (2006). Control of developmental regulators by Polycomb in human embryonic stem cells. Cell *125*, 301-313.

Lehr, H.A., Leunig, M., Menger, M.D., Nolte, D., and Messmer, K. (1993). Dorsal skinfold chamber technique for intravital microscopy in nude mice. The American journal of pathology *143*, 1055-1062.

Leong, K.G., Niessen, K., Kulic, I., Raouf, A., Eaves, C., Pollet, I., and Karsan, A. (2007). Jagged1-mediated Notch activation induces epithelial-to-mesenchymal transition through Slug-induced repression of E-cadherin. The Journal of experimental medicine *204*, 2935-2948.

Levayer, R., and Lecuit, T. (2012). Biomechanical regulation of contractility: spatial control and dynamics. Trends in cell biology *22*, 61-81.

Levy, L., Howell, M., Das, D., Harkin, S., Episkopou, V., and Hill, C.S. (2007). Arkadia activates Smad3/Smad4-dependent transcription by triggering signal-induced SnoN degradation. Molecular and cellular biology *27*, 6068-6083.

Li, A., Dawson, J.C., Forero-Vargas, M., Spence, H.J., Yu, X., Konig, I., Anderson, K., and Machesky, L.M. (2010a). The actin-bundling protein fascin stabilizes actin in invadopodia and potentiates protrusive invasion. Current biology : CB *20*, 339-345.

Li, G., Margueron, R., Ku, M., Chambon, P., Bernstein, B.E., and Reinberg, D. (2010b). Jarid2 and PRC2, partners in regulating gene expression. Genes & development *24*, 368-380.

Li, X., Kumar, A., Zhang, F., Lee, C., and Tang, Z. (2012). Complicated life, complicated VEGF-B. Trends in molecular medicine *18*, 119-127.

Li, Y., Zhang, F., Nagai, N., Tang, Z., Zhang, S., Scotney, P., Lennartsson, J., Zhu, C., Qu, Y., Fang, C*., et al.* (2008). VEGF-B inhibits apoptosis via VEGFR-1-mediated suppression of the expression of BH3-only protein genes in mice and rats. The Journal of clinical investigation *118*, 913-923.

Li, Z., Cao, R., Wang, M., Myers, M.P., Zhang, Y., and Xu, R.M. (2006). Structure of a Bmi-1-Ring1B polycomb group ubiquitin ligase complex. The Journal of biological chemistry *281*, 20643-20649.

Liu, J., Yue, P., Artym, V.V., Mueller, S.C., and Guo, W. (2009). The role of the exocyst in matrix metalloproteinase secretion and actin dynamics during tumor cell invadopodia formation. Molecular biology of the cell *20*, 3763-3771.

Liu, Z.J., Xiao, M., Balint, K., Smalley, K.S., Brafford, P., Qiu, R., Pinnix, C.C., Li, X., and Herlyn, M. (2006). Notch1 signaling promotes primary melanoma progression by activating mitogen-activated protein kinase/phosphatidylinositol 3-kinase-Akt pathways and up-regulating N-cadherin expression. Cancer research *66*, 4182-4190.

Lizarraga, F., Poincloux, R., Romao, M., Montagnac, G., Le Dez, G., Bonne, I., Rigaill, G., Raposo, G., and Chavrier, P. (2009). Diaphanous-related formins are required for invadopodia formation and invasion of breast tumor cells. Cancer research *69*, 2792-2800.

Lockman, K., Hinson, J.S., Medlin, M.D., Morris, D., Taylor, J.M., and Mack, C.P. (2004). Sphingosine 1-phosphate stimulates smooth muscle cell differentiation and proliferation by activating separate serum response factor co-factors. The Journal of biological chemistry *279*, 42422-42430.

Lorentzen, A., Bamber, J., Sadok, A., Elson-Schwab, I., and Marshall, C.J. (2011). An ezrin-rich, rigid uropod-like structure directs movement of amoeboid blebbing cells. Journal of cell science *124*, 1256-1267.

Lucitti, J.L., Jones, E.A., Huang, C., Chen, J., Fraser, S.E., and Dickinson, M.E. (2007). Vascular remodeling of the mouse yolk sac requires hemodynamic force. Development *134*, 3317-3326.

Machacek, M., Hodgson, L., Welch, C., Elliott, H., Pertz, O., Nalbant, P., Abell, A., Johnson, G.L., Hahn, K.M., and Danuser, G. (2009). Coordination of Rho GTPase activities during cell protrusion. Nature *461*, 99-103.

Machesky, L.M., and Li, A. (2010). Fascin: Invasive filopodia promoting metastasis. Communicative & integrative biology *3*, 263-270.

Magdalena, J., Millard, T.H., and Machesky, L.M. (2003). Microtubule involvement in NIH 3T3 Golgi and MTOC polarity establishment. Journal of cell science *116*, 743-756.

Malanchi, I., Santamaria-Martinez, A., Susanto, E., Peng, H., Lehr, H.A., Delaloye, J.F., and Huelsken, J. (2012). Interactions between cancer stem cells and their niche govern metastatic colonization. Nature *481*, 85-89.

Maney, T., Wagenbach, M., and Wordeman, L. (2001). Molecular dissection of the microtubule depolymerizing activity of mitotic centromere-associated kinesin. The Journal of biological chemistry *276*, 34753-34758.

Mangeat, P., Roy, C., and Martin, M. (1999). ERM proteins in cell adhesion and membrane dynamics. Trends in cell biology *9*, 187-192.

Mani, S.A., Guo, W., Liao, M.J., Eaton, E.N., Ayyanan, A., Zhou, A.Y., Brooks, M., Reinhard, F., Zhang, C.C., Shipitsin, M.*, et al.* (2008). The epithelial-mesenchymal transition generates cells with properties of stem cells. Cell *133*, 704-715.

Margueron, R., Justin, N., Ohno, K., Sharpe, M.L., Son, J., Drury, W.J., 3rd, Voigt, P., Martin, S.R., Taylor, W.R., De Marco, V.*, et al.* (2009). Role of the polycomb protein EED in the propagation of repressive histone marks. Nature *461*, 762-767.

Margueron, R., and Reinberg, D. (2011). The Polycomb complex PRC2 and its mark in life. Nature *469*, 343-349.

Marusyk, A., Almendro, V., and Polyak, K. (2012). Intra-tumour heterogeneity: a looking glass for cancer? Nature reviews Cancer *12*, 323-334.

Marusyk, A., and Polyak, K. (2010). Tumor heterogeneity: causes and consequences. Biochimica et biophysica acta *1805*, 105-117.

Masszi, A., Speight, P., Charbonney, E., Lodyga, M., Nakano, H., Szaszi, K., and Kapus, A. (2010). Fate-determining mechanisms in epithelial-myofibroblast transition: major inhibitory role for Smad3. The Journal of cell biology *188*, 383-399.

Matsui, T., Maeda, M., Doi, Y., Yonemura, S., Amano, M., Kaibuchi, K., and Tsukita, S. (1998). Rho-kinase phosphorylates COOH-terminal threonines of ezrin/radixin/moesin (ERM) proteins and regulates their head-to-tail association. The Journal of cell biology *140*, 647-657.

McDonald, D.M., and Baluk, P. (2002). Significance of blood vessel leakiness in cancer. Cancer research *62*, 5381-5385.

McGill, M.A., and McGlade, C.J. (2003). Mammalian numb proteins promote Notch1 receptor ubiquitination and degradation of the Notch1 intracellular domain. The Journal of biological chemistry *278*, 23196-23203.

McHugh, J.B., Fullen, D.R., Ma, L., Kleer, C.G., and Su, L.D. (2007). Expression of polycomb group protein EZH2 in nevi and melanoma. Journal of cutaneous pathology *34*, 597-600.

Medjkane, S., Perez-Sanchez, C., Gaggioli, C., Sahai, E., and Treisman, R. (2009). Myocardin-related transcription factors and SRF are required for cytoskeletal dynamics and experimental metastasis. Nature cell biology *11*, 257-268.

Melnikova, V.O., Bolshakov, S.V., Walker, C., and Ananthaswamy, H.N. (2004). Genomic alterations in spontaneous and carcinogen-induced murine melanoma cell lines. Oncogene *23*, 2347-2356.

Merlot, S., and Firtel, R.A. (2003). Leading the way: Directional sensing through phosphatidylinositol 3-kinase and other signaling pathways. Journal of cell science *116*, 3471-3478.

Michaloglou, C., Vredeveld, L.C., Soengas, M.S., Denoyelle, C., Kuilman, T., van der Horst, C.M., Majoor, D.M., Shay, J.W., Mooi, W.J., and Peeper, D.S. (2005). BRAFE600-associated senescence-like cell cycle arrest of human naevi. Nature *436*, 720-724.

Mikkelsen, T.S., Ku, M., Jaffe, D.B., Issac, B., Lieberman, E., Giannoukos, G., Alvarez, P., Brockman, W., Kim, T.K., Koche, R.P.*, et al.* (2007). Genome-wide maps of chromatin state in pluripotent and lineage-committed cells. Nature *448*, 553-560.

Millard, T.H., and Martin, P. (2008). Dynamic analysis of filopodial interactions during the zippering phase of Drosophila dorsal closure. Development *135*, 621-626.

Miller, A.J., and Mihm, M.C., Jr. (2006). Melanoma. The New England journal of medicine *355*, 51-65.

Min, J., Zaslavsky, A., Fedele, G., McLaughlin, S.K., Reczek, E.E., De Raedt, T., Guney, I., Strochlic, D.E., Macconaill, L.E., Beroukhim, R.*, et al.* (2010). An oncogene-tumor suppressor cascade drives metastatic prostate cancer by coordinately activating Ras and nuclear factor-kappaB. Nature medicine *16*, 286-294.

Minn, A.J., Gupta, G.P., Siegel, P.M., Bos, P.D., Shu, W., Giri, D.D., Viale, A., Olshen, A.B., Gerald, W.L., and Massague, J. (2005). Genes that mediate breast cancer metastasis to lung. Nature *436*, 518-524.

Miralles, F., Posern, G., Zaromytidou, A.I., and Treisman, R. (2003). Actin dynamics control SRF activity by regulation of its coactivator MAL. Cell *113*, 329-342.

Mitra, S.K., Hanson, D.A., and Schlaepfer, D.D. (2005). Focal adhesion kinase: in command and control of cell motility. Nature reviews Molecular cell biology *6*, 56-68.

Mohun, T., Garrett, N., and Treisman, R. (1987). Xenopus cytoskeletal actin and human c-fos gene promoters share a conserved protein-binding site. The EMBO journal *6*, 667-673.

Mootha, V.K., Lindgren, C.M., Eriksson, K.F., Subramanian, A., Sihag, S., Lehar, J., Puigserver, P., Carlsson, E., Ridderstrale, M., Laurila, E.*, et al.* (2003). PGC-

1alpha-responsive genes involved in oxidative phosphorylation are coordinately downregulated in human diabetes. Nature genetics *34*, 267-273.

Morey, L., and Helin, K. (2010). Polycomb group protein-mediated repression of transcription. Trends in biochemical sciences *35*, 323-332.

Morita, T., Mayanagi, T., and Sobue, K. (2007). Dual roles of myocardin-related transcription factors in epithelial mesenchymal transition via slug induction and actin remodeling. The Journal of cell biology *179*, 1027-1042.

Moriyama, M., Osawa, M., Mak, S.S., Ohtsuka, T., Yamamoto, N., Han, H., Delmas, V., Kageyama, R., Beermann, F., Larue, L.*, et al.* (2006). Notch signaling via Hes1 transcription factor maintains survival of melanoblasts and melanocyte stem cells. The Journal of cell biology *173*, 333-339.

Mouilleron, S., Langer, C.A., Guettler, S., McDonald, N.Q., and Treisman, R. (2011). Structure of a pentavalent G-actin*MRTF-A complex reveals how G-actin controls nucleocytoplasmic shuttling of a transcriptional coactivator. Science signaling *4*, ra40.

Mu, Y., Gudey, S.K., and Landstrom, M. (2012). Non-Smad signaling pathways. Cell and tissue research *347*, 11-20.

Muller, A., Homey, B., Soto, H., Ge, N., Catron, D., Buchanan, M.E., McClanahan, T., Murphy, E., Yuan, W., Wagner, S.N.*, et al.* (2001). Involvement of chemokine receptors in breast cancer metastasis. Nature *410*, 50-56.

Murdoch, C., Muthana, M., Coffelt, S.B., and Lewis, C.E. (2008). The role of myeloid cells in the promotion of tumour angiogenesis. Nature reviews Cancer *8*, 618-631.

Nagy, J.A., Chang, S.H., Shih, S.C., Dvorak, A.M., and Dvorak, H.F. (2010). Heterogeneity of the tumor vasculature. Seminars in thrombosis and hemostasis *36*, 321-331.

Nagy, J.A., and Dvorak, H.F. (2012). Heterogeneity of the tumor vasculature: the need for new tumor blood vessel type-specific targets. Clinical & experimental metastasis.

Nakamura, Y., Tanaka, F., Haraguchi, N., Mimori, K., Matsumoto, T., Inoue, H., Yanaga, K., and Mori, M. (2007). Clinicopathological and biological significance of mitotic centromere-associated kinesin overexpression in human gastric cancer. British journal of cancer *97*, 543-549.

Nakasone, E.S., Askautrud, H.A., Kees, T., Park, J.H., Plaks, V., Ewald, A.J., Fein, M., Rasch, M.G., Tan, Y.X., Qiu, J.*, et al.* (2012). Imaging tumor-stroma interactions during chemotherapy reveals contributions of the microenvironment to resistance. Cancer cell *21*, 488-503.

Naumov, G.N., MacDonald, I.C., Weinmeister, P.M., Kerkvliet, N., Nadkarni, K.V., Wilson, S.M., Morris, V.L., Groom, A.C., and Chambers, A.F. (2002). Persistence

of solitary mammary carcinoma cells in a secondary site: a possible contributor to dormancy. Cancer research *62*, 2162-2168.

Nazarian, R., Shi, H., Wang, Q., Kong, X., Koya, R.C., Lee, H., Chen, Z., Lee, M.K., Attar, N., Sazegar, H.*, et al.* (2010). Melanomas acquire resistance to B-RAF(V600E) inhibition by RTK or N-RAS upregulation. Nature *468*, 973-977.

Ng, T., Parsons, M., Hughes, W.E., Monypenny, J., Zicha, D., Gautreau, A., Arpin, M., Gschmeissner, S., Verveer, P.J., Bastiaens, P.I.*, et al.* (2001). Ezrin is a downstream effector of trafficking PKC-integrin complexes involved in the control of cell motility. The EMBO journal *20*, 2723-2741.

Nguyen, D.X., Bos, P.D., and Massague, J. (2009). Metastasis: from dissemination to organ-specific colonization. Nature reviews Cancer *9*, 274-284.

Nieman, K.M., Kenny, H.A., Penicka, C.V., Ladanyi, A., Buell-Gutbrod, R., Zillhardt, M.R., Romero, I.L., Carey, M.S., Mills, G.B., Hotamisligil, G.S.*, et al.* (2011). Adipocytes promote ovarian cancer metastasis and provide energy for rapid tumor growth. Nature medicine *17*, 1498-1503.

Nieto, M.A. (2011). The ins and outs of the epithelial to mesenchymal transition in health and disease. Annual review of cell and developmental biology *27*, 347-376.
Nurnberg, A., Kitzing, T., and Grosse, R. (2011). Nucleating actin for invasion. Nature reviews Cancer *11*, 177-187.

O'Connell, J.T., Sugimoto, H., Cooke, V.G., MacDonald, B.A., Mehta, A.I., LeBleu, V.S., Dewar, R., Rocha, R.M., Brentani, R.R., Resnick, M.B.*, et al.* (2011). VEGF-A and Tenascin-C produced by S100A4+ stromal cells are important for metastatic colonization. Proceedings of the National Academy of Sciences of the United States of America *108*, 16002-16007.

Oberg, C., Li, J., Pauley, A., Wolf, E., Gurney, M., and Lendahl, U. (2001). The Notch intracellular domain is ubiquitinated and negatively regulated by the mammalian Sel-10 homolog. The Journal of biological chemistry *276*, 35847-35853.

Oheim, M., Beaurepaire, E., Chaigneau, E., Mertz, J., and Charpak, S. (2001). Two-photon microscopy in brain tissue: parameters influencing the imaging depth. Journal of neuroscience methods *111*, 29-37.

Olson, E.N., and Nordheim, A. (2010). Linking actin dynamics and gene transcription to drive cellular motile functions. Nature reviews Molecular cell biology *11*, 353-365.

Olson, M.F., and Sahai, E. (2009). The actin cytoskeleton in cancer cell motility. Clinical & experimental metastasis *26*, 273-287.

Orimo, A., Gupta, P.B., Sgroi, D.C., Arenzana-Seisdedos, F., Delaunay, T., Naeem, R., Carey, V.J., Richardson, A.L., and Weinberg, R.A. (2005). Stromal

fibroblasts present in invasive human breast carcinomas promote tumor growth and angiogenesis through elevated SDF-1/CXCL12 secretion. Cell *121*, 335-348.

Ougolkov, A.V., Bilim, V.N., and Billadeau, D.D. (2008). Regulation of pancreatic tumor cell proliferation and chemoresistance by the histone methyltransferase enhancer of zeste homologue 2. Clinical cancer research : an official journal of the American Association for Cancer Research *14*, 6790-6796.

Padua, D., Zhang, X.H., Wang, Q., Nadal, C., Gerald, W.L., Gomis, R.R., and Massague, J. (2008). TGFbeta primes breast tumors for lung metastasis seeding through angiopoietin-like 4. Cell *133*, 66-77.

Paez-Ribes, M., Allen, E., Hudock, J., Takeda, T., Okuyama, H., Vinals, F., Inoue, M., Bergers, G., Hanahan, D., and Casanovas, O. (2009). Antiangiogenic therapy elicits malignant progression of tumors to increased local invasion and distant metastasis. Cancer cell *15*, 220-231.

Paget, S. (1989). The distribution of secondary growths in cancer of the breast. 1889. Cancer metastasis reviews *8*, 98-101.

Palumbo, J.S., Talmage, K.E., Massari, J.V., La Jeunesse, C.M., Flick, M.J., Kombrinck, K.W., Hu, Z., Barney, K.A., and Degen, J.L. (2007). Tumor cell-associated tissue factor and circulating hemostatic factors cooperate to increase metastatic potential through natural killer cell-dependent and-independent mechanisms. Blood *110*, 133-141.

Parks, A.L., Klueg, K.M., Stout, J.R., and Muskavitch, M.A. (2000). Ligand endocytosis drives receptor dissociation and activation in the Notch pathway. Development *127*, 1373-1385.

Parri, M., Taddei, M.L., Bianchini, F., Calorini, L., and Chiarugi, P. (2009). EphA2 reexpression prompts invasion of melanoma cells shifting from mesenchymal to amoeboid-like motility style. Cancer research *69*, 2072-2081.

Pasini, D., Cloos, P.A., Walfridsson, J., Olsson, L., Bukowski, J.P., Johansen, J.V., Bak, M., Tommerup, N., Rappsilber, J., and Helin, K. (2010). JARID2 regulates binding of the Polycomb repressive complex 2 to target genes in ES cells. Nature *464*, 306-310.

Peng, J.C., Valouev, A., Swigut, T., Zhang, J., Zhao, Y., Sidow, A., and Wysocka, J. (2009). Jarid2/Jumonji coordinates control of PRC2 enzymatic activity and target gene occupancy in pluripotent cells. Cell *139*, 1290-1302.

Pertz, O., Hodgson, L., Klemke, R.L., and Hahn, K.M. (2006). Spatiotemporal dynamics of RhoA activity in migrating cells. Nature *440*, 1069-1072.

Pflicke, H., and Sixt, M. (2009). Preformed portals facilitate dendritic cell entry into afferent lymphatic vessels. The Journal of experimental medicine *206*, 2925-2935.

Phng, L.K., and Gerhardt, H. (2009). Angiogenesis: a team effort coordinated by notch. Developmental cell *16*, 196-208.

Pierrat, M.J., Marsaud, V., Mauviel, A., and Javelaud, D. (2012). Expression of microphthalmia-associated transcription factor (MITF), which is critical for melanoma progression, is inhibited by both transcription factor GLI2 and transforming growth factor-beta. The Journal of biological chemistry *287*, 17996-18004.

Pinner, S., Jordan, P., Sharrock, K., Bazley, L., Collinson, L., Marais, R., Bonvin, E., Goding, C., and Sahai, E. (2009). Intravital imaging reveals transient changes in pigment production and Brn2 expression during metastatic melanoma dissemination. Cancer research *69*, 7969-7977.

Pinner, S., and Sahai, E. (2008). PDK1 regulates cancer cell motility by antagonising inhibition of ROCK1 by RhoE. Nature cell biology *10*, 127-137.

Pinnix, C.C., Lee, J.T., Liu, Z.J., McDaid, R., Balint, K., Beverly, L.J., Brafford, P.A., Xiao, M., Himes, B., Zabierowski, S.E.*, et al.* (2009). Active Notch1 confers a transformed phenotype to primary human melanocytes. Cancer research *69*, 5312-5320.

Plath, K., Fang, J., Mlynarczyk-Evans, S.K., Cao, R., Worringer, K.A., Wang, H., de la Cruz, C.C., Otte, A.P., Panning, B., and Zhang, Y. (2003). Role of histone H3 lysine 27 methylation in X inactivation. Science *300*, 131-135.

Poincloux, R., Collin, O., Lizarraga, F., Romao, M., Debray, M., Piel, M., and Chavrier, P. (2011). Contractility of the cell rear drives invasion of breast tumor cells in 3D Matrigel. Proceedings of the National Academy of Sciences of the United States of America *108*, 1943-1948.

Pollock, P.M., Harper, U.L., Hansen, K.S., Yudt, L.M., Stark, M., Robbins, C.M., Moses, T.Y., Hostetter, G., Wagner, U., Kakareka, J.*, et al.* (2003). High frequency of BRAF mutations in nevi. Nature genetics *33*, 19-20.

Potente, M., Gerhardt, H., and Carmeliet, P. (2011). Basic and therapeutic aspects of angiogenesis. Cell *146*, 873-887.

Prezioso, C., and Orlando, V. (2011). Polycomb proteins in mammalian cell differentiation and plasticity. FEBS letters *585*, 2067-2077.

Qin, J.Z., Stennett, L., Bacon, P., Bodner, B., Hendrix, M.J., Seftor, R.E., Seftor, E.A., Margaryan, N.V., Pollock, P.M., Curtis, A.*, et al.* (2004). p53-independent NOXA induction overcomes apoptotic resistance of malignant melanomas. Molecular cancer therapeutics *3*, 895-902.

Rak, J., Mitsuhashi, Y., Bayko, L., Filmus, J., Shirasawa, S., Sasazuki, T., and Kerbel, R.S. (1995). Mutant ras oncogenes upregulate VEGF/VPF expression: implications for induction and inhibition of tumor angiogenesis. Cancer research *55*, 4575-4580.

Rando, O.J. (2012). Combinatorial complexity in chromatin structure and function: revisiting the histone code. Current opinion in genetics & development *22*, 148-155.

Rath, O., and Kozielski, F. (2012). Kinesins and cancer. Nature reviews Cancer *12*, 527-539.

Ren, G., Baritaki, S., Marathe, H., Feng, J., Park, S., Beach, S., Bazeley, P.S., Beshir, A.B., Fenteany, G., Mehra, R.*, et al.* (2012). Polycomb Protein EZH2 Regulates Tumor Invasion via the Transcriptional Repression of the Metastasis Suppressor RKIP in Breast and Prostate Cancer. Cancer research *72*, 3091-3104.

Reya, T., Morrison, S.J., Clarke, M.F., and Weissman, I.L. (2001). Stem cells, cancer, and cancer stem cells. Nature *414*, 105-111.

Ribeiro, C., Ebner, A., and Affolter, M. (2002). In vivo imaging reveals different cellular functions for FGF and Dpp signaling in tracheal branching morphogenesis. Developmental cell *2*, 677-683.

Ridley, A.J. (2011). Life at the leading edge. Cell *145*, 1012-1022.

Ridley, A.J., and Hall, A. (1992). The small GTP-binding protein rho regulates the assembly of focal adhesions and actin stress fibers in response to growth factors. Cell *70*, 389-399.

Ridley, A.J., Schwartz, M.A., Burridge, K., Firtel, R.A., Ginsberg, M.H., Borisy, G., Parsons, J.T., and Horwitz, A.R. (2003). Cell migration: integrating signals from front to back. Science *302*, 1704-1709.

Rinn, J.L., Kertesz, M., Wang, J.K., Squazzo, S.L., Xu, X., Brugmann, S.A., Goodnough, L.H., Helms, J.A., Farnham, P.J., Segal, E.*, et al.* (2007). Functional demarcation of active and silent chromatin domains in human HOX loci by noncoding RNAs. Cell *129*, 1311-1323.

Robinson, B.D., Sica, G.L., Liu, Y.F., Rohan, T.E., Gertler, F.B., Condeelis, J.S., and Jones, J.G. (2009). Tumor microenvironment of metastasis in human breast carcinoma: a potential prognostic marker linked to hematogenous dissemination. Clinical cancer research : an official journal of the American Association for Cancer Research *15*, 2433-2441.

Roesch, A., Becker, B., Meyer, S., Wild, P., Hafner, C., Landthaler, M., and Vogt, T. (2005). Retinoblastoma-binding protein 2-homolog 1: a retinoblastoma-binding protein downregulated in malignant melanomas. Modern pathology : an official journal of the United States and Canadian Academy of Pathology, Inc *18*, 1249-1257.

Roesch, A., Fukunaga-Kalabis, M., Schmidt, E.C., Zabierowski, S.E., Brafford, P.A., Vultur, A., Basu, D., Gimotty, P., Vogt, T., and Herlyn, M. (2010). A temporarily distinct subpopulation of slow-cycling melanoma cells is required for continuous tumor growth. Cell *141*, 583-594.

Rolny, C., Mazzone, M., Tugues, S., Laoui, D., Johansson, I., Coulon, C., Squadrito, M.L., Segura, I., Li, X., Knevels, E.*, et al.* (2011). HRG inhibits tumor growth and metastasis by inducing macrophage polarization and vessel normalization through downregulation of PlGF. Cancer cell *19*, 31-44.

Rosemblat, S., Durham-Pierre, D., Gardner, J.M., Nakatsu, Y., Brilliant, M.H., and Orlow, S.J. (1994). Identification of a melanosomal membrane protein encoded by the pink-eyed dilution (type II oculocutaneous albinism) gene. Proceedings of the National Academy of Sciences of the United States of America *91*, 12071-12075.

Ross, S., Cheung, E., Petrakis, T.G., Howell, M., Kraus, W.L., and Hill, C.S. (2006). Smads orchestrate specific histone modifications and chromatin remodeling to activate transcription. The EMBO journal *25*, 4490-4502.

Rousseau, S., Houle, F., Kotanides, H., Witte, L., Waltenberger, J., Landry, J., and Huot, J. (2000). Vascular endothelial growth factor (VEGF)-driven actin-based motility is mediated by VEGFR2 and requires concerted activation of stress-activated protein kinase 2 (SAPK2/p38) and geldanamycin-sensitive phosphorylation of focal adhesion kinase. The Journal of biological chemistry *275*, 10661-10672.

Roussos, E.T., Balsamo, M., Alford, S.K., Wyckoff, J.B., Gligorijevic, B., Wang, Y., Pozzuto, M., Stobezki, R., Goswami, S., Segall, J.E.*, et al.* (2011). Mena invasive (MenaINV) promotes multicellular streaming motility and transendothelial migration in a mouse model of breast cancer. Journal of cell science *124*, 2120-2131.

Sadi, A.M., Wang, D.Y., Youngson, B.J., Miller, N., Boerner, S., Done, S.J., and Leong, W.L. (2011). Clinical relevance of DNA microarray analyses using archival formalin-fixed paraffin-embedded breast cancer specimens. BMC cancer *11*, 253:251-213.

Safer, D., Elzinga, M., and Nachmias, V.T. (1991). Thymosin beta 4 and Fx, an actin-sequestering peptide, are indistinguishable. The Journal of biological chemistry *266*, 4029-4032.

Sahai, E. (2005). Mechanisms of cancer cell invasion. Current opinion in genetics & development *15*, 87-96.

Sahai, E., Garcia-Medina, R., Pouyssegur, J., and Vial, E. (2007). Smurf1 regulates tumor cell plasticity and motility through degradation of RhoA leading to localized inhibition of contractility. The Journal of cell biology *176*, 35-42.

Sahai, E., and Marshall, C.J. (2002). RHO-GTPases and cancer. Nature reviews Cancer *2*, 133-142.

Sahai, E., and Marshall, C.J. (2003). Differing modes of tumour cell invasion have distinct requirements for Rho/ROCK signalling and extracellular proteolysis. Nature cell biology *5*, 711-719.

Sahlgren, C., Gustafsson, M.V., Jin, S., Poellinger, L., and Lendahl, U. (2008). Notch signaling mediates hypoxia-induced tumor cell migration and invasion. Proceedings of the National Academy of Sciences of the United States of America *105*, 6392-6397.

Sakurai, T., and Kudo, M. (2011). Signaling pathways governing tumor angiogenesis. Oncology *81 Suppl 1*, 24-29.

Sala, A. (2005). B-MYB, a transcription factor implicated in regulating cell cycle, apoptosis and cancer. Eur J Cancer *41*, 2479-2484.

Sanz-Moreno, V., Gadea, G., Ahn, J., Paterson, H., Marra, P., Pinner, S., Sahai, E., and Marshall, C.J. (2008). Rac activation and inactivation control plasticity of tumor cell movement. Cell *135*, 510-523.

Sanz-Moreno, V., Gaggioli, C., Yeo, M., Albrengues, J., Wallberg, F., Viros, A., Hooper, S., Mitter, R., Feral, C.C., Cook, M.*, et al.* (2011). ROCK and JAK1 signaling cooperate to control actomyosin contractility in tumor cells and stroma. Cancer cell *20*, 229-245.

Sauka-Spengler, T., and Bronner-Fraser, M. (2008). A gene regulatory network orchestrates neural crest formation. Nature reviews Molecular cell biology *9*, 557-568.

Schiller, M.R. (2006). Coupling receptor tyrosine kinases to Rho GTPases--GEFs what's the link. Cellular signalling *18*, 1834-1843.

Schmidt, S., and Friedl, P. (2010). Interstitial cell migration: integrin-dependent and alternative adhesion mechanisms. Cell and tissue research *339*, 83-92.

Schmierer, B., and Hill, C.S. (2007). TGFbeta-SMAD signal transduction: molecular specificity and functional flexibility. Nature reviews Molecular cell biology *8*, 970-982.

Schoumacher, M., Goldman, R.D., Louvard, D., and Vignjevic, D.M. (2010). Actin, microtubules, and vimentin intermediate filaments cooperate for elongation of invadopodia. The Journal of cell biology *189*, 541-556.

Schoumacher, M., Louvard, D., and Vignjevic, D. (2011). Cytoskeleton networks in basement membrane transmigration. European journal of cell biology *90*, 93-99.

Schroeter, E.H., Kisslinger, J.A., and Kopan, R. (1998). Notch-1 signalling requires ligand-induced proteolytic release of intracellular domain. Nature *393*, 382-386.

Scott, G., and Leopardi, S. (2003). The cAMP signaling pathway has opposing effects on Rac and Rho in B16F10 cells: implications for dendrite formation in melanocytic cells. Pigment cell research / sponsored by the European Society for Pigment Cell Research and the International Pigment Cell Society *16*, 139-148.
Scully, R. (2000). Role of BRCA gene dysfunction in breast and ovarian cancer predisposition. Breast cancer research : BCR *2*, 324-330.

Shaner, N.C., Campbell, R.E., Steinbach, P.A., Giepmans, B.N., Palmer, A.E., and Tsien, R.Y. (2004). Improved monomeric red, orange and yellow fluorescent proteins derived from Discosoma sp. red fluorescent protein. Nature biotechnology *22*, 1567-1572.

Sharma, S.V., Lee, D.Y., Li, B., Quinlan, M.P., Takahashi, F., Maheswaran, S., McDermott, U., Azizian, N., Zou, L., Fischbach, M.A.*, et al.* (2010). A chromatin-mediated reversible drug-tolerant state in cancer cell subpopulations. Cell *141*, 69-80.

Shen, X., Kim, W., Fujiwara, Y., Simon, M.D., Liu, Y., Mysliwiec, M.R., Yuan, G.C., Lee, Y., and Orkin, S.H. (2009). Jumonji modulates polycomb activity and self-renewal versus differentiation of stem cells. Cell *139*, 1303-1314.

Shields, J.D., Fleury, M.E., Yong, C., Tomei, A.A., Randolph, G.J., and Swartz, M.A. (2007). Autologous chemotaxis as a mechanism of tumor cell homing to lymphatics via interstitial flow and autocrine CCR7 signaling. Cancer cell *11*, 526-538.

Shields, J.D., Kourtis, I.C., Tomei, A.A., Roberts, J.M., and Swartz, M.A. (2010). Induction of lymphoidlike stroma and immune escape by tumors that express the chemokine CCL21. Science *328*, 749-752.

Shojaei, F., Wu, X., Malik, A.K., Zhong, C., Baldwin, M.E., Schanz, S., Fuh, G., Gerber, H.P., and Ferrara, N. (2007a). Tumor refractoriness to anti-VEGF treatment is mediated by CD11b+Gr1+ myeloid cells. Nature biotechnology *25*, 911-920.

Shojaei, F., Wu, X., Zhong, C., Yu, L., Liang, X.H., Yao, J., Blanchard, D., Bais, C., Peale, F.V., van Bruggen, N.*, et al.* (2007b). Bv8 regulates myeloid-cell-dependent tumour angiogenesis. Nature *450*, 825-831.

Shweiki, D., Itin, A., Soffer, D., and Keshet, E. (1992). Vascular endothelial growth factor induced by hypoxia may mediate hypoxia-initiated angiogenesis. Nature *359*, 843-845.

Simon, J.A., and Kingston, R.E. (2009). Mechanisms of polycomb gene silencing: knowns and unknowns. Nature reviews Molecular cell biology *10*, 697-708.

Simons, P.C., Pietromonaco, S.F., Reczek, D., Bretscher, A., and Elias, L. (1998). C-terminal threonine phosphorylation activates ERM proteins to link the cell's cortical lipid bilayer to the cytoskeleton. Biochemical and biophysical research communications *253*, 561-565.

Sitaram, A., Piccirillo, R., Palmisano, I., Harper, D.C., Dell'Angelica, E.C., Schiaffino, M.V., and Marks, M.S. (2009). Localization to mature melanosomes by virtue of cytoplasmic dileucine motifs is required for human OCA2 function. Molecular biology of the cell *20*, 1464-1477.

Sitohy, B., Nagy, J.A., Jaminet, S.C., and Dvorak, H.F. (2011). Tumor-surrogate blood vessel subtypes exhibit differential susceptibility to anti-VEGF therapy. Cancer research *71*, 7021-7028.

Sotiropoulos, A., Gineitis, D., Copeland, J., and Treisman, R. (1999). Signal-regulated activation of serum response factor is mediated by changes in actin dynamics. Cell *98*, 159-169.

Stark, G.R., and Darnell, J.E., Jr. (2012). The JAK-STAT pathway at twenty. Immunity *36*, 503-514.

Stehbens, S., and Wittmann, T. (2012). Targeting and transport: How microtubules control focal adhesion dynamics. The Journal of cell biology *198*, 481-489.

Stenzel, D., Franco, C.A., Estrach, S., Mettouchi, A., Sauvaget, D., Rosewell, I., Schertel, A., Armer, H., Domogatskaya, A., Rodin, S.*, et al.* (2011). Endothelial basement membrane limits tip cell formation by inducing Dll4/Notch signalling in vivo. EMBO reports *12*, 1135-1143.

Stock, J.K., Giadrossi, S., Casanova, M., Brookes, E., Vidal, M., Koseki, H., Brockdorff, N., Fisher, A.G., and Pombo, A. (2007). Ring1-mediated ubiquitination of H2A restrains poised RNA polymerase II at bivalent genes in mouse ES cells. Nature cell biology *9*, 1428-1435.

Straussman, R., Morikawa, T., Shee, K., Barzily-Rokni, M., Qian, Z.R., Du, J., Davis, A., Mongare, M.M., Gould, J., Frederick, D.T.*, et al.* (2012). Tumour micro-environment elicits innate resistance to RAF inhibitors through HGF secretion. Nature.

Strom, M., Hume, A.N., Tarafder, A.K., Barkagianni, E., and Seabra, M.C. (2002). A family of Rab27-binding proteins. Melanophilin links Rab27a and myosin Va function in melanosome transport. The Journal of biological chemistry *277*, 25423-25430.

Stroschein, S.L., Wang, W., Zhou, S., Zhou, Q., and Luo, K. (1999). Negative feedback regulation of TGF-beta signaling by the SnoN oncoprotein. Science *286*, 771-774.

Su, I.H., Dobenecker, M.W., Dickinson, E., Oser, M., Basavaraj, A., Marqueron, R., Viale, A., Reinberg, D., Wulfing, C., and Tarakhovsky, A. (2005). Polycomb group protein ezh2 controls actin polymerization and cell signaling. Cell *121*, 425-436.

Subramanian, A., Tamayo, P., Mootha, V.K., Mukherjee, S., Ebert, B.L., Gillette, M.A., Paulovich, A., Pomeroy, S.L., Golub, T.R., Lander, E.S.*, et al.* (2005). Gene set enrichment analysis: a knowledge-based approach for interpreting genome-wide expression profiles. Proceedings of the National Academy of Sciences of the United States of America *102*, 15545-15550.

Tachibana, M., Takeda, K., Nobukuni, Y., Urabe, K., Long, J.E., Meyers, K.A., Aaronson, S.A., and Miki, T. (1996). Ectopic expression of MITF, a gene for Waardenburg syndrome type 2, converts fibroblasts to cells with melanocyte characteristics. Nature genetics *14*, 50-54.

Taddei, M.L., Parri, M., Angelucci, A., Bianchini, F., Marconi, C., Giannoni, E., Raugei, G., Bologna, M., Calorini, L., and Chiarugi, P. (2011). EphA2 induces metastatic growth regulating amoeboid motility and clonogenic potential in prostate carcinoma cells. Molecular cancer research : MCR *9*, 149-160.

Tagami, S., Okochi, M., Yanagida, K., Ikuta, A., Fukumori, A., Matsumoto, N., Ishizuka-Katsura, Y., Nakayama, T., Itoh, N., Jiang, J.*, et al.* (2008). Regulation of Notch signaling by dynamic changes in the precision of S3 cleavage of Notch-1. Molecular and cellular biology *28*, 165-176.

Takaishi, K., Sasaki, T., Kato, M., Yamochi, W., Kuroda, S., Nakamura, T., Takeichi, M., and Takai, Y. (1994). Involvement of Rho p21 small GTP-binding protein and its regulator in the HGF-induced cell motility. Oncogene *9*, 273-279.

Tavares, L., Dimitrova, E., Oxley, D., Webster, J., Poot, R., Demmers, J., Bezstarosti, K., Taylor, S., Ura, H., Koide, H.*, et al.* (2012). RYBP-PRC1 complexes mediate H2A ubiquitylation at polycomb target sites independently of PRC2 and H3K27me3. Cell *148*, 664-678.

Tcherkezian, J., and Lamarche-Vane, N. (2007). Current knowledge of the large RhoGAP family of proteins. Biology of the cell / under the auspices of the European Cell Biology Organization *99*, 67-86.

Thiery, J.P. (2003). Epithelial-mesenchymal transitions in development and pathologies. Current opinion in cell biology *15*, 740-746.

Thiery, J.P., Acloque, H., Huang, R.Y., and Nieto, M.A. (2009). Epithelial-mesenchymal transitions in development and disease. Cell *139*, 871-890.

Thurber, A.E., Douglas, G., Sturm, E.C., Zabierowski, S.E., Smit, D.J., Ramakrishnan, S.N., Hacker, E., Leonard, J.H., Herlyn, M., and Sturm, R.A. (2011). Inverse expression states of the BRN2 and MITF transcription factors in melanoma spheres and tumour xenografts regulate the NOTCH pathway. Oncogene *30*, 3036-3048.

Tong, Z.T., Cai, M.Y., Wang, X.G., Kong, L.L., Mai, S.J., Liu, Y.H., Zhang, H.B., Liao, Y.J., Zheng, F., Zhu, W.*, et al.* (2012). EZH2 supports nasopharyngeal carcinoma cell aggressiveness by forming a co-repressor complex with HDAC1/HDAC2 and Snail to inhibit E-cadherin. Oncogene *31*, 583-594.

Toyofuku, K., Valencia, J.C., Kushimoto, T., Costin, G.E., Virador, V.M., Vieira, W.D., Ferrans, V.J., and Hearing, V.J. (2002). The etiology of oculocutaneous albinism (OCA) type II: the pink protein modulates the processing and transport of tyrosinase. Pigment cell research / sponsored by the European Society for Pigment Cell Research and the International Pigment Cell Society *15*, 217-224.

Tozer, G.M., Kanthou, C., and Baguley, B.C. (2005). Disrupting tumour blood vessels. Nature reviews Cancer *5*, 423-435.

Treisman, R. (1986). Identification of a protein-binding site that mediates transcriptional response of the c-fos gene to serum factors. Cell *46*, 567-574.

Trenkmann, M., Brock, M., Gay, R.E., Kolling, C., Speich, R., Michel, B.A., Gay, S., and Huber, L.C. (2011). Expression and function of EZH2 in synovial fibroblasts: epigenetic repression of the Wnt inhibitor SFRP1 in rheumatoid arthritis. Annals of the rheumatic diseases *70*, 1482-1488.

Tsai, M.C., Manor, O., Wan, Y., Mosammaparast, N., Wang, J.K., Lan, F., Shi, Y., Segal, E., and Chang, H.Y. (2010). Long noncoding RNA as modular scaffold of histone modification complexes. Science *329*, 689-693.

Urban, E., Jacob, S., Nemethova, M., Resch, G.P., and Small, J.V. (2010). Electron tomography reveals unbranched networks of actin filaments in lamellipodia. Nature cell biology *12*, 429-435.

van Kemenade, F.J., Raaphorst, F.M., Blokzijl, T., Fieret, E., Hamer, K.M., Satijn, D.P., Otte, A.P., and Meijer, C.J. (2001). Coexpression of BMI-1 and EZH2 polycomb-group proteins is associated with cycling cells and degree of malignancy in B-cell non-Hodgkin lymphoma. Blood *97*, 3896-3901.

van Meeteren, L.A., and ten Dijke, P. (2012). Regulation of endothelial cell plasticity by TGF-beta. Cell and tissue research *347*, 177-186.

van Tetering, G., van Diest, P., Verlaan, I., van der Wall, E., Kopan, R., and Vooijs, M. (2009). Metalloprotease ADAM10 is required for Notch1 site 2 cleavage. The Journal of biological chemistry *284*, 31018-31027.

Varambally, S., Cao, Q., Mani, R.S., Shankar, S., Wang, X., Ateeq, B., Laxman, B., Cao, X., Jing, X., Ramnarayanan, K.*, et al.* (2008). Genomic loss of microRNA-101 leads to overexpression of histone methyltransferase EZH2 in cancer. Science *322*, 1695-1699.

Varambally, S., Dhanasekaran, S.M., Zhou, M., Barrette, T.R., Kumar-Sinha, C., Sanda, M.G., Ghosh, D., Pienta, K.J., Sewalt, R.G., Otte, A.P.*, et al.* (2002). The polycomb group protein EZH2 is involved in progression of prostate cancer. Nature *419*, 624-629.

Vartiainen, M.K., Guettler, S., Larijani, B., and Treisman, R. (2007). Nuclear actin regulates dynamic subcellular localization and activity of the SRF cofactor MAL. Science *316*, 1749-1752.

Vaughan, R.B., and Trinkaus, J.P. (1966). Movements of epithelial cell sheets in vitro. Journal of cell science *1*, 407-413.

Verhey, K.J., Kaul, N., and Soppina, V. (2011). Kinesin assembly and movement in cells. Annual review of biophysics *40*, 267-288.

Verona, R., Moberg, K., Estes, S., Starz, M., Vernon, J.P., and Lees, J.A. (1997). E2F activity is regulated by cell cycle-dependent changes in subcellular localization. Molecular and cellular biology *17*, 7268-7282.

Vicente-Manzanares, M., Ma, X., Adelstein, R.S., and Horwitz, A.R. (2009). Non-muscle myosin II takes centre stage in cell adhesion and migration. Nature reviews Molecular cell biology *10*, 778-790.

Vignjevic, D., Kojima, S., Aratyn, Y., Danciu, O., Svitkina, T., and Borisy, G.G. (2006). Role of fascin in filopodial protrusion. The Journal of cell biology *174*, 863-875.

Villanueva, J., Vultur, A., Lee, J.T., Somasundaram, R., Fukunaga-Kalabis, M., Cipolla, A.K., Wubbenhorst, B., Xu, X., Gimotty, P.A., Kee, D.*, et al.* (2010). Acquired resistance to BRAF inhibitors mediated by a RAF kinase switch in melanoma can be overcome by cotargeting MEK and IGF-1R/PI3K. Cancer cell *18*, 683-695.

Wang, C., Liu, X., Chen, Z., Huang, H., Jin, Y., Kolokythas, A., Wang, A., Dai, Y., Wong, D.T., and Zhou, X. (2011). Polycomb group protein EZH2-mediated E-cadherin repression promotes metastasis of oral tongue squamous cell carcinoma. Molecular carcinogenesis.

Wang, H.R., Zhang, Y., Ozdamar, B., Ogunjimi, A.A., Alexandrova, E., Thomsen, G.H., and Wrana, J.L. (2003). Regulation of cell polarity and protrusion formation by targeting RhoA for degradation. Science *302*, 1775-1779.

Wang, R., Chadalavada, K., Wilshire, J., Kowalik, U., Hovinga, K.E., Geber, A., Fligelman, B., Leversha, M., Brennan, C., and Tabar, V. (2010a). Glioblastoma stem-like cells give rise to tumour endothelium. Nature *468*, 829-833.

Wang, W., Eddy, R., and Condeelis, J. (2007). The cofilin pathway in breast cancer invasion and metastasis. Nature reviews Cancer *7*, 429-440.

Wang, W., Goswami, S., Lapidus, K., Wells, A.L., Wyckoff, J.B., Sahai, E., Singer, R.H., Segall, J.E., and Condeelis, J.S. (2004). Identification and testing of a gene expression signature of invasive carcinoma cells within primary mammary tumors. Cancer research *64*, 8585-8594.

Wang, W., Goswami, S., Sahai, E., Wyckoff, J.B., Segall, J.E., and Condeelis, J.S. (2005). Tumor cells caught in the act of invading: their strategy for enhanced cell motility. Trends in cell biology *15*, 138-145.

Wang, X., He, L., Wu, Y.I., Hahn, K.M., and Montell, D.J. (2010b). Light-mediated activation reveals a key role for Rac in collective guidance of cell movement in vivo. Nature cell biology *12*, 591-597.

Watanabe, N., Kato, T., Fujita, A., Ishizaki, T., and Narumiya, S. (1999). Cooperation between mDia1 and ROCK in Rho-induced actin reorganization. Nature cell biology *1*, 136-143.

Watanabe, T., Noritake, J., and Kaibuchi, K. (2005). Regulation of microtubules in cell migration. Trends in cell biology *15*, 76-83.

Webb, D.J., Donais, K., Whitmore, L.A., Thomas, S.M., Turner, C.E., Parsons, J.T., and Horwitz, A.F. (2004). FAK-Src signalling through paxillin, ERK and MLCK regulates adhesion disassembly. Nature cell biology *6*, 154-161.

Weissleder, R., Tung, C.H., Mahmood, U., and Bogdanov, A., Jr. (1999). In vivo imaging of tumors with protease-activated near-infrared fluorescent probes. Nature biotechnology *17*, 375-378.

Wheeler, A.P., and Ridley, A.J. (2004). Why three Rho proteins? RhoA, RhoB, RhoC, and cell motility. Experimental cell research *301*, 43-49.

Widmer, D.S., Cheng, P.F., Eichhoff, O.M., Belloni, B.C., Zipser, M.C., Schlegel, N.C., Javelaud, D., Mauviel, A., Dummer, R., and Hoek, K.S. (2012). Systematic classification of melanoma cells by phenotype-specific gene expression mapping. Pigment cell & melanoma research *25*, 343-353.

Wiley, H.E., Gonzalez, E.B., Maki, W., Wu, M.T., and Hwang, S.T. (2001). Expression of CC chemokine receptor-7 and regional lymph node metastasis of B16 murine melanoma. Journal of the National Cancer Institute *93*, 1638-1643.
Wilkinson, S., Paterson, H.F., and Marshall, C.J. (2005). Cdc42-MRCK and Rho-ROCK signalling cooperate in myosin phosphorylation and cell invasion. Nature cell biology *7*, 255-261.

Wolf, K., and Friedl, P. (2011). Extracellular matrix determinants of proteolytic and non-proteolytic cell migration. Trends in cell biology *21*, 736-744.

Wolf, K., Mazo, I., Leung, H., Engelke, K., von Andrian, U.H., Deryugina, E.I., Strongin, A.Y., Brocker, E.B., and Friedl, P. (2003). Compensation mechanism in tumor cell migration: mesenchymal-amoeboid transition after blocking of pericellular proteolysis. The Journal of cell biology *160*, 267-277.

Wolf, M.J., Hoos, A., Bauer, J., Boettcher, S., Knust, M., Weber, A., Simonavicius, N., Schneider, C., Lang, M., Sturzl, M.*, et al.* (2012). Endothelial CCR2 Signaling Induced by Colon Carcinoma Cells Enables Extravasation via the JAK2-Stat5 and p38MAPK Pathway. Cancer cell *22*, 91-105.

Wolven, A.K., Belmont, L.D., Mahoney, N.M., Almo, S.C., and Drubin, D.G. (2000). In vivo importance of actin nucleotide exchange catalyzed by profilin. The Journal of cell biology *150*, 895-904.

Wu, Y.I., Frey, D., Lungu, O.I., Jaehrig, A., Schlichting, I., Kuhlman, B., and Hahn, K.M. (2009). A genetically encoded photoactivatable Rac controls the motility of living cells. Nature *461*, 104-108.

Wyckoff, J., Wang, W., Lin, E.Y., Wang, Y., Pixley, F., Stanley, E.R., Graf, T., Pollard, J.W., Segall, J., and Condeelis, J. (2004). A paracrine loop between tumor cells and macrophages is required for tumor cell migration in mammary tumors. Cancer research *64*, 7022-7029.

Wyckoff, J.B., Jones, J.G., Condeelis, J.S., and Segall, J.E. (2000). A critical step in metastasis: in vivo analysis of intravasation at the primary tumor. Cancer research *60*, 2504-2511.
Wyckoff, J.B., Pinner, S.E., Gschmeissner, S., Condeelis, J.S., and Sahai, E. (2006). ROCK- and myosin-dependent matrix deformation enables protease-independent tumor-cell invasion in vivo. Current biology : CB *16*, 1515-1523.

Wyckoff, J.B., Wang, Y., Lin, E.Y., Li, J.F., Goswami, S., Stanley, E.R., Segall, J.E., Pollard, J.W., and Condeelis, J. (2007). Direct visualization of macrophage-assisted tumor cell intravasation in mammary tumors. Cancer research *67*, 2649-2656.

Xie, S., Luca, M., Huang, S., Gutman, M., Reich, R., Johnson, J.P., and Bar-Eli, M. (1997). Expression of MCAM/MUC18 by human melanoma cells leads to increased tumor growth and metastasis. Cancer research *57*, 2295-2303.

Xing, F., Saidou, J., and Watabe, K. (2010). Cancer associated fibroblasts (CAFs) in tumor microenvironment. Frontiers in bioscience : a journal and virtual library *15*, 166-179.

Xu, L., Kang, Y., Col, S., and Massague, J. (2002). Smad2 nucleocytoplasmic shuttling by nucleoporins CAN/Nup214 and Nup153 feeds TGFbeta signaling complexes in the cytoplasm and nucleus. Molecular cell *10*, 271-282.

Yana, I., Sagara, H., Takaki, S., Takatsu, K., Nakamura, K., Nakao, K., Katsuki, M., Taniguchi, S., Aoki, T., Sato, H.*, et al.* (2007). Crosstalk between neovessels and mural cells directs the site-specific expression of MT1-MMP to endothelial tip cells. Journal of cell science *120*, 1607-1614.

Yang, L., Pang, Y., and Moses, H.L. (2010). TGF-beta and immune cells: an important regulatory axis in the tumor microenvironment and progression. Trends in immunology *31*, 220-227.

Yasumoto, K., Yokoyama, K., Takahashi, K., Tomita, Y., and Shibahara, S. (1997). Functional analysis of microphthalmia-associated transcription factor in pigment cell-specific transcription of the human tyrosinase family genes. The Journal of biological chemistry *272*, 503-509.
Yin, J.J., Selander, K., Chirgwin, J.M., Dallas, M., Grubbs, B.G., Wieser, R., Massague, J., Mundy, G.R., and Guise, T.A. (1999). TGF-beta signaling blockade inhibits PTHrP secretion by breast cancer cells and bone metastases development. The Journal of clinical investigation *103*, 197-206.

Yokoyama, S., Woods, S.L., Boyle, G.M., Aoude, L.G., MacGregor, S., Zismann, V., Gartside, M., Cust, A.E., Haq, R., Harland, M.*, et al.* (2011). A novel recurrent mutation in MITF predisposes to familial and sporadic melanoma. Nature *480*, 99-103.

Yonemura, S., Hirao, M., Doi, Y., Takahashi, N., Kondo, T., and Tsukita, S. (1998). Ezrin/radixin/moesin (ERM) proteins bind to a positively charged amino acid cluster

in the juxta-membrane cytoplasmic domain of CD44, CD43, and ICAM-2. The Journal of cell biology *140*, 885-895.

Yonenaga, Y., Mori, A., Onodera, H., Yasuda, S., Oe, H., Fujimoto, A., Tachibana, T., and Imamura, M. (2005). Absence of smooth muscle actin-positive pericyte coverage of tumor vessels correlates with hematogenous metastasis and prognosis of colorectal cancer patients. Oncology *69*, 159-166.

Yu, W., Feng, S., Dakhova, O., Creighton, C.J., Cai, Y., Wang, J., Li, R., Frolov, A., Ayala, G., and Ittmann, M. (2011). FGFR-4 Arg(3)(8)(8) enhances prostate cancer progression via extracellular signal-related kinase and serum response factor signaling. Clinical cancer research : an official journal of the American Association for Cancer Research *17*, 4355-4366.

Zabierowski, S.E., Baubet, V., Himes, B., Li, L., Fukunaga-Kalabis, M., Patel, S., McDaid, R., Guerra, M., Gimotty, P., Dahmane, N.*, et al.* (2011). Direct reprogramming of melanocytes to neural crest stem-like cells by one defined factor. Stem Cells *29*, 1752-1762.

Zavadil, J., Cermak, L., Soto-Nieves, N., and Bottinger, E.P. (2004). Integration of TGF-beta/Smad and Jagged1/Notch signalling in epithelial-to-mesenchymal transition. The EMBO journal *23*, 1155-1165.
Zetter, B.R. (1998). Angiogenesis and tumor metastasis. Annual review of medicine *49*, 407-424.

Zhang, F., Tang, Z., Hou, X., Lennartsson, J., Li, Y., Koch, A.W., Scotney, P., Lee, C., Arjunan, P., Dong, L.*, et al.* (2009). VEGF-B is dispensable for blood vessel growth but critical for their survival, and VEGF-B targeting inhibits pathological angiogenesis. Proceedings of the National Academy of Sciences of the United States of America *106*, 6152-6157.

Zhang, K., Wong, P., Zhang, L., Jacobs, B., Borden, E.C., Aster, J.C., and Bedogni, B. (2012a). A Notch1-neuregulin1 autocrine signaling loop contributes to melanoma growth. Oncogene.

Zhang, L., Zhou, F., Drabsch, Y., Gao, R., Snaar-Jagalska, B.E., Mickanin, C., Huang, H., Sheppard, K.A., Porter, J.A., Lu, C.X.*, et al.* (2012b). USP4 is regulated by AKT phosphorylation and directly deubiquitylates TGF-beta type I receptor. Nature cell biology *14*, 717-726.

Zhang, S., Fei, T., Zhang, L., Zhang, R., Chen, F., Ning, Y., Han, Y., Feng, X.H., Meng, A., and Chen, Y.G. (2007). Smad7 antagonizes transforming growth factor beta signaling in the nucleus by interfering with functional Smad-DNA complex formation. Molecular and cellular biology *27*, 4488-4499.

Zhao, J., Sun, B.K., Erwin, J.A., Song, J.J., and Lee, J.T. (2008). Polycomb proteins targeted by a short repeat RNA to the mouse X chromosome. Science *322*, 750-756.

Zhao, X.D., Han, X., Chew, J.L., Liu, J., Chiu, K.P., Choo, A., Orlov, Y.L., Sung, W.K., Shahab, A., Kuznetsov, V.A.*, et al.* (2007a). Whole-genome mapping of histone H3 Lys4 and 27 trimethylations reveals distinct genomic compartments in human embryonic stem cells. Cell stem cell *1*, 286-298.

Zhao, X.H., Laschinger, C., Arora, P., Szaszi, K., Kapus, A., and McCulloch, C.A. (2007b). Force activates smooth muscle alpha-actin promoter activity through the Rho signaling pathway. Journal of cell science *120*, 1801-1809.

Zipfel, W.R., Williams, R.M., and Webb, W.W. (2003). Nonlinear magic: multiphoton microscopy in the biosciences. Nature biotechnology *21*, 1369-1377.